



COST is supported by the EU RTD Framework Programme and ESF provides the COST Office through an EC contract.

Proceedings of International Conference  
Prague, 19 - 20 April 2013

# Applications of Structural Fire Engineering



**COST**- the acronym for European **CO**operation in the field of **Scientific and Technical Research**- is the oldest and widest European intergovernmental network for cooperation in research. Established by the Ministerial Conference in November 1971, COST is presently used by the scientific communities of 35 European countries to cooperate in common research projects supported by national funds.

The funds provided by COST - less than 1% of the total value of the projects - support the COST cooperation networks, COST Actions, through which, with only around € 20 million per year, more than 30.000 European scientists are involved in research having a total value which exceeds € 2 billion per year. This is the financial worth of the European added value which COST achieves.

A bottom up approach (the initiative of launching a COST Action comes from the European scientists themselves), à la carte participation (only countries interested in the Action participate), equality of access (participation is open also to the scientific communities of countries not belonging to the European Union) and flexible structure (easy implementation and light management of the research initiatives ) are the main characteristics of COST.

As precursor of advanced multidisciplinary research COST has a very important role for the realisation of the European Research Area (ERA) anticipating and complementing the activities of the Framework Programmes, constituting a bridge towards the scientific communities of emerging countries, increasing the mobility of researchers across Europe and fostering the establishment of Networks of Excellence in many key scientific domains such as: Biomedicine and Molecular Biosciences; Food and Agriculture; Forests, their Products and Services; Materials, Physics and Nanosciences; Chemistry and Molecular Sciences and Technologies; Earth System Science and Environmental Management; Information and Communication Technologies; Transport and Urban Development; Individuals, Society, Culture and Health. It covers basic and more applied research and also addresses issues of pre-normative nature or of societal importance.

Web: <http://www.cost.eu>

**Proceedings of International Conference  
Application of Structural Fire Engineering  
in Prague, 19 - 20 April 2013**

The production of this publication was supported by COST, [www.cost.esf.org](http://www.cost.esf.org)  
COST Action TU0904

**Integrated Fire Engineering and Response**

Ed. Wald F., Burgess I., Horová K., Jána T., Jirků J.

ISBN – 978-80-01-05204-4

CTU Publishing House, Czech Technical University in Prague

April 2013

250 copies, 516 pages

© COST Office, 2013

No permission to reproduce or utilise the contents of this book by any means is necessary, other than in the case of images, diagrammes or other material from other copyright holders. In such cases, permission of the copyright holders is required. This book may be cited as: Application of Structural Fire Engineering, Prague 19-20 April 2013.

## LIST OF CONTENTS

<b>Preface</b> .....	9
Wald F., <i>Czech Republic</i> , Burgess I., <i>United Kingdom</i>	
<b>Session 1: Structural fire design modelling</b>	
Principles of verification and validation .....	13
Kwaśniewski L., Bojanowski C., <i>Poland</i>	
Car fires with sprinklers: A study on the Eurocode for sprinklers.....	23
Partanen M., Heinisuo M., <i>Finland</i>	
Benchmark example problems for beams at elevated temperatures .....	29
Sawicki B., Pełczyński J., Kwaśniewski L., <i>Poland</i>	
Benchmarking for the inclusion of shear studs in finite element models .....	36
Anderson K., Gillie M., <i>United Kingdom</i>	
The use of optimization in fire development modelling .....	42
Ira J., Hasalová L., Jahoda M., <i>Czech Republic</i>	
A qualitatively model to describe the influence of boundaries on the energy density by considering the energy leakage, and its extension on the system ventilation and fire fighting systems .....	49
Simon P., Schlee S., Schmidt J., Dehn F., <i>Germany</i>	
Comparison of CFD modelling with fire tests .....	55
Sekret R., Saleta D., Sztarbała G., Smardz P., <i>Poland</i>	
FDS versus EN-models .....	61
Molkens T., <i>Belgium</i>	
The comparison of the results of a full scale evacuation test to the calculation method of Hungarian regulations and to the Pathfinder software.....	67
Szilagyí C., <i>Hungary</i>	
CFD modelling of the braced barrel vault made from rectangular hollow sections in natural fire .....	73
Polus L., Szumigala M., Kurzawa Z., Malendowski M., <i>Poland</i>	
Experimental and numerical study of balcony effect in external fire spread into upper floors .....	79
Morgado H.J.L., Rodrigues J.P.C., Laim L.M.S., <i>Portugal</i>	
<b>Session 2: Structural fire design application</b>	
On the use of fire brigade statistics for structural fire safety engineering .....	89
De Sanctis G., <i>Switzerland</i> , Kohler J., <i>Norway</i> , Fontana M., <i>Switzerland</i>	
Stochastic finite element methods for the reliability-based fire-resistant design of structures .....	96
Guo Q., Jeffers A.E., <i>USA</i>	
Interactive interoperability between firefighters and fire protection equipment.....	102
Horová K., Entler S., <i>Czech Republic</i>	
An approach for evaluating vulnerability of bridges against fire hazard.....	108
Kodur V., Naser M., <i>USA</i>	

Performance-based fire safety design of different types of constructions in Germany .....	114
Zehfuss J., Klinzmann C., Paliga K., <i>Germany</i>	
Reducing the risk on a food industry “serious” fire .....	120
Tsatsoulas D., <i>Greece</i>	
Predicting the behaviour of steel fire doors subjected to fire endurance test.....	125
Tabaddor M., Jadhav S., <i>USA</i>	
Numerical simulation of natural fire in an industrial building considering earthquake damage of non-structural members .....	131
Zografopoulou K., Pantousa D., Mistakidis E., <i>Greece</i>	
Robustness of the Vesuvian roofs under the combined overload and high temperatures due to air falls .....	138
Faggiano B., Formisano A., Mazzolani F.M., <i>Italy</i>	
Damage control of intumescent painting .....	144
Molkens T., <i>Belgium</i>	

### **Session 3: Structural response – Steel structures**

Steel temperature calculations in performance based design.....	153
Sandström J., Wickström U., <i>Sweden</i>	
Fire protection of tall steel columns using water sprinklers.....	160
Outinen J., Vaari J., <i>Finland</i>	
A simplified model for modelling flexible end-plate connections in fire .....	166
Lin S., Huang Z., Fan M., <i>United Kingdom</i>	
Fire tests on beams with class 4 cross-section subjected to lateral torsional buckling .....	173
Prachař M., Jandera M., Wald F., <i>Czech Republic</i>	
Resistance of T- and K-joints to tubular members at elevated temperatures.....	179
Ozyurt E., Wang Y.C., <i>United Kingdom</i>	
Post-impact fire resistance of T-stub joint component.....	186
Ribeiro J., Santiago A., Rigueiro C., <i>Portugal</i>	
Finite element analysis of fire resistant reinforcement of end-plate connections .....	193
Tsapara K., <i>Greece</i> , Drosopoulos G.A., <i>Germany</i> , Stavroulakis G.E., <i>Greece</i>	
Protected steel and composite connections in fire .....	200
Schaumann P., Kirsch T., <i>Germany</i>	
Development of a general component-based connection element for structural fire engineering analysis .....	207
Dong G., Burgess I., Davison B., Sun R., <i>United Kingdom</i>	
Behaviour of axially loaded structural bolting assemblies in fire.....	214
Johnson L., Palmiere E., Thackray R., Burgess I., Davison B., <i>United Kingdom</i>	
Structural response under natural fire of barrel shell construction .....	220
Malendowski M., Glema A., Kurzawa Z., Polus L., <i>Poland</i>	
Class 4 sections at elevated temperature .....	226
Hricák J., Wald F., Jandera M., <i>Czech Republic</i>	
Fire design of steel beams with welded class 4 cross-section.....	232
Couto C., Vila Real P., Lopes N., <i>Portugal</i> , Zhao B., <i>France</i>	

Interactive shear resistance of corrugated web in steel beam exposed to fire.....	238
Maślak M., Łukacz M., <i>Poland</i>	
Fire resistance of cold-formed C steel columns .....	244
Lopes N., Arrais F., Vila Real P., <i>Portugal</i>	
Baseline study on the behaviour of cold-formed steel columns subjected to fire.....	251
Craveiro H.D.S., Rodrigues J.P., Laím L., <i>Portugal</i>	
The structural behaviour in fire of a cold-formed steel portal frame having semi-rigid joints.....	258
Johnston R.P.D., Lim J.B.P., Sonebi M., Wrzesien A.M., Armstrong C., <i>United Kingdom</i>	
Fire-induced collapse of steel structures .....	265
Dondera A., Guiliani L., <i>Denmark</i>	
Numerical study of steel beams in sub-frame assembly .....	272
Iqbal N., Heistermann T., Veljkovic M., <i>Sweden</i> , Lopes F., Santiago A., Simões da Silva L., <i>Portugal</i>	
Reduction of connection resistance during Veselí fire tests .....	278
Jána T., Wald F., <i>Czech Republic</i>	
Steel structural fire-resistance design for protecting the world cultural heritage .....	284
Du Y., <i>China</i>	
Reducing design steel temperature by accurate temperature calculations.....	290
Wickström U., Byström A., Sandström J., Veljkovic M., <i>Sweden</i>	
Influence of zinc coating to a temperature of steel members in fire.....	294
Jirků J., Wald F., <i>Czech Republic</i>	
<b>Session 4: Structural response – Concrete structures</b>	
Bending analysis of beams affected by fires.....	301
Salaverry M., Gillie M., <i>United Kingdom</i>	
Influence of high temperature on stiffness of R/C beams.....	307
Kowalski R., Abramowicz M., Glowacki M., <i>Poland</i>	
Analysis of curved reinforced concrete beam in fire conditions.....	314
Ružić D., Saje M., Planinc I., Hozjan T., <i>Slovenia</i>	
Fire resistance performance of welded built-up square CFT columns with reduced intumescent paint.....	320
Kim S., Yom K., Choi S., <i>Korea</i>	
Flexural check at high temperatures of reinforced concrete bridge decks strengthened with EBR-FRP.....	326
Nigro E., Bilotta A., Del Prete I., <i>Italy</i>	
Simplified method for predicting deformations of RC frames during fire exposure .....	334
Youssef M.A., El-Fitiany S.F., <i>Canada</i>	
The impact of car park fire on concrete structure .....	340
Weisenpacher P., Glasa J., Halada L., Valasek L., Dobrucky M., <i>Slovak Republic</i>	
Temperature analysis of lightweight aggregate concrete slab members at elevated temperatures for predicting fire resistance .....	346
Hora M., Štefan R., Procházka J., <i>Czech Republic</i>	

Reinforced concrete walls during fire .....	352
Hayhoe W., Youssef M.A., El-Fitiany S.F., <i>Canada</i>	

### **Session 5: Structural response – Composite structures**

An alternative simplified model of tensile membrane action of slabs in fire .....	361
Burgess I.W., Dai X., Huang S-S., <i>United Kingdom</i>	
Effect of unprotected interior beams on membrane behaviour of composite floor systems in fire I: Experimental investigation.....	368
Tan K-H., Nguyen T-T., <i>Singapore</i>	
Effect of unprotected interior beams on membrane behaviour of composite floor systems in fire II: Numerical assessment.....	374
Nguyen T-T., Tan K-H., <i>Singapore</i>	
Thermomechanical analysis of composite structures using OpenSees .....	380
Jiang J., Li G-Q., <i>China</i> , Usmani A., <i>United Kingdom</i>	
Steel fibre reinforced concrete for floor slabs.....	386
Bednář J., Wald F., Vodička J., Kohoutková A., <i>Czech Republic</i>	
Fire resistance of steel-concrete side-plated beams .....	392
Kolšek J., Hozjan T., Saje M., Planinc I., <i>Slovenia</i>	
Fire performance of an unprotected composite beam .....	399
Selamet S., <i>Turkey</i>	
Fire resistance of steel frames under different fire-after-earthquake scenarios based on scaled design accelerograms .....	405
Pantousa D., Mistakidis E., <i>Greece</i>	
Fire test of timber-fibre concrete composite floor .....	411
Caldová E., Wald F., Kuklíková A., <i>Czech Republic</i>	

### **Session 6: Structural response – Timber structures**

Numerical analysis of timber beam exposed to fire.....	417
Pečenko R., Hozjan T., Turk G., <i>Slovenia</i>	
Numerical modelling of the behaviour of protected and unprotected wooden members under fire .....	423
Dufková M., Kuklík P., <i>Czech Republic</i>	
Estimation of fire resistance by means of calculation performed for atypical exterior wall of a woodstructure .....	427
Vargovský K., Sedlák P., Zachar M., <i>Slovakia</i>	
Cone calorimeter tests on FR treated Norway spruce.....	433
Hartmann P., Kögl J., Beikircher W., <i>Austria</i>	

### **Session 7: Structural response – Material behaviour**

Behaviour of the headed stud shear connectors on composite steel-concrete beams under elevated temperatures utilising carbon nanotube .....	441
Mirza O., Wilkins K., <i>Australia</i>	
Investigations of steel elements with intumescent coating connected to space-enclosing elements in fire .....	447
Kraus P., Mensinger M., Tabelaing F., Schaumann P., <i>Germany</i>	

Numerical and experimental analysis of reactive fire protection systems applied to solid steel rods in tension .....	454
Häßler D., Hothan S., <i>Germany</i>	
Lean duplex stainless steel material tests at elevated temperatures using steady state method .....	461
Huang Y., Young B., <i>China</i>	
Mechanical properties of self-compacting concrete with different additives after high temperature exposure .....	467
Rukavina M.J., Bjegovic D., Gabrijel I., <i>Croatia</i>	
Microstructural and mechanical characterisation of post-tensioning strands following elevated temperature exposure .....	474
Robertson L., Dudorova Z., Gales J., Vega E., Smith H., Stratford T., Blackford R., Bisby L., <i>United Kingdom</i>	
Modelling of the influence of creep strains on the fire response of steel elements .....	480
Torić N., Harapin A., Boko I., Peroš B., Ban M., <i>Croatia</i>	
Strengthening of heat damaged reinforced concrete cylinders .....	486
Roy Danie A.B., Sharma U.K., Bhargava P., <i>India</i>	
Comparative fire performance of high strength concrete columns with different types of fiber reinforcement.....	493
Khaliq W., <i>Pakistan</i> , Kodur V., Raut N., <i>USA</i>	
On the thermo-mechanical characterisation of cement mortars exposed to high temperature.....	501
Bamonte P., Gambarova P.G., <i>Italy</i>	
Evaluation of the fire separating wall after the fire.....	507
Król P.A., <i>Poland</i>	
<b>Author Index</b> .....	513
<b>Scientific and Organizing Committee</b> .....	516





## PREFACE

The current practice in the European Union is that safety, including fire safety, is nationally managed, and requirements are determined by each country's specific experiences. While the political motivations for this approach are obvious, and local circumstances vary between countries, it can easily lead to similar processes having to be re-researched and re-invented country by country. In the context of the European Union, fire safety requirements are based on EU Regulation 305/2011. This document, published by the European Parliament and Council, sets out harmonised conditions for the marketing of construction products as an essential requirement for construction works. In Annex I of this document the basic requirements for mechanical resistance, stability and fire safety are summarised. Construction works must be designed and built in such a way that, in the event of fire: The load-bearing capacity of the construction can be assumed for a specific period of time; The generation and spread of fire and smoke within the works are limited; The spread of the fire to neighbouring construction works is limited; Occupants can leave the works or be rescued by other means; The safety of rescue teams is taken into consideration. The load-bearing capacity of the construction may be modelled on the principles summarised in the parts of the structural Eurocodes which deal with fire. The introduction of common standards in areas related to fire safety, it seems obvious that in such an important area the sharing of experience and research should be facilitated, and hence the need for networks in the COST model.

However, the need for integration has a further dimension. Fire engineering researchers tend to specialise in areas such as fire dynamics, structural fire engineering, active/passive fire protection, environmental protection or human response. Since the background sciences of these disciplines are different there is little interaction between them. Practitioners, including fire engineers, building/fire control authorities, and fire-fighters tend to consider fire safety as a whole, but lack in-depth awareness of recent advances in research and are outside the academic research networks. Through encouraging the exchange of information on different aspects of fire engineering and response between researchers in different countries, the COST TU0904 network "Integrated Fire Engineering and Response" was set up with the intention of fostering an awareness of the current state of the art, and to avoid continual repetition of research. The non-research fire safety community should benefit from exposure to advanced research findings, discussion with researchers, and the sharing of best practice. The input from this community gives researchers an awareness of real-world constraints, and an appreciation of where new research and standards are needed.

The TU0904 Action divides its membership loosely into three themed Working Groups, although clearly its overall mission of promoting integration means that these groups interact on many of the key activities. The Working Groups are: WG1 (Fire Behaviour and Life Safety) which focuses on the behaviour and effects of fire in buildings, combining this research-based knowledge

with the most effective means of protecting human life against the occurrence of fire in the built environment. This includes active fire-fighting measures and the effects of building form on the inherent risk to inhabitants. WG2 (Structural safety) covers the response of different building types to fires and the rapidly-developing research field of structural fire engineering, including new materials and technologies and the effectiveness of passive protection measures. Crucial problems of structural fire engineering concern change of use of buildings and the current imperatives of robustness, sustainability, energy saving and protection of the environment after fire. WG3 (Integrated Design) brings together design, practice and research across the disciplines of fire in the built environment. In structural design this includes integration of fire resistance with all the other functional requirements of a building, from conceptual design onwards, rather than simply adding fire protection after all other processes are complete. Active input from practitioners, regulators and fire-fighters through this group has been vital to the success of the Action.

The Action started in March 2010, and now has 22 nations of the EU, plus New Zealand, among its participants. Its first deliverable, a State of the Art Report attempted to bring together the current state of research, mainly in the participating countries but set into the context of knowledge world-wide. The second deliverable, the Proceedings of the Action's conference in April 2011, allowed the Action to be informed by current research findings from both within and outside the Action. The third deliverable, a volume of Case Studies, presented state-of-the-art examples of current best practice in performance-based practical fire engineering design, based on recent research knowledge. These explained the decision processes, scientific assumptions and practical constraints, as well as the ways in which different aspects of fire engineering were integrated into practice. The fourth deliverable, on Fire Brigade Reports and Investigations, consisted of contributions on the organisation of national fire and rescue arrangements in different EU countries, comparisons of national statistics, recommendations for questions to be included in standardised national fire fighters' reports, and lessons gained from experience of particular disasters.

This volume consists of the Proceedings of the Action's second Conference, held in Prague on 19-20 April 2013. The current activity of the Action, which is visible in the Proceedings, is focused on production of a series of Benchmark Studies, for use by researchers and practitioners. Remaining deliverables of the Action will be contributions to the future development of the fire-related Eurocodes and the educational dimension in the area of structural fire design.

František Wald and Ian Burgess

24 March 2013





## PRINCIPLES OF VERIFICATION AND VALIDATION

Lesław Kwaśniewski <sup>a</sup>, Cezary Bojanowski <sup>b</sup>

<sup>a</sup> Warsaw University of Technology, Faculty of Civil Engineering, Warsaw, Poland

<sup>b</sup> Transportation Research and Analysis Computing Center, Argonne National Laboratory,  
Argonne, IL, USA

### Abstract

This paper discusses the concepts of verification and validation in computational mechanics with special attention to structural fire engineering, by referring to recently published papers and guides on V&V that define some best practices and show directions for future development. The perspective of an analyst, who develops computational models, makes runs, and analyses numerical results mostly using software based on the finite element method, is presented. The considerations emphasize practical problems encountered in the V&V process, potential sources of errors and uncertainties, the importance of sensitivity study, new ideas regarding the relationship between validation and verification, differences between calibration and validation, new aspects of the validation metrics, and guides for designing validation experiments. The discussion is illustrated by computational problem examples.

**Keywords:** benchmark, calibration, fire, sensitivity study, system response quantity, validation, verification

### INTRODUCTION

Wide application of numerical models in structural engineering raises the question about their predictive capability. This question is especially legitimate in the research areas where complex, highly nonlinear structural behaviour is of interest. One of such research areas is the structural fire engineering where interaction of additional effects due to elevated temperatures has to be considered. Among such effects there are: thermal reduction of material properties, generation of additional forces due to constrained thermal deformation, complex thermo, chemical and mechanical effects such as dehydration and vapour pressure leading to premature concrete failure and spalling.

The high, steady interest in computational research for structural fire engineering can be observed based on the simplified statistics presented in Fig. 1 which shows number of related papers recorded in the Google Scholar database (with FIRE in the title and FIRE + "FINITE ELEMENT" anywhere in the article). There can be an expectation for more precise evaluation procedures, specifically dedicated to the considered research area such as structural fire engineering however, in the topic literature definitely dominates opinion that a general procedure applicable to what is called Computational Science and Engineering (CS&E) or Computational Engineering and Physics (CE&P) should be developed, (Oberkampf et al, 2004). The mentioned broad areas encompass many fields of engineering and physics, characterized usually by adjective "computational" such as (computational) fluid dynamics, solid mechanics, and structural dynamics. Even though, it is clear that the expected predictive capability for linear FE static analysis is different than for structural fire engineering, as it is shown schematically in Fig. 2, the same principles of V&V are applicable to all these research fields.

Report (Oden et al, 2006) describes the importance of computer simulation for the development of technical ideas today and predicts a sharp increase in the near future. We are witnessing the continuation of the computer revolution, which, according to Moore's law recognizes (Moore, 1998) a two-fold increase in computing power over the 18 months. In the

80's and 90's it was represented by doubling of the processor clock speed and now represented by an increase of number of transistors that can be packed in a standard chip size. The hardware development is followed by the rapid advancement of numerical programs. For example, based on the finite element method (FEM) commercial program LS-DYNA®, whose source code had 50,000 lines in its early days, in the 70s, now has more than 2.5 million lines in little more than a decade (Kwasniewski, 2009). The improvements in computational capabilities are well illustrated by an example presented in (Belytschko et al, 2000): in the 1970s, a 20 ms crash test simulation using a 300-element vehicle model took about 30 hours of computer time at a cost equivalent to the three-year salary of a university professor. Today's multiprocessor machines allow using a much higher number of finite elements - tens of millions in some FE models. Rapidly increasing number of users or of such programs, with the increasing access to multiprocessor computers with high-performance computing, degrades the computational resource limitations as an excuse for simplified computer simulations. The only limitation left for the use of multiple processors to solve a given problem is scalability of the software for a given problem.

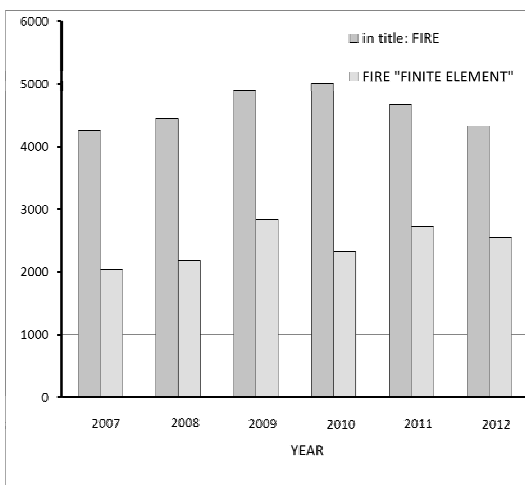


Fig. 1 Number of articles according to Google Scholar

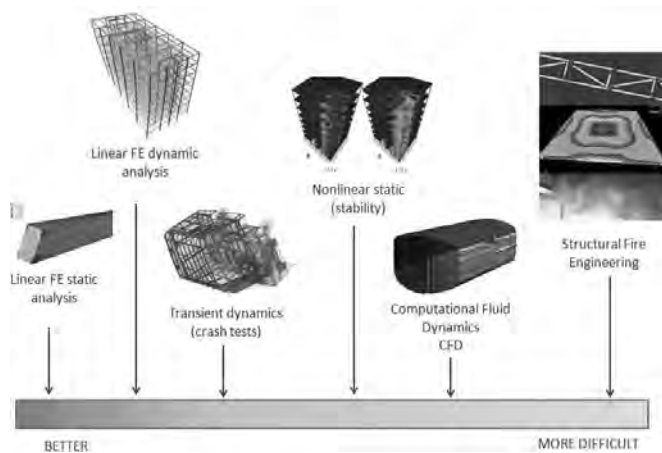


Fig. 2 Predictive capabilities of computer simulations

Despite the rapid hardware and software development there are many contradictory opinions about the reliability of computer predictions (Babuska & Oden, 2004), best expressed by a famous statement: “Essentially, all models are wrong, but some are useful” (Box & Draper, 1987). It is almost impossible to model all the aspects of a complex event, yet valuable conclusions from a series of simulations can be concluded if proper tools and statistical measures are used through the V&V procedures. Early in the development of the finite element method, the Journal of Applied Mechanics rejected FE papers for being insufficiently scientific (Belytschko et al, 2000). Today's general attitude is definitely evolving towards more acceptance of computer predictions, and the numerical results obtained using the dominant FE method are present in numerous technical and scientific papers from many different research areas.

## 1 MODELLING, VERIFICATION AND VALIDATION

Today verification and validation (V&V) is recognized as the primary method for evaluating the confidence of computer simulations (Oberkampf et al, 2004). The relationships between activities involved in the development of mathematical and computational models and in their verification and validation, are often schematically presented using diagrams such as the one shown in Fig. 3 (Kwasniewski, 2009). In Fig. 3, the boxes represent four main concepts: reality of interest, mathematical model, computer models, and validation experiments. Reality of interest relates itself to two aspects: to the physical system containing objects as well as to

the processes intended for analysis. Reality of interest can apply to existing objects or to new solutions (prototyping) but always refers to somehow defined physical objects, for example to a structural element subjected to furnace test or to a whole structure subjected to full scale fire test.

The mathematical (or conceptual) model comprises all assumptions and definitions characterizing the mathematical representation of the reality of interest formulated generally as a system of partial differential equations (PDEs) complemented by boundary and initial conditions (Oberkampff et al, 2004). The transition from reality of interest to mathematical model depends on the objective of the analyses, understanding of physics, the analyst's experience, and resources. Formulation of the mathematical model is the first step in the model development and the first source of errors.

Usually, physical problems of a practical nature, represented by such mathematical models, cannot be solved analytically due to the complexity of, for example, their geometry. To find the solution, a mathematical model is replaced by an approximate computer (computational) model using the process of numerical discretization, which replaces PDEs with sets of algebraic (matrix) equations more suitable for computers. The discretization of space and time can be done using procedures such as the finite element, finite difference, finite volume, and boundary element methods. In solid mechanics and structural dynamics, space discretization is dominantly done with the finite element (FE) method. Time domain of transient events is discretized with finite difference method. In practice FE model development, especially when a commercial code is used, requires many decisions on selection among numerous options.

The last box in Fig. 3 contains a set of validation experiments designed using the validation hierarchy (Oberkampff et al, 2004). The objective of these tests is to increase the accuracy and predictive capability of computer models. Specially designed additional experiments are supposed to provide answers for the questions raised during model development and to quantify the model's uncertainties.

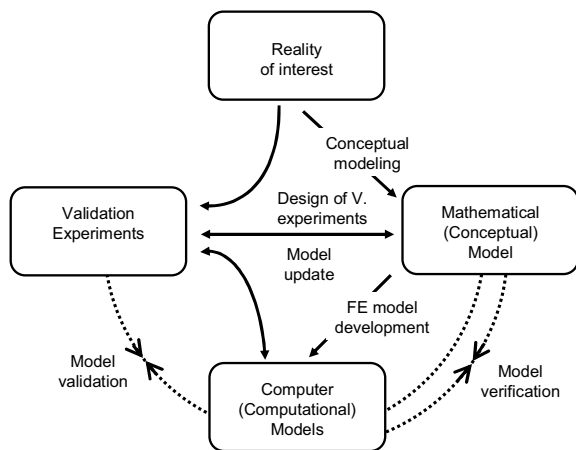


Fig. 3 Relations between modelling, verification and validation (Kwasniewski, 2009)

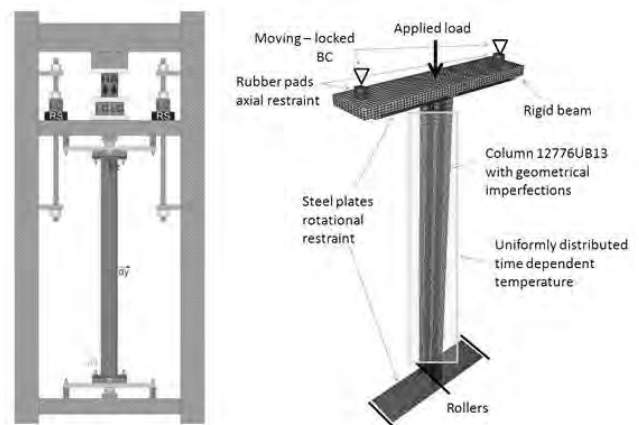


Fig. 4 Example parametric study of furnace test on rotationally restrained steel columns in fire

The solid lines indicate the activities of general model development, including conceptual modelling, computer (FE) model development (i.e., software implementation), and design of validation experiments. Some of these activities are marked with arrows on both sides to show their interactive character, and especially good cooperation between analysts and experimentalists is recommended (Kwasniewski, 2009). The assessment activities, marked with dashed lines, involve verification and validation. Verification and validation should be performed with respect to assumed objectives defining the quantities of interest. The difference between verification and validation is probably most accurately expressed by

Roache's informal statement: "Verification deals with mathematics; validation deals with physics" (Roache, 1998). Verification uses comparison of computational solutions with highly accurate (analytical or numerical) benchmark solutions and among themselves, whereas validation compares the numerical solution with the experimental data. Verification comprises of model and code verification stages. The analyst is usually provided with a software and the code verification stage is usually performed by for software developer. The objective of V&V practices, which is generally to corroborate (mathematical and computational) model for its intended use, can be practically split into three tasks: to detect and separate the model's significant discrepancies, to remove and reduce removable and unavoidable errors, and to evaluate uncertainties in the results. A very important aspect of the V&V process is the proper determination of sources for all significant errors. The dashed line representing validation connects experiments with both the computer and mathematical models. Although validation involves direct comparison of computational results and experimental data, the differences encountered have their sources in both models. It has been pointed out (ASME, 2006) that verification should precede validation, but even the most extensive verification cannot remove all errors (e.g., due to discretization) so validation evaluates the whole modelling process, and some of the errors that originated in different modelling phases cannot be completely separated, compare (Schwer, 2006).

## **2 DIFFICULTIES WITH EXPERIMENTAL VALIDATION IN STRUCTURAL FIRE ENGINEERING**

Experimental validation in the structural fire engineering through comparison between numerical results and experimental data obtained using furnace tests is difficult and has many limitations which are not only economical but also are due to inevitable uncertainties characterising the specimen behaviour (Gillie, 2009). Practically, always limited number of measurements during such tests cannot provide entire information about the space and time distribution of temperatures, evolution of boundary conditions, or generation of additional forces due to constrained thermal and mechanical deformation. The limitations of experimental validation increase the importance of verification which is supposed to deliver evidence that mathematical models are properly implemented and that the numerical solution is correct with respect to the mathematical model.

The problems with experimental validation of computer simulations of structures subjected to fires can be illustrated using the following parametric study (Kwasniewski et al, 2013) where a furnace test (Ali F & O'Connor, 2001) on restrained steel columns was replicated using a coupled structural-thermal numerical calculations, see Fig. 4. The objective of the study was to identify and quantify all possible modelling parameters which can affect the numerical results. The study was focused on improving prediction capabilities for the purpose of virtual testing.

Common model calibration was replaced by experimental validation and extensive parametric study. The calibration is understood here as a posteriori procedure where through repeated calculations with modified input parameters we try to find an "optimal" set of input data which can provide the model's response closest to the actual experimental data. It can happen that due to superimposing of errors we can get good correlation between experimental and numerical results for a wrong model, defined by incorrect input parameters. Often, such a situation can be detected when the model is used for a different case with changed input conditions. Also, a complex model with only some of the input parameters "correctly" calibrated should give a response different from the experimental data due to the indeterminacy of other parameters. This is why validation based on more than one experiment is considered as more reliable (Oberkampf et al, 2004).

In the considered parametric study the comparison of the numerical results and the experimental data was presented for the relationships between column's average temperature and axial force, axial displacement, and lateral displacement in the middle section. Three



critical modelling characteristics were determined: material behaviour, geometrical imperfections, and longitudinal variation of the column temperature. It was found that the postponed buckling occurring at higher furnace temperatures is due to a non-uniform temperature distribution along the column, caused by heat transfer at the partially insulated furnace openings. The study shows how the modelling factors, initially ignored, may affect the numerical results without calibrating the FE model. In the authors' opinion it is not possible to correlate better numerical results with the existing experimental data without reducing model uncertainties (e.g. imperfection magnitudes and loading variation) through additional experiments and measurements. It seems that due to many uncertainties characterizing the fire experiments, with often their wide variation, it is not justifiable to show the comparison between numerical and experimental results in a traditional deterministic way, where only two numbers or curves (i.e. experimental and numerical) are presented.

### **3 BENCHMARK PROBLEMS AND VERIFICATION**

Verification is supposed to deliver evidence that mathematical models are properly implemented and that the numerical solution is correct with respect to the mathematical model. Due to the high complexity of mostly nonlinear problems that are practically important, such verification can be conducted only empirically using "a posteriori" approach where the reasoning is based on the experience coming from repeated calculations. A standard example is the posteriori error estimation based on numerical results for different mesh resolutions. According to (AIAA, 1998) verification can be conducted through tests of agreement between a computational solution and four types of benchmark solutions: analytical, highly accurate numerical solutions of an ODE or PDE problem, and manufactured solutions. In contrast to numerical solutions used in the validation stage, the numerical solutions applied for verification can represent mathematical models with little physical importance.

The importance and usefulness of benchmark studies for specific areas of CS&E such as structural fire engineering is postulated in many papers and conference proceedings. A benchmark example should satisfy the following requirements. The problem considered should be relatively simple, easy to understand. The considered case can show little of practical meaning. It is supposed to be used for verification of computational models not to solve an engineering problem. The complete input data must be provided in an easy to follow way. All assumptions regarding material properties, boundary conditions, temperature distribution, loading conditions, large/small deformations and displacements should be identified. If a numerical solution is considered as a benchmark problem the mesh density study should also be considered and it should be shown that provided results are within the range of asymptotic convergence. One should also consider as a part of verification to use alternative numerical models e.g. different codes or solid vs. shell finite elements (if possible). Publishing a benchmark study we claim that this is a reliable solution. Hopefully, this assumption will be verified by other users. Benchmark problems can serve for code developers but are probably the most helpful for code users who can verify their modelling assumptions, as most of the errors are due to the analyst's mistakes.

### **4 COMPARISON BETWEEN EXPERIMENTAL AND NUMERICAL RESULTS**

The soundness of an experiment as a source of data for validation depends also on the relationship between the application and the validation domains (Oberkampf et al, 2004). The application domain defines the intended boundaries for the use and predictive capability of the computational model. The validation domain characterizes the representation capabilities of the experiment. When a complex system is modelled, there is a need for many validation experiments capturing different physical aspects of the system (e.g., different loading scenarios, boundary and initial conditions) on different level of complexity of the model. Unfortunately, due to high cost of furnace tests, the experiments are rarely repeated and the

probability distribution of the test results is undefined. This distribution can be dramatically different, depending on the selection of the so called system response quantity (SRQ). Some of the researchers acknowledge large discrepancies between the experiment and the computation especially for concrete structural elements subject to elevated temperatures when the important role of moisture transport on the spalling mechanism is not sufficiently captured in the computational model (Heijden & Bijnen, 2007). The need for multiple experiments and computational probabilistic analysis can be best described by Fig. 5 presenting the difference that can be measured between a single experiment and a single simulation and the actual means of a given measure. Sensitivity of this measure to a given parameter is represented by the shape (width) of the distribution function. When comparing simulated results to just one experimental result the analyst has no confidence about representativeness of the experiment result. In the process of calibrating the computational model to just one experiment actually more errors can be introduced in the model and its predictive capability can be negatively affected for a different set of initial parameters

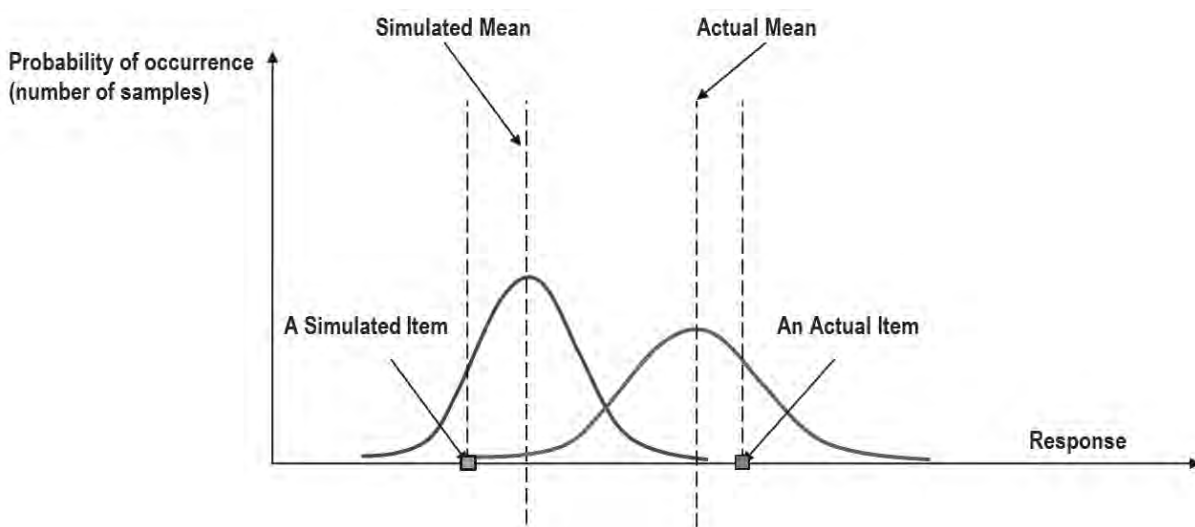


Fig. 5 Difference between simulated and experimental values for a single and item and a population of results

#### 4.1 Validation domains

The ideal situation, possible only for simple systems, is when the validation domain completely overlaps the application domain. This means that the available set of the validation experiments covers all possible parameters defining the computational model within its intended application. When complex systems are analysed, it is sometimes infeasible or even impossible to conduct all necessary experiments to verify all features of the computational model. An example of such a situation is the global analysis of structures in the fire (Foster, 2007). There have been only a few full-scale experimental fire tests (i.e., the Cardington tests) conducted so far, but there are numerical capabilities for such complex analysis. The extreme, theoretical situation is when all possible or available experiments are too far from the application of interest and there is no overlap between the validation domain and the application domain. The credibility of such a computational model, validated only through extrapolation, is obviously much smaller. To improve the predictive capability of computation in such cases, hierarchical validation is introduced where closer correlation of the domains is possible for lower-level experiments and then the gained confidence is extrapolated to the global model.

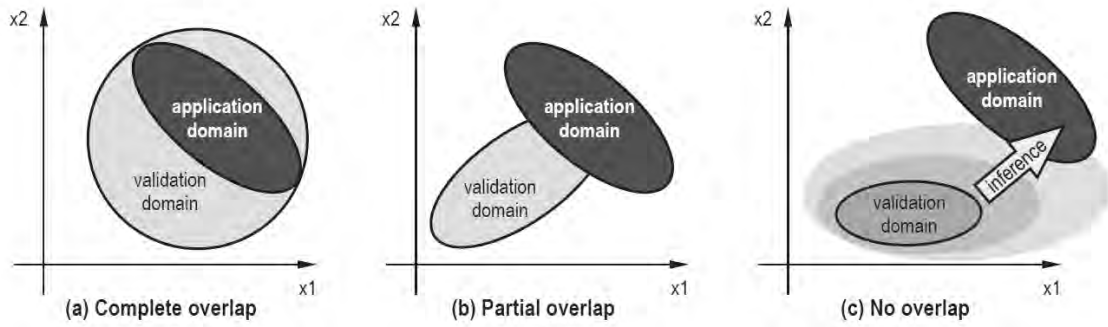


Fig. 6 Possible relations between validation and application domains (Thacker et al, 2004)

## 4.2 Validation metrics

Another important issue affecting the outcome of the comparison between the experimental and numerical results is which parameter (SRQ) we select for the comparison and how it is represented, deterministically or in a probabilistic manner. In (Oberkampff et al, 2004), the authors distinguish six levels of validation comparisons, see Fig. 6. In the first level approach, the simplest and the most common in today's practice, a strictly qualitative comparison is done using plots over the domain, for example, showing the deformation of a structure. The second level represents a more quantitative but still fully deterministic comparison of the numerical and corresponding experimental, single value input-response pairs, using tables or plots. The second and third levels are most common in papers and reports dealing with computational analyses. In the next, higher levels of comparison, the nondeterministic nature of experimental data with both errors and uncertainties is taken into account. Instead of single values for the input and the corresponding result, there are value bars with the centre point representing the mean value and the length equal to two standard deviations (Oberkampff et al, 2004). The value bars provide information on the probability distribution estimated based on the multiple experiments and can be applied to both uncertainties in the input and in the results.

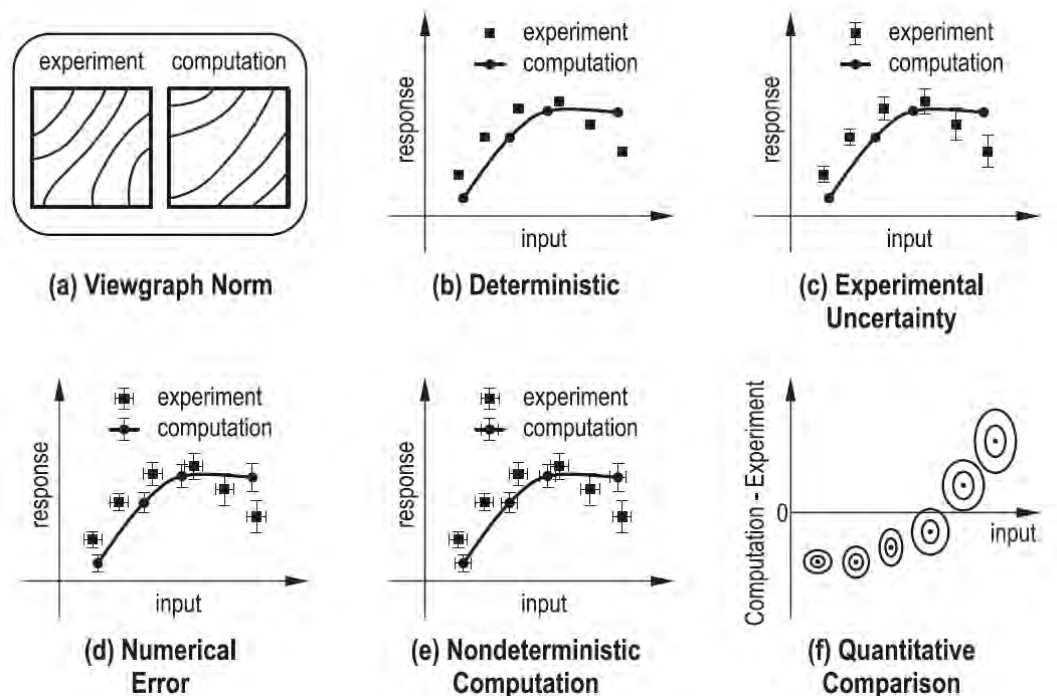


Fig. 7 Quality levels of validation metrics (Oberkampff et al, 2004)

The highest levels are represented by comparison methods where additionally the computational results are treated as nondeterministic, with their own input and output uncertainties. The necessary information is provided by repeated computations for the input variation determined by the experimentally estimated probability distributions (Szabó, 2008). The ideal approach according to (Oberkampf et al, 2004) would show the difference between the computational and experimental probability distributions over the whole possible range of the input quantity, but that would require an enormous effort for any real life application. It should be remembered that for a nonlinear system the relationship between the input and the output can be very complex, and for example, the mean values of the response do not have to be equal to the response for the mean values of the input parameters, compare Fig. 5.

### 4.3 System response quantity

As already mentioned, the validation procedure is based on the comparison between computational results and experimental data. Generally, an experiment can provide much less information than the calculation. The measurements for a quasi-static experiment on an engineering structure usually give us loadings, displacements, and strains. A dynamic experiment provides time histories of loads, strains, displacements, and accelerations. In thermal analysis, the spatial distribution of temperatures is measured. The measurements are done for a limited number of selected locations. Not all the experimental output data is equally representative and has the same importance for comparison with the computation. For example, strain in a uniform beam subject to bending is a local quantity related to internal forces in the considered cross-section. However, the maximum deflection of the same beam is a more representative quantity as it is the result of all deformations along the beam and depends on the whole distribution of internal forces and on boundary conditions. The correlation between the experimental and computational displacements for such a case is more important for the purpose of validation than comparison of local strains. The comparison of stresses instead of strains is more common in engineering practice but requires recalculation of experimentally directly measured strains using material properties affected by their uncertainties. In structural dynamics, we get a better correlation between smoother time histories of displacements than between their second time derivatives—time histories of accelerations that are rougher. The selection of the system response quantity (SRQ) is often limited by the experiment output, e.g., for the earthquake or crash analyses time histories of accelerations are the basic output information.

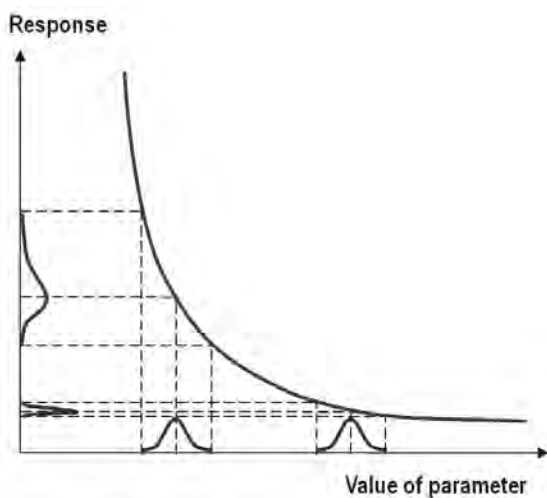


Fig. 8 Different sensitivity of a response on a parameter variation

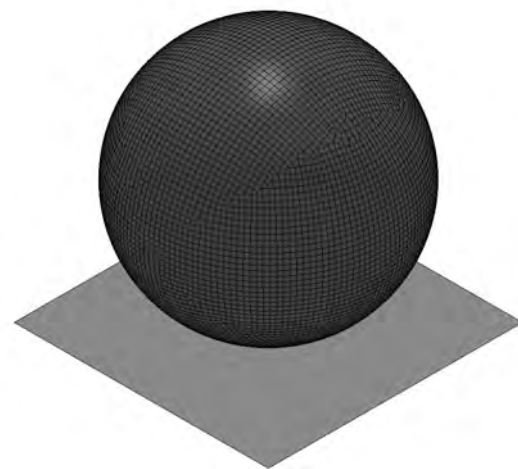


Fig. 9 Model of a hollow glass ball subject to gravity acceleration

Also the range in which we test given response has a great impact on accuracy of the results. If in a given range the response is not sensitive to variation of the input parameter the

accuracy of prediction can be high (See Fig. 8). In some other range the response may be highly sensitive to the variation of the input parameter and the accuracy of the prediction may be significantly lower.

Let's introduce the general idea of predictive capabilities of numerical calculations (i.e. computer simulations) through a simplified example problem of structural mechanics. In this problem we consider a test where a hollow glass ball with external radius of 25mm and the wall 1mm thick is falling under gravity from a prescribed height (2.0 m) and hits a rigid surface. The schematic of the test is shown in Fig. 9. The question is how precisely we can predict the considered process using available nowadays software. From an experimental point of view this test can be performed multiple times and probabilistic values for input parameters characterizing glass as well as response can be measured. Geometrical imperfections on macroscopic level can be also measured for the ball. Although experiments are controlled by many parameters we don't have to measure all of them to be able to perform the tests. For example, not knowing failure parameters in the glass we can drop a hundred balls and measure a radius occupied by all the shattered pieces of the ball. To perform an equivalent simulation many more parameters has to be measured or provided to the analyst. Performed here simulation in LS-DYNA software required detailed material properties of the glass including failure and erosion criteria to allow for material separation. Such process, although non-physical, is often used in simulations that pertain to material separation. If any of the SRQ is related to the failure it may be predicted with large error or uncertainty. Mesh size and mesh pattern are directly influencing the patterns of cracks that can develop only through the eroded elements. On the other hand for example the maximum force that is exerted by the ball on the ground is less affected by the mesh pattern and primarily depends on the mass and the drop height of the ball.

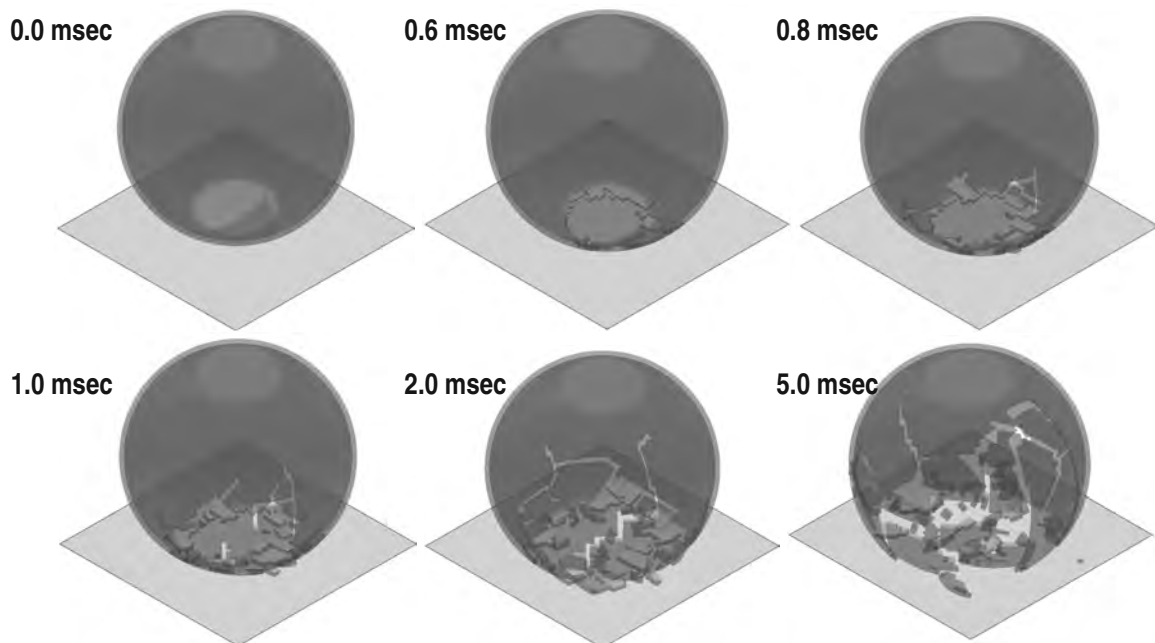


Fig 10. Evolution of glass ball failure upon impact on rigid surface

## 5 SUMMARY

Recently in the literature, some guidelines for improving validation procedures have been formulated. Validation hierarchy, placed in opposition to the model calibration common today, and new validation metrics are examples of such improvement concepts. The examples presented in this paper show how much the result of validation can be affected by the selection of the system response quantity and that there is no universal metrics. The importance of the comparisons using view graphs, often considered in the literature as lower-

level practice, is also emphasized as an efficient method for checking the physical validity of mathematical models. What should be recommended, especially for complex problems with practical meaning, is the design of simple experimental tests placed on different levels of hierarchical validation. Such simple and less expensive tests can provide more valuable material for comparison than costly experiments on entire structure.

## REFERENCES

- AIAA. Guide for the Verification and Validation of Computational Fluid Dynamics Simulations, American Institute of Aeronautics and Astronautics, AIAA-G-077-1998, Reston, VA, 1998.
- Ali F., O'Connor D. 2001. Structural performance of rotationally restrained steel columns in fire, *Fire Safety Journal* 36.
- ASME Guide for Verification and Validation in Computational Solid Mechanics, The American Society of Mechanical Engineers, ISBN #: 079183042X, 2006.
- Babuska I., Oden J. T., Verification and validation in computational engineering and science: basic concepts, *Computer Methods in Applied Mechanics and Engineering*, Elsevier, 193 (36-38) 2004, 4057-4066.
- Belytschko T., Liu W. K., Moran B., Nonlinear finite elements for continua and structures, Wiley New York, 2000.
- Box G. E. P., Draper N. R., Empirical model-building and response surfaces, John Wiley & Sons., pp. 669, 1987.
- Foster S., Chladna M., Hsieh C., Burgess I., Plank R., Thermal and structural behaviour of a full-scale composite building subject to a severe compartment fire, *Fire Safety Journal*, 42- 3, 183-199, 2007.
- Gillie M., Author's Analysis of heated structures: Nature and modelling benchmarks, *Fire Safety Journal* 44, pp. 673–680, 2009.
- Kwasniewski L., Ali F., Balcerzak M., Coupled structural-thermal calculations for restrained steel columns in fire, *Journal of Structural Fire Engineering* vol. 4, no. 1, March 2013, pp. 59-70, 2013.
- Kwasniewski L., On practical problems with verification and validation of computational models, *Archives of Civil Engineering*, 55 (3), 323-346, 2009.
- Moore G.E., Cramming more components onto integrated circuits, *Proceedings of the IEEE*, Institute of Electrical and Electronics Engineers, 86 (1), 1998, 82-85.
- Oberkampf W.L., Trucano T.G., Hirsch C., Verification, validation, and predictive capability in computational engineering and physics, *Appl. Mech. Rev.* 57 (5), 345–384, 2004.
- Oden J. T., Belytschko T., Fish J., Hughes T. J., Johnson C., Keyes D., Laub A., Petzold L., Srolovitz D., Yip S., Revolutionizing engineering science through simulation, National Science Foundation Blue Ribbon Panel Report, (65), 2006.
- Roache P.J., *Verification and Validation in Computational Science and Engineering*, Hermosa Publishers, Albuquerque, NM 1998.
- Schwer L.E., An Overview of the ASME Guide for Verification and Validation in Computational Solid Mechanics. LS-DYNA Anwenderforum, Ulm 2006.
- Szabó B.A., Actis R.L., On the role of hierarchic spaces and models in verification and validation, *Comput. Methods Appl. Mech. Engrg.* doi:10.1016/j.cma.2008.04.025, 2008.
- Thacker B. H., Hemez F. M., Anderson M. C., Pepin J. E., Rodriguez E. A., *Concepts of Model Verification and Validation.*, Los Alamos National Laboratory, 2004.
- Van der Heijden G. H. A., Van Bijnen R. M. W., Pel L., Huinink H. P., Moisture transport in heated concrete, as studied by NMR, and its consequences for fire spalling, *Cement and Concrete Research*, Volume 37, Issue 6, 894-901, June 2007.

## CAR FIRES WITH SPRINKLERS: A STUDY ON THE EUROCODE FOR SPRINKLERS

Mikko Partanen<sup>a</sup>, Markku Heinisuo<sup>a</sup>

<sup>a</sup> Tampere University of Technology, Faculty of Business and Built Environment, Tampere, Finland

### Abstract

The effect of sprinklers is taken into account in EN 1991-1-2 using reduction factors for the fire load. The applicability of the Eurocode method to car fires was studied by modelling the fires with Version 5.5.3 of the FDS program by NIST. The computer model is validated against tests completed in the UK in 2006-2009. Three medium-size car fires are modelled without and with the typical sprinklers used in car parks. The validation results showed that the developed car fire model works well with the actual reference fires, with and without sprinklers. The Eurocode reduction of fire load with sprinklers gives the same maximum temperatures as the simulation with sprinklers up to the first peak of the heat release rate (HRR). The Eurocode reduction does not take into account the fact that adjacent cars do not ignite, as is the case with the developed model and as observed in the tests. The Eurocode method is reliable up to the first peak, after that it is very conservative.

**Keywords:** car fire, sprinkler, Eurocode, FDS.

### INTRODUCTION

Fire safety is one of the key issues when designing buildings. Car parks, open or enclosed, are typical in modern urban environments. Car fires have been studied for many years. The study of the of heat release rate (HRR) of cars began only with the car tests of VTT in Finland in 1991 (Mangs & Loikkanen, 1991). After that many researches have been completed (BRE, 2009). Extensive literature references and interesting statistical data are given in (Li, 2004). Not only cars, but also parts of cars, such as tyres (Gratkowski, 2012) and engine compartments (Weisenpacher et al, 2010) have also been studied. The /actual heat release rate as function of time from ignition is generally the main property in the modelling of fires.

Car fires have in many cases been modelled using computational fluid dynamics (CFD), and most of the analyses, such as (Halada et al, 2012), have been completed using a fire dynamics simulator (FDS) by NIST (Mc Grattan et al, 2010, or older version). Only CFD is considered in this study.

Regarding structural design in fire, the most advanced approach is to use the probabilistic method where the effects (mechanical loads, fire) and the resistances, including passive and active fire-fighting, are determined with their statistical values (distribution, mean, variation) up to the required safety index presented in the Eurocodes for accidental events for the design life time of the building. This method is used in (Schaumann et al, 2010) for open car parks. The Eurocodes allow using not only a fully probabilistic method but also the performance based method which uses the relevant HRR data of the fire to determine temperatures in fire. The Eurocode (EN 1991-1-2, 2003) includes reduction factors for fire loads when sprinklers are used. After the determination of the gas and structure temperatures, the resistances of structures can be checked during the entire fire. In most cases heat transfer analysis and mechanical analysis of structures can be done independently.

No design data for car fires are given in the Eurocodes. The main goal of this paper is to provide background data for car fires and to study the usability of the reduction factors for sprinklers mentioned in the Eurocodes. It is believed by the authors that car fires have generally been well studied and documented, starting with typical cars in the car parks of

buildings (Schleich et al, 1997) and ending up with the worst case scenario involving petrol tankers (see Haack et al, 2005).

## 1 FDS MODEL AND ITS VALIDATION

### 1.1 The FDS model for car fires

The developed model for category 2 (Schleich et al, 1997) car fires includes a burning plane of 1.8x4.8 m<sup>2</sup> (Schleich, 2010) located 500 mm above the floor level. The heat release rate (HRR) curve is fitted to (Schleich et al, 1997) with a peak value of 8 MW at 25 minutes from ignition. The design curve is fitted so that the released energy per one car is 7500 MJ, as required by the categorisation. The adjacent cars are located at a distance of 600 mm, and the next car ignites 12 minutes after the previous one (Joyeux et al, 2001). To make it possible for the fire to spread from one car to another, the burning plane is assigned material properties representing the inner parts of the car. The details of the modelling are given in (Heinisuo & Partanen, 2013). Tyres are objects with an independent HRR curve based on (Gratkowski, 2012). Generally the ignition temperature of tyres is 371-425 °C (Gratkowski, 2012) but in this study it is set to 250 °C to make the overall car model work better with the verification tests. Thus, two car fire models were developed. In one model the ignition time of the adjacent car was pre-set to 12 minutes. The second model was fine-tuned to make the second car ignite about 12 minutes after the first one via broken windows and burning tyres. The second model can also be used for other purposes than adjacent car fires, for example, if the ignition source is some other nearby object.

The windows were supposed to break at 300 °C (Weisenpacher et al, 2012). The side windows of the first ignited car are open to have enough oxygen to enable the fire to burn inside the car. The fire spreads via breaking windows and burning tyres from one car to another so that the second car ignites about 720 s (12 minutes) after the first one, and the third car ignites about 1440 s (24 minutes) after the first. Two materials are used for windows. Automotive windscreens are usually made of laminated glass while side and rear windows are of tempered glass. The car itself is modelled using the non-burning wrought aluminium (Bertram & Buxmann, 2007), used in cars today. There are ventilation openings at the front of the cars and around the tyres. Two tyres have thermocouples monitoring the spread of the fire from one car to another. There are also thermocouples at each burning plane to monitor the ignition temperatures inside the car.

The grid size is 100x100x100 mm<sup>3</sup> near the car making the resolution (Heinisuo et al, 2008) 25, which means a rather dense and accurate grid. Some analyses use a grid size of 200x200x200 mm<sup>3</sup> to accelerate computations at the 3 m zone from the edges of the computational space.

The HRR curves for one and three adjacent cars are shown in Figs. 1 and 2.

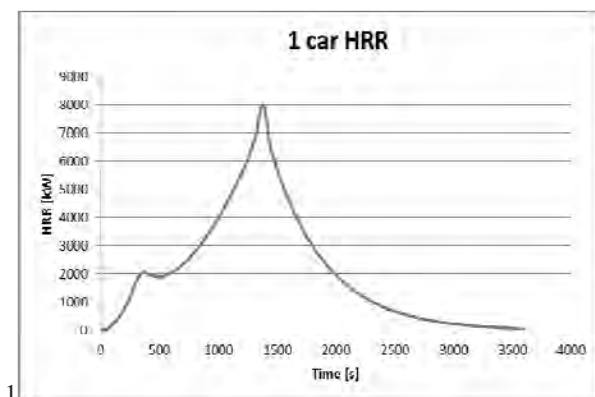


Fig. 1 HRR for one car

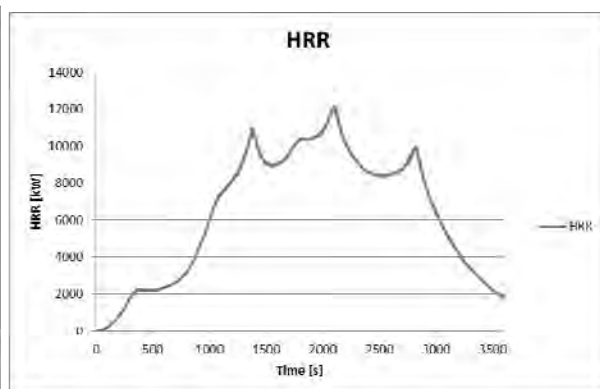


Fig. 2 HRR for three adjacent cars



## 1.2 Validation of the developed model

The FDS car fire model was validated with full scale tests (BRE, 2009). In the first test three cars, a Renault Laguna (car 1), a Renault Clio (car 2) and a Ford Mondeo Estate (car 3) were burned in the absence of sprinklers. They were modelled as category 2 cars, as described above. The computational space was fitted to the tests using initial data describing the test environment. The FDS model is shown in Fig. 3.

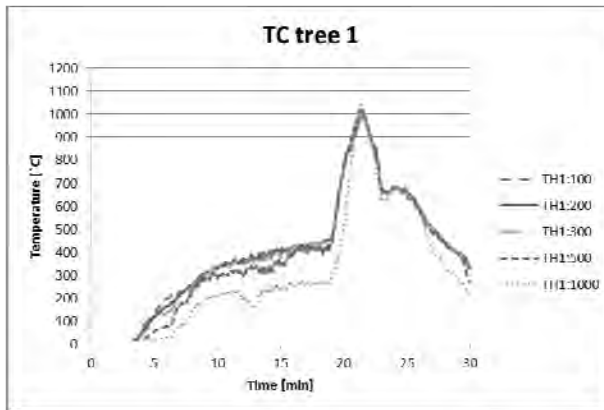


Fig. 3 FDS model of test (car 1 left, etc)

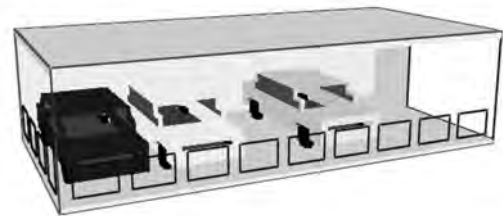


Fig. 4 Temperatures of the model

The fire started at car 1 and continued for about one hour. Temperatures were recorded in the model at thermocouple trees, as in the tests. Fig. 4 illustrates the temperatures in one tree where thermocouples were located 100, 200, 300, 500 and 1000 mm below the ceiling. The temperatures in all recorded thermocouples of the model were about the same as in the test.

In the second test three cars, a Renault Grand Escape, a Seat Ibiza and a Land Rover Freelancer were burned in the presence of sprinklers. These cars were modelled as category 2 cars, as above. The test environment with sprinklers was modelled, too. Six sprinklers of the test had an OH2 classification, 5 mm/min and 12 m<sup>2</sup> per head. In the BRE test only one car ignited, as was the case with the simulation model. The temperatures based on the model were higher in two thermocouple trees and smaller in one tree than in the tests. This is due the fact that the first and only car that burned in the test was a Renault Grand Escape, not a category 2 car as in the simulation. The Renault Grand Escape is a category 5 car that releases 12000 MJ of energy in fire. Category 2 cars, on the other hand, release 7500 MJ.

## 2 CASE STUDY WITH THREE ADJACENT CARS

The virtual car park with a floor area of 8x16 m<sup>2</sup> and a free height of 3 m was modelled with three category 2 cars in the middle. There were no walls in the computational space. The floor and roof were modelled as 100 mm thick non-burning concrete. Four thermocouple trees and nine similar sprinklers as in the BRE test were used in the model, as shown in Fig. 5. The flow rates of the sprinklers in this case were 45 l/min, not 60 l/min as in the BRE test, because the sprinkler coverage area per head was now 9m<sup>2</sup>. Thus, the requirement for sprinkler water flow rate per unit floor area of 5 mm/minute for car parks was fulfilled.

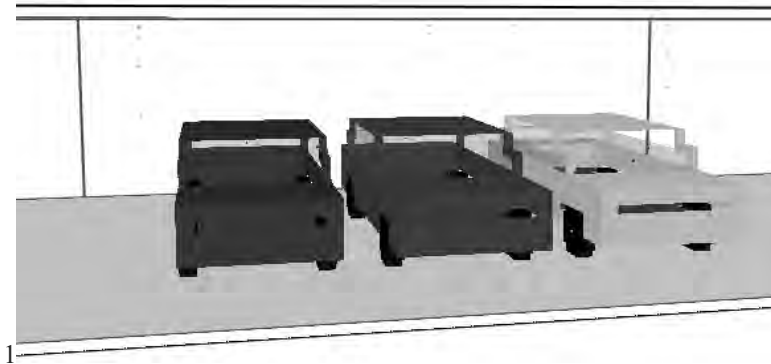
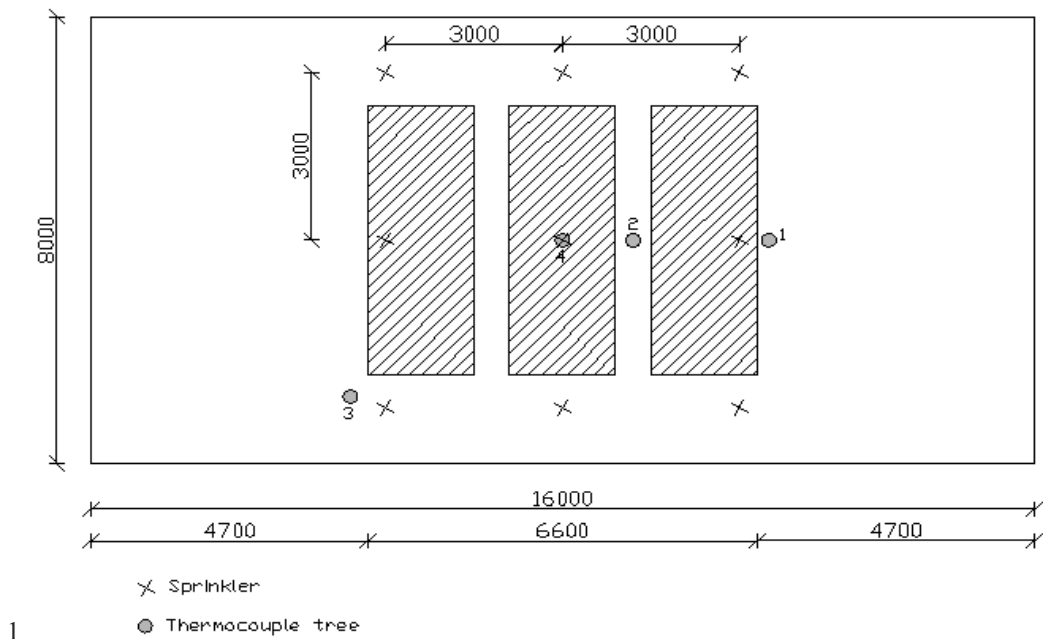


Fig. 5 Virtual car park case

This case was modelled without and with sprinklers. Then, the HRR curve was reduced imitating Eurocodes: The automatic water extinguishing system reduces the design fire load by a factor of 0.61. In the FDS model this reduction was completed by reducing the given HRRPUA value of the burning plane inside the car by a factor of 0.69. Numerical integration was used to calculate the released energy, which with this value was 0.61 times the original energy, referred to as EC0.61. The same technique was used in two other simulations referred to as EC0.43 and EC0.53. The HRR curves for the simulated cases are shown in Fig. 6.

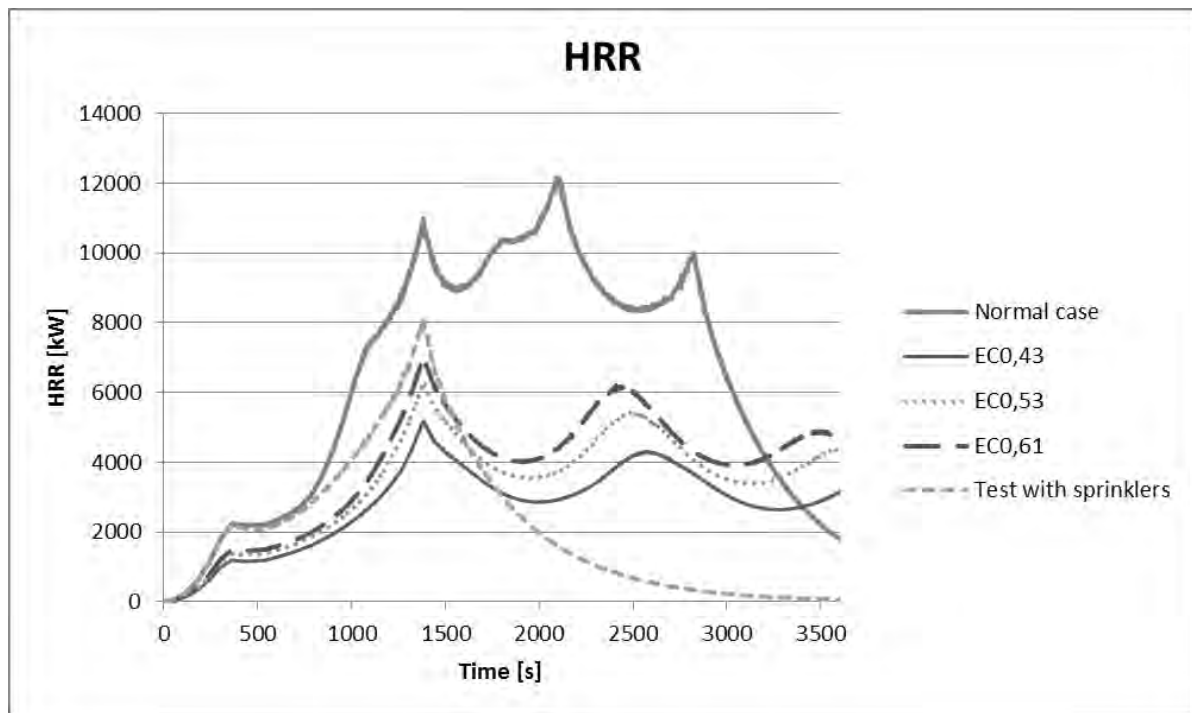


Fig. 6 Virtual car park case

It can be seen that the Eurocode reduction does not take into account the fact that adjacent cars do not ignite, as is the case with the developed model and as observed in the tests. Typical temperatures in the virtual thermocouple trees are shown in Fig. 7.

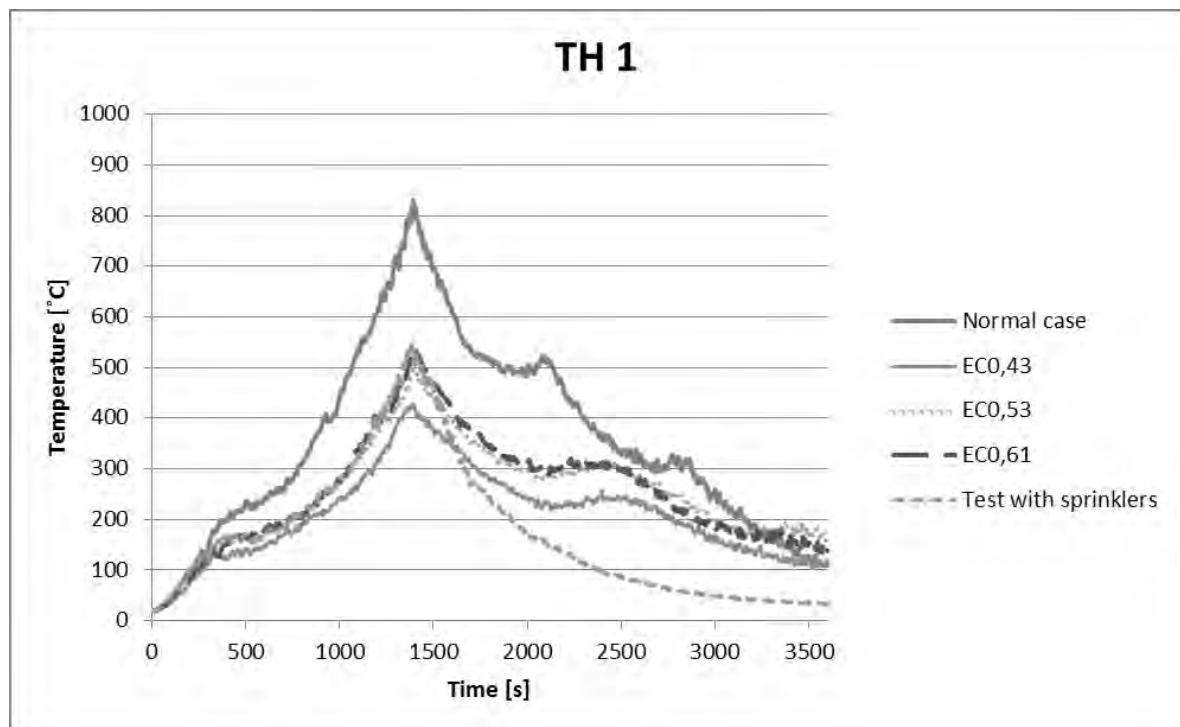


Fig. 7 Temperatures according to simulations

It can be seen that the Eurocode-based reduction of fire load in the presence of sprinklers (see Fig. 7, EC0,61) results in the same maximum temperatures as the simulation with sprinklers at the first peak of HRR. The Eurocode method is reliable for design within this range if the maximum temperatures at the beginning of the fire are those used in the fire design of structures. If it is used to simulate temperatures after the first peak of HRR, the temperatures are very conservative based on these results.

## REFERENCES

- Bertram, M., Buxmann, K., etc., Improving Sustainability in the Transport Sector Through Weight Reduction and the Application of Aluminium, International Aluminium Institute (IAI), 2007, 55 pages
- BRE, Martin M., Fire Spread in Car Parks, Final Research Report BD 2552 (D14 V1)231-569, 16.2.2009, 116 pages
- EN 1991-1-2, Eurocode 1: Actions on structures, Part 1-2: General actions, Actions on structures exposed to fire, CEN, Bryssels, 2003.
- Gratkowski, M.T., Burning Characteristics of Automotive Tires, Fire Technology, United States Department of Justice, Bureau of Alcohol, Tobacco, Firearms and Explosives (ATF), Fire Research Laboratory (FRL), DOI: 10.1007/s10694-012-0274-9, 2012
- Haack et.al., Technical Report – Part 1. Design Fire Scenarios, Thematic Network, FIT – Fire in Tunnels, The Fifth Framework Programme of the European Community ‘Competitive and Sustainable Growth’. Contract no G1RT-CT-2001-05017, 2005.
- Halada, L., Weisenpacher, P., Glasa, J., Computer Modelling of Automobile Fires, Advances in Modeling of Fluid Dynamics, Dr. Chaoqun Liu (Ed.), ISBN: 978-953-51-0834-4, InTech, DOI: 10.5772/48600, 2012.
- Heinisuo, M., Laasonen, M., Hyvärinen, T., Berg, T., Product modeling in fire safety concept, effect of grid sizes and obstacles to steel temperatures, IABSE Helsinki 2008 Congress, 2008.
- Heinisuo, M., Partanen, M., Modeling of Car Fires with Sprinklers, Research Report, Tampere University of Technology, Faculty of Business and Built Environment, Tampere, 2013.
- Joyeux, D., Kruppa, J. Cajot, L.G. Schleich, J.B. Van de Leur, P. Twilt, L. Demonstration of real fire tests in car parks and high buildings (2001), European Research Contract n° 7215 PP 025, Final report.
- Li, Y., Assessment of Vehicle Fires in New Zealand Parking Buildings, MEFÉ Thesis, University of Canterbury, Christchurch, New Zealand, 2004.
- Mangs, J., Loikkanen, P., Fire tests in passenger cars, VTT Research Report No.TSPAL00455/90, VTT Espoo, Finland, 1991.
- Mc Grattan, K., et al., Fire Dynamics Simulator, Technical reference guide. National Institute of Standards and Technology, version 5.5, 2010, USA
- Schaumann, P., Sothmann, J., Albrecht, C. Safety concept for structural fire design – application and validation in steel and composite construction, Proceedings of 11th International Seminar of Fire Protection , June 2010, Leipzig, 2010
- Schleich, J.B., Cajot, L.G., Franssen, J.M., Kruppa, J., Joyeux, D., Twilt, L., Van Oerle, J., Aurtenetxe, G. Development of design rules for steel structures subjected to natural fires in closed car parks (1997), EUR 18867EN, Report.
- Shleich, J.B, Modern Fire Engineering, Fire Design of Car Parks, Arcelor Profil, Luxembourg Research Centre. (Internet publication), 2010.
- Weisenpacher, P., Glasa, J., Halada, L., Computer simulation of automobile engine compartment fire. Proc. of the Int. Congress on Combustion and Fire Dynamics (J. A. Capote, ed.). Santander: GIDAI - Fire Safety - Research and Technology, 2010, p. 257-270. ISBN 978-84-86116-23-1
- Weisenpacher, P., Glasa, J. and Halada, L., Parallel simulation of automobile interior fire and its spread onto other vehicles, Fire Computer Modeling: international congress, [Santander, 19 de 2012]/ edited by Jorge A Capote, Daniel Alvear, ISBN 978-84-86116-69-9, 2012, pp. 329-338, 2012.

## **BENCHMARK EXAMPLE PROBLEMS FOR BEAMS At Elevated Temperatures**

Bartłomiej Sawicki<sup>a</sup>, Jan Pełczyński<sup>a</sup>, Lesław Kwaśniewski<sup>a</sup>

<sup>a</sup>Warsaw University of Technology, Faculty of Civil Engineering, Warsaw, Poland

### **Abstract**

The paper presents development of a series of solutions for beams at elevated temperatures which are supposed to serve as benchmark problems for applications of computational models in fire structural engineering. Three cases of loading i.e. pure bending, central force, and uniformly distributed loading, are considered for a simply supported, and fixed on both ends beams at uniformly distributed elevated temperature varying in time. The results are provided in terms of the midspan deflection for specified loading levels and temperatures. The results mainly obtained using finite element (FE) models and two commercial codes, are verified through comparison with analytical solutions for simplified cases and through parametric study aimed to examine the effect of modelling parameters. The numerical results are subjected to mesh density study using the grid convergence index (GCI) concept.

**Keywords:** beam, benchmark, fire, finite element, verification

### **INTRODUCTION**

Nowadays verification and validation (V&V) is recognized as the primary method for evaluating the confidence of computer simulations (Oberkampf et al, 2004). V&V is especially important in the research areas where complex, highly nonlinear structural behaviour is considered. One of those is the structural fire engineering where interaction of additional effects due to elevated temperatures has to be considered such as reduction of material properties and generation of additional forces due to constrained thermal elongation. Validation in the structural fire engineering through comparison between numerical results and experimental data obtained using furnace tests is difficult and has many limitations due to inevitable uncertainties characterising the specimen behaviour (Gillie, 2009). This fact enhances the importance of verification which is sought as a comparison of computational solutions with highly accurate (analytical or numerical) benchmark solutions and among themselves, for example using mesh density study (Santiago et al, 2009).

The benchmark solutions can serve for both code developers, to check the corrections of new features introduced in the code, and for code users who can check if their models are developed correctly. They should represent a good balance between simplicity and applicability. Simpler the problem considered, more reliable solution can be obtained, but too simplified problem can miss some important features which need to be taken into account in the study. On the other hand, more complex problem, less reliable solution can be provided. This fact is reflected often when different codes are used for the same problem (Santiago et al, 2009) or different modelling parameters such as finite element formulation, solving procedures, material models are used within the same code. To solve this dilemma a hierarchical approach is proposed in which a series of solutions is developed starting from the simplest cases towards more complex.

The paper presents application of such strategy to the problem of beams at elevated temperatures. The objective of the presented study is to provide not only solutions but also accumulate the evidence that they are correct.

## 1 PROBLEM DESCRIPTION

To define a family of cases characterizing the behaviour of beams at elevated temperatures, several parameters need to be identified as listed below. Some of them are taken from the existing studies (Gillie, 2009) and present a good balance between simplicity and correspondence with the real world. The stress is put on description of the numerical models to allow other users to follow calculations and check their simulations. For better comparison of results and for understanding the factors affecting differences between them and analytical solution, two commercial FE codes are used: ABAQUS, very commonly used in such cases (Santiago et al, 2009) and LS-DYNA, less often used in similar problems.

### 1.1 Geometry

Geometry means here a set of data defining all dimensions and shape of the beam. For all the solutions presented in this study a 1000x50x30 mm beam was considered. The ratio of length to depth is 20, so it is assumed that the shear force effect on deflection is negligible.

### 1.2 Material

Similar as in (Gillie, 2009), elastic-perfectly plastic material is considered, with the difference that here both elastic modulus and yield stress are temperature dependent, comparable to (Lin et al, 2010). Stress-strain relationship and temperature dependence are shown schematically in Fig. 1. Elastic modulus at 0°C is  $E_0=200$  GPa and the corresponding yield stress  $\sigma_{y,0}=200$  MPa. Material model is simple enough to allow easy FE modelling but also reflects material properties of structural steel at elevated temperature. In all cases  $\nu=0.3$  and  $\alpha_t=1.2\cdot 10^{-5}$  K<sup>-1</sup>, which corresponds well with steel properties.

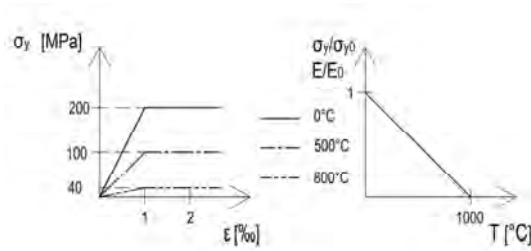


Fig. 1 Material model

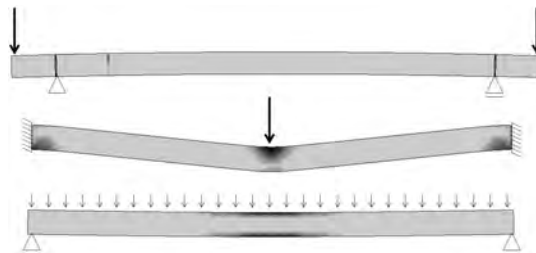


Fig. 2 Plastic regions, loading and boundary conditions – simplified drawings

### 1.3 Mechanical Loading

Three loading cases are considered: pure bending, central force, and uniformly distributed load, see Fig. 2. Pure bending is applied by four point bending test where two equal forces are applied at the top of cantilevers with bigger stiffness than the main beam. The central force is applied at the neutral axis of the beam, and uniformly distributed loading is applied as increased gravity. The first case is considered mainly to verify FE results with analytical solutions for elastic-plastic bending. This solution is also used for the mesh density study. The last case is more realistic and more related to experiments. The magnitude of the loads was chosen to produce bending moment of magnitude 700 Nm in the most stressed cross-section of simply supported beam. This lies between moments in which outer fibres yields (500 Nm) and whole section reaches plasticity (750 Nm) at 800°C, giving good elastic-plastic response of the beam. This gives force of 7000 N at the ends of 100 mm cantilevers in pure bending, 2800 N in point force load and equivalent of 5.6 N/mm distributed loading.

## 1.4 Boundary Conditions

Only two idealized boundary conditions are taken into account: a simply supported beam, where constraints are applied at the neutral axis, and a beam fully fixed on both ends. In the presented study only planar bending is considered with symmetry constraints (transverse y-displacement constrained) applied to all nodes in the vertical symmetry plane.

## 1.5 Temperature variation

Uniformly distributed temperature within the beam (the main span) is assumed. For FE mesh studies with constant temperature, the temperature effect is modelled directly through variation of the material properties and thermal expansion is not taken into account. At the beginning of the simulations the loading is applied gradually and then it is kept constant. For temperature varying in time, the simulations are divided into three steps. In the first step temperature 0°C is constant while the mechanical loading grows from zero to the full magnitude. In next two phases the loading is kept constant and the temperature grows linearly to 800°C and back to 0°C, (Gillie, 2009). All calculations are static, without inertia effects, and with time serving as nonphysical loading parameter.

## 1.6 FE Meshes

Only 3D meshes, as most general, are considered. It is supposed that FE models built of solid elements are able to capture more comprehensively local effects, and eventual deviation of plane cross sections (deplanation) due to shear deformation. Dimensions of FEs for three subsequent meshes used for the mesh density study are 16.67x12.5x7.5, 8.33x6.25x3.75 and 4.17x3.125x1.185 mm. Each of three meshes is built of the same elements with denser meshes generated through dividing each edge in two (one solid is divided into eight).

## 2 ANALYTICAL SOLUTIONS

For validation of FE models, analytical solutions for simply supported beams under pure bending, point force and uniformly distributed loading were obtained below.

### 2.1 Pure bending

Analytical solutions are obtained based on the assumptions that cross sections stay planar and the effect of shear is neglected. It is also assumed that the approximate formula (second derivative) for the curvature can be applied to find beam deflection. For elastic-ideal plastic material with yield stress  $\sigma_y$  the bending moment can be given by

$$M = \sigma_y b \left( \frac{h^2}{4} - \frac{\sigma_y^2}{3E^2} \rho^2 \right) \text{ if } \sigma_y \frac{bh^2}{6} \leq M \leq \sigma_y \frac{bh^2}{4} \quad (1)$$

where  $\rho$  is the radius of curvature which can be approximated by

$$\frac{1}{\rho} = w''(x), \quad w(0) = 0, \quad w(l) = 0 \quad (2)$$

To obtain displacement function  $w(x)$  it is necessary to solve differential Eq. (2) for  $M = const$ . The maximum deflection  $f$  in the midspan is

$$f = \frac{1}{8\sqrt{3}} \frac{\sigma_y l^2}{Eh} \left( \frac{1}{4} - \frac{1}{6} \mu \right)^{-1/2} \text{ and } \mu = \frac{M}{\sigma_y \frac{bh^2}{6}} \quad (3)$$

## 2.2 Concentrated force

For point load *Eqs. (1 )and (2)* are still valid. Maximum bending moment  $M(x)$  and the maximum elastic moment  $M_s$  (at the cross-section  $x = x_0$ ) are given as

$$M(x) = \frac{P}{2}x, \quad M_s = \frac{\sigma_y b h^2}{6} \quad \text{and} \quad M_s = \frac{P}{2}x_0 \quad (4)$$

Beam deflection shape  $w(x)$  is divided into  $w_1(x)$  for  $x \leq x_0$  (elastic behaviour of the cross-section) and  $w_2(x)$  for  $x_0 \leq x \leq l/2$  (elastic-perfectly plastic behaviour of the cross-section). Parameter  $x_0$  results from *Eqs.(4.2)* and *(4.3)*. Displacement function  $w(x)$  is obtained after solving *Eq. (5)*.

$$\begin{aligned} -EIw_1''(x) &= \frac{P}{2}x, \quad w_2''(x) = \frac{1}{\rho} = \frac{\sigma_y}{\sqrt{3}Eh} \left( \frac{1}{4} - \frac{P}{2\sigma_y b h^2}x \right)^{-1/2}, \\ w_1(0) &= 0, \quad w_1(x_0) = w_2(x_0), \quad w_1'(x_0) = w_2'(x_0) \quad w_2'\left(\frac{l}{2}\right) = 0 \end{aligned} \quad (5)$$

Maximum deflection of the beam can be written as *Eq. (6)*.

$$f = \frac{1}{6} \frac{\sigma_y l^2}{Eh} \frac{3\sqrt{3-2\psi} + \psi\sqrt{3-2\psi} - 5}{\psi^2} \quad \text{and} \quad \psi = \frac{P}{\frac{2}{3} \frac{\sigma_y b h^2}{l}} \quad (6)$$

## 3 MESH DENSITY STUDY

For the mesh density study, the maximum deflection for cases with pure bending at 0°C and 800°C was used. The procedure called Grid Convergence Index GCI (Slater, 2008), (Kwasniewski, 2013) was applied. Using concept of Richardson extrapolation, the order of convergence and asymptotic solution is found based on results obtained from three subsequent meshes. The meshes are constructed with a constant grid refinement ratio  $r = 2$

$$r = \frac{h_3}{h_2} = \frac{h_2}{h_1} = \text{const} \quad (7)$$

where  $h_1, h_2, h_3$  are measures of mesh size (e.g. the largest element egde) and  $h_1 < h_2 < h_3$ . In this paper the convergence rate, given as (Slater, 2008)

$$p = \frac{\ln\left(\frac{f_3 - f_2}{f_2 - f_1}\right)}{\ln(r)} \quad (8)$$

where  $f_1, f_2, f_3$  are the results from three subsequent meshes. Next, the asymptotic solution is obtained as

$$f_{h=0} \cong f_1 + \frac{f_1 - f_2}{r^p - 1} \quad (9)$$

The GCI is defined as (Slater, 2008):

$$GCI = \frac{F_s |\varepsilon|}{r^p - 1} 100\% \quad (10)$$



where  $F_s = 1$  is a safety factor, and  $\varepsilon$  defines relative difference between subsequent solutions

$$\varepsilon = \frac{f_1 - f_2}{f_1} \quad (11)$$

As can be seen (Tab. 1) a good convergence and correlation with analytical solutions are obtained for constant 0°C, 800°C (no thermal expansion) and for temperature varying from 0 to 800°C and deflection recorded at 800°C. For all next cases, the finest mesh is applied.

Tab. 1 GCI results for simply supported beam with pure bending

Solver	Temperature [°C]	Result [mm]			$p$	$f_{h=0}$ [mm]	$GCI_{12}$	$GCI_{23}$	$\frac{GCI_{23}}{r^p GCI_{12}}$
		$f_3$	$f_2$	$f_1$					
ABAQUS	0constant	1.367	1.391	1.398	1.778	1.401	0.206	0.710	1.005
	800constant	9.256	10.490	10.970	1.362	11.276	2.786	7.489	1.046
	800 varying	8.478	9.636	9.963	1.824	10.092	1.292	4.729	1.034
LS-DYNA	0constant	1.369	1.393	1.400	1.778	1.403	0.206	0.709	1.005
	800constant	9.640	11.023	11.818	0.799	12.893	9.095	16.963	1.072
	800 varying	8.384	9.228	9.814	0.526	11.145	13.562	20.774	1.064

#### 4 NUMERICAL RESULTS FOR BEAMS UNDER FIRE

Tab. 2 Deflection of simply supported beam with pure bending under fire [mm]

	0°C	200°C	500°C	600°C	700°C	800°C	700°C	600°C	500°C	200°C	0°C
Analytical	1.400	1.750	2.800	3.500	4.667	11.180	-	-	-	-	-
ABAQUS	1.398	1.747	2.796	3.495	4.569	9.963	7.635	6.469	5.770	4.727	4.372
LS-DYNA	1.400	1.743	2.773	3.461	4.609	9.814	7.512	6.358	5.667	4.626	4.275

Tab. 3 Deflection of simply supported beam with concentrated force under fire [mm]

	0°C	200°C	500°C	600°C	700°C	800°C	700°C	600°C	500°C	200°C	0°C
Analytical	0.933	1.167	1.866	2.333	3.111	4.667	-	-	-	-	-
ABAQUS	0.940	1.174	1.882	2.352	3.136	5.074	3.507	2.723	2.253	1.548	1.312
LS-DYNA	0.940	1.172	1.869	2.333	3.108	5.008	3.462	2.688	2.223	1.526	1.293

Tab. 4 Deflection of fixed beam with concentrated force under fire [mm]

	0°C	200°C	500°C	600°C	700°C	800°C	700°C	600°C	500°C	200°C	0°C
ABAQUS	0.239	9.693	29.964	36.008	41.846	47.716	44.456	40.732	36.669	24.472	16.235
LS-DYNA	0.239	9.667	29.877	35.915	41.752	47.627	44.372	40.656	36.608	24.491	16.359

Tab. 5 Deflection of simply supported beam with distributed loading under fire [mm]

	0°C	200°C	500°C	600°C	700°C	800°C	700°C	600°C	500°C	200°C	0°C
Analytical	1.167	1.458	2.333	2.917	3.889	5.833	-	-	-	-	-
ABAQUS	1.172	1.466	2.347	2.934	3.912	7.019	5.065	4.088	3.501	2.621	2.328
LS-DYNA	1.173	1.462	2.331	2.911	3.877	6.920	4.991	4.024	3.444	2.571	2.279

Fig. 3-7 present numerical and analytical results for five selected cases: simply supported beam subjected to four point bending, simply supported and fixed beams subjected to concentrated force and uniformly distributed loading. For all cases the time variation of temperature defined in Section 1.5 is considered. Deflection  $f$  is shown in the relation to the

displacement  $f_0$  at  $0^\circ\text{C}$ , which makes variation of material properties under temperature more visible.

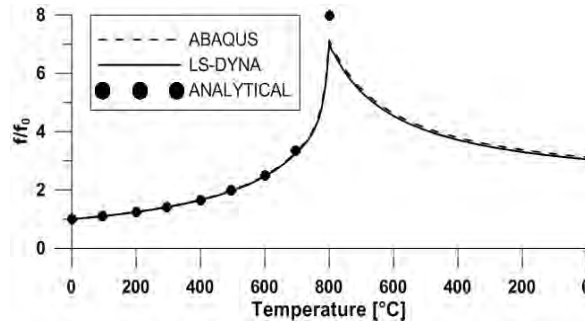


Fig. 3 Deflection of simply supported beam under pure bending and elevated temperature

Tab. 6 Deflection of fixed beam with distributed loading under fire [mm]

	0°C	200°C	500°C	600°C	700°C	800°C	700°C	600°C	500°C	200°C	0°C
ABAQUS	0.239	9.649	29.946	35.996	41.839	47.714	44.449	40.734	36.669	24.386	16.060
LS-DYNA	0.239	9.607	29.810	35.840	41.664	47.514	44.261	40.555	36.503	24.311	16.110

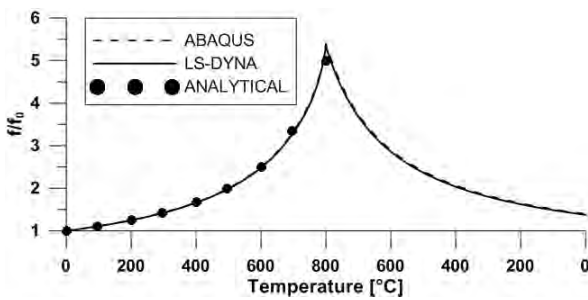


Fig. 4 Deflection of simply supported beam under concentrated force and elevated

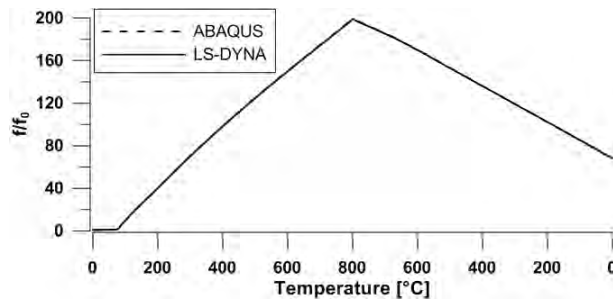


Fig. 5 Deflection of fixed beam under concentrated force and elevated temperature

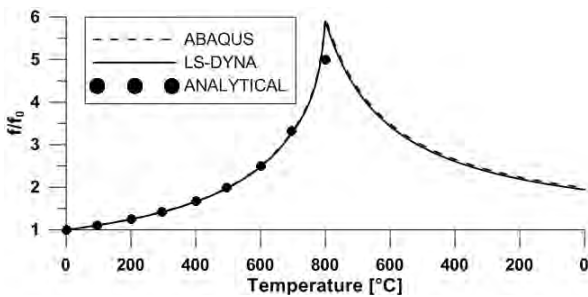


Fig. 6 Deflection of simply supported beam with distributed load and elevated temperature

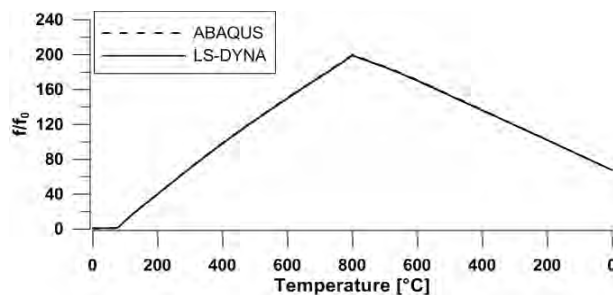


Fig. 7 Deflection of fixed beam under distributed load and elevated temperature

## 5 SUMMARY

A series of solutions for beams at elevated temperatures are presented as benchmark problems for applications of computational models in fire structural engineering. Presented numerical solutions have been verified through comparison with analytical solutions for limited number of simple cases and through comparison of the numerical results obtained using two FE codes. The mesh density study based on the grid convergence index (GCI) concepts is also

presented for beams subjected to pure bending. Comparison of the results shows very good correlation for elastic range however, when plastic deformation is present there is a clear difference between FE and analytical solutions.

## REFERENCES

- Gillie M., Analysis of heated structures: Nature and modelling benchmarks, *Fire Safety Journal* 44, pp. 673–680, 2009.
- Lin T. J., Yang Y. B., Huang C. W., Inelastic nonlinear behaviour of steel trusses cooled down from a heating stage, *International. J. of Mech. Sciences* 52, pp 982-992, 2010.
- Kwasniewski L., Application of grid convergence index in FE computation, *BULLETIN of The Polish Academy of Sciences, Technical Sciences*, vol. 61, (1), 2013, in print.
- Oberkampf W.L., Trucano T.G., Hirsch C., Verification, validation, and predictive capability in computational engineering and physics, *Appl. Mech. Rev.* 57 (5), 345–384, 2004.
- Santiago A., Haremza C., Simoes da Silva L., Rodrigues J. P., Numerical Behaviour of Steel Columns subject to Localized Fire Loading, "Proceedings of the 12th Int. Conf. on Civil, Structural and Env. Eng. Computing", Civil-Comp Press, Stirlingshire, UK, Paper 7, 2009.
- Slater J. W., Examining Spatial (Grid) Convergence, NASA NPARC Alliance V&V, 2008.

## BENCHMARKING FOR THE INCLUSION OF SHEAR STUDS IN FINITE ELEMENT MODELS

Kate Anderson <sup>a</sup>, Martin Gillie <sup>b</sup>

<sup>a</sup> AECOM, Edinburgh, UK

<sup>b</sup> School of Engineering, The University of Edinburgh, Edinburgh, UK

### Abstract

There are many aspects of shear stud behaviour that may affect a heated steel-concrete composite structure in fire such as stud layout, ductility and strength; heated material behaviour; loss of composite action through the failure of multiple studs; and so on. This paper attempts to understand the role of shear studs on full structural behaviour in fire during both heating and cooling. Predictions of stud behaviour at ambient temperature using numerical models are first compared to experimental work to benchmark the modelling approach. A good correlation is found. This is followed by the analysis of full structural behaviour in fire where shear stud properties are varied parametrically. Individual shear studs are modelled so it is possible to identify which studs fail and at what point in the fire. The results demonstrate the importance of ensuring continued composite action in fire.

**Keywords:** Finite element modelling, connections, shear studs

### INTRODUCTION

Shear connectors in steel-concrete composite construction play a vital role in ensuring both strength and serviceability requirements are met at ambient temperature. Their behaviour and design has been extensively studied. In fire conditions it can be expected that shear connectors play a similarly important role, yet their behaviour in fire has received very little attention. This is despite the many studies of composite structures in fire, both experimental and numerical, that have been undertaken over the last 15 years examining almost all other aspects of the behaviour of such structures.

This paper examines how shear connector behaviour may affect the response and strength of heated composite structures by means of a numerical parametric study using Abaqus, the commercial finite element package. Various models were produced which are discussed in detail below; in each case a concrete slab, modelled with 4-noded shell elements, was connected to steel beams, modelled with 2-noded beam elements, to simulate a portion of a steel-concrete composite structure. Steel behaviour was modelled with an elasto-plastic temperature dependent model assuming a von Mises yield criterion. Concrete was modelled using the “damaged-plasticity” model available in Abaqus. Geometric non-linear effects were accounted for. Because of the abrupt changes in stiffness that occur when shear studs fail, it was necessary to use an explicit dynamic solver for all analyses to obtain numerical convergence. This paper explores the effect of the degree of shear connection in fire on structural behaviour. Other parameters are considered by Anderson (2012).

### 1 AMBIENT TEMPERATURE BENCHMARK

In order to gain confidence in later results, an initial model was validated against experimental data. Experimental data on the behaviour of shear-studs in fire is rare so validation was first made against ambient temperature data produced by Chapman and Balakrishnan (1964).

Chapman’s experiments consisted of concrete slab strips attached by shear studs to steel beams. The slabs were loaded uniformly and deflections measured. A span of 5.5 m with

simple supports was used. The steel beams were 305 mm deep and 152 mm wide, with a flange thickness of 18 mm and web thickness of 10 mm. The slab was 152 mm deep and 1.22 m wide. It had 4, 8 mm  $\Phi$  bars top and bottom in the longitudinal direction and 12.7 mm  $\Phi$  bars in the transverse direction at 152 mm spacing at the top and 305 mm spacing at the bottom. Further details of test arrangements are given in Tab. 1.

Tab. 1. Material properties used for validating numerical models against experimental data; starred values are assumed data; all others are taken from Chapman Balakrishnan (1964)

Property	Steel	Concrete	Reinforcement
Compressive strength (MPa)	240	50	500*
Tensile strength (MPa)	240	5	500*
Young's modulus (GPa)	210	26.7	210*
Strain at peak stress (-)	NA	0.003	NA
Strain at failure (-)	NA	0.0045	NA
Poisson's ration	0.3*	0.2	0.3*

Chapman's test "U3" was used for validation. This test was chosen because it most closely reflects a realistic building design and loading scenario. It used T-studs (a form of shear connector commonly used in current construction) evenly spaced at 216 mm centres. The load-slip behaviour of the studs obtained from push-out tests by Chapman is shown in Fig. 2. The numerical model used for validation is shown in Fig 1. In this model, friction between the steel and concrete was included with a coefficient of friction of 0.5, as recommended in EC4 (2004), while a contact condition was specified that prevented the steel penetrating the concrete but left separation free to occur. Twenty-four pairs of shear studs connecting the steel and concrete were modelled explicitly using individual connector elements. These elements were specified rigid in all direction except parallel to the beam axis where the force-displacement relationship followed that shown in Fig. 2. Chapman's test data showed shear studs failed on average at a load of 120 kN with a deformation of 2.54 mm. This failure condition was included in the numerical model. Pinned-boundary conditions were specified at each end of the beam. These provided rather more axial restraint than was present in reality but it was found that assuming no axial restraint (simple supports) produced poorer correlation with test data. A spring support would have been most accurate but the results obtain (Fig. 3) are sufficiently good for the modelling approach used to represent the shear studs to be considered validated at ambient temperature.

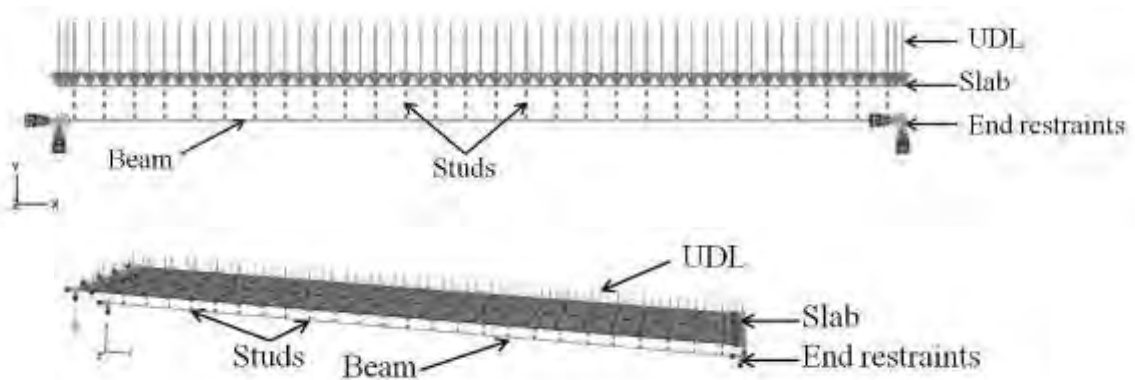


Fig. 1 Numerical model used for benchmarking model

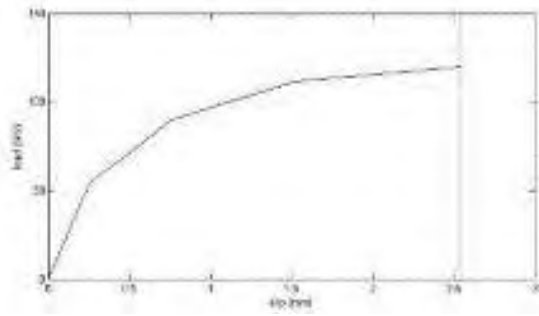


Fig. 2 Shear stud load slip behaviour from Chapman and Balakrishnan (1964)

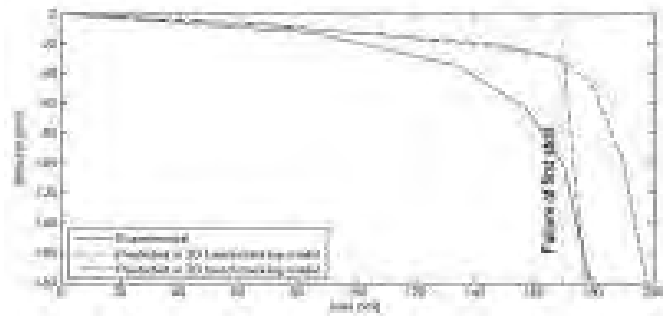


Fig. 3 Load-deflection response of 2D and 3D (discussed here) benchmark models

## 2 NUMERICAL MODEL

With an ambient temperature model validated, a standard model was developed for a parametric study of shear stud behaviour at elevated temperatures. This paper presents only the results from the connectivity study although; other parameters have been considered in Anderson (2012). Full connectivity is defined as the case where the steel or concrete fails before the studs while partial connectivity is the converse. Connectivity therefore relates to the strength of the studs.

### 2.1 Geometry

A 6m by 6m slab has been chosen to represent an average room size. A total imposed load of  $5 \text{ kN/m}^2$  is assumed. Together with the dead load of the slab, a beam size of UB533x210x92 was chosen and a slab depth of 150 mm. Reinforcement bars are provided at 150 centres top and bottom and in both directions, 12 mm  $\Phi$  bars in the bottom and 8 mm  $\Phi$  bars at the top. Shear studs are explicitly included and their spacing is calculated based on the distance between ribs in the profiled steel decking under the concrete slab. This distance can vary between around 150 mm – 300 mm and so an arbitrary figure of 200mm was chosen in this case, (Kingspan, 2009). The stud spacing is assumed to be equal to this distance, (Quiroz, 2009). The studs at each end of the slab were placed at half this distance from the support meaning there are a total of 30 studs in this case. Load-slip behaviour, based on the experimental curve shown in Fig. 2 is defined in the direction of the beam main axis while movement in any other direction is restrained.

Boundary conditions that pinned the ends of the beam and slab were imposed. Symmetry was used at the two edges of the slab parallel to the beam to model continuity.

### 2.2 Heating

A parametric fire was assumed to heat the whole structure. A maximum gas temperature of  $895 \text{ }^\circ\text{C}$  was achieved after 60 minutes and gas temperature returned to ambient after a total time of 190 minutes, 130 minutes after the peak temperature. Heat transfer calculations were carried out to calculate the temperature of the slab at 5 points throughout its depth while the steel beam was assumed to have a uniform temperature. The slab took around 19 hours to return to ambient temperature whereas the beam cooled in about 4 hours.

## 3 PARAMETRIC STUDY

### 3.1 Partial Connectivity

When the strength of an individual shear stud and its spacing along the beam is known, the degree of shear resistance can be calculated. Full shear resistance is not required from the studs and a minimum requirement can also be calculated. The degree of shear resistance can be calculated as follows according to Eurocode 4 as:

$$\eta = \frac{N_c}{N_{c,f}} \quad (1)$$

where  $N_c = 0.5nP_{Rd}$  and  $N_{c,f} = 0.85A_cF_{cd}$  (2) / (3)

In the above equations  $N_c$  is the design value of the compressive normal force in the concrete flange,  $N_{c,f}$  is the design value of the compressive normal force in the concrete flange with full shear connection,  $n$  is the number of shear studs along the length of the beam,  $P_{Rd}$  is the design shear resistance of a shear stud,  $A_c$  is the cross sectional area of the concrete and  $F_{cd}$  is the characteristic design strength of the concrete. The minimum degree of shear resistance required to meet the Eurocode recommendations can be calculated as:

$$\eta_{\min} = 1 - \left( \frac{355}{f_y} \right) (0.75 - 0.03L_e) \quad (4)$$

where  $L_e$  is the effective length and  $f_y$  is the yield strength of steel.

In the benchmark model, the capacity of a shear stud was 120 kN. The level of connectivity was increased or decreased in this study to evaluate the effects on time to stud failure and slab deflection. Stud failure forces of 60 kN, 90 kN, 120 kN, 150 kN and 180 kN were chosen for the study. Degree of connectivity and minimum shear requirement is summarised in Tab. 2.

Tab. 2 Shear connectivity provided based on strength of studs

Required degree of shear connection	Stud Shear strength	60kN	90kN	120kN	150kN	180kN
43%	Actual degree of shear connection	35%	52%	69%	86%	103%

### 3.2 Results

Fig. 4 show the failure temperatures of each shear stud over half the length of the beam for the five analyses. At the top of the diagrams is the layout of the slab and beam assembly where the shear studs are explicitly indicated by a dashed line. On the left hand side is the gas temperature throughout the analysis and adjacent to that the status of each shear stud is given: a line ‘|’ denotes that the shear stud is still intact and a cross, ‘x’ indicates failure.

The following conclusions can be drawn from these figures:

- As the level of connectivity increases, the shear stud failure temperature increases for the studs nearer the centre. This is because the studs near the centre of the beam carry less force and therefore will be the last to fail.
- With increasing connectivity, fewer studs fail over the duration of the analyses
- Most studs that fail do so in heating however there are a few that fail in cooling in the 180 kN model.
- The stud to the far right of each figure is 100 mm from the middle of the beam and as the analysis is symmetrical and ideal, the middle shear stud should not be subject to a significant shear force throughout the analysis. This is highlighted in the fact that this stud does not fail in any of the analyses.

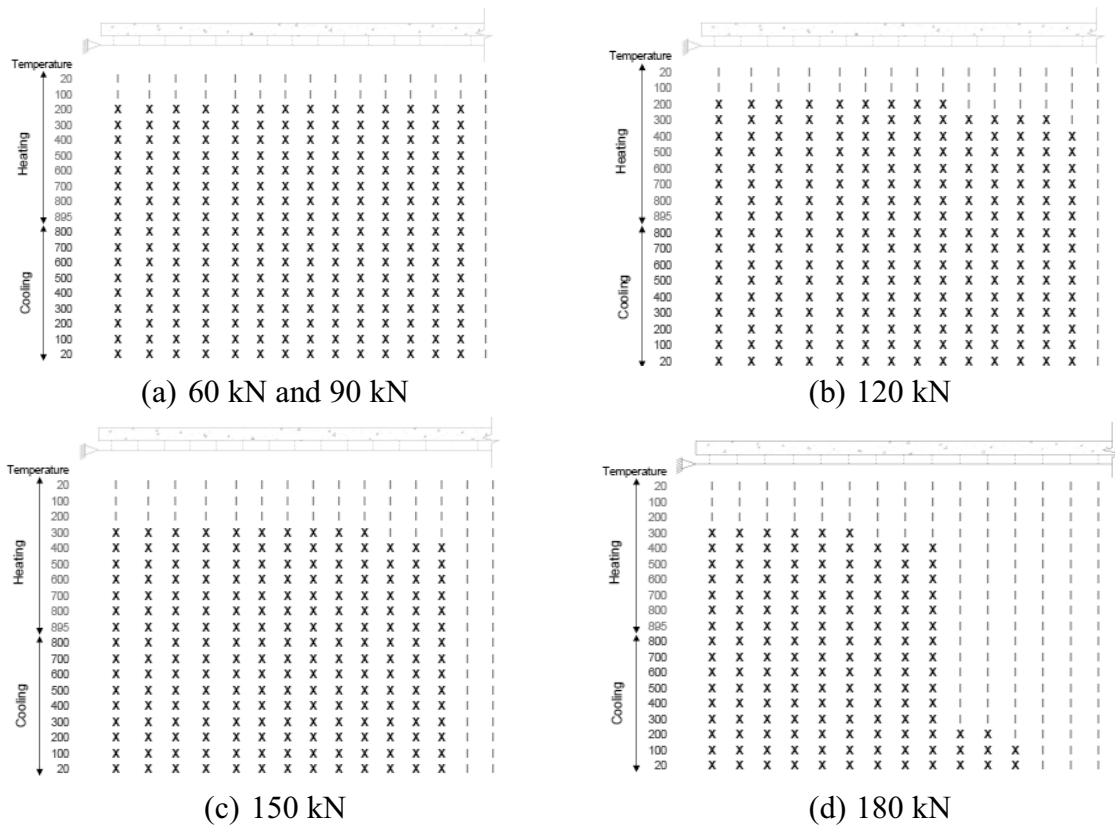


Fig. 4 Failure temperatures of shear studs for different stud capacities

Stud strength also has a marked effect on beam and slab deflection as can be seen from Fig. 5. The beam mid-span deflections increase as the stud strength decreases.

- In the model with the highest level of connectivity, with a stud failure force 180 kN, the maximum deflection during heating is 300 mm.
- In the model with the lowest level of connectivity, where the stud failure force is 60 kN, the maximum deflection during heating is 380 mm.
- The maximum deflection for the model with the lowest connectivity is therefore 25 % higher than that for the model with the highest level of connectivity.
- In cooling, the 180 kN failure model has a residual deflection of 135 mm.
- This is compared to 210 mm for the 60 kN model.
- The residual deflection for the model with the weakest studs is therefore larger by 55 %.

As the structure begins to heat, deflections increase and the slip between the slab and beams also increases. As studs begin to fail at the edges of the beams, where the largest shear forces are, larger rotations are possible and therefore in the models where more shear studs fail, i.e. those with lower stud strength, there will be a larger mid-span deflection. Again, the opposite pattern is seen in the slab deflections: as the stud strength increases, so do the slab edge mid-span deflections, Fig. 5.

- In the model with the highest level of connectivity, where the stud fails at 180 kN, the maximum deflection during heating is 450 mm.
- In the model with the lowest level of connectivity, the maximum deflection during heating is 380 mm.
  - The maximum deflection for the 180 kN failure force model is therefore 20 % larger than that for the 60 kN failure force model.
- In cooling, the 180 kN failure force model has a residual deflection of 295 mm.
- This is compared to 210 mm for the 60 kN failure force model.



- The residual deflection for the model with the highest level of connectivity is therefore 40 % larger than that with the least connectivity.

By considering the relative expansion rates of the beam and slab this can be explained. In each model, the total thermal expansion of both the beam and slab will be the same. As the failure force of the studs increases, the slab deflection over the beam decreases, as explained above. For the total thermal expansion of the concrete to be the same in all models, this will require the concrete expansion to be more prevalent elsewhere in the model. It is therefore evident as a vertical deflection at the slab edges.

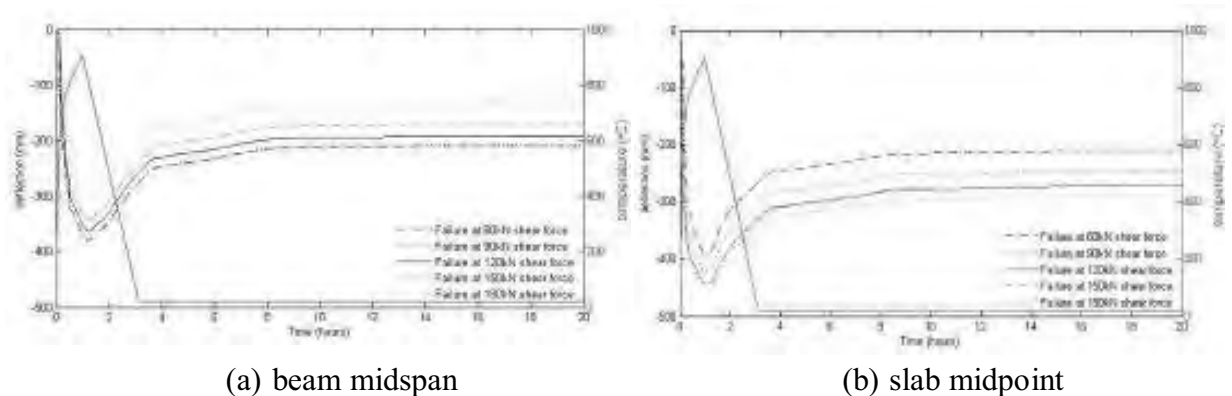


Fig. 5 Deflections at the mid-point of the slab of beam for different shear stud strengths

#### 4 CONCLUSIONS

This study shows that shear studs do effect the predicted response of composite structures in fire. Depending on the design criteria, it may that the degree of shear connectivity appropriate at ambient temperature is not sufficient for high temperature. Therefore, consideration should be given to checking shear stud adequacy at in structural fire design, rather than, as is currently common, simply assuming shear studs will be adequate in the fire limit state.

#### 5 ACKNOWLEDGEMENTS

Funding for this research provided by the EPSRC and Arup is kindly acknowledged.

#### REFERENCES

- Anderson, K, The Effect of Connections on Structural Behaviour in Fire, PhD Thesis, 2012.
- Chapman, J. and S. Balakrishnan, Experiments on composite beams. *The Structural Engineer*, 1964. 42(11): p. 396 - 383.
- CEN, Eurocode 3: Design of steel structures part 1-2: General rules - Structural fire design. 2006b, British Standards Institution.
- EC4, CEN, Eurocode 4: Design of composite steel and concrete structures part 1-1: General rules and rules for buildings. 2004, British Standards Institution.
- Queiroz, F.D., G. Queiroz, and D.A. Nethercot, Two-dimensional FE model for evaluation of composite beams, II: Parametric study. *Journal of Constructional Steel Research*, 2009. 65(5): p. 1063-1074.
- Kingspan Structural Products. 2009 [cited 2010 - 2011; Available from: <http://www.kingspanstructural.com/index.asp>.
- NCCI:AccessSteel, NCCI: Determination of moments on columns in simple construction. 2008.

# THE USE OF OPTIMIZATION IN FIRE DEVELOPMENT MODELING

## The Use of Optimization Techniques for Estimation of Pyrolysis Model Input Parameters

Jiří Ira<sup>a</sup>, Lucie Hasalová<sup>a</sup>, Milan Jahoda<sup>a</sup>

<sup>a</sup> Institute of Chemical Technology, Prague, Faculty of Chemical Engineering, Prague, Czech Republic

### Abstract

This paper deals with the use of the optimization techniques for obtaining the input parameters from the bench scale experimental data that are used for property based fire modeling. Two multidimensional optimization techniques - Genetic algorithm (GA) and Shuffled complex evolution (SCE) - are discussed. Their performance is compared based on the algorithms application to estimation of the material properties of one of the commonly used structural materials – wood.

**Keywords:** fire modeling, genetic algorithm, material properties estimation, global optimization, shuffled complex evolution, wood

### INTRODUCTION

CFD fire modeling quickly emerged as an useful and nowadays quite common tool in fire and safety engineering practice. Commercially affordable CFD fire modeling softwares as FDS, Jasmine or SmartFire are successfully used in many key fire safety applications, e. g. proposing fire evacuation strategies, designing the layout of the active fire protection components etc., where the main objective of the model is to study the consequences of the fire (mainly the evolution of the temperature field and spread of the smoke). When the amount of the heat released during burning (HRR) is known, commercial fire modeling softwares provide good agreement between the model and the real case situations and work as a reliable prediction tool.

Contrary to fire consequence modelling, capabilities of the softwares in case of fire development and spread modelling are still very limited and their use is restricted to research area only. The main challenge in modeling fire spread is to accurately predict the amount of the mass released when the material is exposed to heat as a function of time, i.e. to establish the pyrolysis model together with an appropriate reaction scheme of the material heat degradation.

Considering the basic construction materials, the knowledge of the material mass loss rate when exposed to heat is crucial from the point of view of the buildings static. The amount and the composition of the gases released during pyrolysis significantly influence the evolution of the temperature field and the rate of the heat transfer to the surrounding materials. High temperatures further initiate pyrolysis and leads to the irreversible damage of the building structures (the loss of strength and stiffness of steel beams or the destruction of the concrete components caused by the sudden release of the water vapour from the moisture present in the concrete).

When modeling pyrolysis the main problem is not the insufficient theoretical knowledge of the pyrolysis models, but the lack of the methodology how to determine the model input parameters – kinetic and thermal parameters of the decomposing material. Some of the material properties can be determined from the experimental measurements like thermogravimetric analysis (ISO, 1997), conic calorimetry (ISO, 2002) or differential scanning calorimetry (ISO, 2009). However, most of the parameters have to be determined by

inferring or optimization from the experimental data. The paper deals with using optimization techniques for estimating the pyrolysis model input parameters.

## 1 THE PYROLYSIS MODELING

FDS (McGrattan et al., 2010), Gpyro (Lautenberger, 2007) and Thermokin (Stoliarov & Lyon, 2008) belong currently to the most common pyrolysis models in the fire community. Although these models were developed independently, their mathematical formulation are quite similar. The main differences between the models are the variable specification (e.g. conversion) and the extent of their generality. One of the key governing equations in the pyrolysis model are the condensed phase mass conservation and the condensed phase species conservation. These equations describe the change of the mass of the condensed phase over time in the computational cell, i.e. how quickly the condensed phase species are released into the gas phase. One of the ways to express a mass change is the use of conversion. Therefore the reaction rate of species decomposition is the function of thermodynamic temperature  $T$  and conversion  $\alpha$  (normalized mass fraction). For simplifying the reaction rate is usually expressed as the product of two independent functions

$$r = k(T)f(\alpha) \quad (1)$$

where  $f(\alpha)$  is only a function of conversion and  $k(T)$  is only a function of temperature. The dependence of the reaction rate on temperature is usually expressed by the Arrhenius equation. The function  $f(\alpha)$  is called "reaction model" and may have different forms. The simple form  $(1 - \alpha)^n$  is most commonly used. Than the equation for description of the condensed phase decomposition kinetics has this basic form

$$\frac{d\alpha}{dt} = Z \exp\left(-\frac{E}{RT}\right) (1 - \alpha)^n \quad (2)$$

where  $Z$  is the pre-exponential (frequency) factor,  $E$  is the activation energy,  $R$  is universal gas constant and  $n$  is the reaction order. The Arrhenius equation parameters ( $Z$ ,  $E$ ) together with the reaction order  $n$  are input parameters into models of thermal decomposition of solid materials.

### 1.1 The optimization techniques

The problem of determination of material pyrolysis properties from bench-scale experimental data is an inverse problem. The major complications for solving the inverse problem are the existences of more than one main convergence region and many minor local optima in each region. In general there are many approaches how to solve such global optimization problem (e.g. deterministic methods, stochastic methods, heuristics etc.), but not all can be applied to this problem. The main concern when choosing the optimization method is how close the converged solution is to the global optimum and how quickly the algorithm converge to a solution.

Since 1998, several scientific workers tried to apply different optimization algorithms to the inverse problem of pyrolysis parameters estimation. One of optimization algorithms tested through the fire research community was the genetic algorithm (GA) that belongs to the group evolutionary algorithms. Genetic algorithm is heuristic method that uses the principles of evolutionary biology (natural selection, crossover, mutation, heredity) to find the global optimum. The basic principle of genetic algorithm is described in Fig. 1a. Although the GA was proofed to be very versatile and powerful tool its use has a number of disadvantages. Results obtained by GA are strongly dependent on the initial setup of algorithm parameters such as population size, mutation probability, crossover probability or selection mechanism. Moreover, the GA may have a problem with finding the global optimum. If we change one (or more) parameter we can get qualitatively different solution which meet the optimization criteria as well.

Chaos et al. (2010) used the shuffled complex evolution (SCE) algorithm to estimate the material pyrolysis properties from FPA (ISO, 2011) experimental data. The shuffled complex evolution is the global optimization algorithm developed by Duan et al. (1993) at The University of Arizona. The SCE method combine the strength of Nelder-Mead (downhill simplex) method, controlled random search, genetic algorithm and complex shuffling. The flowchart of SCE algorithm is shown in Fig. 1b. Lautenberger (2011) implemented the SCE algorithm to his pyrolysis model Gpyro and compared its performance over GA using synthetic cone calorimeter experimental data of hypothetical non-charring material. The result suggested that in comparison to GA, SCE converge to a unique solution that corresponds to the global optimum. The normalized deviation between solution was not usually greater than units percent. Moreover, the fitness function reached much higher values (the fitness function is maximized). However, to confirm these conclusions SCE need to be further tested. It is necessary to apply the SCE on various materials and decomposition patterns.

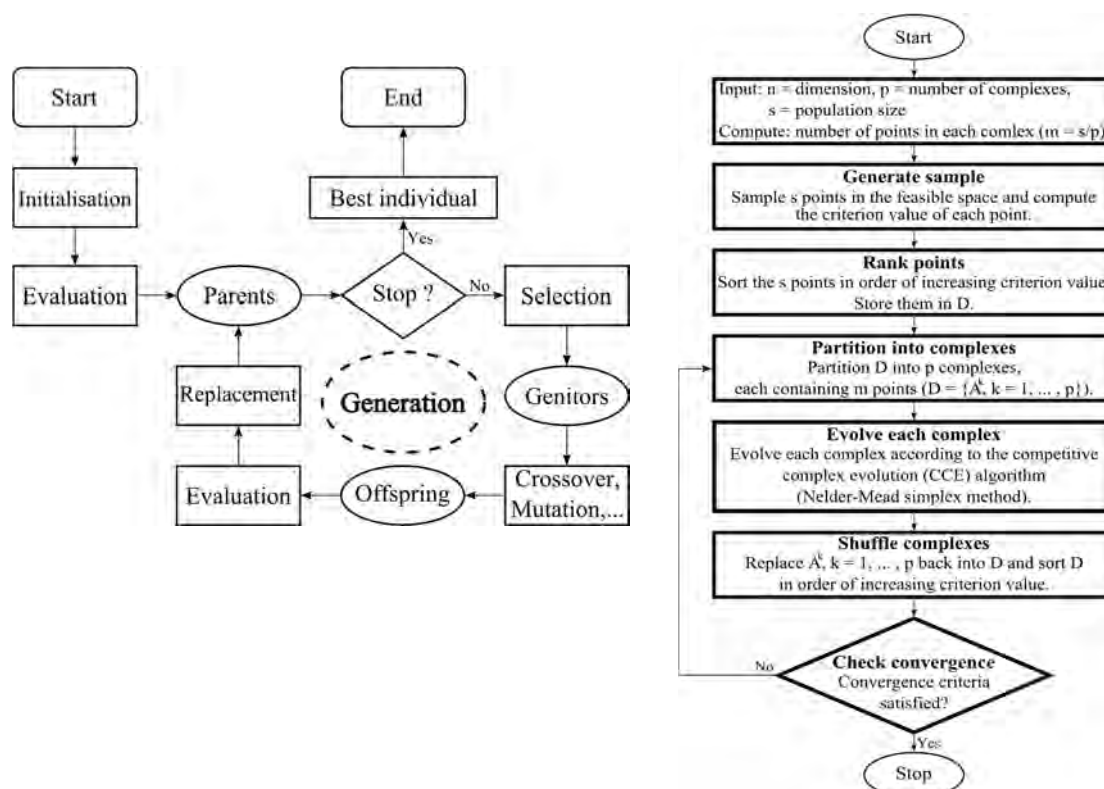


Fig. 1 Optimization algorithm flowcharts a) GA, b) SCE

## 2 COMPUTATIONAL PART

This work deals with the estimation of beech wood decomposition kinetics using GA and SCE optimization algorithm. The experimental data used for the optimization routine were obtained from thermogravimetric analysis (TGA). TGA was carried out in nitrogen atmosphere with heating rate of a sample 5 K/min to the maximum temperature 800 °C.

For the thermal decomposition of beech wood in non-oxidative atmosphere three-step reaction scheme was chosen, shown in Fig. 2. In the first step the water vapour naturally contained in the wood evaporates resulting in the change of the wood density. Subsequently the dry wood decomposes by two independent reactions forming char and gaseous pyrolysate. In the last step, the char transforms to residue again releasing gaseous pyrolysate.

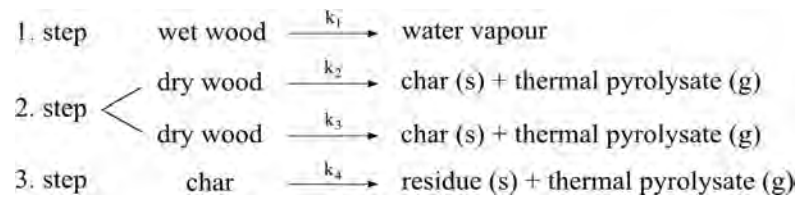


Fig. 2 Beech wood thermal decomposition reaction scheme

For the selected model the total number of parameters to be estimated is 14. 12 parameters ( $Z$ ,  $E$ ,  $n$  for each decomposition reaction) are kinetic parameters for reaction  $k_1$ , ...,  $k_4$  and the remaining two are the density of char and the density of residue.

The estimation of the set of 14 parameters was carried out in program Gpyro. To determine the model kinetic parameters two global optimization methods - genetic algorithm and shuffled complex evolution - were chosen.

One of the main goals of this work was to assess the ability of the optimization algorithm to converge to the unique solution. Therefore ten trials with different initial parameter values randomly generated in the search parameter space (specified by user) were performed both using GA and SCE. At the end model data computed using both GA and SCE estimated parameters were compared to the experimental TGA results. Additionally the rate of convergence and final average value of fitness function were studied to compare which of the algorithms is computationally more efficient.

To investigate the influence of the population size using GA, four calculations with the population size doubling in every run from 125 to 1000 individuals were performed.

### 3 RESULTS

The sets of parameters obtained by optimization using both GA and SCE are summarized in Tab. 1. The parameters listed here are the boundaries of each variable search space, the average values of individual variables calculated from 10 trials with different initial estimate of the parameter values, absolute standard deviation from the average value and normalized standard deviation from the average value in percentages.

Tab. 1 GA settings: 250 individuals, 200 generations, SCE settings - 8 complexes each with 29 points, i.e. 232 points in total

Number	Variable	Units	Boundaries		GA			SCE		
			Minimum value	Maximum value	Average	Absolute standard deviation	Norm. st. dev. (%)	Average	Absolute standard deviation	Norm. st. dev. (%)
1	$\log Z_1$	$\log s^{-1}$	3.5	5.0	4.03	0.39	9.64	3.87	0.22	5.81
2	$E_1$	$\text{kJ/mol}$	35.0	50.0	45.9	2.1	4.57	44.1	2.2	4.98
3	$n_1$	-	0.7	1.5	1.14	0.16	14.21	1.39	0.13	9.27
4	$\log Z_2$	$\log s^{-1}$	10.5	12.5	11.40	0.31	2.72	11.81	0.48	4.05
5	$E_2$	$\text{kJ/mol}$	140.0	160.0	151.0	3.3	2.17	155.5	4.9	3.17
6	$n_2$	-	1.4	3.0	2.18	0.14	6.35	2.13	0.11	5.33
7	$\log Z_3$	$\log s^{-1}$	19.0	21.0	19.84	0.27	1.34	19.14	0.27	1.41
8	$E_3$	$\text{kJ/mol}$	250.0	280.0	262.5	2.8	1.08	255.0	3.1	1.22
9	$n_3$	-	1.0	2.0	1.79	0.17	9.37	1.66	0.10	5.80
10	$\log Z_4$	$\log s^{-1}$	6.0	9.0	6.99	0.38	5.46	6.64	0.14	2.07
11	$E_4$	$\text{kJ/mol}$	140.0	170.0	149.9	4.3	2.86	141.0	2.2	1.54
12	$n_4$	-	2.0	3.5	3.10	0.32	10.19	3.50	0.00	0.11
13	$\rho_{\text{char}}$	$\text{kg/m}^3$	80.0	200.0	196.3	3.1	1.58	198.5	1.53	0.77
14	$\rho_{\text{residue}}$	$\text{kg/m}^3$	80.0	200.0	166.4	1.5	0.90	165.7	0.57	0.34

Absolute average: 5.17

3.28

It can be seen, that both algorithms converged to one same solution within deviation of approximately 5.2 and 3.3 % using GA and SCE respectively. The highest normalized standard deviation from all parameters was approximately 14.5 % with GA and 9.5 % with the SCE algorithm both in the same parameter - reaction order of the first reaction.

In overall, SCE performed slightly better than GA, but our calculations did not confirm that GA should have a problem to find qualitatively the same solution. The Fig. 4 and Tab. 1 suggest that the GA is also able to find "one" solution for our case. This may be due to the fact that the parameter space is very closely specify and does not have to contain a large number of local extremes. However, definition of the close parameter space requires extensive user experience.

The disadvantage of using the real experimental data is, that the exact values of the material parameters are not known, so it is not possible to assess the accuracy of the results. However it is possible to compare the model results using average values from Tab. 1 with the experimental data to verify whether the estimated parameters provide a good fit (Fig. 3). As can be seen, the selected reaction model can describe the experimental curves very well. It describes both the initial mass loss and the secondary peak in the MLR curve.

Fig. 4a shows the GA fitness evolution of the ten trial computations. The group of curves with higher fitness represent the evolution of the best individual (the individual with the highest value of fitness function from all individuals) in the population. The curves below describe average fitness value in the population. For the relatively small population (250 individuals and less) oscillations of fitness function occurs. The part of GA as the evolutionary algorithm are the random processes (e.g. mutation) which can cause that the best individual is knocked out of the population and the fitness function with the number of function evaluations actually decreases.

The SCE fitness evolution for ten different trials with the different random number seeds is shown in the Fig. 4b. Opposed to GA, the SCE fitness evolution is much smoother and without oscillation. The fitness function value increases rapidly in the first approximately 5000 function evaluations and then slowly increase. The fitness evolution follows quite similar pattern in all trials and the fitness level reaches the absolute higher value than in GA.

Fig. 5 shows the effect of population size in the GA on the fitness evolution. With the increasing population size the rate of convergence decrease and decrease the frequency of oscillation - the probability that the best individual will be randomly eliminated decreases with increasing population.

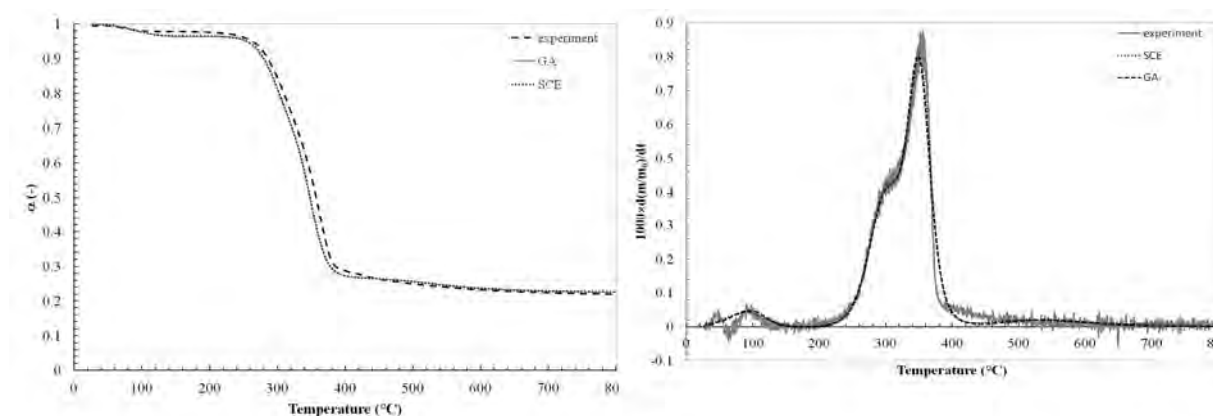


Fig. 3 Comparison of the experimental and model data

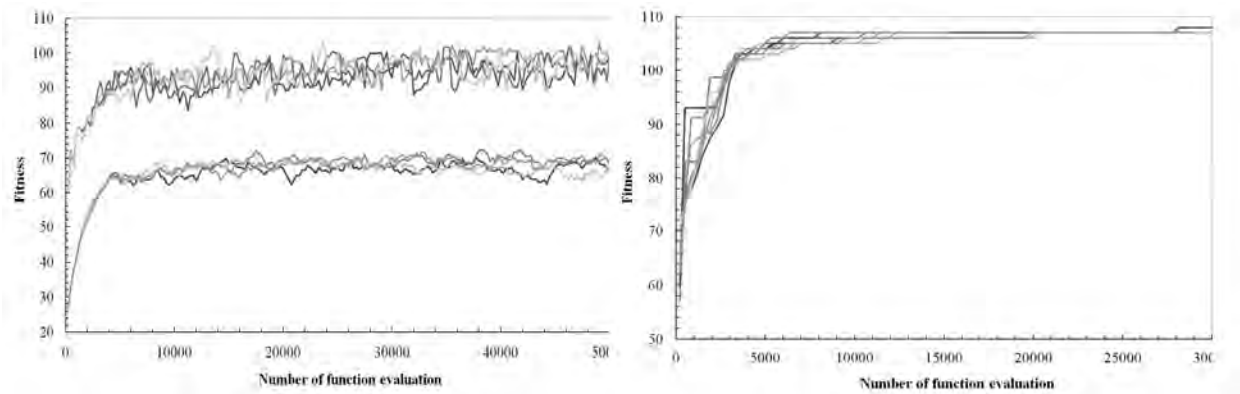


Fig. 4 Fitness evolution a) GA, b) SCE

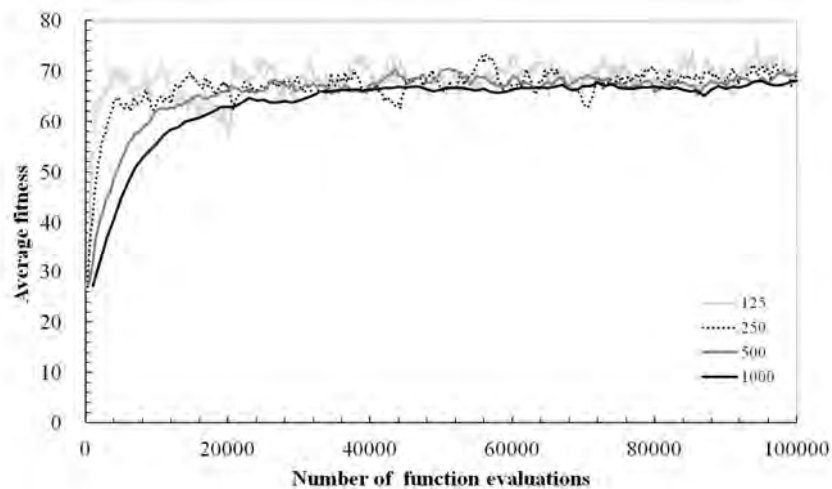


Fig. 5 GA fitness evolution for various population size 125, 250, 500 and 1000 individuals

#### 4 ACKNOWLEDGMENT

Financial support from specific university research (MSMT No 21/2012).

#### REFERENCES

- McGrattan, K., McDermott, R., Hostikka, S., and Floyd, J., "Fire Dynamics Simulator (Version 5) User's Guide," NIST Special Publication 1019-5, National Institute of Standards and Technology, Gaithersburg, MD, 2010.
- Lautenberger, C., Gpyro, A Generalized Pyrolysis Model for Combustible Solids, 2007, <http://reaxengineering.com/trac/gpyro>.
- Stoliarov, S. I., Lyon, R. E., "Thermo-Kinetic Model of Burning," Federal Aviation Administration, DOT/FAA/AR-TN08/17, May 2008.
- Chaos, M., Khan, M. M., Krishnamoorthy, N., de Ris, J. L., and Dorofeev, S.B., Bench-scale flammability experiments: determination of material properties using pyrolysis models for use in CFD fire simulations, Interflam 2010, 2010, pp. 697-708.
- Duan, Q. Y., Gupta, V. K., and Sorooshian, S. Shuffled Complex Evolution Approach for Effective and Efficient Global Minimization, Journal of Optimization Theory and Applications 76: 501-521, 1993. <http://dx.doi.org/10.1007/BF00939380>
- Lautenberger C., Fernandez-Pello C., Optimization algorithms for material pyrolysis property estimation. Fire Safety Science 10: 751-764, 2011.

- ISO 5660-1:2002. Reaction-to-fire tests - Heat release, smoke production and mass loss rate -- Part 1: Heat release rate (cone calorimeter method). International Organization for Standardization, 2012. 39 p.
- ISO 11358:1997. Plastics -- Thermogravimetry (TG) of polymers -- General principles. International Organization for Standardization, 1997. 10 p.
- ISO 11357-1:2009. Plastics -- Differential scanning calorimetry (DSC) -- Part 1: General principles. International Organization for Standardization, 2009. 31 p.
- ISO 12136:2011. Reaction to fire tests -- Measurement of material properties using a fire propagation apparatus. International Organization for Standardization, 2011. 47 p.



# **A QUALITATIVELY MODEL TO DESCRIBE THE INFLUENCE OF BOUNDARIES ON THE ENERGY DENSITY BY CONSIDERING THE ENERGY LEAKAGE, AND ITS EXTENSION ON THE SYSTEM VENTILATION AND FIRE FIGHTING SYSTEMS**

Simon<sup>a</sup> P., Schlee<sup>a</sup> S., Schmidt<sup>a</sup> J., Dehn<sup>a</sup> F.

<sup>a</sup> MFPA Leipzig GmbH Gesellschaft für Materialforschung und Prüfungsanstalt für das Bauwesen Leipzig mbH, Hans-Weigel-Straße 2 B, D-04319 Leipzig

## **Abstract**

Abstract In this paper constitutive models based on physical laws are derived that allow the energy flows and the release of energy to be described and predicted for fires in enclosed spaces and tunnels in particular. The models are generally formulated but are also specifically formulated for practical applications, e.g. for considering the effect of limited burning due to insufficient oxygen supply or the effect of firefighting systems. The solutions agree with the experimentally obtained results in (Carvel et al, 2001 and Carvel et al, 2005). Accordingly, the methods and solutions derived here can be considered adequately validated.

**Keywords:** tunnel fire, heat release rate (HRR), energy density, ventilation

## **INTRODUCTION**

A number of serious tunnel fires, such as those in the Eurotunnel, the Mont Blanc Tunnel and the Tauern Tunnel (Carvel, 2010, Lacroix, 2001, Leitner, 2001, Brousse, 2001), have contributed to the existing interest in methods for determining energy release rates and temperature development in enclosed space. Such methods are of importance not only for tunnel design and, by extension, the economic consequences of fires, but also in the assessment of various rescue scenarios. As part of an international research project (EUREKA) a number of fire scenarios, including a truck fire, were experimentally investigated (Swedish National Testing, 1994, Ingason, 2003, deNenno et al, 2002). Significant differences to known fire scenarios were identified in these experiments in terms of structural engineering. Fire development was much faster, and the temperature gradient at the starting point of the fire was therefore significantly steeper. Significantly higher temperatures were also reached in some cases. In this context, the question was also posed regarding which effect the tunnel geometry or the special conditions of the fire within the tunnel have on the rate of energy release or temperature development. On the basis of experimental investigations, empirically observable relationships were derived taking this effect into consideration (Ingason et al, 2005, Carvel et al, 2005, Carvel et al, 2010, Dehn et al, 2011). Also on the basis of the experimental investigations, temperature-time curves specifically applicable to tunnel structures were incorporated into relevant regulatory guidelines (e.g. ÖVBB, 2005, RABT, ZTV, 2010) in order to enable future tunnel structures to be constructed with adequate safety in terms of the expected fire load. At the same time,

construction materials (see e.g. Dehn et al,2007Dehn et al, 2008) that can withstand the relevant temperature load without loss of integrity and solutions for existing structures or for passive fire protection (see Bergmeister et al, 2003, Clement, 2010). This paper derives constitutive models on the basis of physical laws that allow the energy flows and rates of energy release, and, in turn, temperatures and smoke development, in closed spaces and tunnels in particular to be determined for various boundary conditions. The models are generally formulated and are then further specified for practical applications. The solutions agree with the experimentally obtained results in (Carvel et al, 2005) and (Carvel, 2010), meaning that the methods formulated here (Carvel, 2010, Carvel et al, 2005, Carvel et al, 2004, Dehn et al, 2001) or closed solutions can be considered to be adequately validated.

## 1 THEORETICAL PRINCIPLES FOR THE MODEL

Generally a normal fire is too complex for an analytical approach that is why a simpler source is normally constructed. This source is a superposition of a diffusion source and a radiation source of energy. That is on the first view a strong simplification for the thermal convection, but the thermal convection is the superposition on a direct and an undirect part and so the only mistake of this description seems, to be the handling of the directed part.

The radiation field can thus be described in the following form with the normalization constant (N) and the radius (r).

$$f_{rad}(r) = \frac{1}{N} \begin{cases} (2 - r^2), & 0 \leq r \leq 1 \\ \frac{1}{r^2}, & 1 < r \end{cases} \quad (1)$$

and the diffusion field of energy with the following equation

$$f_{dif}(r) = \frac{1}{N} e^{-\frac{1}{2}r^2} \quad (2)$$

The blending is shown in equation (3) and Fig. 1.

$$f(r) = a f_{rad}(r) + (1 - a)f_{dif}(r), a \in [0, 1] \quad (3)$$

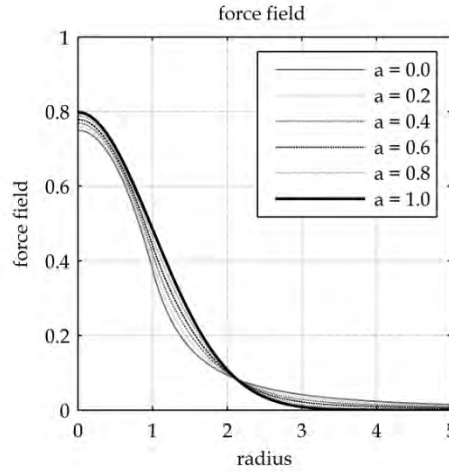


Fig. 1 Transition between a diffuse energy source ( $a = 1$ ) and a radiative energy source ( $a=0$ )

The energy as a field generator size is concentrated in the center, similar to the mass for the gravitational field. In figure Fig. 1 it can be seen more than 80 % of the energy field is in a sector between  $r = 0$  and  $r = 2$  for a source with the radius 1. For a non-spherical approximation for energy density is this good ratio to calculation.

To calculate the leaks the following basis model can be used. A confined space has a border. And on a infinitesimal small borderline the energy has two possibilities, the energy can leave the system (transmission  $\tau \in [0,1]$ ) or the energy can go back into the system (reflection  $\rho \in [0,1]$ ). Every time the energy beak flow ( $E_b$ ) to the system is to calculated by the following general equation ( $E_s$  Energy of the Source,  $E_l$  over the leak lost energy)

$$E_b = E_s \underbrace{(\rho + \tau)}_{=1} \overbrace{\left(1 - \frac{E_l}{E_s}\right)}^{=\rho} \quad (4)$$

This process will be repeated indefinitely and so the energy density increases by a factor of

$$\Phi = \sum_{i=0}^{\infty} (1 - \tau)^i = \sum_{i=0}^{\infty} \rho^i. \quad (5)$$

For a time interdependent spherical geometry it is possibly to calculate the effect of the energy leaks with the equations (4) and (5). For a non-spherical system with some simplifications, such as that the walls are lambertian emitters, that the geometry is easy and that the energy transport from the walls is diffuse, it is possibly to solve the problem analytically.

For a confined non-spherical space the problem is not only defined by the leak, it is as well defined by the ratio of the radii of the source and the confined space. That means that a for flat radiation source the infinitesimal visible surface is a function of the angle  $\alpha_{rad}$  between the normal of the surface and vector between the center of the surface and the point of view. A weak or non-visible surface can be neglected for the energy balance. For a radius higher than the double source radius, the field gradient (Fig. 1) is zero. Or in other term, the reflected energy density is low. For calculating the increasing factor the special case that the confined space has the double radius of the source will be applied. The reason is simple, in this special

case 95 % back flowing energy is captured for  $\alpha_{rad} = 45^\circ$ . The solution for the energy transfer back to confined space form surfaces with greater distances (in a non-spherical system) and a higher angles  $\alpha_{rad}$  amount nearly zero and can be neglected. For a lower ratio between the radii, it needs to be used  $\alpha_{rad}$  higher than  $45^\circ$  and for higher ratio the angle is lower. So, for the approximation the ratio between confined space and source radius of 2:1 was used. That makes it simple to approximation  $\Phi$ .

With all this simplifications, the energy density can be written as ( $r_s$  radius of source)

$$\begin{aligned} \rho_{E,s} r_s^3 &= E = \rho_{E,2s} r_{2s}^3 \\ \frac{\rho_{E,2s} r_s^3}{E^*} &= \frac{\rho_{E,s} r_s^3}{E} \underbrace{\left(\frac{r_s}{r_{2s}}\right)^3}_{=\frac{1}{8}} \end{aligned} \quad (6)$$

To solve this is very easily with a little trick, one writes for  $E^* = \frac{\Phi}{n} E$ . In this case it is directly to see that  $n = 8 \Phi$ . In the studies of Caravel and all [Carvel et al, 2001 Carvel et al, 2005 Carvel, 2010] is  $n = 24$ . And for this experiment is  $\Phi = 3$  by  $E_l = \frac{1}{3} E_s$ .

As result of the superposition on source and reflection term one obtains ( $r_{la}$  radius of limited area)

$$\dot{E}^* = \dot{E}_s (8 \Phi + 1) \underbrace{\left(\frac{r_s}{r_{la}}\right)^3}_{=\alpha^3} \quad (7)$$

The studies of Carvel are for tunnel. In this special case to calculate  $E_l$  is only a geometrical problem. The greatest angle it is to regard is  $45^\circ$  and ratio between the radii of source and confined space is 1:2. In following the leak is calculated for cylindrically symmetrical problem. The leak surfaces ( $A_\tau$ ) and the reflective surfaces ( $A_\rho$ ) are

$$A_\tau = 8 \pi r_s^2 \text{ and } A_\rho = 16 \pi r_s^2 \quad (8)$$

The ratio  $\tau$  between  $E_l$  and  $E_s$  is ratio between the closed surface  $A_\tau + A_\rho$  and leak surface  $A_\tau$

$$\begin{aligned} \frac{E_l}{E_s} &= \frac{A_\tau}{A_\tau + A_\rho} = \tau = \frac{1}{3} \\ \Phi &= \sum_{i=0}^{\infty} \left(1 - \frac{1}{3}\right)^i = 3 \end{aligned} \quad (9)$$

The effect of ventilation and fire fighting systems can be approximated by the Arrhenius equation ( $E_A$  activation energy,  $R$  universal gas constant,  $T$  temperature)

$$\kappa = e^{-\frac{E_A}{RT}} \quad (10)$$

and the ideal gas law ( $p$  pressure,  $V$  volume,  $n$  amount of substance)

$$p V_0 = n R T \quad (11)$$

The ventilation can be approximated with the free volume  $V_\Delta = V_0 (1 - \alpha^3)$  (that means the volume of the system without the volume of the source), that can vary in the ratio to the source from 1 to  $\infty$ . For this reason, the total volume  $V_0$  from equation (11) must be corrected

with a weighting term of  $\frac{V_0}{\alpha^3}$ . With this approximation the exponent of Arrhenius equation can be written as follow:

$$\frac{E_A}{R T} = \frac{n E_A}{\underbrace{p V_0}_{\beta}} \frac{\alpha^3}{1 - \alpha^3}. \quad (12)$$

The effect of ventilation on the HRR (heat release rate) is

$$\dot{E}^* = \dot{E}_s (8 \Phi + 1) \alpha^3 e^{-\beta \frac{\alpha^3}{1 - \alpha^3}} \quad (13)$$

For the fire fighting systems the same procedure can be applied. These systems can reduce the system energy ( $E_T$ , amount of the energy reducing) or the free volume ( $\gamma^3$  expression of the reducing of the free volume). That can be written as an Arrhenius exponent in the following form:

$$\frac{E_A}{R T} = \beta \frac{\alpha^3}{1 - \alpha^3} \frac{p V_0}{p V_0 - E_R} \frac{\gamma^3}{1 - \gamma^3}. \quad (14)$$

In this case one can write equation (13) in the following form:

$$\dot{E}^* = \dot{E}_s (8 \Phi + 1) \alpha^3 \left( e^{-\beta \frac{\alpha^3}{1 - \alpha^3}} \right)^{\frac{p V_0}{p V_0 - E_R} \frac{\gamma^3}{1 - \gamma^3}} \quad (15)$$

## ACKNOWLEDGMENT

The authors are grateful to the Sächsische AufbauBank (SAB) that the project financed by the European Social Fund (ESF) and a fund of the Free State of Saxony. It is promoted as "Investing in your future".



## REFERENCES

- Bergmeister K., Francesconi, S., State of the Art Report on Full Scale Testing of Tunnels under Fire - Upgrading of existing tunnels, 2003.
- Brousse B., Voeltzel A., Botlan Y. L., Ruffin, E., Ventilation And Fire Tests In The Mont-Blanc Tunnel To Better Understand The Catastrophic Fire of 24 March 1999 Proceedings of the 3rd International Conference on Tunnel Fires and Escape from Tunnels, Washington, DC, 9-11 October 2001, 2001, 211-222.
- Carvel R., Beard A., Jowitt, P. W., How much do tunnels enhance the heat release rate of fires? Proceedings of the 4th International Conference on Safety in Road and Rail Tunnels, Madrid, Spain, April 2-6, 2001, 2001, 456-466.
- Carvel R., Beard, A., Jowitt, P. W., The Influence of Tunnel Geometry and Ventilation on the Heat Release Rate of a Fire. Fire Technology, 2004, 40, 5-26.

- Carvel R., Fire Dynamics During the Channel Tunnel Fires. Fourth International Symposium on Tunnel Safety and Security, Frankfurt am Main, Germany, March 17-19 2010, 2010.
- Clement F., Fire protection options for concrete tunnel linings. Fourth International Symposium on Tunnel Safety and Security, Frankfurt am Main, Germany, March 17-19, 2010, 2010.
- Dehn F., Nause P., Hauswaldt S., Abel, F. Willmes, M.: Brand- und Abplatzverhalten von selbstverdichtendem Beton (SVB) für den Tunnelbau Der Citytunnel Malmö als Beispiel Beton- und Stahlbetonbau, 2007, 102, 4-49.
- Dehn, F., Nause. P., Fischkandl, H., Brandresistenter Beton für den Tunnelbau Beton- und Stahlbetonbau, 2008, 103, 271-277.
- Dehn F., Kotthoff I., Neumann N., Hegemann K., Heide U., Schmidt J, Schlussbericht zum BAST-Forschungsprogramm Straßenwesen FE 15.0506/2010/ERB Brandversuche in Tunneln Untersuchungen zum Austritt brennbarer Flüssigkeiten MFPA Leipzig GmbH, 2011.
- deNenno P.J., Drysdale D., Beyler C.I., Walton W.D., Custer R.I.P., Hall J.R., Watts J.M., SFPE Handbook of Fire Protection Engineering, Third Edition. NFPA & SFPE 2002.
- Ingason H, Proceedings of the International Symposium on Catastrophic Tunnel Fires. 2003
- Ingason H., Loennermark A., Heat release rates from heavy goods vehicle trailer fires in tunnels Fire Safety Journal, 2005, 40, 646-668.
- Lacroix D., The Mont Blanc Tunnel Fire: What happened and what has been learned 4th International Conference on Safety in Road and Rail Tunnels, Madrid, 2-4 April 2001, 2001.
- Leitner A., The fire catastrophe in the Tauern Tunnel: experience and conclusions for the Austrian guidelines Tunneling and Underground Space Technology, 2001, 16, 217-233
- ÖVBB-Richtlinie, Erhöhter Brandschutz für unterirdische Verkehrsbauten. Österreichische Vereinigung für Beton- und Bautechnik. 2005.
- RABT, Richtlinien für die Ausstattung und den Betrieb von Straßentunneln. Forschungsgesellschaft für Straßen- und Verkehrswesen, Köln.
- ZTV-Ing, Zusätzliche Technische Vertragsbedingungen und Richtlinien für Ingenieurbauten. 2010.
- Swedish National Testing and Research Institute, Proceedings of the international conference on fires in tunnels. Boras, Sweden, October 1994.

## **COMPARISON OF CFD MODELLING WITH FIRE TESTS**

### **Comparison of CFD Modelling with Results of Full Scale Compartment Fire Tests in a Residential Unit**

Robert Sekret <sup>a</sup>, Damian Saleta <sup>a</sup>, Grzegorz Sztarbała <sup>b</sup>, Piotr Smardz <sup>c</sup>

<sup>a</sup> Politechnika Częstochowska, Częstochowa, Poland

<sup>b</sup> Instytut Techniki Budowlanej, Warsaw, Poland

<sup>c</sup> INBEPO Sp. z o.o., Wrocław, Poland

#### **Abstract**

Two full-scale fire tests were carried out in a derelict apartment block in Bytom (Poland). The primary objective of the tests was to investigate gas temperatures and toxicity conditions during compartment fires in residential units which underwent energy-efficiency improvement works. Such units are typically better sealed and better insulated, in order to reduce heat losses through gaps in the doors, windows and walls. During the tests detailed temperature measurements were collected for both the well-sealed compartment scenario and the benchmark test with included a defined amount of openings in the fire compartment. As a supplementary activity to the main topic of the research it was decided to carry out a-priori and a-posteriori modelling of the thermal conditions within the compartment, using a CFD software package called Fire Dynamics Simulator (FDS). The main purpose was to validate the software for modelling of under-ventilated fires, as the reliability of CFD models in this application is often questioned. The results of the comparison are herewith discussed.

**Keywords:** full scale fire tests, compartment fires, CFD modelling, software validation

#### **INTRODUCTION**

Due to increasing energy costs and more onerous requirements for thermal efficiency many existing buildings in Poland are currently being improved with respect to insulation properties of the enclosures as well as their air-tightness. This process (often referred to as thermo-modernization) is beneficial in terms of the environmental performance of the residential units. However, it is believed that the reduced ventilation rate within the units can increase the risk of carbon-monoxide poisoning in flats equipped with individual gas boilers or stoves and that it can affect tenability conditions in the event of a fire.

On 20 September 2012 two fire tests were carried out in order to examine fire development in real-life conditions. The first test was conducted inside a residential unit with a high degree of air tightness, the second one in a reference unit with typical leakage-paths and openings. The scope of the tests included the analysis of four parameters of fire development, i.e. temperature, toxicity, visibility and pressure (Sekret and Saleta, 2012).

As an additional element of this research work comparisons are being made between experimental results and numerical predictions, in order to validate selected CFD software packages for modelling of under-ventilated compartment fires.

Analysis of the impact of high temperature and concentration of toxic products of combustion on evacuation conditions for the occupants is also being undertaken however it is outside the scope of this paper.

The tests were organized and carried out by the Department of Heating, Ventilation and Air Protection in the Faculty of Environmental Engineering and Biotechnology at Czestochowa University of Technology and Municipal Headquarters of National Fire Service in Bytom with a cooperation of 17 partners representing various industries, i.e. public administration,

rescue services including mining rescue unit, research organisations dealing with fire safety engineering in construction and last but not least the leading fire safety companies in Poland.

## 1 EXPERIMENTAL SETUP

The tests were conducted in a derelict apartment building, situated in Bytom (Silesian Voivodeship). Characteristics of the apartment building:

- five-storey apartment block built in late seventies, prefabricated reinforced concrete structure (walls and floor slabs) with lightweight concrete infill walls;
- due to structural damage (i.e. wall cracks, expansion joint damage etc.) caused by mining exploitation, the building was vacated and earmarked for demolition;
- the tests were carried out in the gable wall apartment block.

Two fire tests in two residential unit of the same layout were conducted: test number one was a sealed-room fire on the fourth floor, test number two was a normal (non-sealed) room fire on the second floor. Residential units used for the fire tests were as follows:

- 4<sup>th</sup> floor flat with total floor area of approx. 37 m<sup>2</sup> and the volume of approx. 91 m<sup>3</sup>; the fire test was carried out from in the sitting room of 15,41 m<sup>2</sup>.
- 2<sup>nd</sup> floor flat with total floor area of approx. 38 m<sup>2</sup> and the volume of approx. 94 m<sup>3</sup>; the fire test was carried out in the sitting room of 15,41 m<sup>2</sup>.

Each residential unit consisted of: a sitting room (15,41 m<sup>2</sup>), a bedroom (9,88 m<sup>2</sup>), a kitchen (5,07 m<sup>2</sup>), a bathroom (3,30 m<sup>2</sup>) and an entrance hall (3,93 m<sup>2</sup>).



Fig. 1 External view of the building

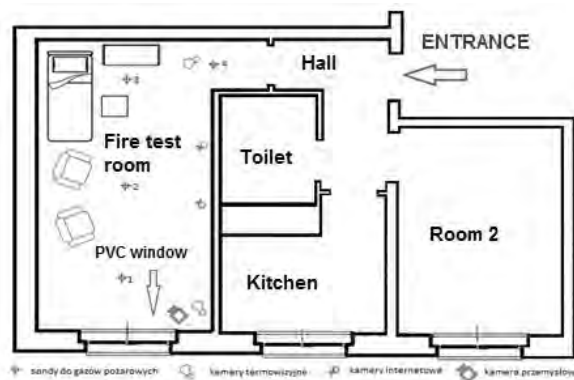


Fig. 2 Geometry of the apartment (test no.1)

During the fire tests temperature inside the compartment was measured using thermocouple trees and infrared cameras. The temperature data was recorded with thermocouples inside the fire room and additional thermocouples positioned outside the building.

- thermocouples t1 and t2 fixed at 200 cm.
- thermocouple t3 fixed at 150 cm.
- thermocouple t4 and thermocouple tree t5 with 3 measurement point – were measuring the parameters of external environment in the vicinity of the window.
- thermocouple trees t6, t7, t8, t9 with 6 measurement points at 110 cm, 150 cm, 190 cm, 215 cm, 230 cm, 245 cm.

In the first fire test flat door and entrance door to the staircase were closed, whereas doors in a flat were open. In the second fire test all doors in a flat were open and the window was open 15 cm wide. Data loggers and other recording equipment were located in flats directly below the test location.

Both tests were ignited with a small wood crib (BS 5852, „wood crib 7”), placed on the central arm-chair.



In the first test (sealed room) the fire has quickly involved the entire chair and has then subsided due to lack of oxygen. The chair initially ignited was completely burnt in the test. The bed positioned next to the chair was also ignited and partially burnt during the 30 min duration of the test. Other items placed in the room (i.e. the second chair, the coffee table and the book-case with books / cardboard boxes) were not ignited.



Fig. 3 Experimental set-up for test no.1



Fig. 4 Fire compartment after test no.1

In the second test (room with limited ventilation) the initial fire growth was slightly slower, probably due to a quicker collapse of the source crib. After involving the first chair the fire has spread to the adjacent bed which was also totally burned during the 30 minutes of the test. Other items placed in the room were not ignited (except for limited charring at edges).



Fig. 5 Experimental set-up for test no.2



Fig. 6 Fire compartment after test no.2

Both fires were extinguished by the fire brigade personnel after 30 minutes of the test.

## 2 NUMERICAL MODELLING

Numerical modelling of the fire scenarios corresponding to the two fire tests was carried out using CFD software package called Fire Dynamics Simulator (FDS, version 5). Detailed information about the programme can be found in the User's Manual and the Technical Reference Guide (McGrattan et al., 2010).

The computational domain was set-up to include the geometry of the relevant areas of the fire test apartment. In all simulations a uniform mesh was adopted. Simulations were run using a coarse mesh (10 cm) and a fine mesh (5 cm), resulting in the total number of 147,456 grid cells and 1,179,648 grid cells respectively.

The initial fire was defined as an input, based on the HRR curve obtained from literature. The fire curve selected was a fire test of a single 2-cushion mock-up chair, with peak heat release rate of 260 kW, attained after 5 minutes (Sardqvist, 1993).

Thermal and ignition properties were applied to obstacles defining adjacent objects such as the bed, the second chair and the bookcase so as to allow fire spread from the initial object to the remaining items in the fire room. As the exact properties of the materials used in the tests were not known (i.e. they were not measured), the values used in the simulations were based on the data available in the literature (e.g. Drysdale, 1998).

Combustion was modelled using the default mixture fraction model (a single-step reaction, with local extinction). Default values of the critical flame temperature and lower oxygen limit parameters were used (1427 °C and 0.15 respectively).

Smokeview 5.6 - Oct 29 2010

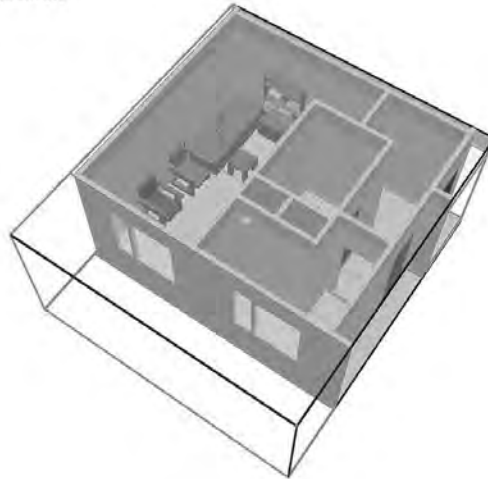


Fig. 7 Geometry of the CFD model

It should be noted that in the post-test simulations the ignition properties of some of the materials were adjusted, in order to achieve better qualitative agreement with fire development observed in the tests. In particular, slightly lower ignition temperatures were adopted compared to the values suggested in the literature.

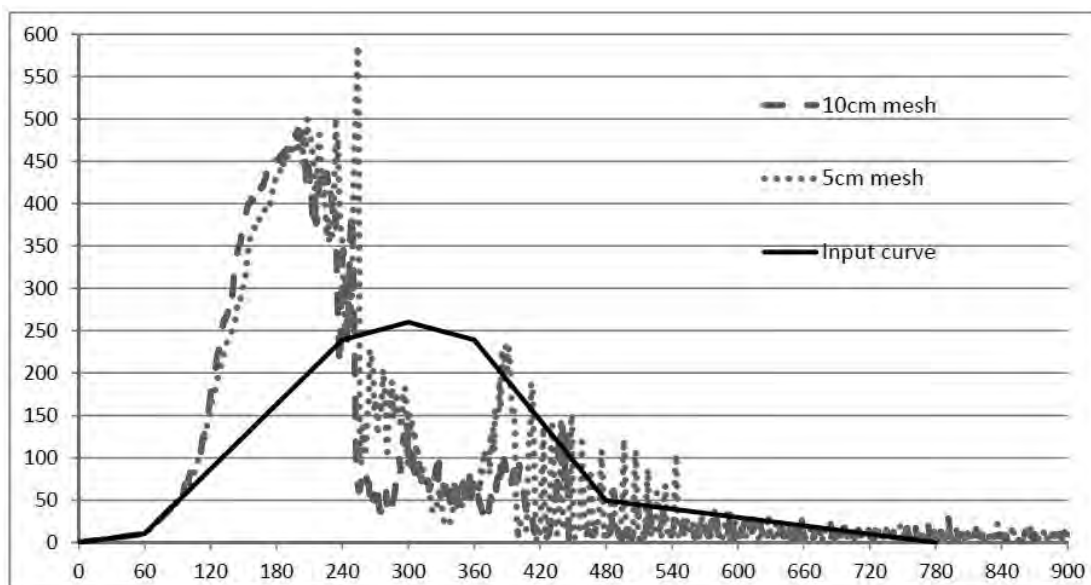


Fig. 8 Comparison of the HRR (in kW) calculated in the simulations for the sealed room scenario with the input curve of a single chair (HRR in kW, time in seconds)

The ventilation conditions in the model were set to replicate the conditions applied in the test. For the fully sealed fire test scenario the only significant opening (leakage path) in the compartment was a ventilation grille in the kitchen.

The rate of heat release computed in the simulation exceeded the growth rate of the initial fire (which was applied as a boundary condition to the top surface of the horizontal cushion of the central chair), which is due to adjacent combustibles being also ignited. After approximately 3.5 minutes the conditions become strongly under-ventilated, which can be seen on the HRR graphs for both 5cm and 10 cm mesh simulations (see Fig. 8).

### 3 COMPARISON OF CFD PREDICTIONS WITH EXPERIMENTAL RESULTS

Numerical simulations were carried out for both the sealed room scenario and the test with additional ventilation paths introduced (window opening, door gaps etc.). This paper will focus on the comparison of the temperature predictions for the sealed compartment scenario (test no.1) as it better highlights the issues arising with modelling of strongly under-ventilated compartment fires.

Fig. 9 and 10 present comparisons of the hot layer temperatures measured in test no. 1 with the values predicted in the simulations, for 10 cm and 5 cm mesh. The values refer to the thermocouple tree located centrally in the room, approx. 1 m away from the first ignited chair.

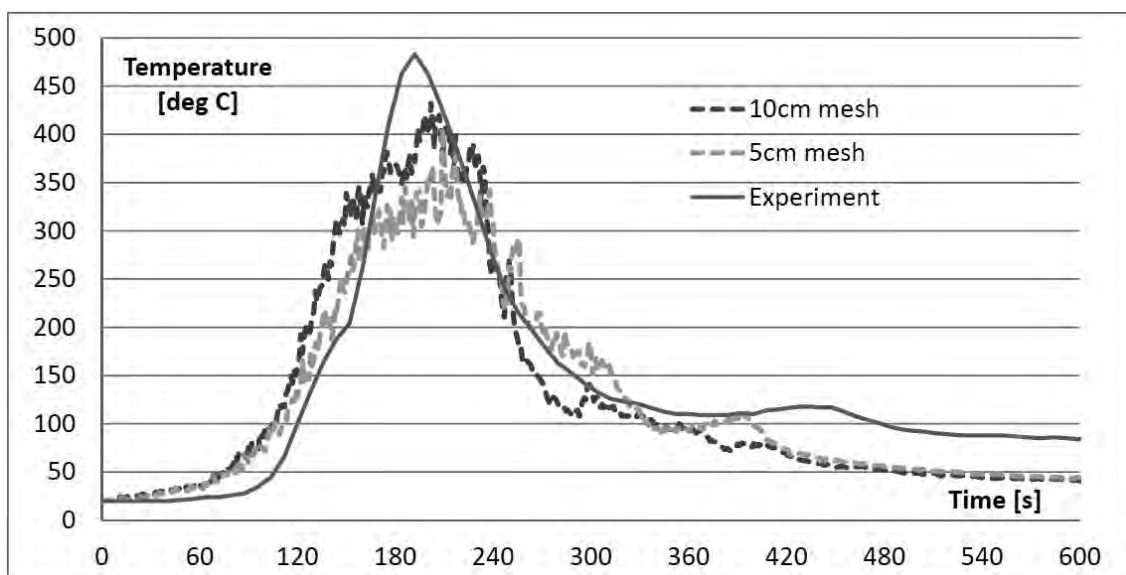


Fig. 9 Temperature 2.40 m above the floor – FDS prediction vs. experimental measurement

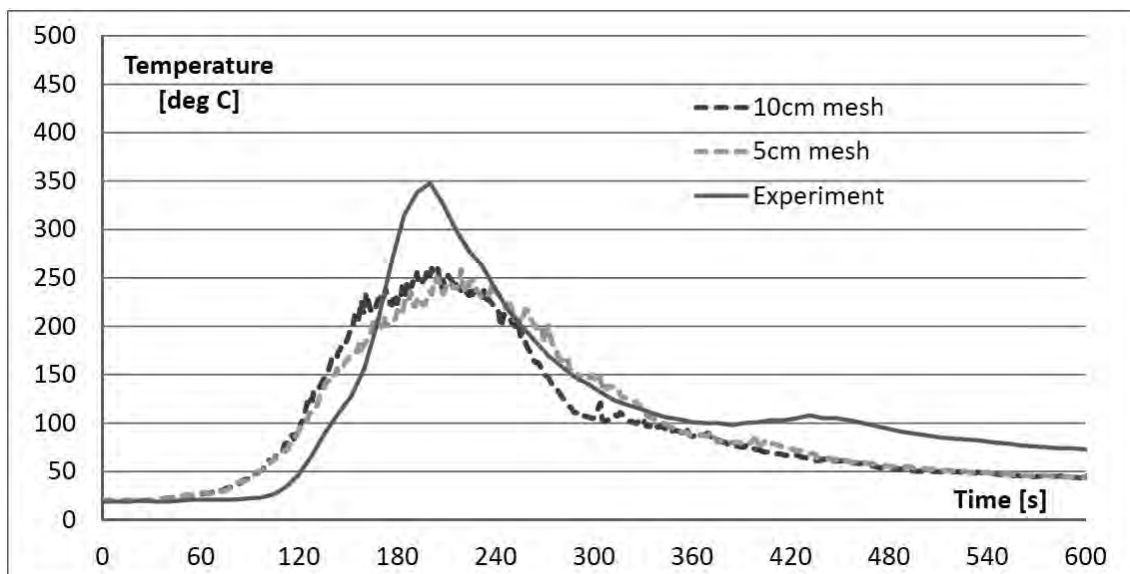


Fig. 10 Temperature 2.00 m above the floor – FDS prediction vs. experimental measurement

Although some allowance should be made for the uncertainties in defining the initial fire and the material properties, it can be generally stated that in the investigated scenario FDS under-predicted the gas temperatures in the hot layer. The peak temperatures in the hot (upper) layer predicted by FDS were 20-25% lower than the measured values.

The relative differences between the numerical and experimental values were even larger for the under-ventilated stage of the fire, when the numerical prediction was 50% lower than the actual temperatures measured in the test. The possible explanation for this may be the following phenomenon observed in the subject simulation undertaken with FDS: in the situation of strong oxygen depletion in the area of fire origin the combustion process (which can be visualized in Smokeview software as the HRR per unit volume) was “shifted” to areas richer in oxygen, even to the room remote from the fire seat and hence much cooler. Such phenomenon was not observed in the experiment. A mixture of air and unburnt fuel gases resulting from an under-ventilated fire can indeed be reignited, however this normally requires high temperature of such gases or an explicit ignition source, neither of which was present in the subject situation.

It is worth to note that the temperature in the cold layer (i.e. 1.00 m above the floor) was generally overpredicted by FDS.

The mesh resolution has a much smaller influence on the predicted temperatures, and no general trend can be identified in this respect. Despite common opinion improved mesh resolution does not seem to lead to higher predicted temperatures for the scenarios investigated.

#### **4 SUMMARY**

CFD models such as Fire Dynamics Simulator used in the subject comparison are very useful for fire engineering work, for example as a tool to predict thermal loading on structural elements exposed to a fire. However, particular care must be taken when applying FDS to strongly under-ventilated fire scenarios. Comparison of numerical and experimental values undertaken as part of a larger research programme and described in this paper indicate that FDS may under-predict peak gas temperatures in the hot zone by up to 25%. In the later phase of the fire, when the conditions in the compartment become severely under-ventilated the difference can be even more significant. The possible cause of this is the difficulty of accurately modeling the combustion processes occurring in severely under-ventilated fires when the simple (default) combustion model is used.

FDS allows more complex approaches to combustion modeling (e.g. two-step reaction or the final-rate, multiple-step combustion model), however these models require more detailed information about the fuel chemistry and much better grid resolutions that would normally be used in practical engineering applications.

#### **REFERENCES**

- Sekret R., Saleta D., Wpływ procesu termomodernizacji budynków mieszkalnych na toksyczność pożaru na przykładzie zabudowy na Górnym Śląsku, 7th International Conference Fire Safety of Construction Works, Warsaw,
- McGrattan K., Baum H., Floyd J., Hostikka S., McDermott R., Mell W., Rehm R. Fire Dynamics Simulator (Version 5) Technical Reference Guide (Volumes 1-3). NIST Special Publication 1018-5, October 2010
- McGrattan K., Floyd J., Hostikka S., McDermott R., Fire Dynamics Simulator (Version 5) User's Guide, NIST Special Publication 1019-5, October 2010
- Drysdale D., An Introduction to Fire Dynamics, Wiley, 1998
- Sardqvist S., INITIAL FIRES RHR, smoke production and CO generation from single items and room fire tests, Lund University, 1993.

## **FDS VERSUS EN-MODELS**

### **Comparison between Heskestad model out of EN and CFD results**

Tom Molkens <sup>a</sup>

<sup>a</sup> StuBeCo bvba, Engineering office, Overpelt, Belgium

#### **Abstract**

For a rather big hippodrome we made a whole FDS model to investigate the influence of a car fire on the structure in terms of smoke and temperature actions on the structure. As fire action we proposed a one or triple car fire. Smoke evacuation is done by natural ventilation; open windows in the roof and doors at ground floor automatically coupled on the detection system. In this particular case we could deliver a report with the guarantee of a smoke free evacuation layer during the required time and no protection is needed for the structure. A guide for the use of the hall was delivered with all the restrictions for a safe use of the construction. At this moment it seems to be useful, for featuring projects, to investigate if there is a difference with the localized fire scenarios from annex C out of EN 1991-1-2. This is of course only valid for the structural impact of the fire load.

**Keywords:** local fire, flame height, temperature, heat flux

#### **INTRODUCTION**

It would be interesting if we could make a comparison between the results of a localised fire following annex C of the EN and the results of the CFD calculation done with the widely known FDS software from NIST. There is a huge time difference to solve both problems, where the EN takes about 5 minutes, the CFD takes sometimes weeks. In the following we like to point out the boundary conditions of room and fire, followed by a discussion of the main parameters such as; flame height  $L_f(z,t)$ , temperature  $\Theta_{(z,t)}$  in the plume, heat flux to the structure  $h_{r+c}$  and at least and most important the steel temperature.

### **1 BOUNDARY CONDITIONS**

#### **1.1 Room geometry**

The hippodrome is a long rectangular building with an insulated double pitch roof, in the sections (Fig. 2 and 3) you'll see some tribune elements which are also a separation or compartment boundary between the hall and secondary rooms like bars, shops and so on. Most important dimensions and materials are listed below:

- Maximum length of compartment = 114,6 m & maximum width = 100,5 m
- Minimum/maximum height of competition hall = 11,4/18,9 m
- Minimum/maximum height of exercise hall = 10,5/12,9 m
- Columns= concrete, steel truss beam for the roof
- Floor, tribunes and walls till about 4,2 m height in concrete, above steel cladding with insulation layer (only insulation in the model).
- Vertical window openings of 6x2,1 m<sup>2</sup> aerologic surface coupled on smoke detection system, ACME smoke detector I2 ( $\alpha_e=1,8$ ,  $\beta_e=-1,1$ ,  $\alpha_c=1$  and  $\beta_c=-0,8$ ).

The model is discretized in 335x382x67 cubes of 0,3x0,3x0,3 m<sup>3</sup>. The size is coming from the smallest dimension of the concrete columns.

Tab. 1 Materials and properties

Material	location	Conductivity (W/mK)	Specific heat (J/(kg.K))	Density (kg/m <sup>3</sup> )	Thickness (m)
Concrete	Floor, walls and columns	1,60	900	2300	0,300
Glass	Wall	0,80	840	2600	0,006
Steel	Beams	50	500	7800	0,020
Insulation	Walls and roof	0,05	1030	40	0,100

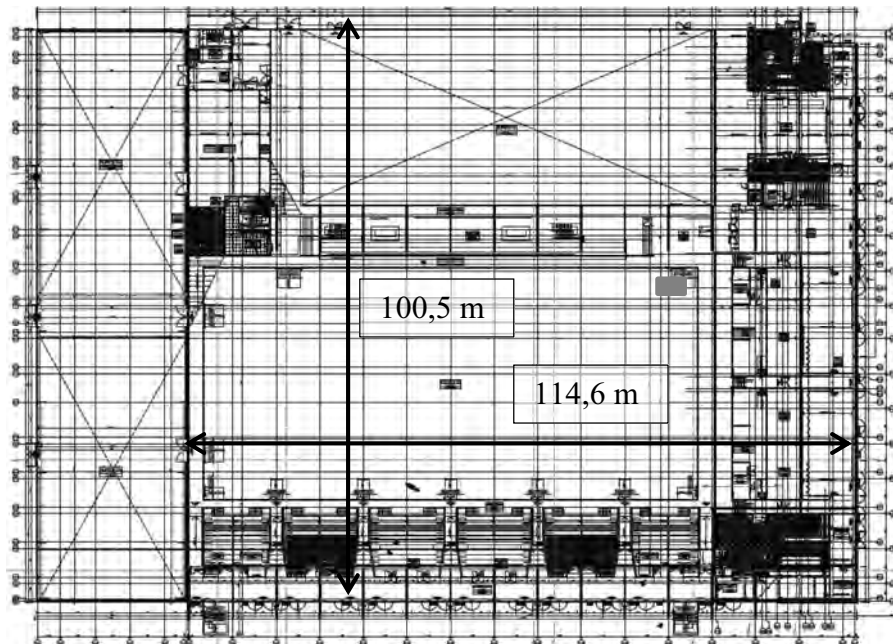


Fig. 1 Floor drawing

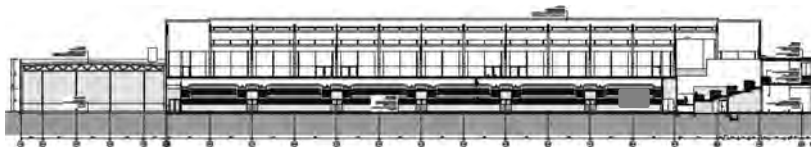


Fig. 2 Longitudinal section

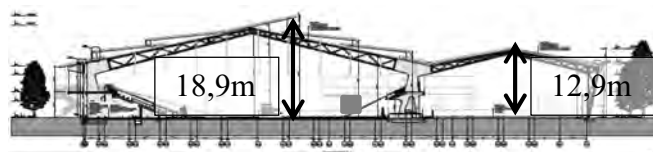


Fig. 3 Cross section

## 1.2 Fire geometry

Neither you investigate a so called Heskestad (flame height bellow ceiling) or Hasemi (flame against ceiling) fire, both of those given formulas in the EN are developed for a circular pool fire. The implantation of the car is determined by the most negative smoke spread which could be obtained out of several simulations.

A conversion must be made between the car fire into an equivalent pool fire. The car was simply modelled as a block with  $L = 4,2$  m length by  $W = 1,8$  m width and  $H = 1,5$  height.

- First we made a FDS calculation where all energy dissipation will be done by the top surface of one car so  $D_{eq,top} = \sqrt{[4/\pi.L.W]} = 3,1$  m and  $RHR_{max} = 1098$  kW/m<sup>2</sup>.

- Secondly all energy dissipation will be done by the top and vertical surfaces of one car so  $D_{eq,top+sides} = \sqrt{[4/\pi \cdot (L \cdot W + 2 \cdot (L+W) \cdot H)]} = 5,7$  m (surf x 3,4) and  $RHR_{max} = 385$  kW/m<sup>2</sup>.
- In a third estimation all energy dissipation will be done by the top surface of three cars so  $D_{eq,top,3} = \sqrt{[3 \cdot 4/\pi \cdot (L \cdot W)]} = 5,4$  m and not three times  $D_{eq,top}$  of 1 car.
- In a fourth estimation all energy dissipation will be done by the top and vertical surfaces of three cars so  $D_{eq,top+sides,3} = \sqrt{[3 \cdot 4/\pi \cdot (L \cdot W + 2 \cdot (L+W) \cdot H)]} = 9,9$  m.
- 



Fig. 4 Real car fire

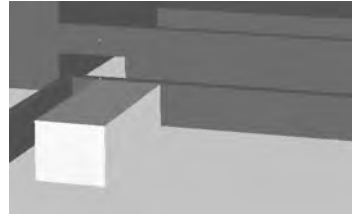


Fig. 5 Only top surface (1car)

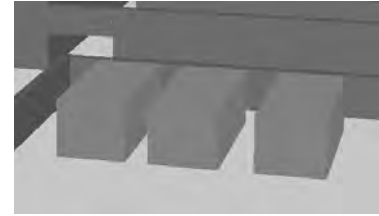


Fig. 6 Top + sides (3 cars)

## 1.2 Fire load

The in our case study applied fire is the one of a medium car, by Joyeux et al. a so called category 3 car of 9500 MJ with a combustion rate of about 71% like can be deduced for new cars. The rate of heat release of one till three cars are presented in the Fig. 7 and Tab. 2 below.

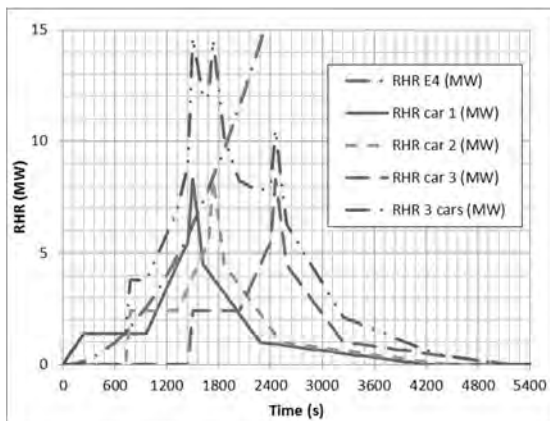


Fig. 7 RHR, Joyeux et al.

Tab. 2 RHR for 1 till 3 cars

time (s)	car 1 (MW)	time (s)	car 2 (MW)	time (s)	car 3 (MW)
0	0	720	0	1440	0
240	1,4	780	2,4	1500	2,4
960	780	1320	2,4	2040	2,4
1440	780	1680	5,5	2400	5,5
1500	780	1740	8,3	2460	8,3
1620	780	1860	4,5	2580	4,5
2280	780	2520	1	3240	1
4200	0	4440	0	5160	0

In Fig. 7. We added also the rate of heat release according to table E.4. from the EN 1991-1-2 for a slow fire in a public space. The grow rate seems to be more or less the same till the peak value for a 1 car fire.

For the description of the fire in the FDS software we used following parameters, we proposed a wood based fire as an approximation:  $C=3.4, H=6.2, O=2.5$ ;  $SOOT\_YIELD=0.08$  and  $HEAT\_OF\_COMBUSTION=17000$  kJ/kg. For smoke particles this can be expected as save sided.

## 2 FLAME HEIGHT

First criteria what must be checked will be the flame height, the choice between an Heskestad fire (flame don't reach the ceiling) or an Hasemi one has an influence on the formulas which must be applied to define the temperature in the Plume and heat flux. In this way this is of an extremely importance.

$$L_f = -1,02 \cdot D_{eq} + 0,0148 \cdot Q^{2/5} > 0 \quad (1)$$

where  $D_{eq}$  Diameter of an equivalent pool, deducted from car surface.  
 $Q$  Rate of heat release in W following Joyeux et al.

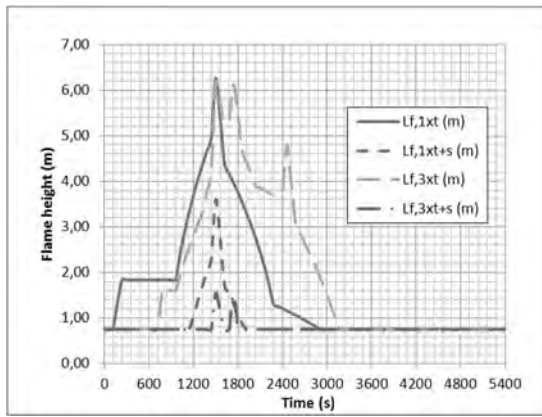


Fig. 8 Flame height following EN

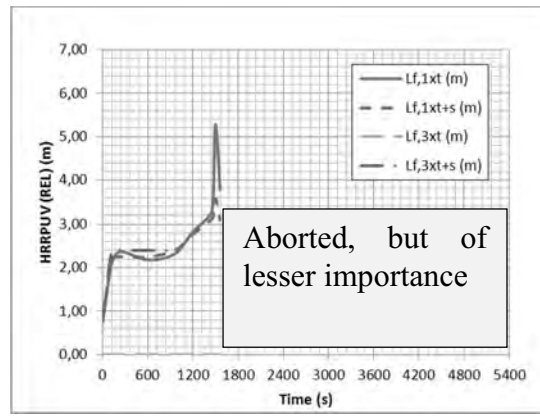


Fig. 9 Flame height following FDS

Following the flame length model included in the EN 1991-1-2, flames will never reach the ceiling, therefore the Heskestad seems to be valid. Because of limited computer capacity we did FDS only simulations for 1 car with energy dissipation on top (t), on top + sides (T+s) and with 3 cars on top + sides.

Maximum flame height following EN is reached with 1 car which is almost the same as for 3 cars and this with energy dissipation only at the top. Results of simulations with also the sides involved lead to very reduced flame height.

To obtain results of the FDS model about the flame height we used a graphical way, by the aid of the  $HRRPUV (REL) > 66 \text{ kW/m}^3$  results. Accuracy is for this reason not famous and in the neighbourhood of 0,20 m. Simulations are done just somewhat further as 1500 s for a one car fire and just till about 1000 s for the 3 cars fire (due to time and computer limitation).

### 3 TEMPERATURE

Where flame height is important to determine the model, it is the temperature which will result in a heat flux on our structural components. The temperature in de plume can be calculated as follows

$$\Theta_{(z)} = 20 + 0,25 \cdot Q_c^{2/3} \cdot (z - z_0)^{-5/3} < 900^\circ\text{C} \quad (2) \quad z_0 = -1,02 \cdot D + 0,00524 \cdot Q^{2/5} \quad (3)$$

- where  $Q_c$  Conductive part of the rate of heat release in W, taken as  $0,8 \cdot Q$ , look (1).
- $z$  level in m along the centre of the plume from mass centre.
- $z_0$  imaginary centre point of the flame in m, if  $< 0$  above mass centre.

At the location of our car the ceiling height is at 14,1 m, we present the calculated results with steps of 2 m just till 2,1 (or 0,6 m above the car) and that in function of time. Because the lower levels of the steel structure are situated at 13,8 m and 11,7 m also measurements this levels are involved. In the FDS software there are simple devices incorporated.

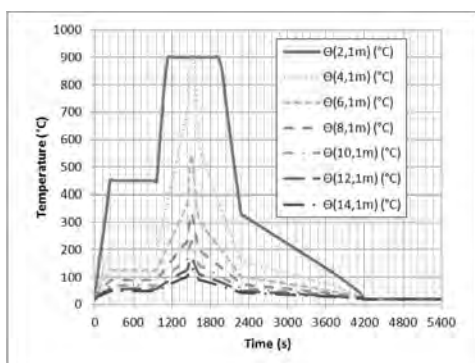


Fig. 10 Temperature for 1 car (t) EN

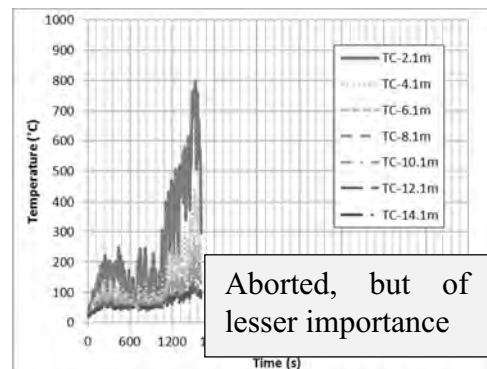


Fig. 11 Temperature for 1 car (t) FDS



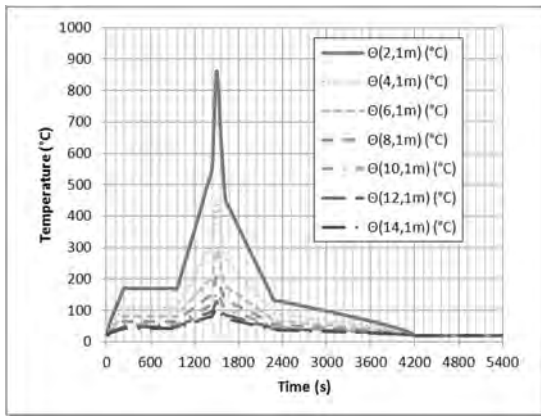


Fig. 12 Temperature for 1 car (t+s) EN

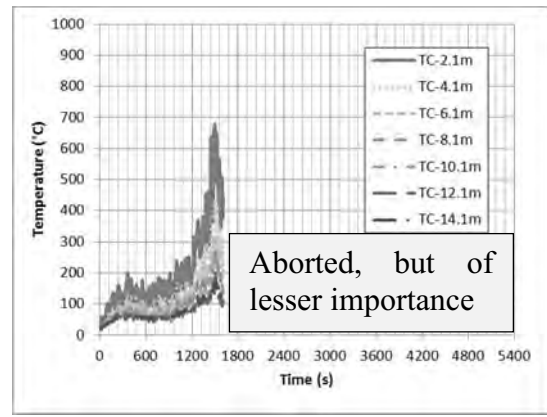


Fig. 13 Temperature for 1 car (t+s) FDS

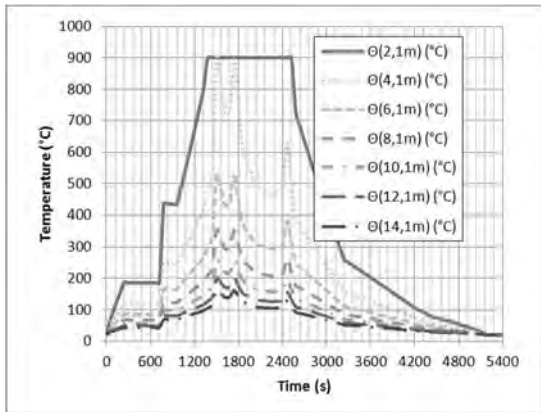


Fig. 14 Temperature for 3 cars (t) EN

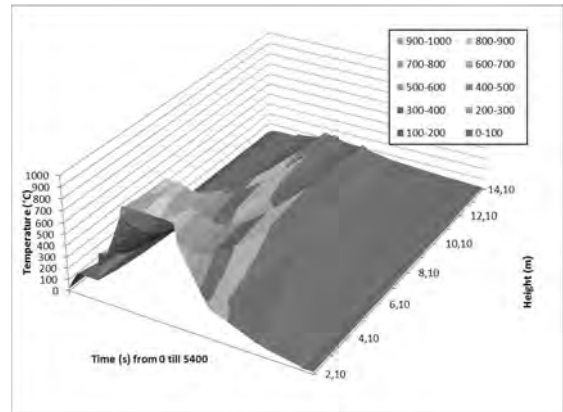


Fig. 15 Temp. for 3 cars (t) EN, 3D impression

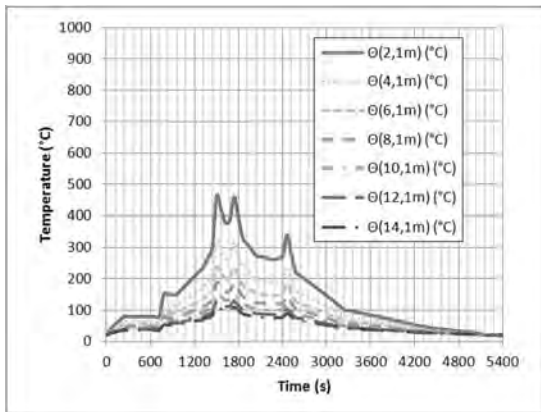


Fig. 16 Temperature for 3 cars (t+s) EN

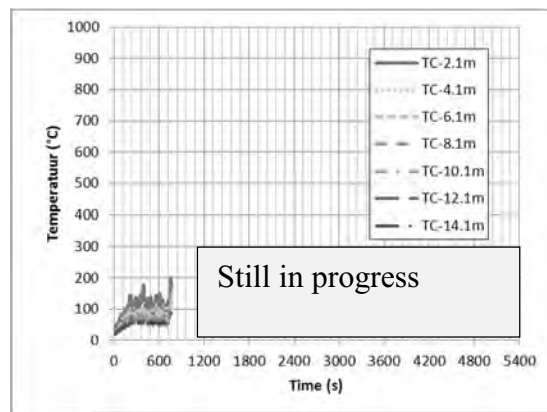


Fig. 17 Temperature for 3 cars (t+s) FDS

Out of the wide range of figures (8 till 14) it becomes clear that our scope of interest can be reduced to what happens at 1500 s. We listed all reading in one table for EN and FDS.

Tab. 3 Temperatures in °C after 1500 s, values in italic are on steel members

Level	2,1 m	4,1 m	6,1 m	8,1 m	10,1 m	12,1 m	14,1 m	<i>11,7 m</i>	<i>13,8 m</i>
1 car t / EN	900	900	544	331	229	172	136	<i>181</i>	<i>141</i>
1 car t / FDS	767	445	289	213	157	125	123	<i>33/111*</i>	<i>30/84*</i>
1 car t+s / EN	861	454	290	207	158	127	106	<i>133</i>	<i>109</i>
<b>1 car t+s / FDS</b>	<b>677</b>	<b>391</b>	<b>317</b>	<b>270</b>	<b>225</b>	<b>200</b>	<b>171</b>	<b><i>39/133*</i></b>	<b><i>32/100*</i></b>
3 car t+s / EN	461	319	238	187	153	129	111	<i>133</i>	<i>113</i>
3 car t+s / FDS	?	?	?	?	?	?	?	?	?

\* = Adiabatic surface temperature / Bold values are probably best match to reality

#### 4 HEAT FLUX TO STEEL AND SURFACE TEMPERATURE

Finally we're most interested in the reaction of our structural component, perhaps errors in flame height and temperature are of lesser importance because the influence on the heat flux is limited. On base of the EN we calculate in the HEA 180 steel truss members a temperature at 11,7 m of 93/72 °C and at 13,8 m of 75/61 °C based on respectively the t/t+s schema for the fire load, look also last two columns of Tab 3.

Tab. 4 Heat flux to the steel in W/m<sup>2</sup> at 1500 s

Level	$h_{r+c,11,7}$	$h_{c,11,7}$	$h_{r,11,7}$	$h_{r+c,13,8}$	$h_{c,13,8}$	$h_{r,13,8}$
1 car t / EN	3507	2456	1052	2449	1822	627
1 car t / FDS	670	117	554	2240	1720	516
1 car t+s / EN	2255	1698	558	1710	1329	380
1 car t+s / FDS	948	159	789	3390	2670	726
3 car t+s / EN	2315	1745	570	1849	1431	418
3 car t+s / FDS	?	?	?	?	?	?

The differences in heat flux (Tab. 4) can be explained by differences in viewing factor, width of the flame (Tondini et al.), radiation from ceiling and smoke flow due to natural ventilation.

#### 5 CONCLUSIONS

It seems that there is a very good agreement between EN and FDS results when comparing the flame height for a car with energy dissipation on the top + side surface (t+s). When we involve only the top surface of the car (t), the EN regulations seems to give an overestimation of the flame height.

On base of the figures, for the temperature the best approach is again achieved with 1 car and t+s burning surface. But with the listed values of Tab. 3 it seems that at higher levels (starting from 6,1 m) this t+s approximation is unsafe sided. Till about 10,1 m the best + save sided approach is obtained by the t system, at higher levels this becomes also an unsafe underestimation. The Horizontal plateaus like obtained by EN are not found.

Regarding the obtained surface temperatures on the structure, again the EN t+s schema fits very well if applied as adiabatic temperature on the steel. It is already shown (Wickström et al.) that this is the best single parameter interface between structural and structural models.

Calculations for a 3 car fire are still in progress, so conclusion can only be made for a local fire with 1 car at this time. Sensibility analyses are on the way to verify influence of material and reaction parameters.

#### REFERENCES

- McGrattan K., McDermott R, Hostikka S, Floyd J., Fire Dynamics Simulator (Version 5) User's Guide, NIST special Publication 1019-5, 2010.
- Joyeux D., Kruppa J., Cajot L.-G., Schleich J.-B., Van De Leur P., Twilt L., Demonstration of real fire tests in car parks and high buildings, European Commission, technical steel research, final report, 2002.
- NBN EN 1991-1-2 + ANB; Eurocode 1: Actions on structures - Part 1-2: General rules – Actions on structures exposed to fire, CEN 2002 + National application document, 2008
- NBN EN 1993-1-2 + ANB; Eurocode 3: Design of steel structures – Part 1-2: General rules – Structural fire design, CEN 2005 + National application document, 2010
- Tondini N., Vassart O., Franssen J.-M., Experimental assessment of the effect of the real flame emissivity for steel elements engulfed into fire, Materials in Fire 2013.
- Wickström U., Robbins A., Baker G., The use of adiabatic surface temperature to design structures for fire exposure, journal of structural fire engineering, Vol 2 , No 1, 2011.

# **THE COMPARISON OF THE RESULTS OF A FULL SCALE EVACUATION TEST TO THE CALCULATION METHOD OF HUNGARIAN REGULATIONS AND TO THE PATHFINDER SOFTWARE**

Csaba Szilagyi <sup>a</sup>

<sup>a</sup> Optomm Ltd. Budapest, Csanyi L. utca 34

## **Abstract**

Action of people in different building has large scale of uncertainty and there is poor availability of experimental data describing it. Evacuation software might be a solution of the problem, but their validation is a key issue. To analyze these key questions, a full scale test was conducted with more than 200 persons participating in it. The test was divided to two phases, first the comparison to Hungarian regulations with a numerical method taking the speed, the width of doors and stairs into consideration and then the comparison to three calculation methods of Pathfinder software. The criteria of calculation defined by the AHJ resulted two different egress scenarios. There were interesting differences between the results of the full scale test, the calculation and the three simulation methods, and also the reasons of the differences were interesting.

**Keywords:** evacuation, experiment, validation, pathfinder, analysing, OTSZ

## **INTRODUCTION**

The evacuation of buildings and open air program areas in Hungary is controlled by the 28/2011. (IX. 6.) BM regulation, concerning the National Fire Safety Codes (NFSC). This regulation is a law, therefore obeying it is obligatory. Designers and authorities began to doubt the evacuation proceedings due to the development of architecture and the needs of the modern age. As a result of architectural development, bigger and bigger buildings are constructed and in such buildings the number of escape routes may rise dramatically. Due to the needs of the modern age, such technological devices are installed into the buildings some of which have a favourable effect and some of which have an unfavourable effect on the evacuation proceedings.

Evacuation aims to provide people a way to leave the building in safety. The method of analysis provided by the law is not detailed enough to reach a safe enough solution. Since the number of variants is high during the evacuation process and also, the effect of these variants on each other is rather high, the analysis without computer simulation is extremely difficult. However, using softwares may generate doubts. The question is whether we can accept these results or not.

Validations can help to answer these questions. Validation is a process during which we analyse a real scale experiment with the help of a software as well, and then the data of the analyses are compared to each other. After the assessment of the comparison we can decide how trustworthy the given software is to be considered. Today in Hungary Pathfinder is one of the most widespread evacuation simulator softwares. This program offers several calculation methods that can be used during a simulation.

There are validation documents available to the software that we all know but we wanted to gather our own experiences concerning the credibility of the program. Thus, the aim of the analysis is to find out how reliable the program is and to decide which of the three calculation methods reflects reality in its fullest, indicating the level of safety as well at the same time.

# 1 REAL EXPERIMENT

## 1.1 Describing the location

According to the evacuation calculation carried out based on the regulation, Dance Club would provide room for too few people, and this way, the club wouldn't be profitable (the owners say). Larger parties have already been organised in the club and authorities did not find the evacuation of the place problematic (only on-sight evaluation was conducted). The owners decided to start an analysis, in order to find real possible solutions that are safe. Evacuation simulations were run with Pathfinder's three simulation modes and one of the results would have been acceptable by the owners but since the results were different, it was necessary to make further calculations. After the discussions with the National Directorate General for Disaster Management, Ministry of the Interior (NDGDM) the next analysis took place on the location.

The NDGDM defined the Dance Club as a disco that can be found on the 3-4-5-6<sup>th</sup> levels of a six-storey building. Its only entrance is on the 3<sup>rd</sup> level at the meeting point of the hanging corridor surrounding the building and the overhead pedestrian crossing that leads to the railway station. Before and after the evacuation, the participants were to be found on the hanging corridor or on the overhead crossing.

The floorspace of the various levels can be seen on Tab. 1. Net floorspace doesn't include areas where built-in furniture and equipment can be found.

Tab 1. Dance Club

Dance Club		
Level	Gross floorspace	Net floorspace
3.	19,76 m <sup>2</sup>	8,35 m <sup>2</sup>
4.	78,25 m <sup>2</sup>	49,4 m <sup>2</sup>
5.	98,64 m <sup>2</sup>	50,3 m <sup>2</sup>
6.	58,75 m <sup>2</sup>	35 m <sup>2</sup>

## 1.2 Variations

Hungarian regulations stipulate that each m<sup>2</sup> of built-in furniture equals (provides room for) 4 people. Therefore, the distribution of the people who is in the club is to be calculated using the most unfavourable scenario, that is, starting with the furthest point from the entrance and using 4 people/m<sup>2</sup> units. Owners said that if the distribution of the people would be like above described, then the club wouldn't be able to work so they set a number limit for the maximum people to be let in. This way, they ensure a comfortable atmosphere on all the levels and the club cannot be overcrowded.



Fig. 1 The Dance floor

### 1.2.1 OTSZ variation

According to Tab. 1, appendix 22 of NFSC the building has to be evacuated in 90 seconds. When defining the number of people to be allowed in, we have taken net floorspace and the number of people allowed/m<sup>2</sup> into account (Tab. 3, appendix 22 in NFSC). In the case of discos, pop concerts and programs that take place in the open (and no seats are provided) this value is 4 people/m<sup>2</sup> (the number of employees wasn't taken into account). We couldn't fill all the levels of the club because only 243 students participated in the analysis. 1022 participants would have been required to fill the whole place (if we count with 4 people/m<sup>2</sup>) so we could only fill the upmost floor (see table).

Tab. 2 2<sup>nd</sup> part of the analysis

Level	Gross floorspace	Visitors	Employees
3.	19,76 m <sup>2</sup>	0	Were not taken into account
4.	78,25 m <sup>2</sup>	0	Were not taken into account
5.	98,64 m <sup>2</sup>	103	Were not taken into account
6.	58,75 m <sup>2</sup>	140	Were not taken into account
Total:		243	Were not taken into account
Total number of participants:		243	

### 1.2.2 Pre-arranged variation

During the analysis we calculated with those numbers (on the three top levels) that were set by the owners (see Tab. 2). We assumed that there are 14 employees and 206 guests can be found in the building (220 total). Participants that were employees had pre-defined points of location. Participants could only begin to leave the building after everyone else has left the level they were on.

Tab. 3 1<sup>st</sup> part of the analysis

Level	Gross floorspace	Visitors	Employees
3.	19,76 m <sup>2</sup>	0	1 (cloakroom attendant)
4.	78,25 m <sup>2</sup>	47	1 barman + 2 security guards
5.	98,64 m <sup>2</sup>	94	1 DJ + 2 barmen + 2 security guards
6.	58,75 m <sup>2</sup>	65	2 barmen + 2 security guards + 1 business manager
Total:		206	14
Total number of participants:		220	

### 1.3 Results of the variations

Tab. 4 Results of the variations

Simulation	Number of simulation	People in the club	Simulation		Number of people exiting in 90 second	Total time required for evacuation
			Beginning	End		
I. Owner	1.	220	10:48	10:50	164	137
	2.	220	11:02	11:04	170	120
II. NFSC	1.	243	11:15	1:17	158	136
	2.	243	11:25	11:27	176	120

## 2 CALCULATIONS OF THE NFSC (ANALYSIS OF THE 1<sup>ST</sup> AND 2<sup>ND</sup> PART)

In Hungary, NFSC is responsible for regulating the evacuation procedures of buildings. Evacuation analyses have two parts: first, they examine the process of leaving the room, and then the exiting of the building is analysed. In the current scenario, only the first section is regulated because the different levels have one airspace (people are outdoors after exiting it). The analysis of the 1<sup>st</sup> section consists of two parts. First, the length of the escape paths is examined, and then they determine how many people can exit the doors in a given period of time. The width of the entrance door is 1.6 m.

Tab. 1, appendix 22 of NFSCSS stipulates that rooms with “C”-“E” flammability class in a building with III fire resistance rating it is required that people are evacuated within one and a half minutes.

NFSC calculations are as follows:

$$t_{1b} = \frac{N_1}{kx_1}$$

where  $t_{1b}$  is the evacuation time of the first section (given in minute, considering how many people can exit the doors)

$N_1$  is the number of people in the room

$k$  is the permeability coefficient (value set to determine how many people leave the exit in a given time period) of the exit that has a constant value of 41,7 people/m/m<sup>2</sup>

$x_1$  is the width of exit  $N_1$ , given in meter

On the basis of this, a maximum of 100 people (who can reach the exit in one and a half minutes) may exit the narrowest cross-section.

- Time required to evacuate 220 people: 3.29 minutes (198 s)
- Time required to evacuate 240 people: 3.59 minutes (216 s)
- Time required to evacuate 243 people: 3.64 minutes (219 s)

## 3 SOFTWARE

### 3.1 Introducing the software

Pathfinder is a simulator program (simulating evacuations and human motion) developed by Thunderhead Engineering.

Pathfinder supports two pathing simulation modes. In “steering” mode doors have no effect on the pathing of the participants; this simulation mode uses a steer-control based system instead. This can ensure an optimal distance between the participants present in a simulation. In SFPE mode participants do not attempt to avoid each other (the small circles, representing participants may overlap) but doors do have an effect on their pathing and velocity is affected by the size of the group of exiting participants.

One may change freely between the different simulation modes in the user’s interface, so the results can be compared this way.

In steering simulation mode Pathfinder combines path design, navigation and the collision of participants to coordinate the movement of the participants.

In SFPE mode Pathfinder uses a flux-based evacuation model, which was published in SFPE Handbook of Fire Protection Engineering (Nelson and Mowrer, 2002) and the SFPE Engineering Guide: Human Behaviour in Fire (SFPE, 2003).

### 3.2 Comparing the results of the three methods of analysis

The mathematic model, run by the computer models evacuation scenarios, which is basically the computerised analysis of a given case. Several difficulties may arise during traditional analysis methods. When carrying out an analogous analysis, it is not possible to examine the

joint effects of geometry, mass or waiting in a line (taking all the details into consideration). This way, all the factors can be analysed that haven't been taken into consideration before. The simulation was made with Pathfinder, which was developed by Thunderhead Engineering.

Two distribution scenarios were analysed. One of these was the one defined by the NFSC (4 people/m<sup>2</sup>) and the other was the one defined by the owners. The simulation aimed to examine what kind of results are produced by the software compared to reality.

### 3.3 Default data of the model

#### 3.3.1 Geometry

The levels of the club were considered rooms in the simulation (as it is given in Pathfinder's user's guide). Thus, we've examined 4 levels as rooms and additional 4 rooms were required as flight of stairs. The rooms were connected by 10 stairs. The size of these stairs was 17.78 cm – 27.94 cm. An entrance door was also modelled on the entry level. The model was built based on the drawings of the building. This model had 4 levels (entry level and three other), The exit was also to be found on the entry level.

#### 3.3.2 Properties of the participants, calculation mode

Width of shoulders: 45.58 cm

Maximum velocity: 1.19 m/s

Calculation mode: steering, SFPE

Evacuation begins at 0.0 s

Number of people to be evacuated:

- 220 (owner's distribution)
- 243 (NFSC scenario)

Tab 5 1<sup>st</sup> simulation (owner's distribution)

Level	Gross floor space	Visitors	Employees
3.	19.76 m <sup>2</sup>	0	1 cloakroom attendant
4.	78.25 m <sup>2</sup>	47	1 barman + 2 security guards
5.	98.64 m <sup>2</sup>	94	1 DJ + 2 barmen + 2 security guards
6.	58.75 m <sup>2</sup>	65	2 barmen + 2 security guards + 1 chief business manager
Total		206	14
Total		220	

Tab. 6 2<sup>nd</sup> simulation (NFSC scenario)

Level	Gross floor space	Visitors	Employees
3.	19.76 m <sup>2</sup>	0	were not taken into account
4.	78.25 m <sup>2</sup>	0	were not taken into account
5.	98.64 m <sup>2</sup>	103	were not taken into account
6.	58.75 m <sup>2</sup>	140	were not taken into account
Total		243	were not taken into account
Total		243	

In the owner's scenario the staff (14 people) began to leave the building with a 60 seconds delay. The reason behind this is the fact that they helped other people during the evacuation.

## 4 CONCLUSION

Tab. 8 Number of people evacuated in 90 s

	Owner's		NFSC		Ratios
	Simulation I.	Simulation II.	Simulation I.	Simulation II.	
Real experiment	164	170	158	176	
Calculations by NFSC	100	100	100	100	1.64 x 1.58
Pathfinder steering	90	90	78	78	1.82 x 2.02
Pathfinder SFPE	90	90	64	64	1.82 x 2.46
Pathfinder SFPE <sup>+</sup>	94	94	63	63	1.74 x 2.50

Tab. 9 Full-time evacuation

	Owner's		NFSC		Ratios
	Simulation I.	Simulation II.	Simulation I.	Simulation II.	
Real experiment	137	120	136	120	
Calculations by NFSC	198	198	216	219	1.44 x 1.58
Pathfinder steering	218	218	261	263	1.59 x 1.91
Pathfinder SFPE	255	255	313	316	1.86 x 2.32
Pathfinder SFPE <sup>+</sup>	250	250	318	338	1.82 x 2.33

It is observable that the 60 seconds latency of the staff in the owner's scenario results in different behaviour on the various levels. There aren't any people on the lower levels but the staff is still at its original spot. On the upper levels, however, the staff begins to exit the building when the area is still crowded. It would be a lot better if they started to exit a given level when it's empty. On the basis of the results, we can safely claim that the evacuation simulations with Pathfinder take more time than the evacuations themselves (in all 3 modes). Calculations take place with 1.82 x safety level in steering and SFPE modes and 1.74 x SFPE<sup>+</sup> mode during the 90 s simulation. When the whole evacuation process is analysed, calculations have a safety level of 1.59 in steering mode, 1.86 in SFPE mode and 1.82 in SFPE<sup>+</sup> mode. The deviation of the simulation modes isn't high but somewhat greater differences are observable between steering mode and the other two modes. This is the result of the two different mathematic models. SFPE modes are flux-based models, where cross-sections of the doors and the level of crowdedness (affecting the pace of advancement) play a major role. Steering mode on the other hand provides a more detailed way of analysis. This is provided by the evasive model, which is a lot more sensitive to a decrease in crowdedness. Due to this sensitivity, an evacuation simulation can speed up to a greater extent (than in SFPE mode) when a decrease takes place. NFSC calculation results fell between real experiment values and simulation values. This leads to the conclusion that the three modes can be considered stricter than the NFSC requirements, thus resulting in more representative results.

## REFERENCES

- Hickernell B. K., Hickernell E. H., Hickernell A. B., Author's Manual for Preparation of Manuscripts for Conference Proceedings, Composite Constructions IV, 2000.
- Dickert D., Book Proceeding: Preparation of Manuscripts, ASCE Publications, 2002.
- Thunderhead Engineering Pathfinder 2011 User Manual
- Thunderhead Engineering Pathfinder 2011 Technical Reference
- Thunderhead Engineering Pathfinder 2009.1.0417 Verification and Validation
- Tadahisa Jin Visibility and Human Behavior in Fire Smoke The SFPE Handbook Of Fire Protection Engineering, . National Fire Protection Association, Quincy, Massachusetts, 3rd edition, 2002. 2-42 – 2-53.



## CFD MODELLING OF THE BRACED BARREL VAULT Made from Rectangular Hollow Sections in Natural Fire

Lukasz Polus <sup>a</sup>, Maciej Szumigala <sup>a</sup>, Zdziaslaw Kurzawa <sup>a</sup>, Michal Malendowski <sup>a</sup>

<sup>a</sup> University of Technology, Faculty of Civil and Environmental Engineering, Poznan, Poland

### Abstract

In the paper the CFD modelling of the complicated braced barrel vault made from rectangular hollow sections in natural fire is presented. The barrel vault is covering a shopping arcade. The covered area of this shopping arcade is 40 m x 80 m. The shopping arcade has two levels. One of the levels is underground. The model is built in full 3D. Natural fire is simulated in FDS software for different fire scenarios. Fire load densities, fire growth rate and rate of heat release are determined from EN 1-1-2: General Actions - Actions on structures exposed to fire. Heat release rate per area is determined for  $t^2$  function. The analysis shows temperature of rectangular hollow sections, distribution of temperature in the shopping arcade, visibility and heat fluxes. The temperatures or heat fluxes can be transferred to the non-linear structural analysis in finite element code Abaqus.

**Keywords:** fire safety, CFD, FDS, natural fire, braced barrel vault

### INTRODUCTION

Nowadays, examples of the expressive use of steel is more and more. Barrel vault is architectural form, used since antiquity (Makowski et al, 1985). The example of braced barrel vault is the construction of the roof of the Atrium Promenada Shopping Center which is presented in Fig. 1. The another example of braced barrel vault is the shopping arcade of the Heart of Atlantis Shopping Centre. The construction of the shopping arcade was designed by Zdzislaw Kurzawa and Lukasz Polus and was presented in Fig. 2.



Fig. 1 Braced barrel vault in the Atrium Promenada Shopping Center

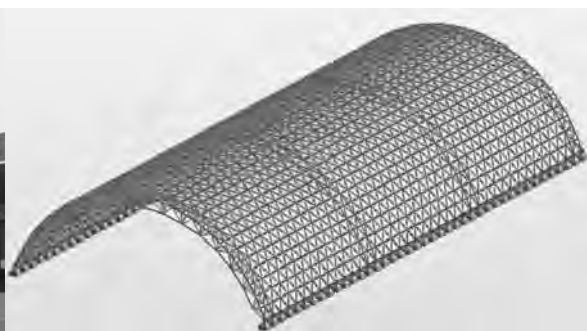


Fig. 2 Braced barrel vault of the shopping arcade in the Heart of Atlantis

Structural members of the construction presented in Fig. 2 are 75mm wide rectangular hollow sections which are 4mm thick. The roof of shopping arcade is a single layer grid structure with four 3D truss which improve the stability of the structure. The covered area is 40 m x 80 m and the shopping arcade has two levels. One of the levels is underground. A lot of people may go shopping and fire is the greatest danger. Design for fire is an important in the design process of the shopping arcade. In the paper, the natural fire in the shopping arcade is presented.

# 1 NATURAL FIRE MODEL IN SHOPPING ARCADE COVERED BY BRACED BARREL VAULT

The model of shopping arcade was created in PyroSim which is a graphical user interface for the Fire Dynamics Simulator and presented in Fig. 3. Model in Smokeview is presented in Fig. 4.

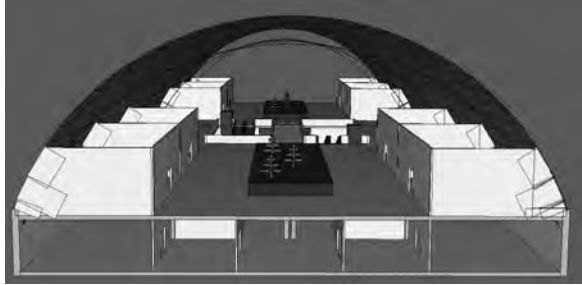


Fig. 3 The model of shopping arcade created in PyroSim

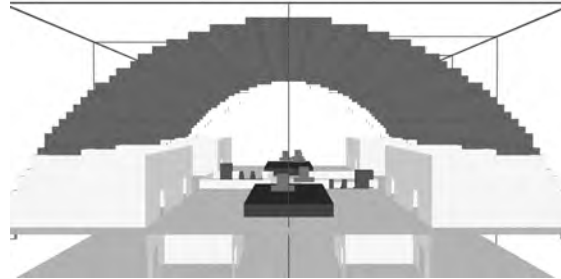


Fig. 4 The model of shopping arcade in Smokeview

The braced barrel vault was modeled as a cylindrical shell with a thickness of 4 mm. Design fire scenarios, characteristic fire load densities  $q_{f,k}$ , compartment floor areas  $A_f$ , fire growth rates, RHR densities, fire growth rates and powers released by the fire  $Q$  are presented in Tab. 1.

Tab. 1 Design fire scenarios

Design fire scenario	$q_{f,k}$ [MJ/m <sup>2</sup> ]	$A_f$ [m <sup>2</sup> ]	Fire grow rate [-]	RHR [kW/m <sup>2</sup> ]	$Q$ [MW]
Fire located to block primary means of escape Public space on the ground floor	122	184	Slow	250	17,64
Fire located to block primary means of escape Public space underground	122	184	Slow	250	17,64
Fire exposing braced barrel vault Shopping centre on the ground floor	730	88	Fast	250	22,00
Fire involving a large area Shopping centre underground	730	182	Fast	250	45,50

The most severe fire is in the shopping centre on the ground floor. Design value of the fire load  $q_{f,d}$  is given in Eq.(1).

$$q_{f,d} = \delta_{q1} \delta_{q2} \delta_n m q_{f,k} \quad (1)$$

where  $q_{f,k}$  characteristic fire load density  
 $m$  combustion factor  
 $\delta_{q1}$  factor for different floor areas  
 $\delta_{q2}$  factor for different types of occupancy  
 $\delta_{qn}$  factor which takes into account the effect of active fire fighting measures

The factor  $m$  is a combustion factor which value is between 0 and 1 (Franssen et al, 2010). The combustion factor is assumed as 0,8. The factor  $\delta_{q1}$  which takes into account the fire activation risk due to the size of the compartment, 88 m<sup>2</sup> is equal 1,212. The factor  $\delta_{q2}$  which takes into account the fire activation risk due to the type of occupancy, shopping centre, is equal 0,78. The factor  $\delta_{qn}$  takes into account the different active fire fighting measures:

- $\delta_{n1} = 1,0$ ; no automatic water extinguishing system
- $\delta_{n2} = 1,0$ ; no independent water supplies

- $\delta_{n3} = 1,0$ ; no automatic fire detection and alarm by heat
- $\delta_{n4} = 1,0$ ; no automatic fire detection and alarm by smoke
- $\delta_{n5} = 1,0$ ; no automatic alarm transmission to the fire brigade
- $\delta_{n6} = 1,0$ ; no fire brigade stationed in the building
- $\delta_{n7} = 0,78$ ; off site fire brigade
- $\delta_{n8} = 1,0$ ; safe access routes
- $\delta_{n9} = 1,0$ ; normal fire fighting devices
- $\delta_{n10} = 1,5$ ; no smoke exhaust system
- $\delta_{qn} = 0,78 \cdot 1,5 = 1,17$

Design value of the fire load is equal  $646,05 \text{ MJ/m}^2$ . The evolution of the RHR is presented in the Fig 5.

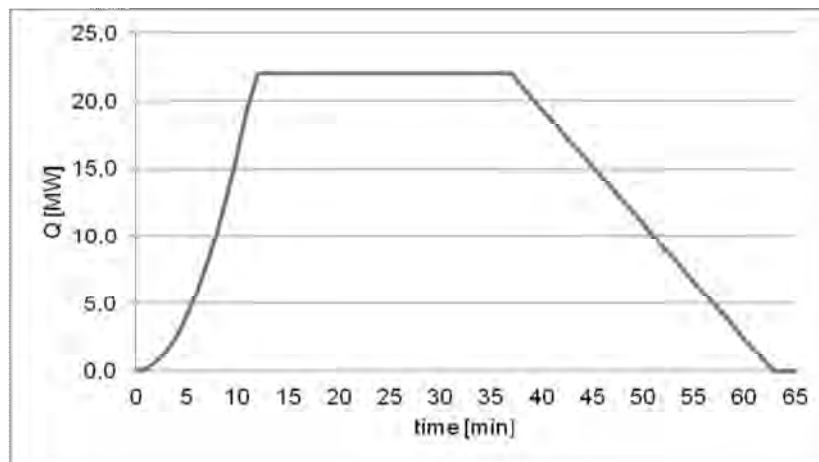


Fig. 5 The evolution of the rate of heat release

## 2 SIMULATION RESULTS

Smokeview 5.6 - Oct 29 2010

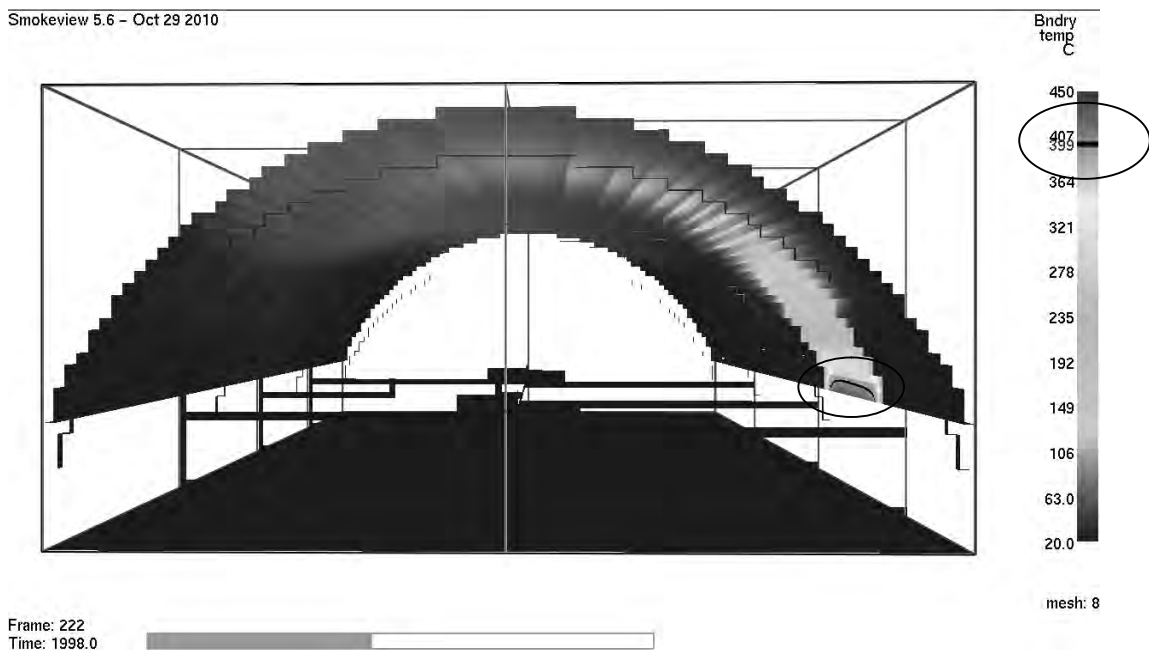


Fig. 6 The wall temperature, mesh  $0,5 \text{ m} \times 0,5 \text{ m} \times 0,5 \text{ m}$  1998 s

The wall temperature and the adiabatic surface temperature were obtained as an output from a fire model. The wall temperature shows the temperature of construction. The adiabatic surface

temperature, which considers a surface as a perfect insulator exposed to heating conditions, should be use to calculating heat transfer to fire exposed structures (Wickstrom et al, 2007). The adiabatic surface temperature is the solution to problems with heat flux boundary conditions like: „the net heat flux to a surface computed by the fire model is dependent on the corresponding surface computed by the same fire model” (Wickstrom et al, 2007). The wall temperature is presented in Fig. 6 and Fig. 7. The maximum wall temperature is equal to 433°C.

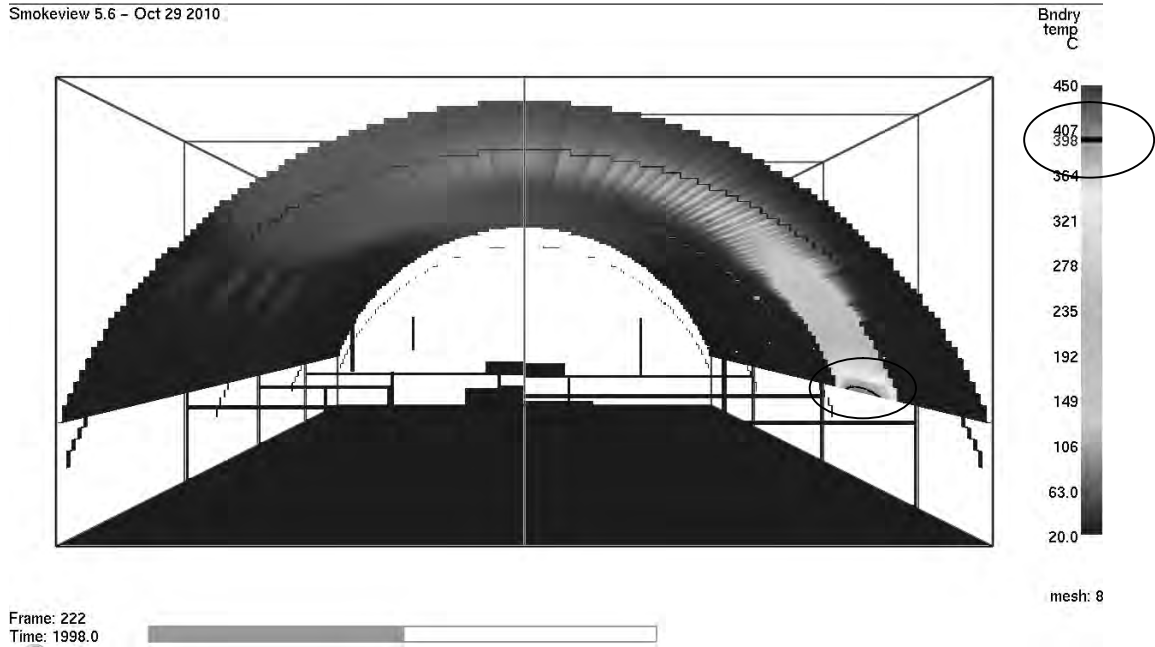


Fig. 7 The wall temperature, mesh 0,25 m x 0,25 m x 0,25 m 1998 s

The adiabatic temperature is presented in Fig. 8.

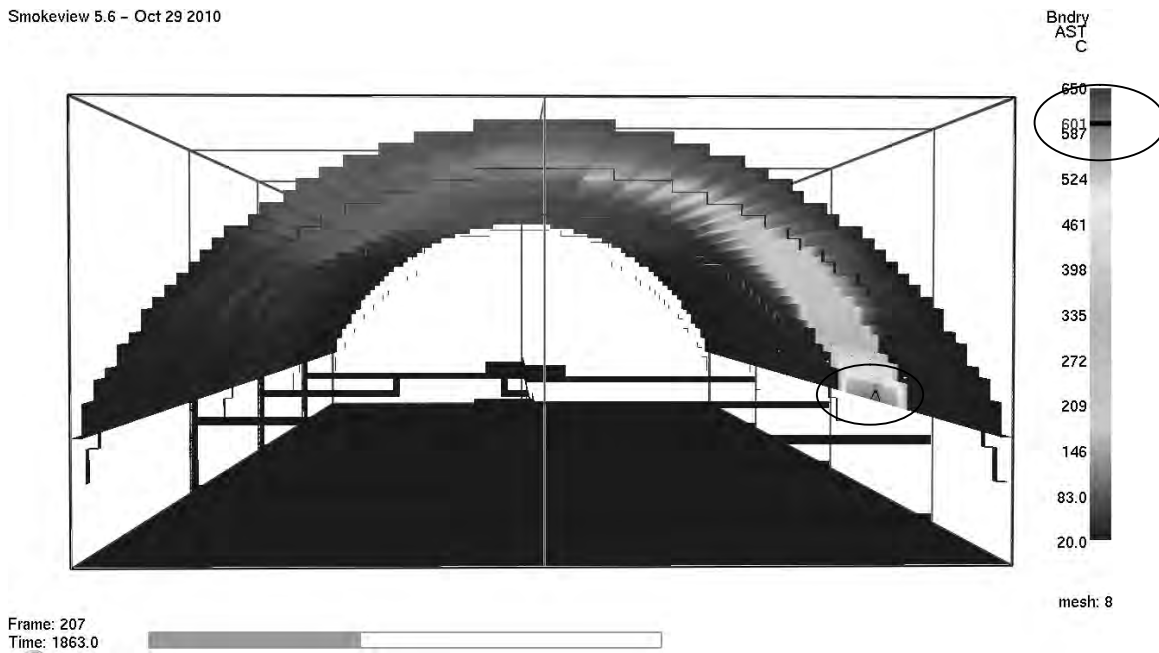


Fig. 8 The adiabatic surface temperature, mesh 0,5 m x 0,5 m x 0,5 m 1863 s

The maximum adiabatic temperature is equal to 623°C. The wall temperature and the adiabatic temperature in the other scenarios are lower.

### 3 CRITICAL TEMPERATURE

According to EN 1993-1-2 the critical steel temperature  $\Theta_{a,cr}$  at time  $t$  for a uniform temperature distribution may be determined for any degree of utilisation  $\mu_0$  at time  $t = 0$  using Eq. (2).

$$\Theta_{a,cr} = 39.19 \ln \left[ \frac{1}{0.9674 \mu_0^{3.833}} - 1 \right] + 482 \quad (2)$$

The degree of utilisation was obtained from Autodesk Robot Structural Analysis Professional software for the fire situation and presented in Fig.9. The combination of actions for accidental situation is given by Eq. (3) (EN 1990).

$$G_k + 0,2S + 0,2W \quad (3)$$

where  $G_k$  all permanent actions  
 $S$  snow loads  
 $W$  wind loads

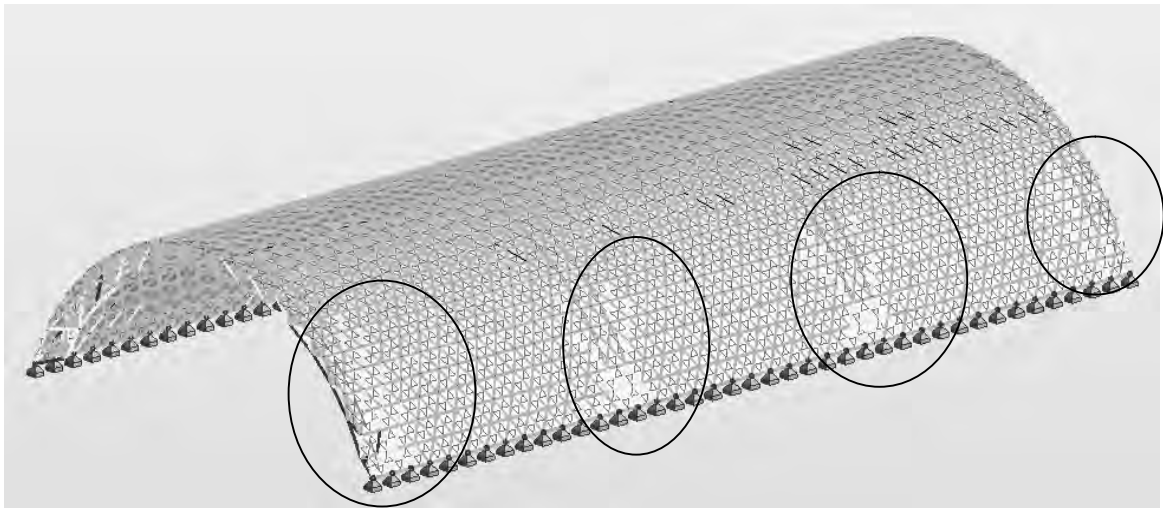


Fig. 9 The degree of utilisation, the most loaded structural members are marked

The critical temperature of the most loaded element,  $\mu_0 = 0.48$ , is equal to 591,2°C.

### 4 SUMMARY

The wall temperature is lower than the critical steel temperature of the most loaded element. The building is huge and hot smoke can easily propagate. The most severe fire is the fire in the shopping centre on the ground floor which has not the highest power of all fires but it exposes braced barrel vault. The adiabatic surface temperature should be use to calculating heat transfer to fire exposed braced barrel vault and can be transferred to the non-linear structural analysis in finite element code Abaqus.

### ACKNOWLEDGMENT

Financial support by the DS grant 11-205/2013 is kindly acknowledged.

### REFERENCES

- Eurocode 0, EN 1990, Basic of structural design. European Committee for Standardization, 2004.
- Eurocode 1, EN 1991-1-2, Actions on Structures Part 1-2 General Actions – Actions on structures exposed to fire, European Committee for Standardization, 2002.

- Eurocode 3, EN 1993-1-2, Design of steel structures Part 1-2 Structural fire design, European Committee for Standardization, 2005.
- Franssen J. M., Vila Real P., Fire Design of Steel Structures, Eurocode 1: Actions on structures Part 1-2: Actions on structures exposed to fire Eurocode 3: Design of steel structures Part 1-2: Structural fire design, European Convention for Constructional Steelwork, 2010.
- Makowski Z. S., et al, Analysis, Design and Construction of Braced Barrel Vaults, Elsevier Applied Science Publishers, 1985.
- Wickstrom U., Duthing D., McGrattan K., Adiabatic surface temperature for calculating heat transfer to fire exposed structures, Manuscripts for Conference Proceedings, International Interflam Conference XI, 2007.

## **EXPERIMENTAL AND NUMERICAL STUDY OF BALCONY EFFECT IN EXTERNAL FIRE SPREAD INTO UPPER FLOORS**

Humberto José L. Morgado <sup>a</sup>, João Paulo C. Rodrigues <sup>a</sup>, Luis Miguel S. Laim <sup>a</sup>

<sup>a</sup> University of Coimbra, Portugal

### **Abstract**

In this paper are presented the results of natural fire tests and numerical simulations using the Fire Dynamics Simulator (FDS) and analytical simulations using the methods of EN 1991-1.2 (2010). The main goal of the investigation is the validation of the values of fire safety regulations on distance between openings corresponding to successive floors in a façade and the effect of dimensions of balconies in the external fire spread into upper floors. It is intended to quantify and measure the height and width of flames projected through the windows and to measure the indoor and outdoor temperatures. The tests were performed in a compartment that was intended to represent a small office with two opposing openings, a door and a window. The distance between the openings in the successive floors was 1.10 m. The test 1 was carried out without any balcony above the opening and tests 2 and 3 had a balcony with different dimensions in length.

**Keywords:** fire simulations, natural fire tests, external fire spread

### **INTRODUCTION**

The fires inside the buildings can sometimes spread to other buildings or from one floor to another floor, because the flames can be projected to outside through windows, doors, roofs or skylights. When projected the flame spreads the fire in façade by convection and radiation. So, limiting the fire spread in the façade is a challenging problem. Reducing the fire spread through the façade openings, many countries created fire safety regulations. The fire safety regulations require a distance between openings to prevent the spread of flames to the top floors and, on the other hand, this risk can also be reduced by a balcony above the openings. In the fire safety regulations around the World exist different proposed distances between openings and sizes of balconies. The distance between openings in Portugal is 1.10 m, but when there is a balcony, with a span at least one meter from each edge of the opening, this distance can be reduced by the span of the balcony. It is noticed that the balconies have to be at least a fire resistance of EI60 (Law 1532/2008). The prediction of the temperature distribution inside and outside (on the facades) a building during a natural fire should be as faithful as possible to the ones observed in reality, in such a way that the fire design of external elements is on the safe side but not too conservative either. Regarding to this matter, for example, Wald et al. (2009) presented an experimental programme to investigate the global structural behaviour of a compartment in the three-storey steel frame building in a plant of the Mittal Steel Ostrava exposed to fire before demolition. Hence this research project was focussed on the examination of the temperature development within the various unprotected structural elements (beams and columns) and its connections during the natural fire. They concluded that (i) the methods for calculating the compartment temperature by the parametric fire curve given in Annex A of EN1991-1-2 compared well with the measured data. (ii) The incremental analytical models allowed presumption of temperatures of the unprotected beams with a good accuracy. (iii) Calculating the temperature of the beam-to-column connection from the measured gas temperature in the fire compartment based on the mass of the connection parts according to Annex D of EN 1993-1-2, was conservative during

the heating phase. (iv) A calculation based on the bottom flange temperature of the supported beam was less conservative. (v) And finally, the prediction of the temperature of the beam-to-beam connections using the measured gas temperature in the fire compartment, based on the mass of the connection parts, was also conservative during the heating phase. The authors still proposed that the calculation based on the bottom flange temperature of the supported beam may be improved by factor 1.0 instead of 0.88. Abecassis-Empis et al. (2008) also carried out natural fire tests, which were conducted in a real high-rise building. The use of these experiments contributed towards extending the current understanding of the complex dynamics of fire and the inherent difficulties of predicting its evolution. They highlighted the strengths and limitations of fire safety tools and practices in real fires. These tests served as a validation tool for certain faculties of CFD models as well as emphasising some of the current limitations of their use. In what concerns to experimental tests focused on the temperature development along the facade of a building between openings, it is observed they are still fairly rare and are mostly of numerical nature. One example, it is the preliminary study published by Weinert and Poh (2006) on the performance of horizontal projections (balcony) in vertical separation of openings in external walls. Three fires were examined with different peak heat release rates. They found that a horizontal projection between about 0.3 m and 0.6 m is equivalent to a 1 m spandrel.

## **1 EXPERIMENTAL TESTS**

The compartment fire was 5.30 m long, 2.03 m wide and 2.10 m tall. The compartment had two openings, one window of 1.23 m width and 0.92 m height, one door of 1.74 m height and 0.73 m width which correspond to an opening factor about 0.30. The façade was 3.30 m long and 3.80 m tall. The distance between the openings in the successive floors was, in the three tests, 1.10 meters. The test 1 was carried out without any balcony above the opening. Tests 2, 3 had a balcony of 0.55 m span and its length was 1.23 m (the same length of window), and 3.23 m (the length of balcony plus 1 m away from each side of the opening), respectively, in tests 2 and 3. The internal walls and ceiling of the compartment were insulated by sandwich panels made of fire resistant gypsum boards and rock wool ( $40\text{kg/m}^3$  for walls and  $150\text{kg/m}^3$  for ceiling). The fire load used in the experimental tests was materialized by means of wood cribs and was obtained by the simplified calculation methods established in EN1991-1-2 (2010). The heat release rate (HRR) used was 4.15 MW, distributed by three piles of wood cribs in the middle of compartment with 1384 kW each one of HRR (Heat Release Rate). For all tests, it was checked the air temperature and the wind speed before the test starts. So, during these tests, practically no wind was detected for all tests, the air temperature was around 30, 15 and 20°C and the relative humidity was 36, 60 and 41% for tests 1, 2 and 3, respectively.

### **1.1 Test 1, 2 and 3**

In test 1 the ignition of wood cribs was a little bit slowly. The time to reach the maximum temperature of 912.5 °C inside the compartment (thermocouple localized in the ceiling) was 26 minutes. The maximum temperature outside, in the middle of the opening of the window of upper compartment, was 260 °C, reached at 15 minutes and 30 seconds. The projection of flame and the plume of smoke in this test were slightly visible. The height of flame above the lintel of window was 0.28 m, the length of flame was 0.10 m and the horizontal projection was 0.88 m (Fig. 1). In test 2 the maximum temperature inside the compartment was 1080.9 °C in ceiling thermocouple reached after 17 minutes and 30 seconds. Outside, below the balcony, was 501.4 °C at 23 minutes and 30 seconds. The flame and the plume of smoke were very visible in this test. The height of flame in projection through the window was 2 m, the horizontal projection was 2.90 m and the lateral projection was 0.20 m (Fig. 2). In test 3 the temperature inside was 1088 °C, obtained in the ceiling at 18 minutes. In the outside, the



maximum temperature obtained below the balcony, was 659.8 °C, at 22 minutes. The flame and smoke plume were very visible. The vertical and the horizontal projections of flame obtained were 2 m and the lateral projection was 0.20 m (Fig. 3).



Fig. 1 Test 1

Fig. 2 Test 2

Fig. 3 Test 3

In test 1 the plume of smoke and the scanty flame up to the superior floor close to the façade (fig. 1). The flame in test 2 bended towards the superior window and surrounded the balcony (fig. 2). In test 2 the flame was projected to outside the façade after hit the balcony (fig. 3).

## 2 NUMERIC SIMULATIONS

In numerical simulations, the FDS program, version 5.5.3, was used. This program is a computational fluid dynamics (CFD) model of fire-driven flow. It is a large-eddy simulation code for low-speed flows with an emphasis on smoke and heat transport from fires (MacGrattan et al, 2010). For visualization of results was used the smokeview interface. The characteristics of fire compartment and façade were the same as in all experimental tests. A finite element mesh of 0.15x0.16x0.17 m was generated automatically by the program and used in all simulations. The time period of analysis was 1470 seconds, corresponding to time when the HRR started to decrease.

### 2.1 Numerical simulation 1, 2 and 3

In numerical simulation 1 (FDS1) the maximum temperature inside the compartment obtained was 947.2 °C in the wall at 9 minutes approximately. The outside maximum temperature, below the window of upper floor, was 849.3 °C at 10 minutes after begins fire. The height of flame obtained by simulations was 3.29 m upper the lintel of fire compartment window. The lateral and horizontal projection was 0.30 m and 1.20 m, respectively. The maximum temperature inside compartment in simulation 2 (FDS2) was 936.5 °C at 8.74 minutes of fire. The maximum temperature outside the compartment was 1118.1 °C, in the balcony thermocouple (end edge), at 10.34 minutes. The height of the projection of flame was 2.20 m and the lateral projection was 0.53 m. The horizontal projection was 1.20 m. In numerical simulation 3 (FDS3) the maximum temperature inside the compartment fire, was 936.1 °C at 9.36 minutes. The outside maximum temperature was 1110.7 °C at 11.34 minutes in front of balcony. The height of flame projection was 3.29 m, the lateral projection was 1 m maybe due to the balcony effect. The horizontal projection was 2 m.

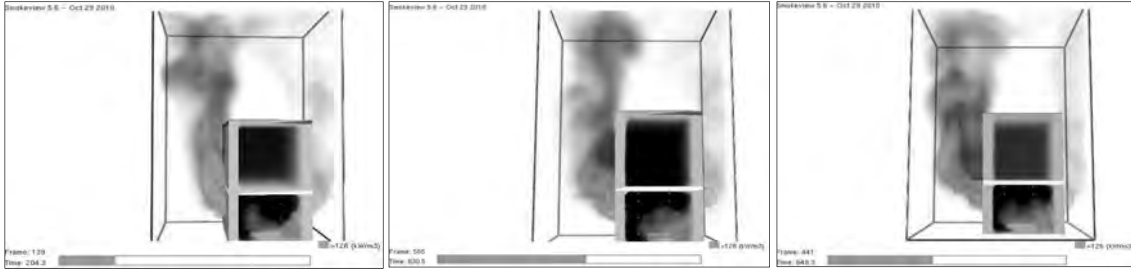


Fig. 4 Simulation 1

Fig. 5 Simulation 2

Fig. 6 Simulation 3

In numerical simulation 1 the flame rose up to the successive floor along the façade (Fig 4), but in the simulation 2 the flame surrounded the balcony and bended toward the window above (Fig. 5). The flame in the simulation 3 rose up parallel to the façade at a distance equal to the balcony span (Fig. 6).

### 3 ANALYTICAL SIMULATIONS

It was also carried out analytical simulations using the method of the parametric fire curves (annex A of EN 1991-1.2, 2010) and the simplified calculation method (annex B of EN 1991-1.2, 2010). The same compartment characteristics as the experimental tests were used in this analytical simulations. The method of parametric curves gave a maximum temperature ( $\theta_g$ ) of 989 °C at 0.480 h inside the compartment (eq. (1)).

$$\theta_g = 20 + 1325 \left( 1 - 0,324 e^{-0,2t^*} - 0,204 e^{-1,7t^*} - 0,472 e^{-19t^*} \right) \quad [^{\circ}\text{C}] \quad (1)$$

where  $\theta_g$  – gas temperature in fire compartment [ $^{\circ}\text{C}$ ]

$t^*$  –fictitious time

In the simplified calculation method used the equations of forced draught. The temperature ( $T_f$ ) inside compartment was 775.4 °C by (eq. (2)).

$$T_f = 1200 \left( 1 - e^{-0,0028 \cdot \Omega} \right) + T_0 \quad [\text{K}] \quad (2)$$

where  $T_0$ , initial temperature [K]

$$\Omega, (A_f \cdot q_{f,d}) / (A_v \cdot A_t)^{1/2}$$

$A_f$ , floor area of the fire compartment [m<sup>2</sup>]

$A_v$ , total area of vertical openings on all walls

$A_t$ , total area of enclosure (walls, ceiling and floor, including openings)

$q_{f,d}$ , design fire load density related to the surface area  $A_f$

The height of flame ( $L_L$ ) projected through the window was 0.58 m given by Eq. (3).

$$L_L = \left( 1,366 \left( \frac{1}{u} \right)^{0,43} \frac{Q}{A_v^{1/2}} \right) - h_{eq} \quad [\text{m}] \quad (3)$$

where  $Q$ , rate of heat release of the fire

$h_{eq}$ , weighted average of window heights on all walls

$u$ , 6 m/s

The horizontal projection ( $L_H$ ) obtained was 2.17 m given by eq. (4).

$$L_H = 0,605 \left( \frac{u^2}{h_{eq}} \right)^{0,22} (L_L + h_{eq}) \quad [m] \quad (4)$$

The width of flame (lateral projection) ( $W_f$ ) was 2.62 m given by eq. (5).

$$w_f = w_t + 0,4 L_H \dots [m] \quad (5)$$

where  $W_t$ , sum of window widths on all walls

The temperature of flame at the window was 746.9 °C and the flame temperature along the axis of one meter was 737.7 °C. In the forced draught the trajectory of the flame may be directed horizontally if there are balconies. The flame is deflected outwardly at a distance equal to the width of the balcony, but the length not change. The  $L_f$  is the same and equal to 2.25 m.

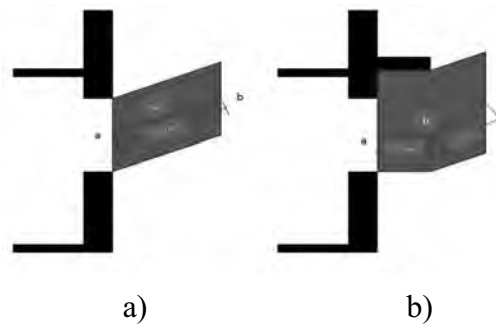


Fig. 4 Flame deflection: a) without balcony; b) with balcony

#### 4 COMPARISON AND VALIDATION OF RESULTS

The maximum temperatures inside compartment were obtained in the ceiling on experimental tests and in the two smaller walls in the numerical simulations. The time to reach the maximum temperature was 9 minutes (FDS 1), 8.70 minutes (FDS 2) and 9.36 minutes (FDS 3) for the numerical simulations and 26 minutes (Test 1), 17.5 minutes (Test 2) and 18 minutes (Test 3) for experimental tests and 29 minutes (Parametric curve) for analytical simulations (Fig. 5).

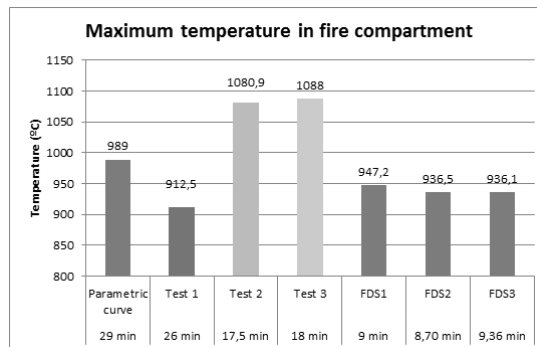


Fig. 5 Maximum temperature in fire compartment

In experimental tests the temperatures inside compartment were higher than outside. In the numerical simulations the temperatures outside were higher than inside compartment. It was noted that the time was not the same when the maximum temperature was reached outside and

inside the compartment both in the experimental tests and in the numerical simulations. The existence of a balcony larger than the window (Test 3 and FDS3) led to that the temperatures above it are smaller than in the case of the balcony ending on the border of the window (Test 2 and FDS2) and much smaller than comparing with the case of inexistence of balcony (Test 1 and FDS1). The results showed that temperatures along the façade do not decrease as a function of height. At different points above the balcony and below the window of the upper compartment were registered temperatures below the ones in the centre of the window of that compartment. It can also be seen clearly in Fig. 6 e 7 that the numerical temperatures at points corresponding to thermocouples T80, T81 and T82 (above the balcony) of the experimental tests, were lower than the ones at points located below it.

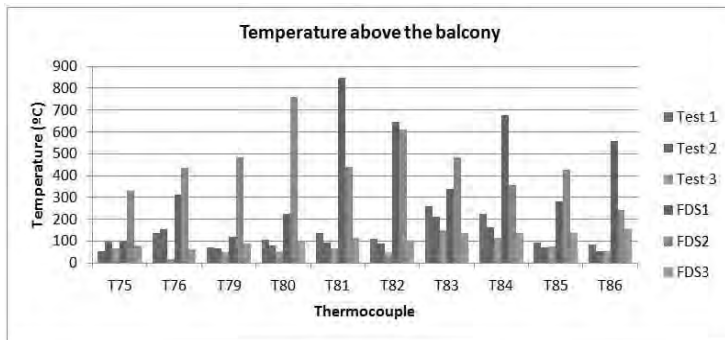


Fig. 6 Temperature above the balcony

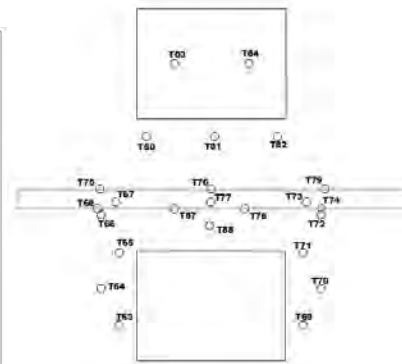


Fig. 7 Measuring temperature points

In Eurocode 1 part 1-2 (EN 1991-1.2, 2010) for forced draught the flame occupies the entire window when occurs the flame projection. In experimental tests this situation didn't occur, (Fig. 7, 8 and 9). This can be observed by a dashed line in Figure 8, where the flame and the plume of smoke do not occupy the entire opening. From these figures it can be assessed that about 20% of the window was used by the fresh air to entry in the compartment while in numerical simulations the flame occupied practically the entire window. The height of flame projection in experimental tests 2 and 3 was 2 m being smaller than test 1 that was 0.28 m. In numerical simulations, it was verified that the height of flame in FDS 2 was (2.22 m) smaller than the ones obtained in FDS 1 and FDS 3 (3.29 m). Concerning the simplified calculation method the height of flame was 0.58m. The horizontal projection in experimental tests was higher in test 3 where the flame was away from the façade. In the numerical simulations FDS 1 and 2, it was observed an equal horizontal projection of flame from the wall, which was 1.20m. In the simplified calculation method the horizontal projection of flames was 2.17m that is the highest value relating to the experimental and numerical tests, exception for test 2. The width of flame enlarged from each side of the window in all experimental and numerical tests, but in experimental test 2 the enlarging is higher than in the others. In the simplified calculation method the flame width was 0.70m that was smaller than in numerical simulation FDS3 (1.0m) and higher than in the other numerical and experimental tests (see Fig. 9).

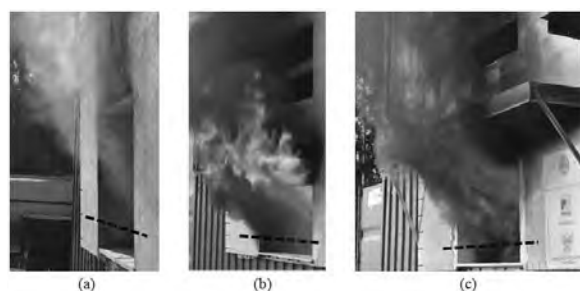


Fig. 8 Flame projection in forced draught

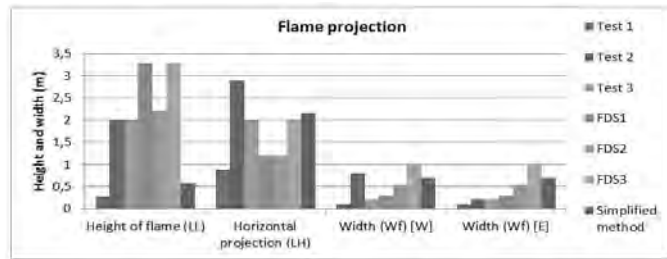


Fig. 9 Flame projection

The presence of a balcony with 1 meter to each side of window was the most viable option, since because of it the flame was kept away from the façade and so the temperatures in the wall above the balcony were lower than the ones recorded in other tests. Therefore, with a balcony between successive openings, the risk of fire propagation to the upper floors will be much smaller. In FDS 2 the height of flames is smaller than the other cases however the flame surrounded the balcony increasing lateral spread of the fire to the upper floors.

## REFERENCES

- Abecassiss, C., Reszka, P., Steinhaus, T., Cowlard, A., Biteau, H., Welch, S., Rein, G. and Torero, J.L., “Characterisation of Dalmarnock fire test one”. *Experimental Thermal and Fluid Science*, Vol. 32, pp. 1334-1343, 2008.
- EN 1991-1-2. “Eurocode 1 – Actions on structures Part 1-2: General actions – Actions on structures exposed to fire”, 2010.
- MacGrantt, K. et al. “Fire Dynamics Simulator (Version 5) - User’s Guide and Technical Reference Guide”. National Institute of Standards and Technology, 2010.
- Decree-Law 220/2008, November 12, Legal Regime for Fire Safety in Buildings.
- Law 1532/2008, December 29, Technical Regulations of Fire Safety in Buildings.
- Wald, F., Chlouba, J., Uhlir, A., Kallerová, P. and Stujberová, M., “Temperatures during fire tests on structure and its prediction according to Eurocodes”. *Fire Safety Journal*, vol. 44, pp. 135-146, 2009.
- Weinert, D. and Poh, W., “Performance of horizontal projections in vertical separation of openings in external walls – comparison with BCA solutions”. *Proceedings of the International Conference on Fire Safety Engineering*, Gold Coast, Australia, 2006, 15 p.









# ON THE USE OF FIRE BRIGADE STATISTICS FOR STRUCTURAL FIRE SAFETY ENGINEERING

Gianluca De Sanctis<sup>a</sup>, Jochen Kohler<sup>b</sup>, Mario Fontana<sup>a</sup>

<sup>a</sup> ETH Zurich, Institute of Structural Engineering, Zurich, Switzerland

<sup>b</sup> NTNU Trondheim, Department of Structural Engineering, Trondheim, Norway

## Abstract

In this paper the fire brigade intervention is considered for the assessment of structural fire safety through the concept of a maximal controllable fire area. Based on a literature survey probabilistic models are developed to consider the uncertainties associated with the fire development and the fire brigade intervention. A sensitivity analysis identifies the most important parameters and suggestions for future data collection are made to improve the probabilistic models.

**Keywords:** fire brigade intervention, statistical data, probabilistic models, sensitivity analysis

## INTRODUCTION

The fire brigade intervention is an important fire safety measure and an integral part of the fire safety concept of a building. Therefore, it should be considered in structural fire safety design. This paper focuses on the probabilistic modelling of the fire brigade intervention including the discovery of the fire, the emergency call as well as the response and fire suppression by the fire brigade.

In this paper literature on fire brigade statistics is listed and used to develop probabilistic models. The listed literature provides a methodical basis for future statistical fire brigade surveys. Limitations and problems using the literature when developing the probabilistic models are discussed and methods to address these problems are presented.

Fire development has a mayor influence on structural safety. Therefore, the effect of the fire brigade on the development of natural fire conditions must be carefully modelled. Early detection by a smoke alarm system should also be considered. In a sensitivity study the most important parameters affecting the impact of a fire on a steel structure are analysed. Based on this sensitivity analysis, suggestions for further data collection and studies are made to improve the probabilistic models and consistently implement fire brigade intervention into fire safety design.

## 1 FIRE MODELING CONSIDERING THE FIRE BRIGADE INTERVENTION

This chapter emphasises on engineering models used to assess the thermal action on the structure taking into account the fire brigade intervention.

### 1.1 Compartment fire model

A fire can be characterized through three phases: the pre-flashover phase, the full engulfed fire (post-flashover) and the decay phase. According to Eurocode 1 (EN 1991-1-2:2002) the pre-flashover phase is modelled by a t-square approach characterizing the increase of the rate of heat release  $Q$  before the maximal rate of heat release per  $m^2$   $RHR_f$  is reached (see Fig. 1). The fire growth parameter  $t_\alpha$  is the basic parameter in this model and is defined by the time needed for the fire to reach a rate of heat release of  $1 MW$ . The basis for this model is the assumption of a constant radial fire spread velocity in all directions. Given the maximum rate of heat release  $RHR_f$  (per  $m^2$ ) the fire spread area  $A_F$  can be assessed through Eq. (1).

$$A_F(t) = \begin{cases} 10^3 \left( \frac{t}{t_\alpha} \right)^2 \frac{1}{RHR_f} & \text{before flashover} \\ A_{Comp} & \text{after flashover} \end{cases} \quad (1)$$

The full engulfed fire – when the fire engulfs the total compartment area  $A_{Comp}$  – is characterized through a constant rate of heat release depending on the fire regime, limited by the fuel or the oxygen. A fuel controlled fire reaches the maximal rate of heat release  $RHR_f$  per  $m^2$  and depends on the surface and the material properties of the combustible material. For ventilation controlled fires the maximal rate of heat release is limited by the available oxygen. The fire load  $q$  determines the full engulfed fire. Eurocode 1 proposes the start of the linear decay phase after 70% of the fire load has been combusted.

## 1.2 Intervention of the fire brigade

The intervention of the fire brigade in the European standard Eurocode 1 is considered through a reduction of the design fire load. Thus, the decay phase of the fire will start earlier. This reduction of the fire load can barely be quantified through statistical data. Therefore, in this paper a model is presented that considers the fire brigade intervention based on measurable quantities.

The success of the fire brigade depends among other parameters (e.g. crew size, equipment etc.) on the intervention time  $T_I$  when the fire brigade starts with the fire suppression activities. This time  $T_I$  consist on several consecutive time intervals as illustrated in Fig. 2. The time when the extinguishment procedure starts is expressed through the sum of all these times:

$$T_I = T_{Detect} + T_{Call} + T_{Disp} + T_{Turnout} + T_{Travel} + T_{Setup} \quad (2)$$

If the fire is grown too large, the suppression of the fire cannot be successful and a full burnout will occur. The fire brigade must then focus on preventing further fire spread. Hosser et al. (2008) proposed a model based on a maximal controllable fire size  $A_{Limit}$  used as an indicator for the fire suppression capability of the fire brigade. If the fire grows larger than this area  $A_F(t) > A_{Limit}$  then a complete burnout must be accepted; otherwise the fire suppression action starts reducing the rate of heat release. Then, the decay phase occurs earlier compared to the complete burnout fire (Fig. 1). It is assumed that the decay phase starts at the intervention time  $T_I$  of the fire brigade. The relation  $A_F(T_I) > A_{Limit}$  determines the probability of failure for fire suppression by the fire brigade.

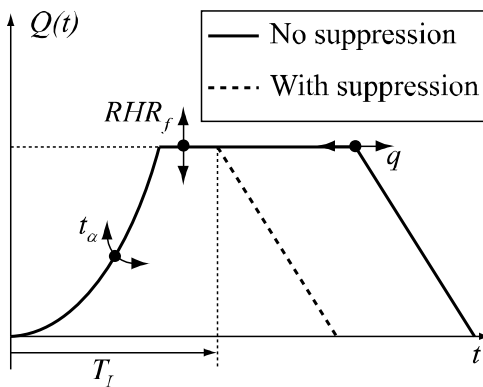


Fig. 1 Rate of heat release including the fire suppression

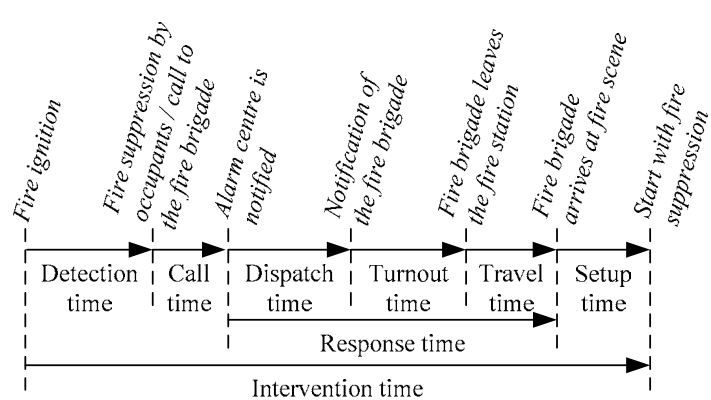


Fig. 2 Time intervals for the fire brigade intervention

## 2 DATA AND LITERATURE SURVEY

Statistical analyses of different authors are performed by different authors (see references) based on national or local fire brigade reports with the aim to quantify the parameters

introduced in Chapter 1. The literature contains summarized and structured information on fire brigade statistics.

The most difficult time interval to quantify is found to be the detection time. The difficulty is that the time of ignition is unknown. Thus, the time has to be estimated indirectly through some physical relationships. Holborn et al. (2004) estimated the detection time as well as the fire growth time based on *Eq. (1)* and providing some sample statistics. The data they used were collected by fire investigators interviewing persons who discovered the fire. It should be noted that not all of the fires merit such an investigation. Only fires which meet some criteria, i.e. fires where four or more fire engines are sent to the scene and fires where persons has to be rescued, have been reported (584 reported fires). Besides the detection time and the fire growth rate Holborn et al. provide sample statistics for the call time as well. The same database has been used by Sårdqvist (2000) to analyse the correlation between the fire spread and the different time intervals of the fire intervention. Because of the small number of data, the results of this analysis should be treated carefully.

Lots of information on the response time of the fire brigade is given, e.g. Holborn (2004), London Fire Brigade (LFB 2011), Schwanitz (2009), Tómasson et al. (2008), Tillander (2004), etc. The reason is that the response time is easy to measure and is often used to check if the performance criteria of the alarm centres and the fire brigades are fulfilled. Some authors provide suggestions for probabilistic models, too (e.g. Schwanitz, Tillander, Tomasson et al.).

### ***Limitations in the use of fire brigade statistics***

Fire brigade statistics do not include fires where no fire brigade attention is needed, e.g. small fires which can be extinguished by occupants. This implies that the probability of a fire event is underestimated when fire brigade statistics are used to assess this probability. Moreover, the efficiency of detection systems and smoke alarm is underestimated, because the rate of small fires extinguished by the user increases. However, insurance data includes also small damages (see Fontana et al. 1999) and could be used – also in combination with fire brigade statistics – to assess the probability of a fire event as well as the efficiency of smoke alarms and detection systems. Further, fire brigade statistics are always related to the fire brigade performance level and local conditions e.g. target criteria for fire brigades (e.g. target response time). Therefore, it is difficult to compare the response times of different fire brigades. Fire brigade statistics should include the performance level of the fire brigade that reported the data as done by the London Fire Brigade (LFB 2011) and Schwanitz (2009).

Often, severe fire incidents merit a detailed investigation and additional valuable data are collected and reported. It is important to report the number of such detailed investigations related to all cases. Otherwise, the results of a statistical analysis might be biased.

## **3 PROBABILISTIC MODELS BASED ON FIRE BRIGADE REPORTS**

Probabilistic models are developed to address the stochastic variation of the parameters defined in Chapter 1. These models are intended to be used for risk analysis or for code calibration. The probabilistic models are developed for Switzerland based on the literature (see Tab. 1).

### **3.1 Fire growth rate**

The probabilistic model of the fire growth rate is chosen based on the analysis done by Holborn et al. (2004). Because they included also smouldering fires a large scatter of the fire growth time has been observed. As the impact of a smouldering fire is negligible for structural engineering, it is assumed that only fires with a fire growth rate  $t_\alpha$  of less than 800sec might affect the structure considerable. Therefore, a Truncated Lognormal (TruncLN) distribution is used to model this parameter.

### 3.2 Detection time

Holborn et al. (2004) estimated the detection time based on reports of London's fire brigade and Eq. (1). The data indicate a large scatter of the discovery time. A Gamma distribution is fitted to the 95% fractile (53 min) and the 51% fractile (5 min) of the data. The distribution of the detection time in Switzerland is assumed to be identical as in London. As the detection time for flaming fires (which affect the structure) is probably shorter as for smouldering fires, it is assumed that the detection of the fire occurs in less than 15 min. Therefore the Gamma distribution is truncated at 15 min. Holborn et al. supposed the existence of a dependency between fire growth rate and detection time. This is not considered in the present model.

Tab. 1 Probabilistic models (related to Swiss office buildings)

		<b>Distr.</b> $X$	<b>Mean</b> $E[X]$	<b>Std. dev.</b> $\sqrt{Var[X]}$	<b>Reference</b>	
<b>Fire</b>	<b>Fire load</b> [MJ/m <sup>2</sup> ]	$q$	Lognormal	420	126	Eurocode 1
	<b>Heat release rate</b> [kW/m <sup>2</sup> ]	$RHR_f$	Normal	250	50	Hosser et al. (2008) (est.)
	<b>Fire growth parameter</b> [sec]	$t_\alpha$	TruncLN	454	197	Holborn et al. (2004)
	<b>Max. controllable fire size</b> [m <sup>2</sup> ]	$A_{Limit}$	Normal	200	30	Hosser et al. (2008) (est.)
<b>Fire brigade</b>	<b>Detection time</b> [min]	$T_{Detect}$				
	without fire alarm		TruncGam	3.67	4.09	Holborn et al. (2004)
	with fire alarm		TruncGam	2.74	3.77	Holborn et al. (2004)
	with detection system		Eq.(4)	(1.53)	(0.70)	Fischer et al. (2012)
	<b>Call time</b> [min]	$T_{Call}$				
	without detection system		Lognormal	2.50	1.88	Holborn et al. (2004)
	with detection system		Det.	0	0	estimated
	<b>Dispatch Time</b> [sec]	$T_{Disp}$				
	without detection system		Lognormal	155.39	31.01	estimated
	with detection system		Lognormal	77.69	15.54	estimated
<b>Turnout and travel time</b> [min]	$T_{T+\tau}$	Lognormal	6.60	3.41	LFB (2011)	
<b>Setup time</b> [min]	$T_{Setup}$	Lognormal	3.50	0.50	estimated	

### 3.4 Influence of a fire detection system (with automatic alarm transmission)

Fire detection systems detect smoke or heat, raise an alarm and call the fire brigade automatically. The detection time is reduced because the alarm of the detection system notifies automatically the alarm centre. The reduction of the detection time depends on the fire growth rate. The faster the fire develops the faster the detection system will raise an alarm. Fischer et al. (2012) proposed a regression model for office buildings (Eq. 3) to quantify the activation time of the devices. The detection time depends only on the fire growth parameter  $t_\alpha$ .

$$\ln(T_{Detect,FDS}) = \beta_0 + \beta_1 \ln\left(\frac{1}{t_\alpha^2}\right) \quad (3)$$

### 3.5 Influence of a fire alarm without automatic alarm transmission (home detectors)

A detached fire alarm raises an alarm when the device detects smoke. But in contrast to the detection systems they do not transmit an alarm to an alarm centre. A fire alarm which only raises an alarm increases just the probability of an early detection of the fire and reduces the discovery time. According to fire brigade statistics from UK (NFBS 2011) the detection time of a fire with the presence of a detached fire alarm will occur in 63% of the fires within 5 min. The probabilistic model for the detection time is adjusted to this value.

## 4 SENSITIVITY ANALYSIS

A probabilistic approach is used to assess the maximum steel temperature of a beam under natural fire conditions as an indicator for structural safety. The room temperature is assessed with the two-zone model OZone (Cadorin et al. 2001) and the maximal steel temperature is

assessed with the simplified calculation method described in Eurocode 3 (EN 1993-1-2:2005). Using the probabilistic approach the uncertainties of the input variables (Tab.1) are considered consistently leading to a variation of the steel temperature (output). With this approach the sensitivities of the input parameters to the output are assessed. This paper distinguishes between local and global sensitivity analysis.

#### 4.1 Local sensitivity analysis

A measure of the sensitivity of an output  $Y_j$  versus an input  $X_i$  can be estimated by the derivate  $\partial Y_j / \partial X_i$ . This derivate can only be computed at a base point defined through a set of input variables  $X_i$ . In the context of code calibration the most common base point is usually chosen by the set of variables which lead to the most probable failure based on a limit state function. This point is defined as the design point. An efficient algorithm to find the design point is provided by the First Order Reliability Method (FORM). The derivate of the input variables at the design point indicates the relative influence on the failure state and can be used for code calibration. This paper focuses on the enhancement of the probabilistic models by improving the input parameters through statistical data. Therefore, no local sensitivity analysis is carried out.

#### 4.2 Global sensitivity analysis

A measure to decide what kind of data should be collected is to assess the relative participation of the input parameters (see Tab.1) on the variance of the output (e.g. maximal steel temperature). Saltelli et al. (2008) propose a decomposition of the variance of the output in first-order effects and total effects. The first-order effect represents the main contribution of an input factor  $X_i$  to the variance of the output  $Y$  and is defined through the first-order index  $S_i$ . The total effect  $S_{Ti}$  is a measure for the total contribution of an input parameter  $X_i$  including the interactions with the other parameters  $X_{-i}$ . The total effect index  $S_{Ti}$  provides an indication whether the variance of an input parameter  $X_i$  can be neglected ( $S_{Ti} \cong 0$ ). The total effect and the first-order- index are defined in Eq. (3) (Saltelli et al. 2008).

$$S_i = \frac{Var[E(Y|X_i)]}{Var(Y)} \quad \text{and} \quad S_{Ti} = 1 - \frac{Var[E(Y|X_{-i})]}{Var(Y)} \quad (3)$$

The difference of the first-order indices and the total effect indices of a variable provides an indication of the interaction effects of the model (non-linearity of the model). Parameters with high interaction effects should be considered accordingly in the assessment of the model output.

The sensitivity indices are assessed for different compartment areas. Further, it is distinguished between the cases where the uncertainties related with the fire brigade intervention are considered (Fig. 3a) and where they are not considered (Fig. 3b) (only non-zero parameters are illustrated).

The highest indices are obtained for the fire growth time  $t_\alpha$  in the case where the fire brigade is considered (Fig. 3a). One of the reasons is due to the high variability of this parameter. The detection time and the turnout and travel time have also a major influence on the outcome.

Interaction effects of all the parameters have a large influence (non-linearity) and should be considered in the assessment of the temperature when considering the fire brigade. The fire load has only a minor influence on the variability of the outcome.

Without considering the uncertainties related with the fire brigade (Fig. 3b) the variation of the output is only dominated through the uncertainty of the fire load. It is seen that the interaction effects of all parameters have only a minor effect on the variance of the output (linear model).

## 5 CONCLUSIONS AND SUGGESTIONS FOR DATA COLLECTION

The sensitivity analysis shows that reducing especially the uncertainty of the fire growth time  $t_\alpha$  will reduce the variance of the steel temperature. A way to reduce the variance of the fire growth time is to report pre-flashover data of fire incidents that affect only the structure, respectively excluding smouldering fires. In this context all data which describe the pre-flashover phase are helpful. For example, data about the time and the area of fire spread (encountered by occupants or by the fire brigade) could be reported to enlarge the knowledge about the fire spread in the pre-flashover phase. The knowledge about the detection time could be increased simultaneously. Additionally, reporting the presence and the operability of fire safety measures helps assessing the effect of the measures on the time intervals.

Often the turnout and travel times are already reported from fire brigades. Such data should be included in the assessment of structural safety. In doing so, the performance criteria of the fire brigade should be reported, too. In this way a comparison of different fire brigades might be possible.

Data on suppression capability of the fire brigade should be collected to verify the engineering model used in this paper. The maximal treatable fire size could be an indicator for this capability. Accordingly, data on the fire size and success of the fire brigade should be collected.

It is seen that the interaction of the parameters is important for determining the outcome. Therefore, data should be reported completely as possible for fire incidents. This provides a basis to assess the correlation between the different parameters. Further, if the fire brigade intervention is considered in the structural safety design then the interaction effects of the parameters should be considered, too.

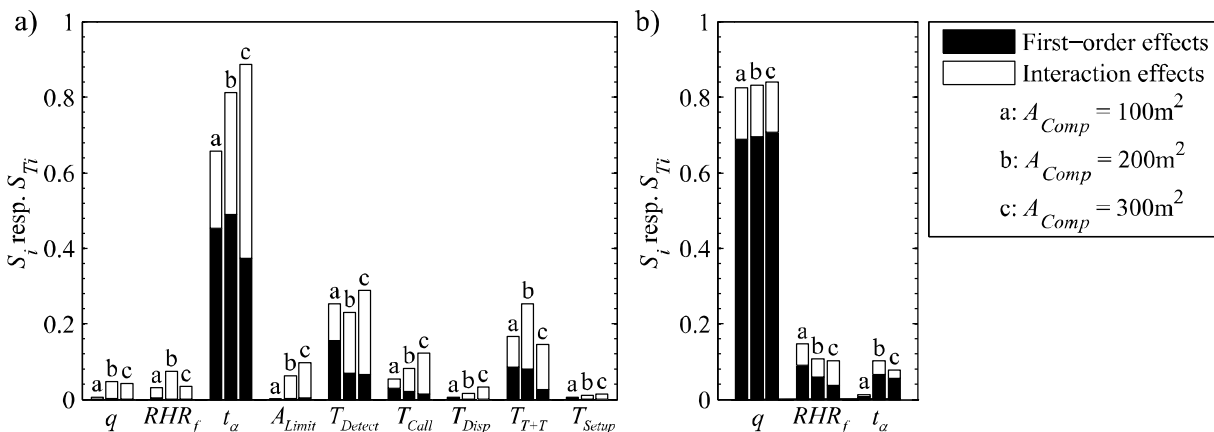


Fig. 3 Sensitivity indices with (a) and without (b) considering the uncertainties associated with the fire brigade intervention

## REFERENCES

- Cadorin, J., D. Pintea & J. Franssen (2001) The Design Fire Tool OZone V2.0 - Theoretical Description and Validation on Experimental Fire Tests, University of Liege, Belgium.
- Fischer, K., J. Kohler, M. Fontana & M. H. Faber (2012) Wirtschaftliche Optimierung im vorbeugenden Brandschutz, Institut für Baustatik und Konstruktion, ETH Zürich.
- Fontana, M., J. P. Favre & C. Fetz (1999) A survey of 40,000 building fires in Switzerland, Fire Safety Journal.
- Holborn, P. G., P. F. Nolan & J. Golt (2004) An analysis of fire sizes, fire growth rates and times between events using data from fire investigations, Fire Safety Journal.

- Hosser, D., A. Weilert, C. Klinzmann, R. Schnetgöke & C. Albrecht (2008) Sicherheitskonzept zur Brandschutzbemessung, Braunschweig, Institut für Baustoffe, Massivbau und Brandschutz.
- London Fire Brigade (2011) Our Performance 2010/11, London, UK, LFB.
- NFBS (2011) Fire Statistics - Great Britain, 2010-2011, Department for Communities and Local Government.
- Saltelli, A., M. Ratto, T. Andres, F. Gampolongo, J. Cariboni, D. Gatelli, M. Saisana & S. Tarantola (2008). Global sensitivity analysis, John Wiley.
- Särdqvist, S. (2000) Correlation between firefighting operation and fire area: analysis of statistics, Fire Technology.
- Schwanitz, B. (2009) Bewertung der Versagenswahrscheinlichkeit von Löschmassnahmen der Feuerwehr durch Auswertung von Einsatzstatistiken und Integration der Ergebnisse in ein probabilistisches Versagensmodell, TU Braunschweig, Diploma Thesis.
- Tillander, K. (2004) Utilisation of statistics to assess fire risks in buildings VTT Building and Transport, Espoo, Finland, Helsinki University of Technology, Ph.D.Thesis.
- Tómasson, B., J. Bengtsson, D. Thorsteinsson & B. Karlsson (2008) A Probabilistic Risk Analysis Methodology for High-rise Buildings taking into Account Fire Department Intervention Time, Proceedings of the 9th International Symposium on Fire Safety Science, Karlsruhe, Germany.

## STOCHASTIC FINITE ELEMENT METHODS FOR THE RELIABILITY-BASED FIRE-RESISTANT DESIGN OF STRUCTURES

Qianru Guo<sup>a</sup> and Ann E. Jeffers<sup>a</sup>

<sup>a</sup> University of Michigan, Department of Civil and Environmental Engineering, Ann Arbor, MI, USA

### Abstract

A reliability-based design methodology is needed to reconcile the uncertainty and ensure a consistent level of safety is provided in engineered structural fire designs. This paper presents the application of two stochastic finite element methods, namely the First- and Second-Order Reliability Methods and Monte Carlo Simulation, to the design of structures subjected to fire. An example of a protected steel column subjected to natural fire is presented. A numerical investigation of the evolution of the failure probability with time demonstrates that analytical reliability methods improve the efficiency of the simulation, although significant errors arise when treating the fuel load as a random parameter. Further analysis reveals a “kink” in the response surface due to the lack of sensitivity to the fuel load during the heating phase of fire development. Utilization of an alternative fire model overcomes this limitation.

**Keywords:** stochastic finite element method, first-order reliability method, Monte Carlo simulation, structural reliability

### INTRODUCTION

The primary objective of engineering design is to produce a system that has strength that exceeds the load demand. However, both the strength and demand of a system naturally exhibit a large amount of randomness. In the fire-resistant design of building structures, the fuel load density, thermal and mechanical properties of materials, and mechanical loads are random in time, leading to a considerable amount of uncertainty in the structural response. Safety factors are often used in engineering design to limit the failure probability in light of uncertainty. Although such design philosophies generally lead to an acceptable level of safety and are easy to implement due to the straightforward manner of the design, they are only the first level of reliability-based design, i.e., the randomness has been taken into account but the reliability of the system is not explicit quantified.

In recent decades, with major developments in the field of structural fire engineering, there is a tendency to replace current prescriptive codes with performance-based design codes. The performance-based design focuses on meeting target levels performance for given design events, thus encouraging engineers to apply new materials and technologies to achieve solutions that are beyond the prescriptive codes. In performance-based design, reliability evaluation plays an important role in ensuring that the limit state requirements are achieved with an acceptable level of safety. A number of researchers have conducted reliability analyses and safety assessments for structures exposed to fire in recent years (Magnusson and Petterson 1980/81; Mehaffey and Harmathy 1984; Beck, 1985; Shetty et al., 1998; Fellingner and Both, 2000; Iqbal and Harichandran, 2010, 2011; Khorasani et al., 2012; Guo et al., 2012; Guo and Jeffers, 2012)

This paper presents the application of two stochastic finite element methods, namely the First- and Second-Order Reliability Methods (FORM/SORM) and Monte Carlo Simulation (MCS), to evaluate the reliability of a column that was designed according to the prescriptive code in the U.S. A comparison was conducted between the analytical reliability methods (FORM/SORM) and Monte Carlo Simulation. The SORM shows a potential to evaluate the reliability problem of a nonlinear limit state curve with improved accuracy and computational efficiency. However, the following study demonstrates that challenges arise when treating the



fuel load density as a random parameter for a parametric fire model (e.g., the Eurocode parametric fire) that is not sensitive to the fuel load during the heating phase.

## 1 METHODS OF ANALYSIS

Three sequentially coupled processes are needed to simulate the structural response under fire: (1) a fire simulation (i.e., parametric fire curve, zone model, or computational fluid dynamics model) to determine the thermal boundary conditions at the structural surface, (2) a heat transfer analysis to determine the temperatures within the structure under the specified boundary conditions, and (3) a structural analysis to determine the mechanical response of the structure. Uncertain parameters appear in each domain, and all of them will affect the final structural response due to the coupling of the various models.

Monte Carlo Simulation (MCS) is the most popular sampling method to evaluate the reliability of structures in fire. It is a versatile tool that can account for uncertainty in any number of parameters as well as the coupling between various domains. However, MCS requires a large sample of parameters, particularly for quantifying the reliability in systems with low probabilities of failure. MCS therefore involves excessive computational costs, although some advanced MCS methods have been introduced in recent years to improve the efficiency of the method.

The First-Order and Second-Order Reliability Methods (FORM/SORM) are a class of analytical reliability methods. These two methods simplify the limit state function by a first-order and second-order Taylor expansion about the “design point,” as shown in Fig. 1. The design point is defined as the point on the limit state curve which has the shortest distance to the origin in standard normal space. The probability of failure evaluated by FORM and SORM is equal to the integration of the joint probability density function on one side of the approached limit state function. As all parameters have been transformed to standard normal space as independent, normally distribution parameters, the integral can be simplified as

$$P_{f\_FORM} = 1 - \Phi(\beta) \quad (1)$$

and

$$P_{f\_SORM} = \Phi(-\beta) \prod_{i=1}^{n-1} \frac{1}{\sqrt{1 + \psi(\beta) \kappa_i}} \quad (2)$$

where  $\beta$  is the distance from the design point to the origin,  $\Phi$  is cumulative density function for a standard normal distribution,  $\kappa_i$  is the principle curvature, and  $\psi(\beta)$  is given as

$$\psi(\beta) = \frac{\varphi(\beta)}{\Phi(-\beta)}, \quad (3)$$

where  $\varphi$  is the probability density function for a standard normal distribution.

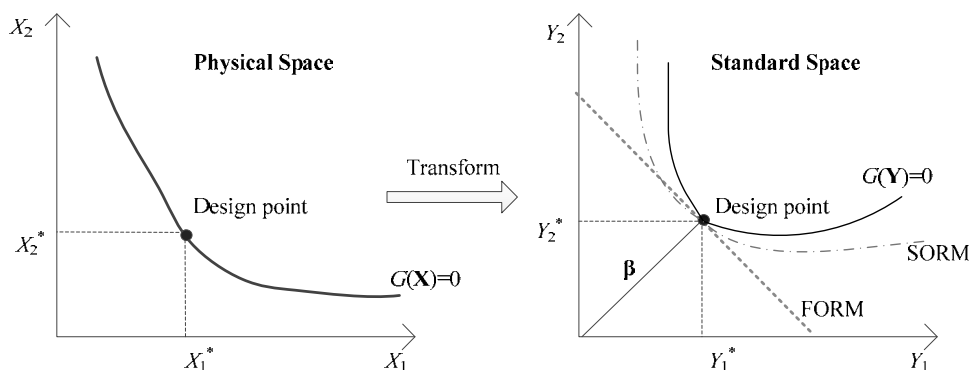


Fig. 1 Calculation of failure probability using FORM/SORM (Haldar and Mahedevan, 2000)

## 2 CASE STUDY

A protected and ideally pinned steel column subjected to natural fire is analysed here. As shown in Fig. 2, the column is the interior column D2 in the second floor of a four-story building introduced in AISC (2011). According to the design requirement, a W12x65 section was chosen for strength, and its geometric properties are shown in Fig. 3. The fire resistance design used a cementitious spray-applied fire resistant material (SFRM). In order to achieve a 2-hour fire resistance rating, the thickness of 28.6mm (9/8 in.) was selected from UL fire resistance directory, although in the reliability analysis the thickness was taken to be 1.6mm greater than the design thickness based on the fact that the actual thickness tends to be larger than the design value in construction (Iqbal and Harichandran, 2010).

Natural fire exposure was modelled by the Eurocode parametric fire (EC1, 2007). The column shown in Fig. 3 was first modelled deterministically to evaluate response under natural fire exposure. The column was given a rather large initial imperfection of  $L/100$  to increase the failure probability of the structure; this was done to ensure that discrepancies in the computed failure probabilities were due to the FORM/SORM calculation rather than inadequate sampling in the MCS. The opening factor  $O$  was assumed to be  $0.04 \text{ m}^{1/2}$  to ensure that the fire was ventilation controlled. The values of thermal inertia  $b$  and fuel load density  $e_t$  shown in Table 1 were based on the mean values reported in (Culver, 1976; Iqbal and Harichandran, 2010). In the heat transfer analysis, the exposed surface was heated by convection and radiation assuming that the convection heat transfer coefficient  $h$  was  $35 \text{ W/m}^2\text{K}$  and the effective emissivity  $\varepsilon$  of the structural surface was 0.8. The SFRM was assumed to have a density of  $300 \text{ kg/m}^3$ , a conductivity of  $0.12 \text{ W/mK}$ , and a specific heat capacity of  $1200 \text{ J/kgK}$  (Buchanan, 2002). In the structural model, the design dead and live loads were 1226 kN and 605 kN respectively. In the reliability analysis, the design dead load was multiplied by a factor of 1.05 and the design live load was multiplied by a factor of 0.24 to get the values at an arbitrary point in time (Ellingwood, 2005). The total column load  $w$  was calculated by

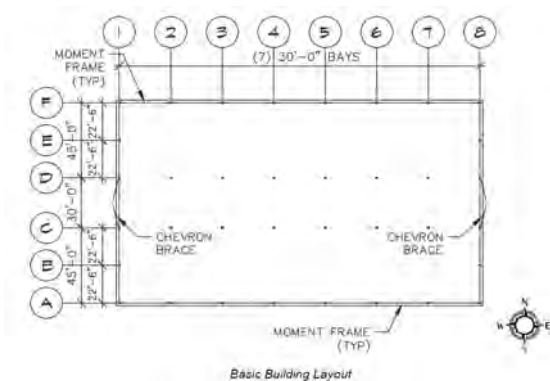


Fig. 2 Floor plan

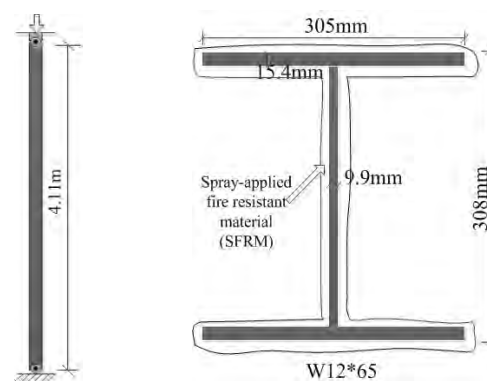


Fig. 3 Geometric properties of the column

Table 1. Statistical properties for the uncertain parameters

Parameter		Mean Value	Distribution	COV	Sensitivity
Room Properties	Fuel Load	564 MJ/m <sup>2</sup>	Gumbel	0.62	1.161
	Thermal Initial	423.5 W s <sup>0.5</sup> /m <sup>2</sup> K	Normal	0.09	0.0058
Properties of SFRM	Thickness	30.2 mm	Lognormal	0.2	-1.561
	Conductivity	0.120 W/mK	Lognormal	0.12	1.342
Parameters in structural model	Yield (at 20C)	359 MPa	Normal	0.08	-1.740
	Dead Load	1287.6 kN	Normal	0.1	2.729
	Live Load	145.3 kN	Gamma	0.24	0.308
	A Factor	1	Normal	0.04	2.729
	B Factor	1	Normal	0.2	0.308
	E Factor	1	Normal	0.05	3.037

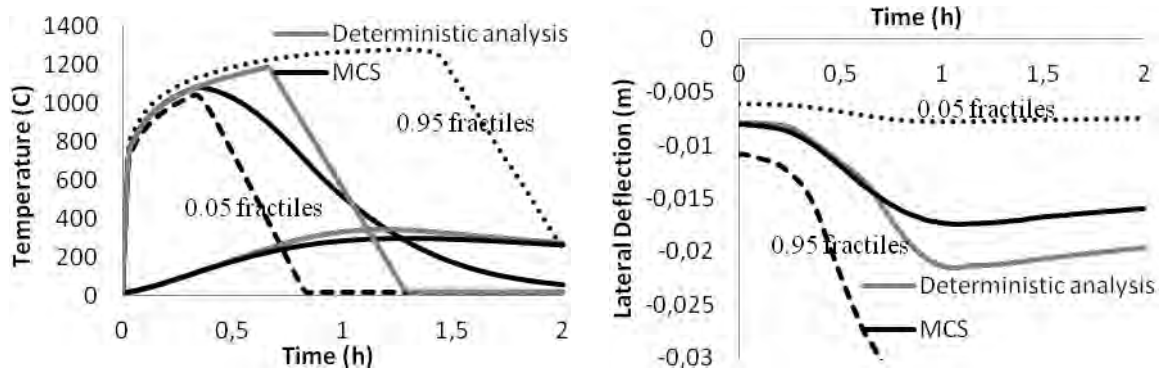


Fig. 4 Simulation results: (a) Fire and column temperatures, and (b) Structural response

$$w = E \times (A \times P_{DL} + B \times P_{LL}). \quad (4)$$

where  $A$ ,  $B$ , and  $E$  are load factors given by (Iqbal and Harichandran, 2010).

The fire and steel temperature from the deterministic analysis (using mean values for the input parameters) are shown in Fig. 4a as the red solid line. The maximum fire temperature arrived around 45 min and was approximately  $1100^{\circ}\text{C}$ . Under this heating, the column reached a maximum temperature of approximately  $400^{\circ}\text{C}$  around 75 min. As shown in Fig. 4b, the column maintains structural stability for the duration of the fire exposure.

A Monte Carlo Simulation with a sampling space of 10,000 was conducted here. In order to reduce the number of random parameters, a sensitivity analysis had been conducted and ten “key” parameters (given in Table 1) were chosen as random based on their sensitivity coefficient and range of variability. A group of natural fire curves were obtained using the statistical properties for the fire parameters. The mean fire temperature with the 0.05 and 0.95 fractiles is shown in Fig. 4a. The maximum fire temperature exceeded  $1,200^{\circ}\text{C}$  in the most severe case. The mid-height lateral deflection is plotted in Fig. 4b for the mean value as well as the 0.05 and 0.95 fractiles.

To evaluate the reliability of the system, failure was defined as the maximum mid-height lateral deflection of  $L/150 \approx 0.028\text{m}$ . In the MCS, the probability of failure was calculated by evaluating the total ratio of failed simulations, i.e.

$$P_f = \frac{n_f}{n}, \quad (5)$$

where  $n_f$  is the number of failed simulations and  $n$  is the total number of simulations. The failure probability as a function of time is shown in Fig. 5a for both the MCS and FORM analysis. As the FORM uses a first-order Taylor expansion of the limit surface, there is significant error in the calculation, although it is noted that the result is conservative. It should also be noticed that the column which was considered to be safe by the deterministic analysis had a 30% probability of failure under natural fire exposure. However, the large probability of failure was likely due to the large initial imperfection that was assumed.

### 3 COMPARISON OF METHODS

To better understand the source of the discrepancies between the FORM and MCS results, an in-depth study of the response and response surface was conducted for various combinations of the parameters given in Table 1. It was found that the FORM gave excellent agreement with the MCS for all combinations of parameters *except* when the fuel load  $e_i$  was treated as a random parameter. It was hypothesized that the error could result from the fact that the response surface was possibly nonlinear. However, a second-order reliability analysis using the SORM gave equally poor results for this case, as illustrated in Fig. 5b.

The problem was reduced to two random parameters and the response surface plotted in Fig. 6. In Case 1, the fuel load  $e_i$  and the thermal inertia of the compartment  $b$  were treated as random parameters. To simplify the analysis, the distribution of the fire load was assumed to

follow a lognormal distribution rather than Gumbel distribution. The response surface for Case 1 illustrates a “kink” in the response surface, which resulted in a limit state function that was practically bilinear. This resulted in significant error in the failure probability for both FORM and SORM, as illustrated in Fig. 5b. For comparison, Case 2 considered the dead load  $P_D$  and thermal inertia  $b$  as random. It can be seen that the response surface for Case 2 was close to linear, giving reason as to why the FORM was able to yield a high level of accuracy for this case.

The source of the bilinear nature of the response surface was suspected to stem from the fact that the fire temperature from the parametric fire curve was not sensitive to the fuel load during the heating phase (i.e., the fuel load only affects the *duration* of heating in the Eurocode parametric fire). Therefore, the problem was reanalysed using the fire model proposed by Ma and Makelainen (2000), which uses an exponential function that depends on the fuel load during both heating and cooling phases of development. The response surface for this case (Case 3) is shown in Fig. 6c. It can be seen that the fire temperature computed by the Ma and Makelainen model leads to a smooth (albeit nonlinear) response surface. The failure probability for this case (shown in Fig. 6c) illustrates that the FORM is not able to capture the nonlinear behaviour of the response. However, the SORM yields excellent agreement with the MCS, as shown in Fig. 6c. The FORM and SORM are more efficient than the MCS. In case 3, FORM and SORM spent around 2.6 hours and 3.3 hours respectively to obtain the reliability curve, but the MCS need 7 hours running in 20 parallel high-performance computing nodes.

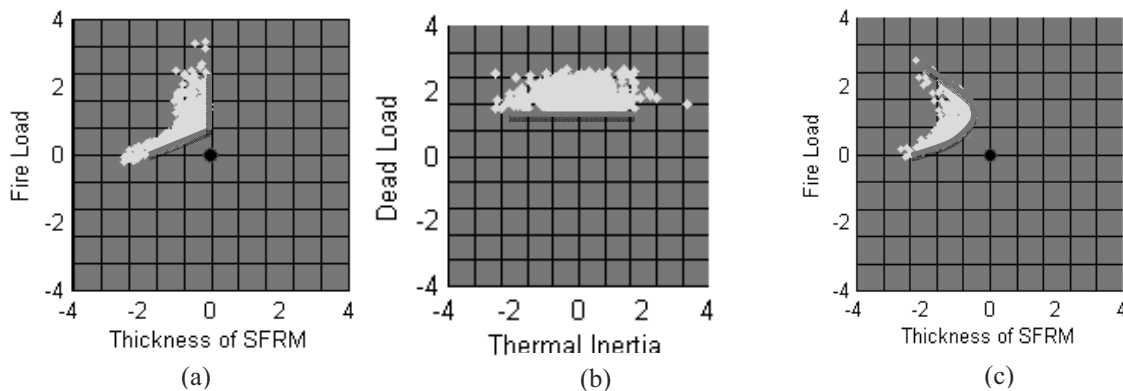


Fig. 6 Response surface (a) Case 1, (b) Case 2, (c) and Case 3

## 4 CONCLUSION

Two kinds of reliability methods were used to analyse the structural response in fire where uncertain parameters appeared in multiple physical domains. The comparison between the analytical method (FORM) and the Monte Carlo simulation demonstrates that the FORM exhibits acceptable accuracy and offers significant saving in computational cost. Furthermore, the accuracy of the analytical reliability methods can be improved by the SORM with a second-order approximation of the limit state function. However, the accuracy of both FORM and SORM is dependent on the shape of the response surface. For the Eurocode parametric fire curve, the response surface has a kink, which leads to significant error that cannot be resolved with a higher order analysis. Nevertheless, this novel application of the analytical reliability method provides an efficient computation of the time-variant probability of failure, which allows the realization of high-level reliability-based designs in fire engineering.

## ACKNOWLEDGEMENTS

This work was supported by the U.S. National Science Foundation under Grant No. CMMI-1032493. Any opinions, findings, conclusions or recommendations are those of the authors and do not necessarily reflect the views of the sponsoring agency.

## REFERENCES

- AISC (2011), 'Steel Construction Manual Design Example v14.0', American Institute of Steel Construction
- Beck, V.R. (1985). "The Prediction of Probability of Failure of Structural Steel Elements under Fire Conditions," Transactions of the Institution of Engineers, Australia: Civil Engineering, 27, 111-118.
- Buchanan AH (2002), "Structural design for fire safety". Wiley, Chichester
- Culver, C.G. (1976). Survey results for fire loads and live loads in office buildings, National Bureau of Standards, Washington, DC.
- EC1 (2007), "Eurocode 1: actions on structures, part 1-2: general actions—actions on structures exposed to fire", BSI EN 1991-1-2. British Standards Institution, London
- Ellingwood, B.R. (2005). "Load combination requirements for fire-resistant structural design," Journal of Fire Protection Engineering, 15, 43-61.
- Fellinger, J.H.H., and Both, C.K. (2000). "Fire resistance: reliability vs. time analyses," Proceedings of Composite Construction in Steel and Concrete IV, Hajjar, J.F. (Ed.), ASCE, USA, 816-827.
- Guo, Q., and Jeffers, A.E. (2012). "Finite element reliability analysis for structural safety evaluation in fire," Proceedings of the 7th International Conference on Structures in Fire, Fontana et al. (Eds.), ETH Zurich, Zurich, 469-478.
- Guo, Q., Shi, K., Jia, Z., and Jeffers, A.E. (2012). "Probabilistic evaluation of structural fire resistance," Fire Technology, DOI:10.1007/s10694-012-0293-6.
- Haldar, A., and Mahadevan, S. (2000). "Reliability Assessment Using Stochastic Finite Element Analysis," John Wiley and Sons, New York.
- Iqbal, S., and Harichandran, R.S. (2010). "Capacity reduction and fire load factors for design of steel members exposed to fire," Journal of Structural Engineering, 136, 1554-1562.
- Iqbal, S., and Harichandran, R.S. (2011). "Capacity reduction and fire load factors for LRFD of steel columns exposed to fire," Fire Safety Journal, 46, 234-242.
- Khorasani, N.E., Garlock, M.E., and Gardoni, P. (2012). "Reliability analysis of steel perimeter columns under fire," Proceedings of the 7th International Conference on Structures in Fire, Fontana et al. (Eds.), ETH Zurich, Zurich, 541-550.
- Ma, Z.C. and Makelainen, P. (2000) "Parametric temperature-time curves of medium compartment fires for structural design", Fire Safety Journal 34:361-375
- Magnusson, S.E., and Pettersson, O. (1980/81). "Rational design methodology for fire exposed load bearing structures," Fire Safety Journal, 3, 227-241.
- Mehaffey, J. R. and Harmathy, T. Z. (1984), Failure probabilities of constructions designed for fire resistance. Fire and Materials, 8: 96-104.
- Shetty, N.K., Guedes Soares, C., Thoft-Christensen, P., and Jensen, F.M. (1998). "Fire safety assessment and optimal design of passive fire protection for offshore structures," Reliability Engineering and System Safety, 61, 139-149.
- Vaidogas, E.R., and Juocevicius, V. (2008). "Reliability of a timber structure exposed to fire: estimation using fragility function," Mechanika, 73, 35-42.

# INTERACTIVE INTEROPERABILITY BETWEEN FIREFIGHTERS AND FIRE PROTECTION EQUIPMENT

Kamila Horová<sup>a</sup>, Slavomír Entler<sup>b</sup>

<sup>a</sup> Czech Technical University, Faculty of Civil Engineering, Prague, Czech Republic

<sup>b</sup> Profitech Ltd., Prague, Czech Republic

## Abstract

An operation of fire protection equipment may be dangerous for intervening fire-fighters in some cases. Therefore, it is necessary, in addition to the analysis of fire development which includes a description of real fire scenarios, to affect active response of fire safety measures.

In 2009 the complex automatic fire protection equipment of coal handling route was installed into operation in Tušimice power plant. However, after starting the operation it showed that activation of the extinguishing system on the inclined conveyor bridge threatened the health and life of fire-fighters conducting an intervention.

In the paper an interactive algorithm that ensures a flexible cooperation intervening fire-fighters and automatic extinguishing system without a risk of fire-fighters life is investigated. Possible fire scenario is analysed in FDS. By numerical simulation applicability of the algorithm is confirmed. Development of gas temperatures in strong chimney flow gives also a view into part of mechanical response of structure.

**Keywords:** coal handling bridge, fire-fighters intervention, automatic extinguishing system, numerical simulation, fire development

## INTRODUCTION

In 2009 the installation of a complex fire protection equipment of coal handling route was started in Tušimice power plant. Equipment consisted of sensors of temperature above and under belts, coal dust sucking off, alarm system and automatic extinguishing system with sending signals to 3 different surveillance locations. Automatic extinguishing system was set to start in 5 min after fire alarm. However this time limit was insufficient to complete a fire survey by fire-fighters. In case of automatic extinguishing, very dangerous conditions for fire-fighters originated from the water flowing down on inclined coal handling bridge. Moving on inclined greasy floor covered with continuous flush of water (about 6760 l/min) was found as life-threatening. In the first moment there were two solutions. To stop using of automatic start of extinguishing system – the solution could lead to a big fire, or to do not realize fire surveys. The second solution was not acceptable because of high number of false alarms (in last 8 years - 676 false alarms). Extinguishing by false alarm would cause several days of lay-by of power plant and loss of 40.000 Euros per day.

The solution was found as an interactive algorithm of interoperability, which enables both an elimination of false alarms or competent control of fire-fighting and automatic extinguishing and cooling of construction in the shortest possible time in difficult conditions of the inclined coal conveyor bridge.

## 1 DESCRIPTION OF INCLINED COAL HANDLING BRIDGE

Coal handling bridge T12 of Tušimice power plant consists of coated steel truss construction inclined in angle of 16°, see Fig. 1 and Fig. 2. Total length of 170 m reaches the height of 47 m. The bridge is 7 m width and 3,3 m high. Steel structure consisted of trusses with upper and lower stiffening trusses is covered by aluminium sheet, window openings are made of

reinforced glass. Massive rigid frames are spaced at 3 m. Bottom deck laying below two conveyors with rubber belts is made of reinforced concrete. By the aid of fire protection walls the coal handling bridge is divided into 2 fire compartments of lengths 102 m and 68 m. However, because of conveyors going through there are big holes in the fire partitions.

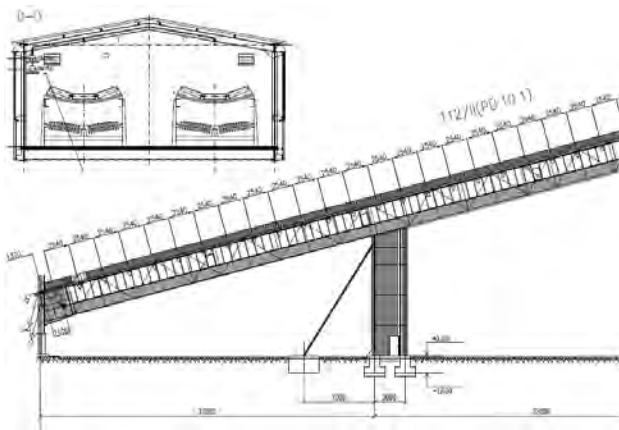


Fig. 1 Construction of coal handling bridge T12



Fig. 2 Tušimice power plant

## 2 DESIGN FIRE SCENARIOS

Four main reasons of the fire on the coal handling bridge can be specified:

- seized rollers under the belt causes ignition of the elastic rubber belt (ignition temperature – 460 °C), after burning the coal on the belt can ignite, the belt may sever, and swirling coal dust can explode (scenario A)
- sparkle from the seized roller can initiate ignition of coal dust – thanks to regular cleaning it is not probable
- transport of fire outbreak from outside – burning of coal followed by burning of belt or reversely (scenario B)
- failure of wiring, human mistake, nature element – burning of coal or coal dust, ignition of belt (with previous reason compiled to scenario B)

### 2.1 Scenario A

Burning of the bottom of belt and its subsequent rupture causes whirling of burning materials and the coal dust. This may exceed the limits of coal dust explosion. Early detection of fire from the bottom of the belt is possible only by monitoring the temperature in the area of rollers. Linear heat detectors are installed in the area of conveyors rollers. When the detected temperature is higher than 80 °C, signal is sent to local fire station. However indication of higher temperature does not start any extinguishing sequence. Starting of automatic extinguishing system is not favourable in this case because of a small effect of extinguishing during burning at the bottom side of the belt and conveyors cannot be stopped, because the belt does not ignite during movement. This fire scenario is not further considered because automatic extinguishing does not start.

### 2.2 Scenario B

In this scenario fire detection is possible by monitoring the temperature above the belt. After detection of the temperature higher than 80 °C belts are stopped and fire intervention is

started. The fire development can be determined by calculation of the design fire with following conditions:

- the most conservative case is considered (both belts are full of coal)
- a rupture of the belt is not reached
- an explosion of coal dust is not included

### 3 NUMERICAL SIMULATION

In inclined bridge there is a strong chimney effect, which accelerates the combustion on one side and intensively cools the construction of the bridge on the other side. Cold air is sucked by lower openings and heated by burning of coal on handling bridge. Holes in fire walls allow air flow to upper part of the bridge where the hot air can leave by upper openings. Numerical simulation based on CFD analysis is the most suitable method for solution of this problem. Fire scenario B is studied numerically by FDS 5 (McGrattan, 2010).

#### 3.1 Description of model

One of the FDS model of inclined bridge is shown in Fig. 3. The dimension of the computational domain is 165 m by 7 m by 50,5 m. The size of openings for conveyors in the lower, middle and upper fire walls is 2 x 2 m by 1,3 m, middle fire wall is placed in two-thirds of the bridge. In the model there are 6 different materials including steel, concrete, plaster, fire brick, coal and rubber. The detailed properties of these materials are described in (Entler, 2013). Properties of burning materials come from Catalogue of brown coal 2009-2010 of mining company SD a.s. and Czech standard CSN 73 0804. Surface properties of the obstructions in the FDS model include steel sheets, concrete bottom deck, plaster and fire brick walls, coal layer and rubber belts. Nominal movement of the conveyor belt of 2 m/s is simulated by air flow. Heat release rate, air velocity above the centre of fire, the air temperature below the ceiling and the wall temperature of the structure of the bridge are measured in 10 min (time needed for fire-fighters intervention).

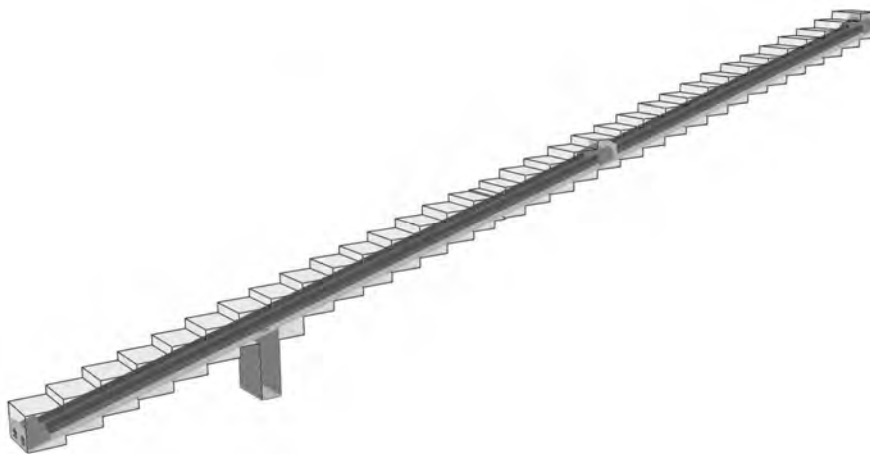


Fig. 3 FDS model of inclined coal handling bridge

Minimum flaming core which causes stopping of belts was found by iteration method. This size depends on parameters of a specific used coal. In this case the minimum flaming core is 40 x 40 x 30 cm. The focus of these dimensions stops the belt after driving of 40m.

During the study two different approaches were analyzed: a model of bridge with inclined construction and ranked grid as stairs (approach A) and a model of bridge with horizontal construction and horizontal cells of grid with inclined vector of gravitational forces (approach B). The final model leading to probable results (approach A) was compiled from a total of 35



computational grids of two sizes of cells. Basic cell size was 6 x 6 x 6 cm, cell size on continuous parts of the bridge was 12 x 24 x 12 cm. The total number of computational grid cells reached 1,8 mil.

### 3.2 Fire development

Based on the above findings, the fire outbreak is placed at 40 m from the beginning of the bridge. After 20 s of moving on the belt, the temperature of 80°C is detected and belt is stopped. Diagram of relative air flow shows fast movement of the flaming core inside the bridge, then stopping of the belts is proved, see Fig. 4. After stabilization of air flow equilibrium the fire starts to burn up and the flow rate gradually increases. From development of rate of heat release shown at Fig. 5, it is obvious that burning the fire up starts after 2 min. The fire spreads upward, in the direction of air flow. Till the 7th min the fire involves only one belt of the bridge. Then it starts to spread to its width - to the second belt. Because of lack of oxygen in upper part of the bridge flames start to spread in the down direction after 7 min.

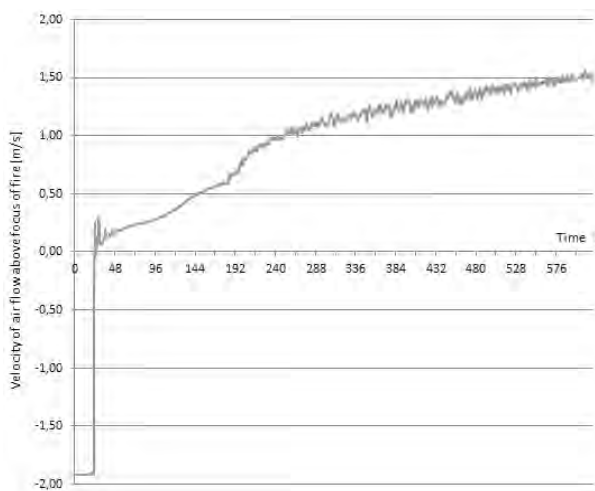


Fig. 4 Air flow above the fire outbreak

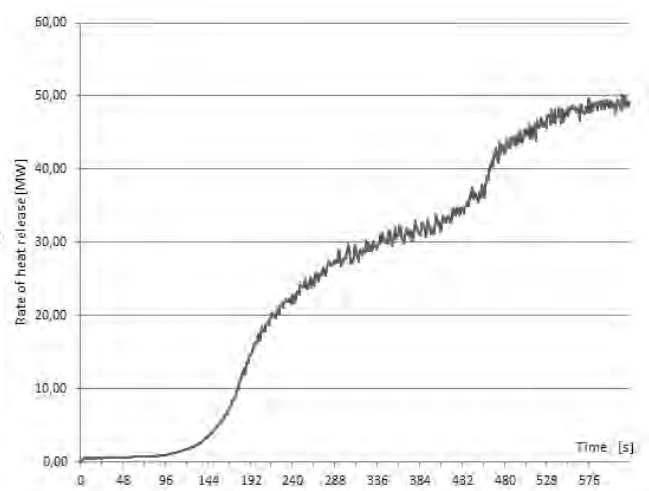


Fig. 5 Rate of heat release

The gas temperature measured below the ceiling, fluctuates significantly. Development of gas temperature in several locations in longitudinal direction of the bridge, below and above the place of ignition is calculated. The trend of the transfer of warm air along the air flow direction is evident. The highest gas temperatures occur between 40 m and 70 m from the beginning of the bridge (450 -950 °C). Maximum temperature of the structure which forms the ceiling reaches more than 800 °C in the most affected part. However the highest temperatures occur only at small areas for short intervals of time. Average temperatures of members of ceiling construction are less than 300 °C.

## 4 INTEROPERABILITY ALGORITHM

The solution of interoperability interactive algorithm is based on an analysis of fire-fighters intervention of fire scenarios. The necessary fire precautions, however, varies according to the fire scenario:

- Detection of elevated temperature in the area of rollers (scenario A) does not start any extinguishing sequence and requires immediate control of coal handling operation by fire-fighters. Until the belts stop, there is sufficient time for the fire survey.
- When a fire on belt is detected (scenario B) automatic extinguishing is started within 2 min from the announcement of a fire to prevent the risk of ignition of a conveyor belt.

- Before the activation of automatic extinguishing the fire-fighters intervention is expected. Within 1 min after fire alarm head of the fire intervention decides. To carry out a comprehensive survey of the conveyor bridge time of 10 min is required. Therefore, the delay of automatic extinguishing for management of fire intervention is allowed to the head of the intervention by technically interactive form, but no longer than 10 min from the fire alarm announcement.
- In order to prevent the spread of fire and prevent rupture of a conveyor belt, fire-fighting must be started manually immediately after the confirmation of a fire by fire-fighters, at latest 7 min after alarm.
- Elimination of risk of breakage of conveyor belt, which is critical for both fire scenarios, can be ensured by excluding stopping of belts. In practice it is still considered to be the only method to prevent the breakage.
- Delay of automatic extinguishing is made by mechanism of interactive algorithm that allows changing of fire safety operations in accordance with the current development of a fire.

Fig. 6 shows 3 phases of the interoperability. The phase 1 describes a situation when the fire-fighters intervention is not realised. The phase 2 shows a fire safety process when the intervention is carried out. In case the fire is not confirmed or cancelled during fire-fighters intervention, the process follows algorithm described in phase 3.

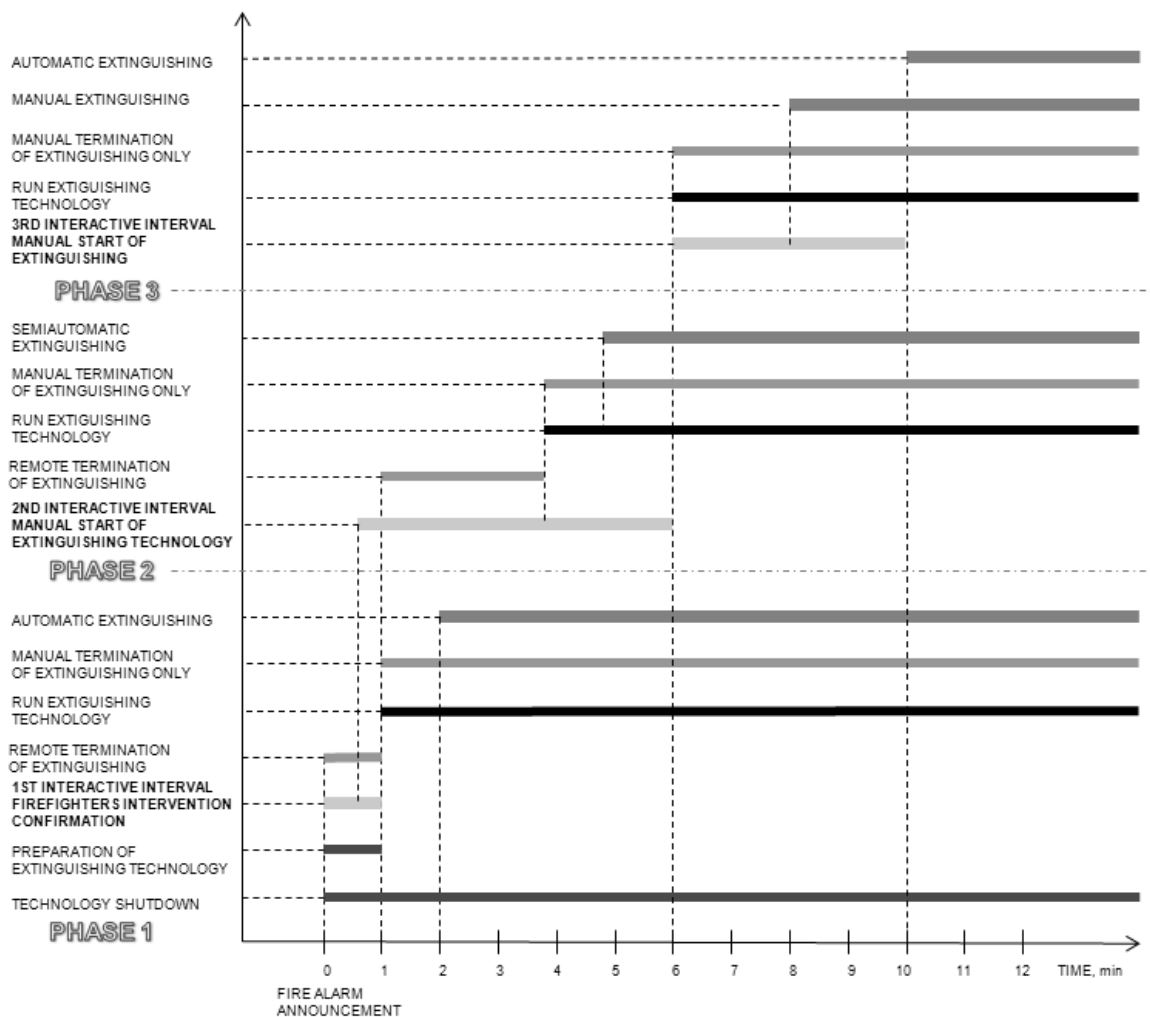


Fig. 6 Interoperability interactive algorithm

## 5 SUMMARY AND ACKNOWLEDGMENT

Based on the requirements for the interaction of fire safety equipment and fire-rescue units new interactive algorithm was developed. This algorithm has been successfully operated since 2010 in power plant Tušimice II. Number of tests was performed to confirm its functionality. The algorithm has been further improved and has already been installed on another power plant Tisová.

Numerical simulation proved that the evolution of the fire is based on flammability of coal and rubber conveyer belts. Brown coal burned in the power plant is less flammable compared to the material of belts. In case the coal is ignited, fire development is very slow and due to the high speed of conveyors transporting the coal it is unlikely probable that the fire occurs on the coal handling bridge. The development of the fire, therefore, depends on the ignition of the conveyor belt, because the fire will spread rapidly at the moment of ignition of a rubber belt. Analysis of all forms of design fire scenarios and CFD models proved that rubber-textile conveyor belts are critical site of fire safety on coal handling bridge. To avoid the risk of fire, regardless its place of origin it is therefore necessary to use a self-extinguishing (fire and flame resistant) conveyor belts.

Analysis of the main design fire scenario in FDS which shows probable fire development confirmed the applicability of the algorithm. By calculation of gas temperature and average temperature of the structure at the most affected part of the bridge in 10 min (time needed for fire-fighters intervention), it is proved that upper construction of the bridge should in the worst case of fire survive only with local damages.

Work on the research presented in this paper is supported by project grant LD11039 and SGS12/122/OHK1/2T/11.

## REFERENCES

- Hladík, 2005: Hladík V., Šetření nehod a havárií na tepelných zdrojích z pohledu Hasičského záchranného sboru, Judicial review of the event of fire in Opatovice power plant, Prague, 2005.
- Catalogue of brown coal 2009-2010: Katalog hnědého uhlí 2009-2010, Severočeské doly a.s., Chomutov, in Czech.
- ČSN 73 0804, 2002: ČSN 73 0804 Požární bezpečnost staveb – Výrobní objekty, Fire protection of building – Industrial buildings, 10/2002, Reichel V., ÚNMZ, in Czech.
- McGrattan, 2010: McGrattan K., McDermott R., Hostikka S., Floyd J., Fire Dynamics Simulator (Version 5) – User guide, NIST Special Publication 1019-5, 2010.
- Thunderhead Engineering 2010: Thunderhead Engineering, PyroSim User Manual, 2010.2, [www.thunderheadeng.com](http://www.thunderheadeng.com).
- Entler, 2013: Entler S., Horová K., Wald F., Fire fighting on inclined coal handling bridge, Integrated Fire Engineering and Response, Fire Brigade Reports and Investigations, 2013, ISBN 978-80-01-05200-6.
- Entler, 2012: Entler S., Požární zásah na šikmém zauhlovacím mostě, Konstrukce 3/2012, ISSN 1213-8762, in Czech.

## AN APPROACH FOR EVALUATING VULNERABILITY OF BRIDGES AGAINST FIRE HAZARD

Venkatesh Kodur<sup>a,\*</sup>, Mohannad Naser<sup>b</sup>

<sup>a</sup>Professor, Civil and Environmental Engineering, Michigan State University

<sup>b</sup>Ph.D. Candidate, Civil and Environmental Engineering, Michigan State University

### Abstract

In recent years, bridge fires are becoming a growing concern, however there is no specific requirements in codes and standards for design of bridge structural members against fire hazard. This paper presents an approach for developing an importance factor for design of bridges against fire hazard. The proposed importance factor takes into account the degree of vulnerability of a bridge to fire and also the critical nature of a bridge from traffic functionality point. The proposed importance factor for fire design, which is similar to the one currently used for evaluating wind, and snow loading in buildings, is validated against previous bridge fire incidents. It is shown through this validation that the proposed method for importance factor can be used as a practical tool for identifying critical bridges from the point of fire hazard and also to develop relevant design strategies for mitigating fire hazard in bridges.

**Keywords:** fire hazard, importance factor, bridges, fire protection, bridge collapse.

### 1 INTRODUCTION

There have been numerous fire incidents in bridges in recent years and in some cases these fires lead to significant damage or collapse of bridges (Kodur et al, 2010). The majority of these bridge fires are caused by collision of vehicle with other automobiles or bridge structural members (Garlock et al, 2012; Bai et al, 2006; Guthrie et al, 2012), hence fires in bridges can be explosive in nature. This has been attributed to the fact that collisions occur at high speeds leading to burning of highly flammable hydrocarbon based fuels. Thus, bridge fires can reach extremely high temperatures (in the range of 1000°C or more) in the first thirty minutes. In some cases, fires can induce significant capacity degradation in structural members, due to loss of strength and stiffness properties of constituent materials, which often lead to partial or full collapse of bridges (Bai et al, 2006; Guthrie et al, 2012). Even in the case of minor fire incidents, where no collapse occurs, proper investigation, inspection and maintenance, in the aftermath of a fire incident, is required before the bridge is opened to traffic. Shutting down a bridge for maintenance would require traffic detouring to nearby routes which can impose significant traffic delays in the affected region.

Bridges during their servicelife are exposed to multiple loadings and various risks. In recent years, there is an increase in shipping of hazardous materials; spontaneously combustible materials and dangerous materials (U.S. Department of Transportation, 2012). Further, bridges are open to general population and easily accessible to public; with minimum or no security at all, hence they are susceptible to vandalism which can often lead to fires (SAIC, 2002).

Although fire represents a significant hazard to bridges, it is still of a rare occurrence and in many cases these fires may burn-out quickly or are extinguished through firefighting. As a result, it is not economical or practical to design all bridges for fire hazard. Only bridges that are at high risk from the point of fire hazard are to be designed for fire safety. Fire hazard in bridges can be overcome to a certain extent through provisions of appropriate fire resistance to structural members, such as girders, piers, etc. (Garlock et al, 2012). For evaluating fire

risk, an importance factor similar to that used for evaluating snow or wind loading in the design of buildings, can be quite useful. In general, fire resistance is achieved via proper design, selection of materials and detailing of the structural members. Unfortunately, at present, there are no specific requirements in codes and standards for fire resistance of structural members in bridges. Hence, this paper presents the development of an importance factor for fire design of bridges.

## **2 FACTORS INFLUENCING FIRE PERFORMANCE OF BRIDGES**

The importance factor for assessing fire risk in a bridge is mainly a function of fire performance of structural members in a bridge and impact of fire on traffic flow. The fire performance of a bridge is influenced by the degree of vulnerability of structural members to a fire. On the other hand, the impact of fire on a bridge is dependent on the critical nature of the bridge from the point of traffic functionality. Some of the key factors that influence the fire performance of bridges are discussed below.

### **2.1 Vulnerability of bridges to fire**

The key factors that contribute to vulnerability of bridges to fire hazard are geometrical features, materials used in construction, loading and restraint conditions and fire intensity. For instance, slenderness and lateral restraint to structural members used in steel bridges can significantly affect local or torsional buckling of girders under fire conditions. On the other hand, concrete cover thickness to internal steel reinforcement has a direct bearing on the fire response of reinforced concrete structural members in concrete bridges. Further, the thermo-physical and mechanical properties of constituent materials significantly affect the response of structural members under fire. In general, all materials experience loss of strength and elastic modulus properties at high temperatures and rate of loss vary depending on the composition of these materials. The type and intensity of loading, as well as restraint conditions, can influence the fire performance of structural members. High load levels subject the members to additional stresses; hence rapid degradation of available capacity occurs under fire. Restrained support conditions can significantly enhance fire resistance of flexural members due to development of fire induced restraint forces that can counter balance the load induced moments. Further, fire intensity in a bridge fire and its duration depend mostly on the fuel type and quantity. Presence of highly flammable hydrocarbon products, unlimited oxygen supply and lack of active and passive fire protection measures can accelerate the rate of growth of fires, producing high intensity fires.

### **2.2 Critical nature of bridges**

The second major factor that is to be considered in evaluating the importance of a bridge, from the point of fire hazard, is the critical nature of the bridge which is mainly influenced by the bridge location and traffic density. If the bridge is located in a route connecting natural obstacles (such as valleys or rivers) and if there are no alternative routes for traffic detours, then any closure of that bridge due to fire damage will significantly slow down or shut down the traffic in the region. Similarly, traffic density can determine the critical nature of the bridge. If a bridge is located on a congested highway or in the surroundings of urban area that serves large number of vehicles daily, loss of operation of such a bridge due to fire will cause significant traffic disruptions in the region.

## **3 APPROACH TO EVALUATE IMPORTANCE FACTOR**

The proposed approach for importance factor is derived by taking into account the vulnerability of bridge structural members to fire, as well as the critical nature of the bridge to the traffic flow. The steps associated in the development of importance factor of bridges are explained below.

### 3.1 Calculation of the importance factor

In order to evaluate the importance factor of a given bridge, several factors and parameters are to be considered. The parameters are based on the vulnerability of bridge structural members to fire, as well as the critical nature of the bridge from traffic flow consideration. The vulnerability of a bridge to fire arises from geometric dimensions and design features of its structural members and likelihood of fire occurrence in the vicinity of that bridge. Based on the previous fire incidents in bridges, those factors were found to be the major contributing factors to the bridge's state of vulnerability (Kodur et al, 2010).

On the other hand, traffic demand, economic consequences in the aftermath of a fire incident and expected fire losses define the critical nature of a bridge. Bridges with high traffic volumes are more prone to higher losses and traffic disruption due to fire. Further, closure of a fire damaged bridge due to post-fire inspection or maintenance would require detouring traffic to nearby routes. Such detouring would amplify traffic intensity in the nearby highways and affect the traffic flow in the region.

For deriving an importance factor, the key characteristics that define the importance of a bridge; vulnerability to fire and critical nature to traffic flow, are grouped into five classes (Kodur and Naser, 2013). Each class is comprised of different parameters that contribute to the importance factor. Within each parameter, there are various sub-parameters that determine the conditions of a specific bridge. Based on engineering judgment and recommendations of previous studies (Garlock et al, 2012; Elhag and Wang, 2007; Wardhana and Hadipriono, 2003; Scheer, 2010), weightage factors are assigned to different sub-parameters. The weightage factors ( $\varphi_{i,x}$ ), on a scale from 1 to 5, are shown in Table 1.

Table 1 Weightage factors based on the different features of a bridge

<i>Class I: Geometrical properties and design features</i>				<i>Class II: Hazard (fire) likelihood</i>			
<i>Param.</i>	<i>Sub-parameters</i>	<i>(<math>\varphi_{i,x}</math>)</i>	<i><math>\varphi_{i,x}(max)</math></i>	<i>Param.</i>	<i>Sub-parameters</i>	<i>(<math>\varphi_{i,x}</math>)</i>	<i><math>\varphi_{i,x}</math></i>
Structural system	Truss/Arch	1	5	Response time (min)	<5	1	5
	Girder - continuous	2			5-10	2	
	Girder - simply supported	3			10-20	3	
	Cable-stayed	4			20-30	4	
	Suspension	5			>30	5	
Material type	Reinforced concrete	1	5		Hist./arch. significance	Conventional	
	High strength/(pre-stressed) concrete	2		Landmark		2	
	Steel-concrete composite	3		Prestigious		3	
	Concrete members strengthened with FRP	4		Threat perception	None (low)	1	3
		Steel and timber			5	Not available (medium)	
Span (m)		<50	1		Frequent (high)	3	
	50-200	2	Fire scenario	A small vehicle fire above /under the bridge	1	5	
	200-500	3		A large truck collision and fire with other vehicles	2		
	>500	4		A fuel tanker collision and fire with bridge sub-structure	3		
	No. of lanes	2		1	Major fuel tanker collision and fire with multiple vehicles and against bridge sub-structure		4
2-4		2		Fire due to fuel freight ship collision with a bridge pier	5		
>4		3	Age (years)	<15	1	4	
15-29	2	60-80		2			
30-50	3	40-60		3			
>50	4	20-40		4			
Current rating	100	1	5	<20	5		
	60-80	2					
	40-60	3					
	20-40	4					
	<20	5					

Additional service features	1 deck	1	5	Class IV: Economic impact				
	2 decks + pedestrians	2		Param.	Sub-parameters	$(\varphi_{i,x})$	$\varphi_{i,x}$	
	Accommodates railroad	3		Closes routes to alt.		<10 km	1	3
	Multi-level	4				10-20 km	2	
	Above water	5				>20 km	3	
Class III: Traffic demand				Time expected for repair			3	
Param.	Sub-parameters	$(\varphi_{i,x})$	$\varphi_{i,x(max)}$					
ADT (vehicles/day)	<1,000	1	5					<3 months
	1,000-5,000	2		3-9 months	2			
	5,000-15,000	3		>9 months	3			
	15,000-50,000	4		Cost expected for repair	< 1 million	1	3	
	>50,000	5			1-3 million	2		
Facility location	Rural	1	3	>3 million	3	3		
	Class V: Expected fire losses							
	Sub-urban	2		Param.	Sub-parameters		$(\varphi_{i,x})$	$\varphi_{i,x}$
Urban	3	Life/property losses			Minimum to no injuries	1	3	
Class V: Expected fire losses								
Env. damage	Minor damage				1	3		Minimum casualties
	Significant damage	2	Many casualties	3				
	Unacceptable damage	3	Minor damage	1	3			
Class V: Expected fire losses								
Env. damage	Significant damage	2	3	Significant damage		2		
	Unacceptable damage	3		Unacceptable damage	3			

Knowing the maximum weightage factors for various parameters in a bridge (from Table 1), a class factor ( $\psi_x$ ) is calculated as:

$$\psi_x = \frac{\sum \varphi_{x(max)}}{\varphi_{total}} \quad (1)$$

where  $\varphi_{x(max)}$  is the maximum weightage factor of each parameter in class (x)

$\varphi_{total}$  is the summation of maximum weightage factors of all parameters in all five classes

Then, a class coefficient ( $\Delta_x$ ) is calculated as the ratio of the summation of the weightage factors of all sub-parameters in class (x) to the summation of the maximum weightage factors of all the parameters in the same class:

$$\Delta_x = \frac{\sum \varphi_{i,x}}{\sum \varphi_{x(max)}} \quad (2)$$

where  $\varphi_{i,x}$  is the weightage factor of sub-parameter (i) in class (x)

$\varphi_{x(max)}$  is the maximum weightage factor of each parameter in class (x)

Finally, an overall class coefficient ( $\lambda$ ) is evaluated as the summation of the product of class coefficient ( $\Delta_x$ ) and corresponding class factor ( $\psi_x$ ).

$$\lambda = \sum \Delta_x \psi_x \quad (3)$$

The overall class coefficient ( $\lambda$ ) is then utilized to assign fire risk grade for a bridge. This is done by comparing the value of the overall class coefficient ( $\lambda$ ) with numerical scores given in Table 2 and arrive at a risk grade and importance factor (IF). The risk grades and related overall class coefficient ( $\lambda$ ) scores are given in Table 2. It should be noted that, about 5% of bridges fall under “critical” risk category and appropriate fire protection to structural members in “critical” bridges can minimize the adverse effects of fire hazard to a great extent. Further information on the classes, parameters, rationale for assigning weightage factors and risk grades can be found elsewhere (Kodur and Naser, 2013).

Tab.2 Risk grades and associated importance factors for fire design of bridges

Risk grade	Overall class coefficient ( $\lambda$ )	Importance factor ( $IF$ )
Critical	$\geq 0.95$	1.5
High	0.51-0.94	1.2
Medium	0.20-0.50	1.0
Low	$< 0.20$	0.8

### 3.2 Validation of the proposed approach

The above developed approach was validated by evaluating importance factor for several bridges that experienced major fire incidents. One such incident is the bridge fire that occurred at the I-95 Howard Avenue Overpass in Bridgeport, CT. Full details of validation and additional case studies are provided else where (Kodur and Naser, 2013).

In Bridgeport, CT, fire a car crashed into a fuel tanker transporting 50,000 liters of heating oil on the I-95 Howard Avenue Overpass on March 23, 2003. The bridge was supported by 30-inch deep steel girders that had a span of 22 meters. The truck slipped along the overpass's concrete barrier and hit two light poles after an unsuccessful maneuvering attempt. The heating oil spilled over a length of 100 meters and ignited. The fire broke and lasted for two hours with peak temperatures of about 1100°C. The high intensity of fire initiated significant buckling in steel girders carrying the overpass. This resulted in partial collapse of steel girders causing both northbound and southbound lanes to collapse. Following the fire, traffic in both directions had to be detoured. The refurbishment of this fire damaged bridge costed about \$11.2 million (Van Horn, 2012).

The above developed approach is applied to evaluate the importance factor for this bridge against fire hazard. The importance factor was found to be 0.64. Using Table 2, the risk grade for fire hazard is determined to be high and thus the importance factor is 1.2. Since the bridge falls under high risk category, fire proofing of steel structural members would enhance the fire performance of the bridge. Hypothetically, the bridge could have survived if the steel girders were protected with 1-hour fire insulation.

## 4 DESIGN IMPLICATIONS

The vulnerability of a bridge to fire hazard can be assessed using the proposed importance factor. The proposed importance factor is similar to the one used for evaluating wind and snow loading in buildings and can be applied in the design of new bridges or in retrofitting of existing bridges. If a bridge is found to be in "critical" or "high" fire risk category, the vulnerability of such a bridge to fire hazard can be minimized by providing fire protection to structural members based on conventional prescriptive approaches. Alternatively, advanced approaches such as performance based fire design methods can be applied to develop unique solutions to overcome fire risk in critical bridges. Hence, the above developed fire-based importance factor can provide a mean to identify critical bridges from fire hazard risk and develop appropriate strategies to enhance fire safety of such bridges.

### SUMMARY

Based on the information presented in the paper, the following conclusions can be drawn.

- Fire represents a severe hazard in bridges and can induce significant damage or collapse of structural members.
- A methodology for evaluating importance factor for fire design of bridges is presented. The approach takes into account the level of vulnerability and critical nature of the bridge from the point of traffic functionality.



- The importance factor can be used as a benchmark to assess relative fire risk in bridges and also develop appropriate strategies for mitigating fire hazard in bridges.

## ACKNOWLEDGMENTS

This material is based upon the work supported by the National Science Foundation under Grant number CMMI-1068621 to Michigan State University. Any opinions, findings, and conclusions or recommendations expressed in this paper are those of the authors and do not necessarily reflect the views of the sponsors.

## REFERENCES

- Kodur V., Gu L., Garlock M., Review and Assessment of Fire Hazard in Bridges, Transportation Research Record: Journal of the Transportation Research Board, 2010.
- U.S. Department of Transportation, Federal Highway Administration, Highway Statistics, 1995-2010: Ibid., Highway Statistics (Washington, DC: Annual Issues), 2010.
- Garlock M., Paya-Zaforteza I., Kodur V., Gu L., Fire hazard in bridges: Review, assessment and repair strategies, Engineering Structures, 2012.
- A Guide to Highway Vulnerability Assessment for Critical Asset Identification and Protection, Prepared by Science Applications International Corporation (SAIC), Transportation Policy and Analysis Center, Vienna, VA 22182, 2002.
- Bai Y., Burkett W., Nash P., Rapid Bridge Replacement under Emergency Situation: Case Study, J. Bridge Eng., 2006.
- Guthrie D., Goodwill V., Hicks M., Tanker fire shuts down I-75, collapses Nine Mile bridge, The Detroit News, 2009.
- Payá-Zaforteza I., Garlock I., A numerical investigation on the fire response of a steel girder bridge, Journal of Constructional Steel Research, 2012.
- Elhag T., Wang Y., Risk assessment for bridge maintenance projects: neural network versus regression techniques, Journal of Computing in Civil Engineering, 2007.
- Wardhana K., Hadipriono F., Analysis of Recent Bridge Failures in the United States, J. Perform. Constr. Facil., 2003.
- Scheer J., Failed Bridges: Case Studies, Causes and Consequences, John Wiley & Sons, 2010.
- Kodur V., Naser M., Importance Factor for Design of Bridges Against Fire Hazard, Engineering Structures, 2013, Submitted.
- Van Horn J., Crews Reopen Fire-Closed I-95 in Six Days, Construction Equipment Guide, 470 Maryland Drive, Fort Washington, PA 19034. Retrieved on January 22<sup>nd</sup>, 2012. <http://www.constructionequipmentguide.com/Crews-Reopen-Fire-Closed-I-95-in-Six-Days/4416/>

# **PERFORMANCE-BASED FIRE SAFETY DESIGN OF DIFFERENT TYPES OF CONSTRUCTIONS IN GERMANY**

## **Global Structure behaviour of Steel Constructions**

Prof. Dr. Jochen Zehfuss <sup>a</sup>, Dr. Christoph Klinzmann, Dr. Karen Paliga <sup>b</sup>

<sup>a</sup> Technical University of Braunschweig, Institute for Building Materials, Concrete constructions and fire protection, Braunschweig, Germany

<sup>b</sup> hhpberlin Ingenieure für Brandschutz GmbH, Berlin, Germany

### **Abstract**

The objective of this article is the illustration of the calculation of natural fires and fire resistance of structural members based on the Eurocodes of three types of special structures, in this case a railway bridge, a parking deck and an airplane hangar. The railway bridge has a width of nearly 70 meters and consists of steel beams and a massive concrete slab that are supported by massive columns and walls and for that reason can be compared to a tunnel. The parking deck was calculated on the basis the FE program ANSYS. The load-bearing capacity as well as the reactive internal forces in the case of fire were investigated. The load-bearing structure of the roof of the hangars is made of steel and is supported by steel columns. The choice of a fire scenario on the safe side is crucial for the design process of the unprotected steel structure.

**Keywords:** Natural Fires, Global structural behaviour, Steel, thermal and mechanical analysis, non-linear material properties, reactive internal forces

### **INTRODUCTION**

Improvements in performance-based design allow for a more realistic and cost effective fire safety design of structures. Within the year 2012, the fire parts of the Eurocodes and the included methods for the calculation of natural fires and the resistance to fire of structural members are introduced into the German building laws. For that reason the application of these methods is generally permitted by the authorities having jurisdiction (AHJ) and it can be assumed that they will become more and more important in years to come.

Thereby simplified or general calculation methods of the according European standards for structural fire safety design can be used, depending on application case. To adopt this method of calculation finite element analysis is required, which considers nonlinear material properties and nonlinear thermal loads in structural elements. In this contribution the application of these methods using the FE-program ANSYS shall be described by means of two types of realistic building projects.

### **1 GENERAL PROCEDURE**

The first step in fire safety design is the definition of design fires in the form of heat-release-time curves specially adapted to the building in question and the relevant fire scenarios. Subsequently, the effects of a design fire on a building and its load bearing structure are evaluated using simulation models, depending on the complexity of the building with zone or CFD-models. The temperatures calculated in these analyses are the basis of the simplified and advanced calculation methods of the Eurocodes.

In Germany the fire safety design of large railway structures like tunnels and stations can rely on special pre-defined design fires that were developed by the German railway services on the

basis of Eurocode 1-1-2 (DIN EN 1991-1-2, 2010) and the specific geometric properties and fire loads of typical train cars.

Design fires for buildings like airplane hangars are not standardized in Germany and have to be derived for the special case. Similar to the design fires for train cars, the special geometric properties (like width and height of airplanes) are taken into account.

## 2 PROJECT EXAMPLE: TRAIN STATION “OSTKREUZ” IN BERLIN

### 2.1 Description of the Construction

The building in consideration is a crossing station in the city of Berlin, where the S-Bahn and long distance train lines intersect on two levels (see figure 1). The platform and the tracks supports of the upper level are made from steel girder grids supporting a concrete slab. The girders are single span beams carried by solid supports and supporting walls. The width of the superstructure is approx. 70 m and has almost the dimension of a tunnel.

A burning train located directly below the superstructure carrier represents the worst case fire scenario. The main task for the fire safety design of the superstructure was to prove that the steel parts of the structure withstand the effects of a fire long enough without loss of load carrying capacity and to devoid fire protection measures such as covering or coating.

### 2.2 Fire Scenarios and Design Fires

By means of a CFD simulation (computational fluid dynamics) the determination of temperature over the period of the fire is calculated using the program FDS (McGrattan, K. B. et al., 2010).

In fig. 2 the relevant time-temperature-curve of the train fire is shown. This time-temperature curve has been measured at the open carriage door one metre above the roof of the car.



Figure 1 Crossing station in Berlin with overlapping platforms (Source: Deutsche Bahn)

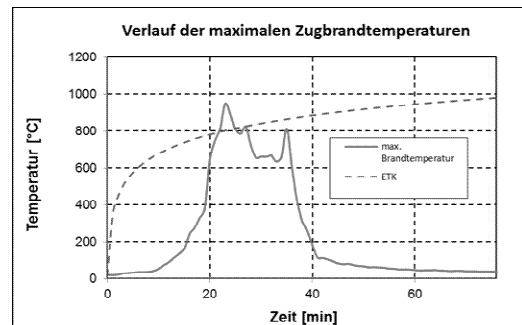


Figure 2 Development of the maximum fire temperature

The time period during which temperatures  $> 200$  °C act on the structure, is approx. 25 minutes. At the time of the maximum impact 950 °C are reached for a short time. For comparison, the uniform-temperature-time-curve (UTTC) is also shown in Fig 2.

### 2.3 Thermal and Mechanical Analysis

The thermal and mechanical analysis was performed with the FE program ANSYS. The mechanical analysis examined the load bearing and deformation behaviour of the construction. The temperatures acting on the structure over the duration of the fire, as well as the mechanical loads and the non-linear temperature-dependent material properties were taken into account.

Fig. 3 shows the vertical deformation of the loaded cross member over the period of fire exposure. It is clearly visible how the course of the deformations corresponds with the natural

fire curve of the thermal load (fig. 2). At the end of the fire, the influences of the temperatures on the load-bearing structure are getting smaller and the deformations are reduced.

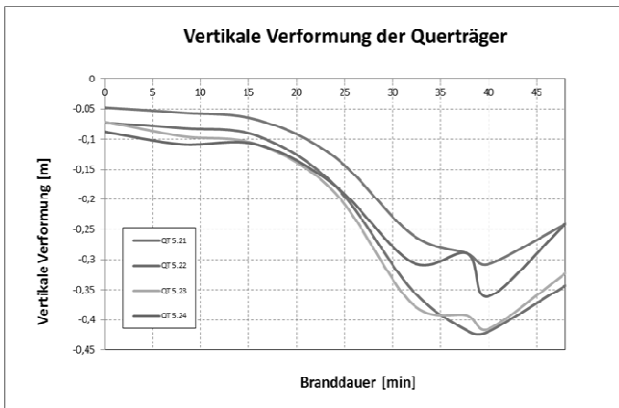


Fig. 3 Deformation of the cross-members during the time of the fire

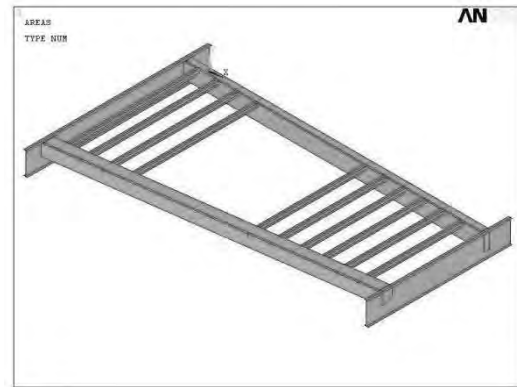


Fig. 4 Three-dimensional model of the steel girder grid of the platform level

The calculations showed that the failure criteria of the distortion were met over the entire period of stress. The results of the simulation show that the girder grid made from unprotected steel resists a natural train fire with temperatures above 900 °C and does not fail in the event of a fire. No fire protection measures such as insulating surface protection for the steel are required.

### 3 PROJECT EXAMPLE: PARKING DECK

#### 3.1 Description of the Construction

The BBC Böblingen Center has a length of 190 m and a width of approx. 130 m. It consists of six floors. The ground floor and the first floor are intended for trade. Above this three levels of parking are located. The structure consists of steel-reinforced concrete, steel columns and composite beams. The steel girders of the composite slab and steel supports in the garage are to be classified in fire resistance class F 90. It is planned to provide the support beams and supports with an intumescent coating which allows a classification in fire resistance class F 30. Proof is required that the objectives with regard to stability are not compromised during the course of fire. This is done on the basis of natural fire scenarios, where it has to be ensured that the device successfully endures the entire fire load and does not fail.

#### 3.2 Thermal and mechanical Analysis

As fire scenario a burning of 8 cars in parking deck 1 was analyzed. The fire flashover time from car to car was established at 10 minutes. The resulting load temperatures of the burn-up of the cars for the structure were determined using a general nature fire model (CFD simulation). The steel frame is protected with a layer of intumescent coating with the fire resistance rating R 30. The thermal material properties of the coating, such as the thermal conductivity and heat capacity, are specified according to (Dorn 2003).

The warming and the carrying- and distortion behavior of the structure was then simulated according to the General calculation method with the help of ANSYS.

The results were evaluated and compared with selected failure criteria. It was found that the failure criteria for bending and deformation were not exceeded.

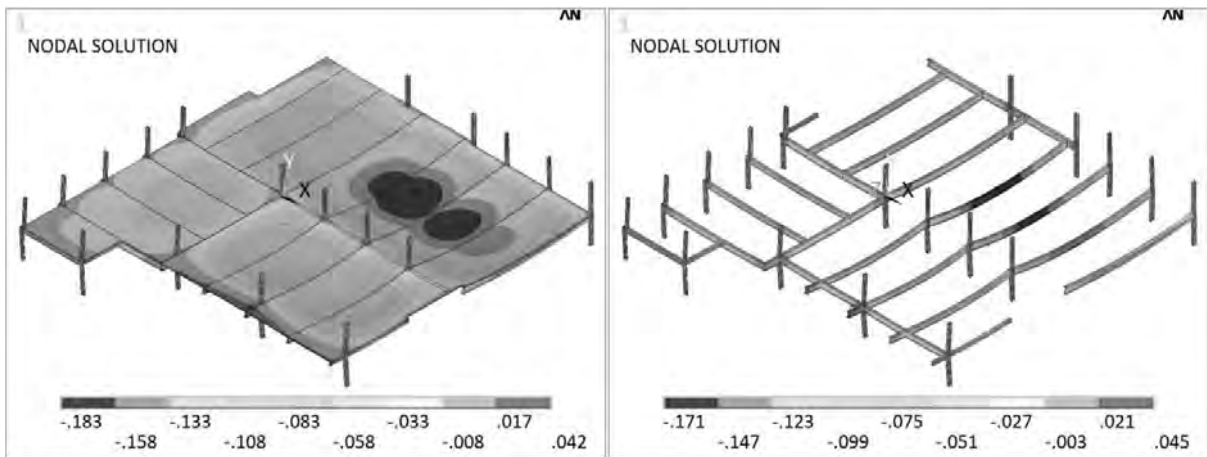


Fig. 5 Deformation in the vertical direction to the 90th minute (left - total system; right - steel construction)

As a result of the compressions in the connections occurring in the heating phase of the fire there will be tensile stresses during the cooling phase. These restraining forces must be considered when the connections are determined. The restraining forces are calculated by multiplying the normal tension with the respective tensioned cross sectional area of the connection. The maximum restraining forces amounted to up to 1300 kN, so that an assessment of the connections for these restraining forces was not possible. As a result, cleats were arranged below the carriers in the connection area, taking over the bearing in the failure of the connection.

## 4 PROJECT EXAMPLE: AIRCRAFT HANGAR

### 4.1 Description of the Construction

The hangar discussed here has the outer dimensions of 83.40 m width and 77.60 m depth and an inner area of 6,472 m<sup>2</sup>. The hangar has a horizontally orientated roof, which is supported by the main load-bearing system which consists of an external two truss girders on steel supports. The hangar has a mean interior height of approximately 18.10 m.

### 4.2 Safety Objectives

Alike to the train station, the main objective that has to be fulfilled by the fire safety design of the construction was a sufficient structural safety in case of fire. Therefore the results from CFD-Simulations should be used for the structural fire design of the steel structure according to the simplified calculation procedures of Eurocode 3 (columns and roof structure). The objective was to use the least possible amount of fire protection measures.

### 4.3 Fire Scenarios

The fire scenarios are compiled according to the various aircrafts that are to be serviced in the hangar:

- Scenario 1: fire in the cabin of a B747-400 with participation of part of the wings (plastics and kerosene fire), fire surface 100 m<sup>2</sup>, fires in a height of approx. 6 m.
- Scenario 2: cabin fire in a B747-400 in the upper-deck (plastics) without participation of the wings, fire area 50 m<sup>2</sup>, fires in a height of approx. 8 m.
- Scenario 3: local fire, for example larger car or a similar major technical device or storage good, fire area 10 m<sup>2</sup>, fires at a height of 4.0 m.

#### 4.4 Design Fires

To ensure design fires on the safe side, the relevant input parameters must be adopted conservatively, so that all relevant fire events are covered.

It is conservatively assumed that the heat release rate is not reduced after the depletion of the fire load but will remain at the maximum rate of heat release. For that reason, only the nature of the fire load, but not the amount is significant for the fire safety design. This leads to the fact that the safety objectives in the building will be proven when a stationary state, i.e. a balance of the energy supplied by the fire and the energy dissipated by the smoke and heat exhaust measures is reached. In all fire scenarios extinguishing measures, for example, by the extinguishing system or the airport fire brigade, are not considered to have a direct effect on the heat release rate. They are accounted for conservatively by the partial factor  $\gamma_{fi,HRR}$  according to (DIN EN 1991-1-2, 2010).

According to the literature such as the (vfdb-Leitfaden, 2009), area-specific heat release rates of between 150 kW/m<sup>2</sup> and 500 kW/m<sup>2</sup> are realistic. In individual cases also values over 600 kW/m<sup>2</sup> can occur especially in plastics and lubricants. This adds up to the following design fires for the defined fire scenarios (partial safety factors in accordance with (DIN EN 1991-1-2, 2010)):

- Scenario 1 (Fire in cabin + wing):  $q' = 600 \text{ kW/m}^2$
- $Q'_{\max} [\text{kW}] = 600 \text{ kW/m}^2 * 100 \text{ m}^2 * 1,075 = 64500 \text{ kW}$  after approx. 930 s
- Scenario 2 (Fire in upper-deck cabin):  $q' = 450 \text{ kW/m}^2$
- $Q'_{\max} [\text{kW}] = 450 \text{ kW/m}^2 * 50 \text{ m}^2 * 1,075 = 24187.5 \text{ kW}$  after approx. 720 s
- Scenario 3 (Local fire at support):  $q' = 500 \text{ kW/m}^2$
- $Q'_{\max} [\text{kW}] = 500 \text{ kW/m}^2 * 10 \text{ m}^2 * 1,075 = 5375 \text{ kW}$

The mean value of the heat of combustion of the fuel mixture was derived from the specific parameters of the individual substances to be approximately 27 MJ/kg.

The results of the fire simulations carried out have proven to be decisive for the roof structure. Because of the height and the width of an aircrafts and their necessary distance to the steel columns of the building, there was no relevant increase in temperature in their vicinity during the fire simulations. Since no fire scenario could be ruled out, the effects of a localized fire event in the immediate vicinity of the columns were analysed. The temperatures resulting from such a fire were calculated with a Plume-model in accordance with Heskestad (DIN EN 1991-1-2, 2010) using a maximum heat release rate of 5 MW.

#### 4.5 Fire Safety Design

In a next step, a thermal analysis in 3-D was undertaken for the steel columns using the temperatures evolving from the localized fire as thermal load. Here, segments of a height of 2 metres were assumed to receive the same thermal load. It was taken into account that the components were protected by a protective coating up to a height of 8 m.

A thermal analysis for the structure of the roof was not necessary, since the temperatures recorded in the CFD simulation were only at about 400 °C. This temperature is well below the critical temperature of the structural members made of steel, as a result a fire safety design was only required for the columns. This design was carried out using the simplified calculation procedures on resistance level of Eurocodes 3 part 1-2 (DIN EN 1993-1-2, 2005). This was done in the most unfavourable area of the components regarding the internal forces and thermal loads. A fire safety design was not necessary for all stiffening components because they were protected from a critical warming by protective coatings.

### 5 SUMMARY AND ACKNOWLEDGMENT

The application of computational design methods of the Eurocodes for complete or partial structures can only be performed with powerful FEM programs that are able to depict and calculate the non-linearities of material build-ups and design loads. The heat generation in the

cross section of the components is done by FEM programs as well. Usually a thermal analysis of two-dimensional models is of sufficient accuracy due to the material properties of steel that lead to quick uniform temperatures.

Depending on the complexity of the analysed structures the simplified or general calculation methods of the Eurocode. In the first case, the internal force in the fire case can be calculated using simple standard software, in the latter case more complex 3-D mechanical analysis is required.

With the rapid development and the increasing capacity of the computer coupled analysis of 3-D models will be possible in the future. Further research in these areas will extend the possibilities of the design of constructions, reduce the cost of planning the implementation of a project, and shorten the time for the realisation of buildings by the reduced structural fire protection at the same level of safety.

We would like to thank  and the Deutsche Bahn AG for the excellent cooperation.

## REFERENCES

- DIN EN 1991-1-2: Eurocode 1: Einwirkungen auf Tragwerke. Teil 1-2: Allgemeine Einwirkungen - Brandeinwirkungen auf Tragwerke. Deutsche Fassung EN 1991-1-2:2010.
- DIN EN 1993-1-2: Eurocode 3: Bemessung und Konstruktion von Stahlbauten. Teil 1-2: Allgemeine Regeln - Tragwerksbemessung für den Brandfall. Deutsche Fassung EN 1993-1-2: 2005 + AC:2005.
- McGrattan, K. B. a. o.: Fire Dynamics Simulator (Version 5) – User’s Guide. National Institute of Standards and Technology, Gaithersburg, October 2010.
- Institut für Brandtechnologie GmbH: Gutachten Nr. G071201, Entwicklung eines numerischen Brandmodells zum DB-Bemessungsbrand für S-Bahn-Fahrzeuge, Leverkusen, 30.01.2008.
- DIN 4102-2: Brandverhalten von Baustoffen und Bauteilen, Bauteile – Begriffe, Anforderungen und Prüfungen, September 1977.
- Twilt, L et al.: Design tools for the behaviour of multi-storey steel framed buildings exposed to natural fire conditions. Cardington (2) final report, TNO report 2003-CVB-R0088, Final Report Agreement 7210-PA, PB, PC, PD-112, 2002.
- Ryan, J. V.; Robertson, A. F.: Proposed Criteria for Defining Load Failure of Beams, Floors and Roof Constructions During Fire Tests. Journal of research of the National Bureau of Standards, Vol. 63C, No. 2, 1959.
- vfdb-Leitfaden „Ingenieurmethoden des Brandschutzes“, vfdb, Technischer Bericht TB 04/01, Mai 2009.
- Dorn: Rechnerische Simulation der Wirkung dämmschichtbildender Beschichtungen bei der brandschutztechnischen Auslegung von Stahlbauteilen. Dr.-Ing. Thomas Dorn. Brandschutz und mehr... Festschrift zum 60. Geburtstag von Univ.-Prof. Dr.-Ing. Dietmar Hossler, Institut für Baustoffe, Massivbau und Brandschutz, Materialprüfungsanstalt für das Bauwesen, TU Braunschweig, Heft 173, Braunschweig 2003.

# **REDUCING THE RISK ON A FOOD INDUSTRY ‘SERIOUS’ FIRE**

## **A Fire Investigation Case Study**

Dimitrios Tsatsoulas <sup>a</sup>

<sup>a</sup> Greek Fire service, Kritis 46 & Martiou, 54008, Thessaloniki

### **Abstract**

A case study of fire investigation of a ‘Serious fire’ in a food industry located in Northern Greece is presented. This work summarized, analyzes and reports detailed fire experience data through on-site investigation and significant investigation report. This fire investigation provides all evidence, witnesses and suspect statements, as well as conclusions and recommendations offered by the fire investigative team in relation to the fire itself, the suspect and potential prosecution.

Areas documented in this work include details about the place of the onset of fire; ignition sources; first ignited materials; time of ignition; degree of spread; contributions of building construction; suppression scenarios; performance of structures exposed to the fire; smoke and toxic emissions; human reaction (response) and evacuation; and the extent of life loss, injury and property damage. Fire Brigade intervention and the time taken to undertake its activities at a fire scene has been evaluated.

Fire investigation analysis clearly show that the prevention of fire spread beyond the first ignited item would have a major impact on the reduction of fire losses. Experimental analysis included small scale (Cone Calorimeter) and medium scale (Enclosed Fire Rig) equipment combined with online effluent gas analysis equipment (FTIR) were employed to estimate the potential of reducing the probability of breaking out and spreading of fire.

**Keywords:** risk, fire, food industry, ignition, fire fighting, fire prevention

## **1 INTRODUCTION**

This study examines a case of a ‘Serious fire’ in a food industry located in the industrial area of Thessaloniki. This food industry was complied with fire safety measures as predicted by the Greek Government Decision (1589/104/2006) ‘Industrial Fire protection’. (So, it has been supplied with passive protection measures i.e means of escape, emergency lighting and signs, and active measures i.e. fire detection, permanent fire water supply network but with no sprinkler installation.) The food industry was a 10.190 m<sup>2</sup> concrete building with 105 employees. Processed materials were Glucose, ground sesame, sugar, cocoa, vanilla, dried fruit put on many mdf wooden pallets. Also, many wooden (mdf) wrapping material used to pack final products.

## **2 INCIDENT ANALYSIS**

The fire has been caused by ‘electrical spark’ originated in the ‘production and machinery area’ below wooden pallets. First ignited materials were ‘unprotected’ wooden mdf pallets and secondary materials were raw mdf wooden material. These factors were leading to the rapid fire growth and flash over conditions. Fire almost immediately spread from first to second ignited materials. It was not contained to the room of origin and spread beyond to the whole building i.e. first and second fire Compartments were inadequate to stop the fire and fire was not been possible to be suppressed by permanent fire fighting hose reels by industrial fire staff.



Almost the whole processed (raw and secondary) materials, final products and electro-mechanical equipment of industry have been destroyed by the fire. Estimated property loss 1,600,000 euro. On the other hand, the reinforced concrete, columns, beams performed very well in such a severe fire due to high fire resistance of reinforced concrete (above two hours and a half). Estimated property value saved 1,250,000 euro.



Fig. 1 Fire incident during post-flashover period (a) production and maintenance area, (b) storage area

Because of the size of the fire, a site-wide evacuation was immediately initiated. Unfortunately, five workers sustained minor injuries including scrapes and smoke inhalation.

### 3 EMERGENCY RESPONSE

The initial call reporting this incident was at 13.08 hours i.e in the middle of working day at 23-09-11. Food industry had a trained and equipped Emergency Response Team (ERT) that included 25 members. On the day of the incident; 15 trained emergency responders were immediately available. They effectively helped building evacuation and tried to extinguish the fire using permanent fire water supply network of industry. Their effort was unsuccessful due to severe fire conditions.



Fig. 2 Fire fighters efforts to tackle the fire

Firefighters from the surrounding fire stations were at 'emergency alert' providing 27 fire vehicles with 80 fire fighters deployed at the scene of fire. Immediately four firefighters using breathing apparatus invaded into the storage area in the back of the building and rescued three employees that were trapped over there. One aerial ladder truck had been used with effective results in the fire extinguishment efforts (see Figure 1). It was used to fight a fire from above and access the upper reaches of a building from the outside. Simultaneously, fire fighters

deployed 2-1/2" (64 mm) handlines around the burning building (see Fig. 2). All lines were immediately placed into operations.

#### 4 LESSONS LEARNED

It is clear from the above that prevention of fire spread behind the wooden first item ignited would have a significant impact on the reduction of fire losses.

In this case where the first material ignited is wood, it is considered that ignition and fire spread could be prevented or minimized by treating the timber surfaces with suitable flame retardants. Fire data on the effects of flame retardants on wooden surfaces is not available, since the relevant market is quite recent and not particularly widespread in Greece.

#### 5 EXPERIMENTAL INVESTIGATIONS

Therefore, in order to investigate this possibility mdf type of timber (as the same that was mainly used for industry's wooden pallets and other industry's wooden construction), were tested with bare samples, as well as using flame retardants (treated at different percentage (%) of the total surface area with a water – based, intumescent flame retardant, suitable for internal surfaces) ; using small scale (Cone Calorimeter) and medium scale (Enclosed Fire Rig) equipment combined with online effluent gas analysis equipment (FTIR) (Small and Medium scale).



Fig. 3 (a) mdf exposed at heat flux  $35 \text{ kW/m}^2$ , (b) untreated mdf crib at 300 sec into the test

Analysis involved thermal behavior and toxic species analysis of the samples:

- 'No ignition' and lower toxic emissions compared to untreated samples were observed at  $35 \text{ kW/m}^2$  (small scale).
- The same behavior was observed in those cases where wooden surfaces located next to ignition source had been treated (medium scale).

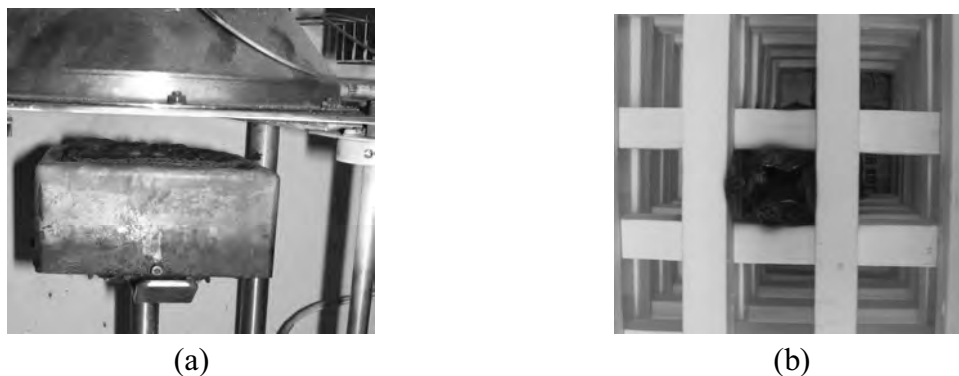


Fig. 4 (a) flame retarded Mdf exposed at Heat flux  $35 \text{ kW/m}^2$ , (b) flame retarded mdf crib at 300 sec into the test

## FTIR Toxic Gas Analysis

The European Community COSHH (COntrol of Substances Hazardous to Health Regulations) workplace 15 minute maximum allowable toxic concentrations are used to evaluate overall toxicity. For untreated mdf, formaldehyde and acrolein were the dominant gases. NH<sub>3</sub> was also significant. CO emissions was significant but not very high. Lower toxic concentrations measured for full (100%) treatment case where acrolein was the dominant toxic.

The effects of flame retardant treatment on major toxic emissions compared with the bare samples are shown on the following Table. In most fully-treated (100%) cases, even in the half-treated (50%) cases, lower or almost equal to unity emissions were measured compared with the bare samples. This is due to the fact that, in such cases, due to the intumescent action, there was either no ignition of the samples (100%-treated cases), or a considerable delay was seen (50%-treated cases). Excessive HCN and NO occurred in 60% of the untreated cases due to the considerable involvement of the flame retardant paint in flaming combustion, since it contains N in its chemical composition.

Tab. 1 Comparative effects of flame retardant treatment on major exhaust emissions

<i>Coated emission</i>	100%F.R. 6 g ethanol	100%F.R. 20 g ethanol	100%F.R. 30 g ethanol	50%F.R. 6 g ethanol	60% Untreated 6 g ethanol	60% Untreated 20 g ethanol
<i>Bare emission</i>						
'Peak CO(ppm) Ratio'	↓ ↓ ↓	↓ ↓ ↓	↓ ↓ ↓	↓ ↓	↓	↓
'Peak HCN(ppm) Ratio'	↓ ↓	↓ ↓	↓	↓	↑ ↑	↑ ↑
'Peak Acrolein(ppm) Ratio'	↓	↓	↓	↓	≈	≈
'Peak NH <sub>3</sub> (ppm) Ratio'	≈	≈	≈	≈	↑	↑
'Peak NO(ppm) Ratio'	↓	↓	≈	≈	↑ ↑	↑ ↑

Each arrow ↓ / ↑ indicates decreasing/increasing up to a factor of three. Two arrows together is equivalent to a change by a factor of 3-6. Three arrows together is equivalent to a change by a factor for greater than 6.

## 6 CONCLUSIONS

The main factors leading to the rapid fire growth and the fire spread to almost the whole building were:

- the lack of effective fire suppression measures close to ignition source;
- the untreated wooden first and secondary ignited materials;
- it is proposed that the application of intumescent flame retardants on wooden surfaces located close to ignition sources in the most probable areas for a fire to break out, could be a safe and approach in reducing fire loss in food industry;
- fire safety management of industry need to be improved following the guidelines below:
  - proper use of fire safety measures from Emergency Response Team. Therefore more fire safety education is needed. Participation in fire fighting exercises in corporation with local fire service is necessary;
  - all building employees were required to participate in periodic emergency evacuation drills;
  - check the company's space; Keep out the flammable substances and sparks and take the necessary fire precautions where is required.

A prosecution may be initiated for industry failing to comply with preventive measures as predicted by government decision 7/1996.

## **7 SUGGESTIONS**

Performing of more small- and medium – scale experiments, treated with the updated technology of the intumescent paints different types of wooden (in the form of cribs or some other form of samples), and using various ventilation rates to achieve both establishing and documentation of the contribution of intumescent technology in fire suppression, are suggested.

## **REFERENCES**

Directorate of Fire Investigations Arson Crimes Control. Greek Fire Service ‘Special investigation reports 2011’, Thessaloniki 2011.

D. Tsatsoulas. ‘Industrial fires in Northern Greece. The influence of Flame retardant on Timber Fires’. Ph.D. Thesis, Leeds (UK) 2008.

D. Tsatsoulas . ‘Thermal behaviour and toxic emissions of various timbers in Cone Calorimeter tests’ ‘International Journal of Safety and Security engineering’, Vol.1, N01(2011) 45-64.

D. Tsatsoulas “Thermal behaviour and toxic emissions of flame retarded timber in Fire Enclosure tests”, pp 295-306. Seventh International Conference on ‘Risk Analysis 2010’, 13-15 September, Algarve, Portugal.

D. Tsatsoulas, H.N. Phylaktou and G. Andrews. ‘Thermal behaviour and toxic emissions of various timbers in Cone Calorimeter tests’. Third international Conference on Safety and Security Engineering, 1-3 July 2009, Rome. In the proceedings of ‘First International Conference on Disaster Management and Human Health Risk’, pp.181-194, 23 -25 September 2009, New Forest, UK.

## **PREDICTING THE BEHAVIOR OF STEEL FIRE DOORS SUBJECTED TO FIRE ENDURANCE TEST**

Mahmood Tabaddor <sup>a</sup>, Sanjay Jadhav <sup>b</sup>

<sup>a</sup> Predictive Modeling CoE, Corporate Research, UL LLC

### **Abstract**

The ability to predict the thermal and structural performances of steel fire doors subjected to fire tests described in safety standards via the finite element method is investigated. These doors must withstand high temperatures without deforming in a manner where gaps might appear allowing flames and smoke to pass through. There are 2 key challenges for modelling: first, deciding how much complexity to include since the tests involve high temperatures and possibly times lasting hours, and second, obtaining the needed material properties over the temperature range seen during the tests. In this investigation, we focus on, one aspect of complexity, the importance in capturing the thermal contact between steel parts within the fire door to improve the predictability of the finite element model.

**Keywords:** Fire Doors, Fire, Structures, Finite Element Analysis, Thermal Contact

### **INTRODUCTION**

Knowledge about the fire resistance of structural components can be derived through physical or virtual testing. Physical testing is expensive due to the destructive nature of the tests. Also physical testing can be limiting due to instrumentation constraints. On the other hand, virtual testing or computer modelling, techniques such finite element analysis (FEA), provide a very data rich output but require tremendous input information such as material properties, loadings, boundary conditions and other details that an experimenter typically need not know in order to conduct experiments.

One method for evaluating the fire resistance of building components, such as fire doors, follows test methods described by fire safety standards (Iwankiw, 2000). Though there have been many numerical and experimental investigations studying various aspects of the standard fire resistance, in this study, we focus on predicting the performance of steel double fire doors subjected to the standard fire test such as described by UL 10 (UL 10 B, 1997). The FEA technique is employed building on previous modelling of steel fire doors (Tabaddor et al., 2009).

### **1 FIRE RESISTANCE TESTING**

The presence of fire doors within a building is meant to prevent the spread of fire with a secondary influence on the smoke and heat exposures to building occupants. As a means of evaluating fire resistance, fire door assemblies are tested according to standards such as the UL standard for fire safety, UL 10B, 'Fire Tests of Door Assemblies' (UL 10B, 1997).

This paper only focuses on the performance of the fire door during the Fire Endurance portion of the test, which is described next. As part of the preparation for this test, the fire door along with supporting structure such as frame and walls are constructed according to specified instructions. The door is part of a restraining frame (Fig. 1) that fits onto the furnace subassembly. With the assembly in place, the fire doors are subjected to a heat flux from gas burners which generate temperatures according to a standard time-temperature curve shown in Fig. 2 (ASTM, 2007). Some tests include a pressurized furnace to capture additional forces

generated during a fire. The conditions of acceptance for the UL 10B standard cover the movement of the door and flaming on the unexposed side.

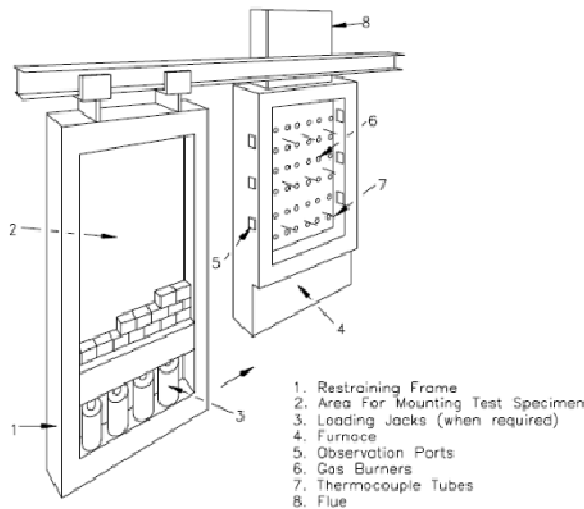


Fig. 1 Schematic of Setup

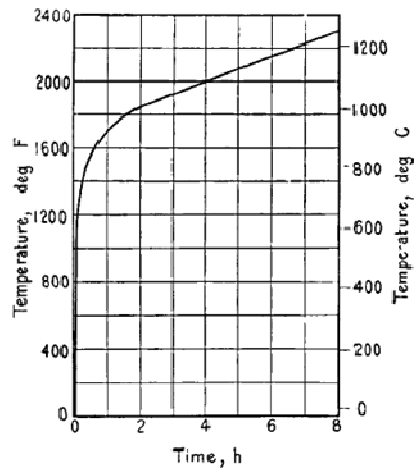


Fig. 2 Standard time-temperature curve

## 2 FINITE ELEMENT MODEL

To build a finite element (FE) model of a fire door assembly, it is prudent to assess the necessary amount of detail that should be captured. As the full complexity of the fire door assembly is transferred into the FE model, both the model-building task and the time to solve the analysis increase substantially.

Fire doors generally consist of steel faces, steel stiffeners and filler insulation material. The fire door in this study was a double door. The door without a lock handle is called the inactive leaf. It included latching bolts that can lock the door into the frame at the top and bottom. During the test, the inactive leaf was latched to the frame. The other door with the lock handle is called the active leaf. The active leaf included the door lock, which was a latch bolt that engaged into the inactive leaf. The inner edges of the two doors facing each other are known as the meeting edge. The gap at the meeting edge was monitored during the test. In addition, fire resistance tests require inclusion of the frame and hinges that connect fire doors to the frame for an assessment of the fire performance of the entire fire door assembly. Some fire doors have windows and glazing. The fire door in this test did not include windows. The general assumptions guiding the model building process were as follows:

- (i) The wall and frame holding the fire door are rigid during the entirety of the test.
- (ii) The thermal insulation does not provide any structural strength to the fire door.
- (iii) The coupling between thermal and structural response is one-way, that is, the structural response has negligible effect on the thermal response.

The software of choice was ANSYS (ANSYS, 2011). For the FE mesh, shell elements were chosen for both the thermal and structural analyses (except for the insulation materials). These 2-D elements are more computationally efficient than 3D elements and are applicable in cases where the thickness of a component is much smaller than its other dimensions (Bathe, 1995). Some idea of the level of detail in the model can be seen in Fig. 3 and Fig. 4. Thermal and mechanical properties over the temperature range of test were found from several public resources (Milke, 2002; NIST, 2005) and can be found in (Tabaddor et al., 2009).

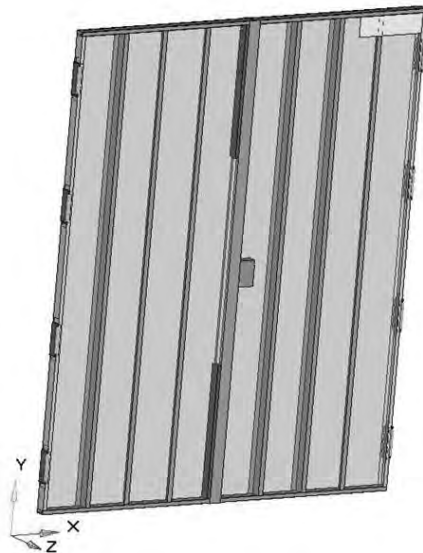


Fig. 3 Solid model of double steel fire door

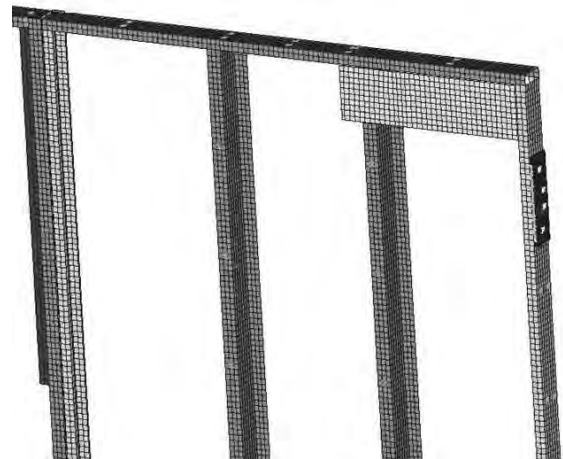


Fig. 4 Detail of connection in FE model

### 3 THERMAL CONTACT

For the transient thermal analysis, it was found that detail of the thermal contact between mating parts was very critical. For example, the steel stiffener is mechanically joined to the steel panel via welds. Clearly the welds will be a critical transfer path. However, depending upon tolerances and deformations, the actual thermal contact region is likely larger and changing. In the fire door, the metal portion on the face exposed to the furnace will be heated via radiation and convection. Heat then flows through the internals mostly through conduction ignoring air gaps between parts and within the insulation. However, due to the differences in thermal conductivities, the steel parts are the most thermally conductive paths and so mating between steel parts can affect the thermal results and subsequent structural predictions. So in this investigation, we developed several different thermal contact configurations.

For the first thermal contact configuration, we assumed only thermal contact via spot welds. Clearly this will lead to the least heat flow through the interior of the door to the unexposed side. The next thermal contact configuration relies upon thermal links placed between all metal surfaces that are expected to be in contact. With the inclusion of thermal links, now an additional variable, the thermal resistance of the thermal link is a required input. As a starting point, we selected the thermal conductivity of air which is  $2.0 \text{ W/(m K)}$ . In this case, now more heat will flow through the stiffeners. Fig. 5 provides some detail on the various thermal contact configurations.

### 4 THERMAL RESULTS

Fig. 6 show a snapshot of the temperature contours at 15 minutes for both the unexposed and exposed surfaces of the fire door assembly for the metal-to-metal thermal contact configuration of only welds. For the unexposed side, hot spots include the lock and the edges of the door. As mentioned previously, the lack of welds on the unexposed side reduces the thermal paths through the stiffeners to the panel. For the exposed surface, cool spots include the lock and edges. Temperatures on the exposed surface reach as high as  $800^\circ\text{C}$ . On the unexposed side, the model predicts that most of the panel surface is below  $130^\circ\text{C}$ . The same general patterns holds as the door heats up further.

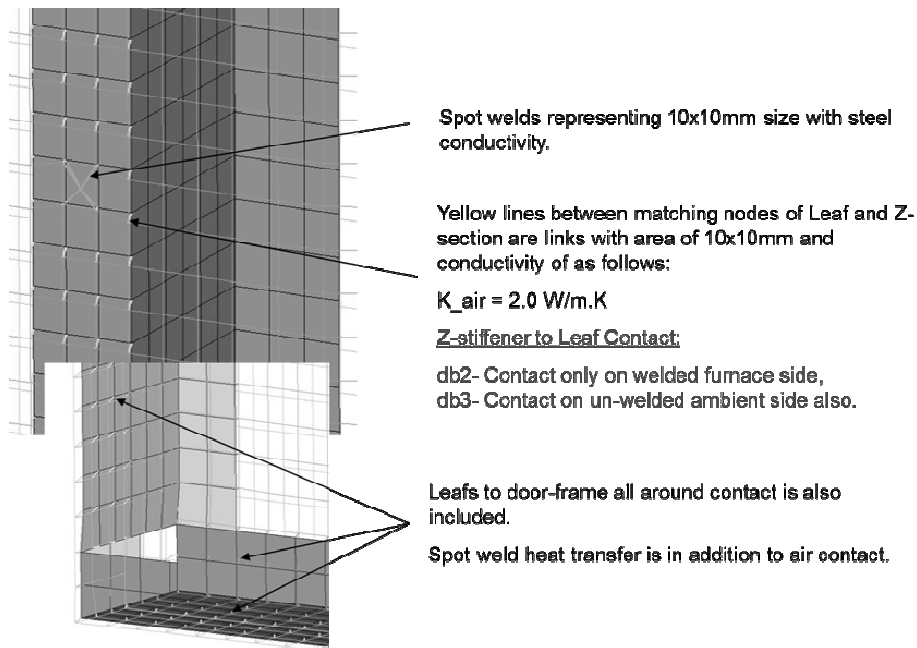


Fig. 5 Description of different thermal contact configurations

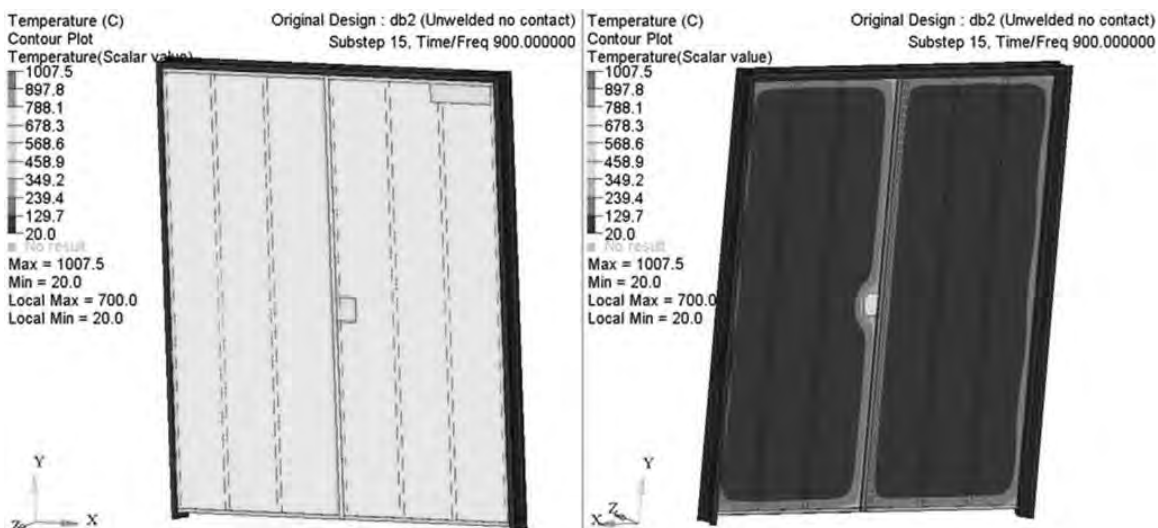


Fig. 6 Temperature contours on exposed (left) and unexposed (right) surfaces at 15 minutes with only thermal contact through the welds

Fig. 7 shows the temperature at 3 different points along one of the unexposed panels, similar to measurements taken during the test. The plot shows that the temperatures on the unexposed side are considerably lower than the temperatures measured during the test. Clearly, this model with no metal-to-metal thermal contact between stiffener and unexposed panel under-predicts temperatures. Despite the presence of welds on only one side of the stiffeners, it is expected that there is more metal-to-metal contact.

Fig. 8 shows the temperature at 3 different points on the unexposed panel similar to measurements taken during the test. As expected, the temperatures on the unexposed panel are much closer to the test temperatures as compared to the previous thermal model which only assumed thermal contact through welds. Clearly, metal-to-metal contact is present and may be changing as the door deforms. This effect is especially more difficult to capture in the absence of welds that would help maintain contact between the stiffener and door panels.



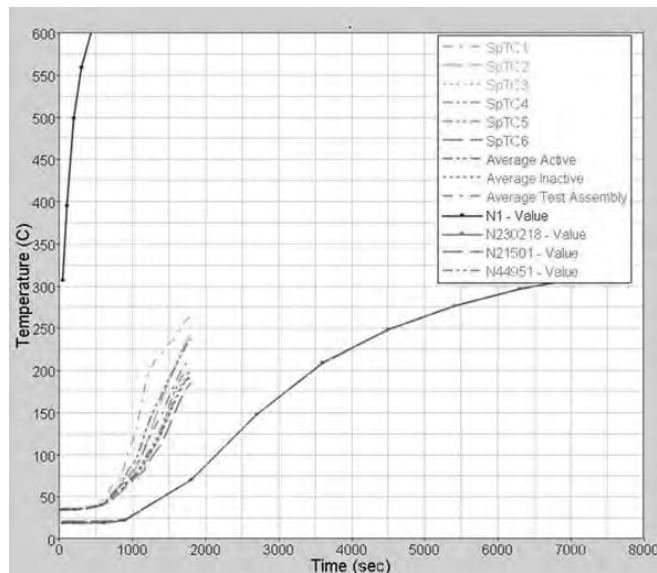


Fig. 7 Temperature over time from unexposed surface with weld only thermal contact

## 5 STRUCTURAL RESULTS

For the structural analysis, it was not necessary to run a transient analysis. Instead, the thermal results at different particular points in time were fed into the structural model to establish heat loads and material properties. This approach is computationally more efficient so that if it shows promise in predicting the structural deflections, a great advantage is gained. However, as noted in the thermal FE results section, the temperature predictions from the original door design show sensitivity to how the thermal contact between metal parts. Therefore the structural analysis results for the original fire door design will show the effect of varying thermal contact conditions. Of course, with this level of uncertainty in the details of the fire door construction, the structural results may not provide accurate quantitative deflection predictions. In addition, the structural analysis was linear not accounting for geometric or material nonlinearities or contact nonlinearity. A nonlinear analysis requires more model building and computational effort and was outside of the scope of the project. Nevertheless, there is value in running a structural analysis for this original door design and comparing the results with the concept fire door design. It is expected that if significant differences exist that they will reflect the proper trends in fire performance simply due to design changes.

Fig. 8 shows the deflection plot for the different cases. The key pattern repeats at all other times, where the basic global feature is bowing of the door towards the furnace. Recall that once the thermal contact condition is set, it does not change. The plot in Fig. 8 compares the deflections at the same point for the original fire door design and the concept fire door design. The first thermal contact configuration (labeled db2) results in higher deflections than the weld/thermal link contact configuration (labeled db3). This suggests that a higher temperature gradient through the thickness of the door will lead to higher deflections from greater bowing of the doors. This effect is documented in the published literature.

Examining the results over time show that deflections increase rapidly during the early part of the test and then exhibit a gradually rising form. Though the deflection values are plotted up to 1 hour, the relative movement of stiffeners and panels for this first-level of modeling is not expected to be applicable beyond 30 minutes. Furthermore, the actual values are not reliable without full model validation. However, the qualitative features of the results for the first 30 minutes are expected to be insightful for design decisions.

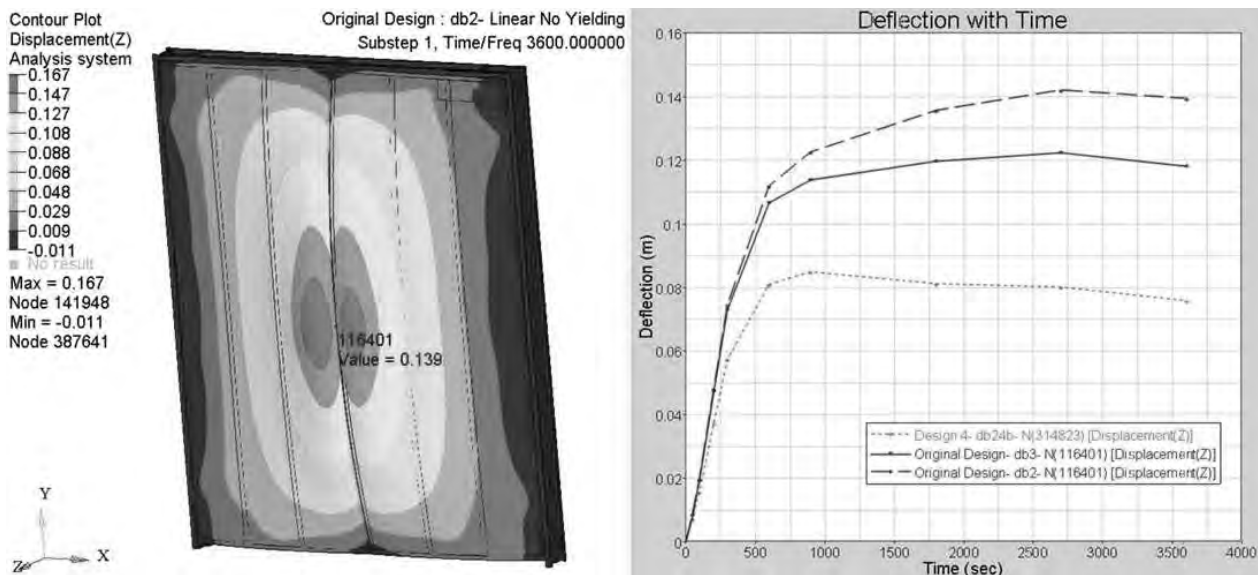


Fig. 8 Normal deflection contours (left) and deflection time plot (right) for 2 different thermal contact configurations and a baseline design

## REFERENCES

- ANSYS User's Guide, ANSYS Inc., Release 12.0, 2011.
- ASTM E119-07, Standard Test Methods for Fire Tests of Building Construction and Materials, ASTM International, 2007.
- Bathe, K.J., Finite Element Procedures, Prentice-Hall, Englewood Cliffs, 1995.
- Iwankiw, N., 'Fire Resistance Design', Practice Periodical on Structural Design and Construction, Vol. 12, Issue 1, February 2007, pp. 3-8.
- Milke, J., "Analytical Methods for Determining Fire Resistance of Steel Members", SFPE Handbook of Fire Protection Engineering, Third Edition, 2002.
- "NIST NCSTAR 1-3: Mechanical and Metallurgical Analysis of Structural Steel", Final Reports on the Collapse of the World Trade Center Towers, National Institute of Standards, 2005, <http://wtc.nist.gov>.
- Tabaddor, M., Gandhi, P.D., 'Thermo-mechanical analysis of fire doors subjected to a fire endurance test', Journal of Fire Protection Engineering, Vol. 19, 2009, p. 51.
- UL 10B Standard for Safety for Fire Tests of Door Assemblies, Ninth Edition, Underwriters Laboratories Inc, 1997.

# NUMERICAL SIMULATION OF NATURAL FIRE IN AN INDUSTRIAL BUILDING CONSIDERING EARTHQUAKE DAMAGE OF NON-STRUCTURAL MEMBERS

Kalliopi Zografopoulou<sup>a</sup>, Daphne Pantousa<sup>a</sup>, Euripidis Mistakidis<sup>a</sup>

<sup>a</sup>Laboratory of Structural Analysis and Design, Dept. of Civil Engineering, University of Thessaly, 38334 Volos, Greece, web page: <http://lsad.civ.uth.gr>

## Abstract

The aim of this paper is to examine the impact of post-earthquake non-structural damages on the development of natural fire in an industrial building, used as storage area. Parametric fire scenarios with various levels of damage (window and door destruction, sprinkler system malfunction) are simulated on a 3D model of the structure, using the Computational Fluid Dynamics software FDS. The fire development is studied and temperature distributions on the structural members are obtained.

**Keywords:** fire-afterearthquake, steelstructures, natural fire

## INTRODUCTION

Post-earthquake non-structural damage can alter significantly the fire behaviour of a building and downgrade the structural safety of the construction. This study examines the impact that such damage has on the development of natural fire, in this case in an industrial building, used as storage area.

The officially approved procedures for estimating the thermal loads for the structural design of industrial facilities under fire require advanced modelling tools for the simulation of the natural fire phenomenon, like the one/two-zone model or the use of Computational Fluid Dynamics (CFD). Simpler approaches such as the parametric temperature-time curves given in Eurocode1,part1-2areonly valid for small compartments, under 500 m<sup>2</sup> and non-industrial occupancies. In this study, CFD analysis is performed with the Fire Dynamics Simulator (FDS) software, to model the fire development in the building. FDS is a CFD code for the simulation of thermally driven flows with an emphasis on smoke and heat transport from fires. The CFD-FDS has two main advantages over the two-zone model: the ability to insert a detailed geometry with a custom-defined burn behaviour of the combustible materials and secondly, the capability of providing time-history temperature results at any position of the modelled structure.

## 1 MODEL

### 1.1 Properties of the examined building

The building under examination has a floor plan of 80x40m with a height of 10 m plus a 2m two-ridge roof. The space is divided in two main compartments, the storage area with dimensions 63x40 m and a 2-storey office/exhibition area of 17x40 m with heights 4 and 6 meters respectively (Fig. 1).The storage compartment has a total of 247 m<sup>2</sup> of windows located in a high row on each of the 63m walls. On the ground and first floor of the office/exhibition area are additional 94m<sup>2</sup>and 58m<sup>2</sup> of windows. In the storage area the supplies are stored in 6.25 m high racks, comprised mainly of electrical appliances and spare parts stored inside cardboard boxes. The structural system of the building consists of seven double-span steel frames. The walls and roof are composed of typical insulation panels. The

base is standard industrial concrete flooring. The two compartments communicate through a 5.00x3.00 m fireproof door. Also, there is a water sprinkler system installed in the storage area.

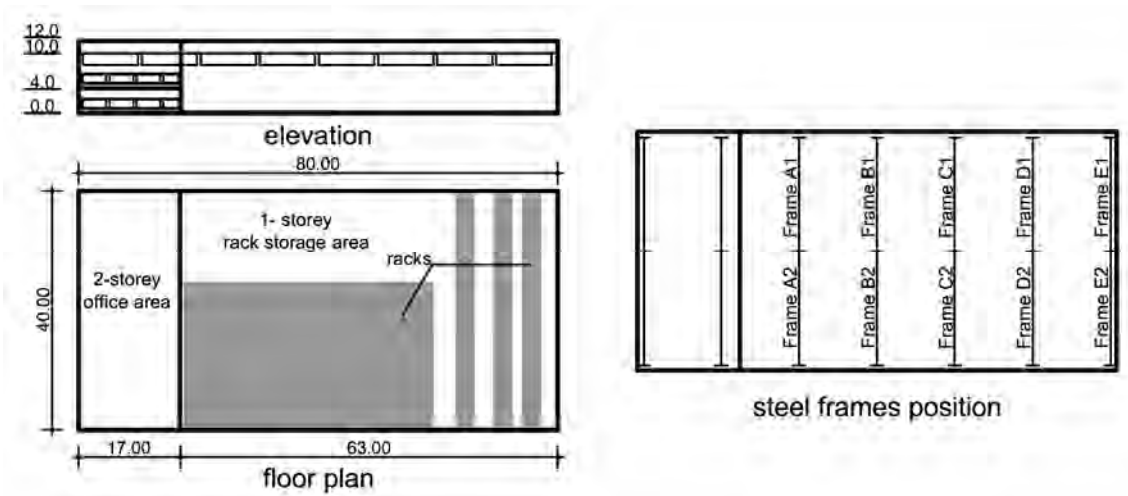


Fig. 1 Building description (dimensions in meters)

## 1.2 Simulation

A full scale 3D model is developed, representing the basic geometry of the building and the construction materials with their thermal properties (steel, concrete, 10cm XPS insulation). A key parameter of the fire simulation is the description of the combustion behaviour of the materials in the storage area. Due to the complex structure of the burning objects, a pyrolysis model would induce uncertainties in the analysis. To avoid such uncertainties a custom Heat Release Rate (HRR) curve is chosen to represent the combustion. The experiments of A. Lönnemark and H. Ingason on fire spread in warehouses (Lönnemark et al., 2005) provided HRR curves of rack storage fire tests that correspond to the storage conditions in the building under examination. The experiments were conducted in 1:5 scale so the results are modified according to the scaling laws, regarding the HRR and the corresponding time (Fong et al, 2003).

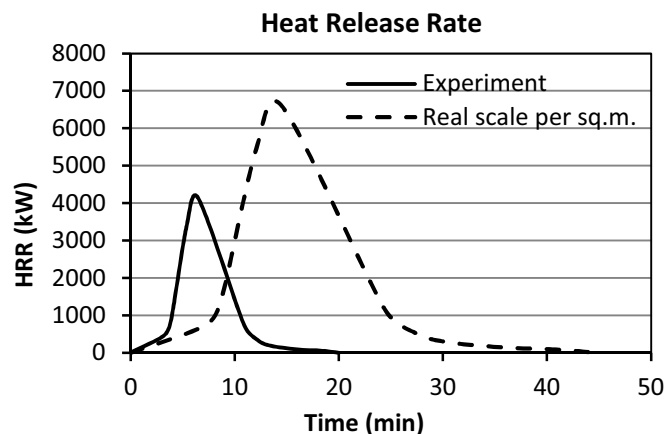


Fig. 2 Experiment and modified real scale Heat Release Rate curve of the rack storage units

The storage racks, are modelled by 156 heat release sections in parallel rows, at a distance of 1.20m, covering the designated area in the floor plan. In order to simulate the fire spread from one rack unit to another, a criterion of the temperature conditions that would ignite the

materials is used. Each heat release section is activated only when the temperature over the section reaches 250°C, the auto ignition temperature of wood (Babrauskas, 2002) and paper (Graf, 1949). This concept is implemented by connecting the activation of each heat release section to a temperature sensor 3m above the centre of the section. This results in a more gradual activation of the heat release sections, dependent on the temperatures of the compartment. It is assumed that the fire does not spread through flames but through radiation and convection flux that starts the pyrolysis of the cellulose materials which produces the combustible gases. A required condition for the combustion to occur is an oxygen index >0.15. If this is not satisfied the fire is suppressed.

The computational mesh consists of 225,000 cells of 0.80x0.80x0.60 m and extends 10 m around and 3m above the building with open boundaries at the end. As ignition of the fire, two of the heat release units in the middle of the compartment are set active in the beginning of the simulation, in order to provide the equivalent amount of heat that was observed at the experiment. The total simulation time is 1 hour and the calculation time steps are set not to exceed 0.1 sec.

### 1.3 Parametric Fire Scenarios

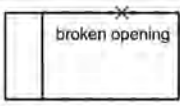
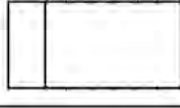
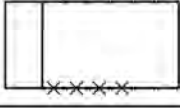


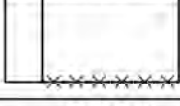

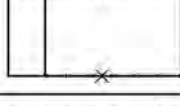
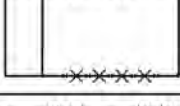

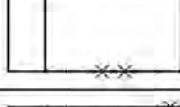
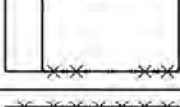

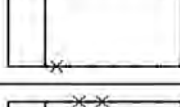
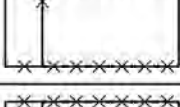
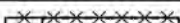
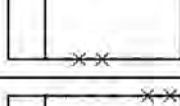


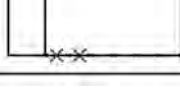
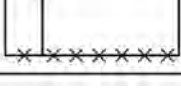

Fire scenario description	Scenario name		
	% of damaged openings		
	% of damaged openings / wall area		
	% of operational water sprinkler system		
<b>SC - 00</b>		<b>SC - 030c</b>	
0 %		27 %	
0 %		3.50 %	
0 %		0 %	
<b>SC - 07</b>		<b>SC - 045</b>	
7 %		43 %	
0.92 %		5.53 %	
0 %		0 %	
<b>SC - 015a</b>		<b>SC - 060a</b>	
14 %		57 %	
1.84 %		7.38 %	
0 %		0 %	
<b>SC - 015b</b>		<b>SC - 060b</b>	
14 %		57 %	
1.84 %		7.38 %	
0 %		0 %	
<b>SC - 015c</b>		<b>SC - 100</b>	
14 %		100 %	
1.84 %		12.96 %	
0 %		0 %	
<b>SC - 030a</b>		<b>SC - 100sp1</b>	
27 %		100 %	
3.50 %		12.96 %	
0 %		100 %	
<b>SC - 030b</b>		<b>SC - 100sp2</b>	
27 %		100 %	
3.50 %		12.96 %	
0 %		50 %	

Fig. 3 Parametric Fire Scenarios

Three types of non-structural “damage” were introduced to the model:

- window breakage, which modifies ventilation conditions,
- fireproof door damage which modifies ventilation and alters the fire compartment
- malfunction of the water sprinkler system.

In total, 14 fire scenarios were tested. Of those, 12 included variations in the ventilation conditions by changing the number and placement of the broken windows and damage of the fireproof door. The remaining 2 had full and half operational the water sprinkler system. A visual description of the scenarios is given in Fig. 3. For every scenario, the following parameters are given: percentage of broken openings to the total area of openings in the storage compartment, percentage of the broken openings to the total wall area, position of the broken openings and percentage of the operational water sprinkler system.

## 2 OUTPUT RESULTS

Tab. 1 Duration (min) of temperature exceeding 600°C on the steel frames for every scenario

Duration over 600 °C	Frames										AVERAGE (min)	ST.DEV. (min)	
	A1	A2	B1	B2	C1	C2	D1	D2	E1	E2			
SC-00	0	2	4	2	0	3	0	0	0	0	0	1	1.4
SC-08	8	2	4	4	0	2	0	0	0	0	0	2	2.7
SC-015a	7	2	12	7	6	2	0	0	0	0	0	4	4.0
SC-015b	2	4	3	14	2	4	0	0	0	0	0	3	4.0
SC-015c	5	8	5	5	0	2	6	0	17	0	0	5	5.0
SC-030a	30	20	44	36	29	26	10	9	6	4	4	21	13.1
SC-030b	8	28	7	20	18	4	40	12	41	20	20	20	12.4
SC-030c	8	30	10	36	6	19	3	5	0	3	3	12	11.6
SC-045	13	28	15	38	14	38	7	37	13	32	23	23	11.6
SC-060a	42	37	46	44	42	41	38	38	35	26	39	39	5.3
SC-060b	43	46	42	40	37	33	37	39	37	38	39	39	3.4
SC-100	20	23	21	36	17	23	15	18	15	16	20	20	6.0
SC-100sp1	0	0	0	0	0	0	0	0	0	0	0	0	0.0
SC-100sp2	0	0	0	5	0	0	0	0	0	0	1	1	1.7

Tab. 2 Average duration (min) and st. deviation of temperature levels on the steel frames

Duration over (minutes)	600 °C		700 °C		800 °C		900 °C		1000 °C	
	average	st. dev.	average	st. dev.	average	st. dev.	average	st. dev.	average	st. dev.
SC-00	1.1	1.4	0.2	0.6	0.2	0.6	0.2	0.6	0.2	0.5
SC-08	2.1	2.7	0.7	1.1	0.2	0.6	0.2	0.7	0.2	0.5
SC-015a	3.6	4.0	1.5	2.7	0.8	1.8	0.2	0.7	0.2	0.7
SC-015b	2.9	4.0	1.7	2.4	0.9	1.9	1.2	2.3	0.8	1.7
SC-015c	4.9	5.0	1.9	3.4	2.0	4.1	0.8	1.4	0.5	0.9
SC-030a	21.3	13.1	8.2	10.0	3.3	5.7	1.9	4.1	1.6	3.4
SC-030b	19.8	12.4	8.2	8.8	5.1	7.5	3.8	6.8	2.0	4.4
SC-030c	11.9	11.6	4.1	4.1	1.9	2.0	1.3	1.6	1.0	1.2
SC-045	23.4	11.6	8.4	5.9	4.5	3.1	3.1	2.3	2.0	1.7
SC-060a	38.9	5.3	23.2	12.2	11.8	9.7	8.3	7.0	6.2	6.7
SC-060b	39.3	3.4	22.8	10.1	11.9	6.9	9.4	6.3	6.8	5.9
SC-100	20.4	6.0	17.8	4.9	15.9	3.9	12.0	4.9	6.6	3.4
SC-100sp1	0.0	0.0	0.0	0.0	0.0	0.0	0.0	0.0	0.0	0.0
SC-100sp2	0.53	1.66	0.39	1.24	0.39	1.24	0.38	1.09	0.14	0.44

Temperature time-histories of the members of the 10 steel sub-frames of the storage compartment which was mainly affected by the fire, are obtained for each fire scenario. The time histories of the frames are difficult to be compared. Instead, the total time that every

frame was subjected to temperatures over 600°C (Table 1), 700°C, 800°C, 900°C and 1000°C is summarized. Due to the non-uniformity of the ventilation and fire development, a number of frames are affected at a different level for every scenario. To include both the degree and spatial extent of the thermal impact on the overall structural system, the average time and standard deviation of the exposure of the frames is computed for every temperature level (Table 2). Among the scenarios with the highest average, the most severe is determined by the smallest standard deviation which indicates that more of the frames are affected by the fire and contribute to the average temperature duration. Also the total HRR curves of the fire scenarios are presented in Fig. 4.

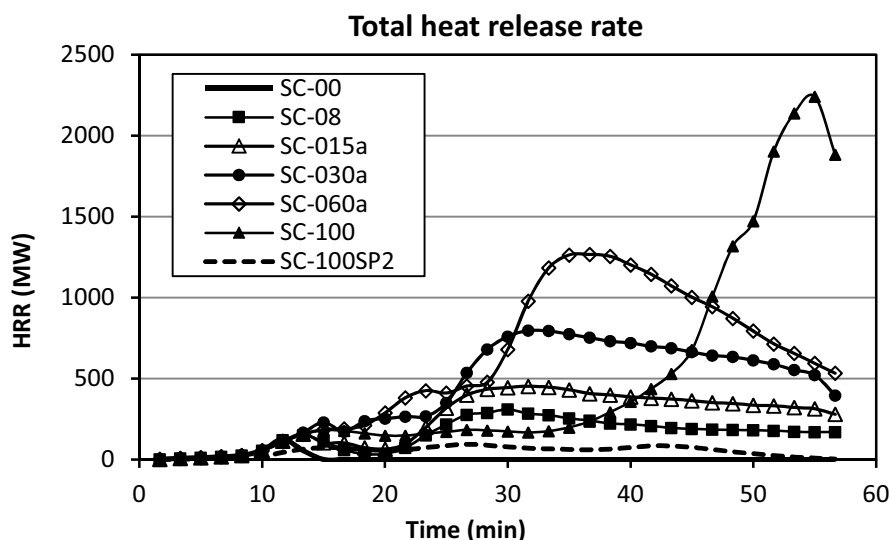


Fig. 4 Total heat release rate for the considered fire scenarios

### 3 DISCUSSION

For the temperature level of 600°C (Table 1) and 700°C (Table 2) the thermal exposure of the steel frames rises as the number of broken windows increases, but reaches a maximum for 60% window damage in scenario SC-060b. As expected, open windows provide fresh air to the fire after the oxygen within the compartment is consumed. Therefore, after some time, the combustion takes place in the vicinity of the openings and affects stronger the nearby frames. As a result, the arrangement of the open windows can lead to a more contained or spatially extended fire (scenarios SC-030a/b/c and SC-060a/b). The scenarios SC-030a/b/c have the same degree of total damage, about 30%, but the position of the broken windows differs. In scenario SC-030a the broken windows concentrate on the right side of the floor plan, in SC-030b are placed diagonally on the opposite walls and in SC-030c only on one side. In Table 1, where the 600°C level is presented on the sub-frames in more detail, it is evident that the damaged windows determine which sub-frames are more affected by the fire. In SC-030a the frames A,B,C are mostly affected, in scenario SC-030b all the frames are affected, especially the ones closer to the openings, and in scenario SC-030c it is clear that the sub-frames A2,B2,C2,D2, placed on the side of the open windows, are the most exposed to heat. The same effect is observed in scenarios SC-015a/b/c, where in scenario SC-015c (with the windows placed diagonally) the most affected frames are the ones next to the windows (frames A2 and E1). Also, the longer distance between the combustion positions (the location of the open windows) generates air flow that spreads in the whole compartment and produces further combustion.

The decrease in the heat exposure that is observed for the temperature level of 600°C for the scenario with all the openings damaged (SC-100), is a result of the slower fire development that has a very steep growth rate after 45 minutes in the simulation (Fig. 4). This situation

leads to higher temperatures with smaller duration and is evident in the higher temperature levels of 800°C, 900°C and 1000°C (Table 2). In these temperature levels the scenario with all the windows broken (SC-100) appears to be the most detrimental, regarding the total thermal exposure. However, the fact that this fire has a significantly slower growth rate, which escalates after 40 minutes in the simulation, provides a better chance of being extinguished by conventional means and the fire-fighting crew. This is probably a result of the air flow that brings colder fresh air in the compartment from the beginning of the simulation and disperses the released heat from the burning racks, increasing the time it takes for the temperature to reach 250°C and activate the rest of the heat release sections. Thus, if the fire is extinguished manually within 40 minutes, the SC-060 leads to higher fire loads. The 100% window damage scenario SC-100 is critical only if the fire is allowed to fully develop and its duration exceeds 1 hour.

Regarding the operation of the sprinkler system, even partially functional can result in the suppression or restriction of the fire, but that highly depends on whether the functional part covers the fire ignition point. The total damage of the sprinkler system is the main reason that extended fire occurs in the compartment so designing a sprinkler system that can withstand seismic displacements is a key factor to the fire design of an industrial facility.

The fire development depends highly on the air supply in the compartment and can even be self-suppressed if there is no ventilation at all (SC-00). A change in the ventilation conditions can be a result of non-structural damage that is most likely to occur during an earthquake. In this case, a fire in addition to a non-functional fire-extinguishing system, can lead to temperatures of magnitude more than 1000°C which are not expected to arise during the fire design process, where the various systems are considered undamaged and fully functional.

#### **4 CONCLUSIONS**

Post-earthquake non-structural damage influences greatly the development of natural fire in an industrial building, especially when combustible materials are in abundance. Although fire loads are not combined in the design with earthquake loads, post-earthquake fire is a probable event and post-earthquake non-structural damage has to be taken into account in the fire design process.

The most influential damage is the malfunction of the active fire protection systems, which are not necessarily designed to withstand seismic forces and displacements. A revision of the design of such systems considering earthquake performance is advised.

Window damage causes change in the ventilation conditions and could lead to temperatures different than the ones considered in the design process. As a result, it is recommended that the fire retardant coating of the steel members should be adequate for the temperature time-histories produced by fire not suppressed by an extinguishing system.

The CFD analysis is a useful tool that can aid the fire design of buildings which do not conform to the provisions for a simpler design approach, though it should be used with caution, as is the case for all advanced computational methods.

#### **REFERENCES**

- Babrauskas V., Ignition of Wood: A Review of the State of the Art, J. Fire Protection Engineering 12, 163-189, 2002
- Eurocode 1: Actions on structures – Part 1-2: General actions – Actions on structures exposed to fire
- Fire Dynamics Simulator and Smokeview, FDS-release5.5.3 SMV-release5.6, website:<http://code.google.com/p/fds-smv/>, 2012
- Graf S. H., Ignition Temperatures of Various Papers, Woods, and Fabrics (Oregon State College Bull. 26), Oregon State College, Corvallis (1949)



- Fong Y.Y. and Fong N.K., Scale Modelling Of Smoke Movement In Linear Atrium, International Journal on Engineering Performance-Based Fire Codes, Volume 5, Number 4, p.149-151, 2003
- Ingason, H., "Experimental and Theoretical Study of Rack Storage Fires", In Department of Fire Safety Engineering, Lund University, Lund, Sweden, 1996.
- JukkaVaari, SimoHostikka, TopiSikanen&AnttiPaajanen, Numerical simulations on the performance of water-based fire suppression systems, VTT Technology 54, 2012
- LönnermarkA, Ingason H., Fire Spread in Large Industrial Premises and Warehouses, SP Swedish National Testing and Research Institute, 2005

# **ROBUSTNESS OF THE VESUVIAN ROOFS UNDER THE COMBINED OVERLOAD AND HIGH TEMPERATURES DUE TO AIR FALLS**

Beatrice Faggiano <sup>a</sup>, Antonio Formisano <sup>a</sup>, Federico M. Mazzolani <sup>a</sup>

<sup>a</sup> University of Naples "Federico II", Dept. of Structures for Engineering and Architecture, Naples, Italy

## **Abstract**

During an explosive eruption, a construction is hit by several actions, always associated to elevated temperatures, causing fires, possible explosions and reduction of the mechanical properties of the structural materials. In this paper, the attention is focused on the analysis of a specific volcanic event, the so-called air fall deposits, generally falling from the eruptive column due to gravity. In particular the robustness against the air fall deposit of the most common roofing structures, typically made of timber, steel and reinforced concrete, in the Vesuvian area is evaluated. Consequently, some protection systems for mitigating the effects of the combination of overloading and high temperatures are identified.

**Keywords:** explosive eruptions, Vesuvian roofs, ash fall deposits, high temperature, robustness evaluation, mitigation systems

## **INTRODUCTION**

Explosive volcanoes, like Vesuvius (Naples, Italy), are extremely dangerous. They are characterized by the violent emission of the so-called eruptive column, formed by gas-solid dispersal, rising vertically from the vent, due to the initial high pressure of the magmatic gas.

An explosive eruption occurring close to an urban area generates several actions that possibly hit a construction: the volcanic earthquake; the additional gravity load on roofs produced by pyroclastic deposits; the horizontal dynamic pressures on façades due to pyroclastic flows and lahars; the impact produced by flying fragments (Mazzolani et al., 2009a,b). All these are associated to elevated temperatures, which either can trigger fires and explosions or induce degradation of the mechanical properties of the structural materials.

Down the century, the volcanic eruptions have produced many fatalities and economic losses all over the world. In Europe, the Vesuvius area is characterise dat highest risk: a probable eruption of Vesuvius menaces the surrounding urban zones, which are very much densely populated, with about 600,000 inhabitants. This hazard situation of the Neapolitan volcano motivated the core committee of European project COST Action C26 "Urban Habitat Constructions under Catastrophic Events" (2006-2010) to introduce the volcanic vulnerability assessment of the Vesuvius area as a case study within the research topics, with the twofold general objectives: the robustness evaluation of the urban environment towards a Vesuvian eruption and the identification of simple and economical mitigation interventions. In this context, the present paper specifically deals with the evaluation of the effects of the combination of overloading and high temperature due to pyroclastic deposits on roofing structures, consequently, leading to the identification of possible mitigation systems.

## **1 NATURE AND MODELLING OF AIR FALL DEPOSITS**

The main products of an explosive eruptions are the pyroclasts, originated by the magma fragmentation. Their deposits are generically called tephra and divided in three basic types: air fall, pyroclastic flows and surges.

The air fall (or tephra fall) deposits are formed by the accretion of clasts, either falling by gravity from the eruptive column or throwing directly in surrounding areas from the crater, according

to ballistic trajectories. Besides, the deposits of pyroclastic flows and surges are produced by gas-solid dispersions with high or low concentration of particles, respectively, which move along the volcano surface, following either the collapse of the eruptive column, or a directional explosion for the sliding of a volcano part, or a lateral explosion at the bottom of a lava dome (Nelson, 2010).

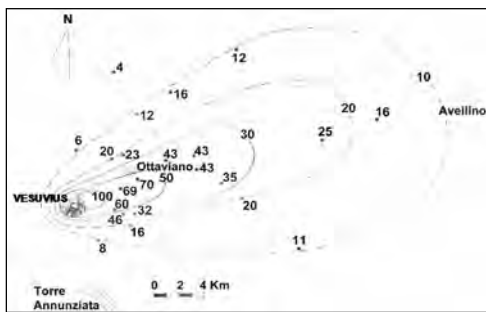
During violent explosive eruptions (Plinian and sub-Plinian), large deposits of tephra fall can cover an area of elliptical shape around the crater, reaching also large distances, according to the direction of stratospheric winds (INGV-OV, 2012). Contrary, moderately explosive eruptions can produce deposits of clasts, whose distribution is symmetrical around the crater, because the launches are not sufficiently high to be influenced by the wind. Generally, the thickness of air fall deposits decreases with the distance from the eruptive centre.

The air fall deposits action on the ground level can be considered as a gravitational distributed load, which can be estimated as it follows:

$$\mathbf{q}_G = \rho \cdot \mathbf{g} \cdot \mathbf{h} \quad (1)$$

where  $\mathbf{g}$  is the gravity acceleration ( $9.81\text{ms}^{-2}$ ),  $\mathbf{h}$  and  $\rho$  are the deposit thickness (m) and density ( $\text{kNm}^{-3}$ ), respectively. The latter depends on the composition and compactness of pyroclasts and the deposit moisture, which is weather dependent. Therefore  $\rho$ , ranges, according to its compactness, from 4 to  $16\text{kNm}^{-3}$  in dry conditions, from 8 to  $20\text{kNm}^{-3}$  in damp conditions (Spence et al., 2005).

The air fall deposits action on the roofs can be modelled by similitude with the snow load (Faggiano et al. 2013), considering  $\mathbf{q}_G$  as characteristic value of the tephra load. In particular with reference to the 1631 sub-Plinian Vesuvian eruption, it being considered in the current Evacuation Plan by the Civil Protection, in Fig. 1 the isopaches of the air fall deposits, which give the distribution of the deposit thickness, are depicted. In the same figure, the air fall deposit loads on the ground ( $\mathbf{q}_G$ ) and on the roof ( $\mathbf{q}_R$ ), corresponding to  $C_E=1$ ,  $\rho = 14\text{kNm}^{-3}$ , different deposits thickness  $\mathbf{h}$  and typical pitch angle  $\alpha$ , according to the technical Italian code for the snow (M.D., 2008), are indicated. In addition to the relationship (2), the model of the air fall deposits action should be completed considering the high temperatures ( $200\text{-}400^\circ\text{C}$ ) of the clasts.



h cm	$\mathbf{q}_G$ $\text{kNm}^{-2}$	$\mathbf{q}_R$			
		$\alpha=0^\circ$ $\text{kNm}^{-2}$	$\alpha=20^\circ$ $\text{kNm}^{-2}$	$\alpha=30^\circ$ $\text{kNm}^{-2}$	$\alpha=45^\circ$ $\text{kNm}^{-2}$
10	1.4	1.1	1.1	1.1	0.6
20	2.8	2.2	2.2	2.2	1.1
30	4.2	3.4	3.4	3.4	1.7
50	7.0	5.6	5.6	5.6	2.8
100	14.0	11.0	11.0	11.0	5.6

(a)

(b)

Fig. 1 Air fall deposits isopaches (cm) (a) and loads on the ground ( $\mathbf{q}_G$ ) and on the roof ( $\mathbf{q}_R$ ) (b), referred to the 1631 sub-Plinian Vesuvian eruption

## 2 IN SITU SURVEY AT THE VESUVIAN URBAN AREA AND CASE STUDIES

The pilot area was identified in Torre del Greco, the most populous town in the volcanic area (about 90,600 inhabitants). Within the COST Action C26, two missions were organized, for investigating three different urbanized zones (De Gregorio et al., 2010), involving members of the partner countries, with the cooperation of the PLINIVS Centre (Hydrological, Volcanic and Seismic Engineering Centre, Naples, Italy; Mazzolani et al., 2010).

The most common constructive types of buildings in the Vesuvius area are masonry and reinforced concrete (RC). The main typologies of roofs are either horizontal (87%), made of timber (4%), steel (58%) and RC (25%) structures, or vaulted (13%).

The examined roof typologies are ventilated and not ventilated timber, steel and RC structures, whose features are represented in Fig. 2.

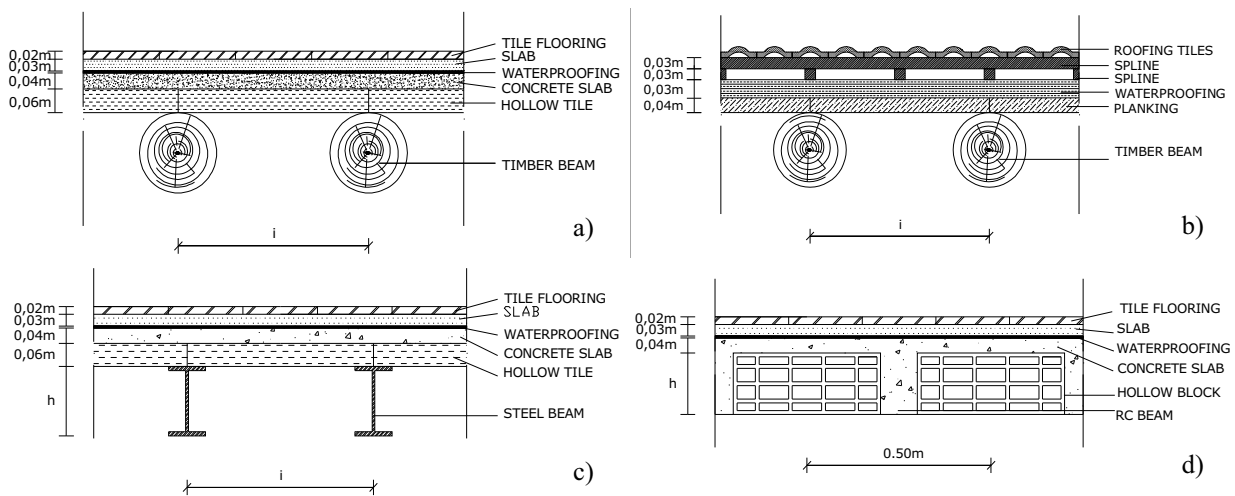


Fig. 2 Main Vesuvian roof types: a) not ventilated timber; b) ventilated timber; c) steel; d) RC

### 3 ROBUSTNESS EVALUATION OF THE VESUVIAN ROOF STRUCTURE

The behaviour of the study roof structures struck by the air fall deposits is evaluated in two steps (Faggiano et al., 2013), considering the combination of the twofold action, such as the additional gravity load and high temperatures. The first one consists in the assessment of the ultimate vertical load which the structure is able to sustain, in addition to permanent design load. In particular, the study is extended to roofs having different geometries and design live loads (0.6 and 2.0 kNm<sup>-2</sup>). The second one is the thermal analysis of the roofs, which aims at evaluating the mechanical degradation due to high temperatures.

The considered static scheme is a simple beam supported at both ends (Fig. 3), subjected to dead load  $g$  and live load  $q_R$  due to the air fall deposits.

Spans:  
L = 3, 4, 5, 6, 7m  
Pitch angles:  
 $\alpha = 0, 20, 30, 45^\circ$   
Interaxes: Timber and steel beams:  
RC beams:  $i = 0.80, 1.00\text{m}$   
 $i = 0.50\text{m}$

BEAM SIZES:			
Timber	Steel	RC	
(chestnut)	FeB360		
Circular ( $\phi$ )	Rectangular (BxH)	IPE	
[cm]	[cm]		
10	12x20	100	Materials, height of beam and reinforcement bars variable according to the different Italian technical codes (RD 1939, MD 1972, MD 1996 and MD 2008), in function of two assumed design live loads equal to 0.6 and 2.0kNm <sup>-2</sup>
12	12x24	120	
14	12x26	140	
16	14x20	160	
18	16x20	180	
20	16x22	200	
22	16x24	220	
24	18x22	240	
26	18x22	270	
28	18x24		
30	20x24		
	20x26		

Fig. 3 Static scheme and geometrical features of the roofs

The mechanical thermal degradation of structural materials (Eurocodes 2, 3 and 5, Parts 1.2) is considered at four temperatures, such as 20, 200, 300 and 400°C, they being assumed as uniformly distributed within the cross section. Thermal analyses are carried out by ABAQUS v. 6.5 nonlinear calculation program (Hibbitt et al., 2010). The FEM model of a 1.50 m x 1.00 m roof area with 16cm depth beams for timber and steel roofs and 12 cm depth beams for RC ones, all of them having a 80cm interaxis, is set up (Fig. 4). The different roof layers (tile, slab, waterproofing), which the thermal properties of the constitutive material (density, conductivity and specific heat) are assigned to, are modelled through **3D heat transfer** elements. With the purpose of increasing the heat transfer time from extrados to intrados of the roof, a layer of a

thermal insulator, constituted by a 3cm thick rock wool with a conductivity coefficient of  $0.04 \text{ Wm}^{-1}\text{K}^{-1}$ , which is considerably smaller than those of timber ( $0.1204 \text{ Wm}^{-1}\text{K}^{-1}$ ), steel ( $53.3004 \text{ Wm}^{-1}\text{K}^{-1}$ ) and concrete ( $1.9104 \text{ Wm}^{-1}\text{K}^{-1}$ ), is also considered.

For each roof types, the ultimate residual live load  $q$  is determined, at different pitch angles  $\alpha$  ( $0-45^\circ$ ) and temperatures  $T$  ( $20-400^\circ\text{C}$ ). In particular, for the sake of example in Fig. 5 for steel roofs the diagrams of  $q$  vs  $L$ , they referring to ambient temperature ( $20^\circ\text{C}$ ) with variable pitch angle (Fig. 5a), and to a  $0^\circ$  pitch angle (plane roof) with variable temperatures (Fig. 5b), and the thermal trend (Fig.5 c) are illustrated.

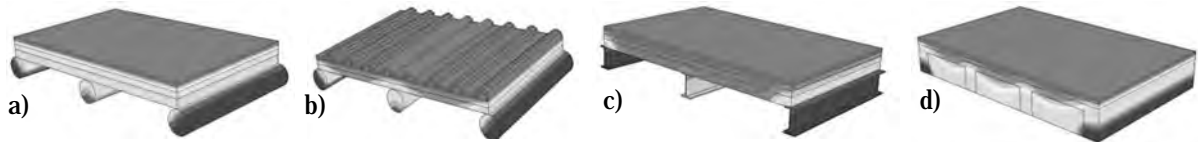


Fig. 4 Portions of roof considered in the thermal analyses: a) not ventilated timber; b) ventilated timber; c) steel; d) RC

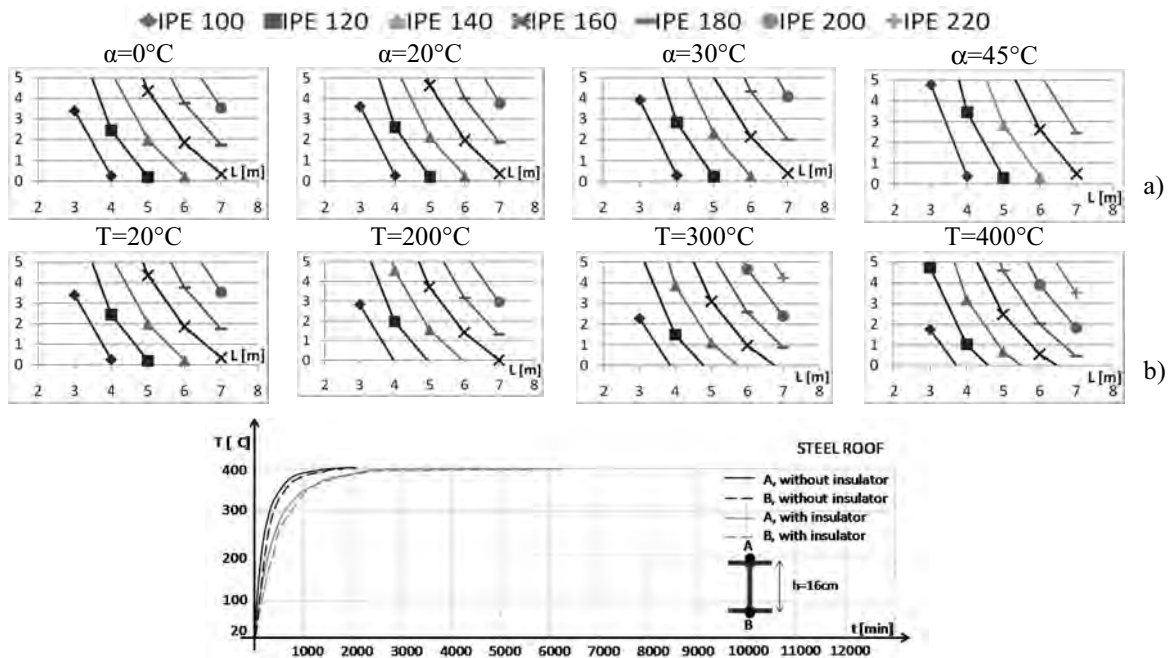


Fig. 5 Steel roofs: air fall deposit collapse loads with different pitch angles (a) and temperatures (b); thermal trend (c)

Results show that the ultimate residual load  $q$  has an increment of about 30-40% as far as the pitch angle  $\alpha$  varies from 0 to  $45^\circ$ . Contrary, high temperatures produce a decrease of the collapse vertical load due to the thermal degradation of the materials, which, as an average, can be quantified as 30% at  $200^\circ\text{C}$  and 50% at  $300^\circ\text{C}$ ; when the clasts temperature reaches  $400^\circ\text{C}$ , for most of the considered sections, any additional load cannot be resisted and the collapse occurs already for permanent loads.

Tab.1 Collapse times with or without an insulator layer

	$T_{cr}$	Time without insulator	Time with insulator
	$^\circ\text{C}$	s	s
Timber roof	100	180	430
Ventilated timber roof	100	120	360
Steel roof	400	2000	6200
RC roof	400	2900	12950

Finally, the maximum collapse time for each roof typology is determined, as reported in Tab. 1, where the beneficial effect of the insulator layer, especially for RC roof structures is apparent (Faggiano et al., 2013).

#### 4 PROPOSED VULNERABILITY CHARTS

In Fig. 6 some vulnerability charts are proposed. With reference to the 1631 Vesuvius eruption, the isopaches corresponding to deposit thicknesses at certain distances from the crater, together with the roof types ( $L=6m$ ,  $C_E=1$  and  $\rho=14kNm^{-3}$ ) and the related collapse times are represented, in the case either of a pitch angle  $\alpha$  equal to  $0^\circ$  without insulator layer (Fig. 6a) or pitch angle  $\alpha$  equal to  $0^\circ$ ,  $20^\circ$ ,  $30^\circ$  and  $45^\circ$  and with the insulator layer (Figs. 6b-e).

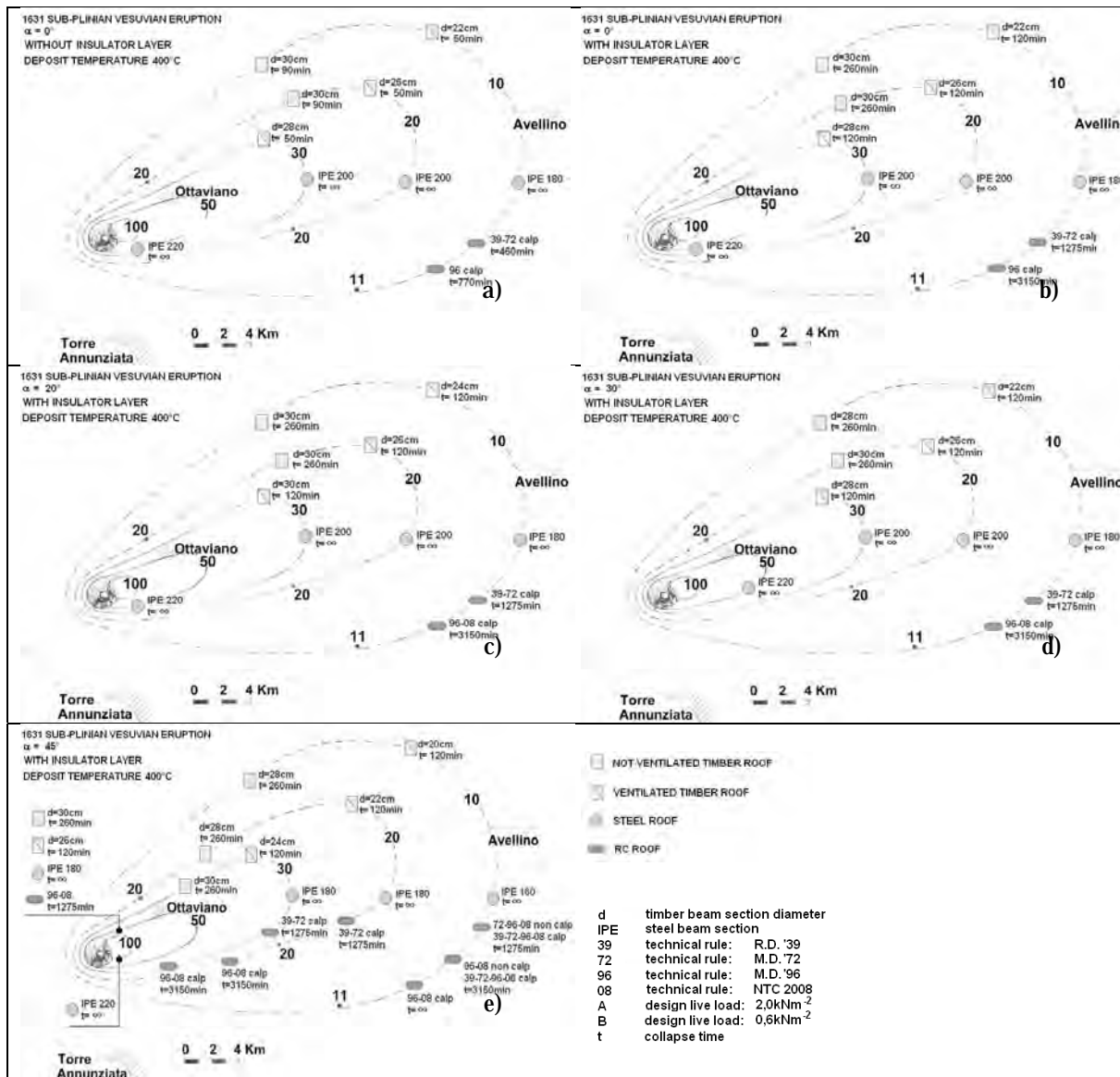


Fig. 6 Maximum collapse time produced by air fall deposits relating to 1631 Vesuvian eruption for roofs without insulator and  $\alpha=0^\circ$  (a) and with insulator and  $\alpha=0^\circ$  (b),  $20^\circ$  (c),  $30^\circ$  (d) and  $45^\circ$  (e)

#### 5 CONCLUSIVE REMARKS AND POSSIBLE MITIGATION SYSTEMS

With reference to the Vesuvius area, roofs designed to resist ordinary vertical loads ( $0.60$  and  $2.00 kNm^{-2}$ ) collapse when subjected to air fall deposits due to a sub-Plinian eruption, as the 1631 one. As it appears, the roofs behaviour under air fall deposits is influenced by two main factors: the materials thermal degradation and the roof pitch angle. The former one is due to the

high clasts temperatures (150-400°C). It can be mitigated through the use of a thermal insulator with a conductivity coefficient of 0.04W/mK, able to triple the collapse time of timber, steel and concrete roofs. Besides, as far as the pitch angle is large, the load on the roof due to the air fall deposits decreases and the ultimate residual vertical load increases; so, in the areas at risk of pyroclastic deposits, a minimum slope of the roofs, such as 30°, should be required. In particular, for the existing plane roofs, a pitch angle can be obtained through the realization of over-structures made of light materials and provided with an adequate thermal insulation.

## 6 ACKNOWLEDGEMENTS

The Authors acknowledge the European Project COST Action C26 ‘Urban Habitat Constructions under Catastrophic Events’ (2006-2010), which has promoted and inspired this research activity, as well as the Institutions involved in the project survey activity (PLINIVS Centre of Naples, ENEA of Bologna, Second University of Naples, University of Aveiro and University of Malta). The contribution of Dr. Daniela De Gregorio, who has developed the numerical analyses within the PhD thesis, is also gratefully acknowledged.

## REFERENCES

- De Gregorio D., Faggiano B., Florio G., Formisano A., De Lucia T., Terracciano G., Mazzolani F.M., Cacace F., Conti G., De Luca G., Fiorentino G., Pennone C., Zuccaro G., Borg R.P., Coelho C., Gerasimidis S., Indirli M., Survey activity for the seismic and volcanic vulnerability assessment in the Vesuvian area: The historical centre and the residential area in Torre del Greco, Proc. of the COST Action C26 Final Conference “Urban Habitat Constructions under Catastrophic Events”, Naples, 2010a.
- Faggiano B., Formisano A., Mazzolani F.M., Robustness evaluation of the Vesuvius roof structures under the air fall deposits due to a Sub-Plinian eruptions, Proc. of the 4<sup>th</sup> Int. Workshop on Performance, Protection and Strengthening of structures under extreme loading (PROTECT 2013), India, 26-27 August 2013 (accepted for publication).
- Hibbit, Karlsson, Sorensen, Inc., Abaqus manuals v. 6.5, 2010.
- INGV-OV, Vesuvian Observatory, [www.ov.ingv.it](http://www.ov.ingv.it), 2012.
- Mazzolani F.M., Faggiano B., De Gregorio D., The catastrophic scenario in explosive volcanic eruptions in urban areas, Proc. of the PROHITECH 2009 Conf., Rome, 2009a.
- Mazzolani F.M., Faggiano B., Formisano A., De Gregorio D., Zuccaro G., Indirli M., Borg R.P., Survey activity for the volcanic vulnerability assessment in the Vesuvian area: The ‘quick’ methodology and the survey form, Proc. of the COST Action C26 Final Conference “Urban Habitat Constructions under Catastrophic Events”, Naples, 2010.
- Mazzolani F.M., Indirli M., Zuccaro G., Faggiano B., Formisano A., De Gregorio D., Catastrophic effects of a Vesuvian eruption on the built environment, Proc. of the 2<sup>nd</sup> International Workshop on Performance, Protection, and Strengthening of Structures under Extreme Loading (PROTECT '09), Hayama, Japan, 2009b.
- M.D. 2008, Ministerial Decree 14 January 2008. New technical rules relating to the constructions (in Italian), Official Journal n.29, 4 February 2008, Ordinary Supplement n.30, 2008.
- Nelson S.A., Introduction & texture & structures of igneous rocks, Tulare University, USA, [www.tulane.edu](http://www.tulane.edu), 2010.
- Spence R., Kelman I., Baxter P.J., Zuccaro G., Petrazzuoli S., Residential building and occupant vulnerability to tephra fall, *Natural Hazard and Earth System Science*.5: 477- 494, 2005.
- Tilling R.I., Lipman P.W., Lessons in reducing volcano risk, *Nature*364: 277-280, 2007.

## **DAMAGE CONTROL OF INTUMESCENT PAINTING**

### **Influence of imperfections in intumescent painting**

Tom Molkens <sup>a</sup>

<sup>a</sup> StuBeCo bvba, Engineering office, Overpelt, Belgium

#### **Abstract**

From daily experience we know that, after erection of a steel structure, damage often occurs on steel columns and beams due to transport and assembly work. In combination with intumescent painting it is normal practice that after some time all paintwork will be touched up and repaired if needed. The problem today is that at that most of the time, steel cladding is already placed and the external parts of columns and beams cannot be reached anymore and stay therefore (partially) damaged.

With the aid of thermoplastic calculation for some case studies, where the outer flange is partially loaded with an external fire instead of an ISO834 fire, we could define how big the damaged area may be and where it could be positioned without influence on the structural integrity of the protection. Until today the SAFIR calculations are done for a R30 protection.

**Keywords:** intumescent painting, damage, imperfections

#### **INTRODUCTION**

Different types of damage or even poor execution of intumescent painting can occur, so this becomes a safety risk if the location of the damage is no longer visible for inspection. Also, to avoid time delays, it is interesting for the constructor to neglect those parts. We did some research at different steel manufacturers to know what the common execution errors could be. From this research it became clear that with application of a painting system on site, completely non-visible or inaccessible areas even remained unprotected.

It is our purpose to simulate these kinds of defects in intumescent coating by means of a thermoplastic model. The scope of our study is limited to industrial buildings with R30 protection. This without counting on the intumescent effect of this kind of protection. To be quite clear; avoiding damage is still the best way forward, however sometimes you just have to deal with it.



Fig. 1. Local damage

#### **1 REFERENCE CASE**

As reference case we used an industrial building with an 18 m span, 4.5 m height and dead load set relatively low (0.30 kN/m<sup>2</sup>), with snow and wind loads according to Belgian standards. The bracing system is schemed with the aid of hollow square sections. Following



first order unity check, the system is well used until 97 % (columns) of the capacity with S235 grade steel.

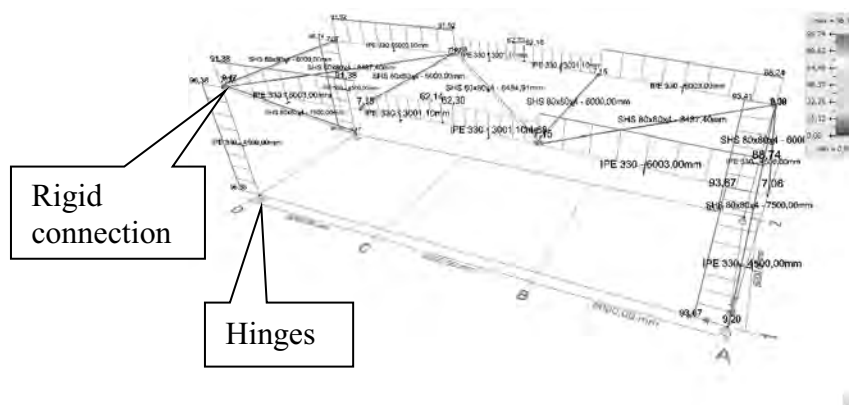


Fig. 2. Reference case, unity check at ambient temperature

## 2 INVESTIGATED SITUATIONS OF MISSING INTUMESCENT PAINTING

### 2.1 Damage pattern of local damage

Most of the damage occurs at the location of temporary support timber for storage and transport or where lifting straps are attached to beams, columns or other members. To obtain uniformly distributed stresses in the elements typically those areas are situated at 1/5<sup>th</sup> of the total length, we have estimated them over the whole width of the IPE 330 and with a length of 200 mm.

On each beam/column we introduced a damaged part at 1/5<sup>th</sup> of the end, in this way the initial hyper-static systems will be reduced to a kinetic one with weaker rotational springs at the referred locations

### 2.2 Inaccessible areas

Differently from what went before in this situation, a complete side of the steel profile will be unprotected in our simulations. This is always the outer (columns) or upper (beam) side. All other sided areas remain always protected as in the previous point.

### 2.3 Situations investigated

Previously, two patterns must be combined with different materials and situations. A steel roof decking profile with a height of 100 mm is always used. It is composed of a 0.75 mm thick (trapezoidal) steel profile and a 100 mm insulation layer = sandwich construction. For the wall cladding the same sandwich construction is used at a distance of 20 or 200 mm away from the column, also concrete at 20 mm distance was investigated.

Tab. 1 Investigated situations

Name	Roof material	Slit (mm)	Wall material	Slit (mm)	Supporting system
R10S-W20S	Sandwich	100	Sandwich	200	Purlins
R10S-W2S	Sandwich	100	Sandwich	20	Liner trays
R10S-W2C	Sandwich	100	Concrete	20	Panels

## 3 TEMPERATURE OF PROTECTED PART OF THE STEEL MEMBER

We start from the idea that the intumescent painting is a well-engineered system with no extra safety built in. Practice (Sanghoon et al. & Schaumann et al.) had already showed that in laboratory tests it seems there is always a certain safety margin in this kind of protection. However it is not our intention to take this into account.

As already applied by ourselves we simulated the behaviour of a steel IPE330 member with the aid of a tri-linear diagram. In the beginning the protection is rather low due to foam growth in an initial phase and in a second phase the rise of temperature slows down. From measurements of the results we could define a slope ratio of 2.69 between the initial and second phase at a temperature of 250°C. Finally at the required protection time of 30 minutes the critical steel temperature of 520°C is reached by the aid of a fictive end gas temperature at the required protection time. The temperature of the steel member is calculated by the aid of the NBN EN 1993-1-2 formula.

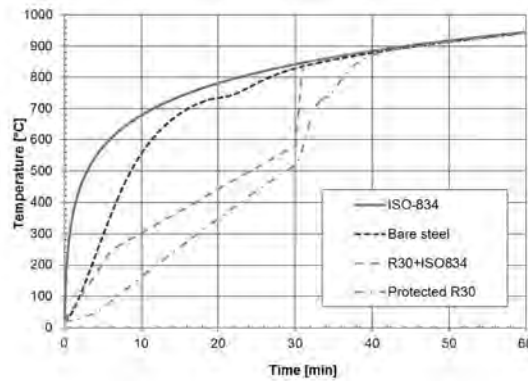


Fig. 2. Assumed tri-linear time-temperature relationship for protected steel (IPE330)

As boundary conditions for defining the curve we used 20°C at 0s, a slope ratio of 2.69 at 250°C end the fictive gas temperature which leads to a steel temperature of 520°C we can describe a bilinear curve. At the end in a time step of 60s the protection is assumed to degenerate completely so the curve fits the ISO834 one = the third part of the curve.

#### 4 HEAT FLUX ON NON PROTECTED PART

It can be imagined that boundary conditions in the neighbourhood of roof or wall cladding are different compared to an open space. It is not at all easy to simulate a temperature profile like that of ISO834 in a numerical way. Results in the narrow space between column and inner side of the elevations (= a slit) seem to be extremely difficult. In addition this would not give any physical insight into the problem. Therefore we apply a modified heat flux on the non-protected part based on the classic time-temperature relationship according to ISO834.

##### 4.1 Numerical model

We built a model for a small room with two insulated borders at the sides (symmetrical boundary conditions), an open space on one end, concrete or sandwich (steel + insulation) at the other end with different spacing to a column, concrete floor and sandwich roof structure. This study was done with a fire load of wood (wooden pellets? of 1400x40x40 mm<sup>3</sup>) equal to 30 kg/m<sup>2</sup> uniformly distributed. In the following table and figures the data is shown.

Tab. 2 Materials and properties

Material	location	Conductivity (W/mK)	Specific heat (J/(kg.K))	Density (kg/m <sup>3</sup> )	Thickness (m)
Concrete	Floor, walls and columns	1,60	900	2300	0,200
Steel (profile)	Beams	50	500	7800	0,010
Steel (sandwich)	Beams	50	500	7800	0,00075
Insulation	Side + sandwich	0,05	1030	40	0,100

In this way we can check the difference between the net heat flux on the directly heated, visible part and the part which stays invisible and therefore unreachable for touch-up work. The same ratios can be applied to the ISO834 heat flux which will lead to a modified one. Measurement devices for temperature, net heat flux, convective and radiation part are located at 1/4 of the profile width (proposed to be the mean value over the width). For the column at 1, 1.5 and 2 m height, for the beam at 1, 1.5 and 2 m from the inner part of the elevation.

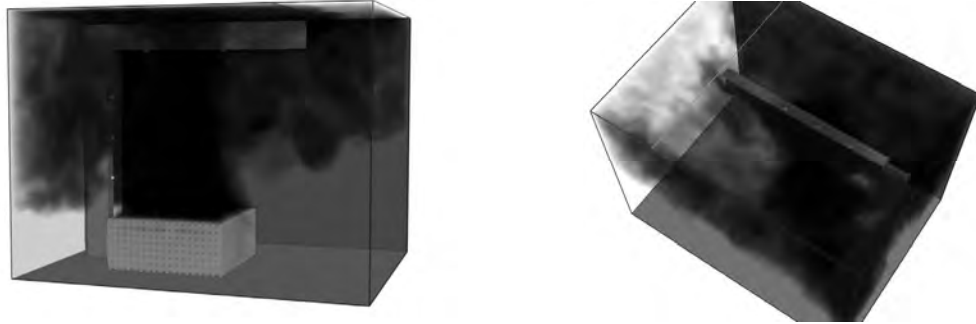


Fig. 3. Isometric view @11.3 s, R10S-W20S Fig. 4 Top view @11.3 s, R10S-W20S

Smoke particles in the figures above show already that smoke can/will penetrate the slits of 200 mm and 100 mm, this is also the case with more narrow spaces of 20 mm. From the measured results it seems that the slit at the column must be treated differently to the one above the beam:

- Most elevated temperature + heat flux and best corresponding to ISO834 is reached at 1m height for the columns and at 1.5m for the beam.
- The convective part for the columns seems to be almost negligible. This is perhaps not the most important because convection is only important in the beginning.
- For the beam the convective part is also more rapidly decreasing as in ISO834.

#### 4.2 Determining reduced heat flux

Based on the formulas 3.1, 3.2 and 3.3 we propose to modify the net heat flux which we are going to apply to the non-protected surface as follows:

$$\dot{h}_{\text{net,column}} = \Phi_{s,c} \dot{h}_{\text{net}} = \Phi_{s,c} [\alpha_c (\theta_g - \theta_m) + \Phi \epsilon_m \epsilon_f \sigma (\theta_g^4 - \theta_m^4)] \quad (1)$$

where  $\Phi_{s,c}$ ,  $\Phi_{s,b}$  general reduction factor for a slit to be applied on column or beam

For other symbols see EN 1991-1-2

Up to now we did not make a separation for the slit factor to be applied on the convective and radiation term, so we only used one general reduction term. From the numerical simulations it emerged that for our purposes, the accuracy was already satisfactory. The factor depends on time (t in s), slit (s in m) and profile width (p in m):

$$\Phi_{s,c} = \frac{1}{1 + 0.6 \frac{p}{s}} 0.210 t^{-0,3840} \quad (2) \quad \Phi_{s,b} = \frac{1}{1 + 0.6 \frac{p}{s}} 2.3406 t^{-0,24} \quad (3)$$

For the beam this approach seems to be very accurate, for the column it is rather conservative due to the "over-estimated" influence of the convective term.

## 5 RESULTS

### 5.1 Temperature profile

For thermal and structural analysis we used the well-known SAFIR software (Franssen). By using this software tool for thermoplastic analysis a temperature profile is independently calculated and applied to a whole structural member. This is of course not the case for the damaged section parts. The following figures shows the differences for the three main sections used in our model, maximum temperature at 1800s respectively 535, 534 and 534°C.



Fig. 5. Protected



Fig. 6 Damaged, s=200mm



Fig. 7 Damaged, s=20mm

### 5.2 Structural behaviour with damage.

For a column slit of 200 mm; a maximum displacement of 44 mm is obtained after 1800s and at the failure time of 1907s, this displacement becomes 744 mm. With a narrow slit of 20 mm, those values become 77 mm @ 1800s and 2828 mm @ 1907s.

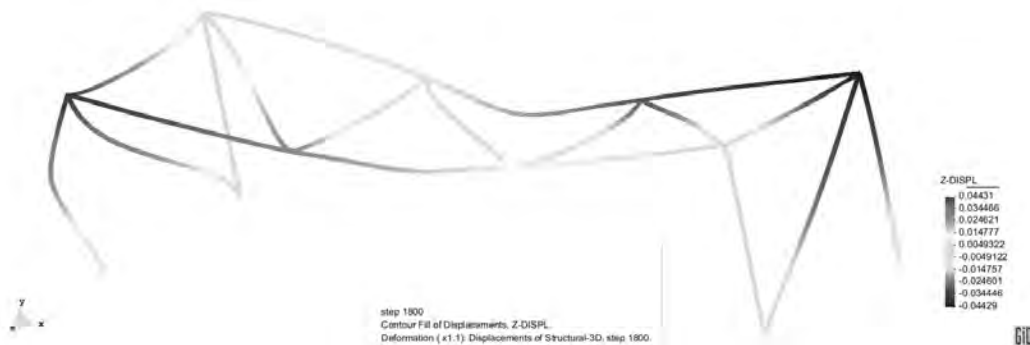


Fig. 8. Structure deformation @ 1800s, 200 mm slit for columns

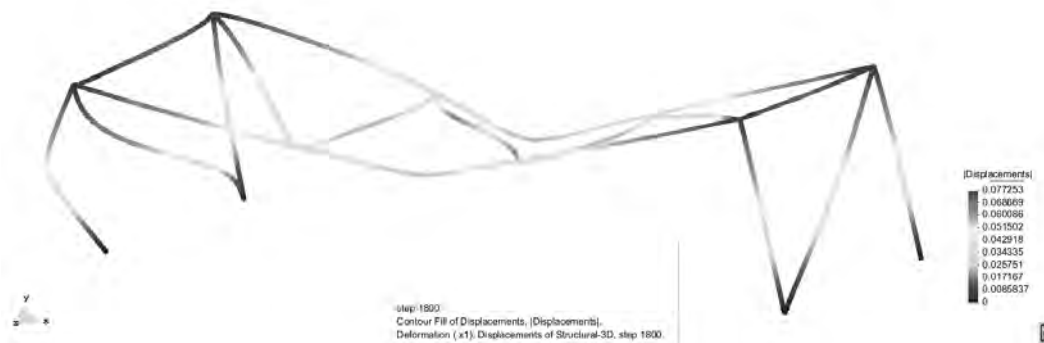


Fig. 9. Structure deformation @ 1800s, 20 mm slit for columns

### 5.3 Structural behaviour with unprotected areas.

For a column slit of 200 mm; a maximum displacement of 76 mm is obtained after 1800s and at the failure time of 1909s, this displacement becomes 1632 mm. With a narrow slit of 20 mm, those values become 76 mm @ 1800s and 2131 mm @ 1910s.

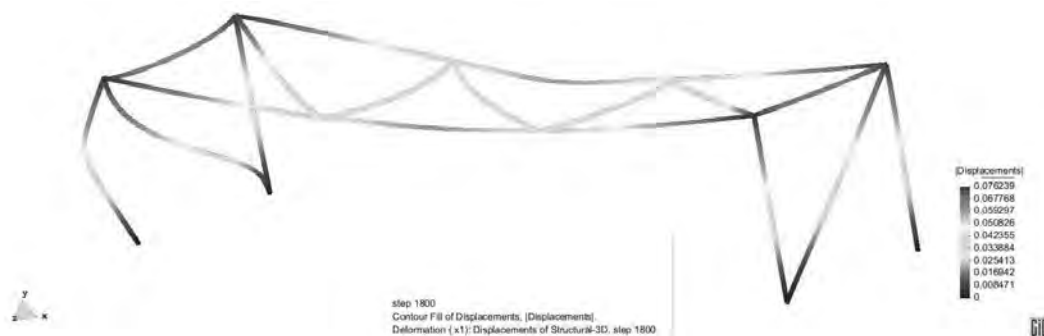


Fig. 10. Structure deformation @ 1800s, 200 mm slit for columns



Fig. 11. Structure deformation @ 1800s, 20 mm slit for columns

## 6 CONCLUSIONS

With the aid of our case study it is numerically proven that the influence of a double local damage at  $1/5^{\text{th}}$  of the length and with a length of 200 mm has no influence on the protection time. Even with the whole surface against roof or wall cladding unprotected, we still fulfil the requirements.

The number of simulation made are still limited but the results are promising, material dependency for wider slits, differentiation from the slit factor to the convective, radiation factor must be done and also the boundary condition of this approach has to be clarified.

## REFERENCES

- EN 1990: 2002 + ANB; Eurocode 0: Basis for structural design, European Committee for Standardization CEN, 2002 + National application document, 2005.
- NBN EN 1991-1-2 + ANB; Eurocode 1: Actions on structures - Part 1-2: General rules – Actions on structures exposed to fire, CEN 2002 + National application document, 2008
- NBN EN 1993-1-2 + ANB; Eurocode 3: Design of steel structures – Part 1-2: General rules – Structural fire design, CEN 2005 + National application document, 2010
- Franssen J.-M., SAFIR. A Thermal/Structural Program Modelling Structures under Fire, Engineering Journal, A.I.S.C., Vol 42, No. 3 (2005), 143-158.
- Molkens T., fire resistance of partially protected steel structures, for use in industrial buildings, PLSE conference Hong-Kong 2012, 479-487.
- Sanghoon H., Petrou K., Naili E.-H. & Faris A., Behaviour of protected cellular beams having different opening shapes in fire conditions, Structures in Fire 2012 – EMPA & ETH Zürich (2012), 75-83.
- Schaumann P., Kirsch T. & Timmen F., Full scale fire test and numerical simulation of a steel connection, Structures in Fire 2012 – EMPA & ETH Zürich (2012), 115-124.









## STEEL TEMPERATURE CALCULATIONS IN PERFORMANCE BASED DESIGN

### Advanced Techniques for Thermal Response Calculations with FE-Analysis

Joakim Sandström<sup>a</sup>, Ulf Wickström<sup>b</sup>

<sup>a</sup> Luleå University of Technology/Brandskyddslaget AB, Karlstad, Sweden

<sup>b</sup> Luleå University of Technology/SP Technical Research Institute of Sweden, Borås, Sweden

#### Abstract

By using advanced FEA techniques, the predicted temperature in steel elements can be reduced significantly (see paper by Ulf Wickström). By in addition assuming a performance based fire exposure obtained with numerical fire models such as Fire Dynamics Simulator, FDS, the steel temperatures can be even further reduced.

Most calculation methods assume the fire exposure of the steel sections to be uniform. By using section factors  $A/V$ , i.e. the circumference over the area, and the most onerous of the fire exposing temperatures from computer fluid dynamics, CFD, calculations, the temperatures is over-estimated which leads to very conservative and costly solutions.

By considering the cooling effect of concrete structures and shadow effects, the temperatures can be reduced in the steel. By combining differentiated fire exposing temperatures from CFD calculations with consideration to shadow effects and the cooling of concrete, the temperature in the steel beam can be reduced even further.

**Keywords:** adiabatic surface temperature, CFD, FEA, shadow effect, thermal response

#### INTRODUCTION

Eurocode 3: Design of steel structures – Part 1-2: General rules – Structural fire design<sup>1</sup> contains various means of calculating temperature in fire exposed steel structures. Most calculation methods assume the fire exposure of the steel sections to be uniform while boundary temperatures from real fires in general are non-uniform<sup>2</sup>. By considering a non-uniform temperature exposure and an advanced FE-analysis set up, there can be a big difference in the calculated temperatures for the same cross section.

When calculating the steel temperature in a beam supporting a concrete slab, these methods for calculation can be illustrated.

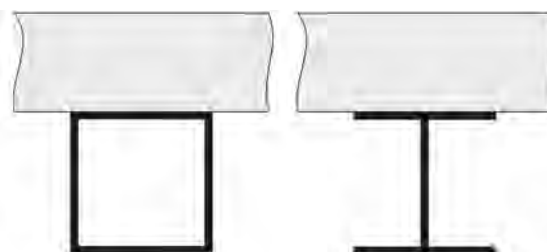


Fig. 1 Concrete slab supported by two different kind of beams

<sup>1</sup>(EN 1993-1-2, 2005)

<sup>2</sup>(Wickström, Jansson, & Touvinen, 2009)

The simplest method is to use section factors  $A_m/V$ , i.e. exposed surface area over the volume of an element, and the most onerous of the fire exposing temperatures from a real fire scenario. The steel temperature tends to gradually adopt the fire exposing temperatures. As the fire exposing temperature is the most onerous it is an over-estimation for the other sides of the steel leading to very conservative and costly solutions. It can be considered an over-estimation as the assumed fire exposure is more severe than the actual fire exposure for most sides of the element. Further, no heat is allowed to leave the cross section to the concrete giving two conservative assumptions.

There are several ways of increasing the accuracy of calculations and thereby often reducing the steel temperatures without reducing the overall safety level.

Firstly, by considering the concrete slab, heat can leave the cross section through the upper flange. This reduces the temperature of the upper flange and to some extent, the web. The cooling effect has little or no impact on the lower flange.

Secondly, by considering the shadowing effects of the flanges in the H-sections the web and inside of the flanges is allowed to “see” other surfaces than only the fire. For simple spread sheet calculations this is done by changing the section factor,  $A_m/V$ , as described in Fig. 2. The effective heated surface,  $A_m$ , is reduced from the actual perimeter to the perimeter of a virtual box,  $[A_m]_b$ , resulting in a lower section factor denoted  $[A_m/V]_b$ .



Fig. 2 The dotted line represents the heated area of the cross section. The left figure is heated with no consideration to shadow effects, whereas the right one does consider shadow effects

In a simplified numerical analysis with no regards to the shadow effects, the development of the steel temperature can be expressed according to EN 1993-1-2<sup>3</sup>.

In an FE-analysis, considering the shadow effect can be done by adding a virtual representation of the box perimeter on a H-section creating a void on each side of the web. Together with the web and flanges, the virtual box perimeter creates a void where the inside of the virtual box perimeter can be modeled with a prescribed temperature. This way, the virtual box perimeter can imitate a black body recreating the fire exposure conditions that exists on the perimeter. A more practical description on how this is done is made in the section 2.

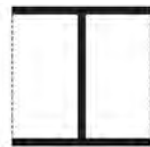


Fig. 3 The virtual box perimeter creates a void with the web and flanges; the dotted line represents the virtual box perimeter

Finally, the non-uniform fire exposure temperatures are considered along with the shadow effects in a FE-analysis.

## 1 CALCULATION OF BOUNDARY DATA

For calculations of steel temperature with non-uniform fire exposure, the fire exposure for each side of the beam and exposed sides of concrete has to be calculated. The boundary data

<sup>3</sup>(EN 1993-1-2, 2005)

for the thermal analysis can be represented by adiabatic surface temperatures,  $AST$ , from FDS<sup>4</sup> which is calculated at the surfaces of the hollow beam and the ceiling as shown in Fig. 4.

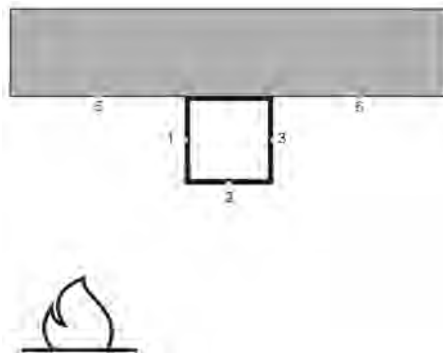


Fig. 4 Set of reference points for transferring data from FDS to FEA; reference point 1 is facing the burner

The modeling domain imitates a room similar to that stipulated in ISO 9705<sup>5</sup>, a room with the dimensions 2.4 m x 3.6 m x 2.4 m and an opening of 0.8 m x 2 m in one end (see Fig. 5). A propane burner is located at one of the far end corners with an elevation of 0.65 m and a constant effect of 450 kW.  $AST$  is obtained at the surface of a modeled hollow steel section with the dimensions 200 mm x 200 mm with flanges and web with a thickness of 10 mm. The beam supports the concrete ceiling.

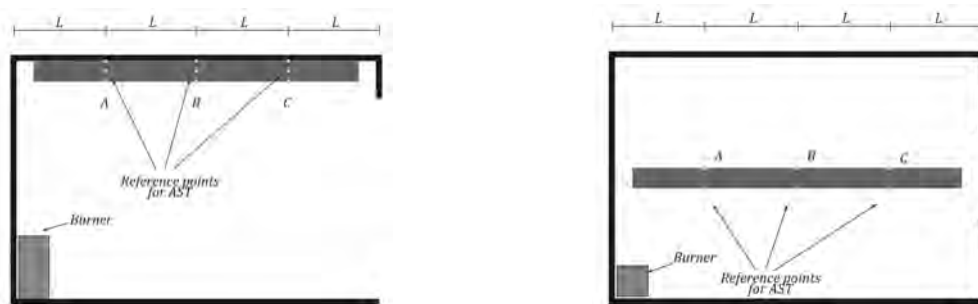


Fig. 5 Setup of calculation for obtaining coupling data for FEA

The data from this calculation represents the fire exposure to the beam. This fire exposure can be assumed equal for structural elements of approximately the same size and shape. As this is the case for the hollow and H-section, calculated  $T_{AST}$  can be used for both of the sections<sup>6</sup>. The H-section has the dimensions 200 mm x 200 mm with flange and a web with a thickness of 10 mm.

The material properties and emissivity are taken from the Eurocodes<sup>7,8</sup> along with the convective properties for natural fires from EN 1991-1-2 (3.3.2)<sup>9</sup> assumed to 10 W/m<sup>2</sup>K for all surfaces.

## 2 EXAMPLES OF COUPLING

When coupling CFD calculations to thermal response calculations there are a few different methods available. The FE-analysis of method 2-5 is performed with TASEF<sup>10</sup>.

<sup>4</sup>(McGrattan, Klein, Hostikka, & Floyd, 2007)

<sup>5</sup>(ISO 9705, 1993)

<sup>6</sup>(Sandström, 2008)

<sup>7</sup>(EN 1992-1-2, 2004)

<sup>8</sup>(EN 1993-1-2, 2005)

<sup>9</sup>(EN 1991-1-2, 2002)

## 2.1 Simplified Eurocode

Spread sheet calculation with fire exposure from a single, uniform temperature. Connection to concrete is ignored.

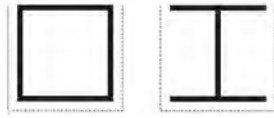


Fig. 6 Fire boundary in calculation 1; the dotted line represents fire exposure

## 2.2 Simplified FEA

Finite element calculation with fire exposure from a single, uniform temperature. No regards to shadow effects for the H-section and the connection to concrete is ignored.

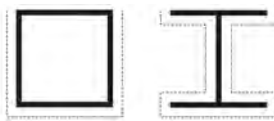


Fig. 7 Fire boundary in calculation 2; the dotted line represents fire exposure

## 2.3 Advanced FEA with uniform fire exposure

Fire exposure from a single, uniform temperature. Concrete is modeled in the calculations but not the shadow effect for the H-section.

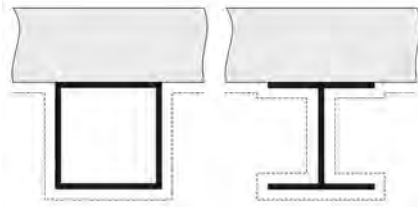


Fig. 8 Fire boundary in calculation 3; the dotted line represents fire exposure

## 2.4 Advanced FEA with uniform fire exposure and shadow effect

Same as above but with regards to shadow effects. This analysis is only performed for the H-section.

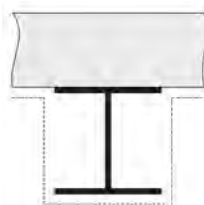


Fig. 9 Fire boundary in calculation 4; the dotted line represents fire exposure

---

<sup>10</sup>(Sterner & Wickström, 1990)

## 2.5 Advanced FEA with non-uniform fire exposure and shadow effect

Full analysis with different fire exposure temperature for each side. The fire exposure temperatures are the corresponding adiabatic surface temperatures for each side.

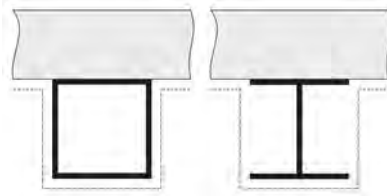


Fig. 10 Fire boundary in calculation 5; the dotted line represents fire exposure

## 3 RESULTS

### 3.1 Fire exposure temperature

The adiabatic surface temperatures in reference point set A are showed in Fig. 11. The highest adiabatic surface temperature is calculated under the bottom flange, i.e. reference point AST A-2, which is used as fire exposure temperature when assuming a uniform fire exposure temperature.

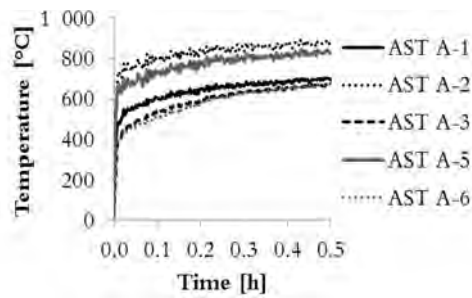


Fig. 11 Adiabatic surface temperatures in reference point set A from CFD calculations

### 3.2 Hollow section

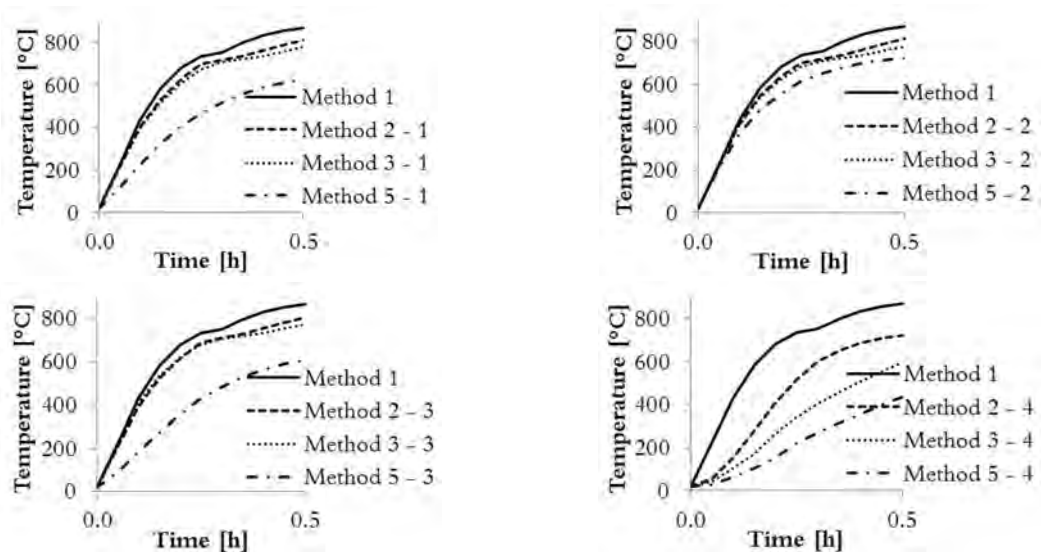


Fig. 12 Temperature development for each of the sides in the hollow section depending on the level of accuracy. Index 4 represents the upper flange in contact with concrete. The other indexes correspond to Fig. 4.

When calculating the temperature in the hollow section, the heat exchange in the void is considered at all times except for the simple spread sheet calculation. The temperature is calculated for all four sides of the hollow section following the same numbering as presented in Fig. 4 with the addition of side 4 which is facing the concrete.

Tab. 1 Temperature distribution in a hollow section with different levels of accuracy

Method	Side 1	Side 2	Side 3	Side 4
1 – simplified EC	877°C	877°C	877°C	877°C
2 – simplified FEA	811°C	809°C	807°C	719°C
3 – advanced FEA, uniform fire exposure	777°C	776°C	772°C	594°C
5 – advanced FEA, non-uniform fire exposure	628°C	719°C	611°C	436°C

### 3.3 H-section

The temperature in the H-section is calculated in the lower flange, the web and the upper flange numbered 2, 3 and 4 respectively.

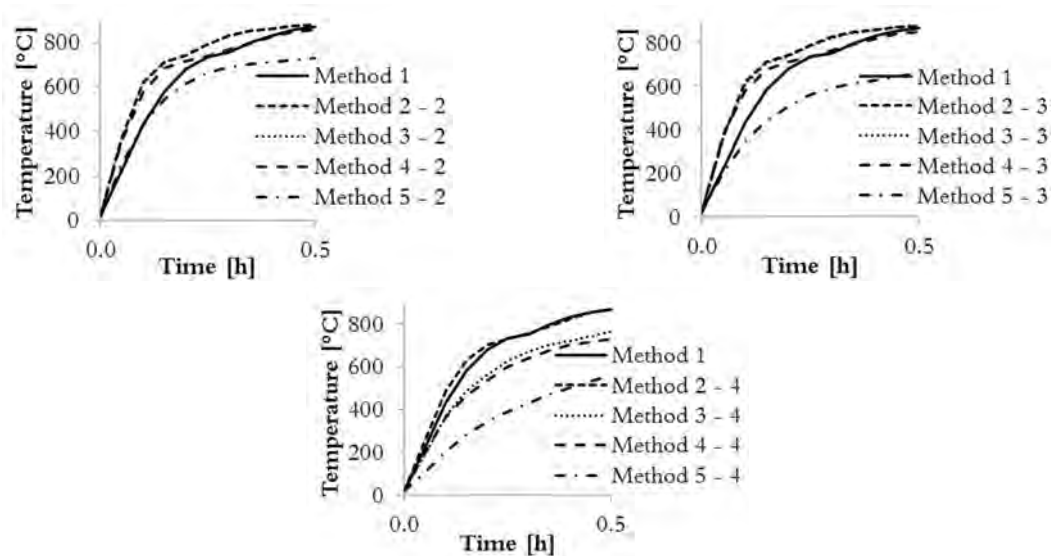


Fig. 13 Temperature development for each of the sides in the hollow section depending on the level of accuracy. Index 2, 3 and 4 represents the lower flange, the web and upper flange in contact with concrete respectively.

Tab. 2 Temperature distribution in a hollow section with different levels of accuracy

Method	Lower flange	Web	Upper flange
1 – simplified EC	869°C	869°C	869°C
2 – simplified FEA	877°C	877°C	868°C
3 – advanced FEA, uniform fire exposure	877°C	876°C	764°C
4 – advanced FEA, uniform fire exposure, shadow	857°C	851°C	731°C
5 – advanced FEA, non-uniform fire exposure, shadow	729°C	658°C	559°C

## 4 COMMENTS ON THE CALCULATIONS

By adopting a more advanced set up of boundary conditions, the steel temperature can be predicted with greater precision and becomes as rule reduced significantly. Only by using FEA considering the cooling effects of concrete on a hollow steel section, i.e. method 3, gives a temperature decrease in the lower flange of close to 100°C and in the upper flange of close to 300°C compared to the simplified method presented in EN 1993-1-2. For the H-section,

this difference is negligible for the lower flange and approximately 100°C for the upper flange.

When adopting different fire exposing temperatures the temperature is even better predicted. This way the analysis consider less onerous exposure on the sides not directly exposed to thermal radiation from the flame. This concept decreases the temperature and the difference compared to the simplified solution for the hollow section is 250°C for the lower flange and 450°C for the upper flange. For the H-section, this difference is 150°C for the lower flange and 300°C for the upper flange.

## **REFERENCES**

- EN 1991-1-2. (2002). Action on structures - Part 1-2: General Actions - Actions on structures exposed to fire. Brussels: European Committee for Standardization, CEN.
- EN 1992-1-2. (2004). Design of concrete structures . Part 1-2: General rules - Structural fire design. Brussels: European Committee for Standardization, CEN.
- EN 1993-1-2. (2005). Design of steel structures - Part 1-2: General rules - structural fire design. Brussels: European Committee for Standardization, CEN.
- ISO 9705. (1993). Fire Tests - Full Scale Room Test for Surface Products. Geneva, Switzerland: ISO.
- McGrattan, K., Klein, B., Hostikka, S., & Floyd, J. (2007). Fire Dynamics Simulator (Version 5) User's Guide, NIST Special Publication 1019-5. Washington: U.S. Government Printing Office.
- Sandström, J. (2008). Calculation of steel temperature with the use of adiabatic surface temperature. Luleå: LTU.
- Sterner, E., & Wickström, U. (1990). TASEF - Temperature Analysis of Structures Exposed to Fire - User's Manual. Borås: SP Report 1990:05.
- Wickström, U., Jansson, R., & Touvinen, H. (2009). Experiments and theory on heat transfer and temperature analysis of fire exposed steel beams. Borås: SP Report 2009:19.

## **FIRE PROTECTION OF TALL STEEL COLUMNS USING WATER SPRINKLERS**

Jyri Outinen<sup>a</sup>, Jukka Vaari<sup>b</sup>

<sup>a</sup>Ruukki Construction Oy, Helsinki, Finland

<sup>b</sup>VTT Technical Research Centre of Finland, Espoo, Finland

### **Abstract**

A known fact is that the water sprinklers cool down the fire and also the structures. In most countries the requirements for fire protection can be lowered, if the building is equipped with automatic water sprinklers. The cooling effect of different kind of sprinkler types, water flows and droplet size to steel structures has been studied for several years in Finland. The outcome has been a national approval for a fire protection system consisting of a selection of steel structures and certain type of sprinkler systems. This research has been presented in ASFE earlier conferences.

The latest research project concerning this is just about to be finished. The objective of this research was to study the behaviour of long steel columns in case of fire in a typical warehouse or a logistic building equipped with adequate sprinkler system. Columns up to 13,7 meters were studied using verified FDS simulation. Fire load scenarios were taken as storage shelves filled with certain material and fire spread. The unknown fact has been how these sprinkler systems cool down the high columns when the sprinkler systems are attached near the roof as normal. The results of this will be presented in this paper together with some other special cases which might occur in a fire in sprinklered building.

**Keywords:** fire protection, water extinguishers, cooling, steel structures, sprinklers

### **INTRODUCTION**

The main idea of this research was to study the effect of ESFR (Early Suppression Fast Response) sprinkler system to cool down the fire and steel structures in fire situation in high storage-type premises. This paper is based on a research report done by VTT (Vaari et al, 2012). The main focus was to study the temperatures in tall columns, when the water extinguishers are attached near the roof as usual and there's no rack sprinklers attached. The benefit is that moving the shelves is not dependent upon the rack sprinklers and still the fire safety stays at adequate level. The cooling effect down to the ground level was the main research issue to be able to design the steel columns to adequate dimensions.

The sprinkler system is based on discharging a large amount of water very fast. The K-value is typically around 200-360 l/min/bar<sup>1/2</sup>.

The research also studied the cooling performance of dry systems. The dry systems are used often in cold storages to avoid freezing of the water in pipes. The functioning differs from the wet system, where there is pressurized water in the pipes and therefore the reaction is faster. In dry systems there's a little delay because of the water coming from the tanks after the system starts, i.e. the sprinkler heads are acting or the fire detectors give the signal.

The height of the columns was limited to 13.7 meters. This comes from the sprinkler design standards

The research was done using FDS (Fire dynamics Simulator) by NIST. The validation was based on experimental research and literature. FDS is the most used fire simulation software and this freeware, open source software is updated actively by the scientific network governed by NIST.



## 1 CALCULATION METHOD

The ability of the sprinklers to cool down steel structures was studied using FDS software, version 6.0.0, SVN12961. This is a tool for especially different flow calculations in fire.

In this work the temperatures of a steel column were studied in cases where the column is either next to the wall or in an open space. The calculation area was 6m x 6m x 13.7m and the resolution was 20cm.

The basic assumption was that the stored things commodities work as an obstacle to the spread of fire and water. The material corresponds to cellulosic, double triwall corrugated cardboard. The fire was modelled as a 2m x 2m burner, in which the time evolution of the heat release rate corresponded to a storage shelf fire. The sprinklers were not assumed to put down the fire, so the heat release rate was allowed to double after the moment the sprinklers activate and then kept steady. This is an assumption often used to be sure of the safety level or overdimensioning.

### 1.1 Sprinkler description

The sprinkler system in the model had 4 nozzles in a 3m x 3m network. The distance to the column wall was 1.5 m. In the case where the column is next to the wall, it is situated in between two nozzles and in the open space-case the column is centered between the four sprinklers. These are illustrated in Fig 1.

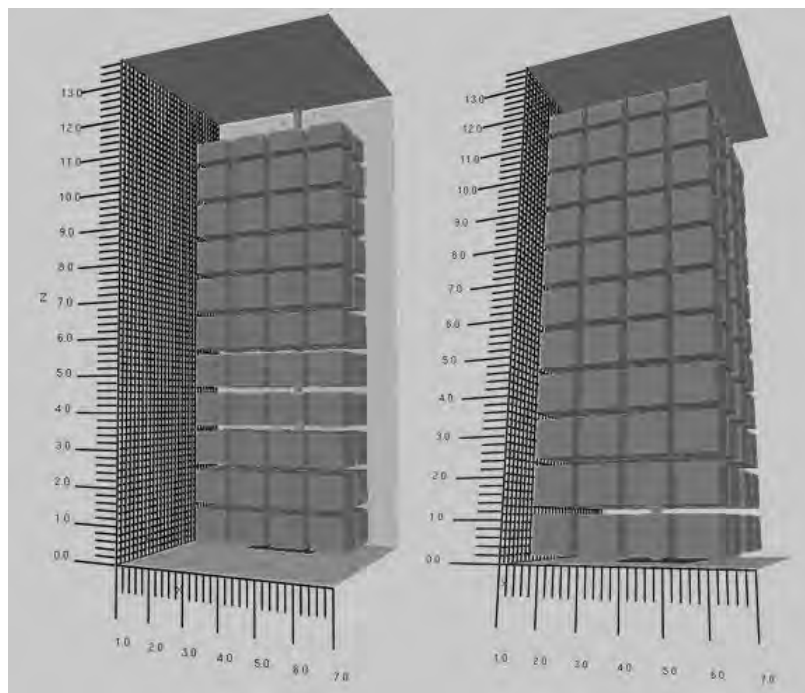


Fig. 1 FDS model for a steel column in local fire in the describes cases.

The spray pattern or spray envelope in these kind of sprinklers is downwards aiming to maximize the water amount watering the area and burning items below. The exact pattern is not very often exactly given.

In this study the water droplets are assumed to be evenly spread in between azimuth angles 50 and 80 to spray sprinklers (used in the dry pipe system) and between 0 and 80 to ESFR sprinklers.

### 1.2 Steel model

The parameters for structural steel follow Eurocode 3 (EN 1993-1-2) values. The temperature dependence was taken into account. The temperatures were determined in 1mm depth underneath the steel surface. Vertical distance between the measuring points was 1 meter.

## 2 RESULTS

### 2.1 Validation of the FDS model

The experimental tests carried out at VTT were used as a validation background. These test results could be used only partly because the situation in this simulation is different from the test. The cooling effect to the gas temperature is less important in this study than cooling down the steel structures.

The freeburn (no sprinklers) case was modelled and compared to the previous test results. It was done with ISO 834 curve. The results can be seen from Fig.2.

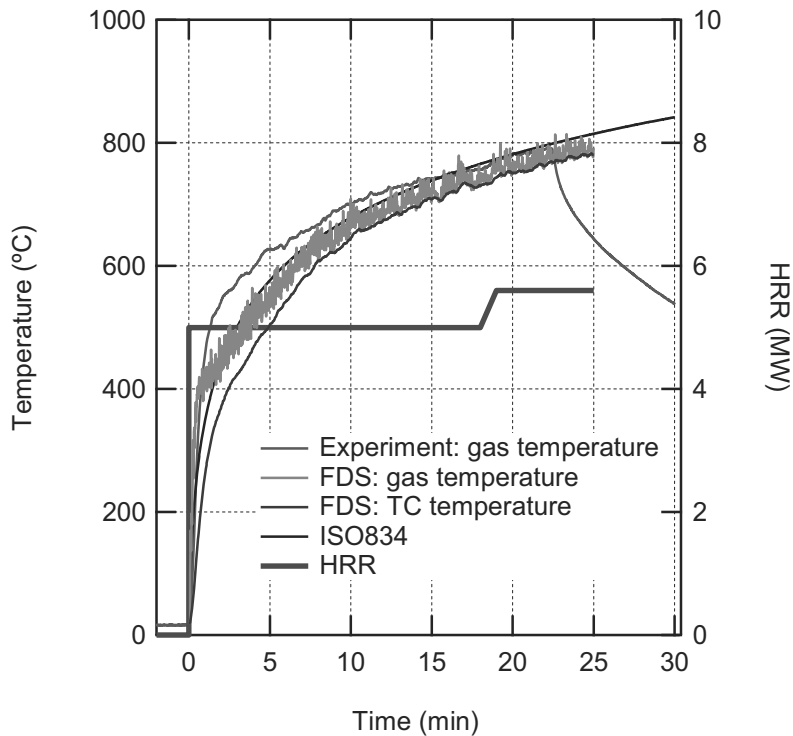


Fig. 2 Time evolution of the heat release rate used in the freeburn experiment, and measured and calculated gas temperatures.

### 2.2 ESFR-system's cooling effect in high storage

ESFR system is based on fast response to fire and very high water amount together with large droplet size which together put down the fire very effectively even from a high distance.

In this research two scenarios were studied in cases where the column is either next to the wall or in an open space. The idea was to study the cooling effect when there's shelves attached and also when there's a lot of fire load but the column is in open space affected by the fire.

The heat release rate was 5.4 MW in the beginning of water discharge and the flame reached about 4-5 meters high. The biggest effect is naturally to the lower part of the column. This is illustrated in Fig 3.

The development of the steel surface temperature in different heights is illustrated in Fig.4. The column wall thickness was in this case 6mm and it can be seen that the maximum temperature is reached at about 2m height with a temperature around 330°C. This shows the cooling power of ESFR system.

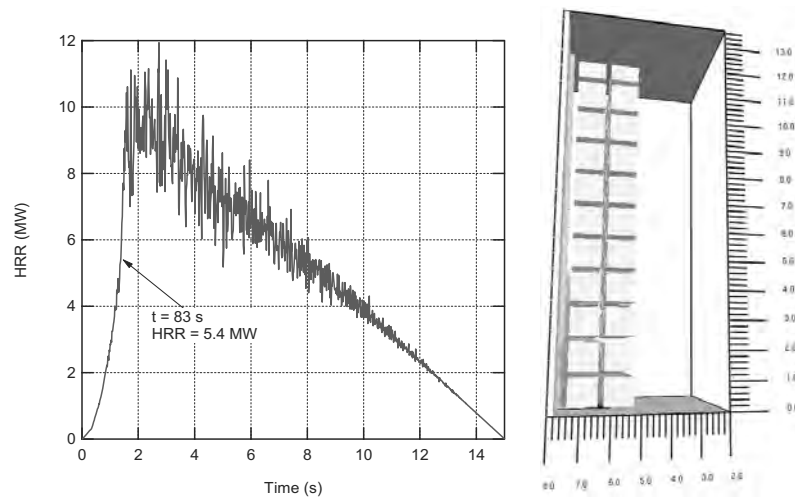


Fig.3 Left: time evolution of the HRR during ESFR cooling experiment with storage racks against a wall. Right: flame shape upon activation of first sprinkler.

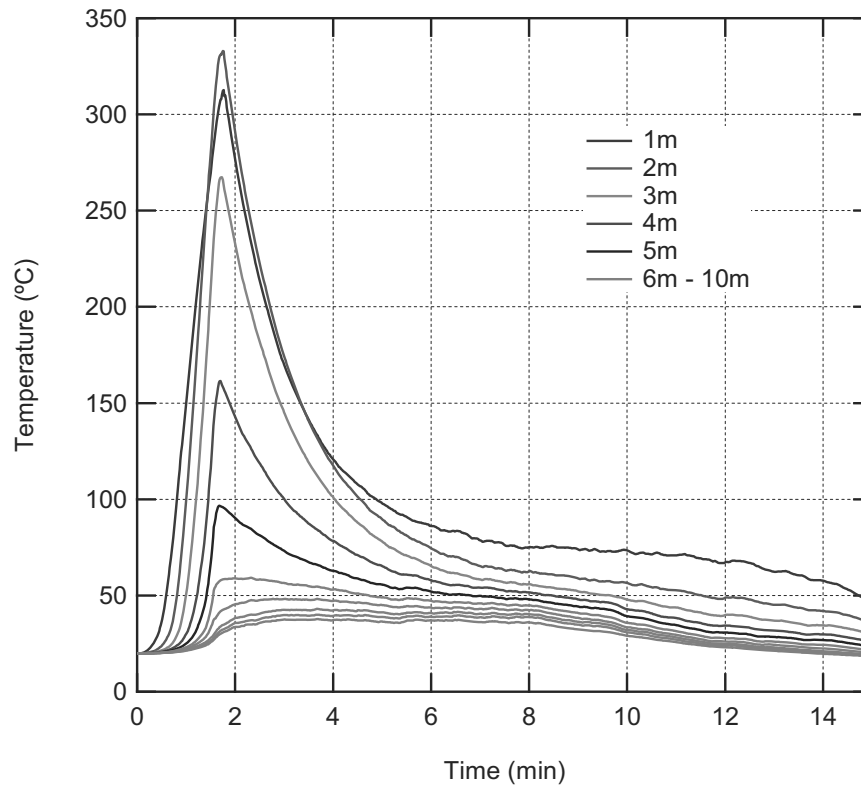


Fig.4 Time evolution of the surface temperature of the steel column during ESFR cooling experiment with storage racks against a wall.

The open space scenario was studied similarly. The heat release rate was 7.6MW in the beginning of water discharge which is a lot higher than used in literature (Kung et.al.) and the flames reached again 4-5 meters in the start. The main effect was to the lower part of the column. The highest temperatures were at 2m height, with maximum of 635°C with 6mm wall thickness. The case, heat release rate and temperature development is presented in Figs. 5 and 6 with a comparison between different wall thicknesses. Naturally this affects the temperature development.

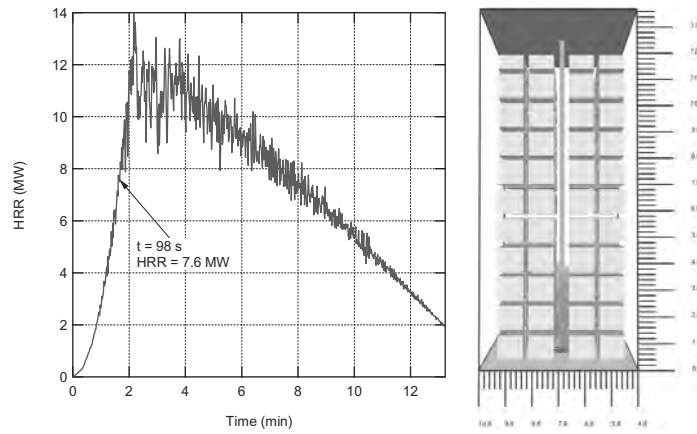


Fig. 5. Left: time evolution of the HRR during ESFR cooling experiment with storage racks in an open space. Right: flame shape upon activation of first sprinkler.

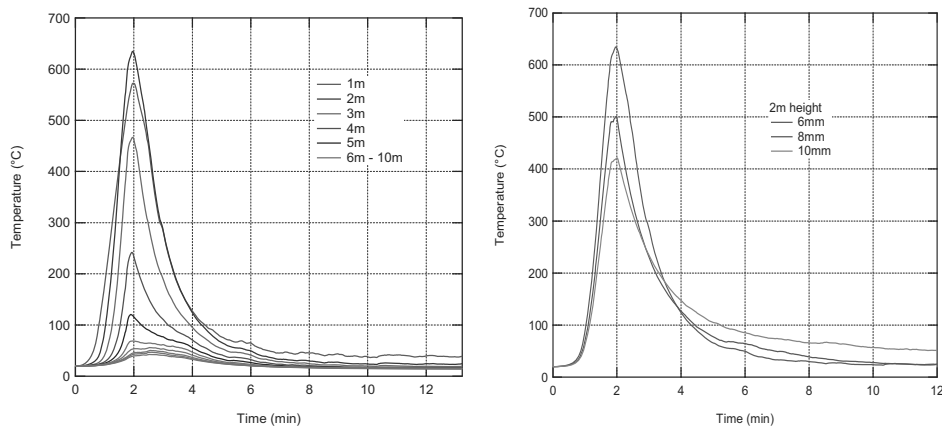


Fig. 6 Left: time evolution of the surface temperature of a 6mm thick steel column during ESFR cooling experiment with storage racks in an open space. Right: the effect of steel thickness on the column surface temperature at 2m height.

### 2.3 Dry system's cooling effect in high storage

One aim was also to study the cooling effect of so called dry system, where there's a delay of the water coming from the nozzles. This was studied with a very maybe too high fire load. The column was in an open space. The heat release rate in the beginning of water discharge was 13.7 MW, because the fire have about 1 minute more to develop before sprinklers work. In Fig. 7 the HRR is presented and in Fig 8 the results are presented for one type column. This has to be studied more thoroughly in the future.

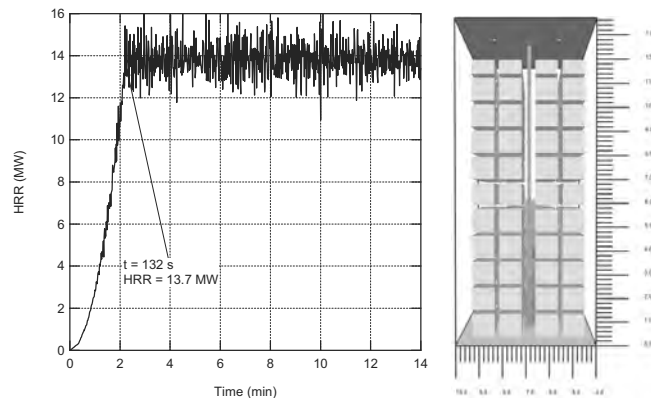


Fig. 7 Left: time evolution of the HRR during dry-pipe system cooling experiment with cold storage racks in an open space. Right: flame shape upon activation of first sprinkler.

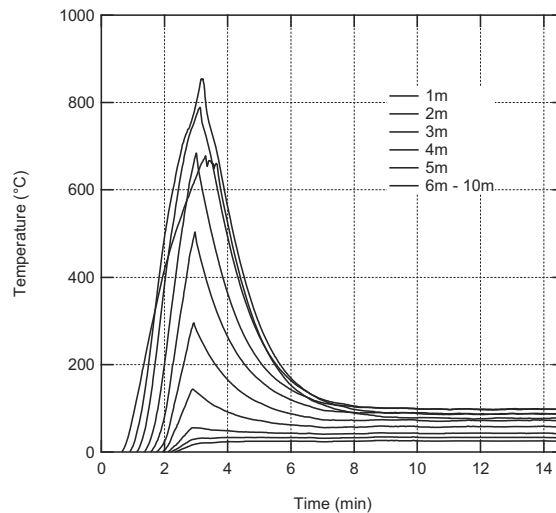


Fig.8 Time evolution of surface temperature of a 10mm thick steel column. Dry sprinkling.

### 3 SUMMARY AND ACKNOWLEDGMENT

The studied ESFR wet sprinkler system can effectively cool down the columns in different cases. The temperatures rise higher only for a short period of time and this will not cause any structural risk. Using dry system, the delay in the activation of the system causes also temperature rise during this time, but when the system starts to work, the temperatures start decreasing strongly to safe level. The structures reach the highest temperatures just before the first sprinkler heads start to work, as was assumed.

The situation of the column of course affects strongly to the temperatures. The studied cases, column in the middle in open space near the shelves with fire load and near the wall varied from each other naturally and the highest temperatures are of course, when the column is engulfed in fire from all sides.

The basic assumption of the fire model in this work might cause too big thermal exposure to the structures and therefore over-estimate the temperatures of the steel columns.

Altogether the results show the effectiveness of sprinkler protection even in this high cases. Of course the functioning of the system has to be reassured to be able to use it as structural fire protection. This is still not an issue when following the sprinkler rules.

More research is planned and will be done in the following years.

The Authors wish to acknowledge the company Ruukki Construction Oy and VTT of good co-operation.

### REFERENCES

- Vaari J, Research report VTT-R-00985-13, Cooling of structures in high storages using sprinkler system, Espoo 2013
- Golinveaux, Sprinkler technology – storage. Presentation at Tyco Storage Summit, Chicago, April 26, 2012.
- Kung, Early Suppression of Rack Storage Fires with K363 Standard Response Sprinkler. Fire Safety Science 10, pp. 403-414, 2011.
- Sheppard, Spray Characteristics of Fire Sprinklers. NIST GCR 02-838. National Institute of Standards and Technology, Gaithersburg, 2002.
- EN 1993-1-2, Eurocode 3: Design of steel structures. Part 1-2: General rules. Structural fire design, 2005.

## A SIMPLIFIED MODEL FOR MODELLING FLEXIBLE END-PLATE CONNECTIONS IN FIRE

Shuyuan Lin<sup>a</sup>, Zhaohui Huang<sup>a</sup>, Mizi Fan<sup>a</sup>

<sup>a</sup>Brunel University, School of Engineering and Design, Uxbridge, UB8 3PH, UK

### Abstract

In this paper a simplified robust 2-noded connection element has been developed for modelling the flexible end-plate connections at elevated temperatures. In this model, the two stage behaviours of flexible end-plate connection are considered. The model has the advantages of both the simple and component-based models. It is computationally efficient and has very good numerical stability under static solver conditions. A total of 14 tests are used to validate the model, demonstrating that this new connection model has the capability to accurately predict the behaviour of the flexible end-plate connections at elevated temperatures. The model can be used to simulate the flexible end-plate connections in real performance-based fire resistance design of steel-framed composite buildings.

**Keywords:** flexible end-plate connection, component-based model, fire resistance, steel structures.

### INTRODUCTION

In recent years considerable research has been done to investigate the performance of steel-framed composite buildings under fire conditions. Current research indicates that the robustness of steel connections is vitally important to the fire resistance of composite buildings. Traditionally, the beam-to-column joints are assumed to be classified as ‘pinned’ or fully ‘rigid’. However, the true behaviour of joints could be classified as ‘semi-rigid’, which is in between the two extremes. A flexible end-plate connection has higher flexibility and larger rotational capacity compared with a flush and extended end-plate connection. Flexible end-plate connection comprises a rectangular plate symmetrically welded to the supported beam web, with the whole assembly then bolted to the supported column flange on site. Because of its simplicity and economy in both fabrication and assembly, flexible end-plate connection is of great popularity in the construction of braced multi-storey steel framed buildings.

Many laboratory tests have been conducted to understand the behaviour of beam-to-column connections at elevated temperatures (Leston-Jones 1997, Al-Jabri et al, 2005). Al-Jabri et al (2005) developed a component-based model to predict the behaviour of flexible end-plate connection under fire conditions. However, the model is only capable of predicting the behaviour of flexible end-plate connection before the beam bottom flange comes into contact with the column flange. In 2008, a series of experimental tests was conducted on the flexible end-plate connections at both ambient and elevated temperatures by Hu et al, (2009), who subsequently developed a component-based model to simulate the response of the flexible end-plate connections at elevated temperatures. In their model, the two stage behaviours of the flexible end-plate connection are taken into account.

The models described so far are component-based models (also known as spring-stiffness models). In these models the connection is regarded as a combination of several basic components. Each individual basic component has its own strength and stiffness characteristics in terms of tension, compression or shear. The overall behaviour of the connection is represented by combining these basic components. The major shortcoming of component-based models is that under a static solver the analysis terminates if one of the components of the connection fails due to numerical singularity. Dynamic solvers need to be

used to overcome this problem, but the computational efficiency of the model is significantly reduced.

Huang (2011) has recently developed a robust 2-noded connection element for modelling the bolted flush and extended end-plate connection between steel beam and column at elevated temperatures. The model has good numerical stability under static solver condition. For this reason this model is employed here as the basis for the current development of a simplified model to simulate the behaviour of the flexible end-plate connections under fire conditions. The two stage behaviours of the flexible end-plate connections are considered in the model presented in this paper.

## 1 DEVELOPMENT OF THE NUMERICAL PROCEDURE

One of the main characteristic of the flexible end-plate connection is that its rotational response comprises two stages, as illustrated in Fig. 1. The first stage is the unimpeded rotation of the connection, and the second stage is when the bottom flange of the beam comes into contact with the flange of the column after sufficient rotation. These two stages comprise the moving of the compression centre of the connection from the end of the endplate to the centre of the beam bottom flange, which leads to an increase of moment resistance and rotational capacity.

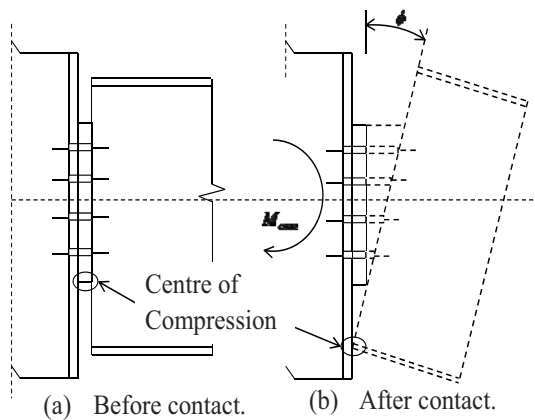


Fig. 1 Movement of centre of compression.

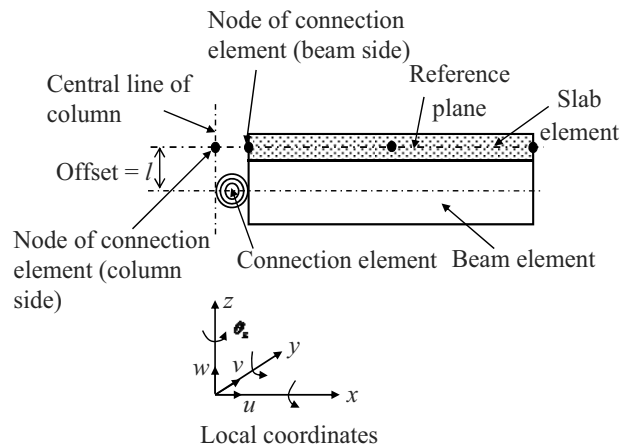


Fig. 2 Two-noded connection element.

These two stages are both taken into account in the model developed in this paper. The proposed numerical procedure is based on the main frame of Huang's two-noded connection element (Huang 2011) with the further developments to analyse the behaviour of the flexible end-plate connections at elevated temperatures. In Huang's original model, the connection is regarded as a two-noded element which has no physical length (see Fig. 2). Each node has six degrees of freedom, three translational degrees of freedom  $u, v, w$ , and three rotational degrees of freedom  $\theta_x, \theta_y, \theta_z$ . Only the in-plane behaviour of the connection element is considered. In order to develop a numerical procedure for determining the bending moment characteristic of the flexible end-plate connection in fire, the connection is divided into tension and compression zones. The developed models for determining the tension, compression and moment resistances of the flexible end-plate connection are based on the component-based method. The moment-rotation characteristic of the connection element is represented as a multi-linear curve at each temperature level (see Fig. 3). In the figure,  $S_{j,int}$  is the initial rotational stiffness of the connection element;  $\phi_{Xd}$  is the rotation when moment of the connection reaches the moment resistance  $M_{j,Rd}$ ;  $\phi_{Contact}$  is the rotation when the bottom flange of beam contacts to the flange of column after sufficient rotation;  $M_{Contact}$  is the

bending moment of the connection when contact happens;  $\phi_{Cd}$  is the maximum rotation of the connection. The rotation  $\phi_{ld}$ ,  $\phi_{Xd}$ ,  $\phi_{Contact}$  are calculated as follows:

$$\phi_{ld} = \frac{2M_{j,Rd}}{3S_{j,int}} \quad (1)$$

$$\phi_{Xd} = \frac{2M_{j,Rd}}{S_{j,int}} \quad (2)$$

$$\phi_{Contact} = \frac{t_p}{0.5 * D_{beam} - d_{beam,plt}} \quad (3)$$

where  $t_p$  is the thickness of flexible end-plate,  $D_{beam}$  is the depth of beam,  $d_{beam,plt}$  is the distance from the bottom flange of the beam to the end of endplate. Because the relative rotation between flexible endplate and the beam is small compared to the geometry of the connection, the value of rotation when contact occurs is calculated directly relate to the geometry of the flexible end-plate and the beam.

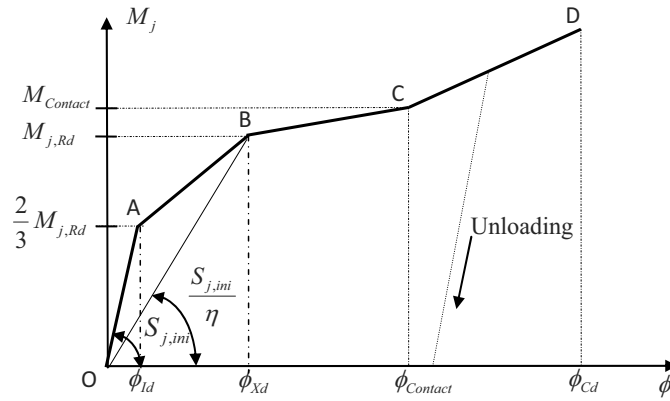


Fig. 3 Multi-linear moment-rotation curve used for the flexible end-plate connection.

Based on comprehensive numerical parametrical studies, the proposed moment-rotation characteristic of the flexible end-plate connection can be expressed as:

$$M_j = \begin{cases} S_{j,int} \phi & \phi \leq \phi_{ld} \\ \frac{M_{j,Rd}}{3(\phi_{Xd} - \phi_{ld})} \times (\phi - \phi_{ld}) + \frac{2}{3} M_{j,Rd} & \phi_{ld} \leq \phi \leq \phi_{Xd} \\ 0.065 \times S_{j,int} \times (\phi - \phi_{Xd}) + M_{j,Rd} & \phi_{Xd} \leq \phi \leq \phi_{Contact} \\ \left( \begin{array}{l} 0.065 \times S_{j,int} \times (\phi_{Contact} - \phi_{Xd}) + M_{j,Rd} \\ + 0.15 \times S_{j,int,II} \times (\phi - \phi_{Contact}) \end{array} \right) & \phi_{Contact} \leq \phi \leq \phi_{Cd} \end{cases} \quad (4)$$

where  $S_{j,int,II}$  is the initial stiffness of the connection for the second stage. If the rotation of connection  $\phi$  is larger than  $\phi_{Cd}$ , it is assumed that the connection is broken, hence the bending moment  $M_j$  is assumed to be zero.

The initial stiffness of the connection  $S_{j,int}$  is calculated based on the model developed by Al-Jabri et al (2005), as shown below:

$$\frac{1}{S_{j,int}} = \frac{1}{K_{eqt} z^2} + \frac{1}{K_c z^2} \quad (5)$$



where  $K_{eqt}$  is the equivalent tension stiffness,  $K_c$  is the compression stiffness,  $z$  is the equivalent level arm.

When the connection has more than one bolt row in tension, the level arm  $z$  is the distance from the centre of compression to the equivalent tension bolt row, which can be expressed as (Al-Jabri et al, 2005):

$$z = \frac{\sum_r (K_{tt,r} h_r^2)}{\sum_r (K_{tt,r} h_r)} \quad (6)$$

where  $K_{tt,r}$  is the tension stiffness of each individual bolt row  $r$ ,  $r$  is bolt row number,  $h_r$  is distance from bolt row  $r$  to the centre of compression.  $K_{tt,r}$  is given as the combination of the stiffness of three components as follows (Hu et al, 2009):

$$\frac{1}{K_{tt,r}} = \frac{1}{K_{plt}} + \frac{1}{K_{weld}} + \frac{1}{N_{bt} K_{bt}} \quad (7)$$

where  $K_{plt}$ ,  $K_{weld}$ ,  $K_{bt}$  are the stiffness for the T-stub assembly, the weld and the bolt respectively.  $N_{bt}$  is the number of bolts in tension at a given bolt row. The detail formulation for calculating the stiffness of these three basic components can be found in the Reference (Hu et al, 2009).

In the tension zone, equivalent tension stiffness  $K_{eqt}$  represents the overall initial stiffness when the connection has more than one tension bolt row. This equivalent tension stiffness can be given from the following expression (Al-Jabri et al, 2005):

$$K_{eqt} = \frac{\sum_r (K_{tt,r} h_r)}{z} \quad (8)$$

When rotation of the connection  $\phi < \phi_{Contact}$  the centre of compression is at the bottom end of endplate. However, when  $\phi_{Contact} \leq \phi \leq \phi_{Cd}$ , the bottom flange of the beam comes into contact with the column flange. At this stage, the centre of compression shifts to the centre of beam bottom flange, which leads to the increase of level arm  $z$ . Hence the initial stiffness  $S_{j,int,II}$  for the second stage is increased.

The tension capacity of each individual bolt row is calculated based on the component-based model proposed by Hu et al (2009). In the current model, the connection is considered as a combination of three basic components, which are the bolt, weld and a T-stub assembly comprising the endplate and the beam web. Each component has its own elastic stiffness and tension resistance. For the T-stub assembly, there are three different failure mechanisms. According to the experimental tests conducted by Hu et al (2009), the failure mechanism for the flexible end-plate connections is mainly the second failure mode. The second failure mechanism is that the T-stub suffers complete yielding, which has a first plastic hinge forming at the flange-to-web intersection and a second plastic hinge occurring in the bolt line. Therefore, in this model, the stiffness and the tension resistance capacity of the T-stub assembly is calculated based on the second failure mode.

For each individual tension bolt row, its tension resistance  $F_{tens,r,bolt}$  can be determined as the minimum value of tension resistance of three basic components as below:

$$F_{tens,r,bolt} = \min(F_{plt}, F_{weld}, F_{bt}) \quad (9)$$

where  $F_{plt}$ ,  $F_{weld}$ ,  $F_{bt}$  are the tension capacity for the T-stub assembly, the weld and the bolt respectively. The detail formulation for determining them can be found in the Reference (Hu et al, 2009). For the compression zone, the rotational stiffness is taken as the value of stiffness of column web, which is calculated based on a simplified model proposed by Block et al (2007).

The moment resistance of a flexible end-plate connection can then be calculated as:

$$M_{j,Rd} = \sum_r h_r F_{tens,r,bolt} \quad (10)$$

where  $F_{tens,r,bolt}$  is the tension resistance of bolt row  $r$ .

In this paper, steel material properties, such as yield strength; ultimate tensile strength and Young's module, are temperature dependent. It is assumed that the material degradation of bolts at elevated temperatures is the same for the beam, column and endplate and the material model specified in Eurocode 3 Part 1.2 (2005) is adopted.

## 2 VALIDATIONS

In order to validate the model presented above 12 tests conducted by Hu et al (2009) have been used, 3 of these were at ambient temperature and 9 at elevated temperatures. In the validation the measured material properties and temperature distribution within the connections are used as input data for the model. The connections tested by Hu et al comprised of a 305x165x40UB beam connected to a 254x254x89UC column, with three M20 Grade 8.8 bolts. The thickness of partial endplate is 10mm. During the tests, the force was applied with inclined angle ( $\theta$ ) to the axis of the connected beam. Three angles,  $\theta = 35^\circ$ ,  $45^\circ$  and  $55^\circ$ , were employed. These three different angles represent three different combinations of vertical shear, axial tension. Three different temperatures of  $450^\circ\text{C}$ ,  $550^\circ\text{C}$  and  $650^\circ\text{C}$  were also employed. According to the test data the two stage behaviours of the partial end-plate connection only occurred in the three ambient temperature tests. In the 9 tests at elevated temperatures the endplate ruptured before the bottom flange of the beam contacted the column.

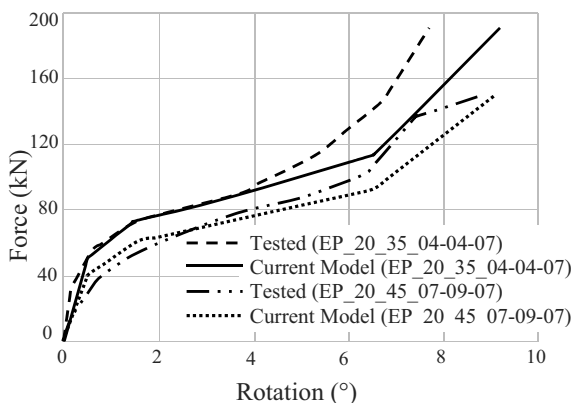


Fig. 4 Comparison results for Tests EP\_20\_35-04-04-07 and EP\_20\_45\_07-09-07(Hu et al, 2009).

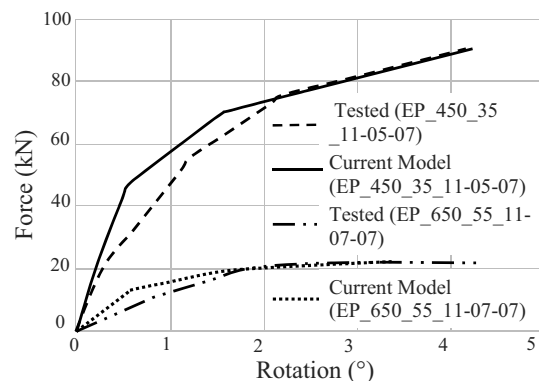


Fig. 5 Comparison results for Tests EP\_450\_35\_11-05-07 and EP\_650\_55\_11-07-07(Hu et al, 2009).

Due to space limitations only five tests are presented here for illustration. Fig. 4 shows a comparison between the results of two ambient tests. Tests of EP\_20\_35\_04-04-07 and EP\_20\_45\_07-09-07 were conducted with the force applied at an angle of  $35^\circ$  and  $45^\circ$ , respectively. In these figures it can be seen that the proposed model provides good agreement with the test data, suggesting that the model predicts the two stage behaviours of the connection well. Fig. 5 and Fig. 6 illustrate three comparisons between predicted and measured connection rotations at elevated temperatures. The tests of EP\_450\_35\_11-05-07,

EP\_550\_35\_15-05-07 and EP\_650\_55-11-07-07 were conducted at 450°C ( $\theta = 35^\circ$ ), 550°C ( $\theta = 35^\circ$ ) and 650°C ( $\theta = 55^\circ$ ), respectively. It is evident that the predicted results by the current model agree well with the tests data.

Two other fire tests conducted by Al-Jabri et al (2005) are also used for the validations. The tested connections consist of two 356x171x51UB beams symmetrically connected to a 254x254x89UC column with M20 Grade 8.8 bolts. The thickness of the flexible endplate is 8mm. The tests were conducted under a constant load with increased temperatures. Two different load levels of 8.2 kNm and 16.5 kNm were applied to the same connection. Fig. 7 shows the comparison of predicted and tested connection rotations for Test 1. It can be seen that the predictions of the current model are in good agreement with the test data.

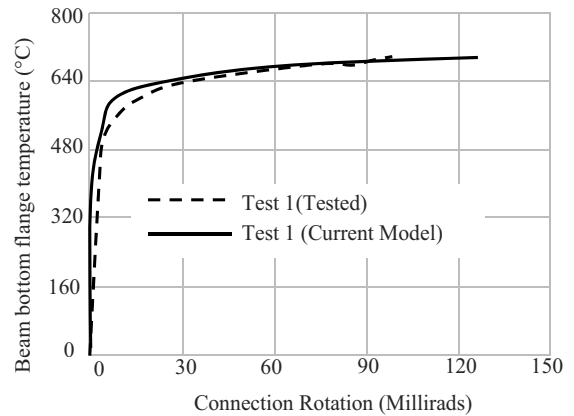
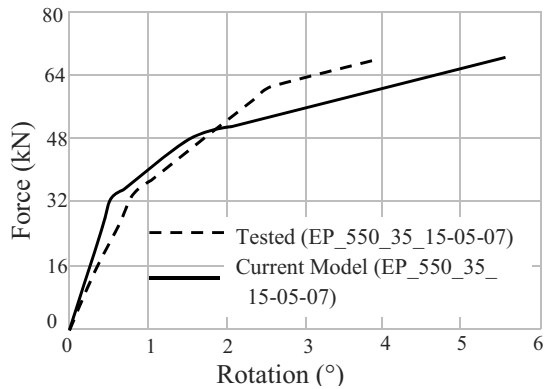


Fig. 6 Comparison results for test EP\_550\_35\_15-05-07 (Hu et al, 2009). Fig. 7 Comparison results for test 1(Al-Jabri et al, 2005).

### 3 CONCLUSIONS

In this paper, a simplified model has been developed for modelling flexible end-plate connections at elevated temperature. The two stage behaviours of the flexible end-plate connection have been explicitly considered in this new model, and the capacities of tension, compression, bending, and the initial stiffness of each connection are all calculated based on the component-based approach. The developed model has very good numerical stability under static solver and it is very computationally efficient. A total of 14 tests was used to validate this model. The validation results show very good correlation between the predicted and tested results at both ambient and elevated temperatures. Hence, it is evident that this new connection model has the capability to accurately predict the behaviour of the flexible end-plate connections at elevated temperatures. The model can be used to simulate the flexible end-plate connections in real performance-based fire resistance design of steel framed composite buildings.

### REFERENCES

- Leston-Jones L.C., The Influence of Semi-Rigid Connections on the Performance of Steel Framed Structures in Fire, PhD Thesis, Department of Civil and Structural Engineering, University of Sheffield, 1997.
- Al-Jabri K.S., Burgess I.W., Plank R.J., Sprint-stiffness Model for Flexible End-plate Bare-steel Joints in Fire, Journal of Constructional Steel Research 61:1672-1691, 2005.
- Hu Y., Davison J.B., Burgess I.W., Plank R.J., Component Modelling of Flexible End-plate Connections in Fire, Steel Structures 9:1-15, 2009.
- Huang Z., A connection Element for Modelling End-plate Connections in Fire, Journal of Constructional Steel Research 67(5):841-853, 2011.

Block F.M., Davison J.B., Burgess I.W., Plank R.J., The Development of a Component-based Connection Element for Endplate Connections in Fire, *Fire Safety Journal* 42:498–506, 2007.

European Committee for Standardization CEN, BS EN 1993-1-2, Eurocode 3: Design of steel structures: Part 1.2: General rules-structural fire design, British Standards Institution, 2005.

## **FIRE TESTS ON BEAMS WITH CLASS 4 CROSS-SECTION SUBJECTED TO LATERAL TORSIONAL BUCKLING**

Martin Prachar <sup>a</sup>, Michal Jandera <sup>a</sup>, František Wald <sup>a</sup>

<sup>a</sup> CTU in Prague, Fac. of Civil Engineering, Department of Steel and Timber Structure, Prague, Czech Republic

### **Abstract**

This paper describes experimental research in behaviour of laterally unrestrained beams (I or H section) of Class 4 constant or variable cross-sections at elevated temperatures. Preparation and design of experiments is described. The design of the test set-up was made by FE modelling and the experiments followed. The test results are given. Future numerical investigation is planned for full understanding of the fire behaviour of steel members of Class 4 cross-sections considering both welded and hot-rolled I or H shape steel profiles.

**Keywords:** steel structure, beam, slender section, lateral torsional buckling, fire design

### **INTRODUCTION**

In the last decade, structural fire design became an inseparable part of structural design. The accuracy of design is essential regarding safety of the structure as well as its economy, concerning also possible additional fire protection costs. Therefore, well representing design models, which simulate the actual behaviour of the structures exposed to fire, are crucial as a base of such design.

Recent design standard EC3 part 1-2 (EN 1993-1-2) contains simple rules for design of Classes 1 to 3 cross-sections under the fire. These rules were based on many experimental and numerical analyses and modified during last decade.

Determination of the bending resistance for members subjected to lateral torsional buckling of Classes 1 to 3 cross sections at elevated temperature is based on the same principles as the design at room temperature according to EC3 part 1-1 (EN 1993-1-1). However it differs in using one imperfection factor only for all types of cross-sections. Informative Annex E of the standard recommends using the design formulas for slender (Class 4) sections as well. But there is a restriction of critical temperature value and different reduction of yield strength is used (0.2 % proof strength for Class 4 instead of 2.0 % proof strength for stockier Class 1 to 3 sections).

Only few experimental data on which the potential refining of the provisions could be based have been collected until now. Therefore, further numerical investigations in lateral-torsional buckling at fire will be made for the slender sections. For the non-uniform members (variable section height), a limited procedure for lateral torsional buckling verification is given in EC3 part 1-1. This is applicable for room temperature only. A development of more general design model is planned to be published for elements at elevated temperature.

### **1 DESCRIPTION OF THE SPECIMENS**

The three tests vary in the cross-sections and considered temperature. Table 1 presents the tests, two beams with constant cross-section and one with variable cross-section (height of the web varies linearly from one end to another). The temperature was chosen based on the most significant changes of plate slenderness calculated using the elevated temperature reduction factors.

Tab. 1 Tested sections

Test number	Figure	Web*	Flange*	Temp [°C]	Non-dimensional slenderness	
					**	***
<b>Test 1</b> <b>IW460/150/4/5</b>	1a	Class 4 $\bar{\lambda}_p = 1.33$	Class 4 $\bar{\lambda}_p = 1.13$	450	1,06	0.86
<b>Test 21</b> <b>IW460/150/4/7</b>	1b	Class 4 $\bar{\lambda}_p = 1.23$	Class 3 $\bar{\lambda}_p = 0.81$	450	0.97	0.79
<b>Test 3</b> <b>IW585-495/150/4/5</b>	1c	Class 4 $\bar{\lambda}_p = 1.45 - 1.76$	Class 4 $\bar{\lambda}_p = 1.13$	650		

- NOTE** \* Classification and plate slenderness - according to EN 1993-1-2 ( $\varepsilon = 0.85[235/f_y]^{0.5}$ )
- \*\* Reduction of material properties - according to EN 1993-1-2 tab. 3.1. ( $\bar{\lambda}_{LT,\theta} = \bar{\lambda}_{LT}[k_{y,\theta}/k_{E,\theta}]^{0.5}$ )  
where  $k_{y,\theta}$  is is reduction factor (relative to  $f_y$ ) for effective yield strength of Class 1 to 3 sections)
- \*\*\* Reduction of material properties - according to EN 1993-1-2 Annex E ( $\bar{\lambda}_{LT,\theta} = \bar{\lambda}_{LT}[k_{0.2p,\theta}/k_{E,\theta}]^{0.5}$ )  
where  $k_{0.2p,\theta}$  is reduction factor (relative to  $f_y$ ) for the design yield strength of hot rolled and welded class 4 sections)
- 1 To avoid shear failure, a thicker plate was used for the side spans. Therefore, two thicknesses were used for the tested beam. 4 mm in the middle span and 5mm in the sidespan.

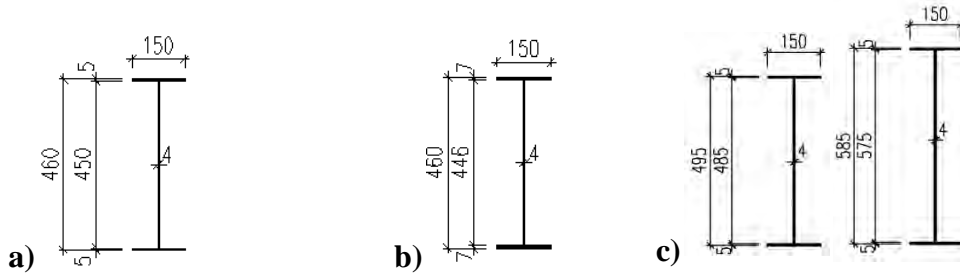


Fig. 1 Cross-section: (a) Test 1; (b) Test 2; (c) Test 3

## 2 NUMERICAL MODEL DEVELOPMENT

First of all, preliminary numerical model for calibration of experiments was made using FE software ABAQUS. The beam was meshed using rectangular shell elements type S4. Failure mode obtained from elastic buckling analysis was used as the initial geometric imperfection shape for post buckling analysis. The initial local and global imperfections were considered using following amplitudes:

- global =  $L/1000$  (where  $L$  is distance between lateral supports)
- local =  $B/200$  (where  $B$  is flange width)

In order to achieve LTB failure mode as main failure mode, different boundary condition and load distributions were modelled. The introduction of stiffeners and different thickness of stiffeners were considered too. Finally, in the location of supports, the pin point supports (one node only) were proposed. The point support allows no displacement in transverse direction as it is much easier to reach in the test and free torsion of the end sections. It has a negligible influence on the resistance and buckling shape. Significant lateral displacement could be observed as result of using pin supports. In the locations of load application, the top and bottom flange were provided with lateral restraints. Elevated temperature was used for the internal span only. Adjacent cross-section and stiffeners were considered at room temperature.

### 3 DESCRIPTION OF THE EXPERIMENTS

During the experiments a simply supported beam with two equal concentrated point loads applied symmetrically was tested. The heated central part of beam where the temperature was aimed to be constant and uniform was therefore subjected to a uniform bending moment. The fire test was performed on steady state, it means that the beam was first heated and then the loads were applied, until failure. The test was controlled by deflection which was estimated as 3.5mm per minute. Final deformation at the end of experiment was 50 mm at midspan. This procedure was the same for all three beams. Figure 2 shows a scheme of experiment.

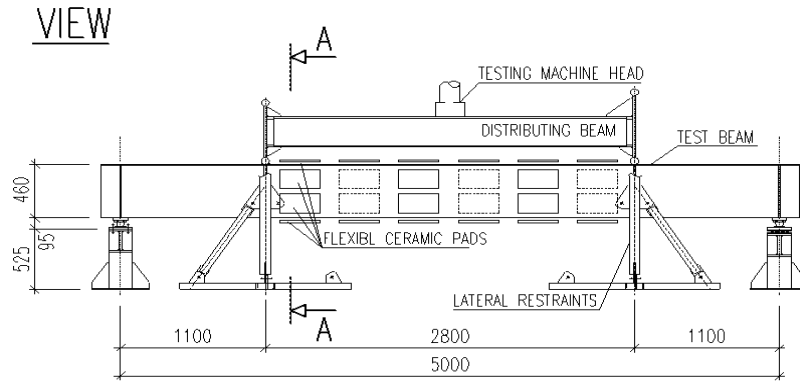


Fig. 2 Scheme of experiment

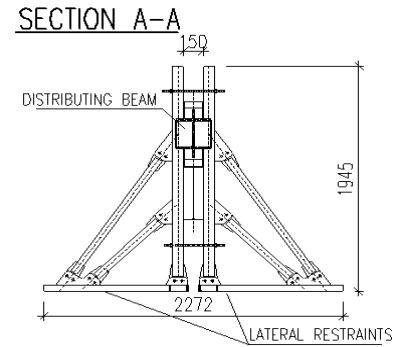


Fig.3 Lateral restraints

#### 3.1 Test set up equipment

Test equipments respected boundary conditions based by the numerical analyses. Their implementation is described below. Figure 3 shows the lateral restraint of the top and bottom flanges in the locations where the load is application (at the edge of heated part). The end supports were considered just by one point support. It was done using a steel sphere bearing placed between two steel plates. As was already described, both end supports allowed free torsion of the end cross-section. One restrains deformations in all directions. The second allows free horizontal displacement in the direction along the beam axis. Figure 4 and 5 shows the fixed pin point support of the beam.

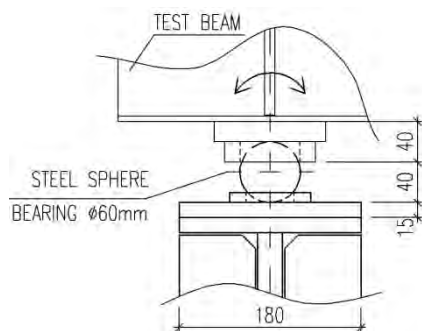


Fig. 4 Fixed pin point support

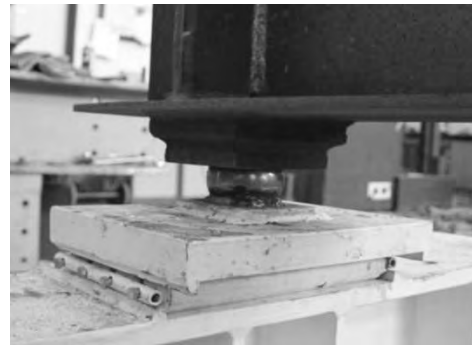
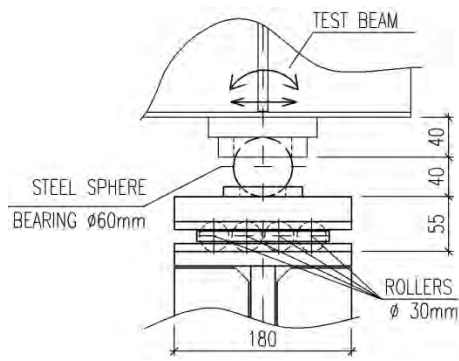


Fig. 5 Free pin point support

### 3.2 Measuring of initial imperfections

The initial geometry of the specimens were established using the two methods, namely laser scanning and manual measurements. The first method - the laser scanning (see Fig. 6) was used for determination of global and local initial imperfections. The second method consists of manual measurement of the exact dimensions of the specimens (width, depth, flange thickness, web thickness) and manual measurement of the amplitude of the local imperfection of the web and the top compression flange (see Fig. 7). The manual measurement was used just to validate the more precise, but not experienced laser-scanning method.



Fig. 6 Laser scanner



Fig. 7 Manual measurement

### 3.3 Heating of specimens

Mannings 70 kVA heat power units with 6 channels were used to heat the specimens. Cable connection of 70 kVA consists of 6 triple cable sets and 4-way splitter cables can accommodate 24 flexible ceramic pads attached. Maximum connected load for the 70 kVA unit is 64.8 kW. One size of the ceramic pads was used: 305 x 165 mm. The power output of the pad was 2.7 kW. Ceramic pads were placed as shown in Fig. 8.

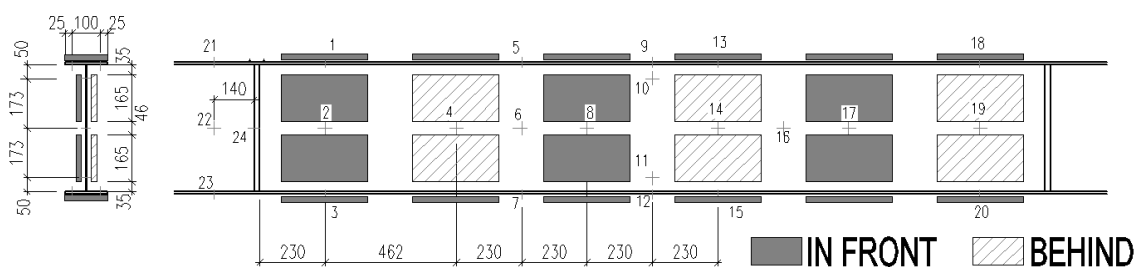


Fig. 8 Layout of flexible ceramic pads and thermocouples



In the first step, the pads were put on the rod rack in order to maintain the position of the heating elements on the web then were fixed by paper adhesive tape on the beam. On the bottom flange, the pads were fixed with the steel wires. On the top flange, the pads were fixed only by adhesive tape to the top of the section.

### 3.4 Measuring of temperatures

Twenty-four thermocouples were used for the temperature measurement. Twenty were placed in the middle span and four were placed in the side spans for monitoring of temperature in not-heated section. The thermocouples were distributed on the beam according to position of ceramic pads, as shown and numbered in Fig. 8. Beam temperatures were recorded from the beginning of heating to the end of experiment.

### 3.5 Measuring of strains

High temperature strain gages were used to measure strain distributions across the depth in the heated section. There were 4 high temperature strain gages attached to the beam at the midspan. Two were in the middle of the top flange and the other two in the middle of the bottom flange. At the side spans, there were 4 room temperature strain gages always one in the middle of the top flange and the second in the middle of the bottom flange. These 4 were attached to control the reactions in the supports and to monitor any frictional losses.

### 3.6 Displacements

The displacements were measured by potentiometers. Two potentiometers were used for measuring displacement in the locations of load application. Vertical (VD), see Fig. 11, and horizontal (HD), see Fig. 12, deflection of the bottom flange centre and lateral rotation (R), see Fig. 13, of the beam at midspan were calculated based on measurement of four potentiometers. Two measured relative vertical deflection and rest of them measured relative horizontal deflection (see Fig.9).

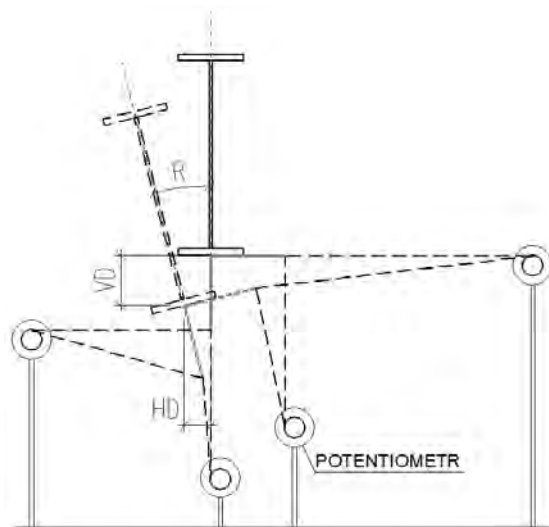


Fig. 9 Measuring of displacement at midspan

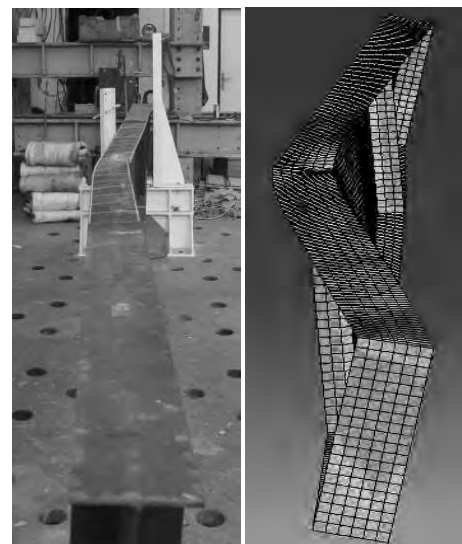


Fig. 10 Comparison of deformed shape (Experiment vs. FEM; test 2)

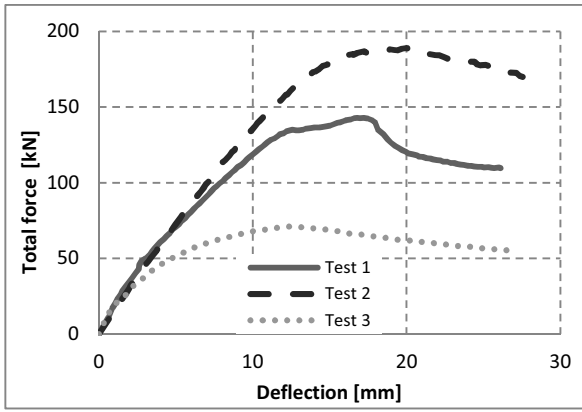


Fig. 11 Vertical deflection of bottom flange at midspan

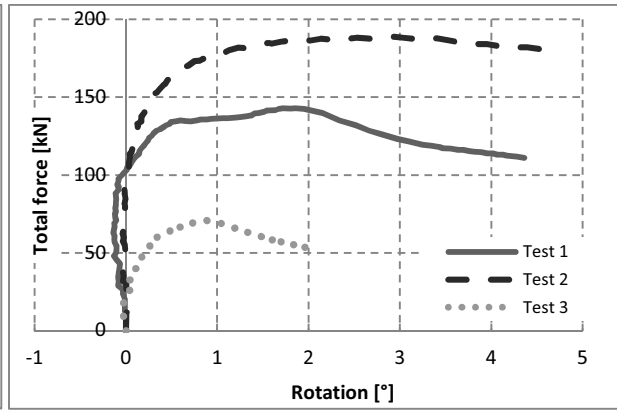


Fig. 12 Rotation about longitudinal axis at midspan

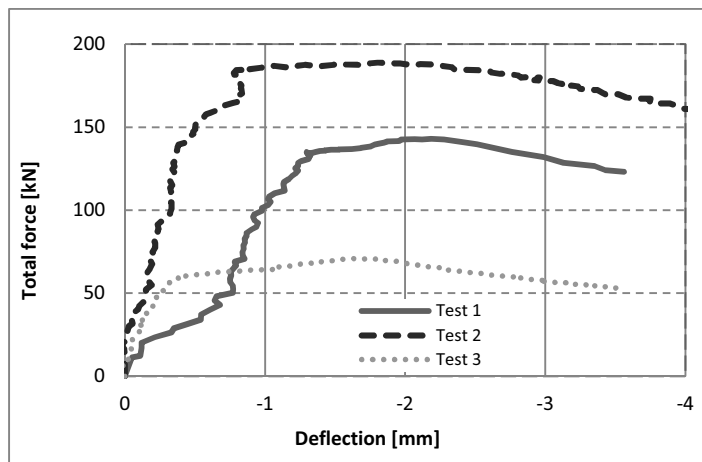


Fig. 13 Horizontal deflection of bottom flange at midspan

#### 4 SUMMARY

In this paper, three experimental tests of laterally unrestrained beams (I or H section) of Class 4 cross-sections at elevated temperatures were described (two beams with constant cross-section one beam with variable cross-section). Several types of displacement and the beam temperatures were measured. Now, these results are used for calibration of numerical model. A numerical validation for beams is currently being carried out (see Fig. 10). Future numerical investigation is planned for full understanding of the fire behaviour of steel members of Class 4 cross-sections considering both welded and hot-rolled I or H shape steel profiles.

#### REFERENCES

- EN 1993-1-2, Eurocode 3, Design of Steel Structures – Part 1-2: General rules - Structural fire design, 2005.
- EN 1993-1-1, Eurocode 3, Design of Steel Structures – Part 1-1: General rules and rules for buildings, 2005.

## RESISTANCE OF T- AND K-JOINTS TO TUBULAR MEMBERS AT ELEVATED TEMPERATURES

Emre Ozyurt<sup>a</sup>, Yong C. Wang<sup>a</sup>

<sup>a</sup> University of Manchester, School of Mechanical, Aerospace and Civil Engineering, Manchester, UK

### Abstract

The purpose of this paper is to investigate the ultimate capacity of welded steel tubular joints at elevated temperatures. Finite Element (FE) simulations of axially loaded tubular T- and non-overlapped K-joints at different elevated temperatures have been carried out using the commercial finite element software ABAQUS v6.10-1. Extensive numerical simulations have been conducted on CHS T- and gap K-joints subjected to brace axial compression or tension, considering a wide range of geometrical parameters. FE simulation results have been compared with the predictions by the CIDECT equations (CIDECT, 2010). It is found that this method overestimates the ultimate load carrying capacity of axially loaded CHS T-joints due to increased tubular wall deformation. For K-joints, this effect is negligible, therefore, the CIDECT equations produces accurate results.

**Keywords:** CHS, T-joints, K-joints, finite element model, ultimate capacity.

### INTRODUCTION

The popularity of hollow structural sections has increased in recent years due to their attractive aesthetics, simplicity, light weight and structural advantages. These sections have been widely used for onshore and offshore structures e.g. bridges, towers, space-truss, offshore platforms etc. Joints are generally the weakest part of the structural components due to stress concentrations.

The behaviour of welded steel tubular structural joints has been extensively studied at room temperatures. However, there is paucity of research on tubular connections under fire conditions. Nguyen et al. (2010) tested five full scale Circular Hollow Section (CHS) T-joints subjected to axial compression in the brace member at different temperatures. Meng et al (2010) and Liu et al (2010) presented experimental and numerical research results of the mechanical behaviour of steel planar tubular truss subjected to fire.

The configurations of a typical circular tubular T-joint and non-overlapped K-joint are presented respectively in Fig. 1 and Fig. 2. The brace members are in axial compression or tension and a wide range of geometrical parameters have been considered. FE simulation results have been compared with the predictions by using the CIDECT equations at ambient temperature but replacing the ambient temperature yield strength of steel by that at elevated temperatures (CIDECT, 2010).

### 1 FINITE ELEMENT MODEL DESCRIPTION

Finite element models of axially loaded tubular in-plane T- (Fig. 1) and non-overlapped K-joints (Fig. 2) at both ambient and elevated temperatures were validated using the general purpose nonlinear finite element package, ABAQUS/Standard v6.10-1 (2011). Numerical results were compared with experimental results of Nguyen et al., (2010) on T-joints, which were carried out at 20°C, 550°C and 700°C and those of Kurobane et al (2010) on K-joints at ambient temperature. To reduce computational time, only a quarter of the T-joints and one half of the K-joints were modelled due to symmetry in geometry and loading, where the

appropriate boundary conditions for symmetry were applied to the nodes in the various planes of symmetry.

### 1.1 Finite element type

Quadrilateral thick shell (S8R) elements for both the chord and brace members are suitable for accurate and economical predictions of T- and K-joints (Van der Vegte, 1992). For modelling welds, quadratic wedge solid elements (C3D15) instead of shell elements were used to allow accurate meshing of the weld geometry (Cofer et al., 1992).

### 1.2 Material properties

For the tubular T-joints tested by Nguyen et al (2010), the steel grade was S355 with a nominal yield strength  $f_y = 380.3 \text{ N/mm}^2$  and an ultimate strength  $f_u = 519.1 \text{ N/mm}^2$  from the coupon test results of Nguyen(2010). The elastic modulus of steel was assumed to be 210 GPa. The elevated temperature stress- strain curves were based on Eurocode EN-1993-1-2 (CEN, 2005a). In the ABAQUS simulation models, true stress – true strain relationships were used.

For the K-joint tests performed by (Kurobane et al., 1986), the nominal yield strengths were  $f_{y,c} = 480 \text{ N/mm}^2$ ,  $f_{y,b} = 363 \text{ N/mm}^2$  and ultimate strengths  $f_{u,c} = 532 \text{ N/mm}^2$ ,  $f_{u,b} = 436 \text{ N/mm}^2$  for the chord and brace members respectively.

### 1.3 Mesh convergence

Mesh convergence study was carried out to determine a suitable FE model for the analysis. The same mesh size was then applied for all models. Model PT3 of the tests by Nguyen et al (2010) was selected for this case.

Fig. 3 presents the mesh sensitivity study results. A mesh size of 10 mm was sufficient. Similarly, mesh convergence study was repeated for the weld geometry and a mesh size of 5 mm was suitable.

Within the joint zone, fine meshes (5 mm, 10 mm for weld and sections respectively) were applied in important regions where high stress gradient occurs, such as the intersection of the brace and chord members. Coarse mesh (20 mm) was chosen in the remaining regions according to the above mesh sizes. Fig. 4 illustrates a typical FE model and the weld detail of a T-joint.

### 1.4 Interactions and load application

In the case of welded models, the brace and chord members were tied with the weld elements using the ABAQUS “tie” function. Discretization method was defined as surface to surface contact. The brace and chord members at the connection region were chosen as a master surface, while the weld elements were slave surface.

Steady state condition was simulated, in which temperatures of the structure were raised to the required level and mechanical loading was then applied. In order to examine the large deformation behaviour, the RIKS method was chosen in ABAQUS. Both geometry and material non-linearities were included. When the arc length increments were arranged its maximum and minimum limitations of 0.1 and 1E-015 respectively, the convergence of iterations was achieved.

Furthermore, in all numerical analyses, the Von-Mises yield surface criterion and isotropic strain hardening rules were used in order to represent the yielding of steel.

### 1.5 Validations against available test data

T- joints of Nguyen et al. (2010) and non-overlapped K-joints of Kurobane et al. (1986) were used for validation. To illustrate the accuracy of the simulation models, T-joint Test PT3 was analysed under brace axial load at 20°C, 550°C and 700°C. One gap K-joint (G2C) was

modelled. The geometric parameters of the T- and K-joints are summarized in Tab. 1. Fig. 5 and Fig. 6 show boundary conditions of the T- and K-joints.

Fig. 7 and Fig. 8 compare the ultimate capacity of the joints and the load-displacement curves. A relative displacement of the brace ( $\delta$ ) was used, defined as the axial displacement of the compression brace relative to the central chord. From the comparisons, it can be concluded that the numerical simulations give close predictions of the test results.

## 2 PARAMETRIC STUDY

In this section, FE analyses were carried out on axially loaded tubular T- and non-overlapped K-joints at different elevated temperatures. The ultimate load ratio was used for comparison of the results. The ultimate load ratio ( $P_{\theta}/P_{20}$ ) was defined as the capacity of the joint at high temperature to that at ambient temperature. Tab 2 lists the parameters considered.

Fig. 9 shows the stress-strain curves for S355 grade steel at different temperatures, based on Eurocode EN-1993-1-2 (CEN, 2005a). Uniform temperature distribution was assumed for both the chord and brace members.

### 2.1 Effects of type of joints

A total of ninety numerical models were performed to understand how the strengths of T- and K-joints vary at different temperatures. Tab. 3 shows the FE results and compares the ratios of elevated temperature joint strength to that at ambient temperature with the reduction factors for effective yield strength based on Eurocode EN-1993-1-2 (CEN, 2005a). It can be seen that for K-joints, the two sets of results are in good agreement, indicating that the strength of K-joints at elevated temperatures can be obtained by using the CIDECT design equations, the only modification being to use the effective yield strength of steel at elevated temperatures. However, for T-joints, the numerical simulation strength ratios are generally lower than the reduction in the yield strength of steel at elevated temperatures.

When a T-joint is under brace compression load, the chord wall is in compression due to global bending and the side faces experience local deformation. The combined effect of a flattened chord (due to side face deformation) and P- $\delta$  effect (due to chord compression from global bending) reduces the yield line capacity of the chord face compared to that based on the original undeformed chord face. At elevated temperatures, both effects increase due to increased deformations as a result of reduced steel stiffness. Therefore, the joint failure loads decrease faster than the steel yield strength at elevated temperatures. This explains the lower joint resistance ratios compared to the steel yield strength reduction factors at elevated temperatures. Indeed, as will be shown in the next section, when the brace load is tensile, the P- $\delta$  effect and chord side face flattening effect disappear and the joint failure loads vary according to the effective yield strength reduction factor at elevated temperatures.

For a K-joint, there is no global bending and no flattening of the chord as the net load perpendicular to the chord face is zero. Hence, the changes in K-joint strength ratios are in accordance with the effective yield strength of steel at elevated temperatures.

### 2.2 Effect of loading conditions

PT4 joint (see Tab. 2) was used as an example to investigate the effects of brace loading directions. Fig. 10 compares the reduction in joint strength (normalised by the joint strength at ambient temperature) at elevated temperatures with the strength reduction factor of steel at elevated temperatures. Also, this figure includes the Eurocode EN-1993-1-2 (CEN, 2005a) reduction factors for elastic modulus of steel at high temperatures.

From the Fig. 10, it can be seen that when the brace is in tensile, the reduction in joint strength is very close to the steel yield strength reduction factor. In the case of brace compression, there is significant difference between the steel strength reduction factor and the numerical simulation result of joint strength ratio at elevated temperatures. The difference is particularly large at temperatures in the region of 200°C-700°C for which the steel elastic

modulus decreases much faster than the steel effective yield strength at elevated temperatures. This temperature region happens to be the most practically relevant. Therefore, it is not appropriate to simply use the high temperature steel yield strength in the ambient temperature equation (e.g. CIDECT or Eurocode EN-1993-1-8) to calculate the joint strength at elevated temperatures for T-joints with the brace in compression. An additional reduction factor, taking into consideration the change in elastic modulus of steel at elevated temperatures, should be introduced. For T-joints with the brace in tension, and as explained earlier for K joints, it is only necessary to replace the ambient temperature yield strength of steel by that at elevated temperatures.

### 3 RESULTS AND CONCLUSIONS

This paper has presented the results of a brief parametric study on the ultimate capacity of welded steel tubular joints at elevated temperatures. Finite Element (FE) simulations of axially loaded tubular T- and non-overlapped K-joints at different elevated temperatures were first validated against available test results. The effect of different joint types and loading conditions on the ultimate carrying capacity of the welded tubular joints at elevated temperatures was carried out to compare with the reduction factor for the effective yield strength of steel based on Eurocode EN-1993-1-2 (CEN, 2005a). It is found that for CHS T-joints under brace compression load, merely changing the ambient temperature yield strength of steel to the elevated temperature strength of steel overestimates the ultimate load carrying capacity of the joints. But this approach produced accurate results for gap K-joints and for T-joints with the brace member under axial tensile load. For T-joints with the brace in compression, the effect of chord face deformation should be considered. This may be done by introducing an additional reduction factor to take account of the steeper reduction in the elastic modulus of steel, compared to the reduction in the effective yield strength of steel, at elevated temperatures.

#### 3.1 Tables

Tab. 1 Joint test specimens used for FE model validation (refer to Fig. 1 and Fig. 2)

Joint Name	D (mm)	d (mm)	T (mm)	t (mm)	g (mm)	$\beta$ (d/D)	$\theta$ ( $^{\circ}$ )
PT3	244.5 (L=2200)	168.3 (l=1100)	6.3	6.3	-	0.69	90
G2C	216.4 (L=1560)	165.0 (l=800)	7.82	5.28	29.5	0.76	60

Tab. 2 Geometrical parameters for T- and K-joints

Joint Name	D (mm)	d (mm)	T (mm)	t (mm)	g (mm)	$\beta$ (d/D)	$\theta$ ( $^{\circ}$ )
KT1	219.1 (L=1500)	193.7 (l=1100)	6.3	6.3	30	0.88	60
KT2	219.1 (L=1500)	168.3 (l=1100)	6.3	6.3	30	0.77	60
KT3	219.1 (L=1500)	114.3 (l=1100)	6.3	6.3	30	0.52	60
PT1	244.5 (L=2200)	168.3 (l=1000)	10	10	-	0.69	90
PT2	244.5 (L=2200)	139.7 (l=1000)	6.3	6.3	-	0.57	90
PT3	244.5 (L=2200)	114.3 (l=1000)	6.3	6.3	-	0.47	90
PT4	323.9 (L=4000)	193.7 (l=1000)	10	10	-	0.60	90
PT5	323.9 (L=3000)	168.3 (l=1000)	10	10	-	0.52	90
PT6	323.9 (L=3000)	139.7 (l=1000)	10	10	-	0.43	90
PT7	323.9 (L=3000)	114.3 (l=1000)	10	10	-	0.35	90

Tab. 3 FE results for T- and K-joints

Joint Name	20° C	200° C	300° C	400° C	500° C	600° C	700° C	800° C	900° C
Eurocode	1.00	1.00	1.00	1.00	0.78	0.47	0.23	0.11	0.06
KT1	1.00	0.99	0.97	0.96	0.76	0.46	0.22	0.11	0.06
KT2	1.00	0.99	0.98	0.96	0.76	0.45	0.22	0.11	0.06
KT3	1.00	0.99	0.96	0.94	0.74	0.43	0.21	0.11	0.06
PT1	1.00	0.98	0.95	0.88	0.70	0.41	0.19	0.10	0.06
PT2	1.00	0.98	0.95	0.90	0.72	0.41	0.20	0.10	0.06
PT3	1.00	0.99	0.96	0.90	0.72	0.42	0.19	0.10	0.06
PT4	1.00	0.95	0.87	0.80	0.64	0.36	0.17	0.09	0.05
PT5	1.00	0.98	0.96	0.89	0.71	0.41	0.20	0.10	0.06
PT6	1.00	0.98	0.96	0.90	0.71	0.42	0.20	0.10	0.06
PT7	1.00	0.98	0.96	0.90	0.72	0.42	0.20	0.10	0.06

### 3.2 Figures

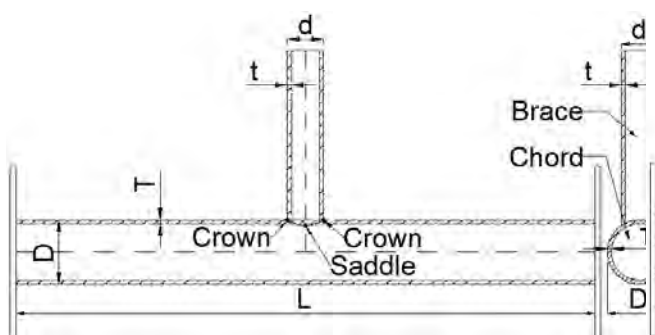


Fig. 1 Configuration of a typical T-joint

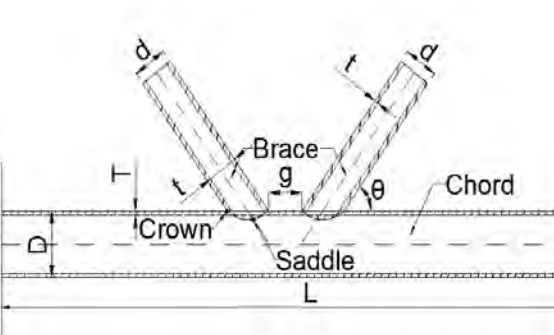


Fig. 2 Configuration of a typical gap K-joint

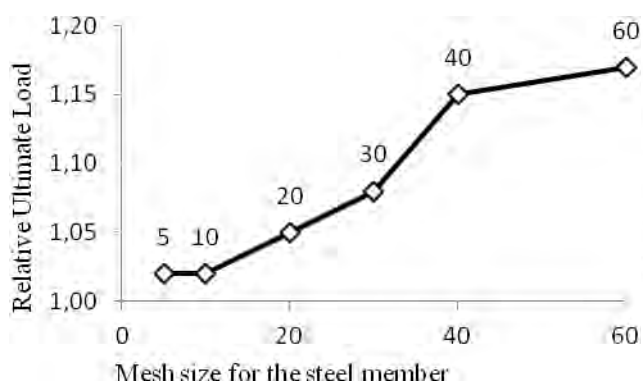


Fig. 3 Mesh convergence

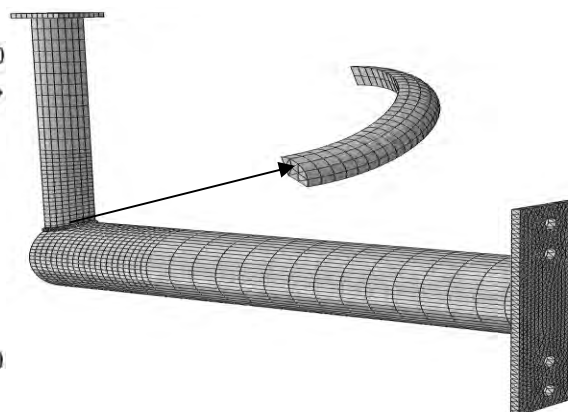


Fig. 4 Finite element mesh

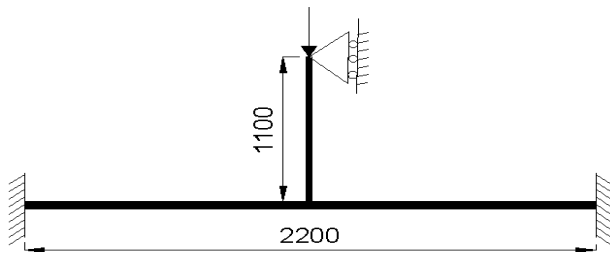


Fig. 5 Boundary conditions of a T-joint

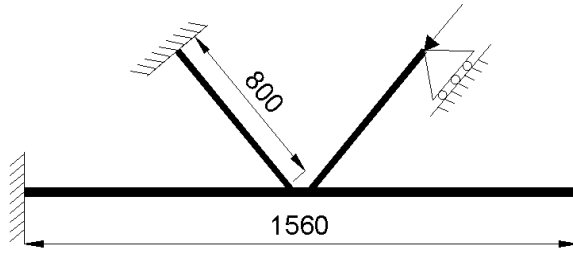


Fig. 6 Boundary conditions of a K-joint

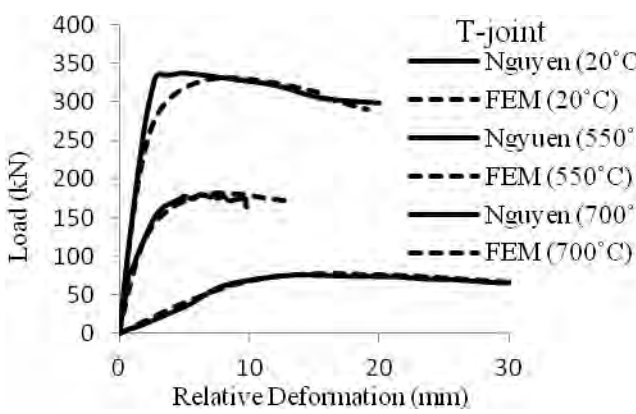


Fig. 7 Validation of the FE model for T-joints

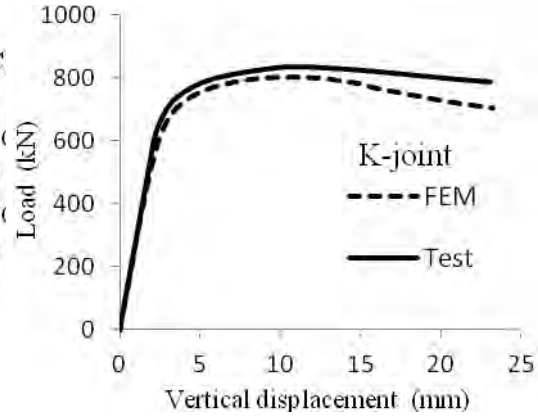


Fig. 8 Validation of the FE model for K-joint

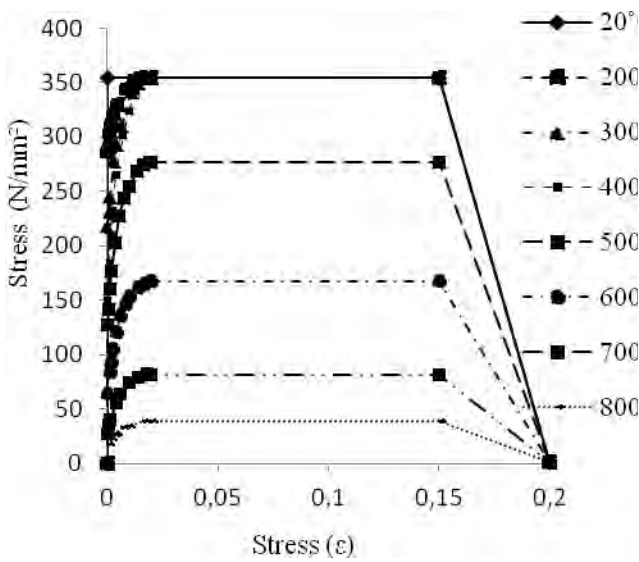


Fig. 9 Stress-strain relationships at elevated temperatures

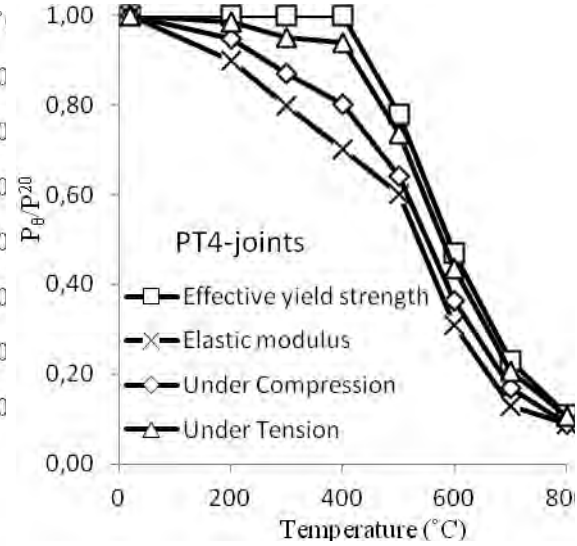


Fig. 10 Comparison of PT4-joints under different loading conditions



## REFERENCES

- Abaqus/Standard, Version 6.11-1, K. a. S. Hibbit, USA, (2011).
- Boresi & Schmidt, Advanced mechanics of materials, 6th Ed., John Wiley and Sons,(2003).
- Cidect, Design Guide for Circular Hollow Section (CHS) Joints Under Predominantly Static Loading, 2th Ed., Verlag TUV Rheinland, Germany, (2010).
- Cofer, William F., and Jihad S. Jubran. "Analysis of welded tubular connections using continuum damage mechanics." **Journal of Structural Engineering** 118.3 (1992): 828-845.
- European Committee for Standardisation (CEN), Eurocode 3: Design of Steel Structure, Part 1.2: General rules-Structural fire Design, Brussels, British Standards Institution, (2005a).
- European Committee for Standardisation (CEN), Eurocode 3: Design of Steel Structure, Part 1.8: Design of joints, Brussels, British Standards Institution., (2005b).
- Kurobane, Ogawa, Ochi & Makino, Local buckling of braces in tubular K-joints, Thin-Walled Structures, vol. 4, pp. 23-40, (1986).
- Liu, Zhao & Jin, An experimental study of the mechanical behavior of steel planar tubular trusses in a fire, Journal of Constructional Steel Research, 66, 504-511,(2010).
- Meng, Jincheng, Minglu & Jing, Parametric analysis of mechanical behaviour of steel planar tubular truss under fire, Journal of Constructional Steel Research, 67, 75-83,(2010).
- Nguyen, Fung & Tan, An experimental study of structural behaviours of CHS T-joints subjected to brace axial compression in fire condition, In: Tubular Structures XIII – Young(ed), 2010.
- Van Der Vegte, The static strength of uniplanar and multiplanar tubular T- and X- joints, Doctoral Dissertation, Delft University of Technology, Netherlands, (1995).

## POST-IMPACT FIRE RESISTANCE OF T-STUB JOINT COMPONENT Numerical Evaluation

JoãoRibeiro <sup>a</sup>, Aldina Santiago <sup>a</sup>, Constança Rigueiro <sup>b</sup>

<sup>a</sup> ISISE, Faculdade de Ciências e Tecnologia, Universidade de Coimbra, Coimbra, Portugal

<sup>b</sup> ISISE, Escola Superior de Castelo Branco, Instituto Superior de Castelo Branco, Castelo Branco, Portugal

### Abstract

Current paper presents a finite element analyses for the characterization of the nonlinear behaviour of bolted t-stub component subject to impact loading followed by fire. The proposed numerical model has previously validated against experimental results under monotonic static loading at ambient and elevated temperatures (Ribeiro *et al.*, 2013). 3D solid and contact elements from the finite element package Abaqus are used to perform the structural model. The temperature dependent material properties, the geometrical and material nonlinearities (including the strain rate sensitivity) were taken into account to predict the failure of the t-stub. A parametric study was conducted to provide insight into the overall behavior, namely their stiffness, resistance, ductility and failure modes due to the effects of dynamic loading followed by fire.

**Keywords:** steel structures, numerical simulation, impact loading, elevated temperatures, T-stub component

### INTRODUCTION

The growing interest in robust design is a consequence of several events that led to the collapse of structures, like for example, the World Trade Centre (WTC) in 2001. The WTC attack has highlighted troublesome weakness in design and construction technologies on structural steel connections which exhibited poor performance when subject to impact loads and fire. The vulnerability of steel connections under dynamic actions has been emphasized by many studies, although most of them were performed for the purpose of mitigating seismic risk (Ellingwood *et al.*, 2007 and Luu, 2009), and few information exists concerning the performance of steel connections under impulsive loads (Yim, 2009, Tyas *et al.*, 2010 and Chang *et al.*, 2011).

Connections performance is directly linked to the robustness of steel structures due to the influence of its ductility and rotation capacity. Currently, the design of steel joints is based on the “component method” established in the Eurocode 3, Part 1.8 (EN1993-1-8, 2005). This method requires the accurate characterization (stiffness, resistance and ductility) of each active component; the t-stub is one of the main components that assure the joint ductility due to its high deformation capacity. This paper intends to study fire and impact loading and apply them to a finite element model for the representation of the nonlinear behaviour of bolted t-stub component under such conditions. Focus is given on the effects of damage due to impact loading on the evolution of structural response.

### 1 STRAIN RATE EFFECT

Strain rate is the deformation, i.e. strain variation, that a material is subject per unit time,  $d\varepsilon/dt$ . Most ductile materials have strength properties which are dependent of the loading speed; mild steel is known to have its flow stress affected. The effects of strain rate on steel strength are illustrated in Fig. 1. The results were obtained from compressive Split Hopkinson Pressure Bar test (SHPB) (Saraiva, 2012); it was observed that yield and ultimate strengths

increase beyond the results obtained with a static test, the rupture strain decreases and the elastic modulus remains indifferent to the loading rate.

Finite element models aiming to simulate the behaviour of structural elements when subject to impact loads require a constitutive law representing the behaviour of materials at high strain rates. Cowper-Symonds and the Johnson–Cook constitutive laws are the widely used in numerical simulations. In the current model, the strain rate effects were considered by the Johnson–Cook law, Eq. (1).

This law describes material hardening through an exponential function and is able to account for strain rate sensitivity and thermal softening behaviours. The constitutive law assumes that the slope of flow stress  $\sigma_y$ , is independently affected by each of the mentioned behaviours; therefore, only the second term (accounting for strain sensitivity) of the equation has been used.

$$\sigma_y = [A + B\varepsilon^n] \cdot [1 + C \ln\dot{\varepsilon}^*] \cdot [1 - (T^*)^m] \quad (1)$$

where:  $A$  is the yield stress;  $B$  and  $n$  represent the effects of strain hardening;  $m$  is the thermal softening fraction;  $\varepsilon$  is the equivalent plastic strain;  $\dot{\varepsilon}$  is the strain rate, and  $\dot{\varepsilon}^* = \dot{\varepsilon}/\dot{\varepsilon}_0$  is the dimensionless plastic strain rate for  $\dot{\varepsilon}_0 = 1.0 \text{ s}^{-1}$ ;  $C$  is the strain rate constant.

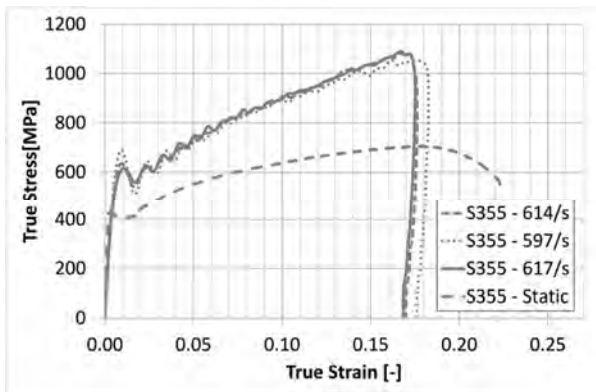


Fig. 1 Stress strain relationship of steel under high-strain rate (approx.  $600 \text{ s}^{-1}$ ) for  $t = 15 \text{ mm}$  plate, S355 (Saraiva, 2012)

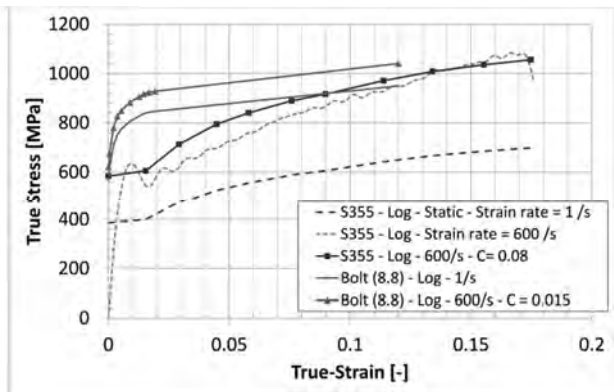


Fig. 2 Stress strain relationship for mild steel and bolts considering Johnson-Cook strain rate sensitivity

## 2 NUMERICAL MODEL

### 2.1 Description of the FE Model

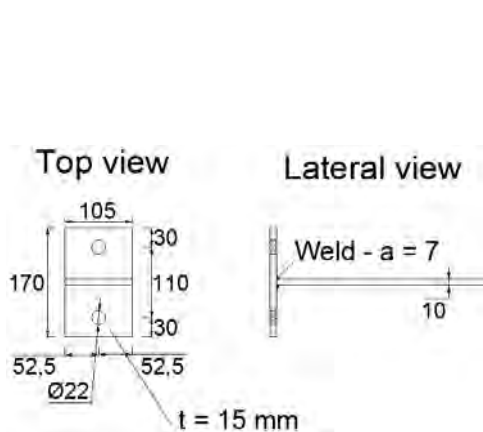


Fig. 3 T-stub geometry

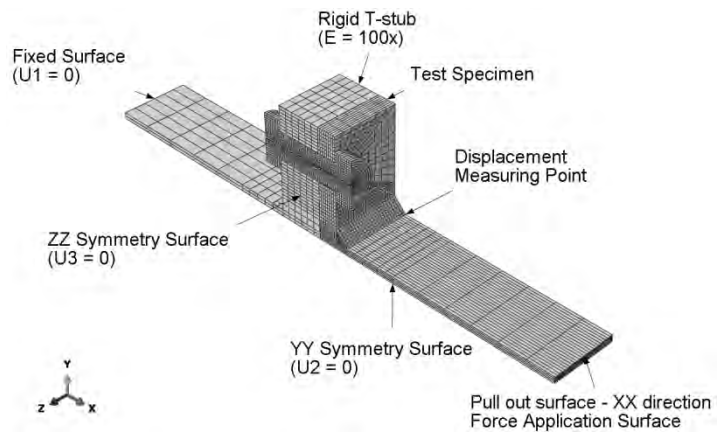


Fig. 4 Numerical model, boundary condition and mesh discretization

The numerical model is drawn from a previous study carried out at University of Coimbra, where numerical models under monotonic static loading at ambient and elevated temperatures (500 °C and 600 °C) were developed (Ribeiro *et al.*, 2013). Fig. 3 and Fig. 4 present the dimensions of the test specimens and the numerical model with boundary condition and mesh discretization. The flange was bolted through two bolts M20, grade 8.8 partially threaded.

The FE model is composed of four parts: (i) rigid back t-stub; (ii) tested t-stub; (iii) bolt, (head and shank as a single piece) and (iv) pull-out plate, as depicted in Fig. 4. Contact conditions are modelled between all the four parts namely: (i) the bottom flange surface with the back t-stub bottom flange; (ii) bolt shank with flanges bolt hole; (iii) top flange surfaces with bolt head; and (iv) pull out plate contact with the tested t-stub once the welds showed very little penetration. The welds have been modelled with tie constraint property linking the pull out plate to the tested t-stub part. Normal contact conditions are accomplished with “hard-contact” property allowing for separation after contact and the tangential behaviour has been assumed with a friction coefficient of 0.2 following “penalty” formulation. Bolt modelling followed the nominal geometry (bolt shank diameter with 20 mm). No pre-load has been considered.

The t-stub model has been simplified by the use of symmetry conditions in axes  $yy$  and  $zz$ ; therefore, displacements in these directions are restrained at the symmetry surfaces (Fig. 4). The model was generated with solid element type C3D8R, allowing large deformations and non-linear geometrical and material behaviour. C3D8R is a valuable choice due to its reduced integration (only 1 integration point) allowing for reductions in calculation time while it provides hour-glass behaviour control. Generally a structured mesh technique with “Hex” element shape is used, except for the weld zone where a “Wedge” element shape was employed.

Mesh discretization studies were previously conducted assuring that a discretization of at least 4 elements through the thickness of bending-dominated plates (t-stub flanges), and a concentric mesh around the bolt area provided accurate results, whilst optimizing calculation time and reducing convergence problems.

## 2.2 Material Properties

Material nonlinearity was included by specifying a non-linear stress-strain relationship for material hardening; Von Mises criterion was considered to establish the yield surfaces with the associated plastic flow for isotropic materials (Abaqus, 2006). Stress-strain relationship has been obtained through uniaxial coupon tests at ambient temperature (Santiago *et al.*, 2013). The mean results are: elastic modulus,  $E = 205500$  MPa, elastic strength,  $f_y = 385$  MPa; ultimate strength,  $f_u = 588$  MPa and ultimate strain,  $\epsilon_{cu} = 24\%$  for the steel. Uniaxial tension test on a M20 grade 8.8 bolt measured  $E = 202500$  MPa;  $f_y = 684$  MPa;  $f_u = 1002$  MPa and  $\epsilon_{cu} = 3.7\%$ . Once the bolt geometry follows nominal dimensions, bolt material properties have been revised to take into account the reduced tensile shank area. Material properties for the weld at ambient temperatures have been assumed equal to the base steel plates. For elevated temperature material models proper reduction factors reported in Eurocode 3, Part 1-2 (CEN, 2005) have been used for the mild steel, bolt, and also the weld. Once large strains and large displacements are expected, material’s constitutive law is included in the numerical model by the *true-stress – logarithmic plastic strain* curves (Fig. 2). As mentioned before, material strain rate sensitivity has been included using the second term of JC model.  $C_{steel} = 0.08$  for  $600 \text{ s}^{-1}$  was calculated from data obtained from SHPB tests (Saraiva, 2012) (Fig. 2). The literature indicate that high strength steels are less sensible to the effects of strain rate variation; According Chang *et al.*(2011) a dynamic increase factor (DIF) of 1.1 may be considered for the bolts; moreover, impact tests on A 325 bolts recovered from the WTC debris showed very low sensitivity to strain rate (Ellingwood *et al.*, 2007). In the current study, a DIF = 1.1 has been considered for bolt grade 8.8 for a strain rate of  $600 \text{ s}^{-1}$ , thus a value of  $C_{bolt} = 0.015$  was adopted (Fig. 2). The welds were assumed to have the same strain rate sensitivity as the base steel.

The Johnson–Cook law provides strain rate hardening varying linearly with the logarithm of strain rate; thus from  $1s^{-1}$  to  $600s^{-1}$  further data is required in case a non-linear variation of the flow stress with strain rate occurs.

### 2.3 Failure criterion

Material damage properties proposed by Hooputra (2004) and Al-Thairy (2011) are assumed in the current study (Fig. 6). These values are based on calibration to the observed failure modes from t-stub static tests and ultimate strain measured in uniaxial tests and SHPB.

### 2.4 Impact and fire loading

The study of rapidly applied loading such as an impact requires a dynamic analysis, once inertia effects of the system can no longer be disregarded; static force equilibrium is not required to be fulfilled. In order to take geometric non-linearities, material plasticity and strain rate behaviour into account, a non-linear dynamic analysis must be put through. In the proposed study the Abaqus dynamic/implicit solver is used.

The numerical analysis is divided in two steps: first, the impact loading is applied using a linear increasing load in 20 milliseconds (from zero to maximum load magnitude); a parametric study of the maximum load ranging from 200 to 900 kN is made. After the impact load reaches the maximum value, the load is decreased to zero in 5 milliseconds; then t-stub is left to vibrate during another 5 milliseconds. Afterwards a static load with magnitude of 70% of the analytical design resistance is set and a linear increase of temperature is applied.

## 3 ANALYSIS RESULT OF T-STUB SUBJECT TO IMPACT AND FIRE

### 3.1 Validation of the numerical model against experimental results under monotonic loading

Fig. 5 compares the numerical predictions (dashed lines) with the experimental results (solid lines) at ambient temperature and elevated temperatures of the t-stub component subject to monotonic static loading. It can be observed that the numerical model can accurately predict the global behaviour of the t-stub component. Considering the failure criteria exposed above, bolt rupture is the ultimate numerical failure mode for all numerical analysis; failure is identified with diamond marker in Fig. 5. Tests at ambient temperature exhibited bolt rupture at 14 mm of web displacement; test at 500 °C exhibited flange cracking around 10 mm of web displacement while for the 600 °C a long horizontal plateau is developed due to long bolt elongation.

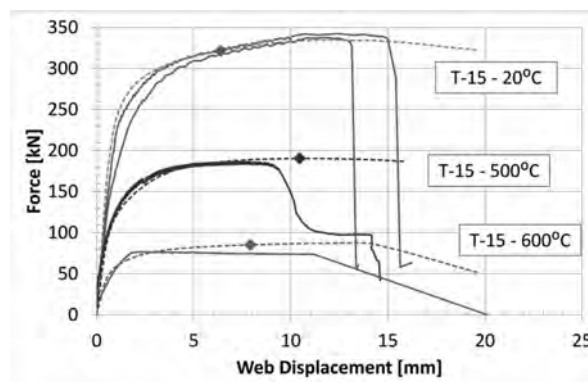


Fig. 5 Response of t-stub at 20, 500 and 600 °C: numerical versus experimental results (Ribeiro *et al.*, 2013)

### 3.2 T-stub subject to impact and fire

For the analysis at elevated temperatures, it has been assumed: (i) temperature variation introduced as a pre-defined field; (ii) high temperature creep effects of steel have not been taken into account; (iii) the temperature has been assumed to be constant throughout the FE model; and (iv) expansion effects due to temperature increase according to EC3 Part. 1-2 (CEN, 2005).

Fig. 7 illustrates the numerical predictions of the t-stub response under the impact loads; comparison with static test can also be made; it can be observed that with the increase of impact loading: i) that the elastic stiffness is not affected, as the elastic modulus remains unchanged; and ii) transition knee caused by the plastic hinge in the t-stub flange is similar for different impact loads; iii) the strain rate variability within the applied force range is very low; also, iv) compared with the static response the force at which the plastic hinge is formed is increased by +8%, far below the  $f_{y,din}/f_y = +51\%$  obtained from coupon tests comparison, Fig. 2. This is because the flange is not subject to a strain rate of  $600 \text{ s}^{-1}$  but mostly below  $80 \text{ s}^{-1}$ , as presented for the 900 kN load case (Fig. 8). For loads over 375 kN the t-stub failed under impact load; Fig. 9 presents results for impact load range of 300 to 375 kN: a critical temperature of  $560 \text{ }^\circ\text{C}$  is predicted for all models with failure due to bolt rupture. Within this study, it was observed, that the impact load imposes damage in the flange next to the weld toe, but not in the bolt; thus, the bolt failure at elevated temperature is not conditioned by previous impact load and all models fail with the same critical temperature. T-stubs subject to lower impact loads exhibit longer displacement development capacity when subject to temperature increase.

		Johnson-Cook C=		Bolt	Weld	Steel
		Strain-rate		0.015	0.08	0.08
				600	600	600
Ductile Dam.	Fracture strain	0.3	0.3	-	-	0.2 0.16
	StressTriaxiality	0.7	0.7	-	-	0.7 0.7
	Strain Rate	1	600	-	-	1 600
	Evolution	0.1		-	-	1
Shear Dam.	ks	0.3	0.3	0.3	0.3	0.3 0.3
	Fracture Strain	0.3	0.3	0.1	0.1	0.1 0.1
	Shear Stress Ratio	0.7	0.7	0.7	0.7	0.7 0.7
	Strain Rate	1	600	1	600	1 600
	Evolution	0.01		1		1

Fig. 6 Material damage parameters

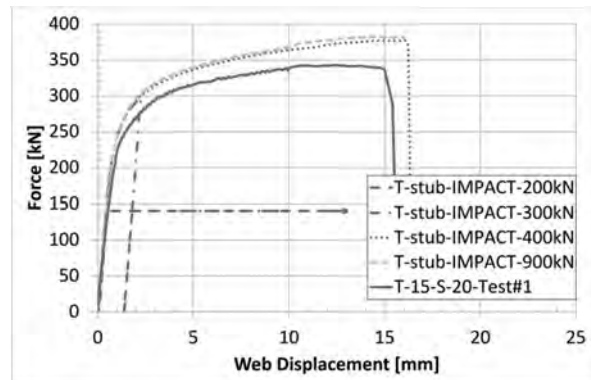


Fig. 7 T-stub response

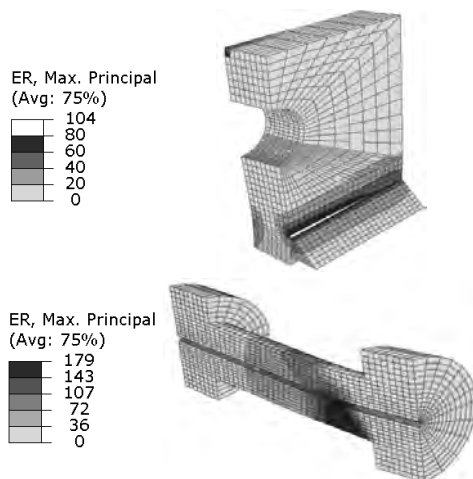


Fig. 8 Strain rate pattern for load of 900 kN

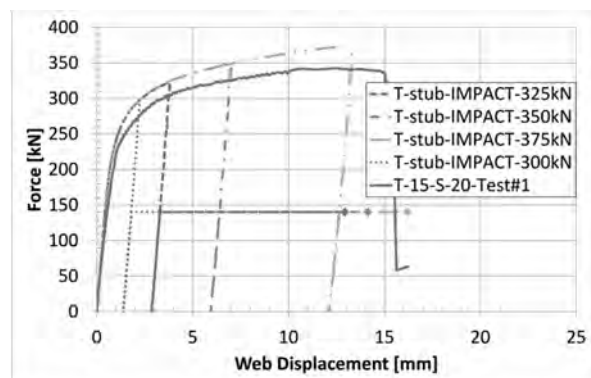


Fig. 9 T-stub response –  $\theta_{crit} = 560 \text{ }^\circ\text{C}$

## 4 SUMMARY

A FE model calibrated to static tests at ambient and elevated temperatures is enhanced to capture the behaviour of the t-stub component subject to several impact load levels, ranging from 200 to 900 kN in 20 milliseconds. Afterwards, the damaged t-stub is subject to a static load equivalent to 70% of the analytical design resistance and the temperature is increased up to failure; predictions of the critical temperature are made. Temperature material softening considers EC3 Part 1.2 (CEN, 2005) reduction factors. Strain rate effects have been taken into account with the Johnson-Cook strain sensitive term calibrated to compressive Split Hopkinson Pressure Bar tests at a strain rate of  $600\text{s}^{-1}$ . Although damage material properties are calibrated to fit observed failure modes from static t-stub tests and static uniaxial tension tests, both ambient and elevated temperatures, there are still great reservations in assessing the damage parameters, especially for high strain rates.

Taking into account the assumed failure criterion, the t-stub is able to resist a maximum impact load of around 375 kN. If the impact load does not damage the bolt, its fire resistance is not affected. Although they exhibit the same critical temperature, those subject to lower impact loads are able to develop longer displacement variation when subject to elevated temperatures; even if the absolute failure displacement is smaller.

## 5 ACKNOWLEDGMENT

The authors acknowledge financial support from Ministério da Educação e da Ciência (Fundação para a Ciência e a Tecnologia) under research project *PTDC/ECM/110807/2009*.

## REFERENCES

- Ellingwood, B.R., et al., Best Practices for Reducing the Potential for Progressive Collapse in Buildings 2007: NISTIR 7396.
- Luu Nguyen Nam, H. Structural response of steel and composite building frames further to an impact leading to the loss of a column. 2009.
- Yim, H.C. and Krauthammer, T., "Load-impulse characterization for steel connections", International Journal of Impact Engineering, Vol. 36, No. 5, pp. 737-745, 2009.
- Tyas, A., Warrem, J. A., Davison J.B., Stoddart E.P., and Hindle, A., Dynamic tests of semi-rigid beam-column connections in Proceedings of the COSTC26 International Conference on Urban Habitat Constructions under Catastrophic Events, Naples 2010.
- Chang, L., Hai, T., Ching, F., Tyas, A., "Numerical simulation of steel bolted beam-column connections subject to dynamic loading" Journal of Applied Mechanics and Materials, 2011.
- CEN, Eurocode 3: Design of steel structures part 1-8: Design of joints, 2005, Brussels: European Committee for Standardization.
- Saraiva, E., Variação das propriedades mecânicas do aço relacionadas com problemas de impacto em estruturas, in portuguese, Master Thesis at University of Coimbra, 2012.
- Barata P., Rigueiro M.C., Santiago A. e Rodrigues J.P., "Characterization of impact scenarios in steel structures"; pp. 242-249, Proceedings of the IABSE Workshop on Safety, Failures and Robustness of Large Structures, Helsinki, Finland, February 2013.
- Ribeiro J. N., Rigueiro C., Santiago A., Numerical behaviour of t-stub joint component at ambient and elevated temperatures, in 2° Cislaci 2013: Coimbra (paper submitted).
- Abaqus, "ABAQUS analysis: user's manual 2006", Providence, RI: ABAQUS Inc.
- Santiago A., Martins D., Barata P. e Jordão S., "Propriedades mecânicas do aço a temperaturas elevadas"; 2° CILASCI - Congresso Ibero-Latino-Americano sobre Segurança contra Incêndio, Coimbra, Portugal, June 2013

- CEN, “Eurocode 3: Design of steel structures. Part 1-2, General rules - Structural fire design”, 2005, Brussels: European Committee for Standardization.
- Seidt, J.D., Gilat, A., Klein, J.A., Leach, J.R., “High Strain Rate, High Temperature Constitutive and Failure Models for EOD Impact Scenarios”, Proceedings of the 2007 SEM Annual Conference and Exposition on Experimental and Applied Mechanics, Springfield, MA, June, 2007
- CEN, “Eurocode 3: Design of steel structures. Part 1-2, General rules - Structural fire design”, 2005, Brussels: European Committee for Standardization.
- Hooputra, H., H. Gese, H. Dell, and H. Werner, “A Comprehensive Failure Model for Crashworthiness Simulation of Aluminium Extrusions,” International Journal of Crashworthiness, vol. 9, no.5, pp. 449–464, 2004
- Al-Thairy, H., Wang, Y.C., “A numerical study of the behaviour and failure modes of axially compressed steel columns subjected to transverse impact”, International Journal of Impact Engineering, vol. 38, pp. 732-744, 2011



## FINITE ELEMENT ANALYSIS OF FIRE RESISTANT REINFORCEMENT ON END-PLATE STEEL CONNECTIONS

Konstantina Tsapara <sup>a</sup>, Georgios A. Drosopoulos <sup>b</sup>, Georgios E. Stavroulakis <sup>a</sup>

<sup>a</sup> Department of Production Engineering and Management, Technical University of Crete, GR-73132 Chania, Greece

<sup>b</sup> Institute of Continuum Mechanics, Leibniz University of Hannover, Germany

### Abstract

In this paper the effect of fire resistant coatings on the mechanical behaviour of steel joints is studied using the finite element method. The proposed finite element model is an extension of a previous one developed for the study of the same connection in elevated temperatures, without fire reinforcement. In particular, the construction used consists of an end – plate steel connection which is covered with panels of lightweight concrete and gypsum board. The behaviour of those two fire resistant materials has been simulated in elevating mechanical and thermal conditions separately and simultaneously. Through this process it is examined the strength of the materials and of the overall construction. Specifically, the action of fire on the strength of the structure may result in an early collapse. In addition, the behaviour of the structure in the connection area and the opening of the interface is investigated.

**Keywords:** fire resistant, steel joint, thermal analysis, fem

### INTRODUCTION

A significant number of scientific projects for the study of steel connections under elevated temperatures has been presented in the past. In particular, both analytical and experimental articles have been published (Lawson, 1990, Al-Jabri et al, 1998, Lien et al, 2009, Kalogeropoulos et al, 2012). On the other hand, scientific work related to the properties and behaviour of fire resistant materials, has been also presented (Jimenez et al, 2006, Weil, 2011, Rahmanian et al, 2012). In the present article an effort is made, for the coupling of structural elements (steel joint) and fire resistant materials (concrete or gypsum boards). Thus, a three dimensional, non-linear finite element model of an end-plate steel connection has been developed. The column, together with the critical bolted parts of the connection, are covered with a fire resistant material of either concrete or gypsum boards. Unilateral contact with friction has been used for the study of contact or separation of the connected parts. In addition, a thermomechanical analysis takes place, for the investigation of the behaviour of the structural system in high temperatures. According to the results presented here, the fire resistant coatings cause a significant reduction of the maximum temperatures developed on the structure, in comparison with the case of no fire reinforcement.

### 1 FIRE RESISTANT MATERIALS AND PROPERTIES

There are different materials available for protecting structural systems during a fire and providing a fire resistant rating. Among them are included insulating materials, which are often used for protecting structures from direct fire exposure. In particular, concrete and gypsum boards are considered to be good insulators and for this reason have been specifically used in this study.

The concrete has low thermal conductivity, and presents endothermic reactions in the cement mass. Under high temperatures, during a fire, a degradation of the mechanical characteristics of the concrete takes place. The compressive strength of the concrete decreases as the

temperature increases due to internal faults caused by the heating of the water and of the uneven distribution of the temperature in the mass of the concrete.

Systems of gypsum boards, as a mean of providing passive fire protection, are used in buildings as fire resistant coatings. The strength of such systems is attributed to the desired thermal properties of the gypsum, as a hygroscopic material.

The thermal properties of these two materials, as well as the mechanical ones slightly differ but in this analysis, the mechanical properties were considered equal, for simplicity. The thermal properties used for concrete and the gypsum boards are shown in Tab. 1.

Tab. 1 Thermal properties of concrete, gypsum board and steel

Temperature (°C)	Conductivity (W/m.°C)		Steel
	Concrete	Gypsum board	
20	0.988	0.200	53.33
100	0.938	0.183	50.67
200	0.875	0.120	47.34
300	0.813	0.100	44.01
400	0.750	0.120	40.68
500	0.688	0.123	37.35
600	0.625	0.130	34.02
700	0.563	0.137	30.69
800	0.500	0.147	27.30
900	0.500	0.160	27.30

The thermal expansion for the steel parts is taken equal to  $12 \times 10^{-6}/^{\circ}\text{C}$ , while the thermal expansion for the bolts is considered equal to  $13 \times 10^{-6}/^{\circ}\text{C}$ . For the thermal reinforcement, the thermal expansion is chosen equal to  $18 \times 10^{-8}/^{\circ}\text{C}$ .

## 2 GEOMETRY AND THE FINITE ELEMENT MODEL

The end-plate steel connection consists of an IPE-360 beam section, an HEA-220 column section, an extended end-plate and eight high strength M20 bolts with average yield and ultimate stresses  $F_y = 600 \text{ N/mm}^2$  and  $F_u = 800 \text{ N/mm}^2$  obtained from coupon tests, were used. The beam, the column, and the end-plate were made of steel having average yield and ultimate stresses  $F_y = 314 \text{ N/mm}^2$  and  $F_u = 450 \text{ N/mm}^2$ , respectively, also obtained from relevant coupon tests. The Young Modulus for the steel parts and the bolts is equal to 120 GPa and the Poisson's ratio to 0.3.

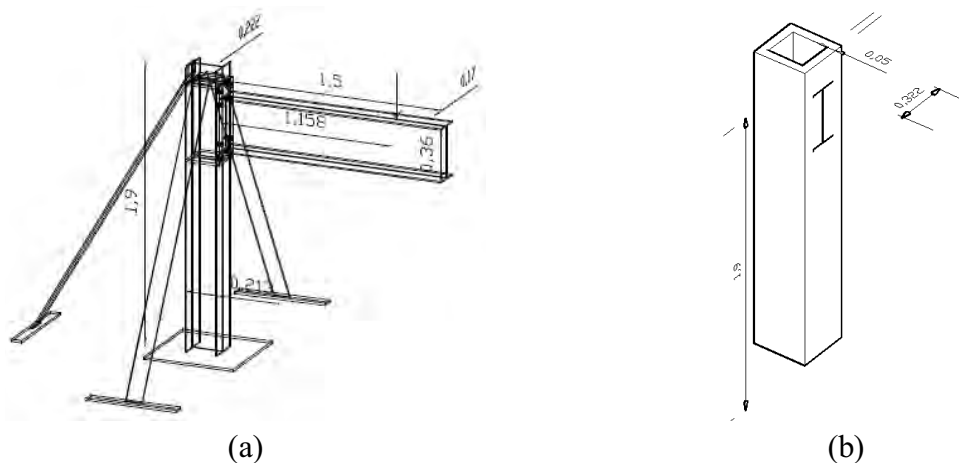


Fig. 1 Geometry of (a) the steel joing and (b) the fire resistant coating

The column, together with the bolted parts of the connection, are covered with a fire resistant panel of steady thickness. The geometry of the connection and the fire resistant coating, are shown in Fig. 1.

For the numerical analysis, three-dimensional 8-node brick finite elements have been used. The mesh of the model becomes denser around the area of the connection. The mesh of the structure is presented in Fig. 2. For the numerical solution of the non-linear problem the Newton–Raphson incremental iterative procedure has been used. For the interfaces between the column, the end-plate and the fire reinforcement, the friction coefficient is taken equal to 0.4.

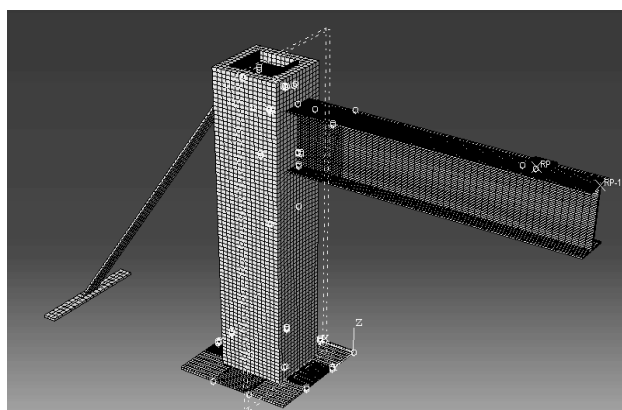


Fig. 2 Mesh of the end-plate connection and the fire resistant coating

Concerning the mechanical properties of the steel material, degradation of the Young Modulus has been considered according to Eurocode 3 (Eurocode 3). The stress–strain laws have been also considered at elevated temperatures (Eurocode 3). Moreover, large displacement analysis as well as the v. Mises plasticity model have been used in the numerical scheme. Finally, for the implementation of the contact and friction laws the penalty method has been chosen.

### 3 CONCEPT OF THE THERMOMECHANICAL ANALYSIS

The numerical analysis has been performed in two phases. In the first phase the pure heat transfer problem is solved. The results of the thermal analysis are imported as a predefined field, into the mechanical finite element model and the thermal-stress analysis is carried out.

It is possible to import the data obtained from the thermal analysis, into any of the steps developed within the thermomechanical model, thus creating the possibility of multiple load steps either thermal or mechanical which will alternate between them with any desired sequence each time. In particular, three main different load cases have been considered for two different fire resistant materials: concrete and gypsum board. In the first case, the thermal and a concentrated mechanical load are concurrently applied in the same analysis step. Within the second load case the thermal load precedes the point loading. The total mechanical load forced is 200 kN. According to the third load case, at the first step half of the initial thermal load is applied ( $1 \text{ kW/m}^2$ ), then follows a mechanical load of 50 kN, in the next step the remaining thermal load is forced ( $1 \text{ kW/m}^2$ ) and finally a mechanical load of 150 kN.

It has to be mentioned that the self-weight has been applied before any other load, at the beginning of the process. It is also noted that for the above load cases, the rate of increase of both the mechanical and the thermal load is linear, within each analysis step.

Among other, in this study are examined:

- The behaviour of the two fire resistant materials and of the overall structure under thermal and mechanical loads.

- The ultimate external vertical load on the beam before failure, the vertical displacements and the force-displacement diagrams.
- The behaviour of the contact–friction interface between the column and the end-plate of the beam (opening and sliding modes).

Finally, for the heat transfer analysis temperature boundary conditions have been applied as shown in Fig. 3. Also, a heat flux equal to  $2 \text{ KW/m}^2$  has been applied to the beam's top flange as it is shown in Fig. 4.

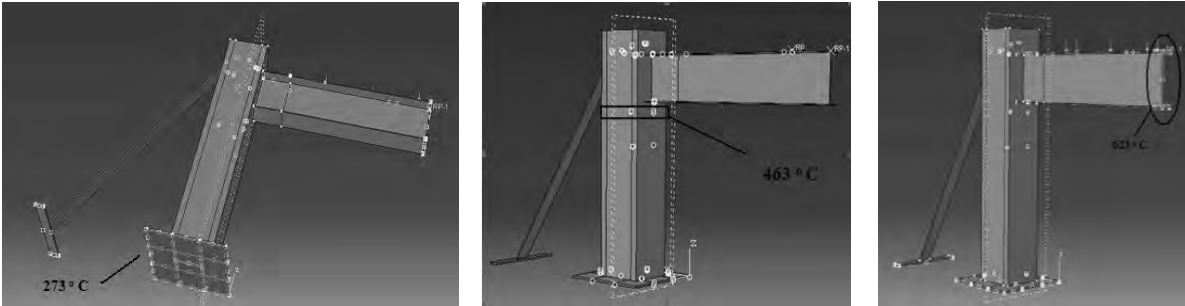


Fig. 3 Temperature boundary conditions

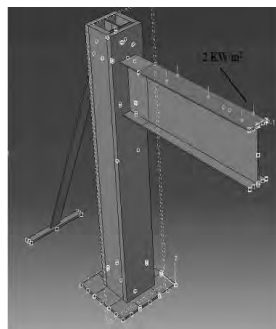


Fig. 4 Thermal heat flux

## 4 RESULTS AND DISCUSSION

### 4.1 Study of the influence of the sequence of thermal and mechanical loads

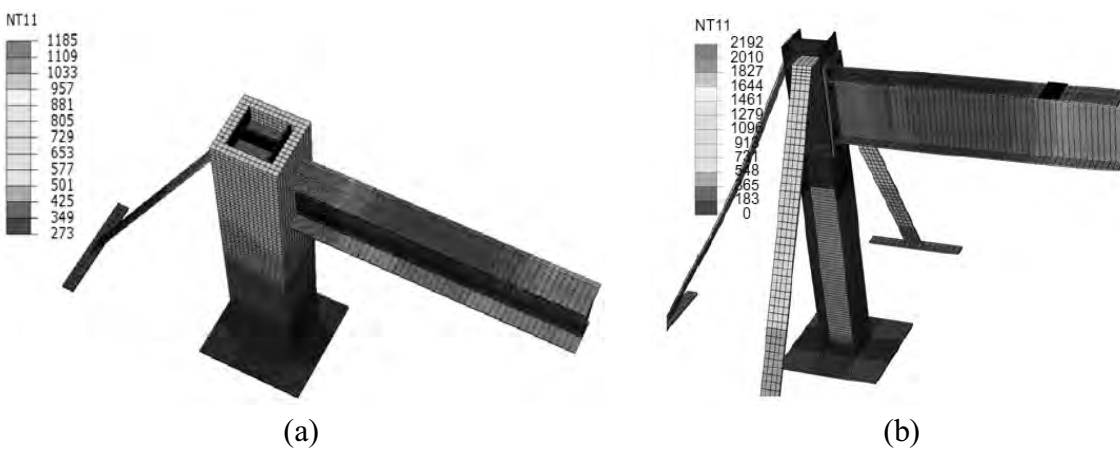


Fig. 5 Temperature distribution for the model (a) with and (b) without thermal reinforcement

By studying the results obtained from the different load cases, it was found that the sequence of the application of thermal and mechanical loads significantly affects the strength of the

overall structure as well as the ultimate load which can be developed, before collapse. Starting with the concrete, in the first case where the thermal and the mechanical load were simultaneously applied the overall temperature reaches the 750 °C. In the second load case where the thermal load precedes a point loading of 200 kN the temperature reaches the 1.185°C. In the last load case, where as mentioned above four steps were applied alternating thermal and mechanical loads, the maximum temperature is equal to 926.6 °C. It has to be mentioned that the third step of this load case, where a thermal load of 1 KW/m<sup>2</sup> is applied to the structure, was not completed while the fourth step of the mechanical loading never started. It is worth noticing that the model of the same joint without fire reinforcement, for the second load case where the thermal load precedes the mechanical one, reached a maximum temperature almost twice bigger than the temperature of the model with the fire reinforcement, Fig. 5. This is an important advantage for the structure with fire reinforcement. For the reinforcement with the gypsum board, the temperature distribution was only slightly different from the previous case of concrete board reinforcement.

According to the load-displacement diagrams on Fig. 6 for the concrete it is shown that the strength is drastically reduced when the thermal load is applied first and the mechanical point load follows. On the contrary, when the thermal and the mechanical loads are concurrently applied the collapse load is of six times greater than the previous case. Also in the third case with the four steps (Fig. 6) the failure load is 50 kN and the connection reaches its highest level of resistance.

The results obtained by using the gypsum board, are similar to the above mentioned results. As it would be expected, the response of the structure is improved when no thermal loading is applied to the structure.

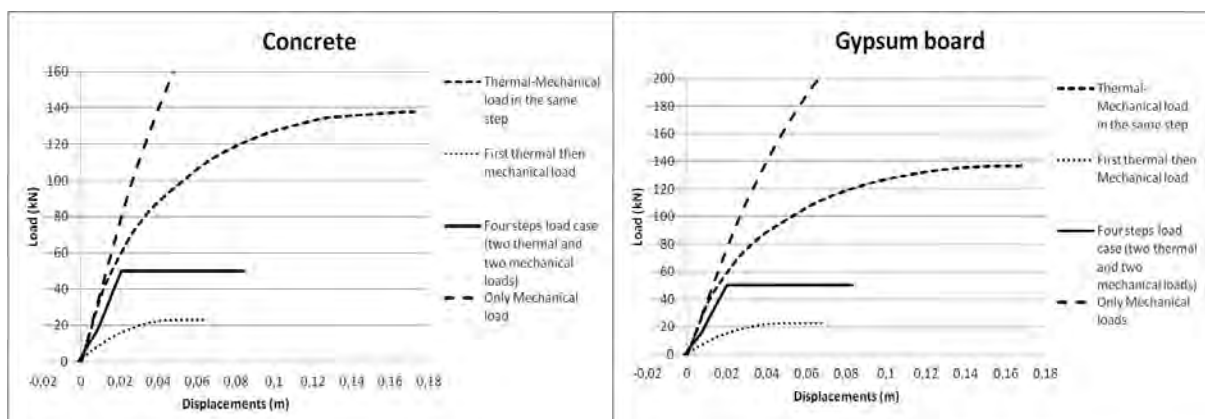


Fig. 6 Force-displacement diagrams

#### 4.2 Behaviour of the contact-friction interface

For the analysis with the concrete fire resistant material and the first load case (Fig. 7a), where the thermal and the mechanical loads are applied simultaneously, the maximum opening of the beam to column interface is 10.3mm. For the second load case, where only the thermal load has been applied to the joint and before the application of the mechanical load, a small opening of 1.1 mm appears (Fig. 7b). This opening appears only due to the heating of the interface, Kalogeropoulos et al, 2012.

For the third load case the maximum opening of the interface becomes approximately five times smaller (2.1mm, Fig. 7c) compared to the first load case. This is attributed to the fact that half of the thermal load is applied first.

Similar opening values for the contact-beam interface is obtained from the model with gypsum board fire reinforcement, Fig. 8.

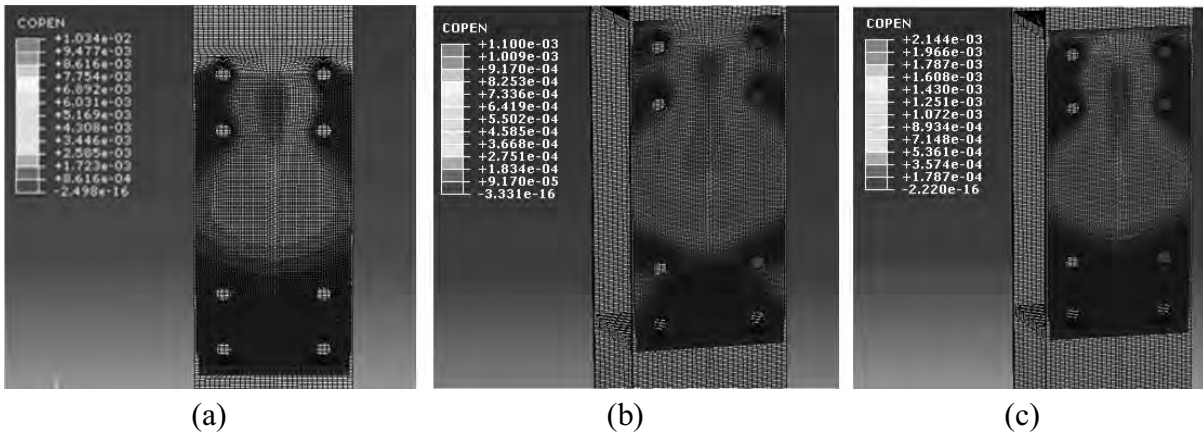


Fig. 7 Opening of the interface (concrete) for the (a) first, (b) second, (c) third load case

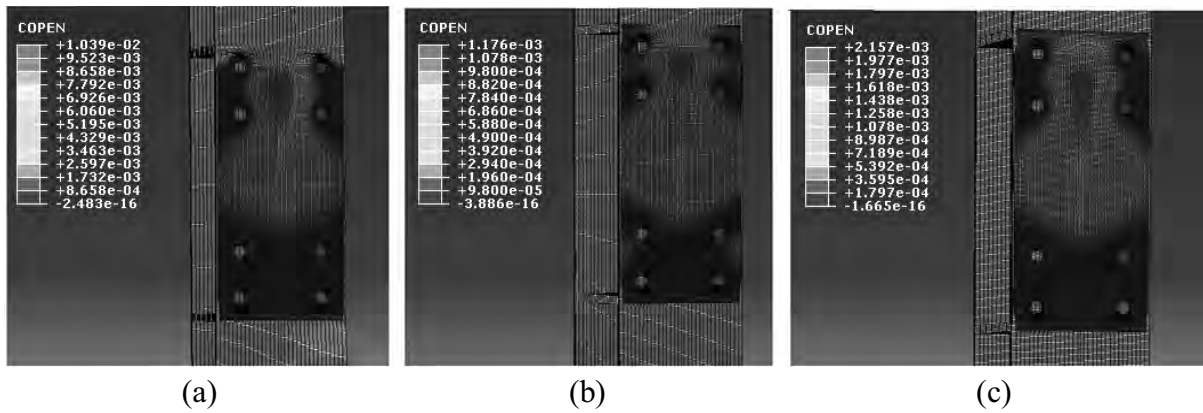


Fig. 8 Opening of the interface (gypsum board) for the (a) first, (b) second, (c) third load case

## 5 CONCLUSIONS

The usage of a fire resistant covering from either concrete or gypsum board in the column of a steel end-plate connection, results in a significant reduction of the maximum temperatures, in comparison with the temperatures developed in the same joint, when no fire reinforcement is applied. The maximum temperature reached 1194 °C in the second load case, for the gypsum board reinforcement.

In addition, it was proved that the resistance of the structure depends on the sequence between the thermal and the mechanical loading. When the thermal and the mechanical load are simultaneously applied to the same step the connection withstands greater load and has increased resistance before it collapses, relative to the case that the thermal load precedes the mechanical one. For this load case, an opening of the column to beam interface appears, when only thermal loads have been applied to the structure, before the application of any mechanical load.

Moreover, when the thermal and the mechanical load are in the same step the displacements become sufficiently large (for application of the both fire coating materials), compared to the case where the thermal load precedes the mechanical one.

Finally, the opening of the column to beam interface for the concrete and the gypsum board reinforcement shows only small differences.

## REFERENCES

- Lawson R. M., Behaviour of steel beam-to-column connections in fire, *The Structural Engineer*, 1990.
- Al-Jabri K. S., Lennon T., Burgess I. W., Plank R. J., Behaviour of steel and composite beam-column connections in fire, *Journal of Constructional Steel Research*, 1998.
- Lien K. H., Chiou Y. J., Wang R. Z., Hsiao P. A., Nonlinear behaviour of steel structures considering the cooling phase of a fire, *Journal of Constructional Steel Research*, 2009.
- Kalogeropoulos A., Drosopoulos G. A., Stavroulakis G. E., Thermal-stress analysis of a three-dimensional end-plate steel joint, *Construction and Building Materials*, 2012.
- Jimenez M., Duquesne S., Bourbigot S., Intumescent fire protective coating: Toward a better understanding of their mechanism of action, *Thermochimica Acta*, 2006.
- Weil E. D, Fire-protective and flame-retardant coatings - A state-of-the-art review, *Journal of Fire Sciences*, 2011.
- Rahmanian I., Wang Y.C., A combined experimental and numerical method for extracting temperature-dependent thermal conductivity of gypsum boards, *Construction and Building Materials*, 2012.
- Eurocode 3, Design of steel structures part 1.2: general rules structural fire design ENV 1993-1-2, Brussels (Belgium): European Committee for Standardization, 2001.

# **PROTECTED STEEL AND COMPOSITE CONNECTIONS IN FIRE**

## **Simulation of the mechanical behaviour of steel and composite connections protected by intumescent coating in fire**

Peter Schaumann<sup>a</sup>, Thomas Kirsch<sup>b</sup>

<sup>a</sup> Leibniz University Hannover, Institute for Steel Construction, Hannover, Germany

<sup>b</sup> Ingenieurbüro Thor-Schipper-Schween, Lohne, Germany

### **Abstract**

Actual developments in numerical simulations of the structural behaviour in fire situation are focussed on taking into consideration the interaction of all structural members in a global approach. Therefore it is necessary to simulate the load bearing behaviour of connections. With this motivation, the authors conducted experiments and thermal FE-simulations on two different connection types. In this paper, the accompanying mechanical FE-simulations of both investigated connection types will be described. The joints are defined as an end plate connection in a steel structure and a fin plate connection in a composite structure. Besides the validation of the numerical models, the results of the described investigations show that it is possible to activate a significant moment resistance within fin plate connections of composite structures. The main requirement for this activation is sufficient reinforcement strength.

**Keywords:** end-plate, fin-plate, bolted connection, fire safety, intumescent coating

### **INTRODUCTION**

Actual developments in numerical simulations of the structural behaviour in fire situation are focussed on taking into consideration the interaction of all structural members in a global approach. Therefore it is necessary to describe the behaviour of connections in detail.

The first step to describe this connection behaviour is to investigate the connection experimentally. This has been conducted by many authors at ambient temperature, beginning in the early 20<sup>th</sup> century (Wilson et al, 1917). Since then, many specialised test setups have been developed to investigate different connection details. Even experiments at elevated temperature and in fire have been conducted in a high number. For example in (Armer et al, 1994) the connection behaviour during some of the Cardington tests is described. Experiments focussed on the connection behaviour have been conducted by (Al-Jabri, 1999), (Wang et al, 2007) and (Schaumann et al, 2008) to mention but a few.

In addition, numerical investigations have been conducted for some elevated temperature tests. For example in (Sarraj et al, 2007) a numerical model of fin plate connections has been developed. In (Yu et al, 2008) a simulation of a steel connection using explicit analysis was presented. The explicit equation solver algorithm was found to be an alternative to the standard algorithm especially if large deformations occur. The authors of this paper also published an FE-analysis and showed that a general damage algorithm can help to increase the accuracy of simulations reasonably (c.f. (Schaumann et al, 2011)).

Although much knowledge has been gained from all these tests and simulations, there are still some unrealistic simplifications concerning the temperature field. In many tests the connection is heated to a constant temperature and then increasingly loaded. As the transient temperature field in a connection is not uniform in a fire situation, this is not realistic. So in other tests the connection is heated following ISO-fire curve or a natural fire curve. Although usual steel constructions are protected against fire to reach a sufficient fire resistance time, most tests are conducted with bare steel connections. For this reason the experiments that underlay this paper have been conducted with protected steel and composite connections.



## 1 EXPERIMENTS

As described, two full scale fire tests have been conducted. The first test dealt with an extended end plate connection within a steel structure and the second was on a fin plate connection within a composite structure. Both connections are displayed in Fig. 1.

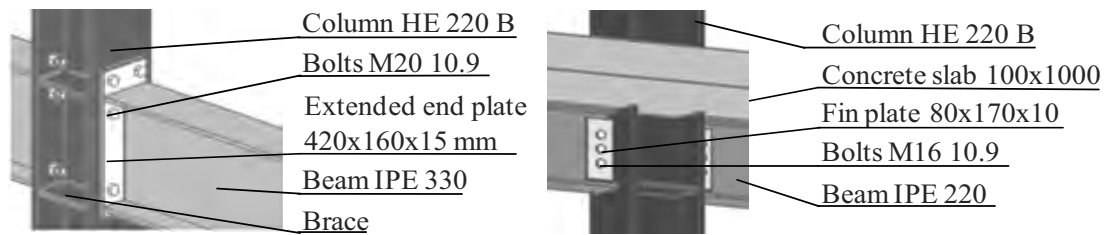


Fig. 1 Scheme of tested connections

As tests and specimen are described in detail in former publications (c.f. (Schaumann et al, 2012) and (Schaumann et al, 2012a)) they will only be mentioned shortly. All steel members consist of S235 steel. The bolts are 10.9 high strength bolts. The concrete slab consists of C25/30 concrete within two layers of Q188 meshes of S500 reinforcing steel. The slab is fully connected to the steel beams by headed studs. All materials have been tested on tensile or compressive strength at ambient temperature. The results are shown in Tab. 1.

Tab. 1 Yield stress and tensile strength of components of tested connections [MPa]

	End plate connection				Fin plate connection				
	Column	Beam	Plate	Bolts	Beam	Plate	Bolts	Concrete	Reinforcement
Yield stress	336	326	314	1039	385	336	1031	39 ( $f_{ck}$ )	600
Tensile strength	465	443	447	1154	506	469	1145	3 ( $f_{ct}$ )	639

As can be seen in Fig. 2 for the end plate connection, the specimen are located inside a load structure with massive steel plates on top. The load of the connection is constant. It is  $M=38.1$  kNm ( $\mu=0,5$ ) for the end plate and  $M=20.5$  kNm ( $\mu=0,7$ ) for the fin plate connection.

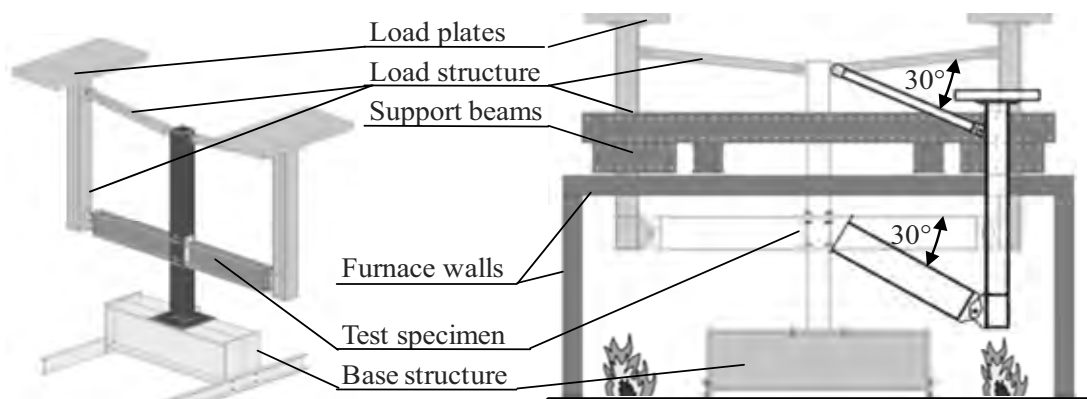


Fig. 2 Scheme of test setup

After the constant loads are applied to the specimen, the furnace temperatures are increased following the ISO-fire curve until connection failure. To ensure a realistic temperature field, the connection and surrounding parts of the specimen are protected by intumescent coating for the fire resistance class R 30. The measured average thickness of the painting is 1 mm.

During the tests, gas and specimen temperatures are measured by 54 thermocouples. The beam deflection is measured by potentiometers. Thickness of the intumescent coating is measured using a furnace camera and small steel bars used as visual gauges.

The experimental results are described in detail in (Schaumann et al, 2012) and (Schaumann et al, 2012a). In this paper, the results are shown within the validation of the FE-simulations.

## 2 GEOMETRY AND BOUNDARY CONDITIONS OF FE-ANALYSIS

To simulate the mechanical connection behaviour in fire, a detailed 3D numerical model of each connection has been developed with the software Abaqus. The geometry of the models is built by solid brick elements (C3D8R) and generally equals the test specimen. Following, only differences between model and specimen are described. One of these differences is the use of the specimen symmetry to reduce the model size. This can be seen in Fig. 3 for the example of the fin plate connection. Another simplification is the use of 1D beam elements for the steel/composite beam (B31) from 400 mm distance from the connection (c.f. Fig. 3). The same elements are used for the reinforcement.

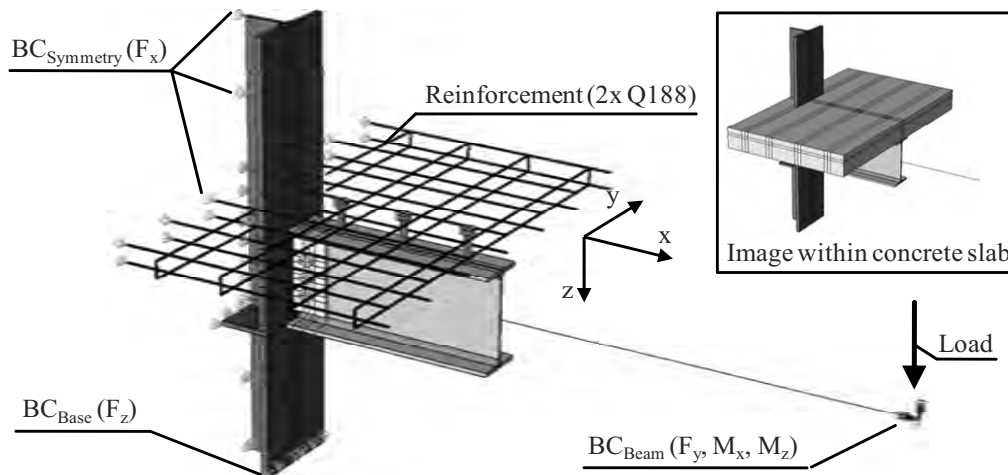


Fig. 3 Numerical model of fin plate connection within boundary conditions (BC)

To simulate the boundary conditions, the model is pinned in x-direction in the whole symmetry area and in z-direction at the bottom of the simulated part of the column (c.f. Fig 3). The end of the lever arm is also pinned in y-direction and the rotation around x- and z-direction is blocked in accordance with the connection between specimen and load structure. The interactions inside the model are simulated using “constraints” between welded members and between the two beam parts. Most other adjacent members (e.g. bolts and fin plate) are connected by a general interaction with a friction coefficient of  $\mu=0.3$  and the ability to separate from each other. The reinforcement is defined as “embedded” in the concrete slab. As described before, the explicit analysis is preferable to simulate connections with large deformations. So this kind of analysis is used. To ensure a stable time increment of  $t=5 \cdot 10^{-7}$ , the element edge size is chosen to be larger than 5 mm. As the model volume of the connection within the concrete slab is higher, element sizes are doubled in parts (c.f. Fig. 3). During the tests it has been observed that failure of one end plate connection occurred by buckling of the lower beam flange. As buckling does not occur in a perfect geometry, the model geometry is set to be imperfect. This is realised using an Eigenvalue-analysis. After this analysis, the local buckling mode with the lowest Eigenvalue is adopted with a maximum deflection of  $u_{\max}=1$  mm. The Buckling mode (with  $u_{\max}=10$  mm) is shown in Fig. 4.

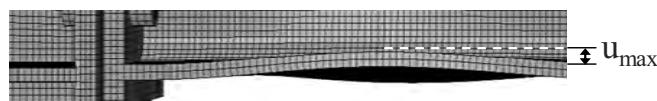


Fig. 4 Numerical model of fin plate connection

As the experiments are conducted in two steps, the numerical simulation follows the same procedure. First the loads are applied using the smooth-step algorithm of Abaqus. Second the temperature is increased. As deflections have only little influence in the temperature field, the thermal simulation is conducted separately. So the temperature field is calculated in advance,

taking into account the nonlinear behaviour of the intumescent coating (c.f. (Schaumann et al, 2012) / (Schaumann et al, 2012a)) and is applied to the mechanical simulation afterwards.

### 3 MATERIAL PROPERTIES OF FE-ANALYSIS

The properties of the used materials are investigated experimentally at ambient temperatures (see Tab. 1). To extend the results for elevated temperatures, Eurocode regulations are used. So for Steel (including reinforcement and bolts), regulations in (Eurocode 3-1-2, 2010), 3.2, based on (Schaumann et al, 1984), are used to determine a stress-strain-behaviour from yield stress at ambient temperature. Differing from the Eurocode, the ultimate stress is added at a strain of  $\epsilon=0.15$  and connected linearly to the stress at  $\epsilon=0.02$  for a better correlation with test results (c.f. Fig. 5). The reduction of the ultimate stress over temperature is realised using results in (Renner, 2005). The resulting stress-strain-diagram for temperatures up to 1000°C is displayed in Fig. 5. While in this figure the nominal stress and strain are displayed for a better comparability with the test results, in the simulation the real stress and strain values are used.

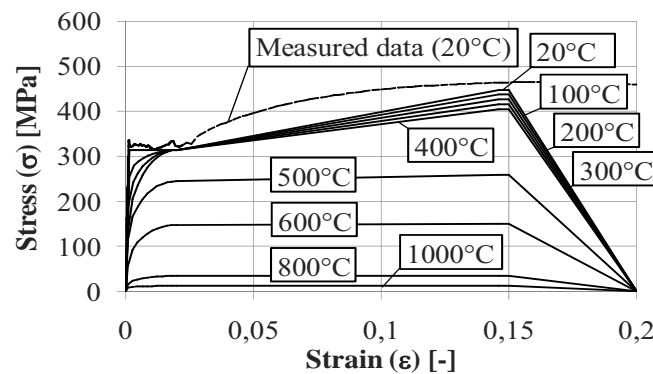


Fig. 5 Temperature dependent stress-strain relationship of end plate

The decreasing parts of the stress values in the diagram are not included in the material behaviour. Instead, the fracture algorithm, presented in (Schaumann et al., 2011) is used.

In the simulation of the fin plate connection, a concrete slab is included and so the material concrete has to be determined as well. The uniaxial compressive behaviour is determined using compressive strength tests, extended for elevated temperatures using regulations in (Eurocode 2-1-2, 2010). For the uniaxial tensile behaviour an approximation in (Hothan, 2004) with a linear increase and bilinear decrease of stress over strain is used.

Further input values for the “concrete damaged plasticity” material law are set to standard values with two deviations. First is the value for dilation angle, defined as  $\psi=30^\circ$  (c.f. (Hothan, 2004)). Second is the relationship between uniaxial and biaxial concrete behaviour, which is defined by the following equation, based on test results in (Ehm, 1986).

$$(f_{ck,bi}/f_{ck}) = 2,27 \cdot 10^{-6} \cdot \theta^2 - 7,31 \cdot 10^{-4} \cdot \theta + 1,16 \quad (1)$$

where  $\theta$  is the temperature [°C]

### 4 VALIDATION OF FE-ANALYSIS

The numerical models are tested and validated against the experimental results. Following the comparison between numerical and experimental results are described for each connection.

#### 4.1 End Plate Connection

During the end plate connection test, the specimen behaved as follows. During the first 10 min, the intumescent coating inflated (c.f. (Schaumann, 2012)), leading to a less fast increase of temperatures afterwards (c.f. Fig 6). With increasing temperatures, the global deflection started to increase as well. During the first 60 min the deflection kept rather low (less than 10 mm). After 60 min of fire exposure the deflection of both beam ends increased

exponentially until the first connection failed after 71 min. This is shown in Fig. 6. As can be seen in the diagram as well, the calculated global deflection of the numerical model is similar.

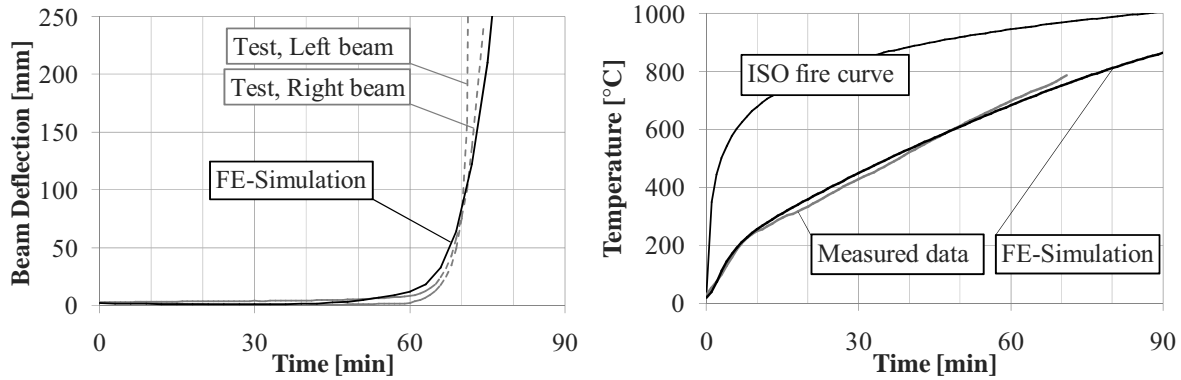


Fig. 6 Global deflection and lower flange temperature of end plate connection during fire

The reason for the connection failure in the experiment and in the FE-analysis was buckling of the component lower flange. As the furnace was stopped for safety reasons with failure of that first connection, the second connection did not fail completely. Nevertheless, the connection kept on deflecting after the end of the test and showed an upcoming combined failure of the lower flange in buckling and the end plate in bending. This occurring failure can be seen in Fig. 7 (right), where the connection after the test is depicted. It can be seen as well that the failure mode of the numerical model is similar. The lower flange is starting to buckle in the same way as seen in the experiment. The loss of contact between end plate and column is less distinct in the simulation but still there.

Moreover, within parametric studies it was found that a slight reduction of the end plate thickness changed the failure mode to end plate bending within bolt fracture. The same failure mode occurred when increasing the load at ambient temperature.

The main result of the investigation concerning the end plate connection is the shown possibility to describe the nonlinear behaviour of the connection using the finite element simulation. Moreover it is shown, that the failure mode of the connection can change due to fire situation and due to change of connection geometry.

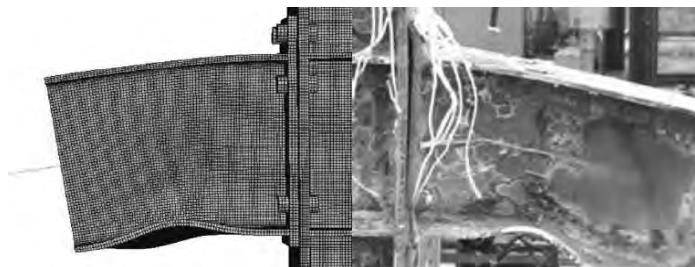


Fig. 7 FE-model just before failure and test specimen after experiment

## 4.2 Fin Plate Connection

In contrast to the investigated end plate, the fin plate connection is usually approximated as a pinned connection at ambient temperature. As a large rotation - exceeding service ability demands - is needed to activate the connections moment resistance, this is reasonable. So it was one aim of the test to show the possibility to activate this moment resistance in fire.

One of the fin plate connections already failed during the loading phase. The unexpected reason for this was found to be the missing ductility of the continuous reinforcement that failed before the lower beam flange got in contact with the column. For this reason the remaining connection was loaded with a reduced moment of  $M=20.5$  kNm.

As can be seen in Fig. 8, the remaining connection resisted the ISO fire for 85 min. Up to 60 min the deflection was neglectable. Afterwards it increased exponentially, until failure occurred due to failure of the pre-damaged reinforcement.

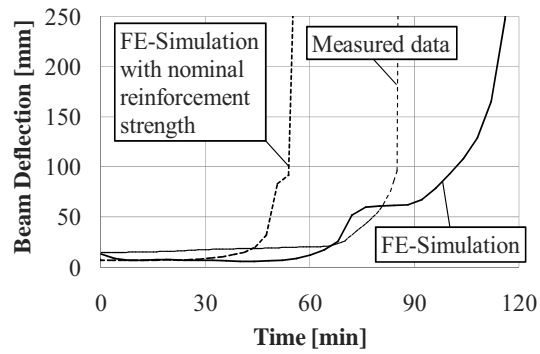


Fig. 8 Beam end deflection in fire test and FE-simulations

As can be seen in Fig. 8 as well, the finite element model behaves slightly different. In the beginning, the deflection decreases with increasing temperatures because of an elongation of the steel beam below the cooler concrete slab. This decrease of deflection was not observed in the experiment for the reason of the pre-damage. After 60 min the FE-model starts to deflect increasingly, as the specimen did in the test.

After about 75 min after ignition, the deflection stops in the FE-model. The reason for this is the contact between lower beam flange and column. Due to this contact, the moment resistance increases significantly. This behaviour was not observed in the experiment, as the contact between column and beam existed from the beginning of the test for the reason of the pre-damage of the reinforcement. Moreover the failure of the pre-damaged reinforcement was the reason of the connection failure in the experiment. So the remaining result of the test is: Even with pre-damaged reinforcement, the connection withstands the fire situation for a significant period. The FE-simulation matches with this result and shows an achievable fire resistance time of nearly 120 min. The final failure of the connection in the FE-simulation is buckling of the lower beam flange (c.f. Fig. 9).

Based on the FE-calculation, it can also be shown that reinforcement resistance is critical for this increase of the moment resistance. When reducing the yield- and ultimate stress of the reinforcement to nominal values, the fire resistance time is reduced to 70 min (cf. Fig 8).

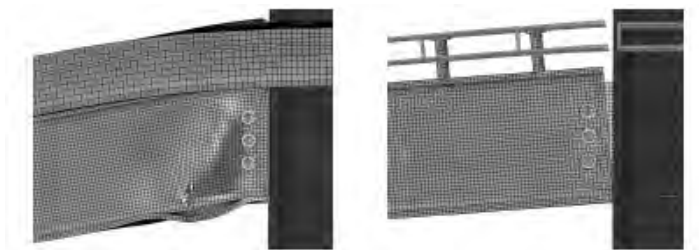


Fig. 9 Failure in FE-model with original (left) and reduced (middle) reinforcement strength

The reason for this can be seen in Fig. 9. As the reinforcement fails before contact between lower beam flange and column exists, the increase of the moment resistance does not occur. The same failure mechanism was found during the loading phase before the fire test.

## 5 SUMMARY AND ACKNOWLEDGEMENT

In this paper experimental and numerical investigations in the load-rotation behaviour of two protected connections in fire situation are presented. The first test specimen is an end plate connection in a steel structure. The second is a fin plate connection in a composite structure. Concerning the first connection it was found that there is a good correlation between numerical investigation and experiment. For this reason, it is possible to use the FE-model to determine the moment-rotation-behaviour for variable connection geometries. Furthermore the model can be used to develop and validate component-method-models for this connection.

Concerning the fin plate connection an unexpected phenomenon has been identified in the load introduction phase of the test. Due to low ductility of the reinforcement, failure occurs before reaching the full plastic bending moment capacity. Using the FE-model in combination with the experiment, the authors were able to show, that this strong moment resistance can be achieved if the design of the reinforcement is improved accordingly.

The IGF-Project No. 16586 N from FOSTA is funded by the German “Federal Ministry of Economics and Technology” via AiF.



Federal Ministry  
of Economics  
and Technology

## REFERENCES

- Al-Jabri, K. S., The behavior of steel and composite beam-to-column connections in fire, Ph.D.-Thesis at the Department of Civil and Structural Engineering, University of Sheffield, Sheffield, 1999.
- Armer, G. S. T., Moore, D. B., Full-scale testing on complete multi-storey structures. *The Structural Engineer* 72 (1994) 30-51, Elsevier, 1994.
- Ehm, C., Versuche zur Festigkeit und Verformung von Beton unter zweiaxialer Beanspruchung und hohen Temperaturen, Dissertation, Institut für Baustoffe, Massivbau und Brandschutz, TU Braunschweig, Braunschweig, 1986.
- Eurocode 2: Design of concrete structures - Part 1-2: General Rules – Structural fire design; German version EN 1992-1-2:2004 + AC:2008, Beuth Verlag, Berlin, 2010.
- Eurocode 3: Design of steel structures - Part 1-2: General Rules – Structural fire design; German version EN 1993-1-2:2005 + AC:2009, Beuth Verlag, Berlin, 2010.
- Hothan, S., Zur dreidimensionalen Simulation von Deckentragwerken im Brandfall, Dissertation, Institute for Steel Construction, University Hannover, Hannover, 2004.
- Renner A., The effect of strain-rate on the elevated-temperature behavior of structural steel, Research dissertation, University of Sheffield, 2005.
- Sarraj M., Burgess I. W., Davison J. B., Plank R. J., Finite element modeling of steel fin plate connections in fire, *Fire Safety Journal* 42 (2007) 408-415, Elsevier, 2007.
- Schaumann, P., Zur Berechnung stählerner Bauteile und Rahmentragwerke unter Brandbeanspruchung, Dissertation, Institut für konstruktiven Ingenieurbau, Ruhr-Universität Bochum, Technisch-wissenschaftliche Mitteilungen Nr. 84-4, Bochum, 1984.
- Schaumann P., Zhao B., Bahr O., Renaud, C., Fire performance of external semi-rigid composite joints, *Proceedings of 6th International Conference Structures in Fire*, Singapore, 2010.
- Schaumann, P., Kirsch, T., Fracture simulation in a steel connection in fire, *Proceedings of Conference: Applications of Structural Fire Engineering*, Prague, 2011.
- Schaumann, P., Kirsch, T., Timmen, F., Full scale fire test and numerical simulation of a steel connection, *Proceedings 7th International Conference on Structures in Fire*, Zurich, 2012.
- Schaumann, P., Kirsch, T., Kressin, H., Full scale fire test and numerical simulation of a fin plate connection protected by intumescent coating, *Proceedings of 10th International Conference ASCCS*, Singapore, 2012a.
- Wang W.-Y., Lia G.-Q., Dong Y.-L., Experimental study and spring-component modeling of extended end-plate joints in fire, *Journal of Constructional Steel Research* 63 (2007) 1127–1137, 2007.
- Wilson, W. M., Moore, H. F., Tests to Determine the rigidity of Riveted Joints in Steel structures, University of Illinois, Engineering Experimentation Station, Urbana, 1917.
- Yu H., Burgess I. W., Davison J. B., Plank R. J., Numerical simulation of bolted steel connections in fire using explicit dynamic analysis, *JConstrStRes* 64 (2008) 515–525, Elsevier, 2008.

## DEVELOPMENT OF A GENERAL COMPONENT-BASED CONNECTION ELEMENT FOR STRUCTURAL FIRE ENGINEERING ANALYSIS

Gang Dong<sup>a</sup>, Ian Burgess<sup>b</sup> and Buick Davison<sup>b</sup>, Ruirui Sun<sup>a</sup>

<sup>a</sup>MMI Engineering, Warrington, WA4 6NL

<sup>b</sup> Department of Civil and Structural Engineering, University of Sheffield, Sheffield S1 3JD,  
e-mails: gdong@mmiengineering.com, ian.burgess@sheffield.ac.uk,  
j.davison@shef.ac.uk, rsun@mmiengineering.com

### Abstract

This paper reports on the development of general-purpose component-based connection finite element intended to model the performance of steel-to-steel joints in fire. The element is generally consistent with Eurocode principles. The development began with the creation of an assembled component-based finite element to represent the flush endplate connection type, in the main using temperature-dependent connection component characteristics which had previously been developed at the University of Sheffield for behaviour up to very high distortions and ultimate fracture, as well as for force reversal. In subsequent work, components for the reverse-channel have been characterized and validated against both numerical modelling and high-temperature testing. The element has been incorporated into the nonlinear global structural analysis program *Vulcan*, developed at the University of Sheffield.

**Keywords:** connections, composite columns, robustness

### INTRODUCTION

The performance of a steel framed structure in fire is significantly influenced by the response of its beam-to-column connections under complex combinations of shear, bending and axial forces. Observations from the full-scale fire tests at Cardington, and the collapse of the buildings at the World Trade Centre in 2001, have raised concerns that joints are potentially the weakest parts of a structure (Burgess, 2007). To accurately predict the behaviour of steel frames in fire, it is essential to include the effects of connection behaviour; in particular the combined effect of axial load and co-existent large rotation, and the reduction of strength and stiffness with increased temperature. This has aroused interest in enabling engineers to predict the behaviour of connections in fire, track the progressive collapse sequence, and design robust structures on performance-based principles.

One approach is to conduct full-scale or isolated fire testing, which is so expensive that it cannot economically produce a sufficient database of results for direct practical design purposes. Alternatively, the creation of detailed FE models of sub-structures can be very accurate, provided that they include the connections and that the analysis is non-linear in terms of material and geometrical changes with temperature. However, the computational expense is often prohibitive for general design purposes.

Tschammernegg (1987) and others proposed the well-known practical approach to representing connections for semi-rigid design, known as the Component Method, which now has been included in Eurocode 3 (2005). This is an intermediate method, requiring the minimum of computational effort while retaining the key characteristics of connection behaviour and offering acceptable predictions of frame behaviour. This paper reports on the development of a general-purpose component-based connection finite element intended to model the large-deflection performance of steel-to-steel joints in fire. The element is generally

consistent with Eurocode principles. This development took place within the COMPFIRE project (RFCS, 2008), on the behaviour in fire of connections to composite (concrete-filled and partially-encased) columns. The reverse-channel connection, shown in Fig. 1(b), has proved to be capable of higher ductility than all conventional types under the large deflections and rotations which can occur in fire (Huang, 2011).

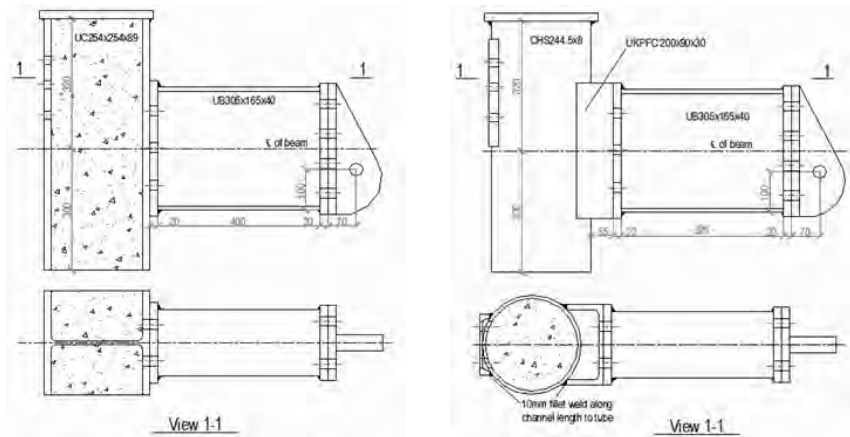


Fig. 1: (a) Endplate and (b) reverse-channel connections to composite columns (Huang, 2012).

## 1 DEVELOPMENT PROCEDURE

Following the principles of the component method, the connection is divided into several key components which contribute to its deformation and ultimately limit its capacity (Block, 2006). Each key component is characterized as a horizontal temperature-dependent non-linear spring which includes inelastic behaviour and a failure limit. These springs are assembled between rigid “bars” to model the connection behaviour. The connection element is then able to deal with very high distortions and ultimate fracture, as well as unloading.

## 2 GENERAL-PURPOSE COMPONENT ASSEMBLY

Fig. 2 presents a schematic illustration of the component assembly of a simple connection. The identified active components are assembled between rigid surfaces to represent the whole connection. In its implementation the connection assembly is designed to include a maximum of five tension spring (bolt) rows and two compression spring rows. Node 1 is located at the intersection between the beam and column reference axes. Node 2 is the end-node of the beam. Vertical shear behaviour has not so far been included in the assembly, and the connection is therefore assumed to be rigid in the vertical shear direction. The connection element is assumed to have no physical length since the modelled connection length (in the vicinity of the column face) is relatively small compared with the attached beams (Li, 1995).



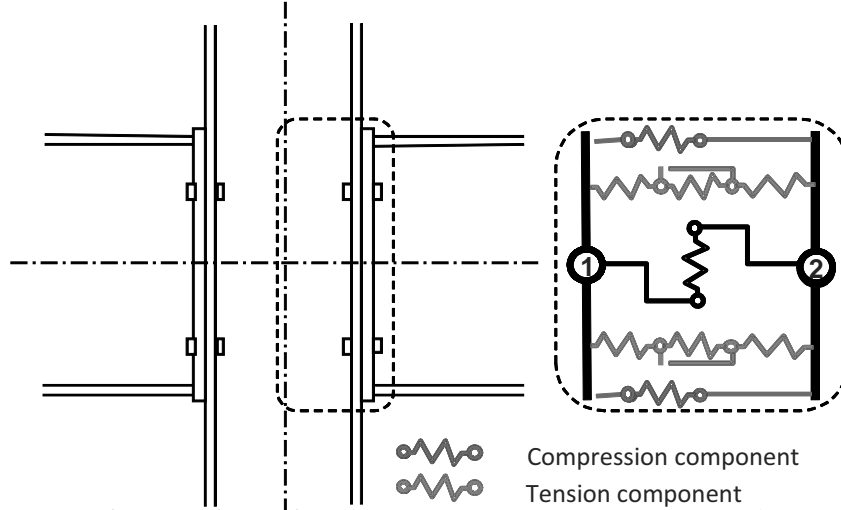


Fig. 2: Schematic component assembly (Block 2006).

### 3 COMPONENT MODELS

Connections in fire are generally subject to extremely large deformations, which take them considerably out of the elastic range, and therefore the adopted component characteristics must not only be able to deal with the initial stiffness and elastic limit for ambient-temperature design, but also to consider the plastic resistance and ductility over a range of elevated temperatures. This connection element largely uses component characteristics which have been developed in previous projects, by Spyrou (2002), Block (2006), and Yu (2009). In addition, component models for the less conventional reverse-channel connection have been characterized in the course of the COMPFIRE project (RFCS, 2012a).

### 4 INCORPORATION OF THE CONNECTION ELEMENT INTO VULCAN

Block (2006) first derived the tangent stiffness matrix ( $K'_c$ ) of the connection element, shown as Eqn. 1. The out-of-plane and torsional DOF are assumed to be connected rigidly, and without interaction, because these are currently under development and are in any case of relatively minor importance in steel or composite building structures.

$$K'_c = \begin{bmatrix} K'_{11} & 0 & 0 & 0 & K'_{15} & 0 & -K'_{11} & 0 & 0 & 0 & -K'_{15} & 0 \\ 0 & \infty & 0 & 0 & 0 & 0 & 0 & -\infty & 0 & 0 & 0 & 0 \\ 0 & 0 & K'_{33} & 0 & 0 & 0 & 0 & 0 & -K'_{33} & 0 & 0 & 0 \\ 0 & 0 & 0 & \infty & 0 & 0 & 0 & 0 & 0 & -\infty & 0 & 0 \\ K'_{51} & 0 & 0 & 0 & K'_{55} & 0 & -K'_{51} & 0 & 0 & 0 & -K'_{55} & 0 \\ 0 & 0 & 0 & 0 & 0 & \infty & 0 & 0 & 0 & 0 & 0 & -\infty \\ -K'_{11} & 0 & 0 & 0 & -K'_{15} & 0 & K'_{11} & 0 & 0 & 0 & K'_{15} & 0 \\ 0 & -\infty & 0 & 0 & 0 & 0 & 0 & \infty & 0 & 0 & 0 & 0 \\ 0 & 0 & -K'_{33} & 0 & 0 & 0 & 0 & 0 & K'_{33} & 0 & 0 & 0 \\ 0 & 0 & 0 & -\infty & 0 & 0 & 0 & 0 & 0 & \infty & 0 & 0 \\ -K'_{51} & 0 & 0 & 0 & -K'_{55} & 0 & K'_{51} & 0 & 0 & 0 & K'_{55} & 0 \\ 0 & 0 & 0 & 0 & 0 & -\infty & 0 & 0 & 0 & 0 & 0 & \infty \end{bmatrix} \quad (1)$$

in which

$$K'_{11} = \sum_{i=1}^n k'_{T,i} + \sum_{i=1}^2 k'_{C,i} \quad (2)$$

$$K'_{15} = K'_{51} = \sum_{i=1}^n l_{T,i} k'_{T,i} + \sum_{i=1}^2 l_{C,i} k'_{C,i} \quad (3)$$

$$K'_{33} = k'_s \quad (4)$$

$$K'_{55} = \sum_{i=1}^n l_{T,i}^2 k'_{T,i} + \sum_{i=1}^2 l_{C,i}^2 k'_{C,i} \quad (5)$$

In which the subscripts 'T' and 'C' represent components working in tension or compression, and  $n$  is the number of bolt rows. The subscript 's' denotes a shear component.

This tangent stiffness matrix has been incorporated successfully into a version of *Vulcan* which incorporates alternate static and dynamic analysis solvers, attempting to use both to best advantage (Sun, 2012). Fig. 3 shows the flow-chart for modelling of a connection failure sequence. Generally a quasi-static analysis solver is used, up to the point at which the first component fails. From this point the dynamic solver is activated to track the structural behaviour. If stability is not regained, this initiates a cascade of failures of the other components, leading to complete detachment of the members.

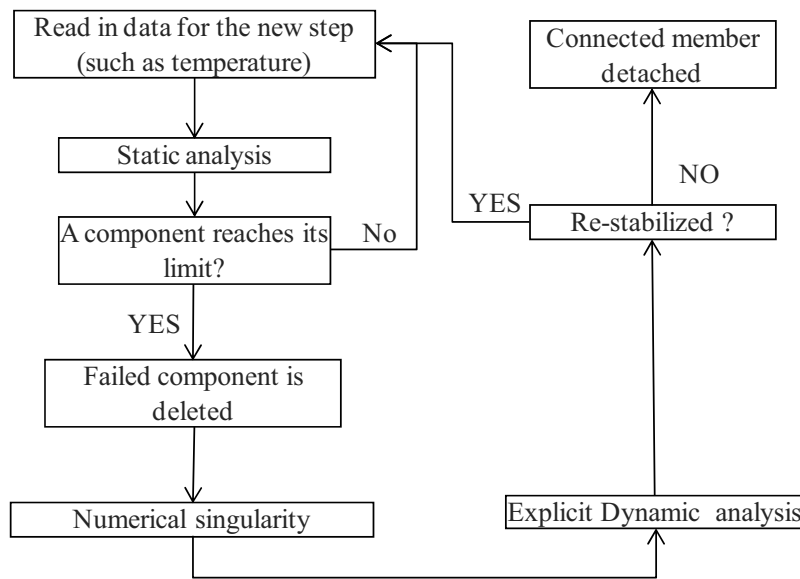


Fig. 3: procedure of connection failure modelling

## 5 APPLICATION OF THE CONNECTION ELEMENT

Within the COMPFIRE project the University of Manchester completed four sub-frame tests with reverse channel connections (RFCS, 2012b). A global finite element model was analysed in *Vulcan* to test the behaviour of the connection element within this subframe. Fig. 4 shows the schematic set-up of the model in *Vulcan* for test TD1. As the applied loads were actually released in an uncontrolled manner during the cooling phase of the test, this analysis does not consider cooling. The column section was CHS 244.5x8, the beam UB 178x102x19 and the connection used a reverse-channel cut from a UK SHS 180x180x42.7. The structure was heated after the applied load ( $F$ ) had reached 40kN, and this applied load was maintained throughout the test.

Fig. 5 shows the curve of beam mid-span deflection against the average temperature in the beam's bottom flange. The analytical curve initially stays close to the test result, but beyond 682°C the deflection begins to rise sharply. At 745°C, the maximum deflection of 220mm is reached, and at this point both of the tension bolt rows are shown as failing due to the bolt heads pulling-out of their holes in the reverse channel. The failure identified in the test was actually bolt thread-stripping, which means that the model used to characterize bolt pull-out is probably on the conservative side.

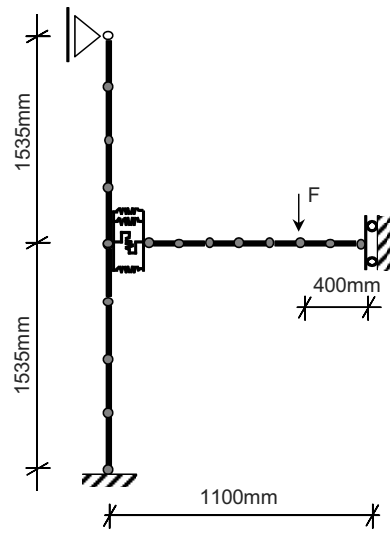


Fig. 4: Sub frame model of Manchester Test TD1 (RFCS, 2012b)

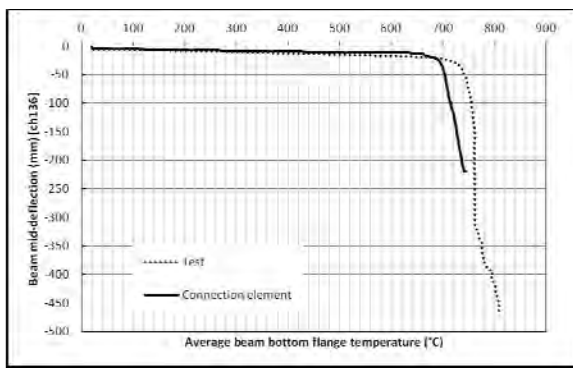


Fig. 5: Mid-span deflection

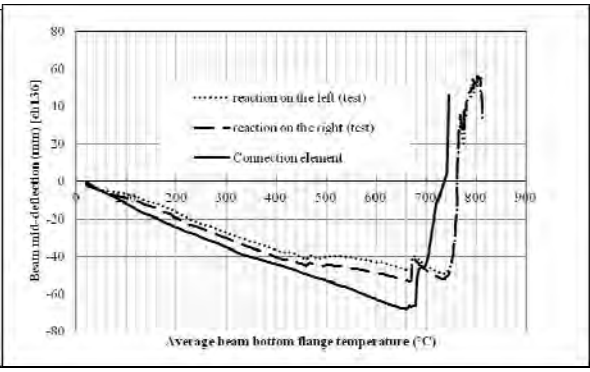


Fig. 6: Axial force in the connection

Fig. 6 presents the connection axial force-temperature relationships; the temperature used for reference is the average test value in the beam bottom flange. The test axial force is the sum of the horizontal reaction forces recorded in the load cells. There is a small initial force, generated when the 40kN load was applied at ambient temperature. The beam's axial compressive force stays close to the test value in the initial heating phase. At around 660 °C the axial force reaches its maximum compressive value, beyond which it declines sharply. At around 745°C the axial force in the connection changes from compression to tension, and the beam enters the catenary-tension phase of its behaviour. Fig. 7 shows the movements of the spring rows in the connection. The movement of the top and bottom spring rows reached over 20mm in the catenary stage. This was possible because the reverse channel connection mobilized considerable ductility. Fig. 7 also shows that the component-based connection element is capable of tracking the behaviour of the reverse-channel connection.

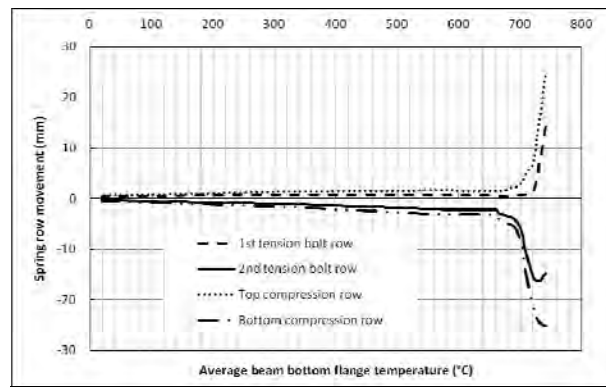


Fig. 7: Spring row movements in Test TD1.

## 6 CONCLUSION

The component-based connection element, implemented in the *Vulcan* software, has been checked against a sub-frame test conducted at the University of Manchester. In Figs 5 and 6 it has demonstrated very acceptable representations of the global test behaviour, and could provide a practical way of modelling the influence of connections in global analysis. The connection element has been shown in this paper to predict the behaviour and ductility of components up to their first fracture within joints in structural fire scenarios. In other recent studies (Sun, 2012) the element has been tested with a dynamic solver to allow progressive failures of components to be tracked. This is intended to make it possible for progressive failure of buildings to be predicted in scenario-based analytical design against fire.

## 7 ACKNOWLEDGEMENT

The research leading to these results received funding from the European Community's Research Fund for Coal and Steel (RFCS) under grant agreement n° RFSR-CT-2009-00021.

## REFERENCES

- Block, F.M. (2006), 'Development of a component-based finite element for steel beam-to-column connections at elevated temperatures', PhD Thesis, University of Sheffield.
- Burgess I.W. (2007), 'Connection modelling in fire', Proc. COST C26 Workshop "Urban Habitat Constructions under Catastrophic Events", Prague, (2007) pp 25-34.
- CEN (2005), EC3: Design of steel structures, Part 1.8: Design of joints, European Committee for Standardization, Document BS EN1993-1-8: 2005.
- Dong, G., Burgess, I.W. and Davison, J.B. (2011), 'Component-based element for endplate connections in fire', Proc. ASFE 2011, Prague, April 2011, pp 195-200.
- Dong, G., Burgess, I.W. and Davison, J.B. (2012), 'Application of a general component-based connection element in structural fire analysis', Proc. 11th Int. Conference on Steel, Space and Composite Structures, Qingdao, China.
- Heistermann, T., Iqbal, N., Veljkovic, M., Lopes, F., Santiago, F. and Simões da Silva, L. (2011) 'Finite element modelling of reverse-channel connections at elevated temperature', EUROSTEEL 2011, Budapest, Hungary. August 31 - September 2, 2011.
- Huang, S.-S., Davison, J.B. and Burgess, I.W. (2011), 'Elevated-temperature tests on joints to composite columns', Proc. 6th European Conference on Steel Structures, Budapest, Hungary, pp1593-1598.
- Huang, S.S., Burgess, I.W. and Davison, J.B. (2012), 'Robustness of joints to composite columns in fire', Proc. 11th Int. Conference on Steel, Space and Composite Structures, Qingdao, China,.

- Li, T.Q., Choo, B.S. and Nethercot, D.A. (1995), 'Connection element method for the analysis of semi-rigid frames', *Journal of Constructional Steel Research*, 32, pp. 143-171.
- RFCS (2008), Design of joints to composite columns for improved fire robustness, Research Fund for Coal and Steel, Grant agreement n° RFSR-CT-2009-00021, European Commission, Belgium.
- RFCS (2012a), Deliverable 3 (D3) Report on simplified structural behaviour of components Research Fund for Coal and Steel, Grant agreement n° RFSR-CT-2009-00021, European Commission, Belgium.
- RFCS (2012b), Deliverable 6 (D6) Recommendations on accurate and efficient FE modelling of composite structures under fire loading incorporating realistic joint behaviour. Research Fund for Coal and Steel, Grant agreement n° RFSR-CT-2009-00021, European Commission, Belgium.
- Tschemmernegg, F., Tautschnig, A., Klein, H., Braun, Ch. and Humer, Ch. (1987), "Zur nachgiebigkeit von rahmenknoten – Teil 1" (Semi-rigid joints of frame structures Vol. 1– in German), *Stahlbau* 56, Heft 10, pp299-306.
- Spyrou, S. (2002), 'Development of a component-based model of steel beam-to-column joints at elevated temperatures', PhD Thesis, University of Sheffield.
- Sun, R.R., Burgess, I.W., Huang, Z.H. and Dong, G. (2012), 'Modelling of progressive failure of connections and ductility demand of connections in fire', 7th International Conference: Structures in Fire, Zurich
- Yu HX, Burgess IW, Davison JB and Plank RJ (2009), 'Development of a yield-line model for endplate connections in fire', *J. Construct. Steel Research*, Vol. 65 (6), pp. 1279-1289.

## BEHAVIOUR OF AXIALLY LOADED STRUCTURAL BOLTING ASSEMBLIES IN FIRE

Lucy Johnson <sup>a</sup>, Eric Palmiere <sup>a</sup>, Richard Thackray <sup>a</sup>, Ian Burgess <sup>b</sup>, Buick Davison <sup>b</sup>

<sup>a</sup> University of Sheffield, Faculty of Materials Science and Engineering, Sheffield, United Kingdom

<sup>b</sup> University of Sheffield, Faculty of Civil and Structural Engineering, Sheffield, United Kingdom

### Abstract

Bolt assemblies used in structural connections may fail in tension via two modes: Necking, which is a ductile failure, and thread stripping, which is a brittle failure mechanism. During a fire, a ductile failure mode is preferable as it provides continued load transfer from beams to columns for the longest amount of time, allowing for building evacuation. Bolt assemblies have been tested under tension at a range of strain rates and temperatures to observe both failure modes. Tests showed that those bolts with a non-martensitic microstructure failed in a beneficial ductile manner, contrary to the current standards.

**Keywords:** Bolt assemblies, ductile and brittle failure, microstructure

### INTRODUCTION

The robustness of connections, and therefore bolt assemblies, is essential for the transfer of loads from beams to columns to avoid progressive collapse. Two failure modes exist under tension; shank necking (breakage) and thread stripping. The latter involves heavy thread deformation causing the nut to pull off the end of the bolt shank. This is a relatively brittle failure compared with shank breakage, and according to published work tends to occur at lower forces. During fire it is essential for bolt assemblies to have sufficient ductility to accommodate thermal expansion and subsequent contraction of adjoining members. Thread stripping should therefore be avoided. This paper investigates the factors which influence the failure mode at elevated temperatures through microstructural characterisation, tensile testing and finite element modelling.

### 1 BEHAVIOUR OF NUTS AND BOLTS UNDER FIRE CONDITIONS

Strength reduction factors prescribed by Eurocode 3 (BSEN1993-1-2 2005) are currently applied to fasteners in structural fire design. These are based on the temperature-dependent strength of steel, and take into account thread deformation or the bolt failure mode. A simplistic assumption is that failure mode depends on thread engagement length and the relative strengths of the mating threads. When the thread engagement length is long and mating thread strengths are comparable, bolt breakage is most likely. When the strength of one thread set is greater than the other and the length of thread engagement is short, thread stripping will occur in the weaker thread set. A detailed model exists for the prediction of failure mode at ambient temperature (Alexander 1977, Ref. No 770420), but as yet no assumptions have been made about the strain rate or temperature dependency of the failure mode.

A number of bolt assembly tests have previously been carried out at elevated temperature under steady-state conditions to evaluate and compare the performance of different bolt assemblies in fire (Kirby 1995; Hu, Davison et al. 2007; Gonzalez and Lange 2009; Gonzalez 2011). These have been carried out on assemblies of different geometrical tolerances; the tighter tolerance, 6g6AZ, as specified in (BSEN14399-4 2005) and (BSENISO10684 2004), and the looser tolerance, 8g7H, for bolts specified to (BS4190 1967; BS4190 2001). The studies also contain different diameters, steel grades, forming methods (hot and cold) and finishes, as detailed in Tab. 1. The test methods employed by the different authors, and their

resultant ultimate tensile capacities and failure modes, are shown in Tab. 2. Some assemblies failed by a single failure mode, while some failed by a combination (where N = necking, S = thread stripping and C = combination).

Normalising the ultimate load capacities of bolt assemblies tested at elevated temperature to those at ambient provides strength reduction factors which can be compared to those used in fire engineering design (BSEN1993-1-2 2005). The traditionally conservative Eurocodes surprisingly suggest reduction factors less severe than those observed in some bolt assemblies at all temperatures, but most significantly at temperatures greater than 300 °C. This may be attributable to the reduced strength in the threads causing greater thread deformation at higher temperatures and potentially a different tempering (softening) behaviour of the bolt material compared to the steel used to create the strength reduction factors available in Eurocode 3.

Tab. 1: Summary of the processing and geometrical tolerances of bolt assemblies tested at elevated temperatures in previously published work

Author	Ref.	Assembly		Bolt				Nut			
		d (mm)	Tolerance	Code	Grade	Formed	Finish	Code	Property Class	Formed	Finish
Kirby	1	20	8g7H	4190	8.8	CF	SC	4190	8	HF	SC
	2	20	8g7H	4190	8.8	CF	SC	4190	8	CF	G
	3	20	8g7H	4190	8.8	CF	SC	4190	8	HF	SC
	4	20	8g7H	4190	8.8	CF	SC	4190	8	CF	G
	5	20	8g7H	4190	8.8	HF	SC	4190	8	HF	SC
Gonzalez	6	16	6g6AZ	14399-4	10.9	CF	G	14399-4	10	-	G
	7	16	6g6AZ	14399-4	10.9	CF	G	14399-4	10	-	G
Hu	8	20	-	4190	8.8	-	-	-	10	-	-
	9	20	-	ISO 4014	8.8	-	-	-	10	-	-

Where CF = cold formed, HF = hot formed, SC = self-colour and G = hot dip galvanised

Tab. 2: Summary of the ultimate load capacities obtained from steady-state tensile tests at a range of temperatures in previously published work

Ref.	Strain rate (min <sup>-1</sup> )	Heating rate (°C/min)	Holding time (min)	F <sub>u</sub> (kN) at Temperature (°C)										Failure mode
				20	100	150	200	300	400	500	550	600	700	
1				226	216	-	215	217	178	126	94	59	24	N
2				198	191	-	177	190	168	118	86	54	23	S
3	0.001-0.003	5-10	15	206	201	-	206	203	168	122	96	62	27	N
4				189	180	-	168	176	158	112	85	54	25	S
5				232	217	-	215	206	183	144	116	80	28	C
6	0.001-0.005	-	30	266	-	-	254	252	210	123	78	47	19	C
7				264	-	-	256	245	203	121	76	50	18	C
8	0.0001*	2-2.5	15	202	-	198	-	187	140	75	-	39	-	N
9				239	-	232	-	225	168	115	-	48	-	N

\* Assuming a 30 mm gauge length

The general trend observed was for necking failures to occur at higher ultimate tensile strengths than stripping failures for 8.8 bolts, while the 10.9 bolts failed at higher ultimate load capacities by a combination of thread stripping, necking and liquid metal embrittlement. Assemblies 6 and 7 were temperature-dependent, so that a combination of necking and thread stripping occurred up to 420°C, liquid metal embrittlement from 420-650°C and pure

stripping above 650°C. Assembly 5 failed by a combination of necking and thread stripping at all temperatures, with both failure modes occurring at similar ultimate load capacities.

## 2 UNIAXIAL TENSILE TESTING

A series of uniaxial tensile tests carried out on turned-down bolts, chosen to eliminate the effects of thread deformation, have been carried out to provide realistic material behaviour to use in a finite element model developed in ABAQUS, using the material properties defined in ISO 898-1, 898-2 and the reduction factors from Eurocode 3. The bolt head is removed and the shank turned-down to a diameter of 7 mm for a parallel length of 35 mm with a 6 mm radius at each end. True thread geometries measured from a number of bolt assemblies from the same batch are included in a pre-existing finite element model. The model will be validated by tensile tests, carried out on bolt assemblies from the same batch as the turned down bolts, at the same temperature and strain rate combinations.

The assembly chosen for this study is typical of that used in UK construction, consisting of a Grade 8.8 galvanised bolt and Property Class 10 galvanised nut to the tighter geometrical tolerance of 6g6AZ. All bolt material and bolt assembly tests were carried out on a single batch from a single manufacturer, to ensure consistent results.

### 2.1 Test setup

The apparatus includes a convection furnace and the same tools used by (Hu, Davison et al. 2007) as can be seen in Fig. 1. Since the test apparatus was designed for tensile testing of bolt assemblies two internally threaded extensions were machined which could accommodate a short M20 bolt at one end and an M20 stub and nut at the other, with the turned-down bolt test piece in-between, as seen in Fig. 2. For both bolt assembly and turned-down bolt tests a tensile force is applied by the top grip to the bottom face of the nut whilst the bottom grip remains stationary.

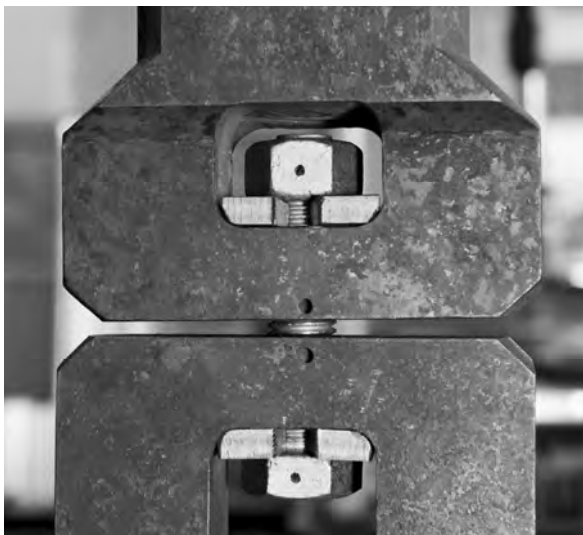


Fig. 1 ESH testing equipment used for turned-down bolt and bolt assembly testing.



Fig. 2 Test setup for turned-down bolt specimen.

Temperature is measured by a thermocouple placed in the bottom shoulder of the turned-down bolts and the centre of the bolt head in the bolt assembly tests. Elongation is calculated by digital image correlation using a Canon EOS 1100D camera with an EFS 18-55mm lens and an automatic trigger system connected to the LabVIEW module. This allows data to be written to file at the same time as the trigger is activated, to allow strain calculation up to failure. Both ends of the gauge length are marked with glass beads attached to the surface of



the specimen with fire cement, so that they are visible in profile without being detrimental to strength.

Based on the test methods used in previous bolt assembly tests it was decided that a study into the failure behaviour of bolt assemblies and bolt material should include a range of temperatures up to 700°C and strain rates ranging from 0.002 min<sup>-1</sup> up to 0.02 min<sup>-1</sup>. The slowest of these is comparable to the strain rates used by (Kirby 1995) and the maximum strain rate at the mid-span of a simply supported beam subjected to an evenly distributed load when calculated on the basis of a limiting deflection of  $L^2/9000d$  (mm/min) (BS476-20 1987). Strain rates of 0.01 and 0.02 min<sup>-1</sup> have also been chosen to reflect the high strain rates experienced during plastic deformation. Unlike the tests shown in Tab. 1 the strain rate is maintained to failure rather than increased beyond 2 – 5 % proof stress, in order to reduce test times. Temperatures set at ambient, 550°C, 620°C and 700°C were chosen, since 550°C is commonly assumed to be the critical or limiting temperature above which steel retains 60% of its ambient-temperature strength and 700°C is a realistic temperature for unprotected connections to reach during a building fire.

## 2.2 Bolt Material Results

The first three tests, carried out at 0.002, 0.01 and 0.02 min<sup>-1</sup> at ambient temperature gave some surprising results, as shown in Fig. 3, exhibiting behaviour characteristic of three different microstructures; pearlite, bainite and martensite. The yield plateau is characteristic of pearlite, but not the martensite that quenched-and-tempered M20 grade 8.8 bolts should contain (90% martensite at their centres, as specified in (BSENISO898-1 2009)). Since all three bolts were from the same batch it can be assumed that they have the same chemical composition, which is within the limits of (BSENISO898-1 2009), and therefore the difference in microstructure is attributed to the cooling rate during quenching. A faster cooling rate leads to transformation from austenite (present at temperatures above around 730°C) to a harder, more brittle, martensite phase, while slower cooling allows for diffusion of carbon atoms and transformation to bainite and pearlite. Hardness readings taken at the bolt neutral axes of the three specimens confirms the presence of different microstructures, with those of the two weaker materials lying below the minimum limit of ISO 898-1.

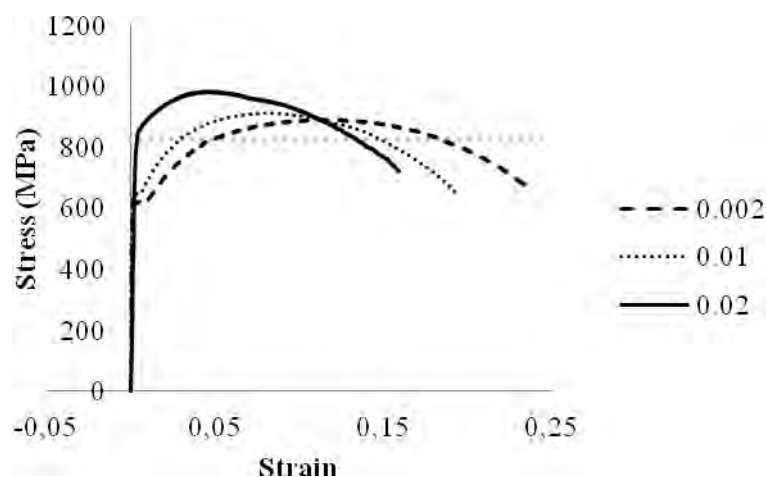


Fig. 3 Ambient-temperature stress-strain curves for 0.002, 0.01 and 0.02 min<sup>-1</sup> showing behaviour characteristic of pearlite, bainite and martensite respectively.

Vickers hardness tests were carried out on the underside of the bolt heads prior to machining test pieces, to ensure that all subsequent specimens contained pearlite to provide worst-case material properties for the finite element model. The repeated test results shown in Fig. 4 exhibit negligible effects of strain-rate on stress; the results were therefore averaged for the three strain rates. At elevated temperatures the strain-rate effect is significant, as shown in

Fig. 5. These results can be simplified to multi-linear curves for input to the finite element model. The resultant strength reduction factors from these tests show that higher strain rates tend to lead to higher reduction factors (less of a reduction in strength) than those from lower strain rates. Most values, however, also fall below those specified in Eurocode 3.

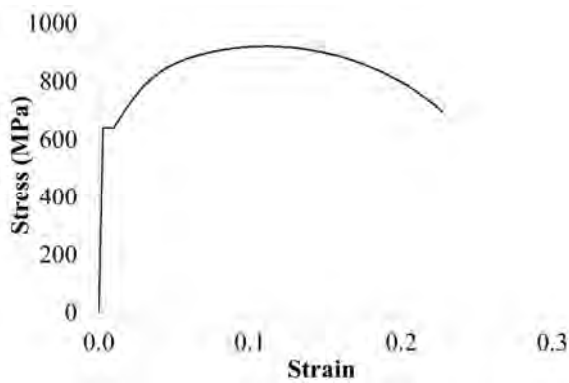


Fig. 4 Average ambient temperature stress-strain curve for turned-down bolts.

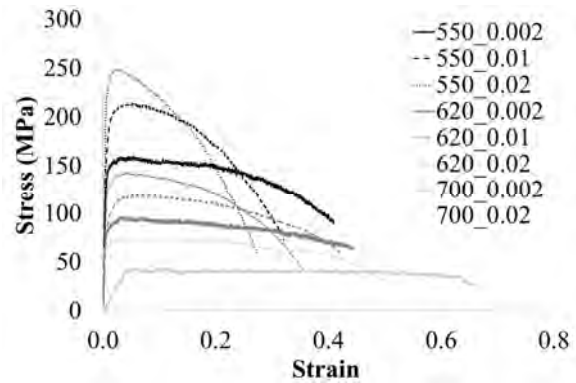


Fig. 5 Elevated temperature stress-strain curves for turned-down bolts.

### 2.3 Bolt Assembly Results

Force is plotted against elongation, measured from the top face of the nut to the bottom face of the bolt head, as shown in Fig. 6.

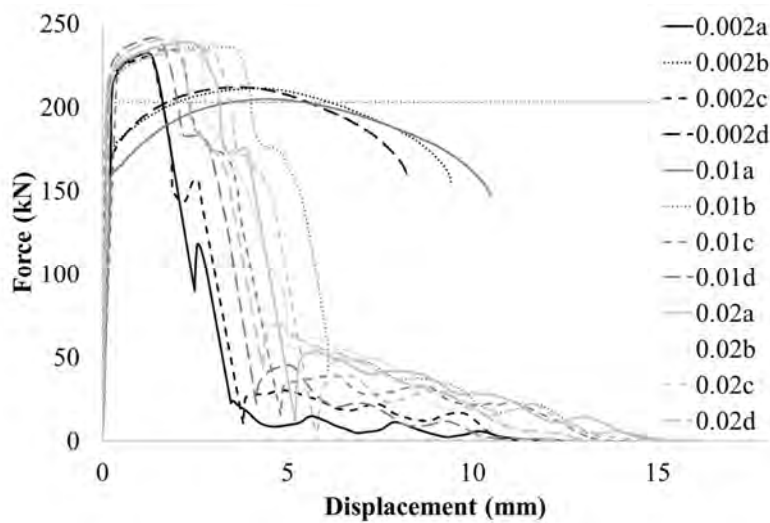


Fig. 6 Ambient-temperature force-displacement curves for bolt assemblies at strain rates 0.002, 0.01 and 0.02  $\text{min}^{-1}$ .

Those assemblies which failed due to thread stripping did so at significantly higher loads than those which failed due to necking, with both failure modes having little strain-rate effect. Hardness testing of the undersides of the bolt heads of the failed specimens shows that those which failed due to necking have lower hardness, so pearlitic or bainitic microstructures can be inferred. All bolt assemblies tested failed above the minimum ultimate tensile load of 203kN prescribed in ISO 898-1. The assemblies that failed through necking did so at significantly lower loads than those which failed through thread stripping, but exhibited ductile failures - bolt assemblies must be ductile in order to continue to transfer loads

effectively from beams to columns during thermal expansion and subsequent sagging of beams during fire.

### 3 SUMMARY AND ACKNOWLEDGEMENT

Despite the lower ultimate load capacities observed in bolt assemblies which failed due to necking, it is still the preferred mode of failure during fire. Tensile testing carried out on bolt assemblies from the same batch has highlighted the importance of tight control during manufacture to ensure consistent material and mechanical properties. Interestingly, the desirable ductile failure mode occurred in bolts which contained a pearlitic or bainitic microstructure, as opposed to the tempered martensite specified. If ductility is essential to ensure structural robustness during fire, it is not apparent why the current objective is to aim for the strong, brittle starting microstructure of tempered martensite. The turned-down bolt test results will provide good material property data as input to finite element models.

### REFERENCES

- Alexander, E. M. (1977, Ref. No 770420). Analysis and Design of Threaded Assemblies. International Automotive Engineering Congress and Exposition. Detroit.
- BS476-20 (1987). "Fire tests on building materials and structure. Method for determination of the fire resistance of elements of construction (general principles)." British Standards Institution.
- BS4190 (1967). "Specification for ISO metric black hexagon bolts, screws and nuts." British Standards Institution.
- BS4190 (2001). "ISO metric black hexagon bolts, screws and nuts - specification." British Standards Institution.
- BSEN1993-1-2 (2005). "Design of steel structures, Part 1-2: General rules - Structural fire design." British Standards Institution.
- BSEN14399-4 (2005). "High-strength structural bolting assemblies for preloading - Part 4: System HV - Hexagon bolt and nut assemblies." British Standards Institution.
- BSENISO898-1 (2009). "Mechanical properties of fasteners made of carbon steel and alloy steel, Part 1: Bolts, screws and studs with specified property classes — Coarse thread and fine pitch thread." British Standards Institution.
- BSENISO10684 (2004). "Fasteners - Hot dip galvanized coatings." British Standards Institution.
- Gonzalez, F. (2011). Untersuchungen zum Material- und Tragverhalten von Schrauben der Festigkeitsklasse 10.9 während und nach einem Brand. PhD, Technischen Universität Darmstadt.
- Gonzalez, F. and J. Lange (2009). "Behaviour of Galvanized High Strength Grade 10.9 Bolts under Fire Conditions." 908-915.
- Hu, Y., J. B. Davison, et al. (2007). Comparative study of the behaviour of BS 4190 and BS EN ISO 4014 bolts in fire.
- Kirby, B. R. (1995). "The behaviour of high-strength grade 8.8 bolts in fire." Journal of Constructional Steel Research 33(1-2): 3-38.

## **STRUCTURAL RESPONSE UNDER NATURAL FIRE OF BARREL SHAPE SHELL CONSTRUCTION**

Michal Malendowski<sup>a</sup>, Adam Gglema<sup>a</sup>, Zdzislaw Kurzawa<sup>a</sup>, Lukasz Polus<sup>a</sup>

<sup>a</sup> Institute of Structural Engineering, Faculty of Civil and Environmental Engineering,  
Poznan University of Technology, ul. Piotrowo 5, 60-965 Poznan, Poland

### **Abstract**

In the paper thermo-mechanical analysis of the structural shell construction with natural fire scenario is presented. The barrel shape coverlet with dimensions 40m x 80m is the roof system for the shopping arcade. The braced shell structure is made of steel rectangular hollow sections. The steel construction is directly covered by special glass system. The interior fire case is considered as the main goal of research. Fire is simulated with the use of FDS software based on computer fluid dynamics. Then the temperatures and/or heat fluxes are transferred to the non-linear Abaqus finite element software system. The 3D geometry FE computational model is prepared using 3D beam finite elements with mechanical and thermal degrees of freedom. CFD and FE analyses are sequentially coupled using special external own scripts. The analyses show influence of the natural fire onto the structural behaviour of the roof.

**Keywords:** fire safety, fire engineering, CFD, FEA, natural fire, coupled problems.

### **INTRODUCTION**

Nowadays a big attention is paid to provide certain level of people's safety in case of fire. So that, especially in large buildings, several active and passive protection systems are installed simultaneously, to assure assumed safety. Number and types of fire protection measures usually came from prescriptive regulations, what leads often to overestimation of needs, and subsequently to excessive costs. From this reason, following paper refers to performance based approach for designing of structures in accidental situation of fire. Particularly, the thermo-mechanical analysis of the braced barrel vault made from rectangular hollow sections in natural fire is provided. Thanks to such formulation, structural response of that construction is approximated more accurately and because of these informations, it is possible to find the golden mean between costs of protection and necessary fire resistance of analysed structure.

### **1 OBJECT OF ANALYSIS**

Analysed structure is the barrel shape vault having dimensions of 40 m x 80 m in plane and about 15 m height. In project, it is a part of bigger leisure and shopping centre, which connect two other parts of this complex of buildings. In this case fully triangulated system has been used in the construction of single-layered braced vault in steel. The steel bar triangles are made from the hollow section which are fixed to each other using special connectors. These connectors allows to make the assembly process satisfactory simple, and after erection they work as rigid connections between bars. Every 25 meters long special spatial truss diaphragms support the coverlet and ensure the spatial stability of whole vault. Fig. 1 shows the isometric view of analysed construction.

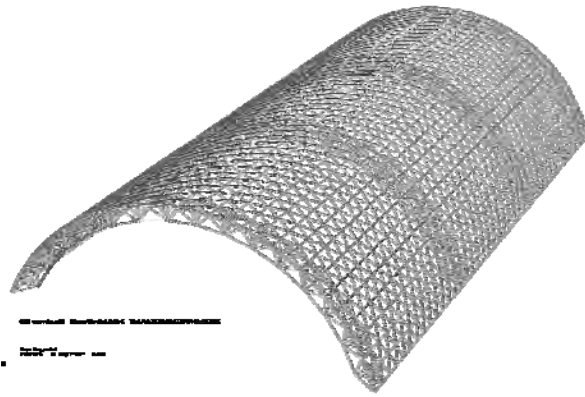


Fig. 1 Isometric view of FEM model

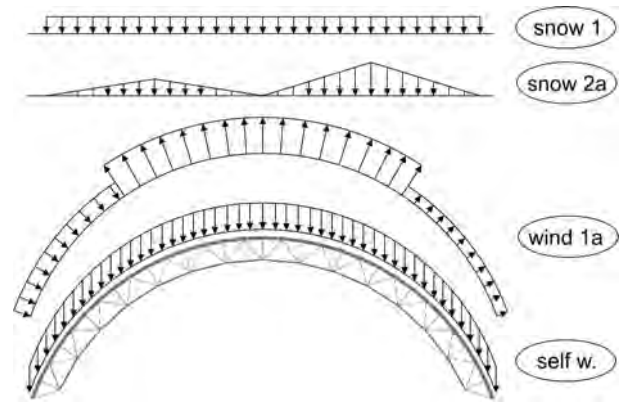


Fig. 2 Types of loads

## 2. ACTIONS

According to PN-EN 1990 (Polish version of Eurocode) the following combination of loads are distinguished:

Tab. 1 Combination of actions

No.	Permanent	Leading accidental action	Variable actions
1.	$1.0 \cdot \text{self\_weight}$	Net heat fluxes comes from natural fire analysis	$0.2 \cdot \text{snow\_1}$
2.			$0.2 \cdot \text{snow\_2a}$
3.			$0.2 \cdot \text{snow\_2b}$
4.			$0.2 \cdot \text{snow\_1} + 0.2 \cdot \text{wind\_1a}$
5.			$0.2 \cdot \text{snow\_2a} + 0.2 \cdot \text{wind\_1a}$
6.			$0.2 \cdot \text{snow\_2b} + 0.2 \cdot \text{wind\_1a}$

Types of variable actions are presented in Fig. 2. Loads having subscript “a” having their symmetric equivalent “b”. The net heat flux to all members of structure are calculated using formulae (3.1) with (3.2) and (3.3) from PN-EN 1991-1-2. To catch whole heat coming into structure, adiabatic surface temperature from natural fire analysis is substituted into those equations. Then temperatures of members are calculated in accordance to equation (4.24) from PN-EN 1993-1-2 like for unprotected internal steelwork.

## 3. CFD ANALYSIS

Computational fluid dynamics analyses were made in FDS (Fire Dynamics Simulator). These analyses are the topic of another paper. For mechanical analysis one fire scenario was chosen and data resulted from analysis of that particular fire scenario are transferred to mechanical model. To do that, in FDS, at surfaces creating analysed vault, boundary data were collected. The quantity of particular interest was adiabatic surface temperature. Thanks to that, both convective and radiative heat flux could be described by one quantity (Wickstrom et.al 2007). The important property of FDS is possibility to use just rectangular geometry. Therefore it is worth to mention that data got from FDS must be treat as some estimation, especially when in this case real geometry of structure is barrel-shape.

FDS is collecting boundary data in so called boundary files. Special scripts are used to read data from these files.

## 4. FEM MODEL

Finite element method calculations are made in Abaqus. Model is composed of 3D beam elements B31 which are able to carry on both large deformations and large strains. Thermal response of these elements is included by thermal strains caused by additional internal forces resulted from temperature gradient along restrained elements. Time step in analysis is set up

to max. 50 sec, so implicit integration is adopted. During analyses, equilibrium at each time increment is found using the Newton-Raphson method. Both material and geometrical non-linearities are taken into account.

Full model is prepared using external scripting interface in Scilab, which is free equivalent for Matlab. Thanks to such process of model preparation, authors have got full control on model properties, and all necessary operations such as: applying both static and thermal boundary conditions, setting the constrains, applying loads, setting the direction of cross-sections, etc..

## 5. TRANSFERING DATA FROM CFD INTO FEM ANALYSES

Temperature history is transferred from FDS results, collected in FDS boundary files, first into Scilab where necessary operations on these data are carried on. At start, comparison of CFD and FEM models have to be done. So some actions on coordinate systems in both models are executed to place FEM model mesh in right place of bigger FDS model. After that's, scripts, already having right coordinates of FEM model, automatically search the nearest nodes from FDS boundary files, and from those, maximum adiabatic surface temperature is chosen. So at the end, temperature history for each node is distinguished.

Because adiabatic surface temperatures got from CFD analysis have got significant noise, it is approximated by multi-linear function. To do it, for each temperature-time curve, minimization problem is solved in the least square sense (Malendowski, 2012).

Next, section temperatures are calculated using Eurocode procedure (formula (4.24) from PN-EN 1993-1-2), with substitution of adiabatic temperature-time curve resulted from above. Such prepared section temperatures are transferred into Abaqus model as boundary conditions at each node. The whole procedure of transferring data between CFD and FEM is presented in Fig. 3.

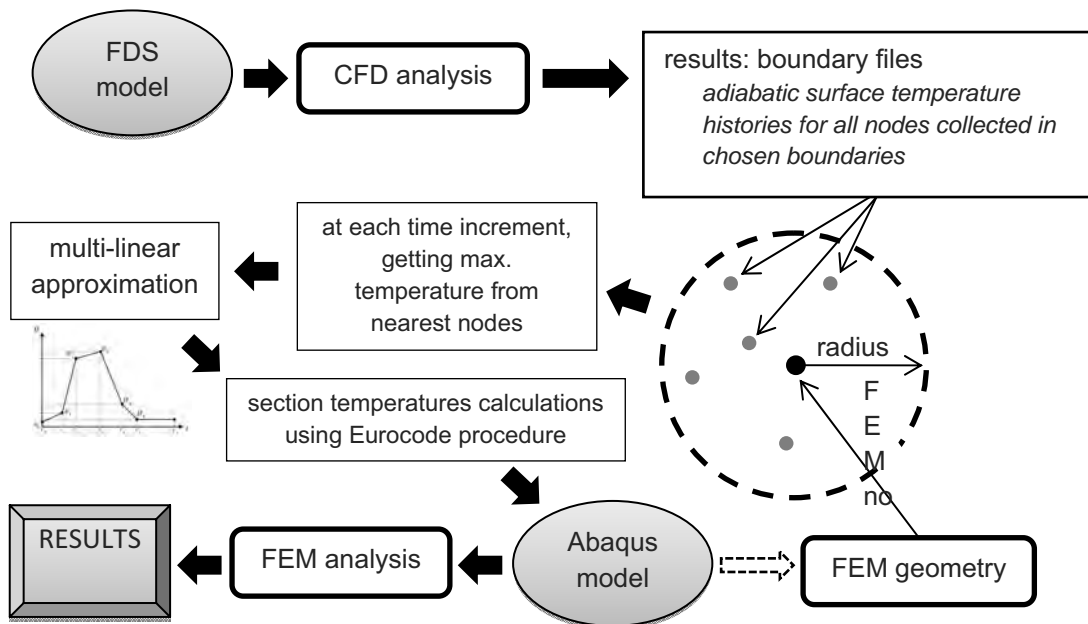


Fig. 3 Data transfer procedure

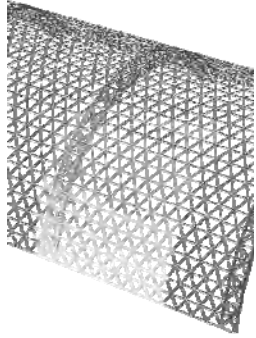
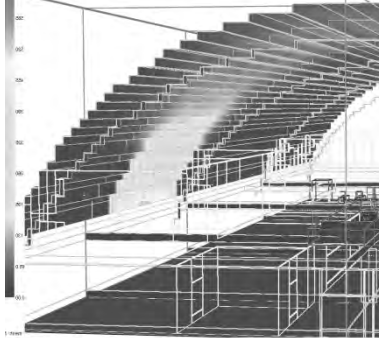
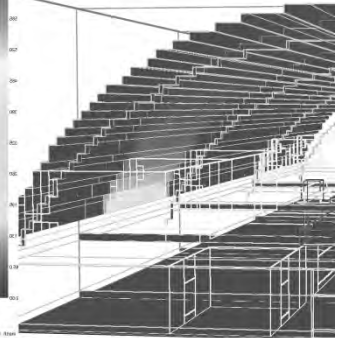
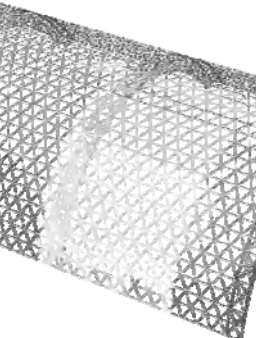
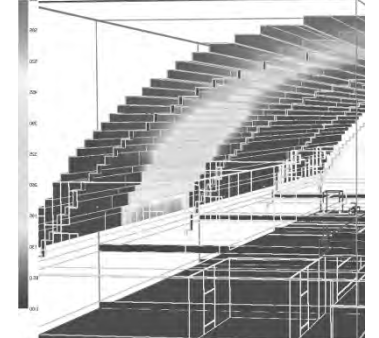
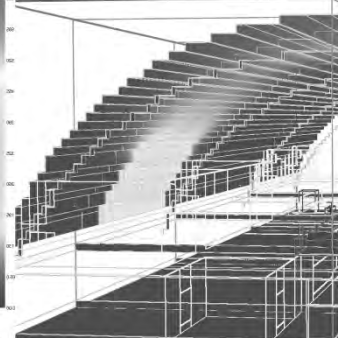
## 6. RESULTS

Results from analyses are collected and distinguished between temperatures of element's nodes, nodal displacements and plastic strains in elements.

### 6.1 Temperatures

In Tab. 2 colour-maps of three comparable quantities are shown. It can be seen that members temperatures calculated according to Eurocode procedure, using adiabatic surface temperature is higher than temperature of surfaces (wall temperatures) from FDS results.

Tab. 2 Comparison between temperatures given in FDS results and calculated in accordance to Eurocode's procedure.

time	Section temperature (EC calc. with AST)	Adiabatic surface temperature (FDS)	Wall temperature (FDS)
10 min			
40 min			

How scripts calculating and transferring temperature work is shown in Fig. 4 at the example of node with maximum reached temperature.

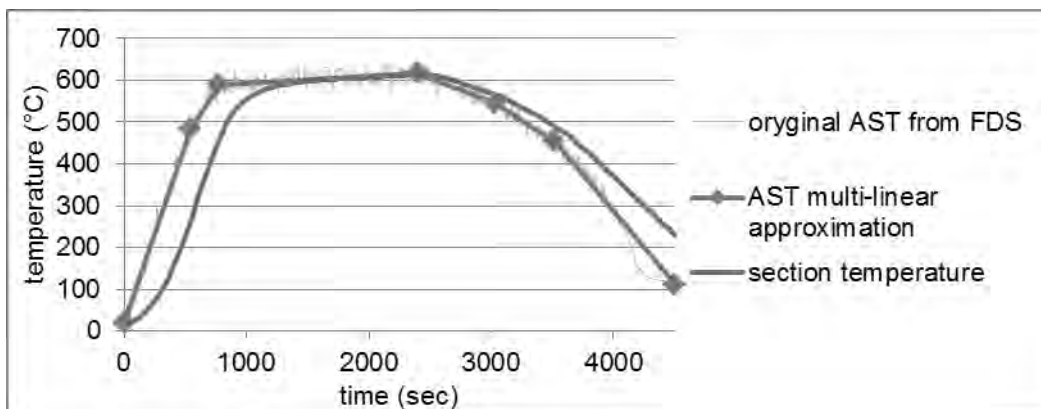


Fig. 4 Temperature history of node with max. temperature

## 6.2 Displacements

Displacement field at time when maximum temperature is reached, show no observable differences with reference to combinations of actions. The magnitude of total deflection is about 15 cm in all cases. Also shape of deformation is similar (Fig. 5).

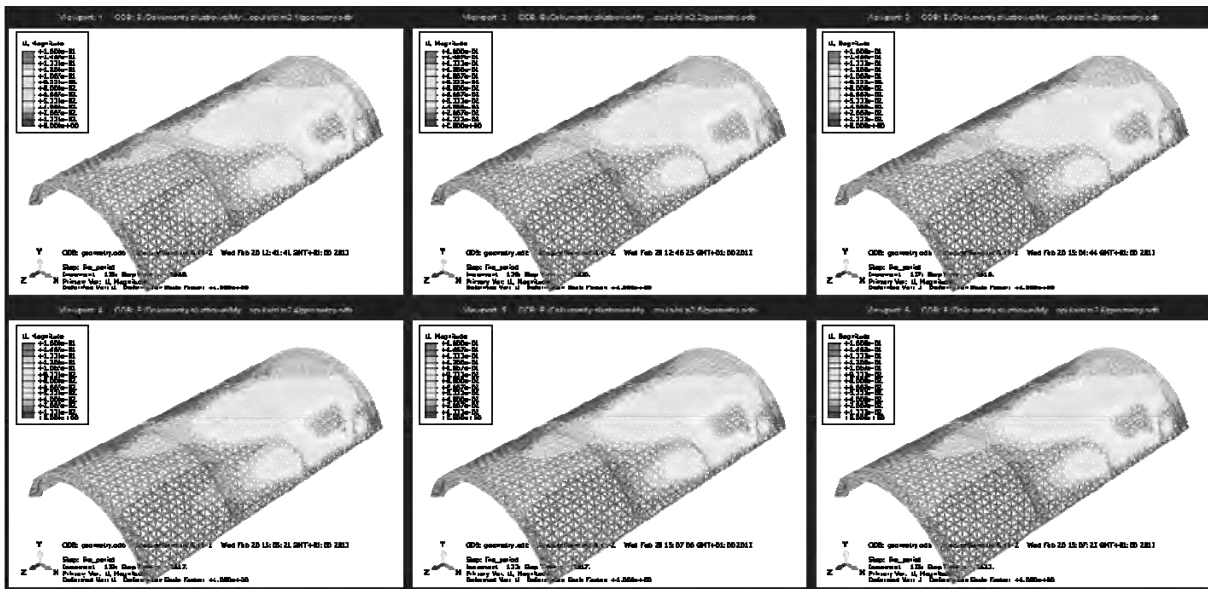


Fig. 5 Shape of deformation for all combinations of actions

### 6.3 Plastic zones

Because it was found, that there are not significant differences between results for different load combinations, just one map of plastic zones is shown in Fig. 6, particularly for load combination number 1 and for time about 40 minutes.. It can be seen from this picture, that only on longitudinal bars stresses reach yield stress, and plastic strains appear.

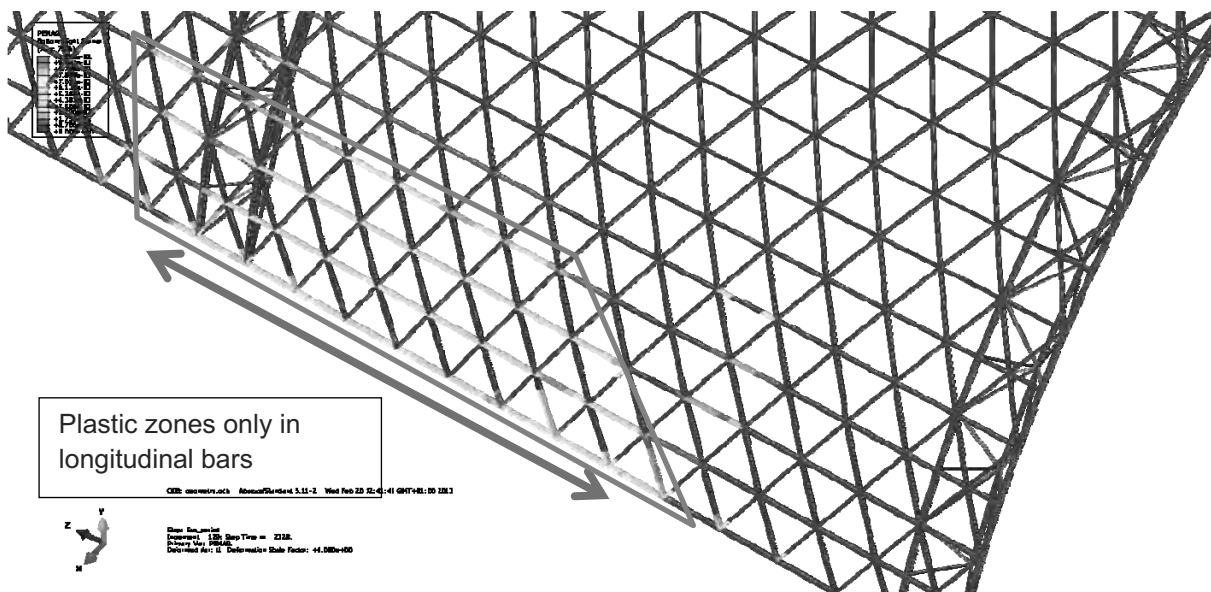


Fig. 6 Plastic zones in bars after 40 minutes of fire

Places where plastic zones propagate coincide with areas having the biggest temperatures. It is worth to mention, that in areas with the biggest temperatures, the largest plastic deformations are near to the support, where structure is most constrained. Supports constrains the structure in longitudinal direction and together with big temperature cause this described phenomena.

## 7. SUMMARY

In this paper, thermo-mechanical analysis of braced barrel vault structure in fire was presented. Analyses were done by solving the coupled CFD-FEM problem, with use of



external scripts, which help with model preparation and transferring data between those two different computational approaches.

Proposed procedure shows how complicated is process of satisfactorily accurate calculation of construction in natural fire. The biggest problem comes from fact, that it needs multi-physical approach, which up to now must be done by coupling different codes (here: FDS and Abaqus).

Results from these analyses show clearly that during fire, thermal action have to be necessarily taken into account, because in situations where construction is several times statically undetermined, thermal elongation of restrained members cause huge damage.

It was shown, that the most suffering members are not those where the biggest deflection was observed, but those which were the most constrained.

Nevertheless, the whole fire course did not threat the overall structural safety of construction. Even if in analysed case always the maximum temperature was chosen and members were threaten as unprotected, global redistribution of forces and stiffness of construction result in safe design from structural point of view. Analysed vault experienced significant thermal deformations, but only a finite number of bars were unable to carry on loads.

Additional finding from these work came from analyses of temperatures. In designing of such big open complexes like upper one, it is unreasonable to use standard ISO curve to describe temperature history. In none of points temperatures reach those from ISO curve.

## REFERENCES

- Eurocode 0, PN-EN 1990, Basic of structural design. European Committee for Standardization, 2004 (in Polish).
- Eurocode 1, PN-EN 1991-1-2, Actions on Structures Part 1-2 General Actions – Actions on structures exposed to fire, European Committee for Standardization, 2002 (in Polish).
- Eurocode 3, PN-EN 1993-1-2, Design of steel structures Part 1-2 Structural fire design, European Committee for Standardization, 2005 (in Polish).
- Wickstrom U., Duthing D., McGrattan K., Adiabatic surface temperature for calculating heat transfer to fire exposed structures, International Interflam Conference XI, 2007.
- Kevin McGrattan et al., Fire Dynamics Simulator (Version 5) User's Guide, NIST, 2007.
- ABAQUS, User's Manual.
- Scilab, Scilab Consortium - Digiteo Foundation ([www.scilab.org](http://www.scilab.org))
- Malendowski M., Approximation of the noisy temperature data got from CFD analysis and its influence onto FE analyses, Fire Safety of Construction Works Conference, ITB, Warsaw 2012.

## CLASS 4 SECTIONS AT ELEVATED TEMPERATURE

Jan Hricák <sup>a</sup>, František Wald <sup>a</sup>, Michal Jandera <sup>a</sup>

<sup>a</sup> Czech Technical University in Prague, Faculty of Civil Engineering, Prague, Czech Republic

### Abstract

The steel cross-sections behave stable or unstable. The behavior of slender cross sections of steel beams is influenced by local buckling. The buckling can be observed on beam web and/or flange and reduce the load bearing capacity of the beam. Design models adopted for daily design procedures are based on the so-called effective width approach. The design at fire situation is simplified which means that the same effective cross section as for cold design is used neglecting the changes of stiffness of steel. The research is focused on getting the knowledge of behaving of steel beams with welded Class 4 cross-sections exposed to high temperatures. This article describes the progress of the experiments.

**Keywords:** compressive resistance, temperature, slender cross-sections, class 4 cross-sections

### INTRODUCTION

A common practice in recent years, thanks to the introduction of European design standards for building construction has become not only an assessment of the structure at normal design situation, but also in the fire. The area of research slender cross-sections is very important, because the assessment and design principles of Class 4 sections are very specific and usually more difficult than for normal sections. Along with any global problems their behavior includes also local buckling of the compressed part of the cross-section.

The research thesis itself is focused on getting the knowledge of behaving of steel beams from the welded cross sections of class 4 (I and H shape) exposed to high temperatures.

### 1 THE DESIGN AND PREPARATION OF THE EXPERIMENTS

The focus of the project is to carry out experiments with I - beams with slender cross-sections, which belong to the class 4. The load capacity of these sections is not directly affected by the yield strength of the steel, but by deformations of the compressed areas of the cross-section, i.e. upper wall and the upper flange. To reach this way of deformation of the samples during the planned experiments, it was necessary to choose the appropriate cross-sectional shape, beam load form and force. Four tests with two types of cross-section loaded by four-point bending were carried out. (see Fig. 1).

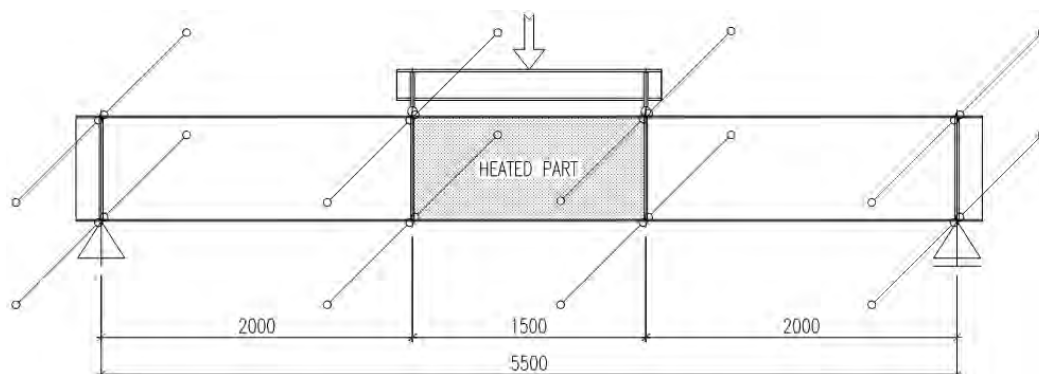


Fig. 1 Static scheme of the experiment

Beams were incur a variable load and they were heated with a constant temperature by an electric heating pads until exhaustion of the load capacity. Each section were heated to a temperature of 450 °C and 650 °C. These experiments were complemented by a number of material tests at high temperatures.

For these experiments, there were two types of welded cross-sections chosen. They represent cross-sections of the 4th class and they are sufficiently burdened by the problematic of local stability of the walls.

- The cross-section A (IW 680/250/12/4) has a vertical strut in the class 4 ( $\bar{\lambda}_P = 1,439$ ) and the flanges are in class 3 ( $\bar{\lambda}_P = 0,661$ ), see Fig. 2a.
- The cross-section B (IW 846/300/8/5) has a vertical strut in the class 4 ( $\bar{\lambda}_P = 1,454$ ) and the flanges are in class 4 ( $\bar{\lambda}_P = 1,182$ ), see Fig. 2b.

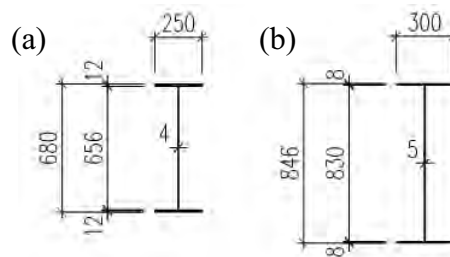


Fig. 2 Cross-sections designed for the experiment: a) Cross-section A, b) Cross-section B

### 1.1 Production of test samples

There were four beams produced for the experiments, with different length of the heated middle part. Due to thermal expansion and to maintain the static scheme (see Fig. 1), the middle heated part was shortened depending on the operating temperature. When heated to a prescribed temperature the middle part of the beam will have a length of approximately 1500 mm.

The A1 beam (cross-section 680/250/12/4 IS) and B1 beam (cross-section 846/300/8/5 IS) for a temperature of 450 °C were made with the middle part length of 1492 mm. The beams A2 (cross-section 680/250/12/4 IS) and B2 (cross-section 846/300/8/5 IS) designated for a temperature of 650 °C were made with the middle part length of 1488 mm.

### 1.2 Tools for the experiment

For the smooth running of the experiment and for taking into account all the boundary conditions according to the static scheme (see Fig. 1), steel tools were designed and manufactured. The scheme of the tools layout, including the location of the test beam is shown in the following figure (see Fig. 3).

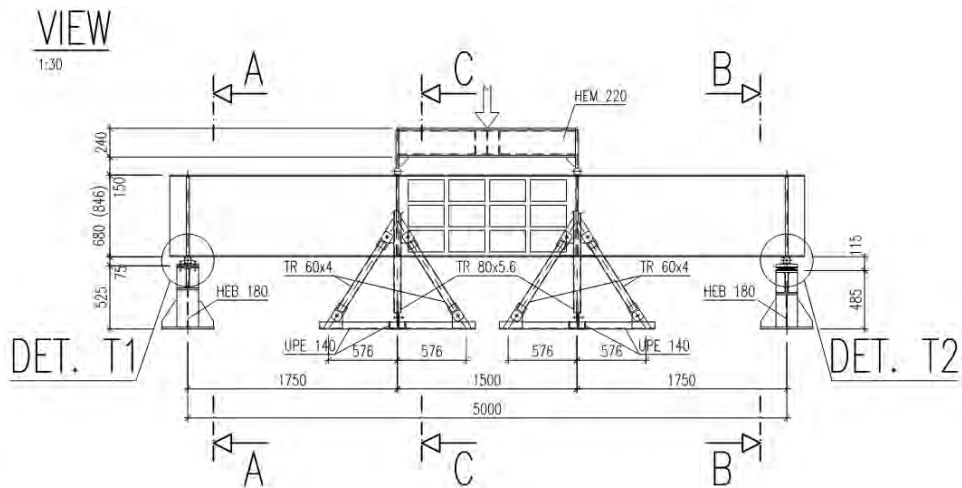


Fig. 3 The scheme of the tools layout

### 1.2.1 The tools for ensuring the torsional stability

The principle of the tools for ensuring the torsional stability at the support points and at the point of the load input is shown in cross sectional views A-A, B-B and C-C (see Fig. 4).

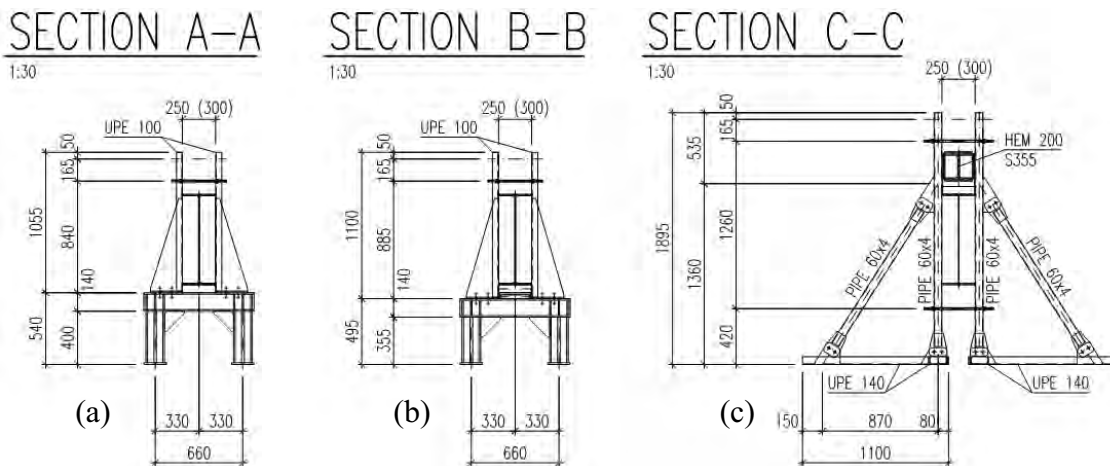


Fig. 4 Views: a) at v the point of the firm joint support, b) at v the point of the sliding joint support, c) at v the point of the load input

The construction of the tools at the support (see Fig. 4a, b) is formed by two vertical guide profiles UPE 100. The horizontal rectification of 240 mm to 310 mm is made possible by a bolt connection with slotted holes in the lower part and the threaded rod at the top part of the tool. The tools for ensuring the torsion stability at v the point of the load input (see Fig. 4c) are formed by the struts, which hold a vertical pair of guide profiles TR 80x5,6. Both the guide profiles are interconnected by a threaded rod at two points.

After placing the test beam to the support, the individual tools will clamp the cross-section of the beam with a small allowance, so a free movement in the vertical and longitudinal directions is not obstructed, but the piece is only prevented from tilting.

### 1.2.2 The design of the supports

The test beam is, according to the scheme (see Fig. 3), placed on the fixed articulated support from the left side (T1 detail - see Fig. 4) and on the sliding joint support (T2 detail - see Fig. 5) from the right side. The sliding articulated support is designed as a rolling bearing.

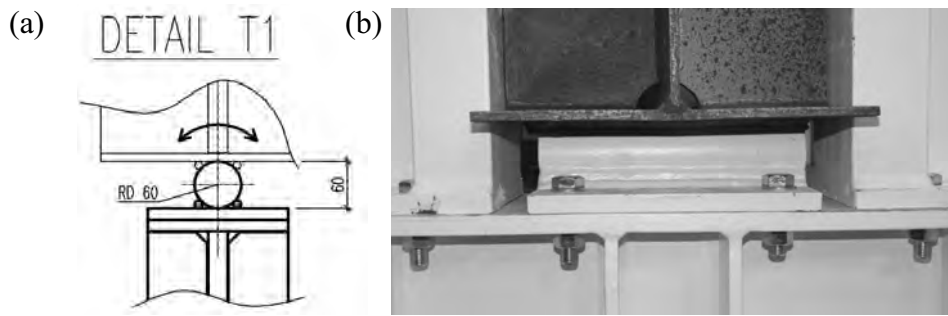


Fig. 5 Fixed articulated support: a) construction detail, b) side view of the finished support

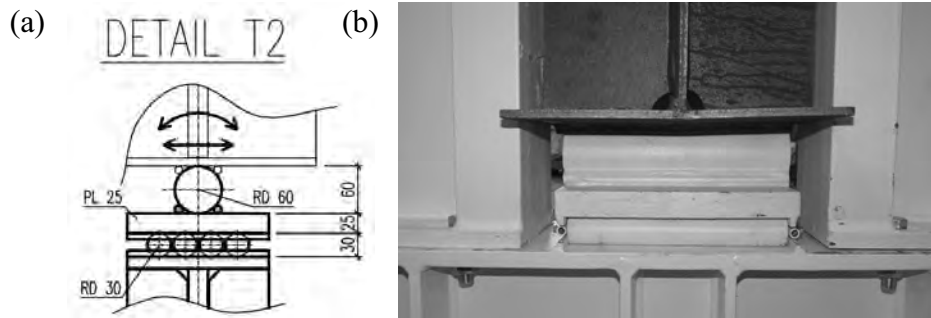


Fig. 6 Sliding articulated support: a) construction detail, b) side view of the finished support

### 1.3 Distribution of heating pads and sensing devices

The distribution of ceramic heating pads, thermocouples and potentiometers was carried out according to the scheme (see Fig. 7).

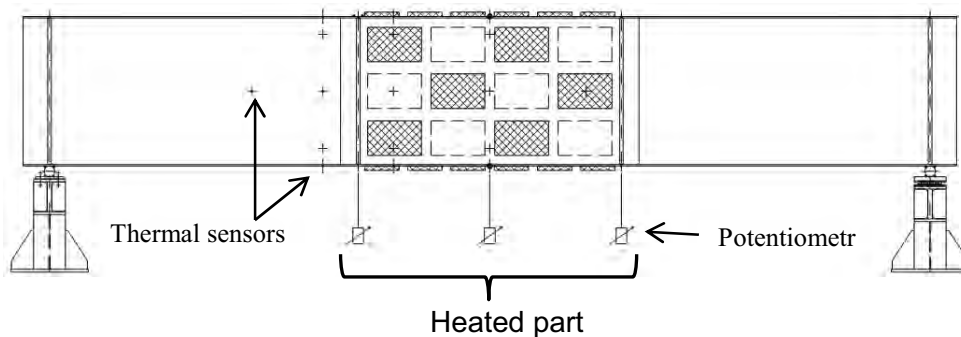


Fig. 7 Scheme of heating pads and sensing devices distribution

#### 1.3.1 Ceramic heating pads

Heating pads 195 x 305 mm were placed on the strut and the flange of the test beam according to the scheme (see Fig. 7). Alternately distributed pads were fastened to the strut using a steel wire grate, which was then fastened by a paper tape. The pads were placed on the flanges only from the outside. The mats on the top flange were loosely laid, and the mats on the bottom flange were fastened by bent wires. The distributed heating pads are seen on these photographs (see Fig. 8). The heating pads are able to reach a maximum temperature of 1200 °C at a heating rate 10 °C/min.

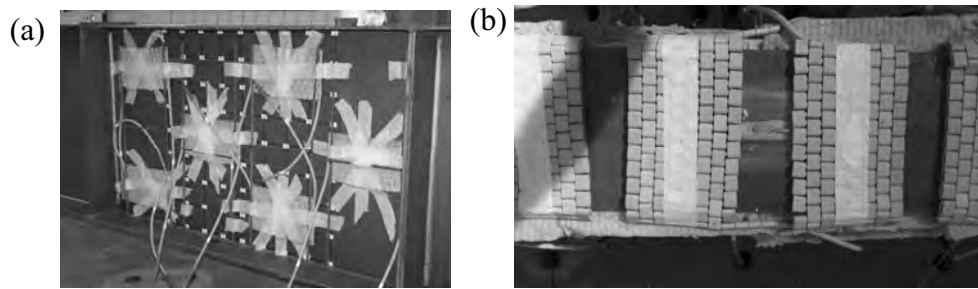


Fig. 8 Photo of the distributed heating mats: a) on the web, b) on the flange

### 1.3.2 Insulation of the heated central part of the beam

The entire heated middle part of the test beam was wrapped by ROCKWOOL Airrock HD thermal insulation boards. The space between the flanges was filled by the Insulation boards and strips of thermal insulation were then placed on both flanges. Thus insulated beam was then tied by a wire. The insulation procedure of the test beam is shown in Fig. 9. Finally, the whole middle part was wrapped by SIBRAL insulating strip.

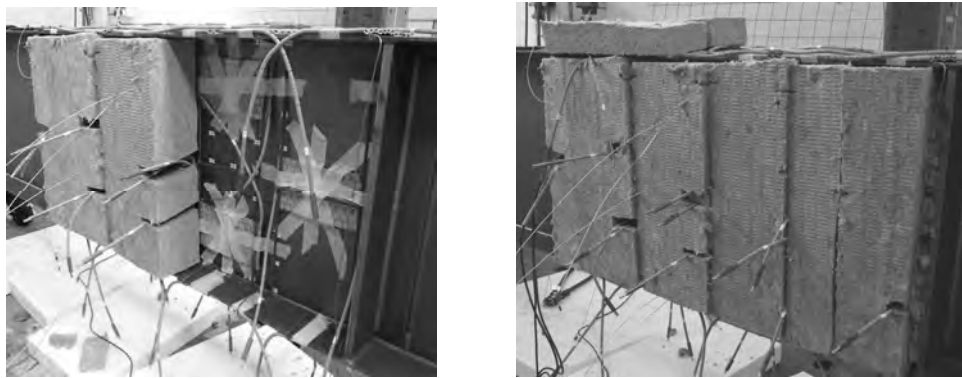


Fig. 9 Insulation procedure of the test beam

## 2 PROGRESS OF THE EXPERIMENT

After connecting all sensing devices (thermocouples, potentiometers, dynamometr in a hydraulic press) to the central measuring equipment and after connection the heating mats to the transformer, the beam was ready for the experiment (see Fig. 10).

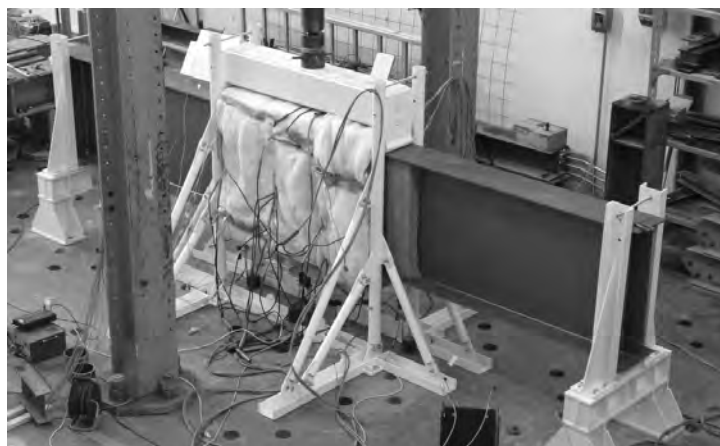


Fig. 10 The prepared test beam prior the experiment

A manual mode was chosen for heating, which allowed controlling of the performance of the heating mats on the basis of information from the thermocouple, displayed on the measuring device. Warm-up time for the temperature  $T \approx 450 \text{ }^\circ\text{C}$  was  $\sim 45$  minutes and  $\sim 65$  minutes for

the temperature  $T \approx 650 \text{ }^\circ\text{C}$ . After reaching the desired temperature in the heated part of the beam, a mechanical loading was started. The hydraulic press, which was controlled by a constant proportion of the deflection path in the middle part of the heated beam, was affecting the test beam through the load beam. The test beam was thus strained by four-point bending. The following load-deflection diagrams for Test 1-4 (see Fig. 11) express the dependence of the applied load of the press and the deflection in the middle of the heated part of the of the test beam. Summary of the results is shown in Tab. 1.

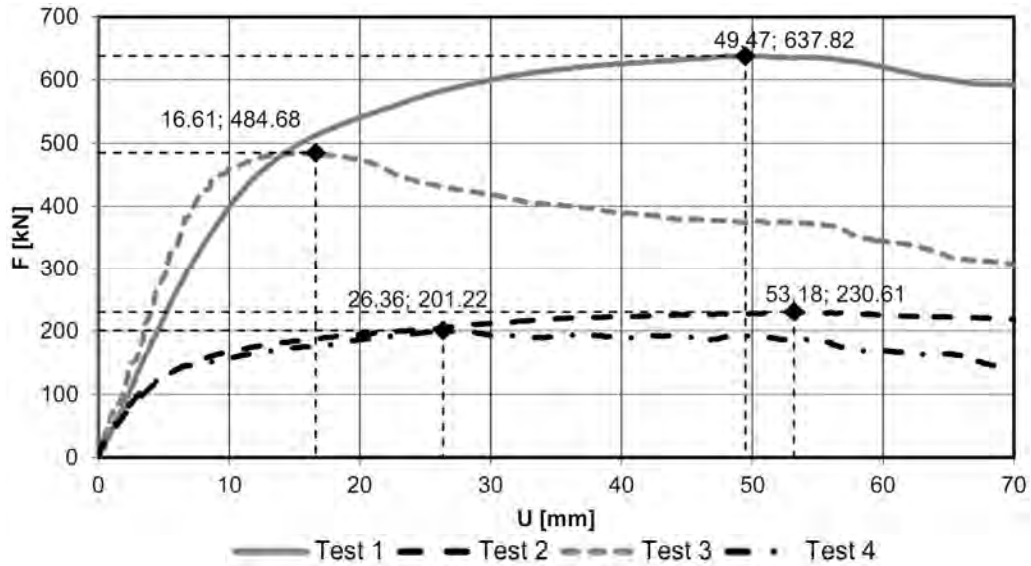


Fig. 11 Load-deflection diagram

Tab. 1 Load capacity from experiments

Tests	Cross-Section	Load capacity [kN]
1	A (IW 680/250/4/12)	637.82
2	A (IW 680/250/4/12)	230.61
3	B (IW 846/300/5/8)	484.68
4	B (IW 846/300/5/8)	201.22

### 3 CONCLUSION

The previous numerical model will be modified according to the actual material properties and according to the actual temperature. In this numerical model will be performed a parametric study. These studies will lead to the formation of a more precise design method for a sections class 4 at a high temperature.

### REFERENCES

- Buchanan A. H., Structural Design for Fire Safety, New Zealand, 2001.  
 Trahair, N. S., Bradford, M. A., Nethercot, D. A., The Behaviour and Design of Steel Structures, London, 2001.

## FIRE DESIGN OF STEEL BEAMS WITH WELDED CLASS 4 CROSS-SECTION

Carlos Couto <sup>a</sup>, Paulo Vila Real <sup>a</sup>, Nuno Lopes <sup>a</sup>, Bin Zhao <sup>b</sup>

<sup>a</sup> LABEST, University of Aveiro, Department of Civil Engineering, Aveiro, Portugal

<sup>b</sup> CTICM, Centre Technique Industriel de la Construction Métallique, Saint-Aubin, France

### Abstract

The present paper deals with the study of the lateral torsional buckling of steel beams with welded class 4 cross-sections in case of fire. A numerical study of several beams with different class 4 cross-sections submitted to uniform bending moment at elevated temperatures has been performed using the finite element method. The results are compared with existing simplified design rules of Part 1.2 of Eurocode 3 showing that these rules are too conservative. A comparison is also made with the proposed method in the French National Annex. Based on these comparisons a new proposal is presented to check the lateral torsional buckling resistance which is validated against the numerical simulations.

**Keywords:** lateral torsional buckling (LTB), beams, class 4, fire, residual stresses

### INTRODUCTION

The lateral torsional buckling (LTB) of steel members submitted to bending is a phenomena that affects the load carrying capacity of these members, in fact, in beams the compression of the flange may lead to a lateral displacement accompanied by a rotation of the cross-section that prevents the full development of the bending resistance. This phenomenon is influenced by a variety of factors, namely the cross-section shape, the loading pattern, the boundary conditions, among others and needs to be considered in the design. Additionally, slender cross-sections may also buckle under compression stresses before attaining the yield stress in one or more parts of the cross-section. This phenomenon is called local buckling.

In Eurocode 3 (CEN, 2005a), lateral torsional and local buckling are treated in separate ways. LTB is accounted for by reducing the cross-sectional bending resistance of the element by a “reduction” factor that takes this phenomenon into consideration. Local buckling can be accounted for by using the effective width method to make the necessary allowances for reductions of the cross-sectional resistance due to the effects of local buckling. The cross-sections where local buckling may occur are classified as class 4, according to Eurocode 3.

The informative Annex E of the Part 1.2 of the Eurocode 3 (EN1993-1-2) (CEN, 2005b) gives some recommendations for the fire design of steel members with class 4 cross-sections. In this annex, it is suggested to use the simple calculation methods with the design value for the steel yield strength as the 0.2% proof strength instead of the stress at 2% total strain as for the other classes, and that the effective cross-section be determined with the effective width method as for normal temperature, i.e. based on the material properties at normal temperature. This procedure is, however, known to be very conservative (Renaud and Zhao, 2006).

This study focus on the LTB behaviour of steel beams with welded class 4 cross-sections submitted to uniform bending moment in fire situation. The LTB resistance of the steel beams evaluated with the fire design rules prescribed in the EN1993-1-2 and also the French National Annex are compared with numerical results obtained with the software SAFIR (Franssen, 2005), showing that EN1993-1-2 is very conservative as mentioned before and the French National Annex could be improved since it has been developed for hot-rolled profiles. Because of that a new proposal has been developed and validated in this study to check for the



LTB resistance of steel beams with welded class 4 cross-sections submitted to uniform bending moment in fire situation.

## 1 LTB RESISTANCE OF BEAMS WITH CLASS 4 CROSS-SECTION

The LTB resistance of beam with class 4 cross-section is evaluated in fire situation with the following expression

$$M_{b,fi,t,Rd} = \chi_{LT,fi} W_{eff,y,min} k_{0.2p,\theta} f_y \gamma_{M,fi} \quad (1)$$

with  $W_{eff,y,min}$  being the section modulus of the effective cross-section calculated with the same rules as for normal temperature,  $k_{0.2p,\theta}$  being the reduction factor for the design yield strength of class 4 cross-sections,  $f_y$  the design yield strength and its respective partial safety factor for fire situation  $\gamma_{M,fi}$ . It may be noted that the values given in the Annex E of EN1993-1-2 for the  $k_{0.2p,\theta}$  are slightly different from the values obtained with the material law model of EN1993-1-2 for steel at elevated temperatures. These values derived from the material law model are given in the French National Annex and are used in this study (see Fig. 1). The reduction factor for LTB in the fire design situation is determined by

$$\chi_{LT,fi} = \frac{1}{\phi_{LT,\theta} + \sqrt{\phi_{LT,\theta}^2 - \bar{\lambda}_{LT,\theta}^2}} \quad (2)$$

and

$$\phi_{LT,\theta} = 0.5 \left[ 1 + \alpha \bar{\lambda}_{LT,\theta} + \bar{\lambda}_{LT,\theta}^2 \right] \text{ and } \alpha = 0.65 \sqrt{235 / f_y} \quad (3)$$

with the non-dimensional slenderness at elevated temperatures given by

$$\bar{\lambda}_{LT,\theta} = \bar{\lambda}_{LT} \sqrt{k_{0.2p,\theta} / k_{E,\theta}} \text{ with } \bar{\lambda}_{LT} = \sqrt{W_{eff,y,min} f_y / M_{cr}} \quad (4)$$

where  $k_{E,\theta}$  is the reduction factor for the *young modulus* at elevated temperature given in EN1993-1-2 and  $M_{cr}$  is the elastic critical moment given in the literature.

According to the French National Annex of EN1993-1-2 the LTB resistance of members with class 4 cross-sections should be checked with the same equation (1) but considering

$$\phi_{LT,\theta} = 0.5 \left[ 1 + \alpha_{LT} (\bar{\lambda}_{LT,\theta} - 0.2) + \bar{\lambda}_{LT,\theta}^2 \right] \text{ with } \alpha_{LT} = 0.34 \quad (5)$$

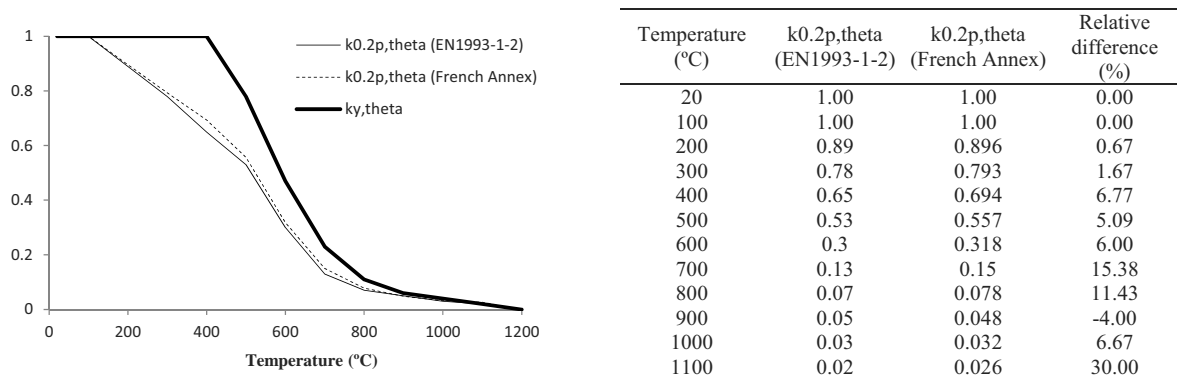


Fig. 1: Variation of the reduction factors with the temperature.  $ky,theta$  is the reduction factor for the design yield strength of class 1, 2 and 3 cross-sections.

## 2 NUMERICAL STUDY

### 2.1 Numerical model

The finite element computer code SAFIR (Franssen, 2005), has been used within this study and the numerical model used is depicted in Fig. 2 and described next.

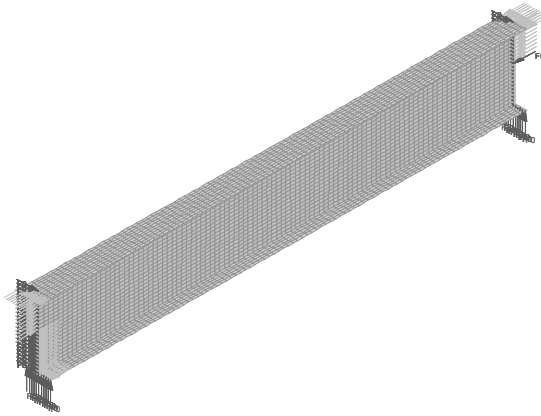


Fig. 2: Numerical model used in this study.

A preliminary study of the density of the mesh has been performed and a total of 10 shell elements for the flange, 22 shell elements for the web and 100 shell elements along the width has been used for the mesh in this study. A uniform bending moment has been applied to the model by means of nodal forces and to prevent numerical problems additional stiff elements along the webs and the flanges have been adopted. The so-called “fork-support” conditions have been considered in the model by restraining vertical displacements of the bottom flange and the out-of-the plane horizontal displacements of the web in the extremities of the beam.

In this study, different temperatures have been considered (350°C, 450°C, 550°C and 700°C). It was established that the temperature along the beam was constant. The steel grade S355 was used and different beam lengths considered, in a total of 240 different cases.

### 2.2 Cross-sections analyzed

A total of 5 cross-sections as indicated in Tab. 1 were analysed. In this Tab. the classification for fire design of each cross-section for bending about major axis is shown, and the classification of the flange and of the web is indicated and also the effective width of the flange and of the web as a % of the gross width is shown. It may be noted that, as a simplification EN1993-1-2 allows that cross-section classification be determined as for normal temperature but using a reduced parameter of  $\varepsilon$  that takes into account the effect of temperature as  $\varepsilon = 0.85\sqrt{235 / f_y}$  . with  $f_y$  being the design yield strength.

Tab. 1: Summary of the cross-sections analyzed and their classification for bending about major axis for fire design (Steel grade S355)

Cross-section	Dimensions (H x B x $t_w$ x $t_f$ ) (mm)	Class of flange in compression	Class of web in pure bending	Effective width (% of gross width)		Classification for bending about major axis for fire design
				flange	web	
A	460x150x4x5	4	4	84%	86%	4
B	460x150x3x4	4	4	70%	64%	4
C	460x150x5x10	3	4	n.a.	100%	4
D	460x150x4x8	3	4	n.a.	90%	4
E	460x150x4x7	4	4	100%	90%	4

All the cross-sections are classified as class 4 for bending about major axis for fire design. Both cross-sections A and B have reduction of the flange and the web, being section B much less effective than A. For cross-sections C and D only the web is classified as class 4 and for the cross-section C no reduction of the web is needed. For cross-section E, despite the flange being classified as class 4 it has no reduction.

### 2.3 Geometric imperfections and residual stresses

The geometric imperfections have been introduced in the model by changing the node coordinates to represent the worst scenario for the assessment of lateral torsional buckling resistance of the beams. This has been considered as the shape given by the eigenmodes of a linear buckling analysis (LBA) performed with the software Cast3M (Cast3M, 2012). In accordance with the finite element method of analysis recommendations given in the Annex C of EN1993-1-5 (CEN, 2012) a combination of global and local modes (see Fig. 3) has been used, where the lower mode has been taken as the leading imperfection and the other one reduced to 70%. The amplitude of the imperfections has been chosen as 80% of the fabrication tolerances given in the EN1090-2 (CEN, 2008) as suggested in the same annex, i.e. global mode has been scaled to 80% of  $L/500$  and the local mode to the maximum between 80% of  $b/100$  or 80% of  $h_w/100$ , where  $b$  is the flange width and  $h_w$  is the height of the web of the cross-section.

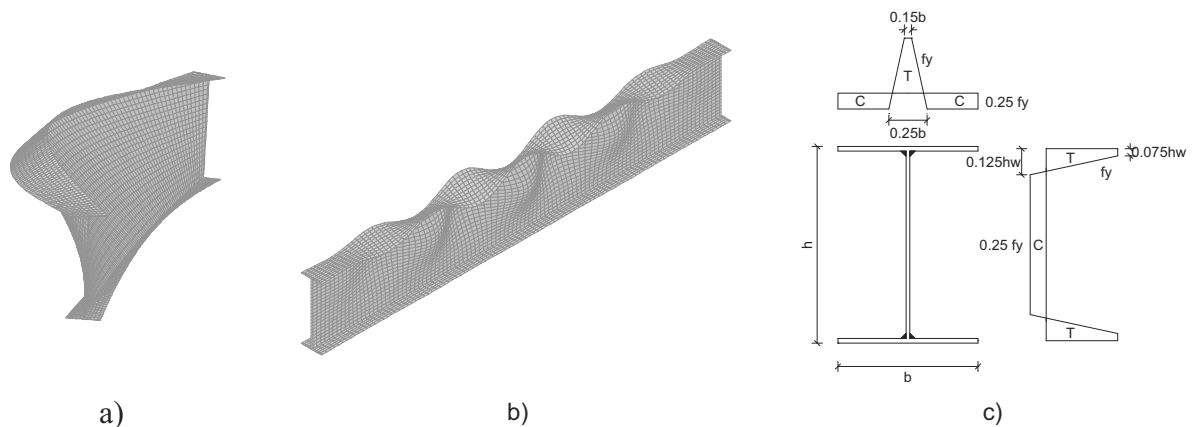


Fig. 3: Geometric imperfections and residual stresses used in the numerical models. a) Global eigenmode, b) local eigenmode and c) pattern of the residual stresses used in this study (taken from (ECCS, 1984)).

Residual stresses have been introduced in the numerical model with the stress pattern depicted in Fig. 3 c), the values adopted for the residual stresses are in accordance with (ECCS, 1976) as used in a previous study (ECCS, 2000).

### 3 LTB RESISTANCE OF STEEL BEAMS WITH WELDED CLASS 4 CROSS-SECTIONS AT ELEVATED TEMPERATURES

In Fig. 4, the results obtained for the LTB resistance of several steel beams with different welded class 4 cross-sections at elevated temperatures is shown and compared to actual design provision of EN1993-1-2. In the left chart results are detailed for one cross-section and in the right chart the results of all cross-sections are plotted. The beams are submitted to uniform bending moment.

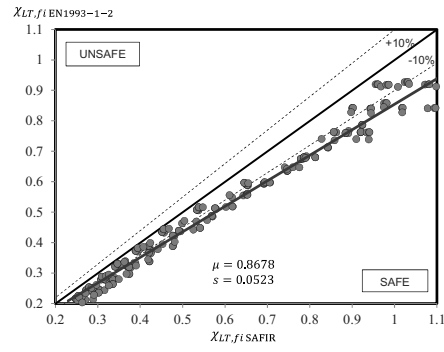
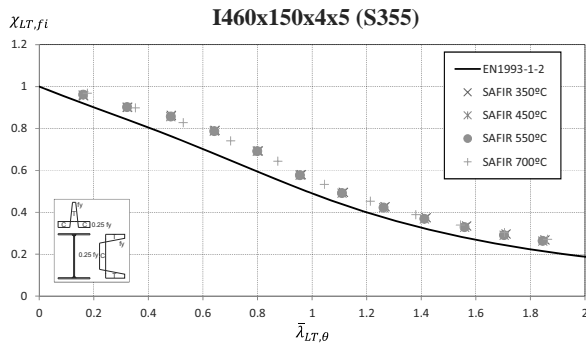


Fig. 4: Comparison between the numerical results calculated with SAFIR and LTB resistance of beams with welded class 4 cross-sections according to EN1993-1-2.

In Fig. 5 the numerical results are again compared with the LTB resistance curve of the French National Annex (see §1). In the left Fig. results are detailed for one cross-section and in the right Fig. the results of all cross-sections are plotted.

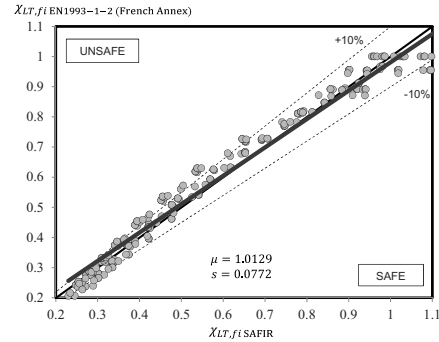
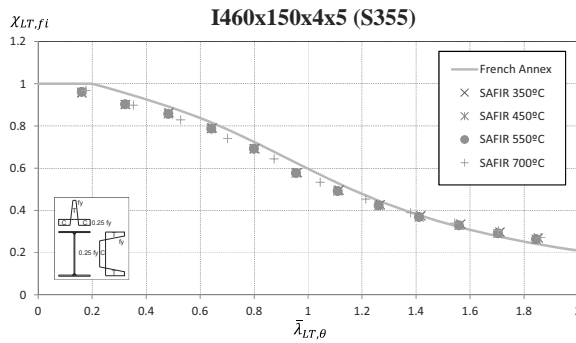


Fig. 5: Comparison between the numerical results calculated with SAFIR and LTB resistance of beams with welded class 4 cross-sections according to French National Annex of EN1993-1-2.

From Fig. 4 it can be seen that the LTB resistance given in the EN1993-1-2 for welded class 4 cross-sections is very conservative. The French National Annex method gives better results as shown in Fig. 5, but it could be improved, mainly because it has been developed for hot-rolled cross-sections. Because of that a new proposal, for the design lateral torsional buckling resistance of beams with welded class 4 cross-sections in fire situation is presented in the next section.

### 3.1 New proposal for LTB resistance of class 4 welded cross-sections

From the basis of the French National Annex proposal, a new proposal for the LTB resistance of steel beams with welded class 4 cross-sections has been developed by curve-fitting the numerical results obtained with SAFIR. This procedure lead to the use of the same equations for checking the LTB resistance of steel members with class 4 cross-sections given in EN1993-1-2 but considering

$$\phi_{LT,\theta} = 0.5 \left[ 1 + \alpha_{LT} \left( \bar{\lambda}_{LT,\theta} - 0.2 \right) + \bar{\lambda}_{LT,\theta}^2 \right] \text{ and } \alpha_{LT} = 0.49 \quad (6)$$

In this case, the imperfection factor  $\alpha_{LT}$  is chosen as the “curve c” in the Tab. 6.4 of EN1993-1-1. The results obtained with the new proposal are shown in the Fig. 7. In the left chart results are detailed for one cross-section and in the right chart the results of all cross-sections are plotted.

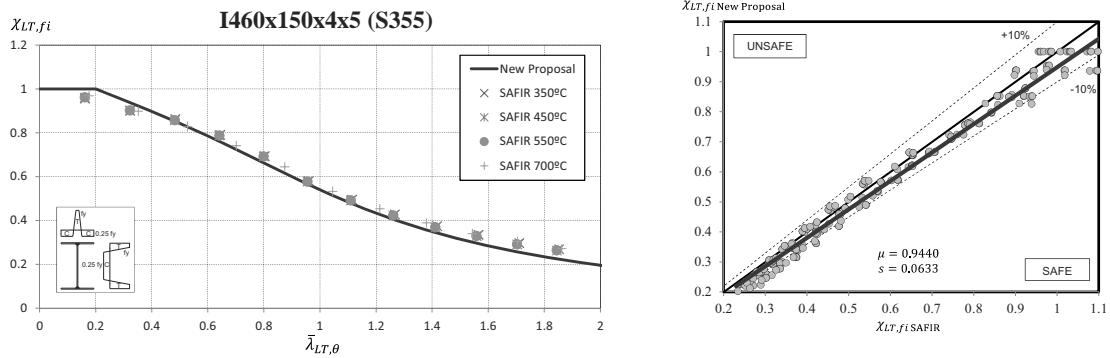


Fig. 6: Comparison between the numerical results calculated with SAFIR and LTB resistance of beams with welded class 4 cross-sections according to the new proposal.

From Fig. 6 it can be seen that this new proposal improves the results and should be used to assess the LTB resistance of steel beams in this case.

#### 4 CONCLUSIONS

In this study the behaviour of beams with welded class 4 cross-section subjected to uniform bending moment was investigated. Using a numerical study with FEM-software SAFIR for different cross-sections, different temperatures and beam lengths, it was possible to observe that the actual fire design rules of EN1993-1-2 for checking the LTB resistance of beams with welded class 4 cross-sections are very conservative. It was also possible to conclude that the French National Annex of the EN1993-1-2, which has been derived for hot rolled profiles, could be improved. For this reason, a new proposal has been developed and validated against numerical results, leading to an improvement of the obtained results.

#### REFERENCES

- CAST3M. CAST 3M is a research FEM environment; its development is sponsored by the French Atomic Energy Commission; 2012. <<http://www-cast3m.cea.fr/>>.
- CEN European Committee for Standardisation, EN 1993-1-1, Eurocode 3: Design of Steel Structures – Part 1-1: General rules and rules for buildings, 2005.
- CEN European Committee for Standardisation, EN 1993-1-2, Eurocode 3: Design of Steel Structures – Part 1-2: General rules - Structural fire design, 2005.
- CEN European Committee for Standardisation. EN 1090-2, Execution of steel structures and aluminium structures - Part 2: Technical requirements for steel structures. Brussels, Belgium, European Committee for Standardisation, 2008.
- CEN European Committee for Standardisation, EN 1993-1-5, Eurocode 3, Design of Steel Structures – Part 1-5: Plated structural elements, 2012.
- ECCS European Convention for Constructional Steelwork TC8, Manual on Stability of Steel Structures. Publication No. 22, 1976.
- ECCS European Convention for Constructional Steelwork TC8, Ultimate limit state calculation of sway frames with rigid joints. Publication No. 33, 1984.
- ECCS European Convention for Constructional Steelwork TC8, New lateral torsional buckling curves  $k_{LT}$  - numerical simulations and design formulae, 2000.
- Franssen, J.-M. (2005). SAFIR, A Thermal/Structural Program Modelling Structures under Fire, Engineering Journal, A.I.S.C. 42(3): 143-158, 2005.
- Renaud, C. and B. Zhao, Investigation of Simple Calculation Method in EN 1993-1-2 for Buckling of Hot Rolled Class 4 Steel Members Exposed to Fire, Fourth International Workshop "Structures in Fire" - SiF'06, Aveiro, Portugal: 119-211, 2006.

## INTERACTIVE SHEAR RESISTANCE OF CORRUGATED WEB IN STEEL BEAM EXPOSED TO FIRE

Mariusz Maślak <sup>a</sup>, Marcin Łukacz <sup>a</sup>

<sup>a</sup> Cracow University of Technology, Faculty of Civil Engineering, Cracow, Poland

### Abstract

The design approach to shear buckling resistance evaluation for corrugated web being a part of a steel beam exposed to fire is presented and discussed in detail. It is based on the experimentally confirmed interaction between the local and global elastic instability failure modes as well as on the possible yielding of the whole web cross – section during fire. Conclusively, the new formulae, adequate for specification of the suitable shear buckling coefficients depend not only on the web slenderness but also on the temperature of structural steel. The methodology proposed by the authors can be added to the current European standard recommendations given in EN 1993-1-2 as a well-justified design algorithm helpful in reliable evaluation of safety level for steel beams with slender corrugated webs subject to fire exposure. It seems to be highly desirable, because at present there are no detailed instructions in this field.

**Keywords:** steel beam, corrugated web, shear buckling coefficient, fire, interaction formulae.

### INTRODUCTION

It is a common knowledge that in the case of a steel beam with corrugated web such web fails due to shear buckling or yielding while its flanges resist the whole bending moment. Therefore, it is usually assumed that the considered web can carry only shear forces applied to the beam and estimation the value of its shear resistance  $V_{Rd}$  becomes the main goal of many analytical models. According to the approach given in EN 1993-1-5 the design value of this resistance is assessed by the specification of the effective shear buckling coefficient  $\chi_c$ :

$$V_{Rd} = \chi_c h_w t_w \frac{f_{yw}}{\sqrt{3}\gamma_{M1}} = \chi_c V_{R,pl,d} \quad (1)$$

In this formula  $h_w$  and  $t_w$  are the web height and its thickness respectively,  $f_{yw}$  is the yield point of the steel the web is made of and  $\gamma_{M1}$  is the suitable partial safety factor. It is important that:

$$\chi_c = \min(\chi_{cL}, \chi_{cG}) \quad (2)$$

where the first coefficient  $\chi_{cL}$  is connected with the local shear buckling failure mode (with buckled areas limited to the single web panels or half-waves), whereas the second one  $\chi_{cG}$  deals with the global shear buckling failure mode. To evaluate the values of such both instability coefficients the web relative slendernesses,  $\bar{\lambda}_{cL}$  and  $\bar{\lambda}_{cG}$ , are defined as follows:

$$\bar{\lambda}_{cL} = \sqrt{\frac{\tau_{pl}}{\tau_{cr,L}}} = \sqrt{\frac{f_{yw}}{\sqrt{3}\tau_{cr,L}}} \quad \text{and} \quad \bar{\lambda}_{cG} = \sqrt{\frac{\tau_{pl}}{\tau_{cr,G}}} = \sqrt{\frac{f_{yw}}{\sqrt{3}\tau_{cr,G}}} \quad (3)$$

Finally:

$$\chi_{cL} = \frac{1,15}{0,9 + \bar{\lambda}_{cL}} \leq 1 \quad \text{and} \quad \chi_{cG} = \frac{1,5}{0,5 + \bar{\lambda}_{cG}^2} \leq 1 \quad (4)$$

## 1 INTERACTIVE SHEAR BUCKLING COEFFICIENT

The standard approach presented above seems to be very simple and easy to use; however, it is necessary to say that it is not fully correct in mathematical sense. Let in random realisation the resistance  $V_R = \min(V_{RL}, V_{RG})$  be the random variable, usually being compared with the associated shear force treated as the concurrent random action effect. Such assumption does not lead to the similar conclusion, dealing with the suitable design values, that  $V_{Rd} = \min(V_{RL,d}, V_{RG,d})$ , suggested by the Eurocode. In this paper the authors propose to replace the classical instability factor  $\chi_c$  (taken from Eq. (2)) by another factor, named the equivalent interactive shear buckling coefficient  $\chi_{c,int}$ . It should give the web shear buckling resistance assessment being significantly more precise because its defining formula is based on the experimentally confirmed interactive relations between the potential elastic – plastic shear stresses. There are a lot of various interactive relations between  $\tau_{cr,L} - \tau_{cr,G} - \tau_y$  (or only between  $\tau_{cr,L} - \tau_{cr,G}$ ), proposed by many authors (Eldib, 2009). In further analysis two most popular of them are considered in detail. The first one is written as follows:

$$\frac{1}{(\tau_{int})^n} = \frac{1}{(\tau_{cr,L})^n} + \frac{1}{(\tau_{cr,G})^n} + \frac{1}{(\tau_y)^n} \quad (5)$$

The exponent  $n$  is here most frequently adopted as  $n = 2$  (El-Metwally, 1998) or even as  $n = 3$  (Sayed-Ahmed, 2001). Let us notice that in case when only interaction between global and local elastic instability failure modes is considered, whereas the influence of web yielding is neglected, this formula is shortened to the following form:

$$\frac{1}{(\tau_{cr,int})^n} = \frac{1}{(\tau_{cr,L})^n} + \frac{1}{(\tau_{cr,G})^n} \quad (6)$$

in which also various values of exponent  $n$  can be used, particularly  $n = 1$  (Bergfelt) (Driver et al., 2006),  $n = 2$  (Abbas) (Abbas et al., 2002) and  $n = 4$  (Hiroshi) (Hiroshi et al., 2003).

Multiplication of both sides of Eq. (5) by  $(\tau_y)^n$  gives:

$$\frac{(\tau_y)^n}{(\tau_{int})^n} = \frac{(\tau_y)^n}{(\tau_{cr,L})^n} + \frac{(\tau_y)^n}{(\tau_{cr,G})^n} + 1 \quad (7)$$

Let  $\chi_{c,int} = \tau_{int}/\tau_y$ , then:

$$\left( \frac{1}{\chi_{c,int}} \right)^n = \bar{\lambda}_{cL}^{2n} + \bar{\lambda}_{cG}^{2n} + 1 \quad (8)$$

Consequently:

$$\chi_{c,int} = \left( \bar{\lambda}_{cL}^{2n} + \bar{\lambda}_{cG}^{2n} + 1 \right)^{-1/n} \quad (9)$$

Similarly, starting from Eq. (6) one have obtained:

$$\chi_{c,int} = \left( \frac{-2n}{\bar{\lambda}_{cL}} + \frac{-2n}{\bar{\lambda}_{cG}} \right)^{-(1/n)} \quad (10)$$

## 2 GENERALIZATION OF THE STANDARD APPROACH TO THE FIRE CASE

To evaluate considered web shear resistance under fully developed fire conditions not only the yield point reduction specified for steel the beam is made of must be regarded through the substitution in Eq. (1) the value  $f_{yw}$  by the product  $f_{yw,\Theta} = k_{y,\Theta} f_y$  (where reduction factors  $k_{y,\Theta} = f_{y,\Theta} / f_y$  are given in EN 1993-1-2 for particular values of material temperature  $\Theta_a$ ) but also the reliable specification of the relation  $\chi_{c,\Theta} = \chi_c(\Theta_a)$  should be made and effectively applied to the analysis. Moreover, the suitable partial safety factor have to be changed, from  $\gamma_{M1}$  into  $\gamma_{M,fi}$ , however in practice such conversion does not give any quantitative difference because in the standard EN 1991-1-2 it is suggested to be used  $\gamma_{M,fi} = 1,0$ . Conclusively, Eq. (1) is rearranged to the form:

$$V_{Rd,\Theta} = \chi_{c,\Theta} V_{R,pl,d,\Theta} \frac{\gamma_{M1}}{\gamma_{M,fi}} = \chi_{c,\Theta} h_w t_w \frac{k_{y,\Theta} f_{yw}}{\sqrt{3} \gamma_{M,fi}} \quad (11)$$

To study the influence of fire temperature on instability coefficients it is convenient to rewrite Eqs. (2 ÷ 4) into the alternative formulae being easier for interpretation:

$$\chi_c = \chi_{cL} \quad \text{if} \quad \bar{\lambda}_{cG} < \bar{\lambda}_c^* = \sqrt{0,674 + 1,304 \bar{\lambda}_{cL}} \quad (12)$$

$$\chi_c = \chi_{cG} \quad \text{if} \quad \bar{\lambda}_{cG} \geq \bar{\lambda}_c^* = \sqrt{0,674 + 1,304 \bar{\lambda}_{cL}} \quad (13)$$

The resultant dependence obtained for persistent design situation (without any fire influence), between the coefficient  $\chi_c$  and the suitable relative web slendernesses,  $\bar{\lambda}_{cL}$  and  $\bar{\lambda}_{cG}$ , is shown in detail in Fig. 1a.

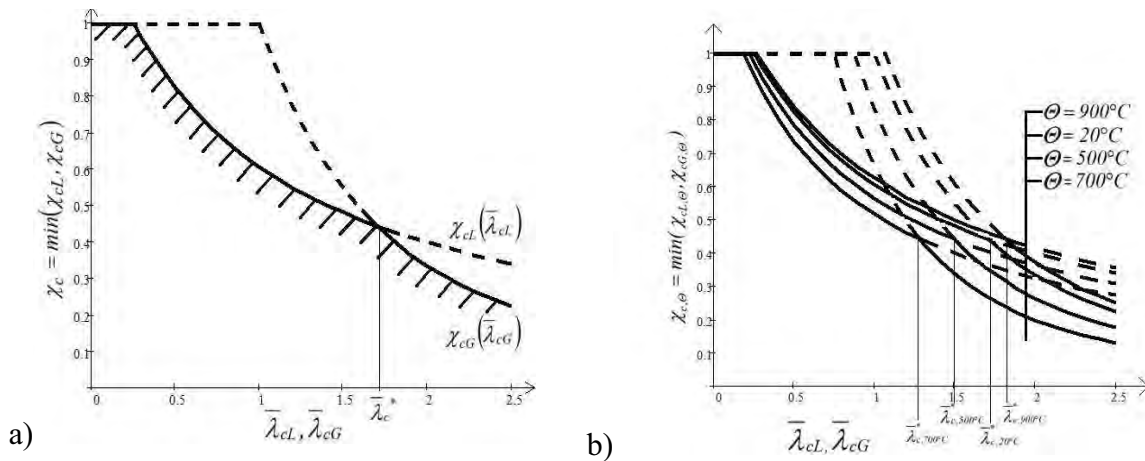


Fig. 1 Relations between shear buckling coefficient  $\chi_c$  and relative slendernesses  $\bar{\lambda}_{cL}$  and  $\bar{\lambda}_{cG}$  a) in persistent design situation - according to Eq. (4), b) under fire conditions - according to Eq. (22).

In further analysis relations between the steel temperature  $\Theta_a$  and the ultimate critical shear stresses are examined, both for local  $\tau_{cr,L,\Theta}$  and for global  $\tau_{cr,G,\Theta}$  instability failure modes. Denotations applied in considered formulae, describing the corrugated web geometry, are illustrated in detail in Fig. 2. Taking from the standard EN 1993-1-5 one can obtain:



$$\tau_{cr,L} = 4,83E_a \left( \frac{t_w}{a_{max}} \right)^2 \quad \text{where} \quad a_{max} = \max(a, c) \quad (14)$$

It is easy to show that, for fire conditions:

$$\tau_{cr,L,\Theta} = k_{E,\Theta} \tau_{cr,L} \quad \text{where} \quad k_{E,\Theta} = E_{a,\Theta} / E_a \quad (15)$$

Values of the reduction factor  $k_{E,\Theta}$  are also collected in the standard EN 1993-1-2.

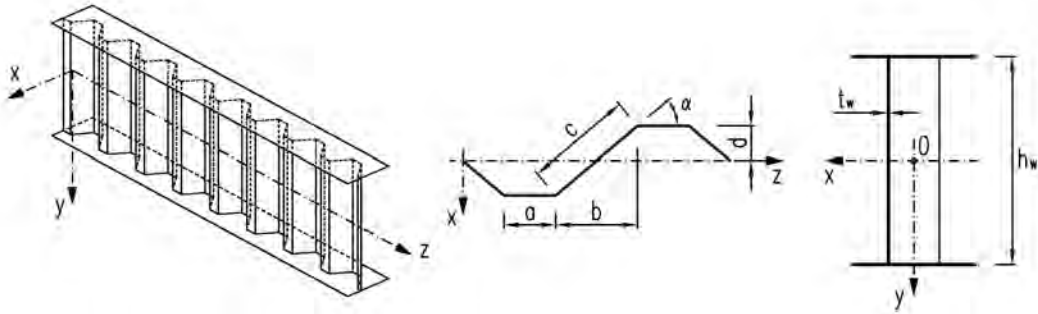


Fig.2. Interpretation of the web dimensions applied to Eqs. (14), (16 and 17).

Similarly, on the base of EN 1993-1-5 occurs:

$$\tau_{cr,G} = \frac{32,4}{t_w h_w^2} \sqrt[4]{D_x D_z^3} \quad (16)$$

where:

$$D_x = \frac{a+b}{a+b \cdot \sec(\alpha)} \frac{E_a t_w^3}{12(1-\nu^2)} \quad \text{and} \quad D_z = \frac{E_a}{a+b} \left( \frac{a t_w (b \cdot \tan(\alpha))^2}{4} + \frac{t_w (b \cdot \tan(\alpha))^3}{12 \cdot \sin(\alpha)} \right) \quad (17)$$

which means that:

$$\tau_{cr,G,\Theta} = k_{E,\Theta} \tau_{cr,G} \quad (18)$$

Let us notice that both Eq. (15) and Eq. (18) are fully adequate not only in relation to trapezoidally but also to sinusoidally corrugated web.

Identification of the relations presented above allows to generalize the definition of the suitable relative web slendernesses, previously specified by Eq. (3). They are now expressed by the following formulae:

$$\bar{\lambda}_{cL,\Theta} = \sqrt{\frac{k_{y,\Theta} f_{yw}}{\sqrt{3} k_{E,\Theta} \tau_{cr,L}}} = \sqrt{\frac{k_{y,\Theta}}{k_{E,\Theta}}} \bar{\lambda}_{cL} \quad \text{and} \quad \bar{\lambda}_{cG,\Theta} = \sqrt{\frac{k_{y,\Theta} f_{yw}}{\sqrt{3} k_{E,\Theta} \tau_{cr,G}}} = \sqrt{\frac{k_{y,\Theta}}{k_{E,\Theta}}} \bar{\lambda}_{cG} \quad (19)$$

In consequence, Eqs. 12 and 13 are changed into the form:

$$\chi_{c,\Theta} = \chi_{cL,\Theta} \quad \text{when} \quad \bar{\lambda}_{cG} < \bar{\lambda}_c^* = \frac{k_{E,\Theta}}{k_{y,\Theta}} \sqrt{0,674 + 1,304 \sqrt{\frac{k_{y,\Theta}}{k_{E,\Theta}}} \bar{\lambda}_{cL}} \quad (20)$$

$$\chi_{c,\Theta} = \chi_{cG,\Theta} \quad \text{when} \quad \bar{\lambda}_{cG} \geq \bar{\lambda}_c^* = \frac{k_{E,\Theta}}{k_{y,\Theta}} \sqrt{0,674 + 1,304 \sqrt{\frac{k_{y,\Theta}}{k_{E,\Theta}}} \bar{\lambda}_{cL}} \quad (21)$$

Finally, having substituted both above equations to Eq. (4), the relations between the instability coefficients and the relative web slendernesses, adequate for fire conditions, can be obtained. They are given as follows:

$$\chi_{cL,\Theta} = \frac{1,15}{0,9 + \sqrt{\frac{k_{y,\Theta}}{k_{E,\Theta}} \bar{\lambda}_{cL}}} \leq 1 \quad \text{and} \quad \chi_{cG,\Theta} = \frac{1,5}{0,5 + \sqrt{\frac{k_{y,\Theta}}{k_{E,\Theta}} \bar{\lambda}_{cG}^2}} \leq 1 \quad (22)$$

and both are illustrated in Fig. 1b for selected values of steel temperature  $\Theta_a$ .

### 3 ALTERNATIVE SHEAR BUCKLING COEFFICIENTS SPECIFIED FOR FIRE CONDITIONS

Regarding an alternative design approach, proposed by the authors (Maślak, Łukacz, 2012) and dealing with the concept of interactive shear buckling coefficients, suitable generalization of the factor defined by Eq. (9), or in the simpler version by Eq. (10), should be made, with respect to the solution obtained by Eq. (19). Consequently, Eq. (9) can be rearranged to the following form:

$$\chi_{c,int,\Theta} = \left( \sqrt{\frac{k_{y,\Theta}}{k_{E,\Theta}}}^{2n} \bar{\lambda}_{cL}^{2n} + \sqrt{\frac{k_{y,\Theta}}{k_{E,\Theta}}}^{2n} \bar{\lambda}_{cG}^{2n} + 1 \right)^{-(1/n)} \quad (23)$$

This formula is possible to be written in a simpler way:

$$\chi_{c,int,\Theta} = \frac{k_{E,\Theta}}{k_{y,\Theta}} \left[ \bar{\lambda}_{cL}^{2n} + \bar{\lambda}_{cG}^{2n} + \left( \frac{k_{E,\Theta}}{k_{y,\Theta}} \right)^n \right]^{-(1/n)} \quad (24)$$

Similarly, considering of Eq. (10) leads to the conclusion that:

$$\chi_{c,int,\Theta} = \frac{k_{E,\Theta}}{k_{y,\Theta}} \left[ \bar{\lambda}_{cL}^{2n} + \bar{\lambda}_{cG}^{2n} \right]^{-(1/n)} \quad (25)$$

### 4 CONCLUDING REMARKS

Both Eq. (22) and Eq. (24) (or alternatively Eq. (25)) give the opportunity to study the beam corrugated web behaviour under fire conditions. In general, the value of the shear buckling coefficient, both  $\chi_{c,\Theta}$  and  $\chi_{c,int,\Theta}$ , decreases when the steel temperature  $\Theta_a$  grows; however, this comment is not accurate when the web temperature is very high ( $\Theta_a \cong 900$  °C), because the inequality  $k_{y,\Theta} < k_{E,\Theta}$  occurs in such circumstances. Nevertheless, the considered web shear resistance is monotonically diminishing in the whole time of fire duration. This effect is not very intense if  $\Theta_a \leq 400$  °C, because then  $k_{y,\Theta} = 1,0$ , but it is significantly strengthened when the web temperature becomes higher.

The alternative approach proposed by the authors to the assessment of the value of shear buckling coefficient specified for fire conditions, in which the experimentally confirmed failure modes interaction formula is taken into account, seems to be more satisfactory and better justified in relation to the commonly used classical standard design technique, when the global and local buckling modes are examined separately.

Detailed relations being the result of application of the formulae recommended in the presented paper are shown in the diagrams completed below (Figs. 3 and 4).

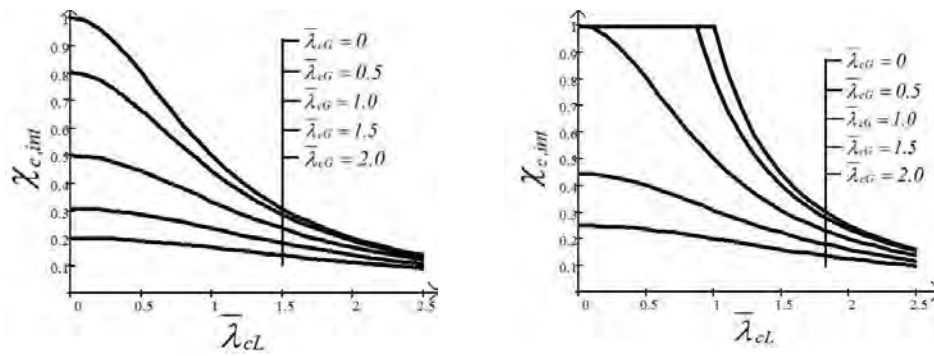


Fig. 3. Relations between the coefficient  $\chi_{c,int}$  and the relative slenderness  $\bar{\lambda}_{cL}$  resulted from the application of Eq. (9) - in the left side, and Eq. (10) - in the right side.

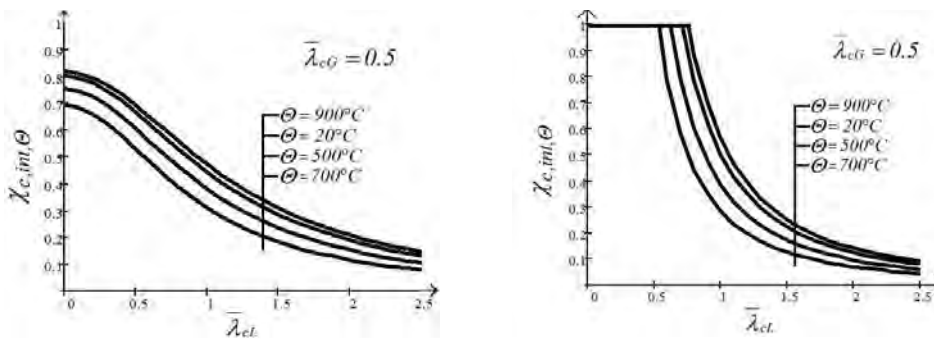


Fig. 4. Relations between the coefficient  $\chi_{c,int,\theta}$  and the relative slenderness  $\bar{\lambda}_{cL}$ , obtained for selected values of web temperature  $\theta_a$ , resulted from the application of Eq. (24) – in the left side, and Eq. (25) – in the right side (it is assumed that  $\bar{\lambda}_{cG} = 0.5$ ).

Suitable relations prepared for fixed value of  $\bar{\lambda}_{cL}$  and being the function of  $\bar{\lambda}_{cG}$  are similar to those, illustrated in the diagrams presented above.

## REFERENCES

- Eldib M.E.A.-H., Shear buckling strength and design of curved corrugated steel webs for bridges, *Journal of Constructional Steel Research*, 65, 2009,
- El-Metwally A.S., Pre-stressed composite girders with corrugated steel webs, Thesis for degree of master, University of Calgary, Calgary, Alberta, Canada, 1998,
- Sayed-Ahmed E.Y., Behaviour of steel and composite girders with corrugated steel webs, *Canadian Journal of Civil Engineering*, 28, 2001,
- Driver R.G., Abbas H.H., Sause R., Shear behaviour of corrugated web bridge girder, *Journal of Structural Engineering*, 132(2), 2006,
- Abbas H.H., Sause R., Driver R.G., Shear strength and stability of high performance steel corrugated web girders, *Proceedings of Structural Stability Research Council Conference*, Seattle, Washington, USA, 2002,
- Hiroshi Shiratoni, Hiroyuki Ikeda, Yohiaki Imai, Koichi Kano, Flexural shear behaviour of composite bridge girder with corrugated steel webs around middle supports, *Japan Society of Civil Engineers J*, 724(I-62), 2003,
- Maślak M., Łukacz M., Shear buckling resistance of steel beam with trapezoidally corrugated web exposed to fire, *Proceedings of International Jubilee Conference UACEG 2012: Science & Practice*, University of Architecture, Civil Engineering and Geodesy, Sofia, Bulgaria, November 15-17, 2012.

## FIRE RESISTANCE OF COLD-FORMED C STEEL COLUMNS

N. Lopes<sup>a</sup>, F. Arrais<sup>a</sup>, Paulo Vila Real<sup>a</sup>

<sup>a</sup> LABEST — Civil Engineering Department, University of Aveiro, Portugal

### Abstract

Steel structural elements composed of cold-formed thin walled sections, are common in buildings due to their lightness and ability to support large spans, however they are more susceptible to the occurrence of local buckling. Additionally, in these members, when subjected to axial compression, the flexural buckling, torsional-flexural buckling and distortional buckling are also common failure modes. These instability phenomena are intensified at high temperatures. This work has the main objective of presenting a numerical study on the fire behaviour of cold-formed thin walled C sections when subjected to compression and high temperatures. The influence of different geometrical imperfections shapes and residual stresses on the ultimate load are evaluated. Comparisons between the finite element numerical results, obtained with geometric and material non-linear analysis, and the Eurocode 3 Parts 1-2 and 1-3 rules are also made.

**Keywords:** steel, cold-formed, columns, buckling, residual stresses.

### INTRODUCTION

The cold-formed steel profiles can be applied to almost all existing buildings typologies. The use of these profiles in construction began around 1850 in the United States and United Kingdom, however, they were not widely used in buildings until 1940. In recent years, it has been recognized that the cold-formed steel profiles can be effectively used as primary structural elements (ASRO, 2008). The cold-formed profiles are commonly used in buildings due to its lightness and ability to overcome large spans, being quite common as roof or walls support elements (Silvestre and Camotim, 2010a).

The structural steel elements with thin walled cold-formed sections, subjected to axial compression, are characterized by being able to have the possibility of failure modes occurrence such as local, distortional and global flexural buckling. These instability phenomena and its influence on the ultimate strength at room temperature have been widely studied in recent years (Gonçalves and Camotim, 2007; Silvestre and Camotim, 2010b). However, its behaviour in fire has not received the same attention. In fact, the fire resistance evaluation of cold-formed profiles has a major role in the design of these elements. The thin walls of these profiles, together with the steel high thermal conductivity, provide a great loss of strength and stiffness on these structural elements (Laim and Rodrigues, 2011; Landesmann and Camotim, 2011; Vila Real and Lopes, 2010).

The manufacturing process of thin cold-formed steel members introduces residual stresses and increases the yield strength in the folding regions. Consideration of residual stresses may be complicated on numerical modelling. It can be idealized as a summation of two types: flexural and membrane. But on cold-formed elements, membrane residual stresses are lower than flexural residual stresses. This variation of residual stresses causes the early yielding of cold-formed steel plate surfaces (Schafer and Peköz, 1998).

This paper presents a numerical study on the behaviour of columns in cold formed C sections in case of fire when subjected to simple axial compression. In this study, the influence of geometrical imperfections and residual stresses on their ultimate load bearing capacity is evaluated.

The programs CUFSM (developed at Johns Hopkins university in the United States) (Schafer and Adány, 2006), and SAFIR (developed at the University of Liege in Belgium) (Franssen, 2005) were used. The program CUFSM performs elastic buckling analysis of thin-walled elements. The thin-walled elements, by their very nature, tend to suffer several instability problems. The CUFSM analysis uses the finite strip method (FSM). In this work, the program CUFSM was used for the purpose of obtaining the local, global and distortional instability modes, comparing these results with the ones from SAFIR. Additionally, the local, distortional and lateral instability modes obtained in CUFSM were used to define the local geometrical imperfections. The program SAFIR uses the finite element method (FEM) for geometric and material non-linear analysis, and was especially developed for the study of structures in fire.

## 1 NUMERICAL MODELLING

Simply supported columns with C cross section were analysed (with height of 155 mm, width of 77 mm, length of the outstand element 31 mm and thickness of 2 mm). A yield strength of 360 MPa was considered, example from Verissimo (2008). It was not considered increased yield strength, due to the cold formed process, in the corners.

The steel constitutive law used for the ultimate load bearing capacity determination with the FEM simulations (sections 3 and 4) was the one prescribed in Part 1-2 of Eurocode 3 (EC3) (CEN, 2005). In section 2 a linear elastic constitutive model, with the young modulus given in this Eurocode in function of the temperature, was used.

In the finite element model, shell finite elements were used due to the walls high slenderness. Concentrated loads were applied, in the parallel directions to the columns axis, along the whole section. The restrictions were imposed in order to reproduce two end pinned supports. The thickness of the shell elements was increased at the column ends to consider a rigid body when loads and restrictions are applied. The mesh was refined to obtain the smaller elements in the positions of maximum deflection and on the supports (see Fig. 1). The temperatures of 350 °C, 500 °C and 600 °C were adopted, they were considered uniform throughout the cross section. In this paper, due to space limitation, only results at 500 °C are shown.

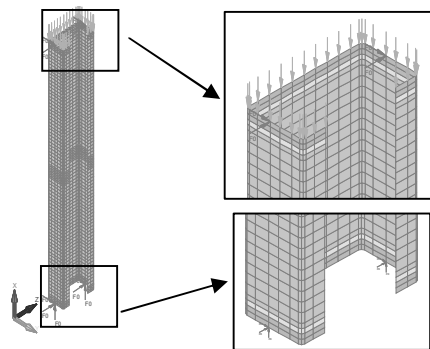


Fig. 1 Adopted numerical model for the C section

## 2 INSTABILITY MODES

With regard to the stability behaviour, a bar with thin wall section can be classified according to their length:

- Short bar - if instability occurs with a local mode;
- Long Bar - if instability occurs with a global mode;
- Intermediate Bar - if instability occurs in a combination of local and global modes (distortional mode).

This section presents the determined critical loads of elastic instability and corresponded modes, through numerical analysis carried out at the columns subjected to high temperatures. Initial geometric imperfections and residual stresses were not introduced and in the finite element analysis it was adopted a linear elastic constitutive law for the material model. Only the reduction factor for elastic modulus at high temperatures has been applied.

In Fig. 2 the comparisons, between the numerical results obtained with SAFIR and the curve corresponded to elastic instability modes obtained with CUFSM, are presented.

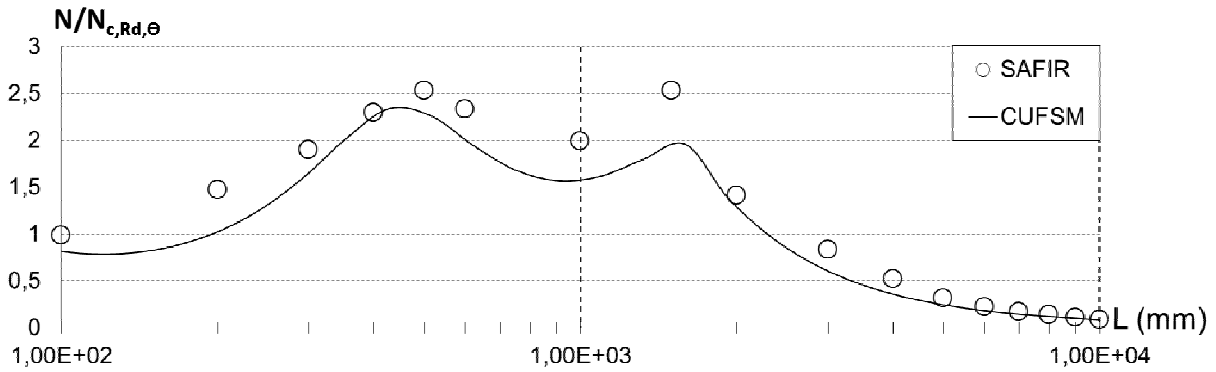


Fig. 2 Comparison between the SAFIR and CUFSM results at 500 °C

The chosen lengths in this study reach local, distortional, global instability modes. For a better understanding of the existing instability modes, it is presented in Fig. 3, a comparative analysis between the instability modes that the profile can suffer, when subjected to simple axial compression.

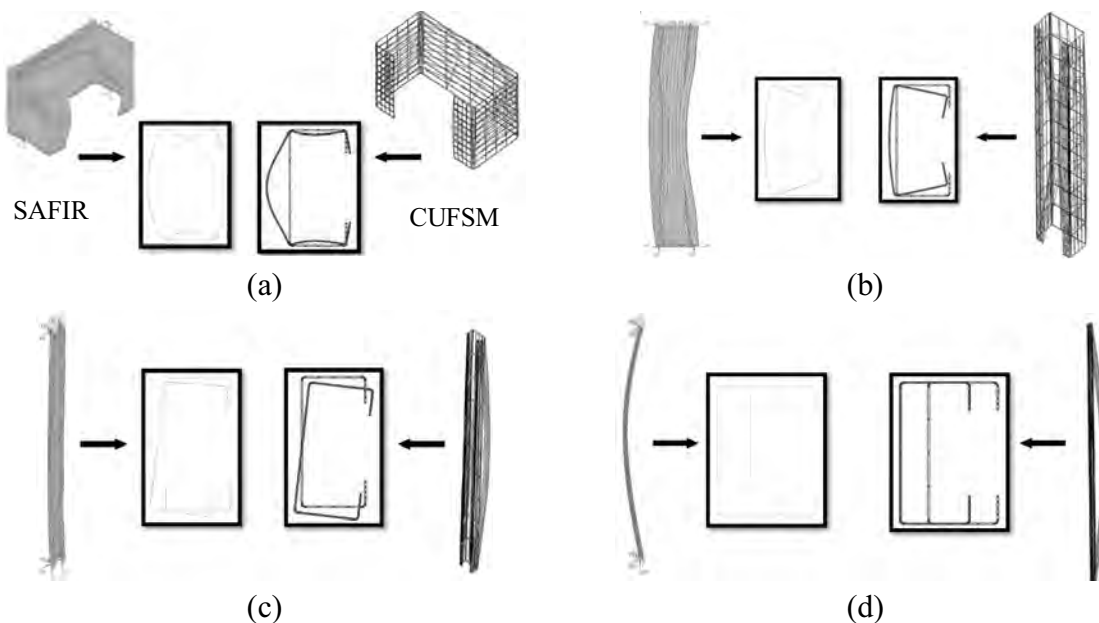


Fig. 3 Instability modes of columns with length of a) 100 mm b) 1000 mm c) 3000 mm and d) 10000 mm

It can be observed the predominance of local buckling on small lengths columns, distortional buckling on intermediate lengths columns and global buckling on long lengths columns.

From the graph in Fig. 2 and from the elastic instability modes shown in Fig. 3, it can observe a good agreement between the results obtained with the SAFIR and CUFSM.

### 3 INFLUENCE OF THE INITIAL GEOMETRIC IMPERFECTIONS ON THE FIRE RESISTANCE

In this section, it is presented a study of the influence of initial imperfections on the ultimate load bearing capacity of cold formed C columns, in fire situation. It were also analyzed the simple calculation rules in Part 1-2 of EC3, when compared to the numerical results.

The geometry of the C section was addressed by the method mentioned in Annex C of EC3 Part 1-3 (CEN, 2004), in the calculation of the resistance. In these prescribed approaches, the calculation methodology for the effective section for the local instability mode differs from the calculation methodology for the distortional mode instability. The local instability mode effective section was based on the concept of effective width, while in the distortional mode instability it was based on the concept of reduced thickness.

#### 3.1 Isolated influence of the geometrical imperfections

To determine the shape of all the imperfections, the analysis performed with CUFSM considering the applied elastic stresses diagram corresponded to axial compression was used. The local, distortional and global instability modes shape obtained in CUFSM were used to define the geometrical imperfections. The following situations were considered:

- without geometrical imperfections;
- with geometrical imperfections corresponded to the local buckling mode;
- with geometrical imperfections corresponded to the distortional buckling mode;
- with geometrical imperfections corresponded to the global (flexural/torsional) buckling mode;
- with geometrical imperfections corresponded to the global (flexural) buckling mode.

The global imperfections were considered with a sinusoidal shape given by the expression

$$y = \frac{L}{1000} \sin\left(\frac{\pi x}{L}\right) \quad (1)$$

The maximum value for the local was of  $b/200$ , being  $b$  the profile height, and for distortional imperfections was of  $b/200$ , being  $b$  the profile width (CEN, 2006).

Fig. 4 shows a column with the different introduced geometrical imperfections.

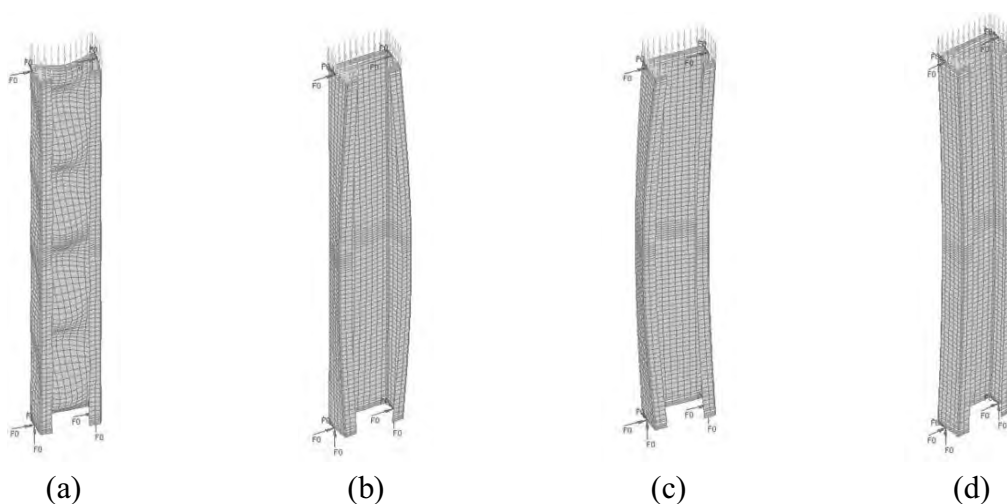


Fig. 4 Geometric imperfections ( $\times 50$ ): a) local; b) distortional; c) global (flexural/torsional); d) global (flexural)

The influence of the introduction of the different geometrical imperfections is presented in Fig. 5. As effective widths were considered for the calculation of the effective section, leading to the appearance of an eccentricity on the load application, instead of a buckling curve a direct comparison between resistances is presented. It is observed that the columns without any imperfections reach higher resistances compared to the ones which take into account initial imperfections. For all slenderness the analysis with local imperfections are the ones that reduce the obtained ultimate loads.

### 3.2 Influence of combined geometrical imperfections

Following Part 1-5 of EC3 a combination of the previous enunciated geometrical imperfections is introduced on the numerical model. According to this norm, in combining imperfections, a leading imperfection should be chosen and the accompanying imperfections may have their values reduced to 70%. As the local imperfections gave the lowest axial compression resistance, they were considered as leading imperfections. Two possible combinations were tested:

- local and global imperfections (being these two the most relevant): columns have local imperfections plus 70% of the global imperfections;
- local, global and distortional imperfections: columns have local imperfections plus 70% of the global imperfections plus 70% of distortional imperfections.

### 3.3 Discussion of the results

From the graph in Fig. 5 it can be observed that the combinations give lower resistances than the ones obtained with the separate imperfections. The observed differences between the two set of combinations are very small, they give almost the same values. Also, for intermediate columns slenderness the design curve proposed by EC3 is too conservative.

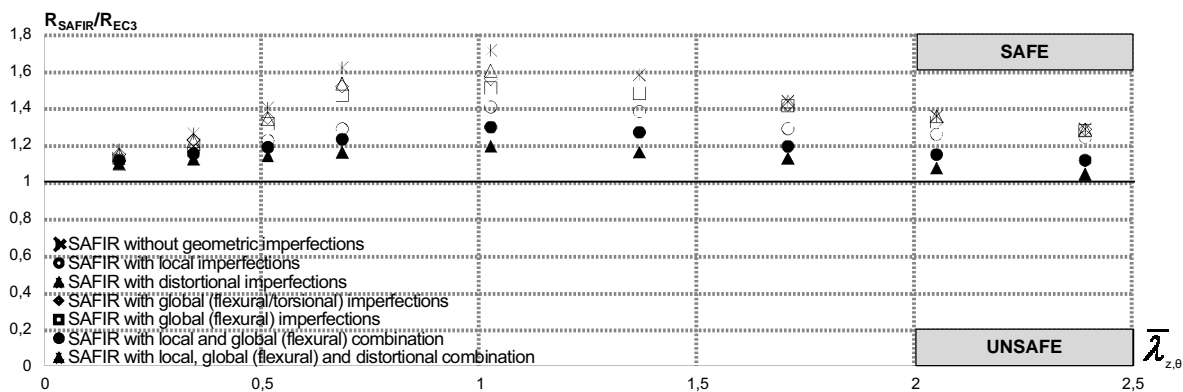


Fig. 5 Comparison of the numerical results at 500 °C

## 4 INFLUENCE OF RESIDUAL STRESSES ON THE FIRE RESISTANCE

In this section, it is presented the influence of the residual stresses on the ultimate load bearing capacity. Fig. 6 shows the considered residual stresses pattern.

Fig. 7 presents the results obtained with and without residual stresses. They were considered on columns with and without geometrical imperfections.

It is observed that the resistance of columns, with intermediate lengths, without any imperfections is affected by residual stresses. In the other hand, considering the geometric imperfections, the residual stresses do not affect the resistance values.



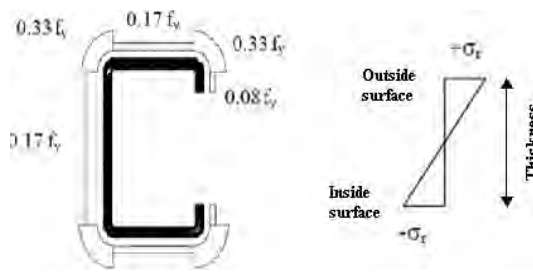


Fig. 6 Definition of residual stresses on cold-formed steel C section (Adapted from (Schafer and Peköz, 1998))

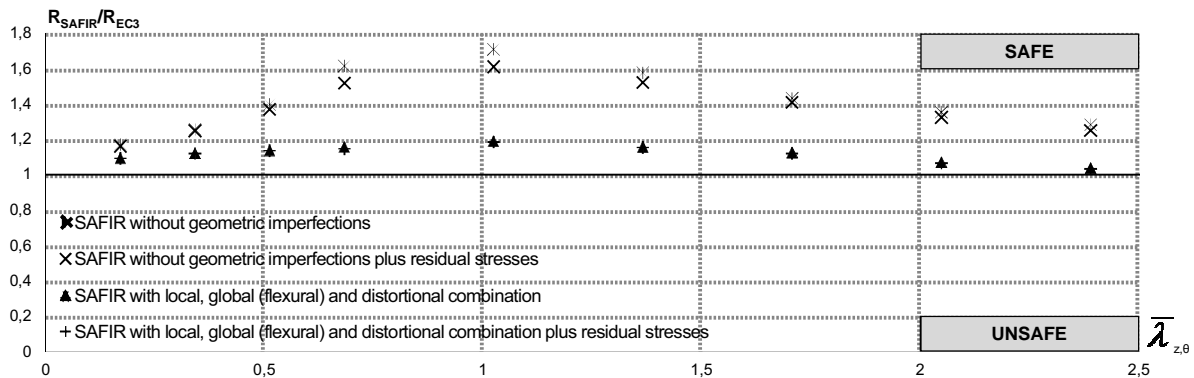


Fig. 7 Comparison of the numerical results with residual stresses at 500 °C

## 5 CONCLUSIONS

In this work it was presented a numerical study on the behaviour of cold formed columns with C cross section in case of fire.

The numerical results obtained at high temperature, for the determination of elastic instability critical loads and buckling modes, were compared using finite element method (FEM) analysis with the program SAFIR with those obtained by finite strips method (FSM) through CUFSM program. It was observed a good agreement between the results obtained with these two programs.

The influence of initial geometrical imperfections (local, distortional, global, and their combination) on the determination of the ultimate loads of these elements at high temperature was analysed, it was concluded that these imperfections are relevant to the determination of those ultimate loads, and that they should be considered.

Considering the residual stresses with the worst initial geometric imperfections combinations was not important, because the ultimate load is extremely affected by all the geometric imperfections and the residual stresses did not have any impact on the resistance values.

Finally, it also performed a comparison between the obtained ultimate loads results and the formulae prescribed in Parts 1-2 and 1-3 of EC3, concluding that the simple calculation rules are on the safe side and sometimes too conservative.

## REFERENCES

- ASRO (Asociatia standardizare din România), Introduction to cold-formed steel design, Technical document ICS 91.010.30;91.080.10, 2008.
- CEN, European Committee for Standardisation “EN 1993-1-2, Eurocode 3: Design of Steel Structures - Part 1-2: General rules - Structural fire design”; Brussels, Belgium, 2005.
- CEN, “EN 1993-1-3, Eurocode 3: Design of Steel Structures - Part 1-3: Supplementary rules for cold-formed members and sheeting”, Brussels, Belgium, 2006.

- CEN, “EN 1993-1-5, Eurocode 3: Design of Steel Structures - Part 1-5: Plated structural elements”, Brussels, Belgium, 2006.
- Franssen, J.-M., “SAFIR. A Thermal/Structural Program Modelling Structures under Fire”; Engineering Journal, A.I.S.C., Vol. 42, No. 3, pp. 143-158, 2005.
- Camotim, D.; Gonçalves, R., “Thin-walled member plastic bifurcation analysis using generalised beam theory”, Advances in Engineering Software, Vol. 38. p. 637-646, 2007.
- Laim, L., Rodrigues, J. P. C., Modelação numérica de vigas em aço enformadas a frio submetidas ao fogo, Congresso de Métodos Numéricos em Engenharia, Coimbra, 2011.
- Landesmann, A., Camotim, D., “On the Distortional Buckling, Post-Buckling and Strength of Cold-Formed Steel Lipped Channel Columns under Fire Conditions”, Journal of Structural Fire Engineering, Vol. 2, nº 1, pp. 1-19, 2011.
- Schafer, B. W., Ádány, S., “Buckling analysis of cold-formed steel members using CUFSM: conventional and constrained finite strip methods”, 18th International Specialty Conference on Cold-Formed Steel Structures, Orlando, Florida, USA, 2006.
- Schafer, B. W., Peköz, T., “Computational modeling of cold-formed steel: characterizing geometric imperfections and residual stresses.”, Journal of Constructional Steel Research, No. 47, pp. 193-210, 1998.
- Silvestre, N., Camotim, D., “Construção em aço leve”, revista da associação portuguesa de construção metálica e mista, year 11, nº20, Marh of 2010a.
- Silvestre, N., Camotim, D., “On the mechanics of distortion in thin-walled open sections”. Thin-Walled Structures, Vol. 48. n.º 7. p. 469-481, 2010b.
- Veríssimo, H., Dimensionamento de elementos estruturais de aço enformados a frio de acordo com o Eurocódigo 3, Master thesis - Universidade Técnica de Lisboa, Portugal, 2008.
- Vila Real, P., Lopes, N., Avaliação da resistência ao fogo da Central de Valorização Orgânica - Unidade de Digestão Anaeróbica, Universidade de Aveiro, Portugal, 2010.

## **BASELINE STUDY ON THE BEHAVIOUR OF COLD-FORMED STEEL COLUMNS SUBJECTED TO FIRE**

Hélder David S. Craveiro<sup>a</sup>, João Paulo C. Rodrigues<sup>a</sup>, Luís Laím<sup>a</sup>

<sup>a</sup> University of Coimbra, Portugal

### **Abstract**

In this paper is presented a state-of-the-art and future research pathways on cold-formed steel (CFS) columns subjected to fire, the experimental set-up built at the University of Coimbra for testing CFS columns and some preliminary results obtained in the tests, comparing them with the ones existing in the literature. The main objective of the experimental research already carried out is to assess the fire resistance, mechanical behaviour and characterize the failure modes of cold-formed steel columns with restraining thermal elongation in case of fire, develop simplified calculation methods and provide experimental data for future numerical studies.

**Keywords:** cold-formed steel, columns, fire resistance, restraining forces, state-of-the-art

### **INTRODUCTION**

Recently the demand of cold-formed steel structures (CFS) has increased significantly, especially for residential, commercial and industrial buildings due to a high strength to weight ratio and an ease to erect when compared to hot rolled-steel structures. In some cases, CFS structures are required to be fire resistant however they present poor fire behaviour because of a combination of the high thermal conductivity of steel and the elevated section factor of the structural member. Despite increasing use there is a lack of research on their behaviour under fire situation. Therefore it is extremely important to investigate and assess the behaviour of cold-formed steel columns subjected to fire.

Due to experimental limitations, so far, most of the experimental studies were performed on stub columns, resulting in a lack of knowledge on the behaviour of CFS slender columns subjected to fire.

A state-of-the-art review is presented in this paper as well as the experimental set-up developed at University of Coimbra for testing of CFS slender columns with restrained thermal elongation subjected to fire and some preliminary experimental results obtained, comparing them with some existing ones in the literature.

### **1 STATE-OF-THE-ART REVIEW**

As mentioned there has been little research on the behaviour of CFS slender columns subjected to fire being most of the studies on stub columns. However these studies are very important and are here presented as baseline studies for future investigations.

A study performed at the Swedish Institute of Steel Construction (Ranby, 1998), for developing structural fire design of thin-walled cold-formed steel sections, was presented in order to find out the steel temperature, how it varies across the steel cross-section and the effect on the load bearing resistance. It was intended to develop a method for designing thin walled cold formed steel sections and to show that limiting the maximum temperature to 350°C for class 4 cross sections, as mentioned in the EN 1993-1.2 (2005), is too restrictive. Results showed that initial deflections have the same influence on the load bearing resistance at ambient temperature and in case of fire and that the calculation of the plate buckling resistance according to EN1993-1.3 (2005) considering the reduced yield strength and elastic

modulus is accurate at elevated temperatures. Results also showed that the 350°C limitation for class 4 cross section is too restrictive.

Feng et al. (2003) performed a total of 52 load-bearing capacity tests at ambient and elevated temperature on compressed short CFS lipped channels, with and without service holes and unlipped channels to assess the physical behaviour and failure modes of this type of structures. The column was heated in an electric kiln and longitudinal distribution of temperature and displacements were measured. Elevated temperatures tests, without thermal restraint, were carried out under steady state condition for four temperature levels (250, 400, 550 and 700°C). When the temperature reached the desired level the axial compression loading was applied until failure. This experimental study showed that depending on the initial imperfections the failure mode of nominally identical columns can be different at both ambient and elevated temperatures. Despite the difference in failure modes the failure loads of nominally identical columns were very close. A numerical analysis was also performed (Feng et al., 2003) based on the experimental work using the design methods presented in some international standards such as the EN 1993-1.3(2006), and a finite element analysis (FEA) using the commercial software ABAQUS (2004) considering geometrical and material non-linearities. Stress-strain relationship of steel at high temperature was determined according to EN 1993-1.2(2005), with a suitable modification in order to use the mathematical equations for the stress-strain relationships at elevated temperatures, or the ones proposed by Outinen et al. (1999). It was found that ambient temperature design guidelines can be used at elevated temperatures providing the reduced yield strength based on 0,2% proof stress and the reduced elastic modulus.

Heva and Mahendran (2008) performed a series of local buckling tests of CFS compression members at elevated temperatures. The tests were carried out at predefined temperatures up to 700°C (100, 200, 300, 400, 500, 600 and 700°C) using a small electric furnace and a special loading set-up made to fit the furnace using 253MA stainless steel and a Tinius Olsen Testing Machine. Ultimate loads were calculated using the available design rules, emphasizing the EN 1992-1.2 (2005) using the effective width method for the local buckling capacity of compression members at elevated temperatures. The yield stress reduction factors at elevated temperatures determined by Ranawaka (2009) and Dolamune Kankanamge (2011) were used since the recommended yield stress reduction factors for both cold-formed and hot-rolled steels were identical in this standard. It was found that using the reduced mechanical properties at elevated temperatures with ambient temperature design guidelines is possible to predict approximately the axial compression capacity of CFS short columns. This study showed once again that limiting the temperature to 350°C as in EN 1993-1.2 (2005) is too restrictive since the CFS columns presented significant capacities beyond this limiting temperature.

Ranawaka and Mahendran (2009) carried out a research based on experimental studies to investigate the distortional buckling behaviour of CFS short compression members under fire conditions. Two types of cross section were tested with different nominal thicknesses, both with low and high strength steels, G250 and G550. Steady state tests were carried out and three types of distortional buckling failure modes were observed at elevated temperature tests, namely by both flanges moving inwards or outwards and by one flange moving outward while the other moving inward. Comparing the ultimate load results with the ones obtained using the direct strength method it was found that they are reasonably accurate when the appropriate reduced mechanical properties are used. Based on this experimental research a numerical study on CFS compression members subjected to distortional buckling at elevated temperatures was developed, considering geometric imperfections, residual stresses and the reduced mechanical properties at elevated temperatures (Ranawaka and Mahendran, 2010). Comparing numerical and experimental results it was found out that the developed finite element models considering accurate mechanical properties and stress-strain characteristics of steels, initial geometric imperfections and residual stresses as a function of temperatures were able to simulate the failure modes, load deflection and ultimate loads.

Ju Chen and Ben Young (2007) developed a numerical study on CFS lipped channel stub and slender columns at elevated temperatures using a finite element software ABAQUS (2004) to investigate the behaviour and design of CFS lipped channel columns at elevated temperatures considering the effects of initial local and overall geometrical imperfections. The nonlinear model was verified against experimental results obtained in the research performed by Young and Rasmussen (1998) at ambient temperature and in the research performed by Feng et al. (2003) at ambient and elevated temperatures, and then the strength prediction of columns was compared with the design strengths using the effective width and direct strength method. It was found that the estimated column strengths using FEA is in good agreement with experimental results both at ambient and elevated temperatures and that the effective width and direct strength method using the reduced material properties conservatively predicted the columns strength.

Almeida et al. (2012) performed some experimental tests on CFS slender columns at elevated temperatures in order to investigate the behaviour of compressed CFS columns considering the influence of the restraining to thermal elongation. Single sections (C), open built-up (I) and closed built-up (2R) sections were tested. Single sections were 1.5 mm thickness and pin ended and semi-rigid boundary conditions were adopted. The applied load corresponds to 30% of the design buckling resistance of a compression member ( $N_{b,Rd}$ ) determined according to the Eurocode 3 Part 1.1 (2005) and Part 1.3 (2006). Some of the results obtained are presented in Fig. 1.

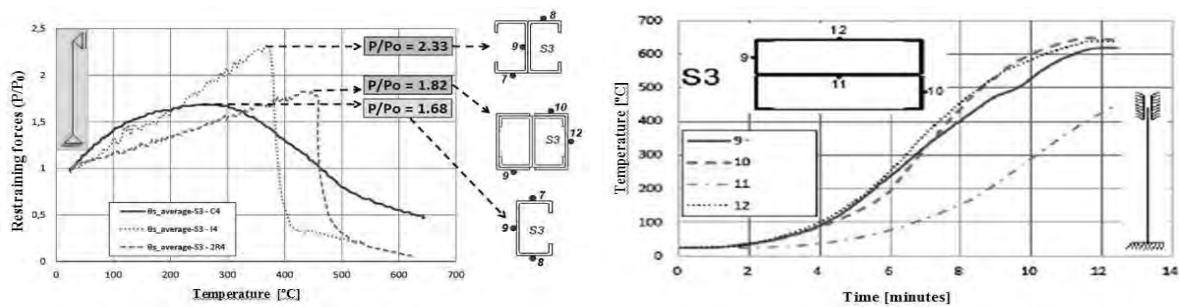


Fig.1 Evolution of restraining forces (a) and temperatures in the column's mid-section in height (b).

So far the absence of experimental fire resistance studies in slender CFS columns is clear. Establishing the presented studies as a starting point and aiming to respond to the existing challenges in this research field a new experimental set-up was developed in order to perform fire resistance tests on cold-formed steel slender columns with restrained thermal elongation.

## 2 FIRE RESISTANCE TESTS ON CFS COLUMNS WITH RESTRAINED THERMAL ELONGATION

The main objective of this experimental research is to assess the influence of the cross section shape, load level ratio, end-support conditions on the fire resistance and structural behaviour of CFS slender columns with restrained thermal elongation in case of fire. Restraining forces, critical times and temperatures, vertical and horizontal displacements were measured and the predominant failure modes characterized. The experimental programme was carried out on CFS slender columns with different types of cross sections, namely single sections, C, open built-up cross sections, I, and closed built-up cross sections, R and 2R (see Fig. 2) with pin-ended support conditions and 3 kN.m of axial restraining provided by the surrounding structure. In Fig. 2 it is possible to see the locations for the thermocouples in the specimens. Longitudinally the thermocouples will be placed in five different sections, in order to evaluate the longitudinal temperature distribution. Columns were 2950 mm long and the cross section 2.5 mm thick and presenting the steel grade S280GD (EN 10147:2000).

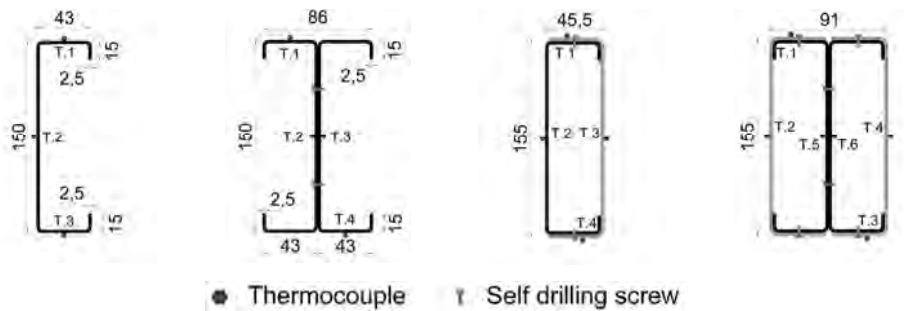


Fig. 2 CFS cross sections tested. Thermocouple's position in each cross section.

## 2.1 Experimental set-up

The experimental set-up system developed at the University of Coimbra (Fig. 3) comprises a 2D reaction frame and a 3D restraining steel frame of variable stiffness in order to simulate the axial stiffness of a surrounding structure to the CFS column subjected to fire. The restraining frame was composed by four columns and two beams placed orthogonally. The connections between columns and top beams were made using threaded rods M24 in order to allow the vertical adjustment of the position of the top beams. The hydraulic jack used to apply the load was placed in the 2D reaction frame. The thermal action was applied using a vertical modular electric furnace programmed to follow the standard fire curve ISO 834. To measure the restraining forces generated during the heating process a special device was built consisting on a hollow steel cylinder with a load cell inside where a Teflon lined solid steel cylinder that was connected to the top of the column, slides through it. The temperatures in each specimen were measured using type K thermocouples placed in the cross section and throughout the length of the column. Vertical displacements were measured using Linear Variable Displacement Transducers (LVDT) placed on top and bottom of the column and the lateral displacements were measured using Wire Displacement Transducers placed throughout the column's length.



Fig. 3 Experimental set-up for CFS slender columns with thermal restrained elongation subjected to fire.

## 2.2 Test procedure

Test specimens were placed in the centre of the restraining structure in the built end-support system that provided pin-ended conditions. All measuring devices were installed in the defined positions. Then the vertical electrical furnace was closed and using a hydraulic jack the correspondent service load was applied. The top beams were connected to the steel columns with M24 grade 8.8 threaded rods. However, during the initial applied load, the vertical displacements of the top beams were allowed, as a slide, in order to guarantee that this load was directly applied to the CFS column. The applied load corresponded to 30% and

50% of the design buckling resistance of a compression member ( $N_{b,Rd}$ ) determined according to the EN 1993-1.1 (2005) and EN 1993-1.3(2006). In Tab. 1 the correspondent loads to the 30% of load level to each cross section considering the pin-ended situation are presented.

Tab. 1 Load values applied.

	C [kN]	I [kN]	R [kN]	2R [kN]
30% $N_{b,Rd}$	8,010	27,200	24,400	95,100

Reaching the established load, vertical displacements of the top beams were blocked, using nuts, and then the electrical furnace, programmed to reproduce ISO 834 fire curve, was turned on. The load applied using the hydraulic jack was kept constant throughout the test and the restraining forces developed by thermal elongation were measured with the load cell placed inside the built device. The test ended when the column no longer supported the applied load and the initial load was reached. Three tests for each type of cross section were carried out.

### 3 RESULTS AND CONCLUSIONS

Since all fire resistance tests were performed inside the vertical furnace, only the final shape of the column could be observed. It was observed that the failure mode involved global buckling and more or less visible local buckling, and that identical columns presented identical deformed shapes.

Some preliminary results for the 50% load level concerning the evolution of temperatures in the mid-section of the column, for each cross section, and the evolution of the restraining forces are presented (Fig. 3 and 4).

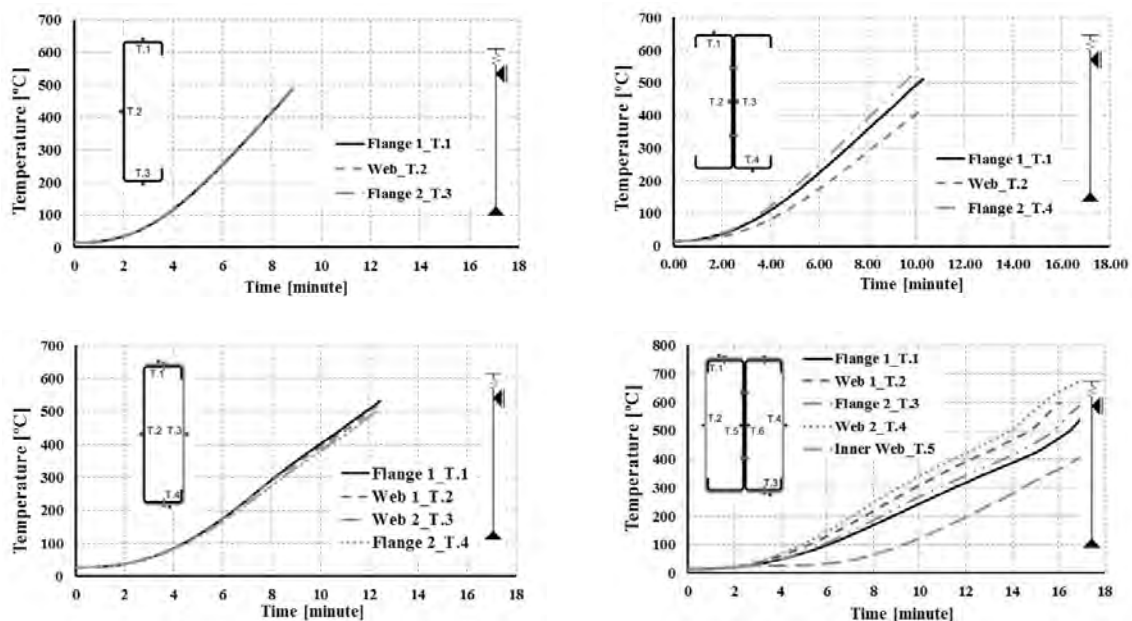


Fig. 3 Evolution of temperatures in each cross section in the mid-section of the column

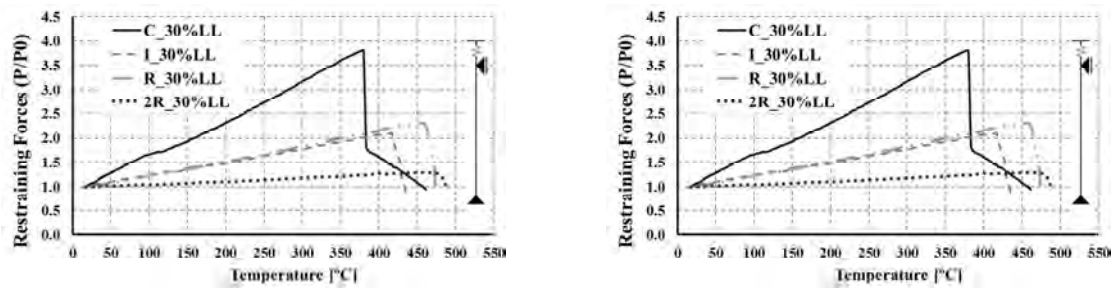


Fig. 4 Evolution of restraining forces vs time and temperature in CFS columns with a 30% load level

It was found that the temperature in each cross section was relatively uniform, except for the closed built-up cross section, 2R, where it was found that the temperature in the inner web is significantly lower. It was observed that for the C cross section the restraining forces increased up to 3.8 times while for I, R and 2R increased up to 2.09, 2.31 and 1.29, respectively and that closed built-up cross sections showed a greater fire resistance. Also it could be observed that the failure temperature was relatively similar for the tested cross sections. Post-critical behaviour at high temperatures was not significant. It was clear that 350 ° C limitation indicated in the Eurocode 3 Part 1.2 is too restrictive since that for temperatures higher than this one the columns still showed load bearing capacity. Comparing these results with the ones presented by Almeida et al. (2012) it was found some similarities between them, both in terms of temperature and restraining forces despite the different thicknesses adopted. Further experimental and future numerical studies will be performed in CFS slender columns in the scope of this research project.

## REFERENCES

- A. Ranby, Structural Fire Design of Thin Walled Steel Sections, Swedish Institute of Steel Construction, J. Construct. Steel Res. Vol 46, Nos. 1-3, pp. 303-304, 1998.
- CEN, EN 1993-1-2, Eurocode 3: Design of steel structures, Part 1.2: General rules, Structural fire design, 2005.
- CEN, EN 1993-1-3, Eurocode 3: Design of steel structures, Part 1.3: General rules, Supplementary rules for cold formed members and sheeting, European Commission for Standardisation, Brussels, 2006.
- M. Feng, Y. C. Wang and J. M. Davies, Structural Behaviour of Cold-Formed Thin Walled Short Steel Channel Columns at Elevated Temperatures. Part 1: experiments, Thin-Walled Structures, 41, 543-570, 2003.
- M. Feng, Y. C. Wang and J. M. Davies, Structural Behaviour of Cold-Formed Thin Walled Short Steel Channel Columns at Elevated Temperatures. Part 2: Design Calculations and Numerical Analysis, Thin –Walled Structures, 41, 571-594, 2003.
- ABAQUS Analysis User's Manual, Version 5.8.1.5 and Version 6.5, Abaqus, Inc., 2004.
- Outinen J., Mechanical Properties of Structural Steels at Elevated Temperatures. Licentiate thesis, Helsinki University of Technology, Laboratory of Steel Structures, Espoo, 1999.
- Yasintha Bandula Heva and Mahen Mahendran, Local Buckling of Cold-Formed Steel Compression Members at Elevated Temperatures, Fifth International Conference on Thin-Walled Structures, Brisbane (Australia), 2008.
- T. Ranawaka and M. Mahendran, Experimental Study of the Mechanical Properties Of Light Gauge Cold-Formed Steels at Elevated Temperatures, Fire Safety Journal, 44, 219-229, 2009.
- N. D. Kankanamge and M. Mahendran, Mechanical Properties of Cold-Formed Steels at Elevated Temperatures, Thin-Walled Structures, 49, 26-44, 2011.



- T. Ranawaka and M. Mahendran, Distortional Buckling tests of Cold-Formed Steel Compression Members at Elevated Temperatures, *Journal of Constructional Steel Research*, 65, 249-259, 2009.
- T. Ranawaka and M. Mahendran, Numerical Modelling of Light Gauge Cold-Formed Steel Compression Members Subjected to Distortional Buckling at Elevated Temperatures, *Thin-Walled Structures*, 48, 334-344, 2010.
- Ju Chen, Ben Young, Cold-Formed Steel Lipped Channel Columns at Elevated Temperatures, *Engineering Structures*, 29, 2445-2456, 2007.
- Young B., Rasmussen KJR, Design of Lipped Channel Columns, *Journal of Structural Engineering*, ASCE 1998, 124(2), 140-8.
- Almeida et al., Behaviour of Compressed Cold-Formed Steel Elements at High Temperatures, 7<sup>th</sup> International Conference on Structures in Fire, Zurich, Switzerland, 2012.
- EN 10147, Specification for Continuously hot-dip zinc coated structural steel sheet – Technical Delivery Conditions, 2000.

## THE STRUCTURAL BEHAVIOUR IN FIRE OF A COLD-FORMED STEEL PORTAL FRAME HAVING SEMI-RIGID JOINTS

Ross P. D. Johnston<sup>a</sup>, James B. P. Lim<sup>a</sup>, Mohammed Sonebi<sup>a</sup>, Andrzej M. Wrzesien<sup>b</sup>,  
Cecil Armstrong<sup>c</sup>

<sup>a</sup> Queen's University Belfast, School of Planning Architecture & Civil Engineering, Belfast, United Kingdom

<sup>b</sup> Department of Civil and Environmental Engineering, University of Strathclyde, Glasgow, United Kingdom

<sup>c</sup> Queen's University Belfast, School of Mechanical and Aerospace Engineering, Belfast, United Kingdom

### Abstract

This paper describes a non-linear finite element study into the effects of elevated temperature on a cold-formed steel portal frame having semi-rigid joints. Numerical modelling was carried out using ABAQUS finite element analysis software with shell elements used to capture localised buckling effects. Results for the ambient shell models are compared against previous full-scale tests. Material properties are taken from the literature, in order to predict the behaviour of the frame at elevated temperature. The results of finite element beam models are compared against those of shell models to enable comparison. At elevated temperature, shell models are shown to detect failure much earlier within the fire. Therefore shell models are recommended for such studies, for a conservative approach.

**Keywords:** cold-formed steel, fire, portal frame, semi-rigid joints, finite element analysis.

### INTRODUCTION

Cold-formed steel portal frames can be a viable alternative to conventional hot-rolled steel portal frames for commercial, industrial and agricultural buildings with spans up to 20 m (Lim and Nethercot, 2004). Despite this, research on the structural behaviour of cold-formed steel portal frames at elevated temperature remains limited. Further research into analysis methods and the collapse mechanism is required, in order to protect fire authorities, persons and adjacent buildings in close proximity to the structure.

Research into the behaviour of hot-rolled steel portal frames at elevated temperature has been carried out by a number of researchers investigating experimental and finite element beam models (Song et al, 2009, Rahman et al, 2011). The Steel Construction Institute (SCI) P313 guidance document (Simms and Newman 2002) outlines the design for hot-rolled steel portal frames in fire boundary conditions. There is no such guidance for structural engineers related to the design of cold-formed steel portal frames in fire boundary conditions.

This paper describes a study of the structural behaviour of a cold-formed steel portal frame at ambient and elevated temperature. Numerical modelling of the frame was carried out using ABAQUS finite element analysis software. The results under loading at ambient temperature were validated against ambient full-scale tests and numerical modelling found in the literature. In order to accurately capture localised buckling effects, shell elements were used to model the back-to-back cold-formed steel members. Spring elements were included to idealise the effects of bolt-hole elongation. Lateral restraint to the frame was provided at both the purlin and side rail locations. The material properties at elevated temperature were taken from literature (Chen & Young, 2004). An additional study was carried out using beam elements, to enable the effect of elevated temperature upon the structural behaviour to be compared. For this preliminary study, initial imperfections were not included within the finite element modelling and columns were assumed as unprotected.

## 1 LITERATURE REVIEW

Previous research investigating cold-formed steel portal frames at elevated temperature tested experimental and numerical models of a frame with modest span (Pyl et al. 2012). The site fire test showed inwards collapse behaviour of the frame with sigma cold-formed steel sections used for the primary load bearing members. In the subsequent SAFIR finite element work, beam elements were used to model the sections with attention made to girders, columns, roof purlins and wall girts only. Experimental and numerical modelling research at ambient temperature (Lim and Nethercot, 2004; Jackson et al., 2012; Wrzesien et al, 2012) have demonstrated the importance of taking the effects of semi-rigid joints into consideration. Recent research indicated that elevated temperature can significantly affect the behaviour of cold-formed steel joints. This is not only in terms of the moment capacity of channel sections in vicinity of the bolt-group, but also in terms of the bearing capacity of the bolt holes (Lim and Young, 2007).

## 2 PORTAL FRAME FINITE ELEMENT MODELS

### 2.1 Structure details

Fig. 1a details the geometry of the frame including the locations of lateral restraint. Fig. 1b shows the typical eaves connection detail used in cold-formed steel portal frame construction.

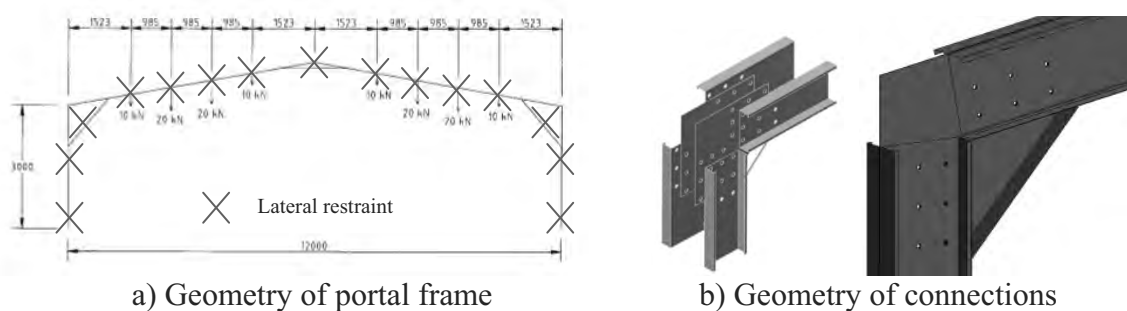


Fig. 1 Geometry of portal frame structure

The frame is formed from bolted back to back channel sections through two 3 mm steel plates (Fig. 2a). A 12 m span frame, with 3 m eaves height and a 10° pitch was considered, using a 315 mm x 230 mm bolt group at both eaves and apex connection (Fig. 2b).

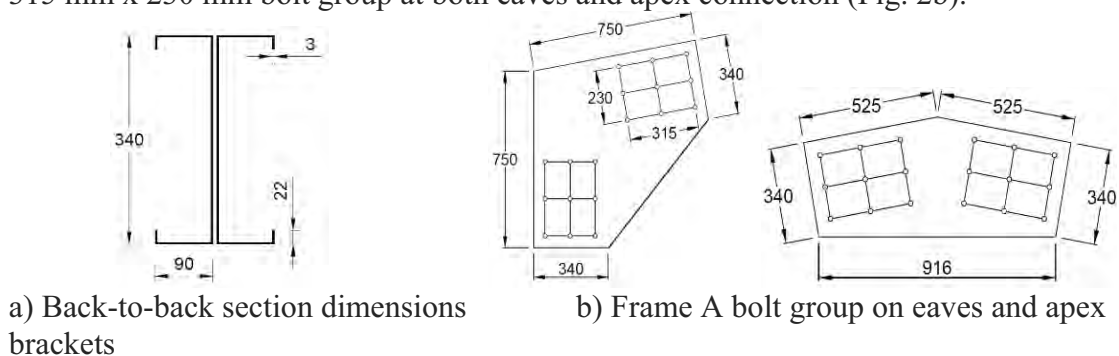


Fig. 2 Details of the frame (mm)

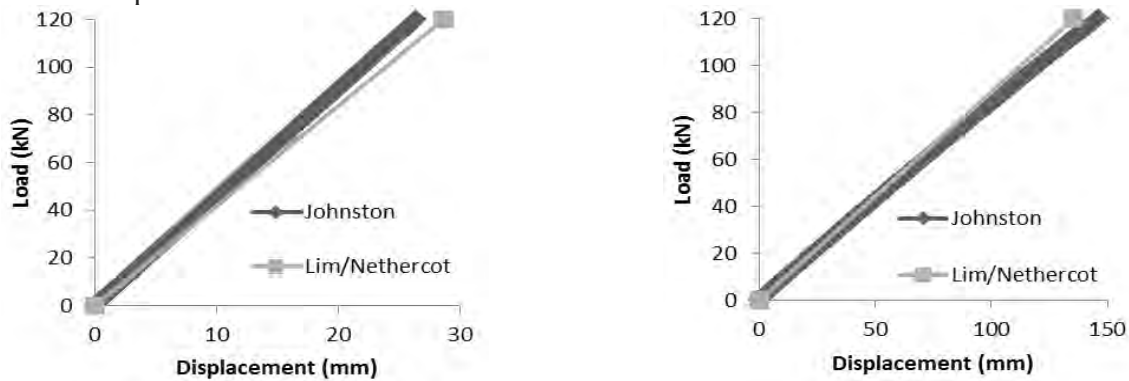
### 2.2 Numerical Modelling

According to Eurocode 3, advanced calculation models (such as the one presented in this paper) may be used for the design of Class 4 sections when all stability effects are taken into account. Therefore, for numerical calculation carried out using the finite element method, shell elements should be used to accurately capture local buckling (Franssen & Real, 2010). A non-linear static riks, elastic-perfectly-plastic model was composed using the finite element

package ABAQUS, with S4R (4-node, reduced integration) shell elements. For the preliminary investigation presented in this paper, initial imperfections were not modelled. At ambient temperature, the following material values were used: Young's Modulus,  $E = 210,000 \text{ N/mm}^2$  and Yield Stress =  $515 \text{ N/mm}^2$ . These were subsequently altered to represent the reduced strength properties of cold-formed steel at elevated temperature. In order to represent the semi-rigid joints, spring elements were used to represent bolt-hole elongation with a stiffness of  $10580 \text{ N}$  in the  $y$  and  $z$  directions.

### 2.3 Ambient Temperature

A finite element shell model was created at ambient temperature and validated using published literature (Lim and Nethercot, 2004). The column bases were treated as pinned supports. The deflection at the apex and eaves levels was compared against an applied load of  $120 \text{ kN}$ . From Fig. 3, it can be seen that the full span ambient frame model shows good agreement with the published literature. Tab. 1 breaks down the exact values, with 7.7% and 8.2% difference in lateral spread at eaves level and vertical apex deflection respectively. This variance can be explained, in part, by the redistribution of forces within the frame. This enabled suitable validation for the preliminary investigation of the frame's behaviour at elevated temperature.



a) Validation at eaves

b) Validation at apex

Fig. 3 Validation of finite element shell model at ambient temperature

Tab. 1 Displacement at  $120 \text{ kN}$  load at ambient temperature

	Lim/ Nethercot (mm)	Ambient frame model (mm)	Difference (mm) [(Lim/Nethercot) - Ambient frame model]	Percentage difference (%)
Lateral spread at eaves	28.6	26.4	2.2	7.7
Vertical at apex	135.2	146.3	-11.1	-8.2

### 2.4 Elevated Temperature

For initial investigation at elevated temperature, a static approach was taken. Models were analysed, with the material stiffness altered for each temperature increment. For each increment, temperature was kept uniform across the entire structure, with the temperature difference between the hot gas and steel section assumed to be negligible for the thin cold-formed steel members. A total load of  $120 \text{ kN}$  was applied, initially at  $250^\circ\text{C}$ , up to a maximum temperature increment of  $700^\circ\text{C}$ . For the semi-rigid joint shell models, eaves and apex brackets were treated as fully restrained. Tab. 2 summarises the material properties used within the models.

Tab. 2 Material properties used in analysis (Chen and Young, 2004)

Steel temperature (°C)	22	250	400	450	500	550	600	700
Young's Modulus E (N/mm <sup>2</sup> )	210000	171696	146496	138096	100609	68632	41427	16200
Yield Stress fy (N/mm <sup>2</sup> )	515	494	454	409	347	267	170	48.9

The ABAQUS beam and shell models of the cold-formed steel portal frame at 250°C are presented in Fig. 4a and Fig. 4b, respectively.

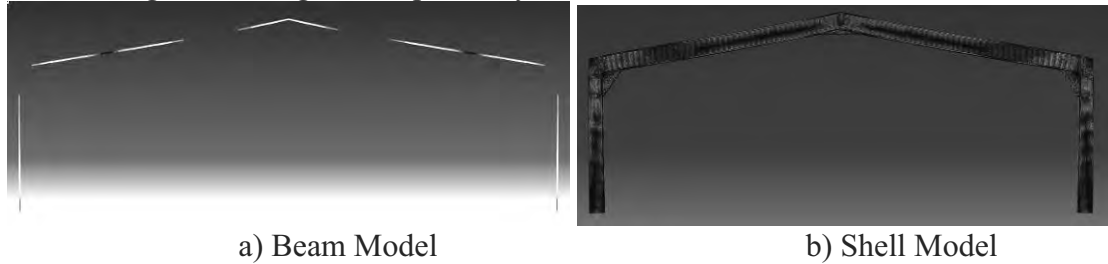


Fig. 4 ABAQUS Beam model and shell model of the cold-formed steel portal frame at 250°C

Fig. 5a and Fig. 5b show the buckling of the shell model, at 550°C and 700°C, respectively. It can be seen that the buckling failure occurs below the eaves bracket, where the stiffness is greatly reduced, through a combination of coupled instability modes. As the brackets were fully restrained, they do not experience buckling, forcing the frame to fail through the channel sections. Fig. 5c demonstrates the behaviour of the column and rafter at 700°C.

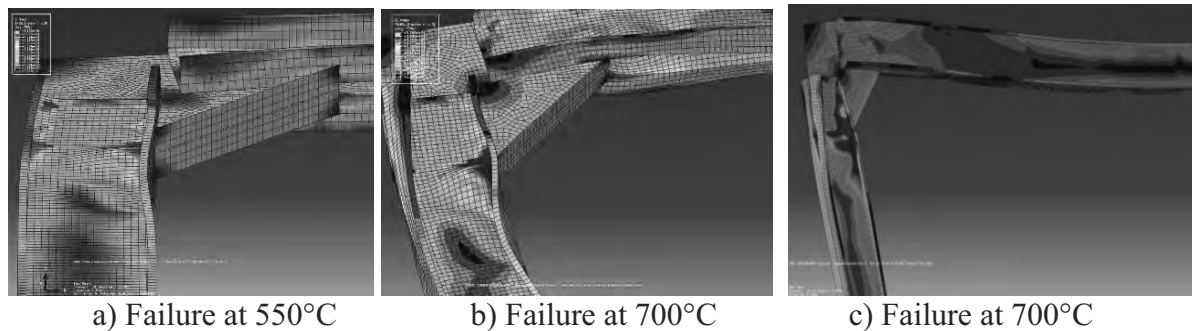


Fig. 5 Failure at eaves bracket connection

### 3 RESULTS

#### 3.1 Shell Models

The results from the ABAQUS finite element shell models demonstrate the high sensitivity of cold-formed steel structures at elevated temperature. Fig. 6 shows the total load carrying capacity of the structure against the mid-span apex displacement for each respective temperature considered.

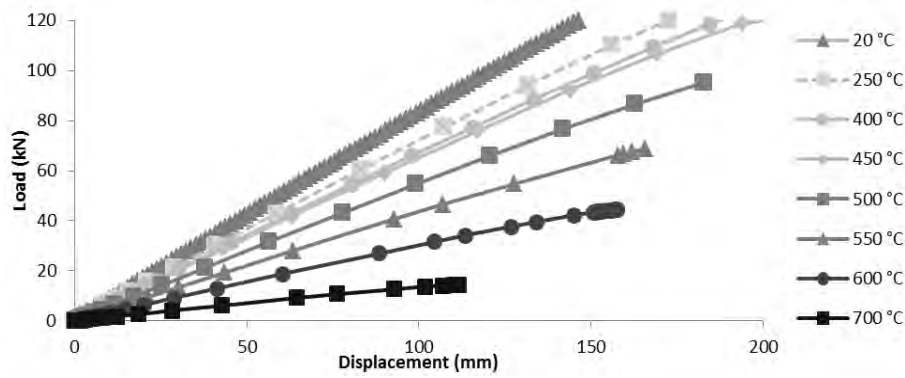


Fig. 6 Load carrying capacity of the structure against apex displacement per temperature interval

From Fig. 6, it can be seen that up to 450°C, the structure can carry a specified load up to 120 kN load. However at 500°C, the structure was only capable of carrying 79% of the specified load (95.4 kN). At 550°C and 600°C, the load carrying capacity was reduced to 57% and 37%, respectively. At 700°C, the highest temperature considered in this study, the structure was only capable of carrying 12% of the specified load (14.4 kN). Fig. 7 illustrates the apex displacement of the structure as a function of the increase in temperature. As the structure is unable to take the full load at temperatures exceeding 450°C, it is compared using a load equal to 10% of the total specified load of 120 kN (equal to 12 kN). From Fig. 7, it can be seen that between 600°C to 700°C, the rafter undergoes the largest relative displacement.



Fig. 7 Apex displacement, per temperature increment for 10% of the total load

The performance of the shell models under loading were compared using the ISO 834 Standard and Hydrocarbon nominal temperature-time curves. Fig. 8 demonstrates the load carrying capacity of the shell model, with respect to the nominal temperature-time curves. For the ISO 834 Standard curve, the structure loses its capacity to carry the specified load of 120 kN between 2-3 minutes (between 400-500°C). For the case of the Hydrocarbon fire curve, the structure loses its capacity to carry the specified load within 1 minute.

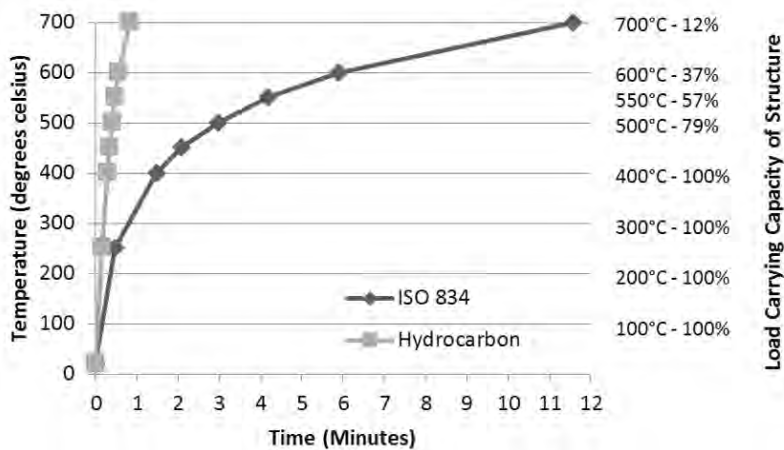


Fig. 8 Load carrying capacity of the shell model with respect to nominal temperature-time curve.

### 3.2 Comparison between shell and beam models

Tab. 3 outlines the comparison between beam and shell models for the temperature range 22°C to 700°C. The shell models show a higher sensitivity to temperature between 450-550°C. At 500°C, the beam model is unable to predict the failure, detected by the shell model. The largest difference in load carrying capacity is 40.8% at 550°C, whereas at 700°C the difference is reduced to 7.8%.

Tab. 3 Comparison between shell and beam models

Tem p (°C)	Load carrying capacity (up to 120 kN)			Apex displacement (mm) <sup>1</sup>		Eaves displacement (mm) <sup>1</sup>	
	Shell (%)	Beam (%)	Difference (B-S) (%)	Shell	Beam	Shell	Beam
22	100.0	100.0	0.0	14.6	6.4	2.6	1.1
250	100.0	100.0	0.0	16.0	7.8	3.2	1.3
400	100.0	100.0	0.0	17.9	9.2	3.5	1.5
450	100.0	100.0	0.0	18.2	9.7	3.7	1.6
500	79.5	100.0	20.5	22.7	13.4	5.0	2.3
550	57.2	98.0	40.8	29.2	19.6	5.5	3.3
600	36.9	61.0	24.1	41.0	32.7	8.0	5.4
700	12.0	19.9	7.8	92.4	85.3	18.7	13.7

Note: <sup>1</sup> To enable comparison, apex and eaves displacement is represented at a load 10% of the total load.

## 4 SUMMARY

This paper has described a preliminary numerical study of a cold-formed steel portal frame, having semi-rigid joints, at elevated temperature. A static finite element numerical analysis has been performed on a loaded frame up to a maximum temperature of 700°C. It should be noted that within this initial study, the stiffness value of the springs which idealize bolt hole elongation have been kept constant for each of the shell models.

The study has demonstrated that beam models are not capable of predicting the same load carrying capacity and displacement when compared to shell models. At elevated temperature, shell models are shown to detect failure much earlier within the fire.

Therefore shell models are recommended for such studies, for a conservative approach. It is suggested that future research investigates a multi-bay portal frame arrangement, using a dynamic analysis which incorporates initial imperfections and actual bolt representation.

## REFERENCES

- ABAQUS standard user's manual, Version 6.11-1 Dassault Systèmes, 2011.
- Chen, J., Young, B., "Mechanical properties of cold-formed steel at elevated temperatures", 17th International Specialty Conference on Cold-formed Steel Structures, Orlando, 2004, pp. 437-65.
- Eurocode 3 design of steel structures part 1-2: General rules - structural fire design. Technical Report BS EN 1993-1-2:2005, British Standard, 2005b.
- Franssen, J., Real, P., "Fire Design of Steel Structures: Eurocode 1: Actions on structures; Part 1-2: General actions -- Actions on structures exposed to fire; Eurocode 3: Design of steel structures; Part 1-2: General rules -- Structural fire design", 1st Edition, ECCS, Ernst & Sohn, 2010, pp.372-373.
- Jackson, C., Wrzesien, A. M., Johnston, R. P., Uzzaman, A., Lim, J. B. P., "Effect of reduced joint strength and semi-rigid joints on cold-formed steel portal frames" in The 6th International Conference on Coupled Instabilities in Metal Structures, Glasgow, 2012, pp. 287-294.

- Lim, J. B. P., Nethercot, D. A., "Finite element idealization of a cold-formed steel portal frame", *Journal of Structural Engineering - ASCE*, Vol.130, 2004, pp. 78-94.
- Lim, J. B. P., Young, B., "Effect of elevated temperatures on bolted moment- connections between cold-formed steel members", *Journal of Engineering Structures*, Vol. 29, 2007, pp. 2419– 2427.
- Pyl, L., Schueremans, L., Dierckx, W., Georgieva, I., "Fire safety analysis of a 3-D frame structure consisting of cold-formed sections; numerical modelling versus experimental behaviour based on a full-scale fire test", *Journal of Thin-Walled Structures*, Vol. 61, 2012, pp. 204-212.
- Rahman M., Lim J. B. P., Xu Y., "Effect of column base strength on steel portal frames in fire", *Proceedings of the Institution of Civil Engineers, Structures and Buildings*, Vol. 165, Issue SB1, 2011, pp.1-20.
- Simms, W., Newman, G., "Single-story steel framed buildings in fire boundary conditions", *The Steel Construction Institute, SCI Publication P313, Berkshire, 2002, 78 p.*
- Song, Y., Huang, Z., Burgess, I., Plank, R., "A new design method for industrial portal frames in fire", *International Conference: Application of Structural Fire Engineering, Prague, 2009, pp. 56-59.*
- Wrzesien, A. M., Lim, J. B. P., Lawson, R. M., "Stressed skin effects on cold-formed steel portal frames with semi-rigid joints", *The 2012 Borneo Engineering Symposium on Cold-formed Steel Innovations, Kuching, 2012, pp. 12-43.*



## **FIRE-INDUCED COLLAPSE OF STEEL STRUCTURES: Basic mechanisms and countermeasures**

Alexandru Dondera<sup>a</sup>, Luisa Giuliani<sup>a</sup>

<sup>a</sup> Technical University of Denmark, Civil engineering Department, Kgs. Lyngby, DK

### **Abstract**

Single-story steel buildings such as car parks and industrial halls are often characterised by stiff beams and flexible columns and may experience an outward (sway) collapse during a fire, endangering people and properties outside the building. It is therefore a current interest of the research to investigate the collapse behaviour of single-story steel frames and identify relevant structural characteristics that influence the collapse mode.

In this paper, a parametric study on the collapse a steel beam-column assembly with beam hinged connection and fixed column support is carried out under the assumption of a protected column and a standard temperature-time curve on the beam. The study shows that sway collapse can be avoided by increasing either the restraint offered by the column or the load-to-resistance ratio of the beam. It seems possible to extend these results to multi-span frames with bracing system, in case of a fire located on one outer span –situation that represents the worst case for the risk of sway collapse.

With respect to this type of frames, a methodology is proposed for the development of design tables that relate the profiles of the elements to the soliciting load on the beam. By means of those tables, a simple method for the assessment and the countermeasure of unsafe collapse mode of single-story steel buildings can be derived.

**Keywords:** steel frames in fire, restraint grade, loading rate, thermo-plastic degradation, thermal expansion, thermal buckling, catenary action, pull-back, sway and non-sway collapse.

### **INTRODUCTION**

Current design procedures for structural fire design are aimed at avoiding structural failures under a pre-determined duration of a standard fire, which defines the resistance class of the buildings and may vary significantly, depending on the type of structure and on the occupancy of the premises. If a minimum resistance of 120 min (R120) is required by most European countries for high rise buildings, single-story buildings such as industrial halls may have much shorter resistance time. According to a review of the Italian Committee for Fire Safety of Steel Construction (Pustorino, et al., 2006), the resistance class of industrial halls with low fire load in Europe varies from a maximum of R60 in Sweden and UK, to a minimum of R15 in Belgium, while in other countries like Finland, Germany and Greece no fire design at all is required for these structures.

The reason of the relaxation of the fire safety requirements of certain national regulations lies in the fact that in case of a fire in an industrial hall less severe consequences are expected than in case of a fire in a tall and complex structure, where the egress of the occupants is hampered by the presence of stairs through many floors and where the costs associated to repair or rebuild of the structure would be huge. Nevertheless, the assumption of limited and acceptable losses for industrial hall fires is only valid in case the collapse of the structure doesn't endanger people and properties on the outside. This circumstance is not unlikely in case of industrial hall collapses, where an outward collapse mode (sway collapse) can be induced by some typical structural characteristics, such as stiff beams and flexible columns.

The problem has been approached by several studies in the last year. However, they are either oriented to explain in details the failure mechanisms of a single steel element under different boundary conditions and thermal actions (Usmani, et al., 2001), (Gillie, 2009), or focused on the design of pitched portals (Song, et al., 2009) and multi-story buildings (Wang, et al., 1995). An attempt to develop a design method for single-story steel frames has been done in the framework of a European research project (EUR 24222, 2010) with respect to pitched portals and lattice steel frames. However, on one side are the proposed empirical formulas not very easy to use, and on the other side the structural characteristics that determine the triggering of one or another failure mechanisms on the other side are not highlighted.

This paper is aimed at describing detail the basic mechanisms that determine the collapse of single-story steel buildings and at identifying the structural properties that influence them. By providing an understanding of the role played by the relevant building characteristics, simple countermeasures aimed at ensuring a safe collapse can be identified and undertaken. Although the results presented in the following refer to a specific frame type, the methodological approach followed in the paper allows for an easy application of the procedure to other frame types and can favour the definition of a general but simple design method for single-story steel buildings in fire.

## 1 BEHAVIOUR OF SINGLE-STORY STEEL FRAMES IN FIRE

As described in several studies (O'Meagher, et al., 1992), (Bong, et al., 2006) and confirmed by the observation of fire tests (Wong, 2001), the behaviour of steel frames in fire is characterized by an outward movement, driven by the thermal expansion of the fire exposed beam, which may be followed by a pullback, driven by the thermal degradation of the steel heated to high temperatures and subjected to the mechanical loads. The predominance of one or another phenomenon will determine the entity of the outward displacement and, ultimately, the collapse mode.

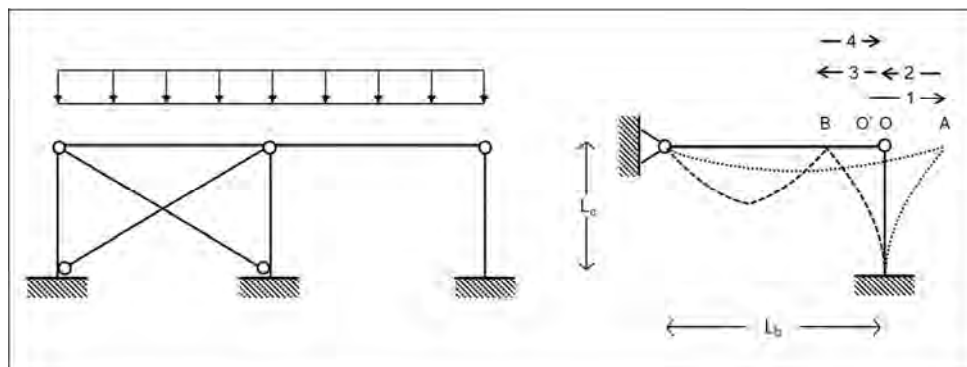


Fig. 1: Two-span braced frame (left) and beam-column assembly (right) with identification of collapse phases.

### 1.1 Collapse phases of a single-story steel frame in fire

In order to better analyse this behaviour and highlight the parameters that play a role in the collapse, reference is made to a simple braced single-story steel frame, as the one shown on in Fig. 1. It is possible to distinguish four phases of the collapse.

#### Phase 1: expansion / sway collapse

At the beginning of the fire, the temperatures are still relatively low and the mechanical properties of the elements have not significantly degraded yet. In this phase, the effect of the thermal expansion is prevailing on the effect of the mechanical loads. As a consequence, an outward displacement will be experienced by the top of column, which will move from the initial position  $O'$  to the maximum outward position  $A$ . In the meanwhile, a compressive force will develop in the beam, while the column will be subjected to shear and moment. The

relative strength and stiffness of the two elements will determine which element fails first, or cause the outward displacement to exceed a safety limit (SN035a-EN-EU, 2006) in case a displacement criterion is adopted for the definition of the collapse. The overcoming of a displacement limit would occur also in case of a column failure, since as soon as no restraint to thermal expansion is provided by the column, the frame collapses outwards in a sway mode.

#### Phase 2: pullback

If the beam fails out of compression, the outwards thrust will cease and the column will start moving backwards towards its rest position O, as the compressive force in the beam will decrease abruptly. As the temperatures get higher the mechanical properties of the steel degrade significantly and a bending failure of the beam will eventually occur. It has to be noted, that in case of a high loading rate of the frame, it is no longer possible anymore to distinguish between buckling and moment failure, as the beam will experience a compressive-bending failure mode. However, the global behaviour of the frame won't be significantly affected by this and the pullback movement will still be sustained by the formation of a three-hinge mechanism in the beam.

#### Phase 3: pull-in

After the bending failure, a transition from bending to tensile resistance occurs in beam. The frame moves from the rest position O inwards, as the catenary that develops in the beam slows down the vertical runaway of the mid-span. The predominance of the inward displacement on the tensile stress depends again on the load and the restraint level and could induce either a tensile failure of the beam or a bending failure of the column. In principle, the rise of tensile stresses in the beam, could induce the failure of adjacent elements and trigger a progressive collapse, as in the case of the Oklahoma Building collapse (FEMA 277, 1996) (Giuliani & Prisco, 2008). However, this seems unlikely to occur in case of fire, as the high material degradation of the beam consequent to the high temperatures that characterize this collapse phase would prevent a significant rise of the forces (Yin & Wang, 2004)

#### Phase 4: relaxation / non-sway collapse

If the beam fails in tension, as typical for frames with fire insulated column, the beam will collapse inside the frame while the column will move outwards towards its rest position, as a consequence of the relaxation of the pull exerted by the beam. If the column fails instead, the beam pull will continue and the frame will collapse inwards. In both cases, an outward collapse is avoided and the frame can be classified as non-sway.

### **1.2 Parametric study**

Single story steel frames are often characterised by hinged beam-column connections and by a bracing system for resisting horizontal actions, as the one shown on the left of Fig. 1. In this case, columns are typically quite flexible, as they only sustain the vertical load of one floor. Beams may have instead relatively big profiles, due to possibly high live loads, such as in case of a travelling crane in an industrial hall or the weight of cars on the roof of a car park.

For what said in the previous section, this organization of the structural system may favour a sway collapse, due to a possible low loading rate of the beam, consequence to the likely absence of live loads at the moment of fire, and to the low restraint offered by the slender column to the thermal expansion of the beam. This is especially true if the fire triggers in an outer span of the frame, as only the outmost column would restrain the beam expansion toward the outside.

The study has been therefore restricted to a worst case, represented by a fire in the outermost span of a braced frame with hinged beam-column connections. Under this assumption, the behaviour of a braced frame can be represented by a model of a beam-column assembly, as the one represented on the right of Fig. 1. In order to reduce the number of variables and favour a clear interpretation of the results, the geometry and the material of the frame has been kept constant and the study refers to a 5 m span, 3 m height frame made of S235 steel.

It is expected the behaviour of the frame will vary significantly, depending on whether the column is insulated or not. As such, the two cases should be investigated separately. In the following, only the results related to the case of an insulated column will be presented. In particular, a thermal action corresponding to the standard fire has been applied to the beam, while the column has been considered to remain cold.

Under these assumptions, the initial resistance and stiffness of the elements only vary with the section profiles, and can be directly related to the solely temperature of the beam. Therefore, the parametric study has been conducted with respect to the following aggregated quantities:

- The initial load-to-resistance ratio  $LLR$  of the beam with respect to bending failure, defined as the ratio between the value of the imposed load  $p$  and the elastic limit load  $p_e$ :

$$LLR = p/p_e \quad \text{where:} \quad p_e = 12 \frac{W_e \cdot f_{s,y}}{L^2} \quad \text{and} \quad 0 \leq p \leq p_e \quad (1)$$

- The initial restrain grade of the beam, which depends on the ratio between the flexural stiffness of the column  $k_{flex,c}$  and axial stiffness of the beam  $k_{ax,b}$ . In the following, the effect of this ratio has been accounted by means of a parameter introduced by Pettersson & Ödeen (1978), named  $\gamma$ -factor and defined as:

$$\gamma = 1/1 + \frac{k_{flex,c}}{k_{ax,b}} \quad \text{where:} \quad k_{flex,c} = \frac{6 \cdot E_s \cdot I_c}{L^3} \quad \text{and} \quad k_{ax,b} = \frac{E_s \cdot A_b}{L} \quad (2)$$

It has to be noted that according to this definition  $\gamma = 1$  corresponds to the case of the free expansion of a simply supported beam, while  $\gamma = 0$  corresponds to the case of a totally hindered expansion of a double-hinged beam. As such, decreasing the  $\gamma$ -factor corresponds to increasing the restrain grade of the beam.

## 2 RESULTS

The results of the parametric studies are presented in Fig. 2 with respect to the variation of  $\gamma$  (left column) and of  $LLR$  (right column). In the Fig., the four phases of the collapse described in the previous section are clearly visible for each of the restrain grade considered. From the Fig. it is also evident that by increasing the restrain grade of the column (i.e. by decreasing the  $\gamma$ -factor), both the horizontal and vertical displacements (indicated with  $u$  and  $\delta$  respectively) decrease, while the sectional solicitations ( $N$  and  $M$ ) increase. As a consequence, the critical temperature of the beam gets lower as the restrain grade increases. The same happens when the  $LLR$  increases. This means that, by increasing either the restrain grade or the loading ratio, the transition from phase 1 to 2 is anticipated and, consequently, the maximum outwards displacement decreases. It is interesting to notice that the transition from phase 2 to 3, which corresponds to the triggering of the catenary effect, doesn't depend instead on the restrain grade, but only on the loading ratio, as visible by observing Fig. 3.

In Fig. 3 the effect of the variation of the restrain grade (left column) and of the loading ratio (right column) is shown with respect to horizontal and vertical displacements corresponding to: i) the beginning of the fire (situation O', corresponding to the initial position before the fire); ii) the transition between phase 1 and 2 (situation A, when the outward horizontal displacement is maximum); and iii) the transition between phase 2 and 3 (situation B, when the inward horizontal displacement is maximum). In the upper part of the Fig., it is observable that maximum outward displacement decreases almost linearly with an increment of the  $LLR$ , while decreases much more rapidly with a decrement of the restrain grade (i.e. increment of  $\gamma$ ). Therefore, in order to avoid a possible excessive outward displacement, an increment of column section is expected to be more effective than an increment of the beam loading. Furthermore, the sensitivity of the horizontal displacements to  $\gamma$  and  $LLR$  is much higher than that one of the vertical displacements, which don't vary much with the two parameters in all three situations O', A, and B.

### 3 METHODOLOGY

The results reported in Fig. 3 refer to an IPE100 beam. The qualitative trend of the displacement with  $\gamma$  and LRR will also apply to different beams; however, the value of the displacements for a given  $\gamma$  and LRR of a bigger profile will be different from that of the IPE100, as the flexural stiffness of the beam will increase. The lower vertical displacements will determine a lower pullback effect and an increment of the outward displacements.

When this displacement becomes significant, even if the column doesn't fail, glasses and other non-structural elements could detach from the façade and endanger people and properties outside the building. It seems therefore sensible to assume a maximum outward displacement  $u_{A,lim}$  as sway failure criterion. According to the indication of the British guidelines (P070, 1991), this displacement has been taken equal to 1/100 of the column height, i.e. to 3 cm.

Then, further parametric analyses have been performed for increasing beam profiles. For each profile and each LRR, the minimum restrain grade  $\gamma_{lim}(LRR, profile)$  corresponding to the achievement of the maximum outward displacement  $u_{A,lim}$  has been assessed.

The results are presented in Fig. 4 in the form of an abacus, which provides the limit restrain grade  $\gamma_{lim}$  for a given profile (horizontal axis) and a given LRR (identified by a colour). In particular the  $\gamma_{lim}$  is found on the vertical axis in correspondence to the limit height of the area hatched with the colour associated to the LRR. This procedure can be repeated for different frames and different fire condition (e.g. frames with fixed connection and uninsulated columns). In this way, a practical design method for assessing a possible outward collapse of a steel frame can be developed and easily integrated in the design practice.

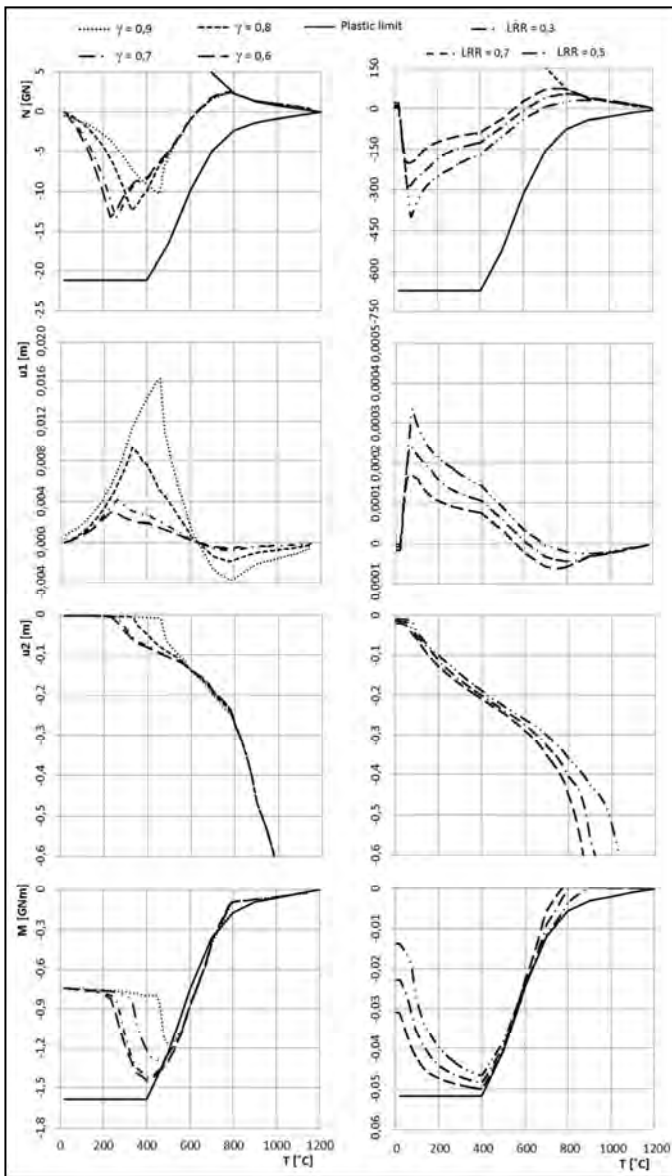


Fig. 2: Increasing restraint grade (left) and loading ratio (right), in term of (top to bottom): horizontal displacement at the top of the column; vertical displacement of the beam mid-span; axial force and mid-span moment in the beam.

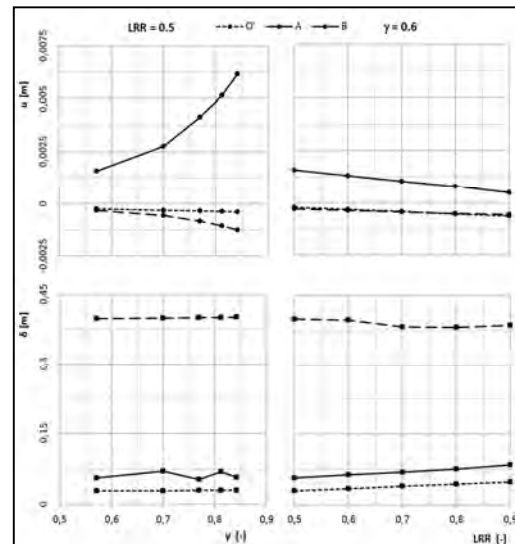


Fig. 3: Horizontal (top row) and vertical displacements (bottom row) in case of variation of  $\gamma$  (left column) and of LRR (right column), with respect to: O' (beginning of fire); A (end of phase 1); and B (end of phase 2).

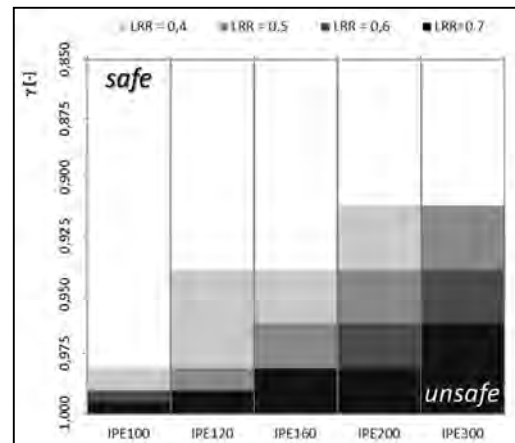


Fig. 4: Abacus for the determination of the collapse mode of a single-story braced frame with hinged beam-column connections and insulated columns fixed to the ground.

## 4 CONCLUSIONS

In this paper, a parametric study on the collapse mode a steel beam-column assembly with beam hinged connections and column fixed to the ground has been carried out under the assumption of a protected column and a standard temperature-time curve on the beam. The study shows that sway collapse can be avoided by increasing either the restraint offered by the column or the load-to-resistance ratio of the beam.

It seems possible to extend these results to multi-span frames with bracing system, in case of a fire located on one outer span -situation that represents the worst case for the risk of sway collapse. With respect to this type of frames, a methodology is proposed for the development of design Tab.s that relates the geometry of the frame to the vertical load of the beam. The methodology described could be applied to different frame type, such as unbraced frames or frames with fir exposed columns, and lead to the definition of a set of simple rules for a safer and more reliable fire design of single-story steel buildings.

## REFERENCES

- Bong, M., Buchanan, A., R.P., D. & Moss, P., 2006. Structural performance of steel portal frame buildings subjected to fire. Christchurch, New Zealand, 19th Australasian Conference on Mechanics of Structures and Materials (ACMSM19), pp. 457-462.
- EUR 24222, 2010. Fire safety of industrial hall - A valorization project, Brussels, Belgium: Research Fund for Coal & Steel - European Commission.
- FEMA 277, 1996. The Oklahoma City Bombing: Improving Building performance Through Multi-Hazard Mitigation, Reston, VA, USA: FEMA Mitigation Directorate and American Society of Civil Engineering (ASCE).
- Gillie, M., 2009. Analysis of heated structures: Nature and modelling benchmarks. *Fire Safety Journal*, 44(5), pp. 673-680.
- Giuliani, L. & Prisco, V., 2008. Nonlinear Analysis for Progressive Collapse Investigation on Reinforced Concrete Framed Structures. Vancouver, Canada, American Society of Civil Engineering (ASCE), pp. 1-10.
- O'Meagher, A., Bennetts, I., Dayawansa, P. & Thomas, I., 1992. Design of Single Storey Industrial Buildings for Fire Resistance. *Steel Construction*, 26(2).
- P070, 1991. Steelwork Design Guide to BS5950- Vol.4: Essential Data for designers, UK: The Steel Construction Institute.
- Pettersson, O. & Ödeen, K., 1978. Brandteknisk dimensionering, principer, underlag, exempel (Fire safety design, principles, basis, examples - in Swedish), Stockholm, Sweden: Förlag Vällingby.
- Pustorino, S., Princi, P., Giomi, G. & Cirillo, V., 2006. Interim Report no.2 - Regola tecnica prescrittiva: Resistenza al fuoco richiesta agli edifici in base alla destinazione d'uso. Riepilogo regolamenti nazionali e confronto con altri paesi Europei. (in Italian), Milan, Italy: Commissione per la Sicurezza delle Costruzioni in Acciaio in caso di incendio - Fondazione Promozione Acciaio.
- SN035a-EN-EU, 2006. NCC1: Practical deflections limits for single storey buildings - Recommendations and guidelines for horizontal and vertical deflection for single storey, Ascot, UK: NCCI - Eurocodes Non Contradictory Complementary Information.
- Song, Y., Huang, Z., Burgess, I. & Plank, R., 2009. A new design method for industrial portal frames in fire. Prague, Czech Republic, Application of Structural Fire Engineering (ASFE).
- Usmani, A., Rotter, J., Lamont, S. & Sanad, A., 2001. Fundamental principles of structural behaviour under thermal effects. *Fire Safety Journal*, 36(1), p. 721-744.
- Wang, Y., Lennon, T. & Moore, D., 1995. The behaviour of steel frames subjected to fire. *Journal of Constructional Steel Research*, 35(1), pp. 291-322.
- Wong, 2001. The structural response of industrial portal frame structures in fire, Sheffield, UK: University of Sheffield.
- Yin, Y. & Wang, Y., 2004. A numerical study of large deflection behaviour of restrained steel beams at elevated temperatures. *Journal of Constructional Steel Research*, Volume 60, pp. 1029-1047.

# NUMERICAL STUDY OF STEEL BEAMS IN SUB-FRAME ASSEMBLY

## Validation of Existing Hand Calculation Procedures

Naveed Iqbal <sup>a</sup>, Tim Heistermann <sup>a</sup>, Milan Veljkovic <sup>a</sup>, Fernanda Lopes <sup>b</sup>, Aldina Santiago <sup>b</sup>,  
Luis Simões da Silva <sup>b</sup>

<sup>a</sup> Luleå University of Technology, Division of Structural and Construction Engineering, Luleå, Sweden

<sup>b</sup> University of Coimbra, Department of Civil Engineering, Coimbra, Portugal

### Abstract

The design methods currently proposed by the codes prescribe the strength assessment of structures to be based on their strength limit state. These design methods can be applied to isolated steel members to determine their design strength in fire. The real response of a structural member is, however, more complex due to the thermal expansion and the presence of restraints against this expansion by the surrounding structure. It is therefore imperative to study the response of a structural member at high temperature in a way which includes its interaction with its surroundings. This paper will focus on the numerical investigation of steel beams in structural frames connected to concrete filled tubular (CFT) columns through reverse channel connections and comparison to hand calculation procedures.

**Keywords:** structural fire design, Abaqus, sub-frames, thermal expansion, catenary action, runaway deflection, artificial damping

### INTRODUCTION

The present design codes prescribe that the fire resistance of structural members should be based on their critical temperature or their strength limit state (Eurocode-3, 2004). These conventional design procedures are based on the assumption that structural members are essentially isolated in their response to fire load. In reality, however, they form a part of a structural frame and their response depends heavily on the way they interact with the surrounding structure. Fire tests conducted on full scale framed buildings at the test facility in Cardington, UK have demonstrated that for the same load levels as a standard fire test, the restrained steel beams can exhibit extensive deflections and still not undergo instability (Kirby, 1997). It has been demonstrated through fire tests on sub-frames and through finite element simulations that beams can exert significant axial forces on the surrounding structure through the connections (Dai et al, 2010).

Temperature dependent variation in the axial force and vertical deflection of a restrained steel beam are important design parameters. Laboratory fire tests are very expensive and time consuming whereas Finite element modelling can be a rather complicated approach (Yin and Wang, 2005). Simplified design procedures have been proposed in order to reduce the complications and make a useful design tool, (Yin and Wang, 2005) and (Dwaikat and Kodur, 2011). The purpose of this paper is to use finite element modelling to validate the proposed hand calculation procedures by comparison to the finite element results. The finite element models in this study are sub-frame models created using the commercial software Abaqus.

### 1 FINITE ELEMENT MODEL (FEM)

The sub-frame models consist of a single I-Profile beam supported by two concrete filled tubular columns. The connection between the beam and columns consist of a reverse channel shown in Fig. 1, which has been shown to have greater rotational capacity at elevated temperatures (Heistermann et al, 2011). Since the test setup is symmetrical about the vertical axis through the mid-span of the beam, only half the setup has been modelled in order to save computation time.



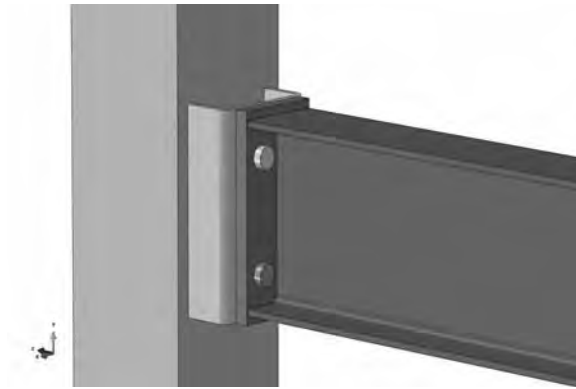


Fig. 1 Reverse channel connection

### 1.1 Material Properties

An elasto-plastic stress vs. strain model without hardening for steel S355 at elevated temperature has been adopted for all steel parts of the FE model (Eurocode-3, 2004). Temperature reduction factors are used to input the temperature dependent material properties. Thermal expansion has also been incorporated into the material model. Following equations relate nominal stresses and nominal strains to true stresses and true strains in Abaqus (Abaqus, 2012).

$$\varepsilon_{true} = \ln(1 + \varepsilon_{nom}) \quad (1)$$

$$\sigma_{true} = \sigma_{nom} (1 + \varepsilon_{nom}) \quad (2)$$

### 1.2 Contact Interactions

Application of small contact pressure for initializing contact between the contact surfaces can prevent any problems of convergence during the analysis. Small bolt load using the ‘Adjust bolt length’ option is applied for this purpose.

### 1.3 Element type

The FE model has been created using solid (continuum) element C3D8R, which is a first order reduced integration 8 node brick element. Reduced integration elements use lower order integration to calculate element stiffness matrix, which reduces the computation time. The drawback of first order reduced integration element like C3D8R is that they are prone to ‘Hourglassing’. However, in Abaqus first order reduced integration elements have ‘hourglass controls’, which if used with finer mesh can solve the problem of hourglassing (Abaqus, 2012).

### 1.4 Numerical Procedure

A static general procedure is performed in the following steps.

- **Pretensioning of Bolts**
- **Load:** 40% of the bending moment capacity at ambient temperature as 4 point load.
- **Heat:** uniform Heat is applied as predefined field according to ISO 824 Fire curve

### 1.5 Boundary conditions

The top end of the column is free to translate longitudinally but restrained from lateral translations whereas the bottom end has all translations restrained. Both ends are free to rotate except about the longitudinal axis. At the free end of the beam a symmetry boundary condition along the longitudinal (z-axis) is defined to simulate the symmetry as discussed earlier.

## 1.6 Pseudo Damping of the Model

Covergence problems in the FE model can be taken care of by using artificial damping. The ratio of the dissipated energy to the total strain energy should be kept below 10% and also the support reaction forces should be checked against the applied load to prevent over damping of the model (Dai et al, 2010).

## 2 HAND CALCULATION PROCEDURE (HCM)

Yin and Wang in their study have proposed a hand calculation procedure, which aims to describe the restrained beam behaviour over the entire temperature range (Yin and Wang, 2005). The general methodology of the procedure is based on the equilibrium of the steel beam at all temperatures as shown in Eq. (3).

$$M_{connection} + M_{midspan} + F\delta = M_{applied} \quad (3)$$

### 2.1 Deflection profile

The deflection profile of the beam is obtained from linear interpolation between deflection profiles for free rotation at supports and full rotational restraints as shown in Eq. (4).

$$deflection\_profile = (1 - c_f) \times free\_rotation + c_f \times restrained\_rotation \quad (4)$$

The degree of end rotational restraint  $c_f$  is defined as the ratio of the rotational stiffness at supports to the beam bending stiffness.

### 2.2 Axial force

Initially, as the temperature increases, the beam expands against the axial restraints offered by the supporting columns. This restrained expansion produces axial compressive force in the beam shown by Eq. (5).

$$F_T = K'_a \left( C_f \times \frac{\delta_m^2}{L} - \alpha \cdot \Delta T \cdot L \right) \quad (5)$$

where  $K'_a$  effective axial support stiffness  
 $C_f$  coefficient derived from the deflection profile of the beam  
 $\delta_m$  mid-span deflection due to mechanical load  
 $L$  span length of the beam  
 $\alpha$  coefficient of linear thermal expansion  
 $\Delta T$  increase in temperature

### 2.2 Midspan deflection

During the elastic phase before the cross section yields, the midspan deflection of the beam is obtained from the equilibrium equation, shown in Eq. (3), through an iteration process. The midspan deflection is relatively small during the elastic phase but starts to increase excessively after yielding happens. The midspan deflection corresponding to maximum catenary force is obtained by the following compatibility equation (Dwaikat and Kodur, 2011).

$$\Delta_c^2 = \left[ \frac{L'}{2} \right]^2 - \left[ \frac{L}{2} + \delta \right]^2 \quad (6)$$

where  $L'$  deformed length of the beam  
 $\delta$  axial deformation of the beam

In the elasto-plastic phase the midspan deflection at any temperature can be obtained through linear interpolation as shown in Eq. (7).

$$\Delta = \Delta_y + \frac{\Delta_c - \Delta_y}{T_c - T_y} \times (T - T_y) \quad (7)$$

where  $\Delta_y$  midspan deflection at yield point  
 $T_y$  temperature at yield point  
 $T_c$  temperature at maximum catenary force

### 3 COMPARISON BETWEEN FEM AND HCM

The test setups are shown in detail in the Tab. 1.

Tab. 1 Test setups used for comparison between FEM and HCM

Model	Column	Beam	Connection	Length
Model01	SHS 250x8	UB 178x102 x19	UK SHS 180x42.7	2 m
Model02	SHS 250x10	IPE300	U200x90x10	5 m

#### 3.1 Axial force and maximum deflection

Fig. 2 and Fig. 3 show axial force in the beam with changing temperature for different values of ‘dissipated energy fraction’ used as to induce damping in the model. The maximum compressive load is reached at approximately the same temperature, however for the model 02 the difference between finite element result and hand calculation result is more than that for model 01. The different values of ‘dissipated energy fraction’ give very little difference between the results. Fig. 4 shows the variation of midspan deflection with temperature for both models. It can be observed from Fig. 4 in comparison to Fig. 2 and 3, that the temperature at which the beam reaches its maximum compressive force is exactly the point where it starts to deflect rapidly. For zero damping the model fails to converge as the compressive force is reducing.

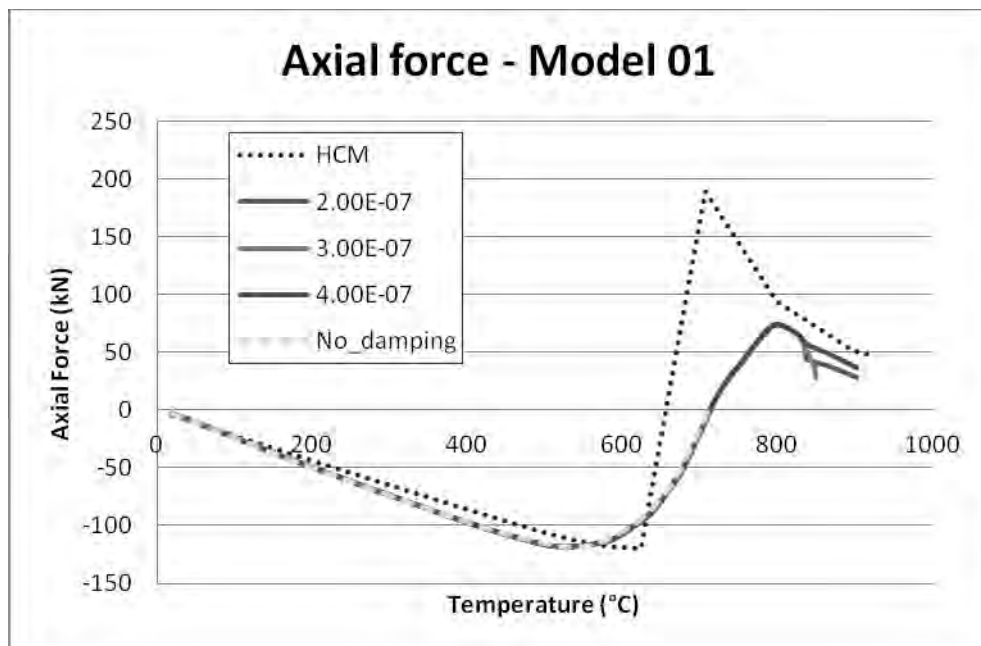


Fig 2: Axial force vs temperature for Model 01

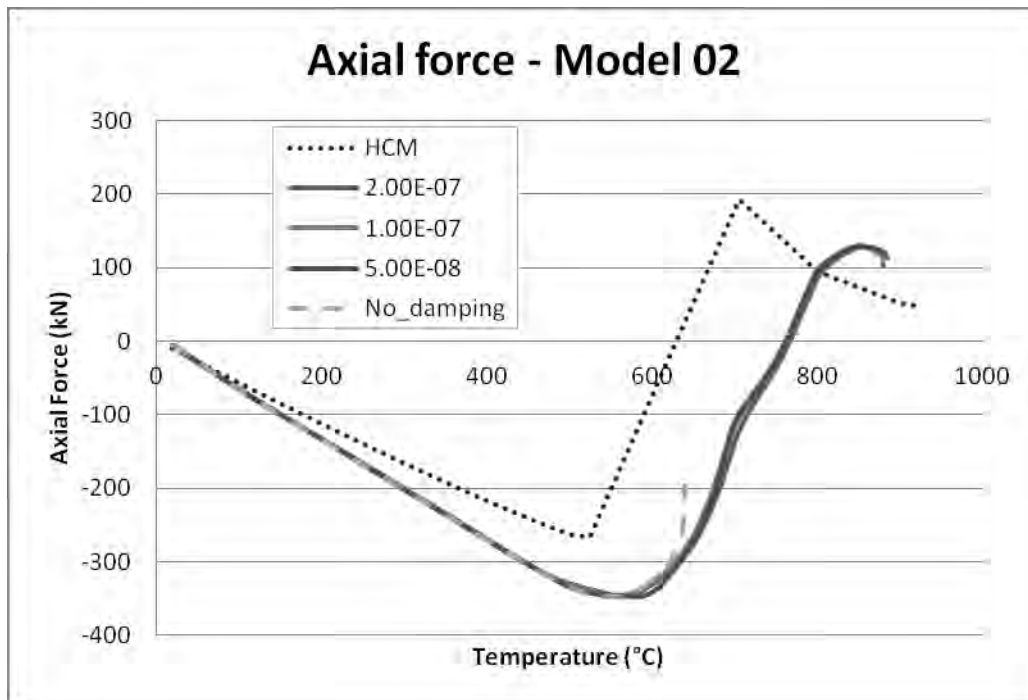


Fig 3: Axial force vs temperature for Model 02

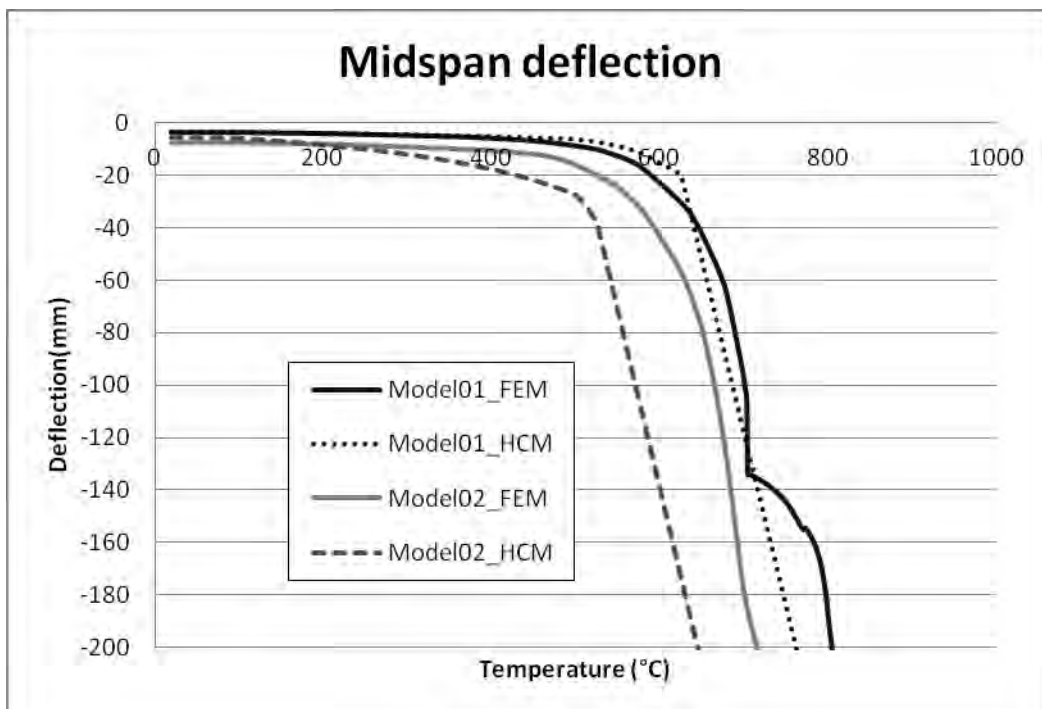


Fig 4: Midspan deflection for both models

## CONCLUSIONS

Following conclusions can be drawn from the comparison between FE-modelling and the hand calculation procedure.

1. The compressive stress predicted by the hand calculation model is 0.62% lower than the result from the FE analysis for model 01 and 23% lower for model 02.
2. The hand calculation model gives conservative estimate for the maximum catenary force in the beam.
3. From hand calculation model, the limiting temperature at which the axial force is zero is lower than the FE analysis results for both models .

4. Damping of the model stabilizes the analysis and solves the convergence problem in both models.
5. The different ‘dissipation energy fraction’ values used here have shown to have very little impact on the results.
6. For model 02 the hand calculation produces results which are much closer to the FE analysis results.

#### **ACKNOWLEDGMENT**

The research leading to these results has received funding from the European Community’s Research Fund for Coal and Steel (RFCS) under grant agreement n° RFSR-CT-2009-00021.

#### **REFERENCES**

- EN 1993-1-2, Eurocode – Design of steel structures – Part 1-2: General rules, Structural fire design, CEN, European Committee for Standardization, Brussels, Belgium, 2004
- Kirby B. R., Large scale fire tests: The British Steel European Collaborative Research Programme on the BRE 8 – Storey Frame, Proceedings of the Fifth International Symposium of Fire Safety Science, 1997
- Dai X. H., Wang Y. C., Bailey C. G., Numerical modelling of structural fire behaviour of restrained steel beam – column assemblies using typical joint types, Engineering Structures, 2010
- Yin Y. Z., Wang Y. C., Analysis of catenary action in steel beams using a simplified hand calculation method, Journal of Constructional Steel Research, 2005
- Dwaikat M. M. S., Kodur V. K. R., A performance based methodology for fire design of restrained steel beams, Journal of Constructional Steel Research, 2011
- Heistermann T., Iqbal N., Veljkovic M., Lopes F., Santiago A., da Silva L. S., Finite Element Modelling of Reverse Channel Connections At elevated temperatures, Proceedings of the Sixth European Conference on Steel and Composite Structures, 2011
- ABAQUS, Abaqus Users’ manual v6.12, Simulia, RI, USA, 2012

## REDUCTION OF CONNECTION RESISTANCE DURING VESELÍ FIRE TESTS

Tomáš Jána <sup>a</sup>, František Wald <sup>a</sup>

<sup>a</sup> Czech Technical University in Prague, Faculty of Civil Engineering, Prague, Czech Republic

### Abstract

The paper is focused to the temperature distribution in the reverse channel connections to concrete filled tubular column during two fire tests on an experimental building in Veselí nad Lužnicí. Temperatures of connections without fire protection as well as fire protected connections were investigated. The connected beams and columns were without fire protection.

**Keywords:** reverse channel, fin plate, heat transfer, fire design, fire test

### INTRODUCTION

The fire design of structures is based on member fire tests in furnaces and connection behaviour is usually neglected. Connections have lower temperature than the adjacent structure during the fire which is caused by the concentration of the material in the connection area and they are protected by a similar thickness of the fire protection as connected members. During the heating and cooling, the connections are subjected to different forces which were not taken into account in the design for the ambient temperature. The connection behaviour is based on the change of mechanical properties of the steel and on the interaction between different parts of the connection. To determine the degradation of the mechanical properties is necessary to find out temperature distribution which can be used in the component method.

The temperature in the connection can be predicted by two methods. According to the first of these methods, the temperature of the beam-to-beam and beam-to column connection with a concrete slab above the connection is calculated from the temperature of the bottom beam flange in the mid-span (CESTRUCO, 2003). The second method is based on the concentrated mass and the temperature is predicted by using the section factor  $A_m/V$  for the each component of the connection. Numerical (Franssen, 2002) and experimental studies (Wald et al., 2006) show necessity to improve the temperature prediction in order to achieve the acceptably accurate description of the connection behaviour during the fire.

The real temperature field in the structure can be obtained from a test on a real object only. Therefore two fire tests on the two-storey building with real fire scenarios create the part of the European project COMPFIRE – Design of Joints to Composite Columns for Improved Fire Robustness. The tests enabled to obtain the temperature developments in the reverse channel connections.

Connections in the partially fire protected steel/composite structure at the fire cannot be critical part of this structure. Heat transfer into the connections can be reduced by fire protection. Temperatures during the fire reach significantly lower values compared with temperatures of unprotected connections. Therefore the selected connections in the experimental building were fire protected.

### 1 EXPERIMENTAL STRUCTURE, CONNECTIONS, FIRE PROTECTION

A two-storey composite steel-concrete experimental structure on the area 10.4 x 13.4, with the height of 9 m was designed and represented a part of an administrative building. Composite ceiling slabs consisted of simple trapezoidal sheets with the rib of 60 mm and 60 mm of

reinforced concrete C30/37. Beams under the slabs designed as IPE 220, 240, 270 and IPE 330 (steel S355) were supported by hollow section columns (TR 245/8, steel S355) filled with concrete and by columns of sections HEB 200. The lateral stiffness of the building was provided by two cross bracings in the both directions. Steel cladding with thermal insulation was used. In each floor there was one window with dimensions 5 x 2 m, see Fig. 1 and (Wald et al., 2011).

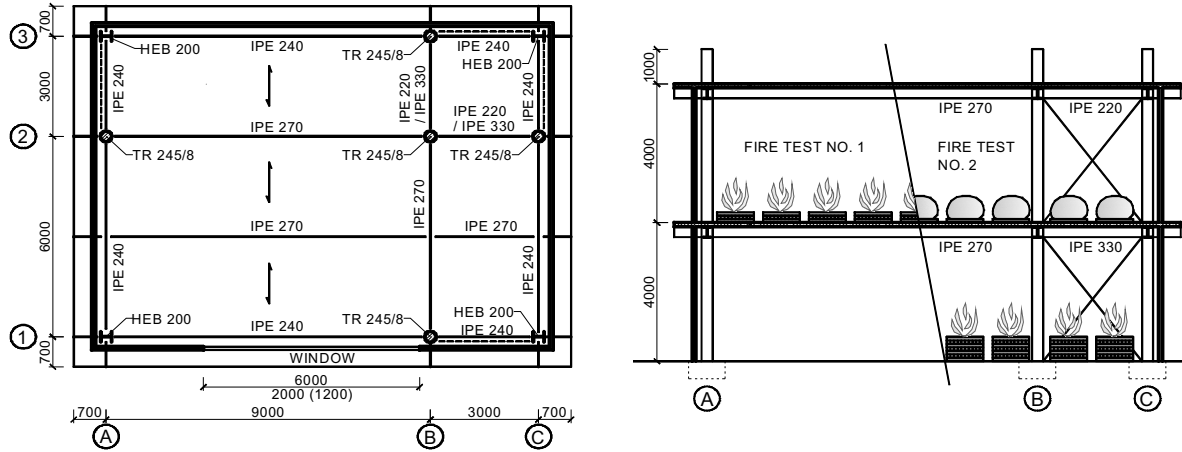


Fig. 1 Experimental structure

Connections were designed according to (EN 1993-1-8, 2005) to resist shear force at ambient temperature and were checked in accordance with European guidelines (ECCS) and (SCI/BCSA). The reverse channel connections connected beams with the cross-sections IPE 220, IPE 270 and IPE 330 to the composite circular tubular column. The reverse channel was formed by standardized rolled section UPE-DIN or by bent sheet metal of the thickness 8 mm. The thickness of the end plates was also 8 mm in all cases. Size of bolts, M12, M16, M20, corresponded with the size of the connected beam. Tab. 1 summarizes the arrangement of the connections which were observed during the fire tests.

Tab. 1 Arrangement of connections

Designation of connection	Beam cross-section	Column cross-section	End plate	Reverse channel	Bolts	Designed thickness of fire protection
First fire test (2 <sup>nd</sup> floor)						
A2-B2 to A2	IPE 270	TR 245/8	165/160/8	sheet 165/200/8	4x M16	20 mm
A2-B2 to B2				UPE 160		
B2-C2 to B2	IPE 220		135/120/8	UPE 120	4x M12	-
B2-C2 to C2				sheet 135/160/8		
Second fire test (1 <sup>st</sup> floor)						
A2-B2 to A2	IPE 270	TR 245/8	165/160/8	sheet 165/200/8	4x M16	-
A2-B2 to B2				sheet 200/220/8		
B2-C2 to B2	IPE 330		200/180/8	UPE 180	4x M20	60 mm
B2-C2 to C2						

Some connections were protected by the fire protection of the thickness 20 mm in the second floor at the first fire test. In the first floor at the second fire test, the fire protection of the thickness 60 mm was applied on the some connections. The reverse channel connections were protected in the length of 250 mm from the edge of the column in the both cases and a mixture of mineral fibres and a cement binder was used as the fire protection.

Fire load was created by piles from softwood dried to moisture of 12 %. The first fire test in the second floor had a character of traveling fire without flashover (fire load was 173.5 MJ/m<sup>2</sup>), the development of the gas temperature at the second fire test in the first floor corresponded with fire scenarios with flashover in a fire compartment of the ordinary administrative building (fire load was 520 MJ/m<sup>2</sup>). The main objective of the fire tests was a monitoring of the heat transfer into the composite structure and a subsequent determination of mutual influence of the fire unprotected and protected parts of the structure. Temperature distribution in the structure and gas temperature in the compartment was measured during the both tests by 120 thermocouples. Typical temperature fields in the reverse channel connections are shown thereafter.

## 2 TEMPERATURES OF FIRE UNPROTECTED CONNECTIONS

### 2.1 Reverse channel connection B2-C2 to B2 at the first fire test

Fig. 2 shows three-metre beam to central column connection with six thermocouples. Thermocouple TC13 was placed into mid-height of the beam web, 100 mm from the end plate, TC14 was installed into the upper bolt, TC15 into the lower bolt. TC16 was placed into mid-height of the end plate between both bolts, TC17 measured temperature in mid-height of the reverse channel flange and TC18 temperature in the steel tube of the column. The connection was not fire protected.



Fig. 2 Fire unprotected beam-to-column connection (B2-C2 to B2) in the 2<sup>nd</sup> floor

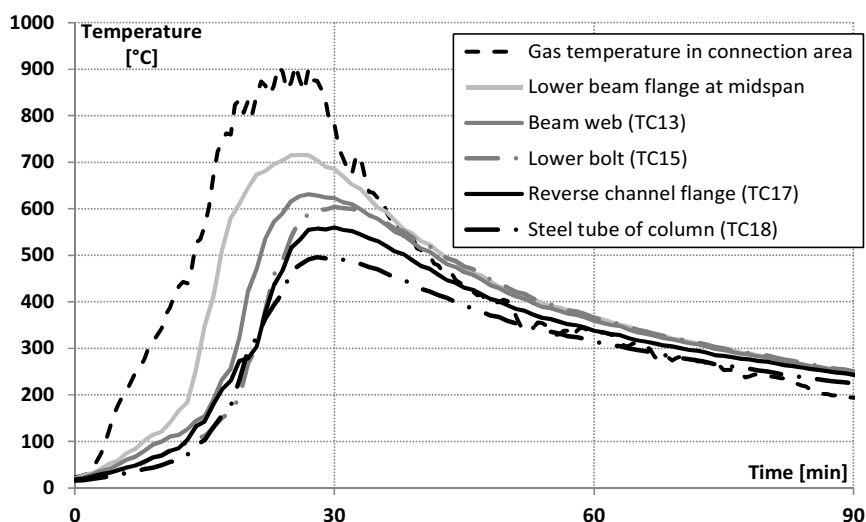


Fig. 3 Comparison of the measured temperatures in fire unprotected reverse channel connection (B2-C2 to B2) with the gas temperature and beam flange temperature in mid-span

In Fig. 3, there are compared the measured temperature in different parts of the connection with the temperature of the bottom beam flange in the mid-span and with the gas temperature. You can see that the connection temperatures were lower than the temperature of the flange



and the parts of the connection close the composite column were lower temperature than the connection components more distant from the column. That shows a positive impact of the great heat capacity of the concrete in the column to reduce the component temperature in the fire unprotected connections.

## 2.2 Reverse channel connection A2-B2 to B2 at the second fire test

The seven thermocouples were on the nine-metre beam to column reverse channel connection without fire protection. The thermocouple TC56 was placed into mid-height of the beam web A2-B2, 150 mm from the end plate, TC57 was installed into the upper bolt, TC58 into the lower bolt. TC59 was placed into mid-height of the end plate between the both bolts, TC60 and TC61 measured temperatures in the middle of the reverse channel flange surface and TC 101 temperature in mid-height of the end reverse channel weld, see Fig. 4.

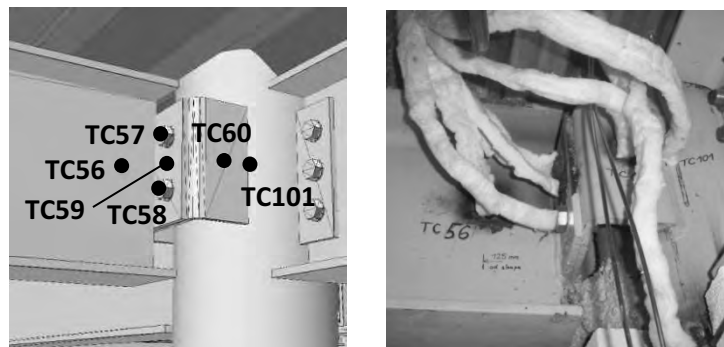


Fig. 4 Fire unprotected beam-to-column connection (A2-B2 to B2) in the 1<sup>st</sup> floor

Temperature distribution of the connection during the second fire test is shown in Fig. 5. Analogous to the temperatures at the first fire test, measured temperature of the each connection component is again significantly reduced in the direction from the beam to the composite column. The connection temperatures are also lower than the temperature of the bottom beam flange in the mid-span.

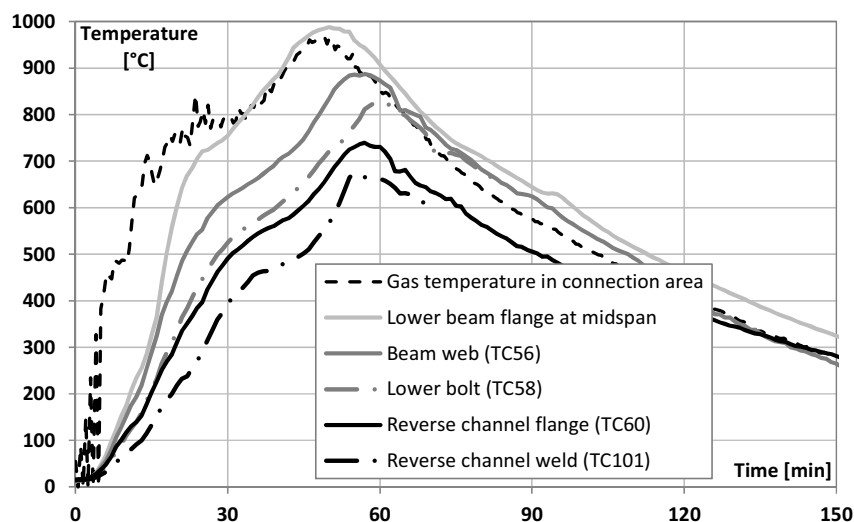


Fig. 5 Comparison of the measured temperatures in fire unprotected reverse channel connection (A2-B2 to B2) with the gas temperature and beam flange temperature in mid-span

### 3 TEMPERATURES OF FIRE UNPROTECTED CONNECTIONS

#### 3.1 Reverse channel connection B2-C2 to B2 at the second fire test

In three-metre beam to column connection, temperature was monitored by five thermocouples. TC62 was placed into mid-height of web of beam B2-C2, 150 mm from end plate, TC63 was installed into upper bolt, TC64 into lower bolt. TC65 was placed into mid-height of end plate between both bolts, TC66 measured temperature in mid-height of reverse channel flange, see Fig. 6. The connection was protected by the fire protection in a length of 250 mm from the edge of the column.

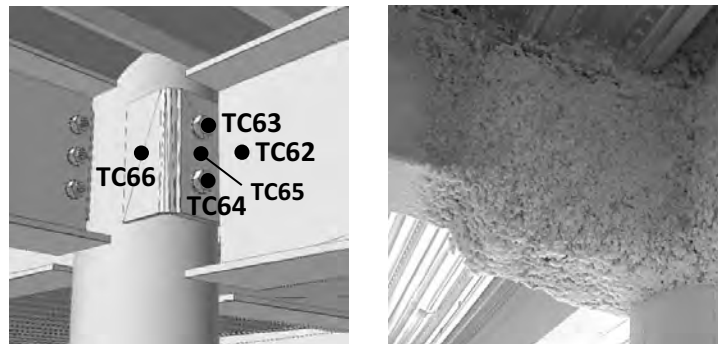


Fig. 6 Fire protected beam-to-column connection (B2-C2 to B2) in the 1<sup>st</sup> floor

Measured temperatures in the fire protected reverse channel connection during the second fire test are shown in Fig. 7. Compared with temperatures in the similar connection without fire protection the applied fire protection with average thickness of 60 mm was able to reduce the temperatures in the connection about 400 °C.

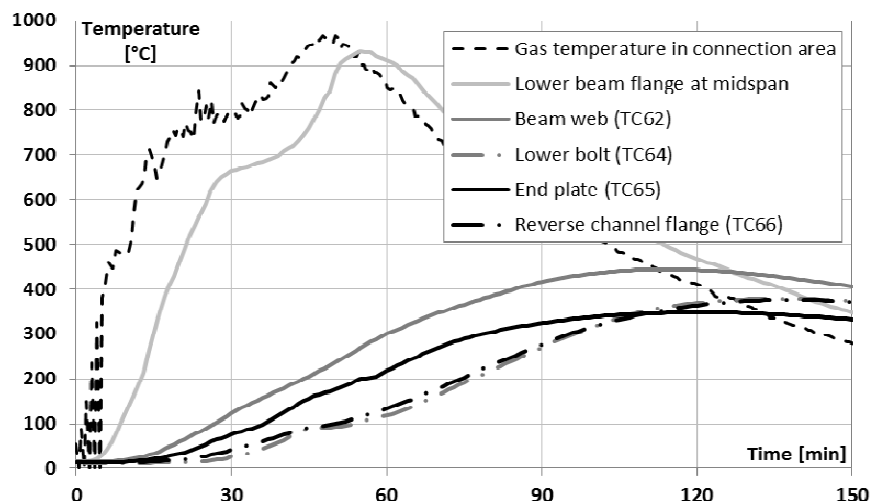


Fig. 7 Comparison of the measured temperatures in fire unprotected reverse channel connection (B2-C2 to B2) with the gas temperature and beam flange temperature in mid-span

### 4 CONCLUSION

Temperature distribution in the connection influences its mechanical behaviour principally through the change in material properties. Steel resistance reduce at elevated temperature. It may be accounted by a factor expressing the ratio between the property at elevated temperature and its ambient temperature value (EN 1993-1-2, 2005).

In Fig. 8 is comparison of the reduction factors for components of reverse channel connection based on the measured temperatures during the second fire test. The figure shows a significant reduction of the mechanical properties of the connection without fire protection unlike fire protected connection. For example at the 45<sup>th</sup> min the value of the reduction factor calculated

from the measured temperature in the fire unprotected lower bolt is 16 %, while the calculated value of the reduction factor is 97 % in the fire protected connection. Utilization of the fire protected connections and beams without fire protection allow to consider the membrane action of a composite ceiling without fire resistance reduction of the connections.

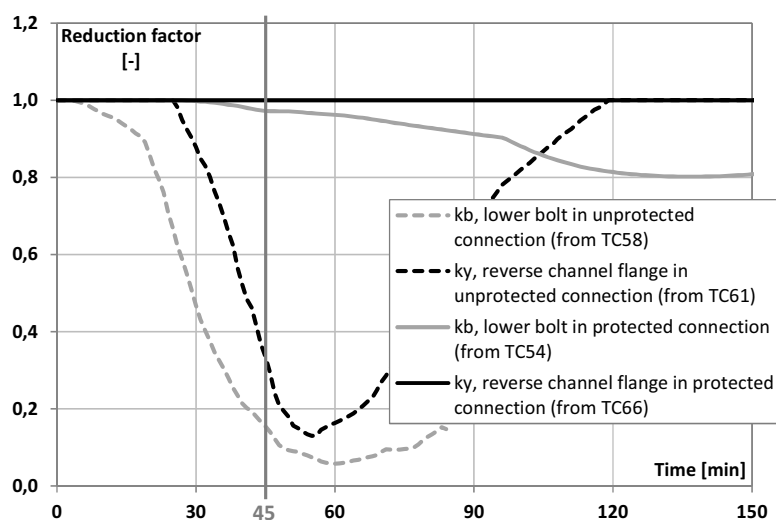


Fig. 8 Reduction of connection resistance through the components in fire unprotected connection (A2-B2 to B2) and fire protected connection (B2-C2 to B2)

## ACKNOWLEDGMENT

This outcome has been achieved with the financial support of grant RFCS COMPFIRE, Design of joints to composite columns for improved fire robustness, and grant SGS12/122/OHK1/2T/11, Modelling of partially protected structures in fire.

## REFERENCES

- CESTRUCO, Design of Structural Connections to Eurocode 3 – Frequently Asked Questions. Ed. Moore D.B., Wald F.: Building Research Establishment Ltd, Watford, 2003, ISBN 80-01-02838-0. URL: [www.fsv.cvut.cz/CESTRUCO](http://www.fsv.cvut.cz/CESTRUCO).
- EN 1993-1-2, Eurocode 3, Design of steel structures - Part 1-2: General rules - Structural fire design, CEN, 2005.
- EN 1993-1-8. Eurocode 3, Design of steel structures - Part 1-8: Design of joints, CEN, 2005
- Franssen, J. M., Numerical determination of 3D temperature fields in steel joints. 2nd International Workshop Structures in Fire, Christchurch, 2002, pp. 2-20.
- Jaspart J.P., Démonceau J.F., Renkin S., Guillaume M.L., European Recommendations for the Design of simple Joints in Steel Structures, ECCS Publ. 126, 90 p., ISBN: 92-9147-000-95.
- SCI P212, Joints in steel construction: Simple connections, London, 2002.
- Wald, F., Simões da Silva, L., Moore, D.B., Lennon, T., Chladná, M., Santiago, A., Beneš, M., Borges, L., Experimental Behaviour of Steel Structure under Natural Fire. Fire Safety Journal 41(7), 2006, pp. 509-522.
- Wald F., Jána T., Horová K., Design of joints to composite columns for improved fire robustness - to demonstration fire tests, Česká technika – nakladatelství ČVUT, 2011, 26 p., ISBN 978-80-01-04871-9.

# STEEL STRUCTURAL FIRE-RESISTANCE DESIGN FOR PROTECTING THE WORLD CULTURAL HERITAGE

Yong Du

Nanjing University of Technology, School of Civil Engineering, Nanjing, China

## Abstract

Minlou is the biggest unit among the world cultural heritage Mingxiao mausoleum erected in A.D. 1405 in Nanjing, China. In A.D. 1853, the timber roof of Minlou collapsed in the fire, and only brick wall survived. To prevent the survival brick wall from weather erosion, a steel truss with timber decorating would be built up in 2008. The finite element analysis was operated to examine the steel truss loading capacity exposed to the most severe fire scenario caused by the combustible timber member. Finally, the fire protection measures were proposed when the structural fire-resistance is satisfied with the objectives of performance-based. The outcome illustrates that steel structural fire-resistance can't depend on results from single element testing in the standard furnace, and provides a snapshot to demonstrate that critical temperature method is efficient for structural fire safety design.

**Keywords:** fire-resistance, fire safety design, steel truss, critical temperature

## INTRODUCTION

Mingxiao tomb buried the first emperor of Ming Dynasty erected in A.D. 1405, composed of a series of buildings. It lies to the east of suburban area in Nanjing, near the west side of Mao Mountain. Minlou is with 39.25m width and 18.4m span which is the biggest building among Mingxiao tomb. The timber roof of Minlou building has been destroyed in the war and brick wall survived in A.D.1853 shown in Fig.1. To prevent the survival brick wall from weather erosion, National Administration of Cultural Heritage approved the emergency measure of rebuilding a roof to cover the survival brick wall. A steel truss with timber decorating was employed shown in Fig.2. There are dozens of corbel arches and hundreds of stock rafters within the steel structural system. Timbers are the fire resource within the service period. To prevent the steel truss from fire, structural design for fire safety is important.



Fig. 1 Minlou building without roof



Fig. 2 Rebuilding roof with ancient shape

## 1 ADVANCED METHOD OF STRUCTURAL FIRE SAFETY DESIGN

The China code CECS200:2006 has been introduced for designing structures to resist fire by calculation. In principle, fire loading can be treated as any other form of loads. However, the structural behaviour in fire in all but the simplest case is much more complex than normal temperature for the material characteristics varied with temperature. Hand calculation

methods aren't suitable to structural thermal analysis. Computer-based finite element methods are employed which include the non-linear material properties temperature dependent and the effects of thermal expansion. The critical temperature method carries out a structural analysis for the fire situation, and check critical temperature in fire limit stat. The basic fire-resistance steps for this project are:

1. Design fire scenario for calculation the maximum temperature of members in the duration.
2. Establish the global finite element model under design loading.
3. Calculate the thermal & mechanical response of global structure at each temperature step ( $\Delta t = 5$  ) and check the loading capacity of each member. When structure collapsed, the critical temperature has been gotten.
4. If the maximum temperature of structures (or elements) subjected to design fire,  $T_m$  , is lower than the critical temperature of structures (or elements),  $T_d$  , given by structural fire analysis, the structural fire-resistance is satisfied without fire protection.
5. If the maximum temperature of members in duration is higher than the critical temperature, design fire protection for steel roof to reduce the temperature. Then go to step3 continued.

## 2 DESIGN FIRE

According to the function of building and the total amount of combustible material, the probable fire scenario can be designed. Fire Dynamics Simulation (FDS developed by NIST) software based on computational fluid dynamic model is employed to simulate the design fire scenario to result the non-uniform fire temperature distribution (Yong, 2005).

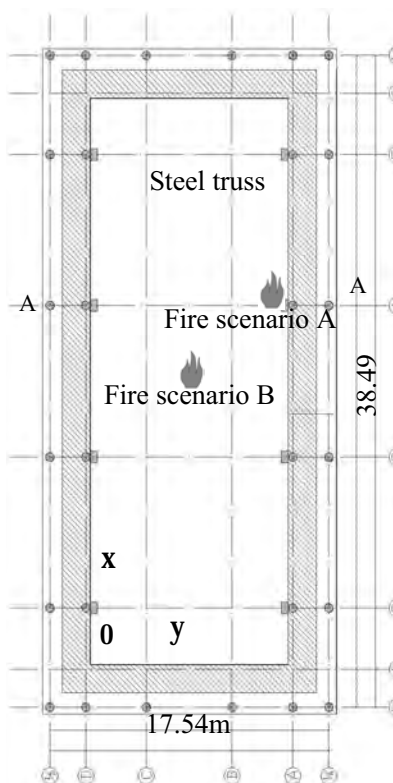


Fig.3 The plane at level 7.15m

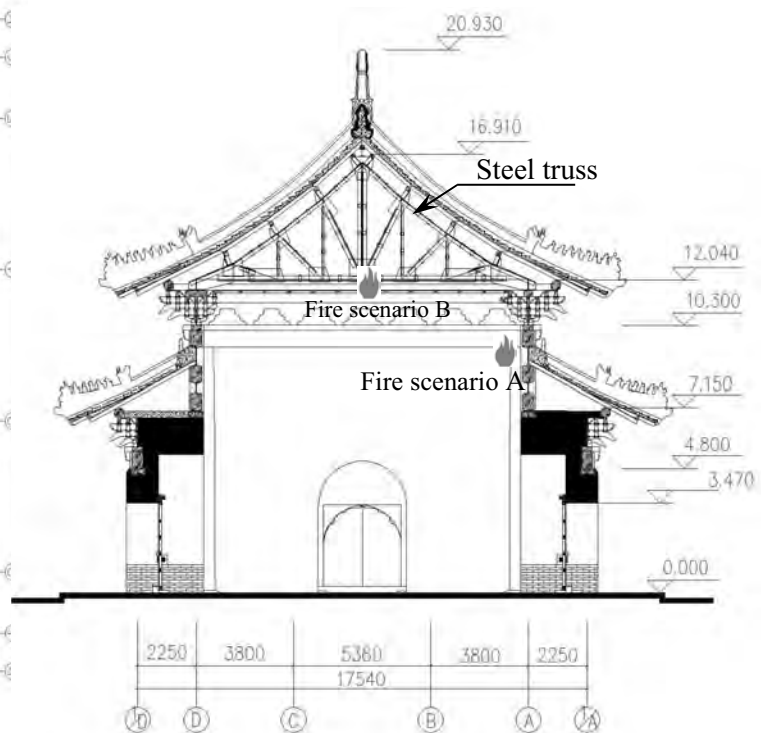


Fig.4 A-A profile

### 2.1 Fire scenarios

Basic premises for design fire are below:

1. There is no heat energy exchange between outside and compartment. The ambient temperature is 20°C.
2. Doors are open as ventilators and the fire is fuel controlled.

3. The fire grows as t-squared type and fire growth coefficient is  $0.04689 \text{ kW/s}^2$ .

Shown in Fig.3 and Fig.4, there is no combustion on the ground, but there are a number of timber elements at the level 7.15m and 10.3m.

Scenario A– dozens of corbel arches are taken for the fire source at the level 7.15m;

Scenario B – a stock beam and wooden ceiling is taken for the fire source at the level 10.3m

## 2.2 Fire heat release rate & smoke temperature

The test on the ratio of heat release (HRR) for wooden piles has been run by Babrauskas and his colleagues since 1980s at NIST. The database is employed to estimate the HRR in Scenario A and B, which is available on NIST web shown in Figure 5 ~ Figure 6. After ignition 10min, the highest HRR is 1.8MW.

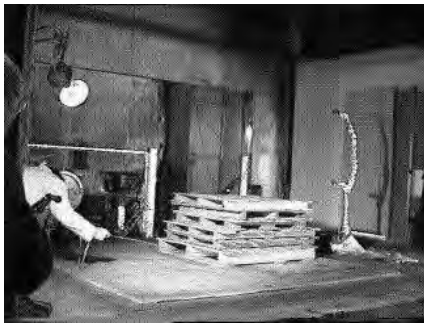


Fig.5 Wooden pile before test



Fig.6 Full development period

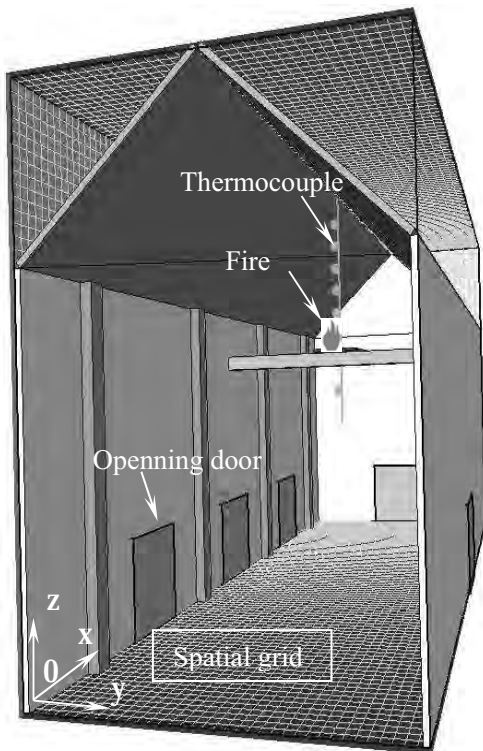


Fig.7 Numerical model for fire

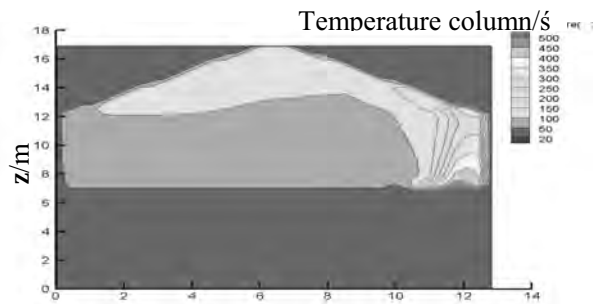


Fig.8 Temperature contours after ignition 30min for scenario A

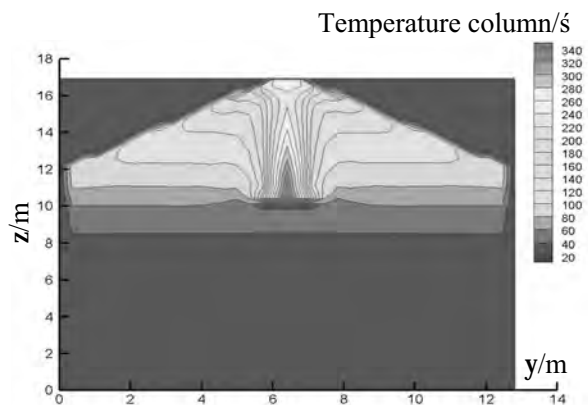


Fig.9 Temperature contours after ignition 30min for scenario B

Considered of fire moving and duration, a conservation fire scenario is designed with 1.8MW heat release for fast T-square growth type and last 1.5h. The fire simulation model shown in Fig. 7 is derived from FDS software to result the non-uniform temperature distribution



Where  $c_s, \rho_s$  specific heat of steel [ $J/(kg \cdot )$ ] and the density of steel [ $7850kg/m^3$ ] respectively

- $\Delta t$  time interval (recommended  $\Delta t$  is not more than 5 seconds)
- $\varepsilon_r$  resultant emissivity representing the radiation transmitted between the hot smoke and the steel member surface [ $\varepsilon_r = 0.5$ ]
- $\varepsilon_s, \varepsilon_f$  emissivity of steel members and flames respectively [ $\varepsilon_s = 0.8, \varepsilon_f = 0.7$ ]
- $\varepsilon_c$  convective heat transfer coefficient [ $25W/(m^2 \cdot )$ ]
- $c_0$  stefan-Boltzmann constant [ $5.67 \times 10^{-8} W/m^2 \cdot K^4$ ]
- $F$  surface area of the unprotected steel member per unit length [ $m^2/m$ ]
- $V$  volume of the unprotected steel member per unit length [ $m^3/m$ ]
- $T_g$  smoke temperature [ $]$ ]
- $T_{sf}$  temperature of the unprotected steel member, which is due to heat transfer by convection and radiant from hot smoke and by flame radiant
- $T_f$  average temperature of flame [ $]$ ]
- $\phi_{sf}$  configuration factor in the particular case of two parallel surfaces
- $\zeta$  ratio of the flame radiated surface for the unprotected steel member

#### 4.1 Configuration factor

The configuration factor is a measure of how much of heat from flames is received by steel member surfaces, between flame area and differential surface of steel members.

The height of flame “ $Z_1$ ” is given by

$$Z_1 = 0.144Q_s^{0.4} \quad (2)$$

where  $Q_s$  is the heat release rate [kW].

Shown in Fig. 13(a), Eq.3 is used, and shown in Fig.13(b) Eq.4 is used.

$$\phi_{sf}^a = \frac{1}{2\pi} \left( \frac{X}{\sqrt{1+X^2}} \tan^{-1} \frac{Y}{\sqrt{1+X^2}} + \frac{Y}{\sqrt{1+Y^2}} \tan^{-1} \frac{X}{\sqrt{1+Y^2}} \right) \quad (3)$$

$$\phi_{sf}^b = \frac{1}{2\pi} \left( \tan^{-1} Y - \frac{1}{\sqrt{1+X^2}} \tan^{-1} \frac{Y}{\sqrt{1+X^2}} \right) \quad (4)$$

where  $X=A/C, Y=B/C; C=H-Z_1$ , shown in Fig. 14.

Induce each geometric parameter into Eq.3 and Eq.4. The configuration factors for each side of the bottom chord, which is made of two angles back to back, can be gotten.

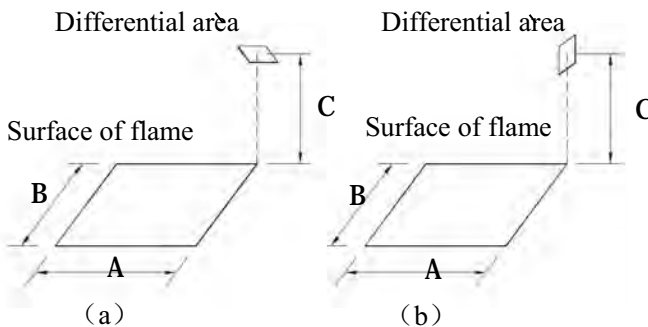


Fig.13 Location of differential area

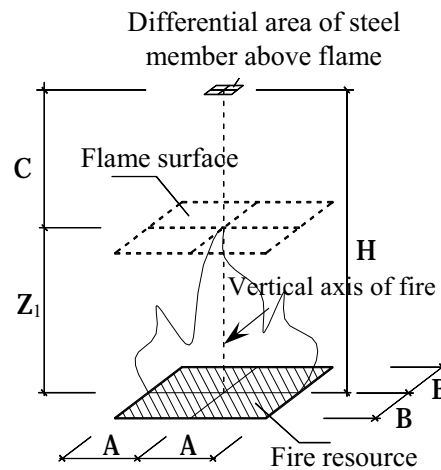


Fig.14 Geometrical data for the configuration factor



### 4.3 Ratio of the effective surface area exposed to flame radiation

$\xi$  is the ratio of the surface area of the unprotected steel member exposed to flame radiation, given by

$$\xi = \sum_{i=1}^n \phi_{sf}^i F_{sr}^i / \phi_{sf} F \quad (5)$$

Where  $F_{sr}^i$  each surface area of unprotected steel members exposed to flame radiation,  
 $\phi_{sf}^i$  configuration factor for each surface of unprotected steel members.

Induce each parameter into Eq.5, the ratio of the surface area of the unprotected chords exposed to flame radiation can be gotten.

Finally, induced parameters given above into the Eq.1, the history of temperature of steel members  $T_{sf}$  can be gotten with step-by-step method. The maximum temperature of steel members in scenario A will reach 550°C during 1.5h duration, and decay from the vertical axis of fires away.

## 5 FIRE PROTECTION

In scenario A the chords above the fire source buckled at the temperature 380°C and regarded as the critical temperature of steel truss.

The fire protect material ensures that the maximum temperature in the steel truss is lower than the critical temperature which would cause structural failure during the fire duration. For given fire protection material properties and the fire duration, the temperature of steel members can be estimated by Eq.6 (Yong, 2006).

$$\frac{T_g - T_s}{T_g - T_g(0)} = -a + (1 + a) \cdot e^{(-b \times 10^{-4} t)} \quad (6)$$

Where  $T_s$  the temperature in steel members,  $T_g(0)$  the ambience temperature (20°C),

$a$  and  $b$  fitting coefficient from reference (Yong, 2006), which are dependent on fire protect material properties  $d_i / \lambda_i$ .

Assuming the rate of the thick of fire protection material  $d_i$  to equivalent thermal conductivity coefficient of fire protection material  $\lambda_i$  is  $d_i / \lambda_i = 0.1$ , then  $T_s = 353$  °C can be derived from Eq.6 for given fire duration 1.5h. The thick of fire protection material  $d_i$  should be determined by  $\lambda_i$  for different fire protection materials.

## 6 CONCLUSIONS

This paper provides a snapshot of information and analysis to demonstrate the critical temperature method is sufficient for fire safety design. A detailed FEA of the space truss was carried out to obtain the critical temperature, and the fire protection measure of the steel roof was carried out. The performance-based structural fire safety design showed that the Minlou roof can maintain its structural loading capacity within 1.5h under fire protection.

## REFERENCES

- CECS 200:2006: National Institute of Standards for Engineering, Technical code for fire safety of steel structures in buildings, CECS 200: 2006 China.
- Yong Du, Guo-qiang Li, Utility temperature elevation empirical formula in large space fire, Fire Science and Technology (in China) 2005; Vol.24 No.3
- Du Yong, Li Guo-qiang. Effects of Flame Radiation on Temperature Elevation of Steel Members in Large Space Buildings Fire. Applications of Structural Fire Engineering, Proceedings of International Conference, Prague, 2009
- Yong Du, Guo-qiang Li, Simplified Algorithm of Temperature in Steel Members in Large Space Fire Based on Field Model, Fire Science and Technology 2006; Vol.25 No.3

## REDUCING DESIGN STEEL TEMPERATURE BY ACCURATE TEMPERATURE CALCULATIONS

Ulf Wickström<sup>a,b</sup>, Alexandra Byström<sup>a</sup>, Joakim Sandström<sup>a</sup>, Milan Veljkovic<sup>a</sup>

<sup>a</sup>Luleå University of Technology, Department of Civil Environmental and Natural Resources Engineering, Luleå, Sweden

<sup>b</sup>Technical Research Institute of Sweden, SP Fire Technology, Borås, Sweden

### Abstract

In this paper an un-insulated I-beam (HE400B) supporting a concrete slab was analyzed. The steel temperature was calculated with the simplest approach according to EC 3 and compared to temperatures calculated considering the cooling by the concrete. In addition the so called shadow effect was considered. The I-beam is then assumed not fully exposed to the incident radiation from the fire as the surfaces between the flanges will be partly shadowed. Temperatures of the I-beam after a fire exposure of 30 minutes was calculated and discussed. The calculations were performed with the finite element code Tasef (Sternier et al, 1990). The mean temperatures of the beam flanges were reduced by more than 200 °C (from 827 °C to 609 °C) when the cooling at the top of the beam and shadow effects were considered. The structure was supposed to be exposed to the standard time-temperature conditions according to EN1363-1 or ISO 834.

**Keywords:** shadow effect, steel structure.

### INTRODUCTION

Eurocode 3: Design of steel structures –Part 1-2: General rules – Structural fire design contains various means of calculating temperature in fire exposed steel structures. For the most commonly used of the calculation methods the temperatures in the steel section are assumed uniform and the thermal properties are assumed constant. However, when following these assumptions the temperatures are often over-estimated which leads conservative and maybe unnecessary costly solutions. In particular the consequences of cooling of steel sections embedded in or in direct contact with concrete structures are not considered in the simplest approximated methods given in EC 3. Only the reduction of the exposed area is taken into account.

In this paper an un-insulated I-beam (HE400B) supporting a concrete slab was analyzed. The steel temperature was calculated with the simplest approach according to EC 3 and compared to temperatures calculated considering the cooling by the concrete. In addition the so called shadow effect was considered. The I-beam is then assumed not fully exposed to the incident radiation from the fire as the surfaces between the flanges will be partly shadowed. Temperatures of the I-beam after a fire exposure of 30 minutes was calculated and discussed. The calculations were performed with the finite element code Tasef<sup>†</sup> (Sternier et al, 1990). The mean temperatures of the beam flanges were reduced by more than 200 °C (from 827 °C to 609 °C) when the cooling at the top of the beam and shadow effects were considered. The structure was supposed to be exposed to the standard time-temperature conditions according to EN1363-1 or ISO 834. Finally it is pointed out that by making more advanced fire modeling including CFD analyses the fire temperatures can be tailored for the particular problem and the calculated temperatures of the steel section can be even more accurate and in most cases further reduced.

## 1 THERMAL MODELING OF AN UNINSULATED I-BEAM

The thermal fire modeling of an uninsulated I-beam can be done more or less accurately. The simplest way is to assume that the beam section is uniformly heated on all exposed surfaces and that the steel at all times reaches the same uniform temperature level. This approximation is often used. The steel section can then be characterized by its section factor only, i.e. the ratio between the exposed area and the volume  $A/V$ , see Eurocode 3 (EN1993-1-2). In the case of a steel beam supporting a concrete slab as shown in Fig.1a only three sides are assumed to be exposed to fire while the fourth side is assumed to neither receive nor lose any heat. In other words it is perfectly insulated, constituting a so called adiabatic boundary. With the simplest assumptions the thermal properties of the steel is constant.

In reality, however, in case of fire heat will be conducted from the steel to the concrete which will reduce the temperature of the steel. In this case the temperature of the steel can no longer be assumed uniform and therefore numerical procedures are needed. Computer codes based on the Finite Element Method are most commonly used for this calculation purpose. By considering a calculation model as indicated in Fig.1b the cooling from the concrete slab, the top flange temperature in particular, will be considerably reduced as well as the average temperature of the steel section. This will be shown by the example below.

Further reduction of the steel temperature are obtained if the so called “shadow effect” is considered. The concept of shadow effects<sup>ii</sup>(Wickström, 2001) was introduced in Eurocode 3 (EN 1993-1-2) to consider the fact that the incident heat radiation received by an open steel section like an I-section is not more than what is received by a so called boxed section. Therefore for the temperature calculation the thermal model is indicated in Fig.1c is applied. Then an artificial surface is introduced between the beam flanges. This surface is then prescribed to follow the fire time-temperature curve. The surface will radiate with an emissivity equal unity to the interior surfaces of the flanges and to the web. Convection may be calculated by assuming convection heat transfer coefficients of the surfaces. In the code Tasef(Sternier et al, 1990)which is used for the calculations reported below the different heat convection transfer coefficients may be applied to the various surfaces creating the void. The introduction of the concept of shadow effects has a similar effect on the temperature calculations as reducing the section factor for the radiation heat transfer part only. The effect on the convection part is not so obvious.

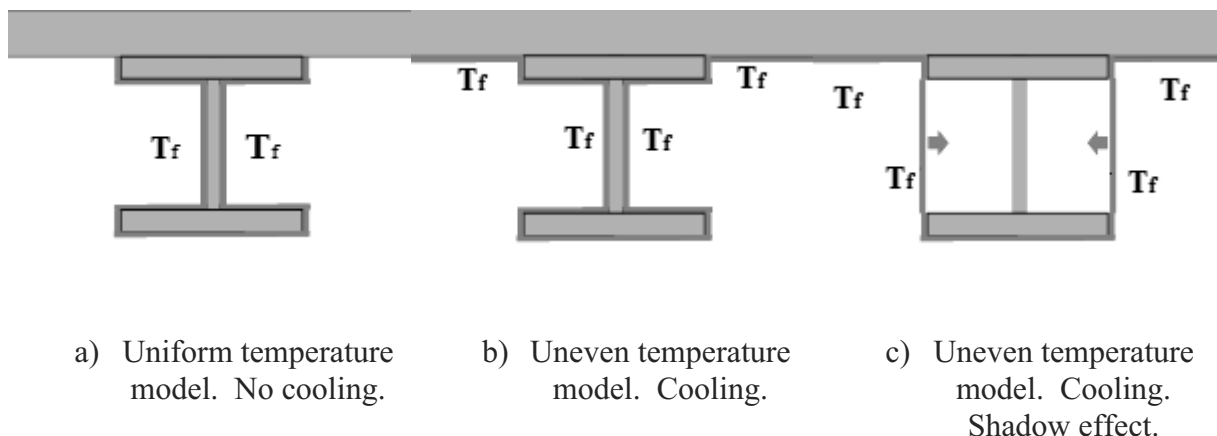


Fig. 1 Three levels of modeling accuracy of an I-beam supporting a concrete slab. The red lines indicates fire boundaries.

### 1.1 An example analyzed with the finite element code Tasef

To illustrate the importance of the various levels of approximations the temperature of an HE400A section was analyzed with finite element code Tasef. The code is a general code for calculating temperature but it is specialized for analyzing fire exposed structures. In

particular the code can be used for calculating heat transfer by radiation and convection in voids or enclosures in structures.

In the example the steel beam supports a 200 mm concrete slab as shown in Fig. 1. The steel beam has a height of 400 mm, 150 mm wide and 40 mm thick flanges, and 30 mm thick web. The thermal properties of the concrete and the steel are according to Eurocode 2 (mean value) and 3, respectively. The boundary conditions are also according to Eurocode when applicable. The surface emissivity of the steel and the concrete are assumed generally to be 0.8.

The beam and a part of the slab were divided into finite element as indicated in Fig. 2. To model the shadow effect an artificial surface is introduced between the flanges as shown in the Fig. 2. The temperature of the inside surface the artificial surface is then prescribed to follow the fire time-temperature curve. The emissivity of the artificial surface shall be unity while the other surfaces around the void are assumed to 0.8 in this case. The heat transfer by convection is calculated by calculating a void gas temperature as the weighted average of the surrounding surface in such a way the total heat transfer between the gas and the surfaces vanishes. Different heat transfer coefficients can be prescribed to the various surfaces. In this case the convection heat transfer at the artificial surface is hard to estimate. Here it is assumed to be as high as  $h_{art} = 50 \text{ W}/(\text{m}^2 \text{ K})$  while for the other surfaces the heat transfer coefficient was assumed to be  $h_{void} = 10 \text{ W}/(\text{m}^2 \text{ K})$ . These estimates are of course uncertain but as the radiation dominates at high temperatures the influence on the steel temperature development is expected to be limited.

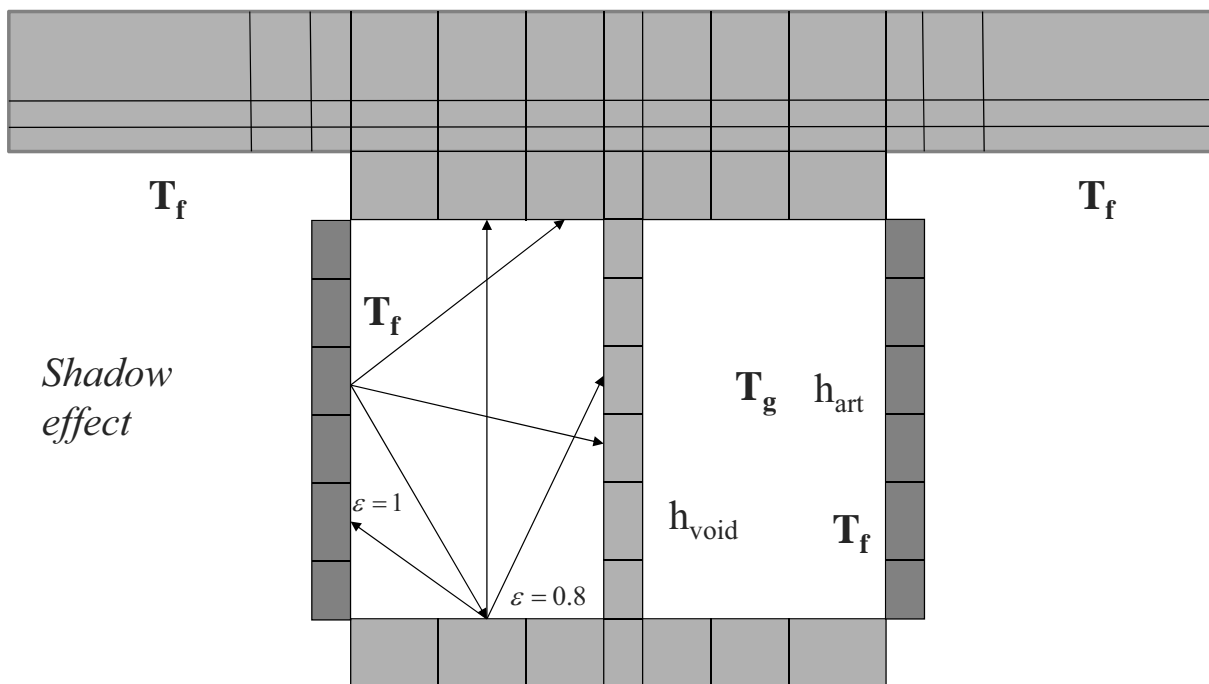


Fig. 2 Finite element model of the beam and slab. The left hand side indicates how the heat transfer by radiation is calculated between each of the element surfaces surrounding the void. The right hand side indicates how the heat is calculated by convection by first calculating the internal gas temperature as a weighted average of the surrounding surfaces.

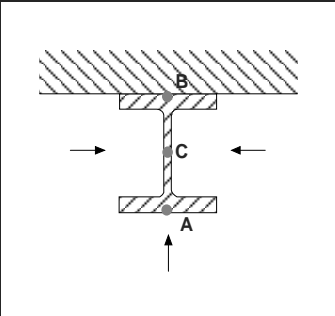
Calculated temperatures after 30 minutes exposure according to the standard fire time-temperature curve according to EN 1361 are given in Tab 1. In all calculations the surface emissivity is assumed equal 0.8 to facilitate the comparisons of the results.

If the simplest method as given in Eurocode 3 is used assuming uniform temperature and constant thermal steel properties the calculated temperature becomes as high as 827 °C. If the cooling of the top flange and varying thermal properties of steel and concrete are considered in a finite element analysis a more accurate temperature distribution can be calculated. The

mean calculated temperature of the flanges then becomes 150 °C lower than the temperature calculated when assuming uniform temperature. The top flange temperature is reduced by almost 220 °C! Note that the middle web temperature is even higher than the lower flange temperature and that it is almost as high as the temperature obtained with the simplest method.

Finally when also considering the shadow effects the calculated steel temperatures become even lower. As shown in Tab 1 the average temperature of the flanges is now almost 220 °C lower than the uniform temperature calculated with the simplest method. The calculated bottom flange temperature is reduced by as much as 325 °C.

Tab 1 Example of calculated temperature in °C of an un-insulated steel I-beam HE400A after 30 min according to five different calculation models. The positions are indicated in the first column.

	Position	Uniform temp Top ins EC	Uneven temp Top cooled Tasef	Uneven temp Top cooled Shadow effect Tasef
	A - top flange	827	749	715
B - bottom flange	827	608	502	
C - web	827	797	719	
<b>Mean (A+B)/2</b>	<b>827</b>	<b>679</b>	<b>609</b>	

## 2 CONCLUSION AND DISCUSSION

The Eurocodes contains simple methods for calculating temperature in structures. These are in general conservative and yields over-estimated steel temperatures and thereby underestimated steel strengths. More accurate and precise estimates can be obtained by considering varying thermal properties and assuming more realistic boundary conditions like cooling from an adjacent structure and shadow effects. In this study only exposure conditions according to standard fire curve has been considered. Even lower steel temperatures can be estimated in some cases by applying more nuanced fire exposures like the parametric curves as presented in Eurocode 1 (EN1991-1-2 Annex A) or by applying advanced CFD calculations. For this purpose considerable interesting work has been carried out by Joakim Sandström using the code FDS. His work will also be presented at this conference.

Several types of insulated steel structures contain real voids where the heat transfer by radiation and convection must be calculated to obtain accurate predictions of steel temperature developments when exposed to fire Fig. 3 shows two examples indicating how an I-section can be insulated with boards of e.g. gypsum or calcium silicate.

## REFERENCES

- Sterner E. and Wickström U., "TASEF – Temperature Analysis of Structures Exposed to Fire," SP Report 1990:05, SP Technical Research Institute of Sweden, 1990.
- Wickström, U. , "Calculation of heat transfer to structures exposed to fire – shadow effects", Interflam 2001.

## INFLUENCE OF ZINC COATING TO A TEMPERATURE OF STEEL MEMBERS IN FIRE

Jiří Jirků<sup>a</sup>, František Wald<sup>a</sup>

<sup>a</sup> Czech Technical University in Prague, Faculty of Civil Engineering, Prague, Czech Republic

### Abstract

This paper describes effect of hot dip galvanizing of steel structure surfaces to temperature of steel members during the fire. Temperature in a set of specimens was measured during the second fire test at experimental building in Veseli nad Luznici. Experiment results show, that the zinc coating can reduce temperature in steel members especially in first fifteen minutes of the fire. The paper describes the process of experiment and analytical evaluation.

**Keywords:** zinc coating, surfacing, emissivity

### INTRODUCTION

Influence of surfacing to the fire resistance is not currently described. A value of surface emissivity of galvanized components for calculations of the fire resistance of steel structures is not specify in Eurocode EN 1993-1-2. Conservatively, the value of surface emissivity  $\varepsilon_m = 0.7$  is considered. This value is used for all steel components.

Surfacing by zinc coating is applied by dipping in zinc bath at a temperature about 450 °C. Therefore, it can reduce emissivity of the surface until the temperature of steel structure reaches this value. After reaching of the temperature about 450 °C, surfacing begins runoff and surface emissivity returns to the value for steel without surfacing. Due to the temperature reduction of a steel member in the initial time of a fire, a temperature curve is moved and fire resistance of steel member 15 or 30 min can be reached without the fire protection.

Experimentally determined value of surface emissivity of galvanized steel members is only valid for the duration of the fire exposure when the temperature of steel member is not higher than approximately 450 °C.

### 1 TEST SPECIMENS

For verification of the effect of surface emissivity of galvanized steel structure to a temperature of steel members in the real fire conditions specimens were placed into compartment in full scale fire test, see Fig 1. The zinc coated specimens were during the second fire test at the first floor of experimental building monitored. The calculated surface emissivity of galvanized elements was verified on the results of fire experiments in a horizontal furnace in 2011. The zinc specimens were hung on logs with a diameter of 10 mm, see Fig 1 under the ceiling structure, in the compartment area with expected highest gas temperature. The arrangement of specimens inside the compartment eliminated an uneven temperature distribution. Members were arranged in pairs, always galvanized and without zinc coated surface. Specimens were isolated at both ends by mineral fiber wool so that the sample simulated the endless element and the heat transfer occur its outer surface only.

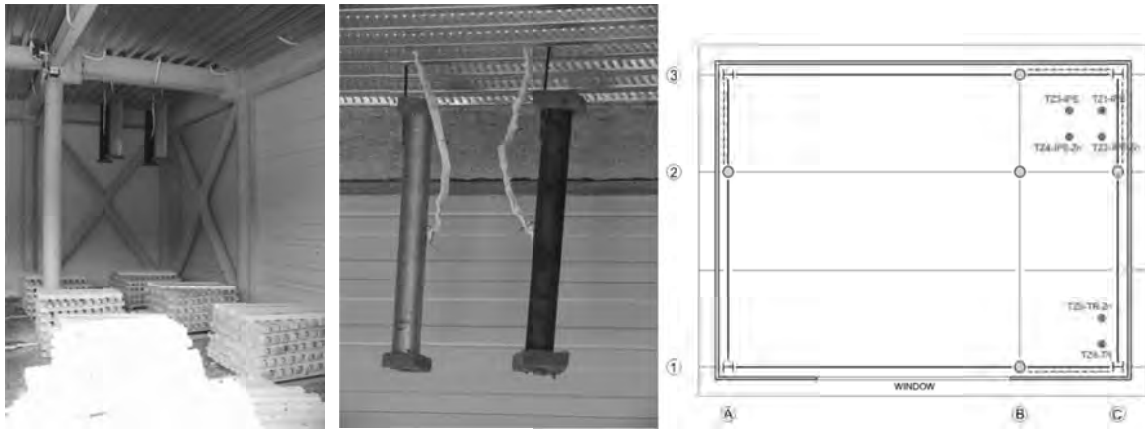


Fig. 1 Specimens under the ceiling of the compartment and location of specimens in the compartment

For the specimens open and closed cross-sections length 1 m were used, see Tab. 1

Tab. 1 Specimens

Specimen	Cross section	Surfacing
TZ1 - IPE	IPE 200	No
TZ2 - IPE	IPE 200	Zn
TZ3 - IPE	IPE 200	No
TZ4 - IPE	IPE 200	Zn
TZ5 - TR	TR 114,3x4	Zn
TZ6 - TR	TR 114,3x4	No

First half of the specimens was done without surfacing – the samples TZ1 - IPE, TZ3 - IPE, TZ6 - TR and second half was galvanized – the specimens TZ2 - IPE, TZ4 - IPE, TZ5 - TR. Identical technology of galvanizing for the both IPE specimens was chosen. Galvanizing temperature reached 447 °C, average coating thickness 157.8 µm, max 171.4 µm, min 138.4 µm. A conventional galvanizing bath without additional chemical elements such as Al, Pb, Bi, Sn, etc. with the chemical composition prescribed for products intended with permanent contact with drinking water was used. A conventional bath for galvanizing of the circular closed cross sections profile TR 114.3 x4, temperature of galvanizing was 458 °C, average thickness of the coating 110 µm was also used.

### 1.1 Specimen's temperature measuring

Temperature of each specimen was measured by one 2 mm diameter thermocouple. This was placed at half height of each specimen. The gas temperature in the fire compartment was measured by twenty 3 mm thermocouples and seven plate thermocouples.



Fig. 2 Detail of surface of zinc coated member after fire

## 2 EVALUATION OF THE FIRE TEST

Step by step method (EN 1993 – 1 – 2, 2005) was for evaluation of the fire test modified. Results are summarized in Tab. 2. Total heat flux increase for galvanized elements was from known gas and steel temperature calculated. Then was a heat transfer coefficient as constant value  $\alpha_c = 4 \text{ W/m}^2\text{K}$  for the specimens without surfacing from the total heat flux and known radiative heat flux calculated. The radiative heat flux of zinc coated specimen and subsequently surface emissivity of zinc coated members from known value of heat transfer coefficient and temperature increase of zinc coated specimen was then derived.

$$h_{net,r} = h_{net} - h_{net,c} \quad (1)$$

where  $h_{net}$  total heat flux [ $\text{W/m}^2$ ]  
 $h_{net,r}$  the radiative heat flux [ $\text{W/m}^2$ ]  
 $h_{net,c}$  convective heat flux [ $\text{W/m}^2$ ]

The calculated values of emissivity for each specimen are shown in the Tab. 2. Resulting emissivity value of zinc coated members was determined as the average from all specimens,  $\epsilon_m = 0.32$ . On Fig 4, 5 and 6 are calculated temperatures with measured with considering an uniform surface emissivity  $\epsilon_m = 0.32$  for all specimens compared. This value is valid until the temperature of steel member reaches the application temperature of zinc coating.

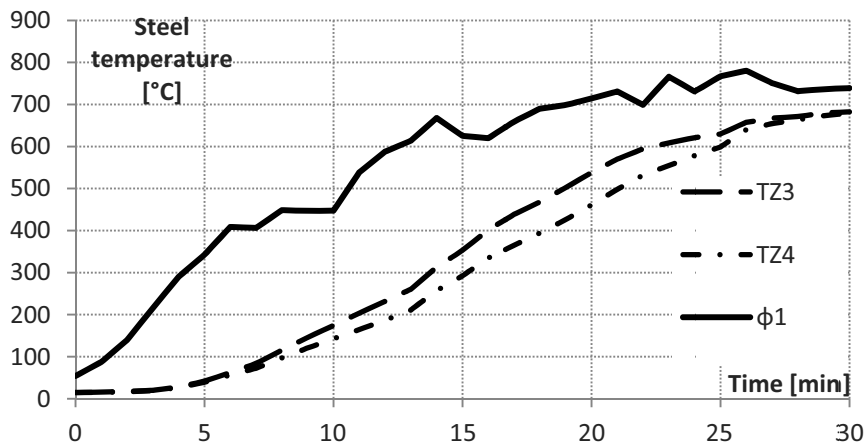


Fig. 3 Comparison of gas temperature ( $\phi 1$ ), measured temperature of zinc coated member (TZ4) and measured temperatures of the element without surfacing (TZ3)



Tab. 2 Calculated surface emissivity of galvanized members

Specimen	Surfacing	Surface emissivity
TZ2 - IPE	Zn	0,290
TZ4 - IPE	Zn	0,280
TZ5 - TR	Zn	0,400

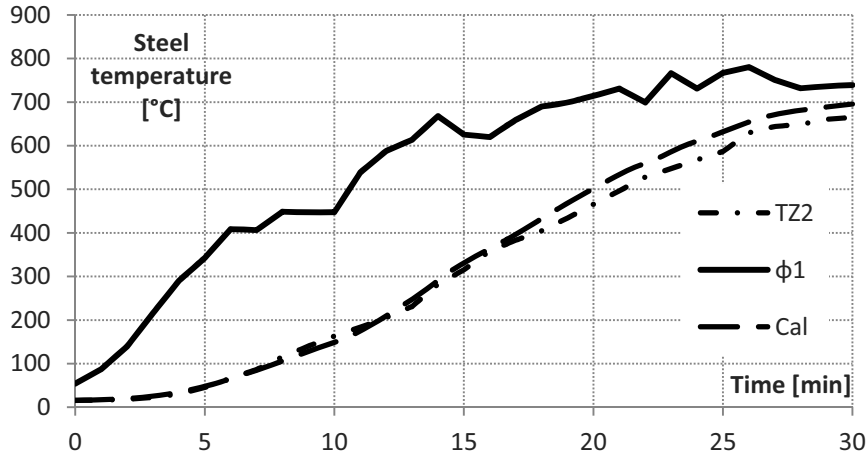


Fig 4 Comparison of gas temperature ( $\phi 1$ ), calculated (Cal) and measured temperature of zinc coated member (TZ2), emissivity 0.32

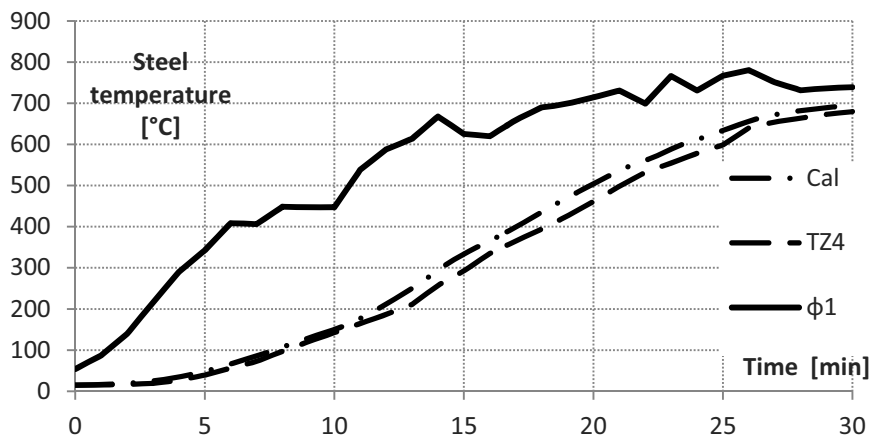


Fig 5 Comparison of gas temperature ( $\phi 1$ ), calculated (Cal) and measured temperature of zinc coated member (TZ4), emissivity 0.32

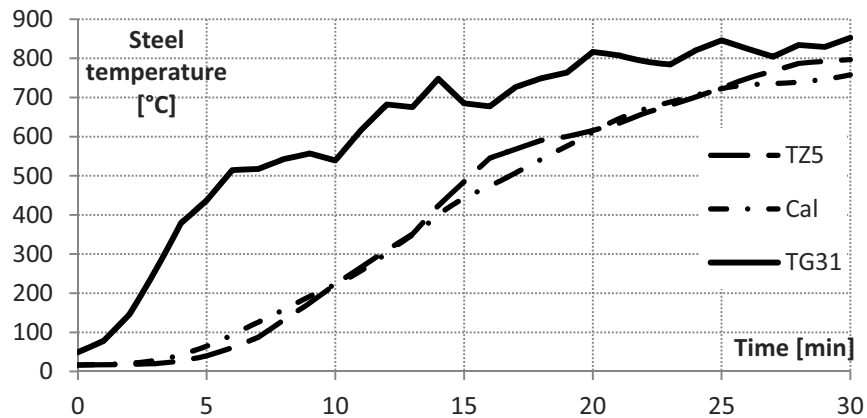


Fig 6 Comparison of gas temperature (TG31), calculated (Cal) and measured temperature of zinc coated member (TZ5), emissivity 0.32

### 3 SUMMARY

Experiment on the real structure shows significant decrease of temperatures of steel members with zinc coated surface in first fifteen minutes of fire. Surface emissivity of zinc coated steel element in the fire (0.32) is less than half of the value of emissivity for steel elements without surfacing (0.7). Next set of specimens is focused on testing influence of zinc coating aging and its effect to surface emissivity in the fire.

### 4 ACKNOWLEDGMENT

This contribution was prepared thanks to support of grant *SGS12/122/OHK1/2T/11, Modeling of partially protected structures in fire.*

### REFERENCES

- EN 1993-1-2, Eurocode 3: Design of Steel Structure, part 1.2: General Rules – Structural Fire Design. British Standards Institution, London, 2005.
- EN 1991-1-2, Eurocode 1: Actions on Structures, Part 1.2: General Actions - Actions on Structures Exposed to Fire, British Standards Institution, London 2002.
- Jirků J., Wald F., Jandera M., Increase of the fire resistance by galvanizing. In: Proceedings: 17<sup>th</sup> Hot Dip Galvanizing Conference. Ostrava, 2011, s. 99-107. ISBN 978-80-254-9364-9.
- Wickström, U.: Heat transfer in fire technology, Luleå tekniska universitet, Luleå 2012, 168 s.





## BENDING ANALYSIS OF BEAMS AFFECTED BY FIRES

M. Salaverry<sup>a</sup>, M. Gillie<sup>a</sup>

<sup>a</sup> University of Edinburgh, School of Engineering, Edinburgh, UK

### Abstract

The fire resistance of reinforced concrete elements can be determined by simple isotherm methods or detailed analyses using a full finite element model. Many design offices do not have sufficient resources to make use of finite element methods and currently must rely on the crude isotherm method. A new methodology of intermediate complexity is presented that determines rapidly the strength of RC beams affected by fire. It is considerably more accurate than existing simple performance based methods, yet is implemented in spreadsheet software that is available to all engineers. Any cross-sectional temperature field can be considered and the method accounts for non-linear and temperature dependent material behaviour in both steel and concrete. It can handle concrete sections of arbitrary cross-section. Results can be numeric or displayed graphically.

**Keywords:** concrete, fire, analysis, excel, isotherm, spreadsheet

### INTRODUCTION

The fire resistance of reinforced concrete elements is normally determined by one of three main procedures which, in increasing order of complexity, are: (i) Using tabulated data from Standard Fire tests which for basic analyses this may be sufficient. (ii) Simple performance based designs using the isotherm method [1]. (iii) More detailed analyses using full finite element models.

A problem with these methods is the enormous gap in complexity between the simplest performance based method (ii) and a full finite element model (iii). Finite element software is expensive to purchase and requires skilled users to produce useful results. Many design offices do not have sufficient funds or expertise to make its use worthwhile for fire design. Consequently they must rely on crude options for assessing the fire resistance of RC structures.

This paper presents a methodology that provides a usable tool to perform calculations to determine the strength of RC beams affected by a fire. It is considerably more accurate than existing simple performance based methods, yet can be implemented in spreadsheet software that is available to all engineers. Any cross-sectional temperature field can be considered and the method accounts for non-linear and temperature dependent material behaviour in both steel and concrete. It can handle concrete sections of arbitrary cross-section. Results can be numeric or displayed graphically.

### 1 OUTLINE OF METHOD

On heating, the key material parameters of a concrete section that affect its capacity to resist load - ultimate stress, ultimate strain change. Since in a typical fire cross-sectional temperatures are non-uniform, the ultimate stress and strain within a concrete section will vary continuously. This has previously been handled very crudely in the “isotherm” method presented in Eurocode 2 [1] where concrete properties are assumed to either remain as at ambient temperature, or be completely removed due to fire. A temperature of 500°C is normally taken as the transition between “strong” and “weak” concrete. This assumption is clearly very crude so to provide a better approach to estimating the strength of concrete members in fire, the method in this paper adopts the following more sophisticated method

1. Determine the temperature field in the cross-section by discretising the section in to (i,j) cells.
2. For each cell, determine the appropriate ultimate strain for its temperature.
3. Determine the cross-section strain distribution assuming i) no cell can exceed its ultimate strain and ii) there is no overall force in the cross-section.
4. For this strain distribution determine the force in each cell based on temperature dependent stress-strain data.
5. Calculate the overall capacity of the section.

The method will be discussed in detail below considering, for simplicity, a rectangular cross-section.

## 2 DETAIL OF METHOD

### 2.1 Heat Transfer

The method requires an estimate of the temperature field in the cross-section being considered in the form of temperatures at each “cell” of a discretization scheme. Cells with typical dimensions of 5 mm are appropriate. The temperature field can be derived by any means and is not, as for the isotherm method, limited to using results from Standard Fire exposure. For this paper, temperatures were derived from an Excel-based 2-d finite difference heat transfer model with an assumption of a Standard fire.

### 2.2 Constitutive Models

Inputs into the method include material constitutive models for both reinforcing steel and concrete. These include temperature dependency of ultimate stress and strain and, if desired, material softening. None of these phenomena are included in the isotherm method. In this paper, data from EC2 has been used but any similar material data would be appropriate.

### 2.3 Strain Distribution

The method presented here modifies the compression block approach typically used at ambient temperature for a different procedure to determine a more accurate shape of the compression zone. Once the temperature field in a section has been obtained, the allowable compressive strain in each cell in the cross-section has to be determined. At ambient temperature a value of 0.003 is widely used in concrete design but this value is not appropriate for elevated temperatures due to the temperature dependency of ultimate strain. Here, a more general value is assumed, the strain at the peak stress  $\epsilon_{c1}$  amplified by a constant  $\beta$  ( $\epsilon_{\text{Allowable}} = \beta \epsilon_{c1}$ ). This value for traditional ambient temperature design takes the value  $\beta_{\text{ambient}} = \epsilon_{\text{design}}/\epsilon_{c1} = 0.003/0.0025 = 1.2$ . Thus, for a given temperature matrix and  $\beta$ , an allowable strain matrix can be determined as indicated for a typical case in Fig. 1.

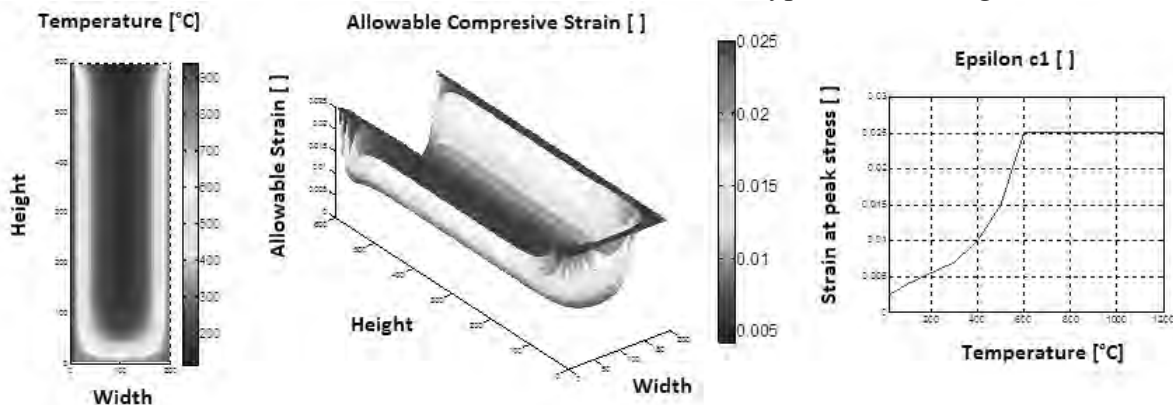


Fig. 1. Temperature profile (Left), Allowable strain  $\beta \epsilon_{c1}$  (Centre) and  $\epsilon_{c1}$  according EC2 (Right).

Assuming that plane sections remain plane after bending, two conditions have to be satisfied in order to calculate the bending resistance of the section: i) The mechanical strain field has to be tangent to the allowable strain field.

$$\max(\epsilon_{\text{mechanical}}^{ij} - \epsilon_{\text{allowable}}^{ij}) = 0 \quad (2)$$

Where  $\epsilon_{\text{mechanical}}^{ij}$  and  $\epsilon_{\text{allowable}}^{ij} = \beta \cdot \epsilon_{c1,T}^{ij}$  ( $\epsilon_{c1,T}^{ij}$  is the concrete strain at peak stress [] and  $\beta$  constant). All parameters are the complete matrices of strains and the difference is taken cell to cell. The point at which this condition is satisfied is the point at which crushing first occurs in the section and corresponds to compression failure of the concrete. The second condition ii) is that there must be no overall axial force in the section, ie:

$$C = T$$

Where  $C$  the total compressive force in the concrete and  $T$  the tensile force in the steel. The strain distribution that satisfies both conditions is determined rotating the mechanical strain plane iteratively. The resulting situation is shown graphically in Figs 2 and 3 for hogging and sagging moment respectively.

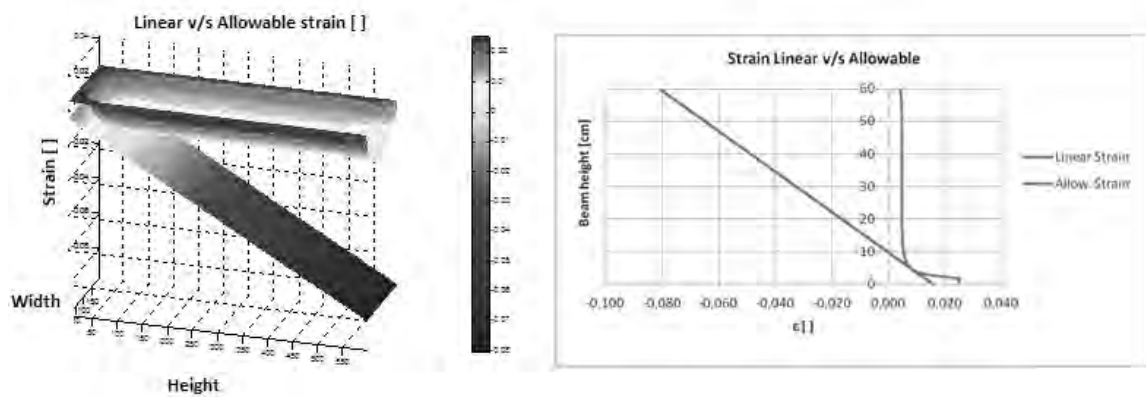


Fig. 2. Interaction between allowable strain and the mechanical strain for hogging moment ( $\beta=1$ ).

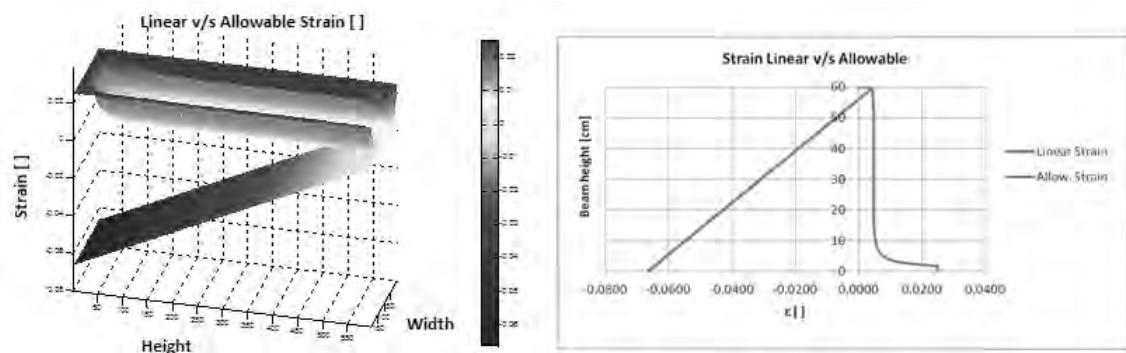


Fig. 3. Interaction between allowable strain and the mechanical strain for sagging moment ( $\beta=1$ ).

#### 2.4 Stress Distribution and Capacity.

With the temperature and strain in each cell determined, it is possible to determine the stress in each cell based on the temperature dependent material data. This leads to a good estimate of high temperature stress block, as indicated in Fig. 4

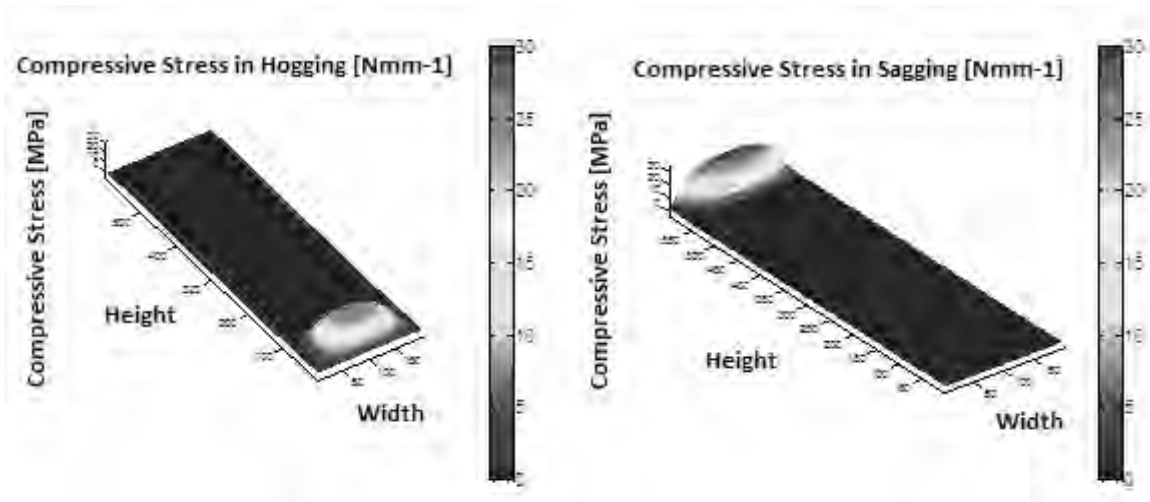


Fig. 4. Stress diagram for hogging (Left) and sagging (Right) moments.

As the coordinates of each cell are known and the value of the stress is also known after the rotation of the mechanical strain plane, the centroid of the compression (C.C) is obtained from.

$$C.C = \frac{\sum f_{ct}^U y_j}{\sum f_{ct}^U} \quad (3)$$

Where  $f_{ct}^U$  is the compressive stress in the concrete cell (i,j) at temperature T [Nmm<sup>-1</sup>] and  $y_j$  the vertical position of the cell. So finally the moment resistance can be determined, as usual.

$$M = (C \text{ or } T) \cdot (d - C.C) \quad (4)$$

### 3 CASE OF STUDY

For this purpose two beams will be compared for two different reinforcement ratios: a) 30 and b) 75% of the maximum reinforcement ratio. For four exposure conditions: a) Ambient T°, b) Standard fire during 60 minutes, c) Standard fire during 90 minutes, d) Standard fire during 120 minutes. And finally, for Sagging and Hogging Moment, totalling 32 cases.

For a beam designed using steel with a yield stress 400 [MPa] and concrete compressive resistance 30 [MPa],  $\rho_{\min}=0.0033$  and  $\rho_{\max}=0.023$ , being  $\rho = A_s/bd$  (ACI 2005, [3]).

#### 3.1 Validation of the method at ambient temperature.

The calculation performed for the four cases was done varying the value of  $\beta$  and studying the flexural resistance. Normalizing the resistance obtained by the resistance obtained at  $\beta=1$  a curve of the enhancement due to  $\beta$  can be obtained.



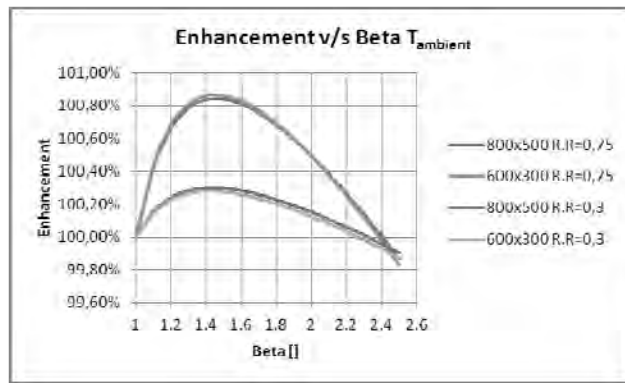


Fig. 5. Enhancement v/s  $\beta$ .

The method captures the fact that the enhancement at ambient temperature is constant for different beam sizes and for different reinforcement ratios. For the cases studied the optimal value of  $\beta$  is 1.4 and the maximum enhancement found was 0.86%. In particular, was found for all cases that when a  $\beta=1.2$  is used, the utilization of the maximum enhancement is 80%.

### 3.2 Behaviour of the method under fire conditions.

A summary of the results obtained is presented graphically for the 32 cases in terms of the enhancement achieved and the optimal  $\beta$  at that point.

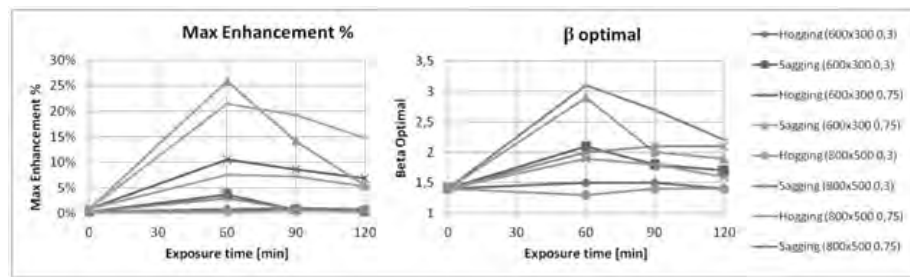


Fig. 6. Maximum Enhancement [%] (Left) and Optimal Beta for max. enhancement (Right).

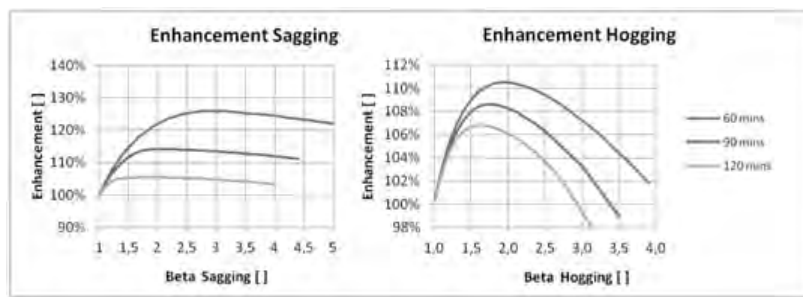


Fig. 7. Enhancement v/s Beta, beam 600x300 with high reinforcement ratio (particular case).

The results for this beam are presented now in detail. The values for resistance obtained by the isotherm method are compared with the resistance calculated from the proposed method for  $\beta=1$  and for the optimal  $\beta$  in each case. The over resistance in the last column correspond to the percentage in resistance obtained from the isotherm method respect to the value at the optimal  $\beta$ .

Tab 1. Summary of the comparison between methods.

Beam	Reinfor. Arrangement.	Moment Type.	Exposure time [min]	Isotherm Resistance [kNm]	Calculated Resistance. ( $\beta=1$ )	Optimal $\beta$	Max. Resistance (Opt. $\beta$ ) [kNm]	Over Resistance (Isotherm Method)
600 x 300	3+3 $\phi$ 16	Sagg.	60	186,97	171,40	2,1	177,69	5%
	3+3 $\phi$ 16	Hogg.	60	247,08	228,38	1,5	230,25	7%
	3+3 $\phi$ 16	Sagg.	90	115,08	117,03	1,8	117,86	-2%
	3+3 $\phi$ 16	Hogg.	90	211,46	196,40	1,5	198,28	7%
	3+3 $\phi$ 16	Sagg.	120	86,94	84,41	1,7	84,75	3%
	3+3 $\phi$ 16	Hogg.	120	179,39	168,68	1,4	170,08	5%
	3+3 $\phi$ 25	Sagg.	60	471,45	323,58	2,9	407,38	16%
	3+3 $\phi$ 25	Hogg.	60	596,42	437,74	1,9	483,85	23%
	3+3 $\phi$ 25	Sagg.	90	318,27	252,47	2	288,09	10%
	3+3 $\phi$ 25	Hogg.	90	525,63	394,90	1,8	428,77	23%
	3+3 $\phi$ 25	Sagg.	120	226,62	199,63	1,9	210,59	8%
	3+3 $\phi$ 25	Hogg.	120	448,75	348,04	1,6	371,81	21%

Note that the highest errors are found in the hogging analysis for high reinforcement ratios and that because no correction due to the high temperature in the corners of the compression block was made.

#### 4 CONCLUSIONS

The proposed method is a useful tool to be used in any engineering office. The results obtained show perfect agreement for ambient temperature using currently recommended allowable strains. Additionally, the traditional method is slightly conservative respect to the method proposed.

A comparison between the isotherm method and the one proposed shows the necessity to correct the isotherm method by considering a compression block with round corners, which reduces its simplicity. In general the results obtained via the isotherm method are slightly higher than the ones obtained with the proposed method, this shows that the isotherm method, while simple, is not as conservative as engineers might think.

Using an approach like the one presented it is possible to study the effect of different assumptions about the allowable compressive strains in concrete. The value of  $\beta$  that produces a maximum resistance varies from 1.4 (In perfect agreement with the value recommended for ambient temperature) to 2.9. In general a good utilization of the enhancement is reached using a value of  $\beta=1.4$  for hogging and  $\beta=2.0$  for sagging moments.

The enhancement achieved is different for different exposures and different fire curves, in this particular case a peak enhancement of 25% was found, which shows the value of studying the maximum allowable strain for design.

#### REFERENCES

- EN1992-1-2: Eurocode 2: Design of concrete structures – Part 1-2: General rules – Structural fire design, 2004.
- Drysdale D; An introduction to fire dynamics, 3rd edition; Wiley, 2011.
- Building code requirements for structural concrete (ACI 318-05) and commentary (ACI 318R-05), ACI American Concrete Institute, 2005

## INFLUENCE OF HIGH TEMPERATURE ON STIFFNESS OF R/C BEAMS

### Experimental stiffness comparison of tensioned or compressed zone of the cross-section

Robert Kowalski<sup>a</sup>, Marian Abramowicz<sup>b</sup>, Michał Głowacki<sup>c</sup>

<sup>a</sup>Warsaw University of Technology, Faculty of Civil Engineering, Poland; r.kowalski@il.pw.edu.pl

<sup>b</sup>School of Fire Service in Warsaw, Poland; marian.abramowicz@sgsp.edu.pl

<sup>c</sup>Warsaw University of Technology, Faculty of Civil Engineering, Poland; m.glowacki@il.pw.edu.pl

#### Abstract

The paper presents results of experimental research whose main topic was determination of stiffness reduction in bent reinforced concrete beams in two cases: when only tensioned or only compressed zone was exposed to high temperature. Twenty four reinforced concrete beams with rectangular cross-section were prepared for the experiment. Eight groups of beams were prepared in total: 2 reinforcement ratio - 0.44 and 1.13% x 2 levels of load - 50 or 70% of destructive force ensuring the constant value of bending moment in the centre part of heated beams x 2 diagrams. Three beams were used in each group. Significant cross-section stiffness reduction was observed in beams where the tensile zone was heated. This was due to considerable elongation of the bars where the steel load elongation summed up with the free thermal strain. In beams where the compressed zone was heated the stiffness reduction was observed only after the time where the tensile zone heated cross-sections were already destroyed.

**Keywords:** reinforced concrete beams, stiffness, fire, high temperature

#### INTRODUCTION

Both load capacity and stiffness of reinforced concrete elements exposed to fire conditions are reduced due to decrease of the mechanical characteristics of concrete and reinforced steel [1, 2]. Sufficiently long exposure of determinable static elements to high temperature resolves in their destruction. In case of indeterminable static structures – leads to a secondary static setup or redistribution of internal forces [3-7].

In bent multi-span elements which are subject to fire exposure in bottom parts it is the tensile zone heated in span cross sections and it is the compressed zone heated in supporting cross-sections. It is well known that as a result of exposure to high temperature the stiffness of span cross sections decreases significantly faster than in support cross-sections [3, 5-7] thus leading to redistribution of internal forces. Adequate quantitative description of stiffness reduction for each cross section has a principal significance for behaviour prediction calculations of the statically indeterminable reinforced concrete elements exposed to fire conditions.

This paper presents a description and results of an experimental program intended to determine the stiffness reduction in cross-sections of bent reinforced concrete beams subject to high temperature only in the tensile or only in the compressed zones.

### 1 EXPERIMENTAL PROGRAM

#### 1.1 Elements

For this high temperature experiment, 24 reinforced concrete beams with rectangular cross-section 140×280 mm, 3500 mm. in length were used. All were made from C25/30 concrete with siliceous gravel aggregate. The main reinforcement was made of two B500SP class steel bars ( $f_{yk}=500$  MPa), diameter 10 or 16 mm (reinforcement ratio  $\rho_1=0.44$  or 1.13%).

Transverse reinforcement with 100 mm spacing made of 6 mm diameter St500b steel bars was applied only in supporting areas. In all beams the reinforcement cover was made in a way that the main reinforcement centre of gravity was 25 mm from the element's front. Dimensions and reinforcement methods are presented on Fig.1.

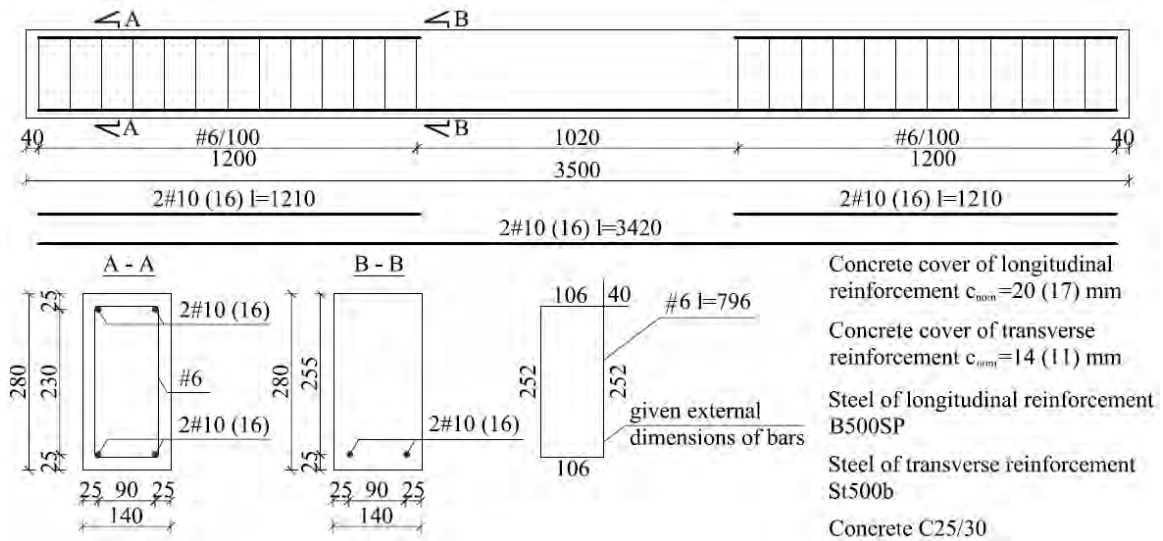


Fig.1. Dimensions and reinforcement of the tested beams

## 1.2 Experiment sequence

There were two static setups used ensuring a constant bending moment in the middle part of the beam heated from the bottom part in both cases. The first setup (Fig. 2a) simply supports the beam at its ends and is loaded with two forces located in 1/3 of the span (tensile zone heated). In the second one (Fig. 2b) the beam was inverted, supports were placed in 1/3 of the span and load applied at its ends (compressed zone heated).



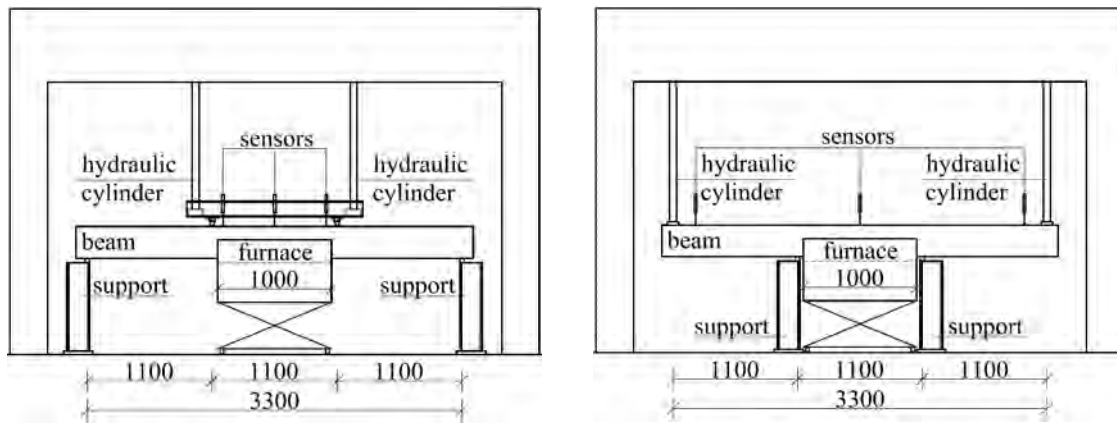


Fig. 2. Photographs and diagrams of the test-bed: a) tensile zone heated, b) compressed zone heated

Experiments in high temperature were executed under application of constant force amounting to 50 % and 70 % of load bearing capacity experimentally determined at room temperature. Overall there were eight series of beams consisting of three equal elements (2 diagrams x 2 reinforcement ratios x 2 load bearing capacity levels) used for the high temperature experiment.

Before high temperature testing a quasi-permanent load action was simulated by loading and discharging each beam eight times to the assumed load bearing capacity level.

Next, a furnace pre-heated to 400°C was placed under the beam reaching about 850°C in 60 minutes. The experiment relied on heating the bottom middle zone of the beam under constant load. The heating time, beam bending and temperature in assigned places were recorded. Fig. 3 presents location of the beam in the furnace cross-section and placement of temperature measurement points.

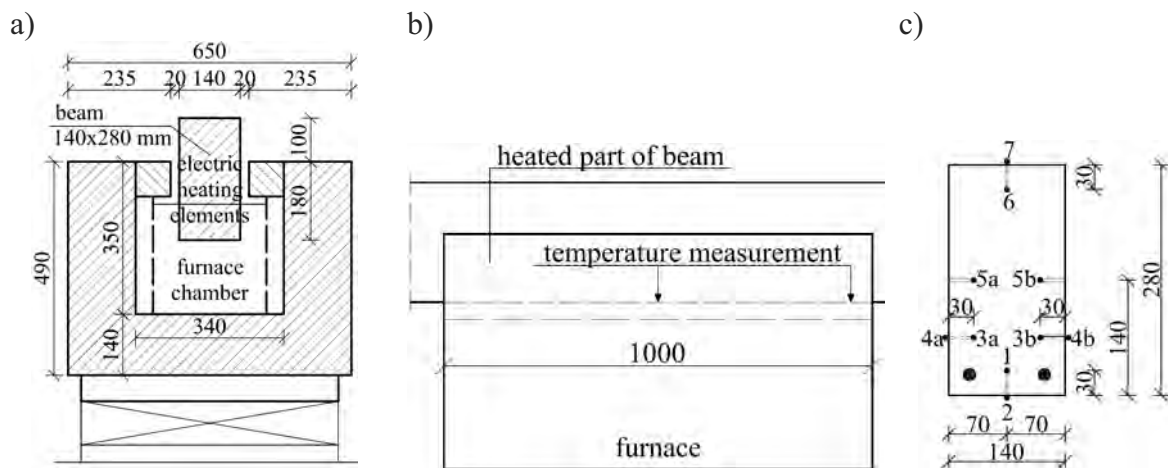


Fig. 3. a) Beam location in furnace cross-section, b) location of temperature measurement cross-sections, c) location of the thermocouples in beam cross-section

## 2 TEST RESULTS

Testing of the beams with tensile heated zone was performed until destruction which occurred after 40-50 minutes. Beams with heated compressed zone showed greater resistance to high temperature and finally were not destroyed during the assigned heating cycle lasting two hours.

Fig. 4, presents median temperature values in the beam's middle cross section in case of compressed zone heated against the standard fire curve.

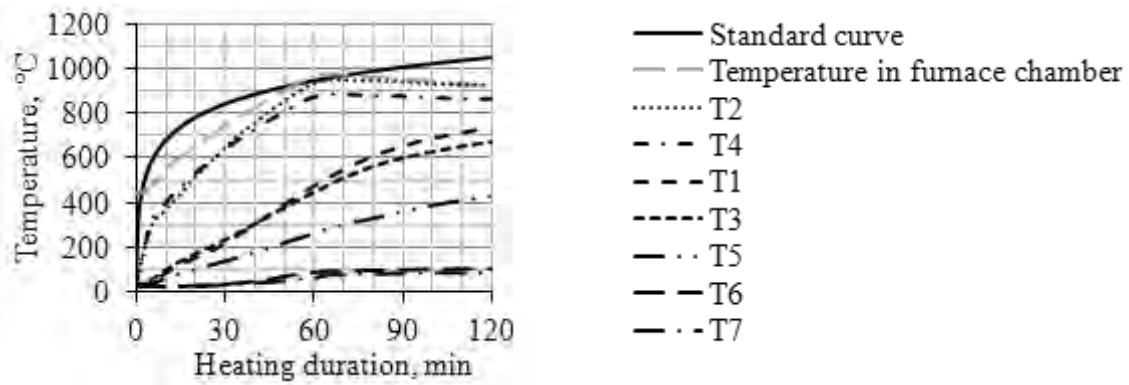


Fig. 4. Graphs for temperature increase in beam middle cross-section and furnace chamber

Fig. 5 presents median deflection graphs from all series of tested beams. In case of the beam's compressed zone heated the deflection value is as sum of results from sensor in the middle of the beam and arithmetic mean from sensors located under the forces.

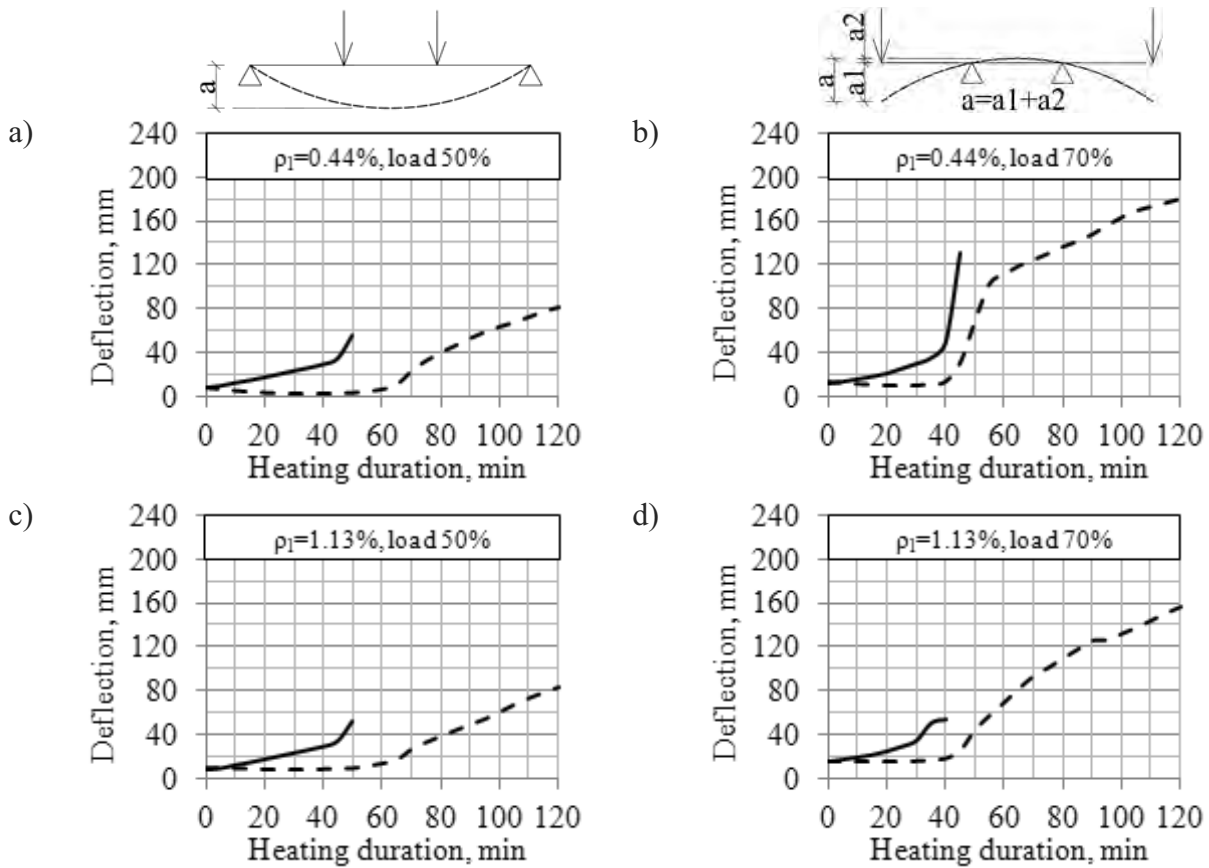


Fig 5. Test results: a)  $\rho_I=0.44\%$ , load 50%, b)  $\rho_I=0.44\%$ , load 70%, c)  $\rho_I=1.13\%$ , load 50%, d)  $\rho_I=1.13\%$ , load 70%; continuous line – tensile zone heated, dashed line – compressed

### 3 RESULT ANALYSIS

In beams with the tensile zone heated there is a significant increase in deflection. Initially it was close to linear then the destruction phase followed. The cross-section stiffness decreased significantly in result of reinforcement temperature increase. This was caused by considerable elongation of the bars where the deflection caused by the load elongation “summed up” with the free thermal steel strain.

In beams with the compressed zone heated there was no deflection increase recorded, in some cases it even decreased while in the same time beams with heated reinforcement were destroyed. This was due to elongation of the fibres in the compressed cross-section zone caused by concrete free thermal strain. The influence of concrete free thermal strain was thus greater than the concrete load induced thermal strain phenomenon [2-5]. This is not surprising as the stress occurring in the compressed zone of the concrete cross-section where not too big. In the initial heating stage median stress levels in the compressed zone can be estimated to: 6-14 MPa, depending on the examined case. The deflection in beams started to increase radically only after about 40-60 minutes, when the temperature of the compressed concrete zone was about 400-600°C.

Basing on the beam deflection one can estimate the cross-section stiffness. It is known that in case of a reinforced concrete element it is relative to the applicable bending moment and is significantly smaller if the cross-section is cracked.

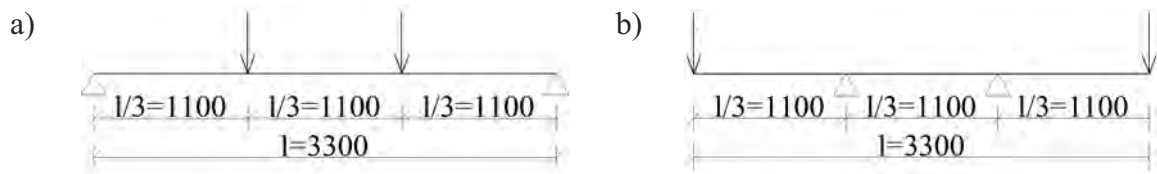


Fig. 6. Static diagram of examined element: a) tensile zone heated, b) compressed zone heated

In practice during calculation of deflections in reinforced concrete elements it is simplified (i.e. [8]) to constant cross-section stiffness in the whole length of the element equalling to a minimal value determined in the location of the maximum bending moment. Thus for further calculations the simplified constant stiffness distribution in the whole length of the examined element was taken. In the applied static setup (Fig. 6) the beam deflection at room temperature (before heating) can be calculated with formula (1):

$$a_{t=0} = \int_0^l \frac{MM}{B} dx = 2 \int_0^{\frac{l}{3}} \frac{MM}{B_{t=0}} dx + \int_{\frac{l}{3}}^{\frac{2l}{3}} \frac{MM}{B_{t=0}} dx = \frac{1}{27} \frac{M_{\max}}{B_{t=0}} l^2 + \frac{5}{72} \frac{M_{\max}}{B_{t=0}} l^2 = \frac{23}{216} \frac{M_{\max}}{B_{t=0}} l^2 \quad (1)$$

where:  $M_{\max}$  – maximal value of bending moment  
 $B_{t=0}$  – beam stiffness at room temperature,  $l$  – beam span.

In the examined beams only the middle section was heated thus it can be assumed that the first element (1) of the formula remained constant during the whole test, while the second one changed its values depending on the stiffness of the cross-section heated to high temperature ( $B_t$ ). The deflection of the heated beam can be calculated for the formula:

$$a_t = 2 \int_0^{\frac{l}{3}} \frac{MM}{B_{t=0}} dx + \int_{\frac{l}{3}}^{\frac{2l}{3}} \frac{MM}{B_t} dx = \frac{1}{27} \frac{M_{\max}}{B_{t=0}} l^2 + \frac{5}{72} \frac{M_{\max}}{B_t} l^2 \quad (2)$$

After transforming dependences (1) and (2) the relative stiffness decrease of the beam heated middle section can be determined from the formula:

$$\frac{B_t}{B_{t=0}} = \frac{15}{23 \left( \frac{a_t}{a_{t=0}} \right) - 8} \quad (3)$$

Fig. 7 presents graphs of relative stiffness decrease in cross-section heated to high temperature depending on heating duration. Values for vertical axis were calculated from formula (3), using experimental deflection values given on graphs at Fig. 5.

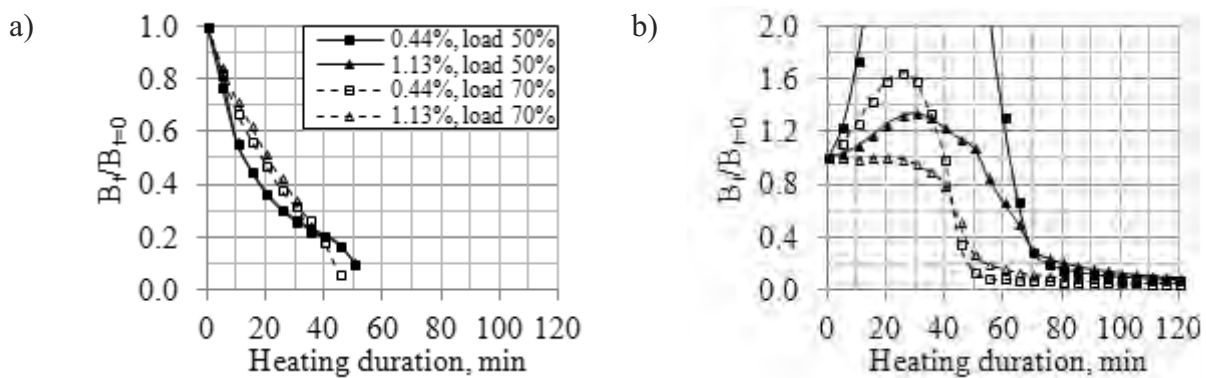


Fig. 7. Graphs of relative stiffness decrease in cross-section: a) tensile zone heated, b) compressed zone heated (descriptions apply to both graphs a & b)

In cases of all beams with heated tensile zone significant stiffness reduction was observed. The relative value decrease was not relative to the beam reinforcement ratio but was relative to their load. In less loaded beams (50% load bearing capacity) already after 12 minutes of heating there was a twofold stiffness reduction. In more loaded beams (70% load bearing capacity) the twofold relative stiffness reduction occurred a little later, after about 20 minutes of heating. This regularity is a consequence of greater deflection values of more loaded beams occurring at room temperature. As it was mentioned before the deflection values in beams with heated tensile zone at initial heating stages decreased a little (or remained roughly constant). Thus values calculated from formula (3) increased. The relatively estimated cross-section stiffness value was increasing more with the decrease of the stress level in the concrete compressed cross-section. This confirms the regularity that concrete in the heated compressed zone expanded freely due to its free thermal strain at the same time contracting due to the load induced thermal strain, [2-5].

Following, after 40 minutes of heating time – in case of bigger load or 60 minutes – in case of smaller load, there was a systematic increase of deflection in the examined beams. This was due to the significant concrete deflection increase (shortening) in the compressed zone heated to about 400-600°C. As a consequence the graphs on Fig. 7b show violent relative reduction of cross-section stiffness, which till the end of the experiment remained on roughly constant low level. However it should be noted that the radical decrease in cross-section stiffness of the heated compressed zone happened only after the cross-sections with tensile zone heated were already destroyed.

#### 4 FINAL REMARKS

In beams with tensile zone exposed to high temperature a significant reduction of cross-section stiffness was observed. This was caused by significant elongation of bars where the deformation due to load action “summed up” with the free thermal strain of steel.

In beams where the compressed zone was heated at initial stages the “fibres” of the compressed cross-section zone elongated. This was caused by the free thermal concrete strain which was greater than concrete deformation due to load (load induced thermal strain).

Results of the performed experiments can be a proof for the regularity that in multi-span reinforced concrete elements exposed to fire conditions at their bottom part one should expect redistribution of bending moments manifested in decrease of sagging moments and increase of hogging moments.



## REFERENCES

- EN 1992-1-2: 2004. Eurocode 2: Design of concrete structures – Part 1–2: General rules – Structural fire design.
- fib Bulletin 38/2007. Fire design of concrete structures – materials, structures and modelling.
- fib Bulletin 46/2008. Fire design of concrete structures – structural behaviour and assessment.
- Kordina K.: Design of concrete buildings for fire resistance. Chapter 6 in: Structural concrete. Textbook on behaviour, design and performance. Second edition. Vol. 4. fib bulletin 54. 2010.
- Kowalski R.: Load bearing capacity calculation of bent RC elements in fire. Publishing house of the Warsaw University of Technology, Warsaw, 2008.
- Kowalski R., Urbański M.: Redistribution of bending moments in multi-span R/C beams and slabs subjected to fire. 7th International Conference AMCM, Kraków 2011, p. 325-326.
- Scott R. H., Whittle R. T.: Moment redistribution effects in beams. Magazine of Concrete Research, 2005, 57, No. 1, February, 9-20.
- EN 1992-1-1;2008. Eurocode 2: Design of concrete structures – Part 1–1: General rules and rules for buildings.

*Experiments performed thanks to financing from the research program of the National Science Centre, Poland no. N N506 431236.*

## ANALYSIS OF CURVED REINFORCED CONCRETE BEAM IN FIRE CONDITIONS

Dušan Ružič<sup>a,b</sup>, Miran Saje<sup>b</sup>, Igor Planinc<sup>b</sup>, Tomaž Hozjan<sup>b</sup>

<sup>a</sup> ELEA iC d.o.o. Civil engineering and consulting, Ljubljana, Slovenia

<sup>b</sup> University of Ljubljana, Faculty of Civil and Geodetic Engineering, Ljubljana, Slovenia

### Abstract

In the paper a novel strain-based finite-element numerical model for the fire analysis of curved reinforced concrete (RC) beams is presented. In addition, the effect of load level and boundary conditions on fire resistance of the curved RC beam is observed.

**Keywords:** curved RC beam, fire, FEM, Reissner beam, moisture transfer, heat transfer, high temperatures

### INTRODUCTION

To design and build significant/important engineering structures properly, such as tunnels, bridges, power plants and dams, certain requirements concerning mechanical resistance and stability of structures must be fulfilled. By fulfilling those requirements we assure engineering structures have sufficient level of safety. Insufficient level of safety can lead into human loss, material damage and pollution of environment. One of the requirements concerning mechanical resistance and stability of structures is fire safety.

Concrete is a heterogeneous material consisting of solid matrix, water and gaseous mixture of dry air and water vapour. When exposed to high temperatures (e.g. in fire) physical and chemical processes within concrete structure occur, such as heat transfer as a result of conduction and convection, release of chemically bonded water and evaporation of free water. This results in lower load bearing capability and higher deformability of concrete structure.

In this paper we present a new numerical model for fire analysis of curved RC beams. Few models for curved beams exposed to fire can be found in the literature, mostly for composite steel-concrete arches (Heidarpour et al., 2010) and steel arches (Bradford, 2006) exposed to thermal loading are presented. The new numerical model consists of three consecutive mathematically uncoupled phases. In the first phase we describe the time dependant change of temperatures of the fire compartment surrounding the beam. In the second (hygro-thermal) phase, heat flux affecting the surface of the beam due to convective and radiative heat flows from the surrounding fire compartment is accounted for in boundary conditions and temperature, pore pressure and free water content in a characteristic cross-section of the curved RC beam are determined implementing the model of Davie (Davie et al., 2006). In the third phase of the analysis the mechanical behaviour (stress-strain state evolution) of the beam during fire employs the geometrically non-linear theory of Reissner (Reissner, 1972) and accounts for axial, shear and flexural deformations. The system of governing equations of the model is solved numerically using the modified principle of virtual work and a strain-based Galerkin-type of FEM. The non-linear stress-strain relations for concrete and rebars at elevated temperatures and the rules for the reduction of material parameters due to an increased temperature are taken from European building code EC2 (EC2, 2004).

### 1 NUMERICAL MODEL

The model for fire analysis of curved RC beams, proposed in this paper, consists of three mathematically uncoupled phases. In the second and the third phase of the fire analysis the

time of fire is divided into time intervals  $[t^{i-1}, t^i]$ , where unknowns are determined with the Newton's iteration method at each time  $t^i$ . In what follows a brief presentation of the three phases will be given.

### 1.1 Fire curves

Time dependent change of temperatures in a fire compartment depends on many parameters and is therefore difficult to predict. Engineers avoid such problem by using simplified parametric temperature-time curves, which define the relation between a gas temperature in the fire compartment and time for standardized situations. One of these fire curves is the hydrocarbon fire curve of the European building code EC1 (EC1, 2004), which represents a fully developed tunnel fire. Once the gas temperature in the fire compartment has been defined, heat and mass transfer in the curved beam can be analysed.

### 1.2 Heat and mass transport model

A coupled heat and moisture transfer in concrete exposed to fire is described by three governing equations of mass conservation of free water, water vapour and dry air and by a governing equation of energy conservation (Davie et al., 2006):

$$\text{Water conservation: } \frac{\partial(\overline{\rho_{FW}})}{\partial t} = -\nabla \mathbf{J}_{FW} - \dot{E}_{FW} + \frac{\partial(\overline{\rho_D})}{\partial t} \quad (1)$$

$$\text{Water vapour conservation: } \frac{\partial(\overline{\rho_V})}{\partial t} = -\nabla \mathbf{J}_V + \dot{E}_{FW} \quad (2)$$

$$\text{Air conservation: } \frac{\partial(\overline{\rho_A})}{\partial t} = -\nabla \mathbf{J}_A \quad (3)$$

$$\text{Energy conservation: } (\overline{\rho C}) \frac{\partial T}{\partial t} = -\nabla \cdot (-k \nabla T) - (\overline{\rho C \mathbf{v}}) \cdot \nabla T - \lambda_E \dot{E}_{FW} - \lambda_D \frac{\partial(\overline{\rho_D})}{\partial t} \quad (4)$$

In Eqs. (1)–(4)  $\overline{\rho}_i$  is the density (mass concentration) of a phase  $i$ ,  $\mathbf{J}_i$  is the mass flux of each phase  $i$  per unit volume of gaseous material,  $\dot{E}_{FW}$  is the rate of evaporation of free water (including desorption), and  $t$  is time. Index  $i$  represents phases of concrete,  $FW$  is free water,  $V$  is water vapour and  $A$  is dry air. In Eq. (4)  $\overline{\rho C}$  is heat capacity of concrete,  $k$  is thermal conductivity of concrete,  $\overline{\rho C \mathbf{v}}$  relates to the energy transferred by fluid flow,  $\lambda_E$  is the specific heat of evaporation,  $\lambda_D$  is specific heat of dehydration and  $T$  is the absolute temperature.

By summing Eq. (1) and (2) we obtain three partial differential equations. The solution is obtained numerically with the finite element method, where the primary unknowns of the problem are temperature  $T$ , pressure of gaseous mixture of water vapour and dry air  $P_G$  and water vapour content  $\overline{\rho}_V$ . For a detailed description of the problem and its numerical formulation, see Davie et al. (2006) or Kolšek (2013) for application to fire analysis of composite structures.

### 1.3 Mechanical model

Once the time and space evolution of temperature and pore pressure in the beam have been obtained, the third phase of the fire analysis can be performed, where the stress-strain state of the beam during fire is finally determined.

In the mechanical model the curved RC beam is modelled by the kinematically exact planar beam model of Reissner (Reissner, 1972). It is assumed that the compatibility of deformations at the contact of the reinforcement and concrete holds. Furthermore, the beam element is

assumed to be under a time-dependant temperature loading and conservative distributed forces  $p_x$ ,  $p_z$  and  $m_y$ . The related governing equations are:

$$\text{Kinematic equations:} \quad x' + u' - (1 + \varepsilon) \cos \varphi - \gamma \sin \varphi = 0 \quad (5)$$

$$z' + w' + (1 + \varepsilon) \sin \varphi - \gamma \cos \varphi = 0 \quad (6)$$

$$\varphi' - \kappa_0 - \kappa = 0 \quad (7)$$

$$\text{Equilibrium equations:} \quad R_x' + p_x = 0 \quad (8)$$

$$R_z' + p_z = 0 \quad (9)$$

$$M' - (1 + \varepsilon) Q + \gamma N + m_y = 0 \quad (10)$$

$$N = R_x \cos \varphi - R_z \sin \varphi \quad (11)$$

$$Q = R_x \sin \varphi + R_z \cos \varphi \quad (12)$$

$$\text{Constitutive equations:} \quad N - N_c = 0 \quad (13)$$

$$Q - Q_c = 0 \quad (14)$$

$$M - M_c = 0 \quad (15)$$

where  $(\circ)'$  denotes the derivatives with respect to  $s$ . Variables  $u$  and  $w$  are the components of a displacement vector and  $\varphi$  is the rotation of a cross-section at the reference axis. Variable  $\varepsilon$  and  $\gamma$  are extensional and shear strains, respectively, while  $\kappa$  represents the pseudocurvature (flexural deformation) of the beam reference axis.  $N$ ,  $Q$  and  $M$  represent equilibrium generalized internal forces, while  $N_c$ ,  $Q_c$  and  $M_c$  denote constitutive generalized internal forces. According to the given stress and strain state on the time interval  $i-1$  and temperature on the time interval  $i$ , the mechanical strains  $D^i = \varepsilon^i + z\kappa^i$  on the time interval  $i$  of any point in the curved beam can be calculated by the equation:

$$D^i = D^{i-1} + \Delta D^i, \quad (16)$$

where  $\Delta D^i$  is the increment of the total strains (also known as the ‘geometrical deformations’) in the time interval  $i$ . Considering the principle of additivity of strains we end up with the strain increment,  $\Delta D^i$ , as the sum of the strain increments due to temperature,  $\Delta D_{th}^i$ , stress,  $\Delta D_{\sigma}^i$ , creep,  $\Delta D_{cr}^i$ , and transient strains of concrete,  $\Delta D_{tr}^i$ :

$$\Delta D^i = \Delta D_{th}^i + \Delta D_{\sigma}^i + \Delta D_{cr}^i + \Delta D_{tr}^i \quad (17)$$

For a detailed description of each strain increment, see Hozjan (2011). The novelty of the presented mechanical model is the introduction of a new strain-based planar curved beam finite-element, which is based on the modified principle of virtual work. For a detailed description of the proposed model a reader is referred to Ružić (2013).

## 2 NUMERICAL EXAMPLE

We consider a curved RC beam exposed to the standard hydrocarbon fire curve as given in EC1 (EC1, 2004) simulating a severe tunnel fire conditions. The curved beam is combined of three radii  $R1$ ,  $R2$  and  $R3$ . The geometrical, cross-sectional, material, reinforcement and loading data of the problem are shown in Fig. 1.

Other data used in the calculations are: density of concrete  $2400 \text{ kg/m}^3$ , density of cement per unit volume of concrete  $300 \text{ kg/m}^3$ , initial temperature  $20 \text{ }^\circ\text{C}$ , initial pore pressure  $0.1 \text{ MPa}$ , initial water vapour content per unit volume of gaseous mixture  $0.013 \text{ kg/m}^3$ , boundary water vapour content per unit volume of gaseous mixture  $0.104 \text{ kg/m}^3$ , initial porosity of concrete

0.15, initial permeability of concrete  $1 \cdot 10^{-16}$  and saturation water content at room temperature  $100 \text{ kg/m}^3$ .

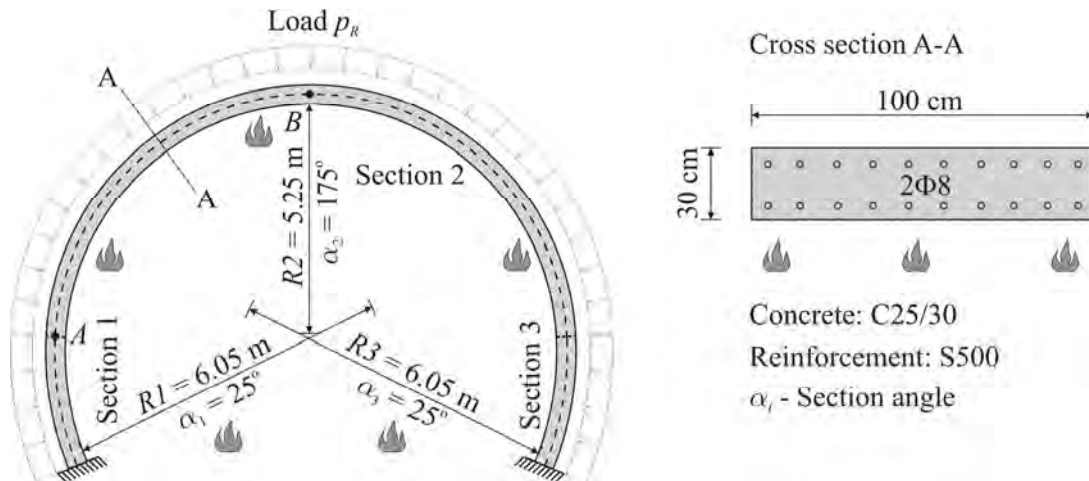


Fig. 1 Geometrical and material properties of clamped curved RC beam

In the hygro-thermal analysis, that we present first, a one dimensional numerical model for a characteristic cross-section of the beam is employed and a mesh consisting of 80 4-noded isoparametric finite elements is used. Furthermore, the time interval  $\Delta t = 0.5 \text{ s}$  is chosen (Hozjan et al., 2011).

The distribution of temperature over the cross-section of the beam at 10, 20 and 30 min is presented in Fig. 2a). As expected we can notice slow heating within the concrete due to its high heat capacity. For instance after 30 minutes of fire, temperature on the boundary is equal to around  $1000^\circ \text{ C}$ , while the temperature in the point of rebar position being 5cm from the exposed surface is equal to only around  $200^\circ \text{ C}$ . This means rebars maintain their initial strength also after 30 minutes of fire exposure.

Fig. 2b) shows the distributions of free water content over the cross-section. As observed from the figure we can notice that captured moisture inside the concrete beam follows the rise of temperature to change partly into vapour while being driven by the water pressure gradient towards the inward of the concrete beam. This driven flow of moisture can be observed in form of increased water front where values of free water content exceed initial values, while region right to the free water front is humid as initially. Region of increased water front mainly occurs due to the condensation of water vapour and by dehydration of chemically bonded water which is released in form of free water.

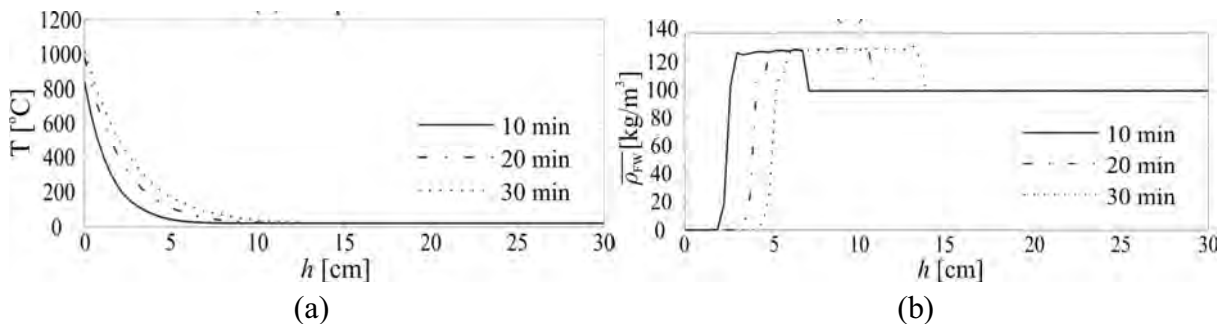


Fig. 2 Distribution of (a) temperature and (b) free water content over the height  $h$  of cross-section at 10, 20 and 30 min

Once the temperature variation in time and space inside a curved RC beam during fire has been obtained, we start with the third phase of fire analysis. In what follows, we first present the convergence tests and then the parametric studies.

We investigated the rate of convergence of the proposed numerical method. Tests were performed for hinged and clamped curved beam with uniform load of  $p_R = 270 \text{ kN/m}$ . In Tab. 1 results for mid span displacement component  $w_B$  (point  $B$ ) of clamped beam with respect to different ratio between the number of finite elements  $N_{el}$  and the degree of the interpolation polynomial  $N_{int}$  are presented. We can notice a good convergence.

Tab. 1 Rate of convergence of clamped curved RC beam

$N_{el} / N_{int}$	8 / 4	16 / 4	32 / 4	64 / 4	128 / 9
$w_B$ (cm)	-2.36	-1.91	-2.12	-2.15	-2.14
Rel. er.(%)	10.048	10.866	1.230	0.181	0.000

In addition we also investigated the rate of convergence for critical time and horizontal displacement component of point  $A$  (see Fig. 1.) which are not presented in the paper. The results were nearly the same as in the previous convergence test. Based on these results we decided to employ 32 finite elements with interpolation polynomial of the 4<sup>th</sup> order for parametric study.

Tab. 2 Critical time, displacement components of points  $A$  and  $B$  for clamped curved RC beam

Load $p_R$ (kN/m)	$N_{el}$	$t_{cr}$ [min]	$w_B$ [min]	$u_B$ [cm]
135	32	20.75	-2.45	1.10
270	32	35.97	-2.12	1.15
540	32	38.89	-1.83	1.44
810	32	17.04	-1.60	1.53

Tab. 3 Critical time, displacement components of points  $A$  and  $B$  for hinged curved RC beam

Load $p_R$ (kN/m)	$N_{el}$	$t_{cr}$ [min]	$w_B$ [min]	$u_A$ [cm]
135	32	10.58	-3.59	2.34
270	32	5.54	-1.92	1.64
540	32	9.87	-6.98	5.37

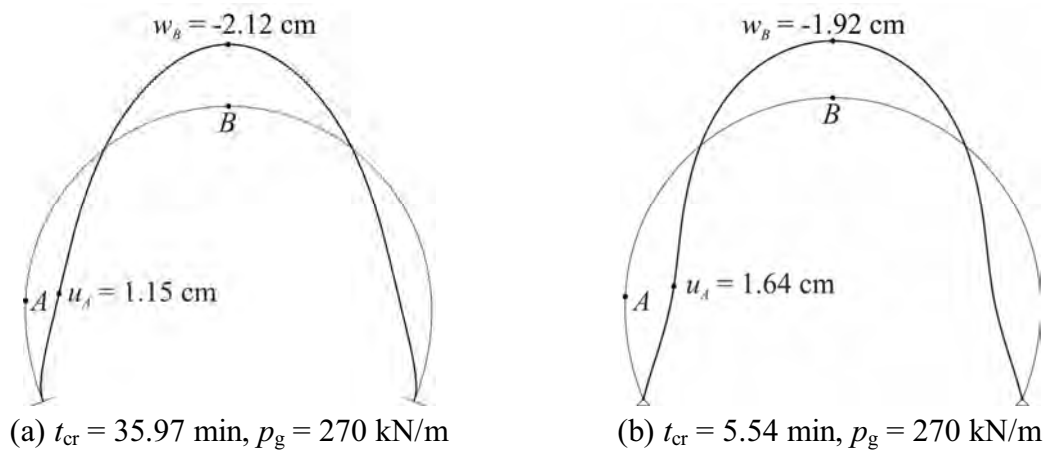


Fig. 3 75 times scaled deformed shape of (a) clamped and (b) hinged curved beam at critical time

In the following parametric study different load levels  $p_R$  are considered for the observed curved RC beam accounting for hinged and clamped boundary conditions. Results are presented in Tab. 2 and 3 as well as in Fig. 3a) and 3b).

The presented parametric study indicates that load level and boundary conditions as well as their coupled interaction significantly affect the stability of the curved beam exposed to thermal loading. Deformed shape of the curved beam due to load and boundary conditions can cause instability as the unsupported lengths of the beam sectors change in the process of deforming.

### 3 ACKNOWLEDGMENT

The work of D. Ružić was partly financially supported by the European Union, European Social Fund. The support is gratefully acknowledged.

### 4 SUMMARY

We presented a new numerical model for the fire analysis of planar curved RC beams accounting for kinematical and material non-linearity. The temperature field in concrete was determined with a coupled model of slow transient phenomena involving heat and mass transport and pore pressure increase in concrete. Furthermore, the strain-based non-linear beam finite-element was involved in mechanical analysis. In the final numerical case the presented beam formulation has been found appropriate for the thermo-mechanical analysis of curved RC beams.

### REFERENCES

- Bažant Z.P., Kaplan M.F., Concrete at high temperatures: material properties and mathematical models. Longman, Harlow, 1996.
- Bradford M.A., Buckling of circular steel arches subjected to thermal loading. Weld World, 50:349–9, 2006.
- Davie C.T., Pearce C.J., Bićanić N., Coupled heat and moisture transport in concrete at elevated temperatures - Effects of capillary pressure and adsorbed water. Numerical Heat Transfer, Part A: Applications 49:733 – 763, 2006.
- Heidarpour A., Pham T.H., Bradford M.A., Nonlinear thermoelastic analysis of composite steel-concrete arches including partial interaction and elevated temperature loading. Eng Struct, 32:3248–3527, 2010.
- Hozjan T., Saje M., Srpčič S., Planinc I., Fire analysis of steel-concrete composite beam with interlayer slip. Comput Struct, 89(1-2):189–200, 2011.
- Kolšek J., Fire analysis of two-layered composite structures, University of Ljubljana, Faculty of Civil and Geodetic Engineering, Doctoral thesis (in Slovene), 2013.
- Reissner E., On one-dimensional finite-strain beam theory: The plane problem. Journal of Applied Mathematics and Physics (ZAMP), 23:795–804, 1972.
- Ružić D., Fire analysis of partially delaminated curved reinforced concrete beam structures, Unpublished manuscript (in Slovene), University of Ljubljana, Faculty of Civil and Geodetic Engineering, 2013.
- SIST EN 1991-1-2, Eurocode 1: Actions on structures – Part 1-2: General actions – Actions on structures exposed to fire, 2004.
- SIST EN 1992-1-2, Eurocode 2: Design of concrete structures – Part 1-2: General rules – Structural fire design, 2005.

# **FIRE RESISTANCE PERFORMANCE OF WELDED BUILT-UP SQUARE CFT COLUMNS WITH REDUCED INTUMESCENT PAINT**

SunHee Kim <sup>a</sup>, KyongSoo Yom <sup>b</sup>, SungMo Choi <sup>c</sup>

<sup>a</sup> University of Seoul, School of Architectural Engineering, Seoul, Korea

<sup>b</sup> Harmony Structural Engineering, Seoul, Korea

<sup>c</sup> University of Seoul, School of Architectural Engineering, Seoul, Korea

## **Abstract**

Welded built-up square CFT columns are widely employed in construction field thanks to their structural efficiencies by avoiding stress concentration area and improving workability in fabrication and maximizing the composite effect enabled by bent ribs. Although welded built-up square CFT columns have structural advantages over other members and are widely used, they are classified as non-fireproof in Korea because the steel tubes are directly exposed to a fire. Thus, fire coating required for the columns by the law results in inefficient design. This study suggests welded built-up square CFT columns with reduced coating to enable improved fire-resistance performance for 2 ~ 3 hours. The purpose of the study is to analyse their fire-resistance performance using the variable of axial ratio which is the major factor in the performance and suggest efficient functional design with reduced coating.

**Keywords:** intumescent paint, BS5950-8, fire-resistance, temperature distribution

## **INTRODUCTION**

In this study, ACT columns without fire protection and fire Intumescent paint were fabricated for loaded heating test to verify the fire resistance performance of interior anchor type concrete filled steel tube columns.

### **1 BACKGROUND OF RESEARCH**

The studies on concrete filled steel tubular columns have been made since early 1990s. Due to the rise in steel price and the development of high-strength materials, the methods to reduce steel amount and use structural members more efficiently have been suggested. Kyongsoo Yom suggested L-channel bending unit with rib shown in Fig 1(a) to utilize the composite effect between the concrete and steel tube. Placing the welding joints at the centre of the 4 sides enhances workability in fabrication and avoid stress concentration area in the corner. Fig. 1(b) shows the cross-section of the column called 'Advanced Construction Technology (ACT)' column developed in 2006. Water pressure test was carried out to verify the welding performance of the columns and evaluate the safety of their welding throat depth. In addition, the studies on the seismic performance and structural behaviour of the columns have been made continuously. Since the construction technology of the ACT columns was certified in Korea in 2011, they have been used in the structures which require high axial force. Although CFT column is recognized as a fire resistant member thanks to its thermal storage effect, it does not provide the fire resistance performance required for high-rise buildings. In order to deal with this shortcoming, reinforcement using steel fibre or steel bar was developed. Most of the studies dealt with the CFT columns less than 400mm in width and those without fire protection. Major studies on the fire resistance of CFT columns were made by the researchers of NRCC (National Research Council of Canada) such as V. K. R Kodur(2004) and T. T. Lie (1995,2005) and those in Fuzhou University, China led by Lin-Hai Han(2003) and sponsored by CIDECT (Comite' International pour le Development et l'E' tude de la Construction



Tubulaire). Kodur and T.T. Lie (2005) observed the thermal and dynamic characteristics of the concrete-filled columns reinforced with steel fibre and developed the numerical approach to forecast the fire resistance of the columns. The employment of CFT columns without fire protection is considered for economic reasons and many studies have been made on their fire-resistance performance. In order to evaluate the fire resistance performance of non-fire protection columns and fire intumescent resistance paint, loaded heating tests were conducted and axial deformation and in-plane temperatures were analyzed.

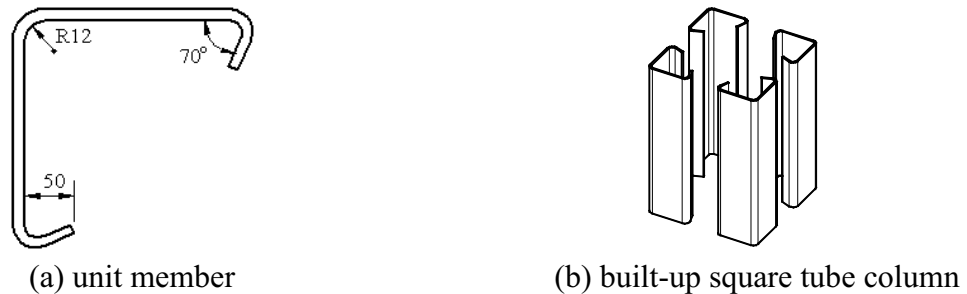


Fig. 1 ACT (Advanced Construction Technology) Column (Choi S.M 2011)

## 2 FIRE RESISTANCE TEST UNDER A LOAD

The columns employed in high-rise buildings should satisfy 3 hour fire resistance requirement. However, it is difficult to secure fire resistance for 3 hours only with steel bar or steel fibre reinforcement because high-rise buildings should deal with greater load. Therefore, fire resistance paint was applied to the ACT columns and their fire resistance was examined. While this method of reinforcement has advantages such as no requirement of finishing touches after painting and easy application of the paint even to joint ends and small spaces, it costs more than fire resistance spray or board. Therefore, thinner layer of the fire resistance paint was applied. Tab. 1 shows the specimen details. All of the 4 columns were made of the same steel ( $F_y = 325$  MPa) and concrete (42.5 MPa). The variables in the test were load ratio and thickness of intumescent coating. Tab. 1 shows the specimens and their specification. 5 thermo couples were installed to measure the temperatures and deformation of the steel and the concrete. The test was carried out in accordance with KS-F 2257-1 standard heating curve and equation 1 and a 1,000 ton heating furnace shown in Fig. 2(a) was used. End-plates (800x800x40mm) were placed at the top and bottom of the specimens to place them at the heating furnace. 6 vent holes consisting of 3 sets were made to release pressure generated in the column. The dimension of the vent holes was 20 mm. Fig. 2(b) shows specimen details including the location of thermo couples and vent holes.

Tab. 1 Specimens List of ACT Column

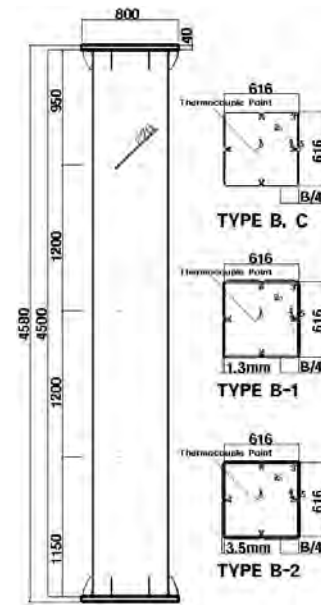
Type	PARAMETER		B(mm)	t(mm)	L(mm)	Load Ratio	Test Load C (kN)
	Main	Sub					
B	Non-Protection	Basic	610	10	4512	0.6	8972
C		Load ratio	611	10	4485	0.5	7476
B-1	Intumescent coating	Paint 1.3mm	616	10	4576	0.6	8972
B-2		paint 3.5mm	616	10	4579	0.6	8972

$$T = 345 \log_{10} (8t + 1) + 20 \quad (1)$$

where T is Heating Temperature ( $^{\circ}$ C), t is time (min)



(a) 10,000 kN heating furnace



(b) specimens details

Fig. 2 Heating furnace, specimen details and location of thermo couples



(a) painting of column



(b) boundary condition

Fig. 3 Application of fire resistance paint and boundary condition

### 3 CROSS SECTIONAL TEMPERATURE DISTRIBUTION

As shown in Fig. 4(a), the temperatures measured at the corners of the concrete (Specimens B and C) rose rapidly. Temperature that measured in specimens B-2 at Concrete centre has decreased. It is estimated that the thermocouple location in an unstable state is gradually stabilized?. The temperatures at 1/4 point from the surface did not exceed 100 °C as shown in Fig. 4(b). The temperatures of the interior anchors in specimens B-1 rose rapidly from 100 minutes due to rapid contraction as shown in Fig. 4(d). Deformation was accelerated when gaps were made between the steel tube and the concrete and interior anchors were separated from the concrete due to the expansion of the steel tube exposed to fire. BS5950-8 has presented simplified equation for the temperature distribution prediction. Predicting Parameter is Fire Resistance time, cross-sectional size and steel tube thickness. Cross-sectional depth of up to 70 mm can be predicted. If the cross-sectional depth greater than 70 mm, can be set to a constant temperature. Simplified method using BS5950 presented internal temperature of steel tube with 600 mm width and 10mm thickness cross-section as shown in Fig. 5. Results are compared with experimental results. Temperature of D/4 point (measurement depth is 150 mm) is less than 100 °C until 60 minutes as shown in Fig. 5.

Temperature of Concrete edge position reaches 400 °C before 30 minutes, which is showing similar behaviour to the experimental results.

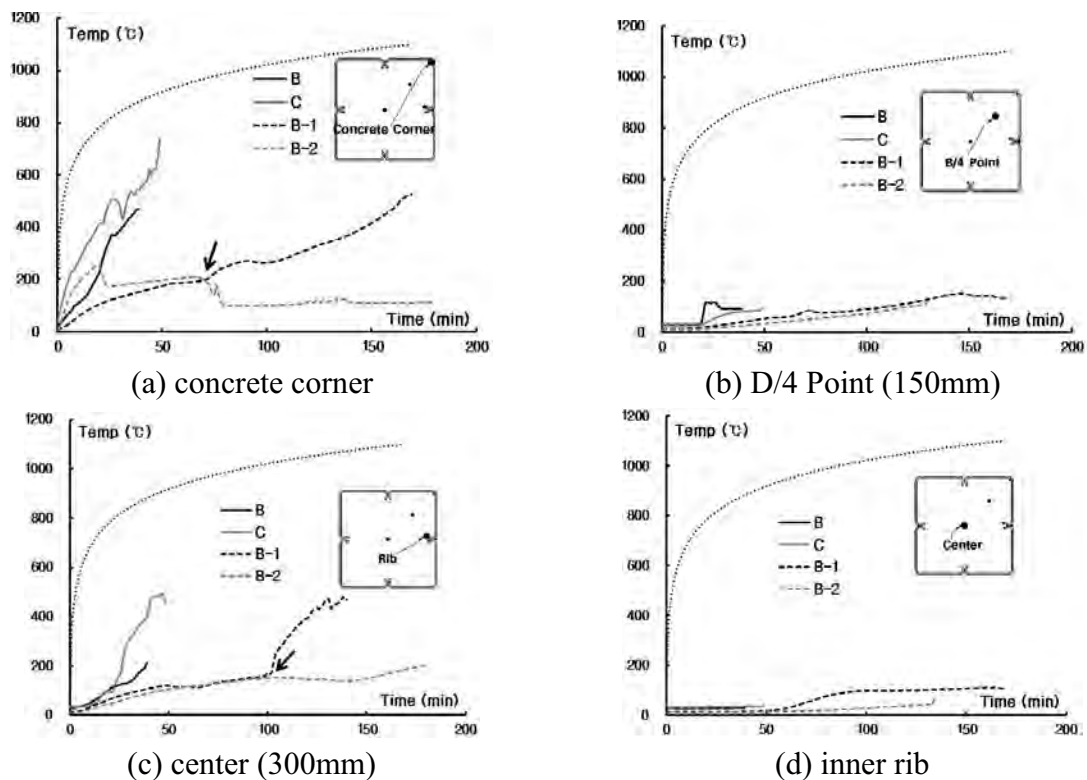


Fig. 4 Cross-sectional temperature distribution of ACT columns

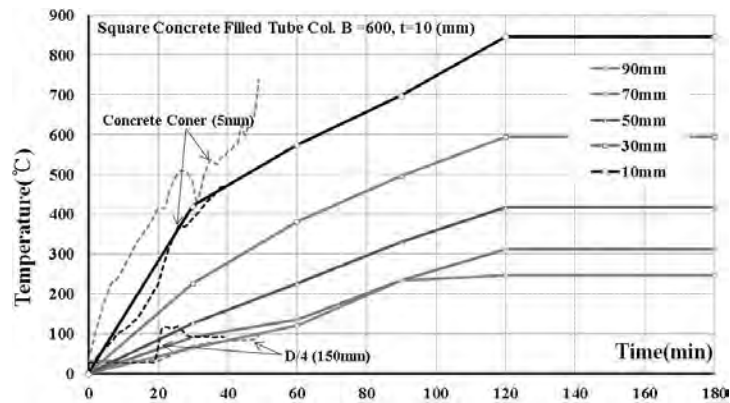


Fig. 5 Temperature distribution verification

#### 4 HIGH TEMPERATURE COMPRESSIVE DEFORMATION BEHAVIOR

Fig. 6 shows the axial deformation of the specimens. The thermal expansion of the steel tubes upon heating caused axial expansion of the specimens B and C. The deformation reached peak in 20 minutes of heating when the furnace temperature was 600~700 °C. Then, axial expansion stopped and contraction deepened due to the deterioration in the load capacity of the steel tubes and the local buckling of the tubes at their ends and the load to the exterior tubes was transferred to the concrete and interior tubes. Therefore, specimens B and C showed rapid contraction. The specimen with 3.5mm-thick-layer of fire resistance paint displayed gradual axial expansion for the 180 minutes of heating and the steel tube did not contract. As the fire resistance paint was exposed to fire, it formed fire-blocking layers. The

layers turned white and finally became like black lumps of charcoals. Since temperature rise was delayed, the specimen resisted fire for 180 minutes. In the specimen with 1.3mm-thick-layer of fire resistance paint, the steel tube expanded gradually and resisted fire for 170 minutes.

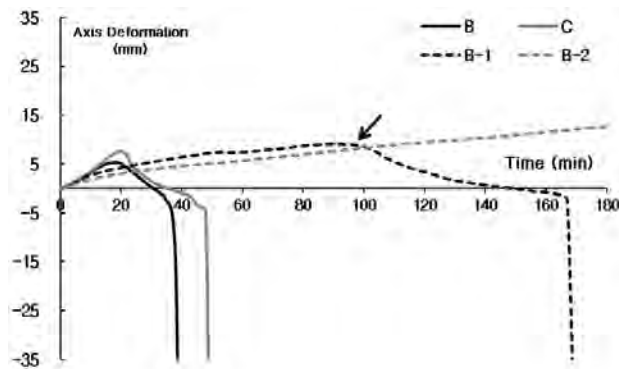


Fig. 6 Axial Deformation of ACT Column as Exposure Time

Tab. 2 summarizes the weight, length and width of the specimens before and after the test. Fig. 7 shows the failure mode of the specimens at the termination of the test. The difference in weight was the biggest in specimen B-2 because the moisture in the concrete vaporized and the surface of the steel tubes was oxidized during the 3 hours of heating.

Tab. 2 The dimensions of Specimens before and after heating  
(A: Before Heating , B : After Heating // Unit : mm or kg)

	A Weight	B Weight	Weight gap	A Length	B Length	Length gap	A Width	B Width	Axial Expansion
B	4820	4740	80	4578	4512	66	610	632	5.3
C	4860	4750	110	4576	4485	91	611	635	7.6
B-1	4910	4710	200	4576	4515	61	612	658	10
B-2	4960	4810	150	4579	4575	4	614	615	13

As shown in Fig. 7, the center of the specimen with 1.3mm-thick-layer of fire resistance paint turned black, while the 3.5mm-thick-layer of fire resistance paint swelled with tiny cracks on it.

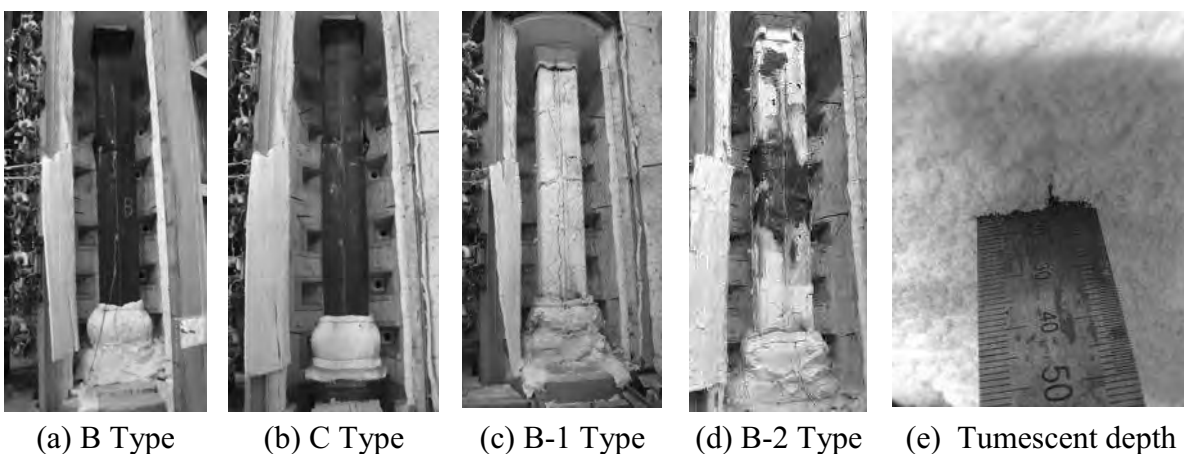


Fig. 7 Failure mode of specimens

In the latter, the swell was about 15mm deep, indicating fire resistance duration of over 180 minutes. It is deduced that 1.8~3.5mm-thick-layer of fire resistance paint is appropriate for economically efficient fire resistance design. Additional studies should be conducted to find the optimal thickness of fire resistance painting. For the verification method, interpretation of the simulation analysis between the result of the experiment and variables is needed. The prime variable is thickness of the steel tube, since the effect of reinforced fire resistant paint in concrete-filled steel tube and general steel tube is different. Therefore, the thickness of the paint can differ by thermal conduction rate of the steel tube. These results could not be included in this study, but continuous research will be in progress.

## 5 SUMMARY

In this study, ACT columns without fire protection and fire intumescent paint were fabricated for loaded heating test to verify the fire resistance performance of interior anchor type CFT columns. The conclusion of the study to enable economically efficient fire resistance design is as follows. In the ACT specimens without fire protection, the interior anchor was exposed to high temperatures and the fire resistance performance of the columns was deteriorated due to thermal expansion. Since the cracks at the concrete reduced confinement effect rapidly, load ratio should be adjusted downward to below 0.5 to secure the fire resistance duration of more than 60 minutes. Also, the temperatures at the ACT columns reinforced with fire resistance paint were stable and noticeably lower until 180 minutes compared with the other 2 groups of specimens. A member with 3.5mm thickness of the fire-resistant paint has shown only axial expansion for 180 minutes and compressive deformation has not appeared. In other words, strength reduction by high-temperature has not happened and could get satisfying result of three hours of fire resistant performance.

## REFERENCES

- D.K. Kim, S.M. Choi, Structural Characteristics of CFT Columns Exposed to Fire, International Japan-Korea Symposium on Advanced Engineering and Science, 2000. 11
- D.K. Kim, S.M. Choi, J.H. Kim, K.S. Chung, S.H. Park, Experimental Study on Fire Resistance of Concrete-filled Steel Tube Column under Constant Axial Loads, International Journal of Steel Structures, Vol.5, No.4, pp.305-313. 2005
- K.S. Chung, S.H. Park and S.M. Choi, Material Effect for Predicting the Fire Steel Tube Column under Constant Axial Load, Journal of Constructional Steel Research, 64, pp.1505-1515. 2008
- S.H Lee, S.H Kim, S.M Choi, Water pressure Test and Analysis for Concrete Steel Square Columns, Journal of Constructional Steel Research 67, pp1065 -1077, 2011
- L.H.Han, Y.F. Yang, Lei Xu, An experimental study and calculation on the fire resistance of concrete-filled SHS and RHS columns, J.Constr. Steel Research 59, pp.427-452. 2003
- T.T.Lie (1980), "New facility to determine fire resistance of columns", Canadian Journal of Civil Engineering 7(3): pp551-558.
- T.T.Lie, R.J.Irwin (1995) Fire resistance of rectangular steel columns filled with bar-reinforced concrete, Journal of Structural Engineering, ASCE, pp.797-805.
- T.T.Lie and V.K.R.Kodur (1996), "Fire resistance of steel columns filled with bar-reinforced concrete", ASCE Journal of Structural Engineering 122(1): pp30-36.
- T.T.Lie and V.K.R.Kodur (1996) Fire resistance of circular steel columns filled with fiber-reinforced concrete, Journal of Structural Engineering, ASCE, pp.776-782.
- V.K.R.Kodur and T.T.Lie (1995), Experimental Studies on the Fire Resistance of Circular Hollow Steel Columns Filled with Steel-Fibre-Reinforced Concrete, IRC Internal Report No.691, National Research Council of Canada, Ottawa, Ontario, Canada.

## **FLEXURAL CHECK AT HIGH TEMPERATURES of reinforced concrete bridge decks strengthened with EBR-FRP**

E. Nigro<sup>a</sup>, A. Bilotta<sup>a</sup>, I. Del Prete<sup>a</sup>

<sup>a</sup> University of Naples Federico II, Department of Structures for Engineering and Architecture, Naples, Italia

### **Abstract**

In this paper the thermo-mechanical behaviour of RC bridge decks strengthened with externally bonded FRP laminates is investigated by considering environmental conditions responsible of thermal states different from the normal ones. A parametric analysis is performed by varying the slab thickness, the FRP reinforcing percentage, the type of fibre and the thickness of the protection layer. The results are given in terms of ultimate bearing capacity of the slabs, which allows individuating the conditions responsible of premature FRP-to-concrete debonding or temperature levels greater than the glass transition temperature of the adhesive.

**Keywords:** concrete slabs, FRP, fire resistance, debonding

### **INTRODUCTION**

Fibre reinforced polymers (FRP) are composite materials successfully applied to repair and/or strengthen RC structures. For external strengthening of reinforced concrete structures the FRP laminates are bonded to the exterior of concrete using adhesive resins, like epoxy resins, phenolic resins and other types, ensuring to transfer forces between the concrete and FRP through shear stresses that develop in the adhesive layer. However, degradation of mechanical properties of composites by various environmental effects such as elevated temperatures, moisture absorption and cycling loads is a very important factor in durability predictions of composite materials (Springer, 1984 – Buggy et al, 1994). Especially, a critical condition occurs when the glass transition temperature  $T_g$  of the polymer matrix is achieved, determining shear capacity reduction in resin and the following fibre's overloading. Application of FRPs have been limited primarily to bridges, where fire is not a primary consideration during design (Bisby et al 2005). Nevertheless, in this paper the thermo-mechanical behaviour of RC bridge decks strengthened with externally bonded FRP laminates is investigated by considering environmental conditions responsible of thermal states different from the normal ones. The examined cases are: (a) bituminous paving cast in place on a bridge deck at temperature  $T=180^{\circ}\text{C}$ ; (b) fire exposure over the bridge deck.

### **1 BEHAVIOUR OF FIBRE-REINFORCED COMPOSITES AT ELEVATED TEMPERATURE**

Several researches on thermal behaviour of FRP materials are nowadays available in the scientific literature. In the following the main results are briefly summarised in order to deduce basic information on the thermo-mechanical properties of the various FRPs types and the FRP-to-concrete interface behaviour at high temperature.

#### **1.1 Thermo-mechanical behaviour of FRPs**

In order to study the behaviour of RC slabs strengthened with FRP at high temperatures it is necessary to know the thermo-mechanical properties of the constituent materials; Eurocode 2 - Part 1-2 gives the thermo-mechanical properties for concrete and steel bars, while the main theoretical and experimental contributions concerning the behaviour of FRP composite materials

and adhesive resins at elevated temperature are summarised in (Blontrock et al, 1999) and in (Bisby et al, 2005). Based on experimental data assembled by (Blontrock et al, 1999). Fig. 1 show exponential best-fit curve of the temperature-dependent reduction coefficient of the tensile strength referred to various types composites with carbon fibres and epoxy matrix. Temperature-dependent curves may be still obtained in an analogous way for the FRP elastic modulus. Finally, the assumption of elastic-brittle constitutive law is still suitable, obviously defined by values of tensile strength and elastic modulus reduced due to elevated temperature.

## 1.2 FRP to concrete bond at elevated temperature

FRP-to-concrete bond ensures to transfer the interaction forces between RC beam and external FRP plate or sheet, assuring suitable performances of the strengthened structural member as a whole. The interaction forces are transferred through the polymer matrix or adhesive, whose mechanical properties deteriorate as temperature increases. In particular, loss of bond may occur if the glass transition temperature  $T_g$  is achieved in the adhesive.

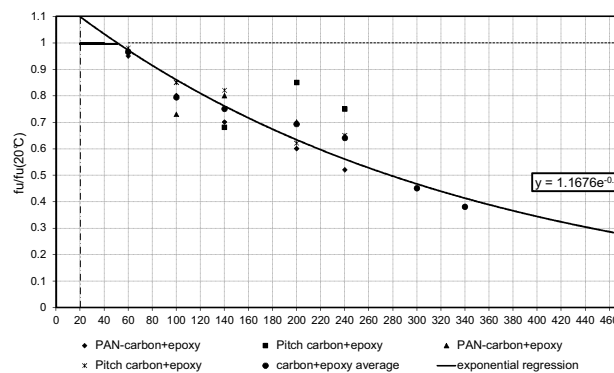


Fig. 1 Temperature-dependent tensile strength reduction of various carbon fibre composites.

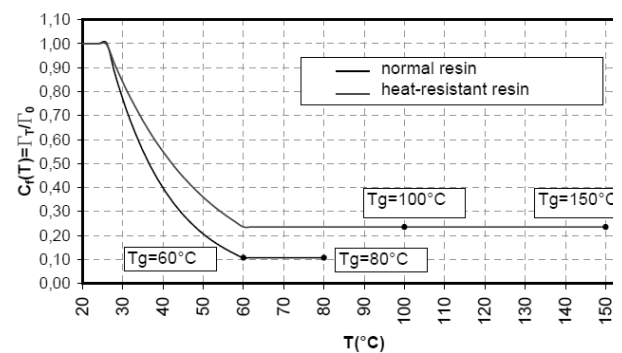


Fig. 2 Temperature-dependent specific fracture energy of the bond law for normal and heat-resistant resins.

In accordance with CNR-DT 200/2004 the maximum force transmitted by the FRP-to-concrete interface in normal temperature condition is related to so called “specific fracture energy”  $\Gamma_F$  of the interface bond law, whose characterization can be found in (Wu at al, 2004), that provides experimental data concerning the reduction of the specific energy fracture with the temperature. Fig. 2 shows typical temperature-dependent reduction curves of the specific energy fracture for normal and “heat-resistant” resins: it has to be remarked the great reduction of the interface effectiveness, in the case of normal resins (NR) which exhibit glass transition temperatures  $T_g$  variable in the range (60÷80°C), whereas heat-resistant resins (HR) are characterised by greater values of  $T_g$  (100÷150°C).

## 1.3 Structural behaviour of FRP-strengthened concrete beams or slabs at elevated temperature

The bond between external FRP reinforcement and concrete beam vanishes suddenly if the member bottom is directly heated by fire, due to the low glass transition temperature of the epoxy resins (Deuring, 1994). In the tests a similar behaviour has been observed when conventional steel strengthening is utilised, although composite sheets without protection behave better than steel plates without protection because of the lower heat conduction in the fibre direction and their smaller weight. Therefore, FRP externally strengthened RC beams or slabs need the protection with supplemental insulation in order to avoid the debonding between FRP sheets or laminates and concrete support. Some researches are devoted to study the performances of FRP strengthened elements protected by different insulation systems in order to individuate the minimum requirements to obtain satisfactory performances in fire

(Bisby et al, 2005). Obviously, if the FRP strengthening is not directly heated by fire or other sources of heat, the performances may be better.

## 2 SAFETY CHECK AT ELEVATED TEMPERATURE AND DESCRIPTION OF NUMERICAL MODEL

According to the provisions of European and Italian codes (EN1991 1-2, D.M. 14-02-08), the safety check of structural members subjected to elevated temperature may be carried out, in strength domain, comparing design value of the relevant effects of actions in the fire situation at time  $t$  ( $E_{fi,d,t}$ ) with the corresponding design value of the resistance of the member in the fire situation at same time  $t$  ( $R_{fi,d,t}$ ):

$$E_{fi,d,t} \leq R_{fi,d,t} \quad (1)$$

Unlike the safety checks in normal temperature conditions, in equation(1) the member resistance decreases due to material thermal damage and the effects of actions may vary due to thermal expansions and deformations.

The relevant effects of actions  $E_{fi,d,t}$  for the fire situation are obtained for time  $t=0$  through the combination of mechanical actions in accordance with EN 1990 “Basis of structural design” for accidental design situations. The design resistance  $R_{fi,d,t}$  of a structural member in the fire situation is evaluated considering the temperature-dependent reduction of the material mechanical properties  $X_{d,fi} = K_T X_k$ , and assuming unit partial safety factors  $\gamma_{M,fi}$ .

The fire resistance assessment of a structural member may be performed through experimental tests in furnaces or applying analytical approaches. In both cases conventional temperature-time laws of the environment may be assumed. For fires characterized mainly on burning of oil or other substances with equivalent rate of heat release, the “hydrocarbure curve”, is suggested by Eurocode 1 - Part 1-2. The mentioned fire curve is represented in Fig. 7.

The assessment of the structural member flexural resistance at elevated temperature is performed, as for normal temperature, determining the bending moment-curvature law ( $M-\chi$ ;  $N$ ) of the critical cross-section for the imposed value of the axial force  $N$  and the current temperature field within the section. The numerical procedure to assess the moment-curvature law of the cross-section is explained in (Nigro et al, 2010).

The failure of the FRP strengthened cross-section is assumed to occur when the ultimate strain is achieved at least in one material. The temperature-dependent ultimate strains of concrete and steel are assumed according to Eurocode 2-Part 1-2, whereas the ultimate strain of the FRP strengthening is assumed as the strain limit for intermediate debonding suggested in CNR-DT 200/2004 and modified according to specific energy fracture reduction shown in Fig. 2. It has to be remarked that if the temperature  $T_i$  in the adhesive layer exceeds the glass transition temperature  $T_g$  of the epoxy resin, the FRP strengthening may be considered lost, but the structural member keeps the residual resistance as a simple RC member.

The hypothesis of decoupling the thermal behaviour of the materials from the mechanical behaviour is the basis of the Fourier equation for the study of the heat propagation within solid bodies and may be usually accepted.

In most practical cases the thermal field may be considered as uniform along the member axis, therefore the actual 3D thermal problem can be reduced to more manageable 2D or 1D problems. Due to the variability of the material thermal properties with the temperature (thermal conductivity, specific heat, density), a numerical solution of the heat transfer problem has to be performed; in the paper the finite element method is used by means of FIRES-T3 computer program in which the heat transfer on the boundary may be assumed to occur through a combination of radiation and convection, linearly or non-linearly modelled.

According to usual FEM approach, the slab or beam cross-section is divided into a sufficient number of layers or elements and in each one the temperature is assumed as uniform and equal to that of its centroid. Each element is characterised by specific thermal properties, different from that of other elements and variable depending on its temperature. In particular,



thermal analyses are performed by considering concrete thermal properties in accordance with EN1992-1-2, whereas FRP thermal properties are defined in (Weidenfeller et al, 2003) and in (Sweeting et al, 2004).

For the considered time of exposure to prescribed environment conditions (fire or others), the thermal analysis gives the thermal field in the cross-section. A specific stress-strain law ( $\sigma-\epsilon; T_i$ ), which is a function of the local temperature and takes into account the variation of the material mechanical properties with the temperature, can be linked to every element of the mesh into which the section has been divided. Obviously different types of constitutive law are employed for concrete, steel rebars and FRP strengthening.

### 3 PARAMETRIC ANALYSES

The thermo-mechanical behaviour of RC bridge decks strengthened with externally bonded FRP laminates is investigated by considering environmental conditions responsible of thermal states different from the normal ones. As already said, the examined cases are:

- a) Maintenance of bituminous paving, cast in place on a bridge deck at temperature  $T=180^\circ\text{C}$ ;
- b) Accidental situation, resulting in a fire exposure over the bridge deck.

The performed applications concern RC bridge slabs 15 or 20 cm thick, symmetrically reinforced with steel bars (the reinforcement percentages at top or bottom side are equal to 1% of the concrete area). The slabs are externally strengthened with C-FRP; laminates or fabrics; positive or negative bending moment strengthening and different strengthening amounts. A typical bituminous paving 8 cm thick is considered over the RC slab. The one-dimensional analysis, carried out through FEM approach, is obviously exact if a continuous FRP strengthening is used. Due to the slight influence of the FRP laminates on the heat transfer, also when discrete FRP plates or strips are employed (Fig. 4-Fig. 5), the difference in terms of temperature at representative points is negligible.

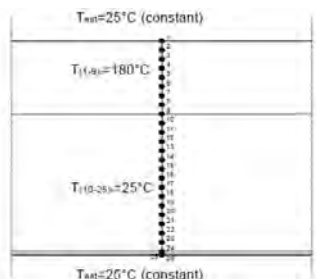


Fig. 3 Slab discretization

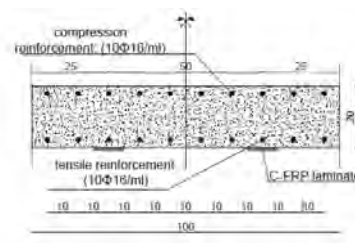


Fig. 4 RC slab strengthened to positive bending moment

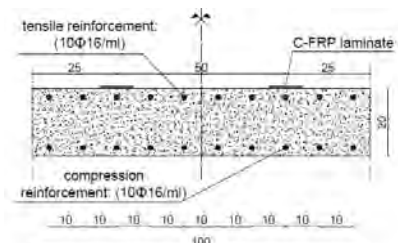


Fig. 5 RC slab strengthened to negative bending moment

#### *a) Maintenance of bituminous paving, cast in place on a bridge deck at temperature $T=180\text{ C}$*

The realization of a bituminous paving on a bridge deck represents a periodic maintenance operation. The cast in situ is carried out at about  $180^\circ\text{C}$ , therefore some significant reduction of safety may arise in the RC slab externally strengthened with FRP. Two schemes of FRP external strengthening are considered: bottom side strengthened slab in the sagging moment zones of continuous or simply supported schemes (Fig. 4); top side strengthened slab in the hogging moment zones of continuous schemes (Fig. 5). For the thermal analysis also the bituminous paving is modelled with appropriate thermal properties; initial temperature conditions  $T(t=0)=180^\circ\text{C}$  are assumed within the paving thickness. Two situations of environment temperature are considered:  $T_e=25^\circ\text{C}$  and  $T_e=35^\circ\text{C}$ .

Based on the performed thermal analyses, Fig. 6 shows the curves of the time-dependent temperature which arises in the FRP strengthening on the slab bottom side after bituminous paving laid at time  $t=0$ . It is possible to remark that in all the examined cases the maximum temperature is always lower than the glass transition temperature  $T_g$  of normal adhesive resins. Moreover, due to the particular heat transfer, the temperature peak occurs some hours after the

paving realization. The obtained results are quite not-dependent on the bituminous mix, which changes mainly the time of maximum temperature.

The safety check of the strengthened slab considering the temperature variation in the materials is summarized in Tab. 1, where  $M_{Ed}$  is the design bending moment in the normal conditions (assumed equal to the “cold” resistant moment  $M_{Rd}$  at ULS),  $M_{Ed,fi} = \eta_{fi} M_{Ed}$  is the design bending moment for the considered situation, and  $M_{Rd,t}$  is the resistant moment at ULS of the cross section taking account of the strength reduction due to elevated temperature. The table shows that the safety control ( $M_{Ed,fi} \leq M_{Rd,t}$ ) is always satisfied in the examined cases. If the design level  $\eta_{fi}$  tends to 1, the check control may become critical in the case of small thickness slab and normal adhesive resin, which exhibits a greater resistance reduction of the strengthened slab.

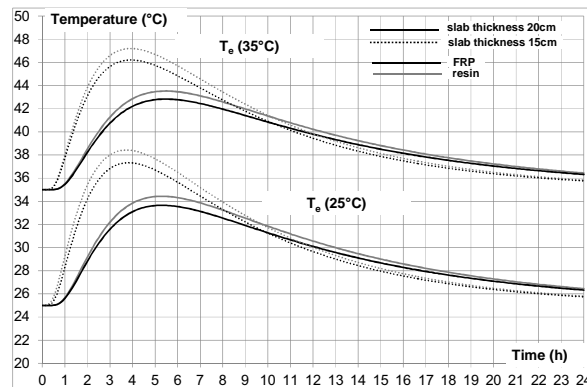


Fig. 6: Time-dependent temperature in resin and FRP strengthening on the bottom side.

When a bridge slab is strengthened with FRP plate or sheets on the top side for negative bending moment (Fig. 5), a protective cover needs to avoid damages in the FRP strengthening during the maintenance operations, as the demolition of the old road surface. The protective layer is required to have a good resistance to abrasion and concentrated loads and, if possible, to ensure also some thermal insulation. In the numerical applications a protective layer of concrete is considered. For the purpose of a parametric analysis, four different thicknesses variable from 1 to 4 cm are considered.

The thermal analyses show that the maximum temperature values in the FRP strengthening reaches about 85°C in the case of 1cm concrete protective layer. The maximum temperature decreases to about 65°C for a thickness of 4 cm. Therefore, the realization of a bituminous paving may lead to overcome the glass transition temperature  $T_g$  of normal adhesive resins. The safety check of the strengthened slab considering the temperature variation in the materials is not satisfied for the considered cases if a normal adhesive resin is utilised, due to the great reduction of the specific fracture energy and, consequently, of the FRP strain limit for intermediate debonding (see Fig. 2).

Only in the case of 4-cm thick layer the temperature in the FRP-to-concrete interface is lower than the expected glass transition temperature  $T_g$  of a normal resin. However, also in this case the significant reduction of the resistant moment at ULS, when normal resins are utilised, leads to a lack of safety with reference to the usual design level  $\eta_{fi} = 0.7$  for elevated temperature (see Tab. 2). On the contrary, if a “heat-resistant” resin is employed, the safety check is satisfied with  $\eta_{fi}$  values greater than 0.7.

Tab. 1: Safety check of the slab in positive moment region  
(maintenance of the bituminous paving).

						Normal resin	High resistant resin
Thickness	N° lam/m	b lamina	$\eta_{fi}$	$M_{Ed}$	$M_{Ed,fi}$	$M_{Rd,t}$	$M_{Rd,t}$
cm	\	mm	\	kNm	kNm	kNm	kNm
15	2	100	0.7	69.75	48.83	63.62	78.65
20	2	100	0.7	128.32	89.92	142.84	147.86

Tab. 2: Safety check of the slab in negative moment region  
(maintenance of the bituminous paving -  $s \leq 3\text{cm}$ ).

						Normal resin	High resistant resin
Thickness	N° lam/m	b lamina	$\eta_{fi}$	$M_{Ed}$	$M_{Ed,fi}$	$M_{Rd,t}$	$M_{Rd,t}$
cm	\	mm	\	kNm	kNm	kNm	kNm
15	2	100	0.7	69.75	48.83	37.43	57.94

Tab. 3: Safety check of the slab in negative moment region  
(maintenance of the bituminous paving -  $s=4\text{cm}$ ).

						Normal resin	High resistant resin
Thickness	N° lam/m	b lamina	$\eta_{fi}$	$M_{Ed}$	$M_{Ed,fi}$	$M_{Rd,t}$	$M_{Rd,t}$
cm	\	mm	\	kNm	kNm	kNm	kNm
15	2	100	0.7	69.75	48.83	45.64	61.94

In conclusion, for slabs with FRP strengthening on the top side the use of “heat resistant” resins is necessary in order to avoid the achievement of the glass transition temperature in the same resins and satisfy the safety check in the presence of maintenance operations on bituminous paving. A protective layer of concrete is however necessary in order to avoid damages in the FRP strengthening and reduce the temperature in the structural materials.

***b) Accidental situation, resulting in a fire exposure over the bridge deck.***

A fire event over the bridge deck may occur because of a vehicular accident. For a bridge slab strengthened with FRP plate or sheets on the bottom side, the numerical analyses show that temperature in FRP and resin (Fig. 8) are generally lower than 60°C. When the FRP strengthening is on the top side of the RC slab, the maximum temperature at FRP-to-concrete interface exceeds generally the glass transition temperature of normal and heat-resistant resins, despite the thermal insulation provided by the road surface and the protection layer. The intersection between the assumed glass transition temperature  $T_g$  of the adhesive resin and the time-dependent temperature curves allows determining the maximum fire exposure time for the considered protection thicknesses (see Fig. 9a for normal resins and Fig. 9b for heat-resistant resins). It has to be remarked the significant role played by the thickness of the protection layer, which leads to greater fire exposure times.

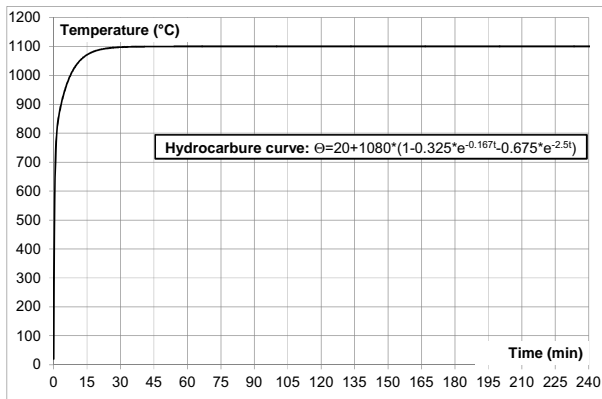


Fig. 7 Nominal Temperature-Time fire curves

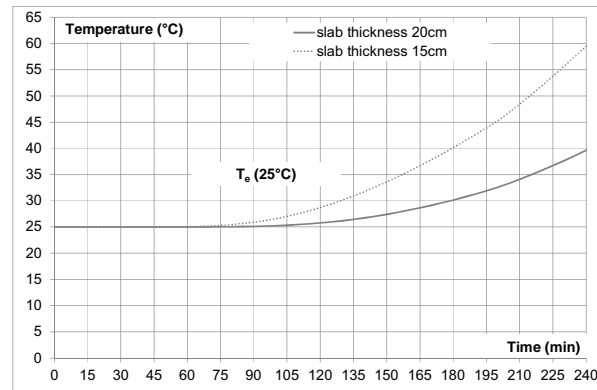
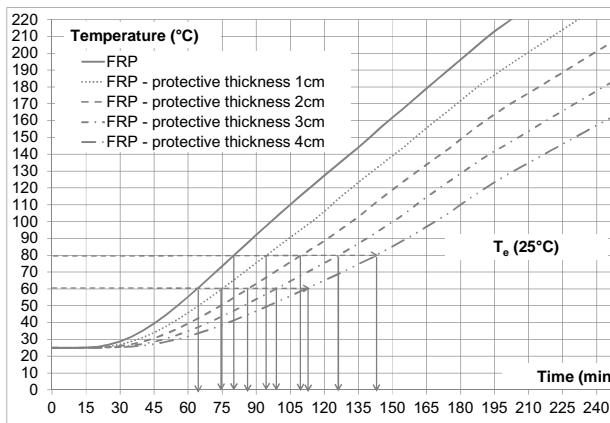
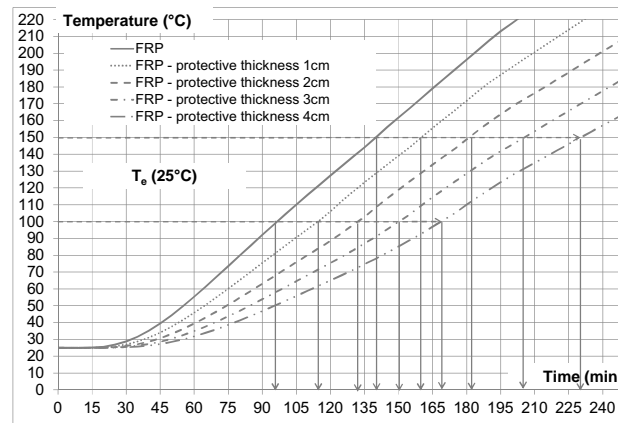


Fig. 8: Temperature in FRP on the bottom side



(a)



(b)

Fig. 9: Temperature in FRP on the top side (a) normal (b) heat-resistant resins

#### 4 CONCLUSION

The paper focused on performing a parametric analysis concerning the behaviour of RC bridge slabs externally strengthened with FRP in the presence of environmental situations responsible of elevated temperatures. In the case of bituminous paving realization, the analyses point out that the use of “heat resistant” adhesive resins is necessary with the aim of preventing the achievement of the glass transition temperature, if the strengthening is located on the top side of the slab. A protective layer of concrete is moreover required in order to avoid damages in the FRP strengthening. For strengthening on the bottom side, if the design level  $\eta_{fi}$  tends to 1, the safety check may become critical in the case of small thickness slab and normal adhesive resin, which exhibits a greater resistance reduction of the strengthened slab. In the case of fire event over the bridge deck and strengthening on the bottom side, the conclusions are quite similar to the ones of the previous environmental situation. If the strengthening is located on the top side of the slab, the use of “heat resistant” resins is recommended in order to increase the maximum time of fire exposure which prevents the achievement of the glass transition temperature in the adhesive resin.

#### REFERENCES

- Springer GS: Effects of temperature and moisture on sheet molding compounds, Springer GS, editor, Environmental effects on composite materials, vol. 2. Technomic Publishing Company, Inc;1984. p. 59–78
- Buggy M, Carew A.: The effect of thermal ageing on carbon fibrereinforced polyether ether ketone (PEEK). J Mater Sci 1994;29:1925–9
- Eurocode 2, Design of Concrete Structures – Part 1-2: General Rules - Structural Fire Design, April 2004

- Blontrock H., Taerwe L., Matthys S.: Properties of Fiber Reinforced Plastics at Elevated Temperatures with Regard to Fire Resistance of Reinforced Concrete Members, FRPRCS-4, Baltimore, SP 188-5, 1999.
- Bisby L.A., Green M.F., Kodur V.K.R.: Response to fire of concrete structures that incorporate FRP, *Prog. Struct. Engng. Mater.*, 7:136-149, 2005.
- fib-Task Group 9.3, Externally Bonded FRP Reinforcement for RC Structures, Technical Report Bulletin 14, fib, 2001
- CNR-DT 200/2004, Instructions for Design, Execution and Control of Strengthening Interventions by Means of Fibre-Reinforced Composites (in Italian), Italian National Research Council, 2004.
- Wu Z. S., Iwashita K., Yagashiro S., Isshikawa T., Hamaguchi Y.: Temperature effect on bonding and debonding behavior between FRP sheets and concrete, *Proceedings of FRP Composites in Civil Engineering – CICE 2004, Adelaide (Australia)*, 905-912, 8-10 December 2004.
- Deuring M.: Brandversuche an Nachtraglich Verstaerkten Tragern aus Beton, Research Report EMPA No. 148'795, Dübendorf, Swiss Federal Laboratories for Materials Testing and Research, 1994.
- UNI EN 1991-1-2, Eurocode 1: Actions on structures Part 1-2: General actions - Actions on structures exposed to fire, November 2002
- UNI EN 1992-1-2, Eurocode 2: Design of concrete structures Part 1-2: General rules - Structural fire design, December 2004
- Ministry of Infrastructure and Transport (Italian Government) 2008. Technical Code for the Constructions. G.U. n. 29 of 14/02/2008
- Iding R., Bresler R., Nizamuddin Z., "FIRES-T3" - A computer program for the fire response of structures-thermal, Fire Research Group, University of California, Berkeley, 1997.
- Bernd Weidenfeller, Michael Hofer, Frank R. Schilling: Thermal conductivity, thermal diffusivity, and specific heat capacity of particle filled polypropylene, *Composites: Part A* 35 (2004) 423-429, Elsevier Ltd. doi:10.1016/j.compositesa.2003.11.005, 2004
- R.D. Sweeting, X.L. Liu: Measurement of thermal conductivity for fibre-reinforced composites, *Composites: Part A* 35 (2004) 933-938, Elsevier Ltd. doi:10.1016/j.compositesa.2004.01.008, 2004
- Nigro E., Cefraelli G., Pustorino S., Princi P.: Progettazione di strutture in acciaio e composte acciaio-calcestruzzo in caso di incendio, Hoepli, 2010

# SIMPLIFIED METHOD FOR PREDICTING DEFORMATIONS OF RC FRAMES DURING FIRE EXPOSURE

M.A. Youssef<sup>a</sup>, S.F. El-Fitiany<sup>a</sup>

<sup>a</sup> Western University, Faculty of Engineering, London, Ontario, Canada

## Abstract

Structural engineers are in need of analytical methods to assess the performance of Reinforced Concrete (RC) frames during fire events. Existing numerical methods require extensive knowledge of heat transfer calculations and the finite element method. This paper proposes a practical approach to track the fire performance of indeterminate RC frames during ASTM-E119 and ISO 834 standard fires exposure. The proposed method utilizes a finite difference method to predict the temperature distribution within the section of the RC frame. The predicted elevated temperatures are then used to conduct a sectional analysis. The effective flexural and axial stiffnesses are evaluated and used to predict the overall behavior of the structure during fire. The proposed approach is validated by comparing its predictions with analytical results by others.

**Keywords:** concrete, fire, elevated temperatures, sectional analysis, indeterminate structures, thermal restraint.

## INTRODUCTION

Fire initiates when combustible materials ignite. Then, it spreads horizontally and/or vertically depending on the compartment boundaries. A temperature gradient is generated through exposed RC elements. These elevated temperatures cause the element's stiffness to degrade and produce thermal deformations. Structural fire safety of RC structures is currently evaluated based on the fire ratings of single elements, i.e. columns, beams, walls, and slabs. However, the overall behavior of the structure during a fire should be assessed to ensure the safety of the occupants and the fire fighters during evacuation.

Fire testing is the most reliable approach to assess the fire endurance of a structure but its use for concrete frames is very limited. This is mainly because of its cost, which makes it unsuitable for regular design. Finite Element (FE) tools are very powerful and capable of analyzing RC structures during fire events. Drawbacks of using the FE method including: the need for a comprehensive computer program, the difficulty to comprehend its results and to identify potential modeling errors, and the long running time make it impractical for design engineers. This paper provides engineers with a practical approach to predict the fire response of statically determinate or indeterminate RC frames. The proposed method extends the work done by El-Fitiany and Youssef, 2009 that proposed a one-dimensional (1D) sectional analysis method to predict the flexural behavior of the heated section at different axial load levels ( $\lambda$ ).

## 1 PROPOSED METHOD

For a given fire duration, the proposed method can be applied using the following steps:

1. determining of an equivalent one-dimensional average temperature distribution for the cross-section of the heated elements.
2. identifying the needed constitutive models for the heated elements.
3. predicting the unrestrained thermal deformations for the heated elements.

4. evaluating the flexural and axial stiffnesses of the heated elements based on their axial forces and moments.
5. Analyzing the fire-exposed frame under the effect of the applied loads while accounting for the thermal deformations using linear elastic analysis. The flexural and axial stiffnesses obtained in step 4 are utilized in this step. The moments and axial forces are redistributed based on the assigned stiffness values.
6. Recalculating the flexural and axial stiffnesses in step 4 for the revised moments and axial forces obtained in step 5.

Steps 4, 5, and 6 are repeated until the change in the obtained axial forces and moments is less than an assumed tolerance. The following sections explain these steps.

## 2 AVERAGE TEMPERATURE CALCULATION

At specific fire duration, a heat transfer analysis is conducted to predict the temperature distribution using the Finite Difference Method (FDM) (Lie et al, 1992). The cross-section is then divided into horizontal layers and an average temperature  $T_{avg}$  is calculated for each layer.  $T_{avg}$  represents the algebraic average temperature, in °C, of the elements within each layer and is suitable for calculating the thermal and transient creep strains as they are temperature dependent (El-Fitiany and Youssef, 2009).

## 3 CONCRETE AND STEEL CONSTITUTIVE RELATIONSHIPS

Fire temperature reduces the mechanical properties of concrete and steel. It also induces new strains, i.e. thermal and transient creep strains. The following sub-sections provide a brief summary of the concrete and steel models used in this paper.

### 3.1 Concrete Strains

The total concrete strain at elevated temperatures ( $\varepsilon$ ) is composed of three terms: unrestrained thermal strain ( $\varepsilon_{th}$ ), instantaneous stress related strain ( $\varepsilon_c$ ), and transient creep strain ( $\varepsilon_{tr}$ ). The total strain is given by Eq. (1).

$$\varepsilon = \varepsilon_{th} + \varepsilon_c + \varepsilon_{tr} \quad (1)$$

The free thermal strain,  $\varepsilon_{th}$ , is a strain resulting from fire temperature and can be predicted using the Eurocode 2 model for siliceous and carbonate concretes.

The value of the instantaneous stress-related strain ( $\varepsilon_c$ ) at the peak compressive stress ( $f'_{cT}$ ), i.e.  $\varepsilon_{oT}$ , defines the stress-strain relationship during fire exposure. For loaded concrete, the effect of elevated temperatures on  $\varepsilon_{oT}$  is negligible. The variation of  $\varepsilon_{oT} + \varepsilon_{tr}$  with fire temperature is proposed by Eurocode 2. A linear relationship, Eq. (2), is chosen to represent the Eurocode 2 recommendation. Such a relationship simplifies the sectional analysis and results in good prediction of the flexural and axial stiffnesses.

$$\varepsilon_{oT} + \varepsilon_{tr} = 2.52 \times 10^{-5} T_{avg} \quad 80 \text{ °C} < T_{avg} \leq 1200 \text{ °C} \quad (2)$$

### 3.2 Concrete Ultimate Strain

Concrete ultimate strain is the strain at which concrete crushing occurs. Elevated temperatures increase this strain. Eurocode 2 proposes a linear relationship between  $\varepsilon_{uT}$  and  $T_{avg}$ . This relationship can be represented by Eq. (3).  $\varepsilon_{uT}$  is defined in Eurocode 2 as the strain corresponding to zero compression stress. The difference between  $\varepsilon_{uT}$  and  $\varepsilon_{oT} + \varepsilon_{tr}$  is constant and equal to 0.02.

$$\varepsilon_{uT} = 2.52 \times 10^{-5} T_{avg} + \Delta\varepsilon = \varepsilon_{oT} + \varepsilon_{tr} + 0.02 \quad (3)$$

### 3.3 Concrete Compressive Strength

Concrete compressive strength experiences significant degradation at elevated temperatures. Eurocode 2 predicts the reduced compressive strength ( $f'_{cT}$ ) for siliceous and carbonate concretes as a ratio from its ambient value ( $f'_c$ ). The reduction in  $f'_{cT}$  for siliceous concrete is represented by Eq. (4), as it allows reaching closed form solution for flexural stiffness.

$$f'_{cT}/f'_c = 1.76 \times 10^{-9} T_{avg}^3 - 3 \times 10^{-6} T_{avg}^2 + 2.5 \times 10^{-4} T_{avg} + 1.00 \quad (4)$$

### 3.4 Concrete Stress-Strain Relationships

A general and simple approach to estimate the  $f_{cT} - \varepsilon_{cT}$  descending branch is proposed by Eurocode 2 and represented by Eq. (5). Eqs. (2) and (4) are used to calculate  $(\varepsilon_{oT} + \varepsilon_{tr})$  and  $f'_{cT}/f'_c$ , respectively.

$$f_{cT} = f'_{cT} \left[ 2 \left( \frac{\varepsilon_{cT}}{\varepsilon_{oT} + \varepsilon_{tr}} \right) - \left( \frac{\varepsilon_{cT}}{\varepsilon_{oT} + \varepsilon_{tr}} \right)^2 \right] \quad \varepsilon_{cT} \leq (\varepsilon_{oT} + \varepsilon_{tr}) \quad (5a)$$

$$= f'_{cT} \left[ \frac{\varepsilon_{uT} - \varepsilon_{cT}}{0.02} \right] \quad (\varepsilon_{oT} + \varepsilon_{tr}) < \varepsilon_{cT} \leq \varepsilon_{uT} \quad (5b)$$

### 3.5 Steel Stress-Strain Relationships

The model proposed by Lie et al (1992), is used to predict the reduced yield strength of reinforcing bars ( $f_{yT}$ ) and the stress-strain ( $f_{sT} - \varepsilon_{sT}$ ) relationship.

## 4 PREDICTION OF THE UNRESTRAINED DEFORMATION

A sectional analysis approach suitable for the analysis of rectangular RC beams at elevated temperatures was proposed by El-Fitiany and Youssef, 2009. Fig. 1a shows the fiber model of a typical RC cross-section subjected to fire from three faces. The average temperature ( $T_{avg}$ ) distribution, Fig. 1b, can be calculated using the Finite Difference Method (FDM).  $T_{avg}$  induces thermal strains that can be evaluated using the following method:

1. The nonlinear thermal strain ( $\varepsilon_{th}$ ) distribution, Fig. 1g, is calculated using  $T_{avg}$ . The thermal strain of steel bars is calculated based on the elevated temperature at their locations.
2.  $\varepsilon_{th}$  is then converted to an equivalent linear thermal strain ( $\overline{\varepsilon_{th}}$ ), Fig. 1d, by considering self-equilibrium of internal thermal forces in concrete and steel layers.  $\overline{\varepsilon_{th}}$  is represented by the value of the center axial strain ( $\varepsilon_i$ ) and the curvature ( $\psi_i$ ).  $\varepsilon_i$  and  $\psi_i$  define the unrestrained thermal deformation of a heated section.
3. Fig. 1f shows the differences between the equivalent linear and nonlinear thermal strains, which represent the self-induced thermal strains ( $\varepsilon_{st}$ ). These strains are assigned as initial strains for the concrete and steel when calculating the flexural and axial stiffnesses. The following sections present a simplified approach to calculate  $\varepsilon_{st}$  using the predicted  $T_{avg}$  distribution and material models presented earlier in this paper.
4. Fig. 1f shows the differences between the equivalent linear and nonlinear thermal strains, which represent the self-induced thermal strains ( $\varepsilon_{st}$ ). These strains are assigned as initial strains for the concrete and steel when calculating the flexural and axial stiffnesses. The following sections present a simplified approach to calculate  $\varepsilon_{st}$  using the predicted  $T_{avg}$  distribution and material models presented earlier in this paper.



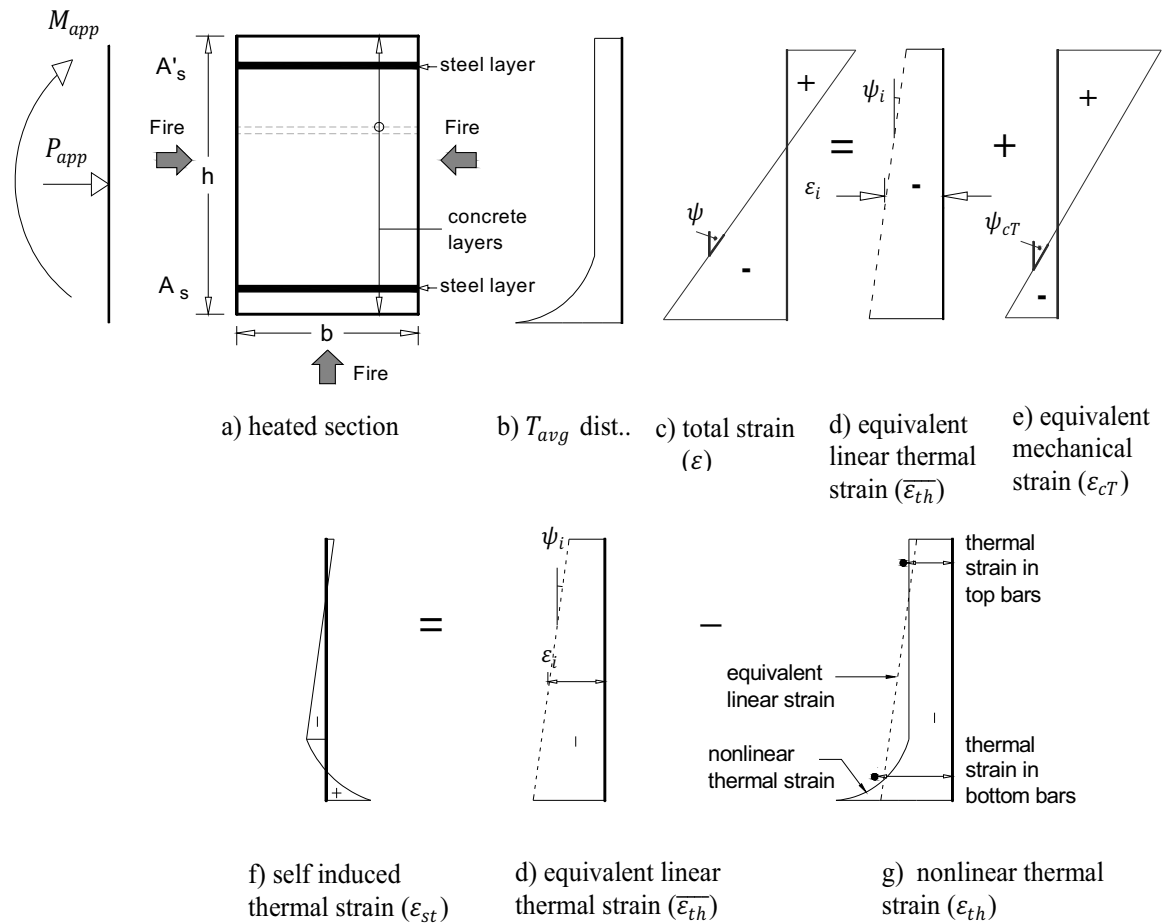


Fig. 1 Sectional analysis approach for heated RC sections

## 5 EVALUATION OF THE FLEXURAL AND AXIAL STIFFNESSES

Fig. 1a shows the applied axial force ( $P_{app}$ ) and moment ( $M_{app}$ ) on a RC section exposed to fire from three faces. The use of sectional analysis to evaluate the flexural and axial stiffnesses for this section involves the following steps:

1. The self-induced thermal strains ( $\epsilon_{st}$ ), calculated in the previous section, are assigned as initial strains for the concrete and steel to model the corresponding self-induced self-equilibrating thermal stresses. The terms  $\epsilon_{st}$ ,  $\epsilon_c$ , and  $\epsilon_{tr}$  are lumped into an equivalent mechanical strain  $\epsilon_{cT}$ , Eq. (6).

$$\epsilon = \overline{\epsilon_{th}} + (\epsilon_{st} + \epsilon_c + \epsilon_{tr}) = \overline{\epsilon_{th}} + \epsilon_{cT} \quad (6)$$

2. For assumed values of  $\epsilon_{cT}$  at the center of the section and  $\psi_{cT}$ , the internal stresses in the concrete and steel are evaluated. The corresponding internal axial forces are then calculated. To satisfy equilibrium between the calculated internal forces and the external loads, i.e.  $P_{app}$  and  $M_{app}$ , iterations are executed by changing the values of center  $\epsilon_{cT}$  and  $\psi_{cT}$ . This process can be repeated for different values of  $M_{app}$ . A typical relationship between  $\psi_{cT}$  and  $M_{app}$ , for a constant  $P_{app}$ , is sketched in Fig. 2.

3. The secant slope of the  $M-\psi_{cT}$  diagram represents the section's effective flexural stiffness ( $EI_{eff}$ ) at  $M_{app}$  (El-Fitainy and Youssef, 2012). The corresponding effective axial stiffness ( $EA_{eff}$ ) equals to  $P_{app}$  divided by the center axial strain ( $\epsilon_{cT}$ ).

As shown in Fig. 2, heating RC sections from the bottom face and the two sides cause the bottom concrete fibers to thermally expand more than the top concrete fibers and results in  $\psi_i$ . The acting moment induces a mechanical curvature ( $\psi_{cT}$ ), which is either added to or

deducted from  $\psi_i$ . As shown in Fig. 2a, a positive (sagging) moment induces a curvature that adds to the initial curvature. For negative (hogging) moments, compression stresses are applied on the bottom fibers. Curvature caused by these stresses opposes the initial curvature, Fig. 2b.

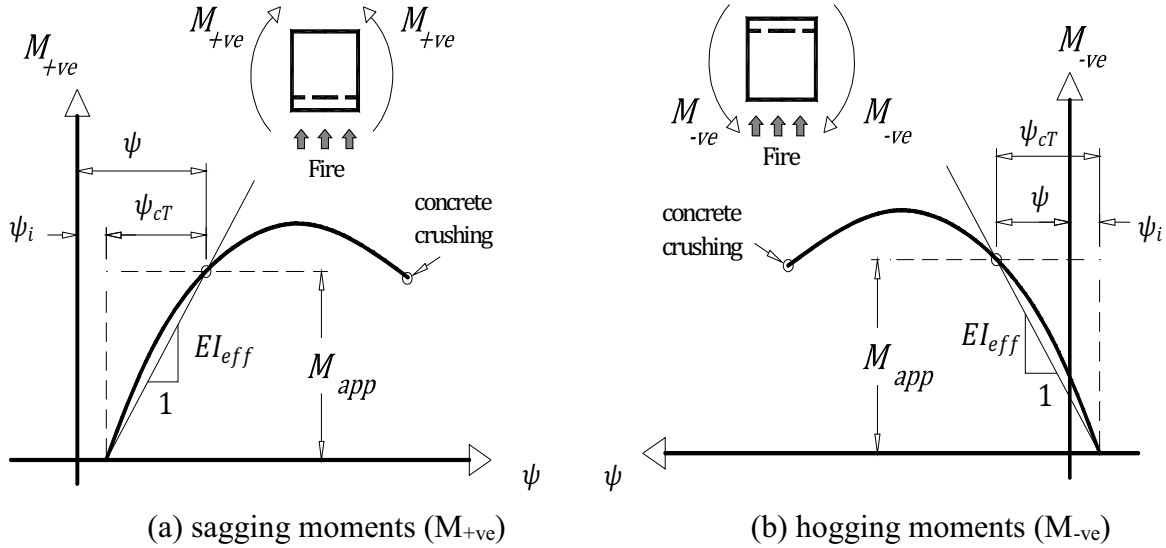


Fig. 2 ( $M$ )-( $\psi$ ) diagrams for RC sections during fire

For a specific fire duration, the effect of thermal strain on the  $M$ - $\psi$  relationship is not governed by  $M_{app}$ . It represents the unrestrained/free thermal expansion of the unloaded concrete element and results in shifting the  $M$ - $\psi$  and diagram by a value  $\psi_i$ , Fig. 2. Consequently, the total curvature ( $\psi$ ) is the sum of the unrestrained thermal curvature ( $\psi_i$ ) and the mechanical curvature ( $\psi_{cT}$ ) and can be expressed in terms of the effective stiffness ( $EI_{eff}$ ) as follows.

$$\psi = \psi_i + M_{app}/EI_{eff} \quad (7a)$$

Similarly, the total center axial strain ( $\varepsilon$ ) is the sum of the unrestrained thermal strain ( $\varepsilon_i$ ) and the center mechanical strain ( $\varepsilon_{cT}$ ) and can be expressed in terms of the effective axial stiffness ( $EA_{eff}$ ) as follows.

$$\varepsilon = \varepsilon_i + P_{app}/EA_{eff} \quad (7b)$$

The following sections present a simplified approach to calculate  $EI_{eff}$  and  $EA_{eff}$  using the predicted  $T_{avg}$  distribution and material models presented earlier in this paper.

## 6 VALIDATION CASE (IDING ET AL., 1977)

Iding et al, 1977 has analytically investigated the behavior of RC frames during fire exposure. Fig. 3 shows a schematic of a single bay RC frame analyzed using FIRES-RC II, a comprehensive FE software developed at University of California, Berkeley. The beam and column dimensions are  $355 \text{ mm} \times 711 \text{ mm}$ . The frame was exposed to a 1.0 hr of ASTM-E119 standard fire over its entire length while supporting the vertical loads shown in Fig. 3. The frame was analyzed assuming siliceous concrete and a compressive strength of  $27.6 \text{ MPa}$ . The yield strength of the reinforcing bars was  $275.8 \text{ MPa}$ .

This frame is analyzed using an elastic FE software SAP2000, and analyzed using the degraded flexural and axial stiffnesses. The effect of thermal expansion is considered by modeling  $\varepsilon_i$  and  $\psi_i$  as an induced deformation for all fire-exposed RC members. The

predicted deformed shape is shown in Fig. 3. A good match is found between the proposed method and the nonlinear FIRES-RC II FE software. The difference in deformations can be due to using different material models.

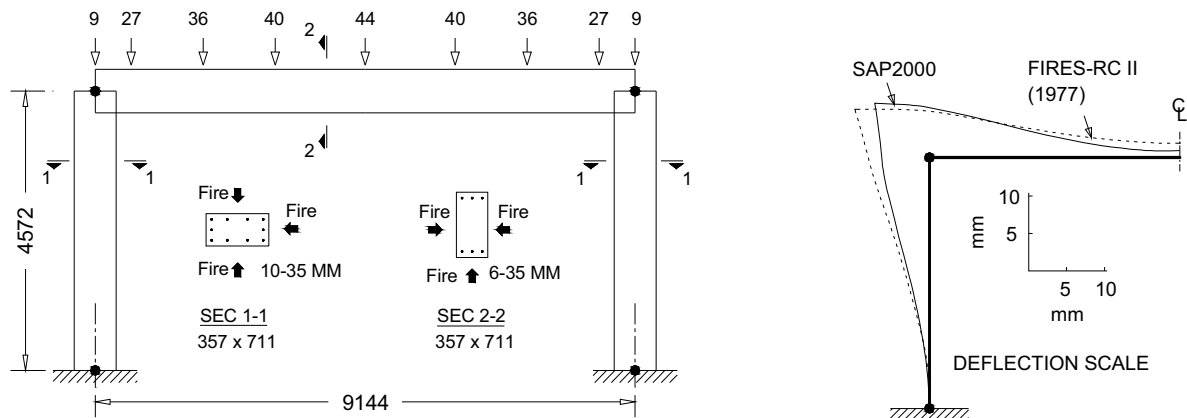


Fig. 3 Layout for a RC frame exposed to ASTM-E119 fire [Dims in mm, loads in kN]

## 7 SUMMARY AND ACKNOWLEDGMENT

The overall behavior of RC framed structures is studied in this paper. A practical approach based on superimposing the effects of thermal expansion and material degradation is introduced. The nonlinear thermal expansion is converted to an equivalent uniform thermal distribution, which can be represented by the unrestrained thermal axial strain  $\varepsilon_i$  and curvature  $\psi_i$ . The degradation effect in material strength is considered by accounting for the reduction in the effective flexural and axial stiffnesses,  $EI_{eff}$  and  $EA_{eff}$ , respectively. The proposed method is validated by comparing its results with a case study for a single storey RC frame analyzed by Iding et al, 1977. A good agreement is found between the finite element method predictions and the results of the proposed method for both case studies. This research was funded by the Natural Sciences and Engineering Research Council of Canada.

## REFERENCES

- Lie, T.T., ed., "Structural Fire Protection", ASCE Manuals and Reports on Engineering Practice, no. 78, New York, NY, 1992.
- El-Fitiany, S., Youssef, M.A., "Assessing the flexural and axial behaviour of reinforced concrete members at elevated temperatures using sectional analysis", FSJ, 2009.
- Iding, R., Bresler, B., Nizamuddin, Z., "FIRES-RC II, A computer program for the fire response of structures-reinforced concrete frames (revised version)", 1977.
- El-Fitiany S.F. Youssef M.A., "Simplified method to analyze continuous RC beams during fire exposure", ACI Struct. J., In press (accepted Oct 2012).
- Eurocode 2, "Design of concrete structures", ENV EC2, 1992.
- Wilson EL. SAP2000 analysis reference manual, Computers and Structures Inc.; 2002.

## THE IMPACT OF CAR PARK FIRE ON CONCRETE STRUCTURE Parallel Computation

Peter Weisenpacher <sup>a</sup>, Jan Glasa <sup>a</sup>, Ladislav Halada <sup>a</sup>, Lukas Valasek <sup>a</sup>, Miroslav Dobrucky <sup>a</sup>

<sup>a</sup> Institute of Informatics, Slovak Academy of Sciences, Bratislava, Slovak Republic

### Abstract

This study examines the influence of automobile fire in a car park on concrete parts of the structure. In 2009, a series of full-scale fire experiments in open air was conducted, including the fire in automobile interior and its influence onto a vehicle in its vicinity. We performed a set of simulations of this scenario, using the NIST FDS system, version 5.5.3. Comparison with experimental data confirmed the simulation reliability. In this paper, we use material properties of car interior materials established by our research to simulate a car fire in a small part of car park containing two burning cars and its influence on concrete ceiling and a pillar in the vicinity of the cars. We use here the calculation with 48 and more MPI processes to evaluate the ability of high performance computing to solve problems of structural fire safety.

**Keywords:** computer simulation, automobile fire, car park, parallel calculation

### INTRODUCTION

A danger of fires in car parks and other transportation structures is still actual. Flames, radiation, smoke and other toxic fire products constitute a direct threat for human lives. However, there is another danger caused by fire, which endangers both people and property. Structures can suffer from intensive fires with long duration and their destruction could lead to severe damages.

This article is focused on support, which can be provided to fire safety precautions by computer fire simulation. Prediction of the fire behaviour and its impact on structure can be an important part of such precautions. Recently, various fire simulation systems have brought the possibility to use computer fire simulation to better understand the dynamics of such fires and enrich results of full-scale fire experiments, which are usually expensive and less flexible with respect to the change of scenario parameters (Heinisuo et al, 2012). We examine the influence of automobile fire in a car park on some concrete parts of the structure. In 2009, a series of full-scale fire experiments with several cars in open air was conducted in testing facilities of Fire Protection College of Ministry of Interior of the Slovak Republic in Povazsky Chlmec. These experiments included a fire in car interior and its influence onto a vehicle in its vicinity.

We performed a set of sequential and parallel simulations of this scenario using the NIST FDS simulation system, version 5.5.3 (McGrattan et al, 2009). The simulation results compared with the experimental data confirmed the simulation reliability and significant performance increase of parallel computation. In this paper, we use material properties of dominant flammable materials in car interior established by our research to simulate car fire in a small part of a car park containing two burning cars and its influence on concrete ceiling, pillar and joist in the vicinity of the cars. The computational domain does not include walls. As our previous research (Weisenpacher et al, 2012) has confirmed the reliability of parallel FDS simulation, we use here cluster computation with 48 and 72 MPI processes to evaluate the ability of high performance computing to solve problems of structural fire behaviour.

## 1 FULL-SCALE EXPERIMENT OF AUTOMOBILE INTERIOR FIRE

The full-scale experiment of automobile interior fire and its spread onto another near standing car (Fig. 1 and 2) was carried out in November 2009 in Povazsky Chlmec (Svetlik, 2010, Polednak, 2010). We used new functional automobile Kia Cee'd with only slightly damaged passenger compartment (scorched driver's seat). The right front and left rear side windows were broken in order to increase the oxygen supply. The second automobile, an older model of BMW, was located lengthwise in the 50 cm distance. Three thermocouples were used to detect the gas temperature: in the interior of the first automobile above the driver's seat, above the roof and in the luggage compartment. One thermocouple was located at the BMW bonnet side. The fire behaviour observations were recorded by digital cameras and an infra-red camera. The fire was ignited by burning of a small amount of gasoline (about 10 ml) poured onto a cloth placed onto the back seat behind the Kia driver's seat (under the broken window).



Fig. 1 Ignition of experimental fire



Fig. 2 Experimental fire behaviour

After several dozens of seconds, the fire became visibly more intensive and after 2 minutes the whole passenger compartment started to burn and flames reached over the roof through the broken windows. During the next minutes, the rest of the windows were broken and the temperature inside the interior reached the value of 1000 °C. After 7 minutes, a rubber sealing of the nearest BMW window ignited. After 12 minutes the fire was suppressed.

## 2 FDS SIMULATION OF EXPERIMENTAL SCENARIO

We created an FDS model of the fire scenario including both tested automobiles (see Fig. 3). composed of aluminium alloy sheets, rubber tyres and glass windows. The first automobile also included interior equipment such as seats, dashboard with a wheel and interior lining. The second automobile model included the window rubber sealing in the location, where ignition occurred during the experiment. We used table values for standard material properties such as parameters of aluminium and rubber, and some parameters from (Andreini et al, 2011) for two interior equipment materials ('UPHOLSTERY' for seats and 'PLASTIC' for other equipment) as their first approximation. Finally, we obtained realistic fire behaviour of simulated fire for the parameters given by Tab. 1.

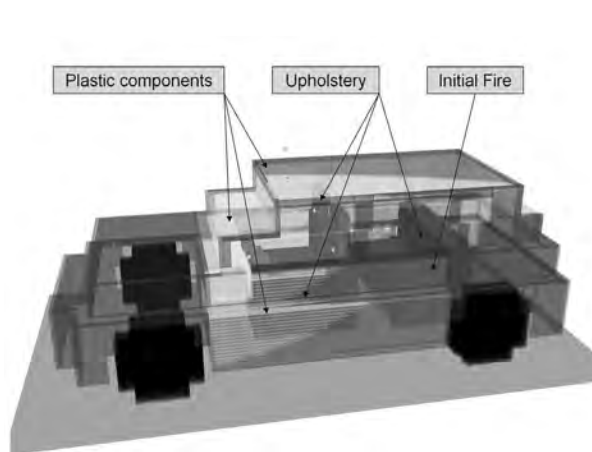


Fig. 3 Automobile interior model

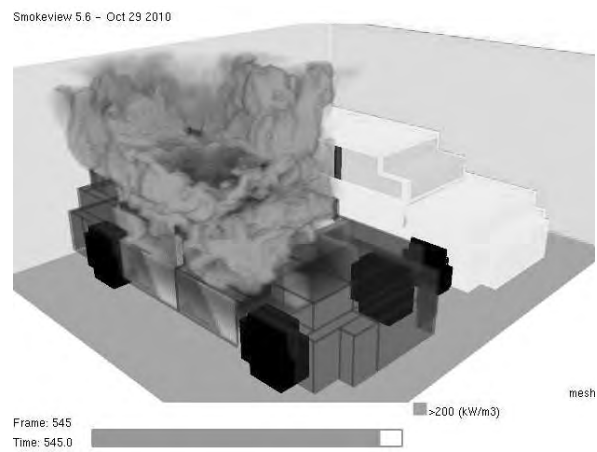


Fig. 4 Simulated fire behaviour

Tab. 1 Optimised properties of car interior materials

Type of Material	$T_{ign}$ [°C]	$H_v$ [kJ.kg <sup>-3</sup> ]	HRRPUA [kW.m <sup>-2</sup> ]	$\rho$ [kg.m <sup>-3</sup> ]
'UPHOLSTERY'	370	4000	200	80
'PLASTIC'	440	4000	250	930

The size of computational domain was 576 x 486 x 240 cm. For the 3 cm mesh resolution, the simulation included 192 x 162 x 80 cells (2,488,320 cells). Qualitative behaviour of the simulated fire was very similar to the fire observed during the experiment (see Fig. 4). Simulation is described in detail in (Weisenpacher et al, 2012). We can conclude that the temperature in the car interior, which was the most important for the results reliability confirmation, was in very good agreement with experimental measurements. The results for exterior thermocouples were less satisfactory. Our results also agree with the main conclusions of the paper (Okamoto et al, 2009), in which the 3 MW HRR peak and 1000 °C interior temperature peak after flashover in the passenger compartment were observed as well as the influence of the windows breakage on burning behaviour, which was also an important factor of our simulation.

### 3 FDS SIMULATION OF CAR PARK FIRE

The simulation described in the previous chapter validated the FDS model of scenario in which two cars with elaborated interior equipment are dominant source of fire. An important question connected with this scenario is what would be the impact of such fire on concrete construction of the car park. We elaborated a scenario of car fire in a small part of a car park containing two burning cars. The computational domain did not include car park walls (boundary condition 'OPEN'), only the concrete floor, ceiling and a pillar and joist in the vicinity of the second car. The computational domain size was 864 x 864 x 300 cm with the 3 cm mesh resolution. The simulation included 288 x 288 x 100 cells (8,294,400 cells). As the previous simulation confirmed the reliability of parallel simulations up to approximately 100 MPI processes, the domain was decomposed to 48 and 72 meshes, each of them assigned to specific CPU core. The source of fire (27 x 27 cm area with 1000 kW HRRPUA) was placed on driver seat, under the broken front left window. The simulation included 45 minutes of fire. The HRR was increasing after windows of the first car were broken and fire afflicted

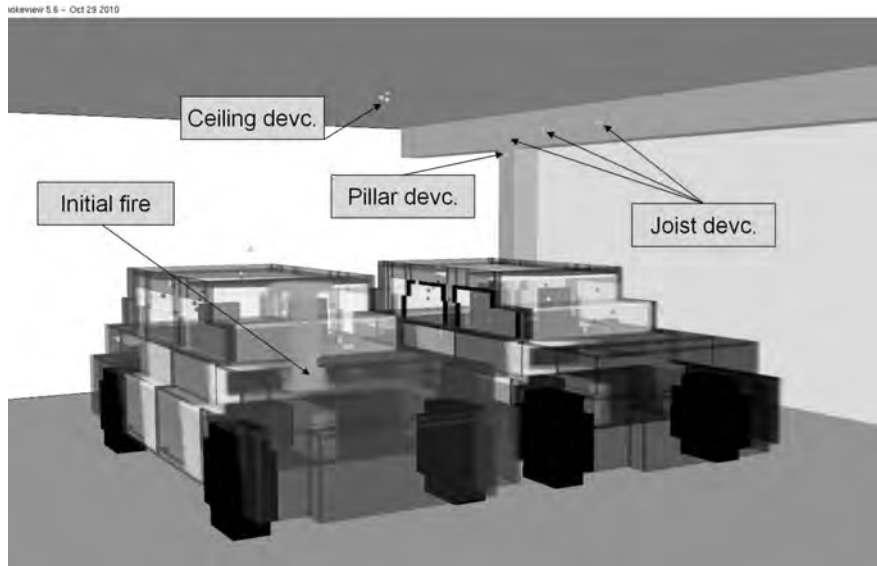


Fig. 5 Simulation configuration: mutual position of automobiles



Fig. 6 Fire behaviour at the 372<sup>nd</sup> second



Fig. 7 Fire behaviour at the 1000<sup>th</sup> second

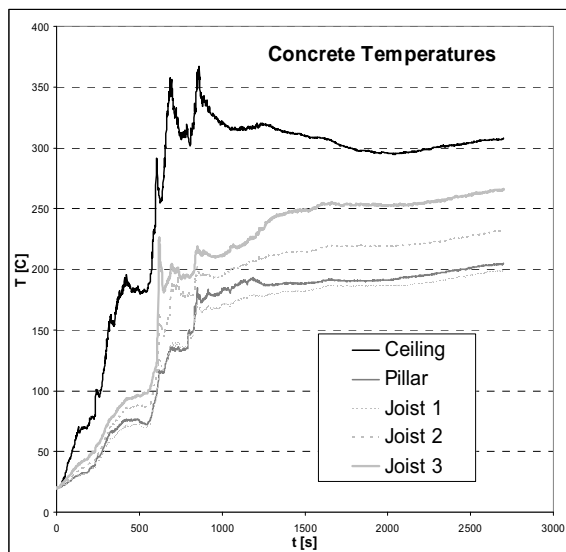


Fig. 8 Concrete temperatures behaviour

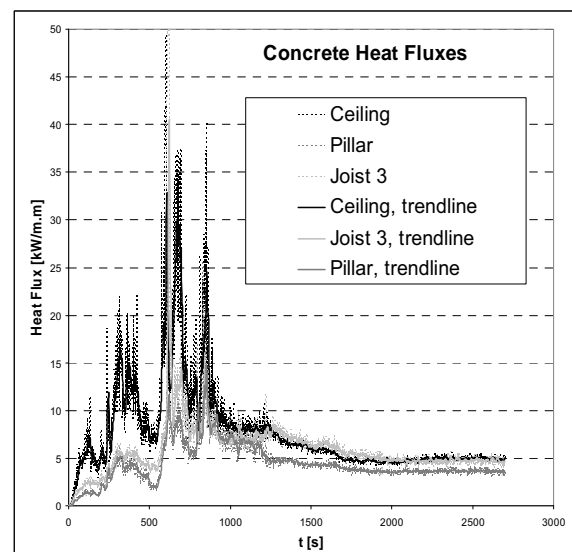


Fig. 9 Concrete heat fluxes behaviour

the second car, until it reached approximately 6 MW at the 15<sup>th</sup> minute and then it dropped slightly and stabilised above 4 MW. The most important devices measuring temperature and heat flux were placed on the ceiling, pillar and joist (see. Figs. 5-7). These quantities as well as HRR behaviour can be seen in Figures 8-13. Some parameters characterising the fire behaviour and simulation performance are presented in Tab. 2. As some uncertainty concerning material properties of main materials must be taken into account, we performed also a simulation in which the 350 kW HRRPUA for both materials was used. In this simulation, significantly higher HRR was achieved (see Fig. 11).

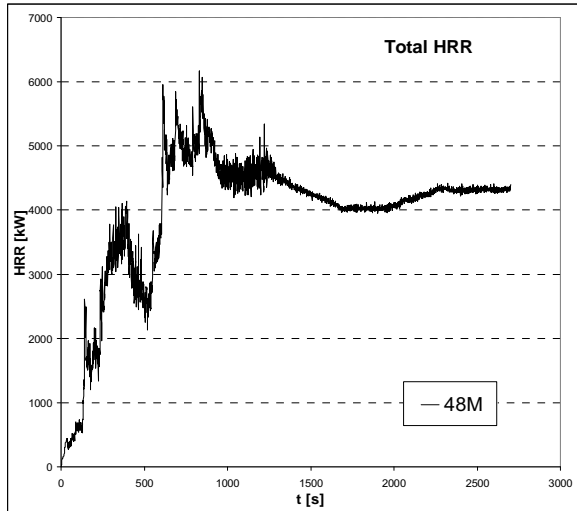


Fig. 10 HRR behaviour for 48M simulation

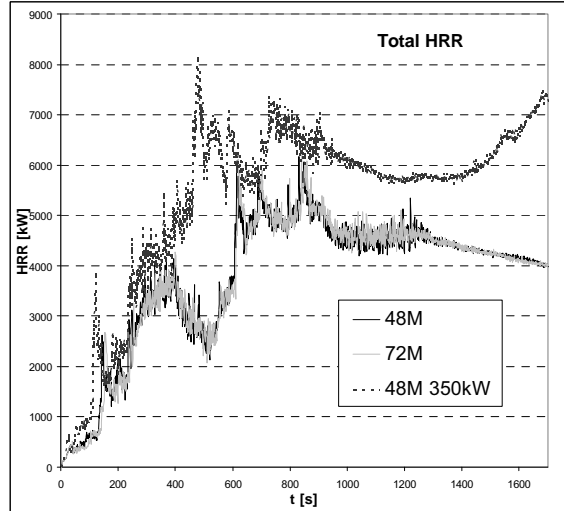


Fig. 11 HRR of different simulations

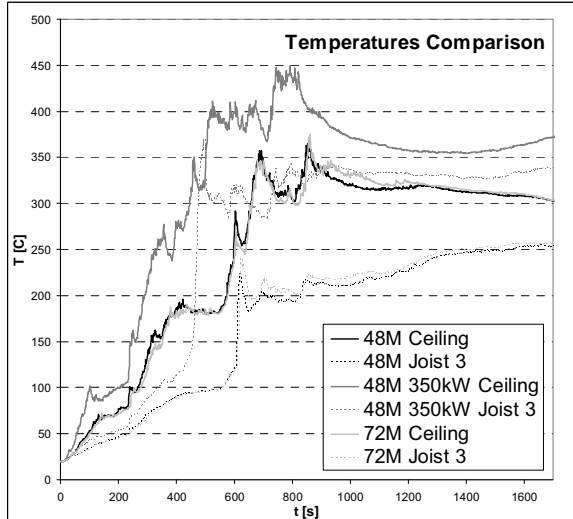


Fig. 12 Temperature behaviour of different simulations

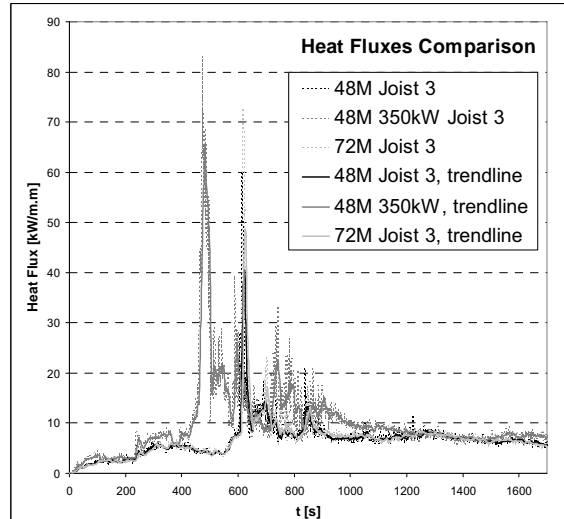


Fig. 13 Heat fluxes of different simulations

Tab. 2 Simulation results and calculations performance.  $t_{FL1}$  and  $t_{FL2}$  is time of flashover of the 1<sup>st</sup> and 2<sup>nd</sup> car interior, respectively,  $t_{IGN}$  is the time of the 2<sup>nd</sup> car bodywork ignition,  $T_{ceil,max}$  is the maximal ceiling temperature,  $t_{ceil,max}$  is the time in which this temperature was achieved and  $T_{j1700}$  and  $q_{j1700}$  is the temperature and heat flux of concrete joist at 1700<sup>th</sup> second.

	$t_{FL1}$ [s]	$t_{IGN}$ [s]	$t_{FL2}$ [s]	$T_{ceil,max}$ [°C]	$t_{ceil,max}$ [s]	$T_{j1700}$ [°C]	$q_{j1700}$ [kW.m <sup>-2</sup> ]
48M	28	224	548	367	861	254	5-6
72M	28	233	553	371	862	255	5-6
48M, 350	20	180	403	448	792	338	7-8



### 3 SUMMARY

The simulation results suggest, that car fire of such extent as was considered in the simulation does not constitute any critical threat for construction stability, which is in accordance with (Zhao et al, 2004). However, the simulation results are strongly dependent on material properties, especially on HRRPUA of interior equipment materials. Further research is required to refine these values in order to increase the simulation reliability. Moreover, the more detailed model of the complete car, not only the passenger compartment is needed to obtain more realistic fire behaviour during the whole period of fire (see the fire behaviour after the 1200<sup>th</sup> second in Fig. 10). Nevertheless, our simulation demonstrated potential of the FDS computer simulation to contribute to solving problems connected with structural fires even in very complex fire scenarios.

### 4 ACKNOWLEDGMENTS

The authors would like to thank to P. Polednak and J. Flachbart for the organization of automobile fire experiments and to J. Aсталos, P. Slizik and V. Sipkova for technical support of cluster calculations. This paper was partially supported by the VEGA (project VEGA 2/0216/10) and ERDF (Operational Programme Research & Development, ITMS 26240220060) agencies.

### REFERENCES

- Andreini, A., Da Soghe, R., Giusti, A. and Caruso, L., Pyrolysis Modeling And Numerical Simulation Of Rail Carriage Fire Scenarios For The Safe Design Of A Passenger Train. Proceedings of 7<sup>th</sup> Mediterranean Combustion Symposium, Chia Laguna, Italy, 2011.
- Heinisuo, M., Laasonen M. and Partanen M., Effect of Eurocode 1 Annex E factors to the gas temperatures in car park fires, [http://people.fsv.cvut.cz/~wald/fire/ifer/2012-Autumn-Meeting/Zadar\\_autopalo\\_Markku.pdf](http://people.fsv.cvut.cz/~wald/fire/ifer/2012-Autumn-Meeting/Zadar_autopalo_Markku.pdf), COST Project Autumn Meeting, Zadar, 2012.
- McGrattan, K., Klein, B., Hostikka, S. and Floyd, J., Fire Dynamics Simulator (Version 5): User's Guide, NIST Special Publication 1019-5, NIST, Washington, 2009.
- Okamoto, K., Watanabe, N., Hagimoto, Y., Chigira, T., Masano, R., Miura, H., Ochiai, S., Satoh, H., Tamura, Y., Hayano, K., Maeda, Y. and Suzuki, J., Burning Behaviour of Sedan Passenger Cars. *Fire Safety Journal*, 44, 2009.
- Polednak, P., Experimental Verification of Automobile Fires (in Slovak). Proceedings of the 4<sup>th</sup> International Conference on Fire Safety and Rescue Services, Zilina, Slovakia, 2010.
- Svetlik, J., Fire in the passenger car engine compartment (in Slovak). Proceedings of the 4<sup>th</sup> International Conference on Fire Safety and Rescue Services, Zilina, Slovakia, 2010.
- Weisenpacher, P., Glasa, J. and Halada, L., Parallel simulation of automobile interior fire and its spread onto other vehicles. Proceedings of the International Congress Fire Computer Modeling (J. A. Capote, ed.), Santander, Spain, 2012.
- Zhao, B. and Kruppa, J., Structural Behaviour of an Open Car Park under Real Fire Scenarios, *Fire and Materials*, 28, 2004.

# TEMPERATURE ANALYSIS OF LIGHTWEIGHT AGGREGATE CONCRETE SLAB MEMBERS AT ELEVATED TEMPERATURES FOR PREDICTING FIRE RESISTANCE

Michal Hora <sup>a</sup>, Radek Štefan <sup>a</sup>, Jaroslav Procházka <sup>a</sup>

<sup>a</sup> Department of Concrete and Masonry Structures, Faculty of Civil Engineering, Czech Technical University in Prague, Czech Republic

## Abstract

This paper is focused on lightweight aggregate concrete with expanded clay and its issues according to fire resistance. The procedures and recommendations for the calculation of fire resistance of lightweight aggregate concrete structures are presented. These procedures are based on nowadays methods for normal-weight concrete structures. These methods are modified in order to cover specific parameters and properties of lightweight concrete structures.

**Keywords:** lightweight concrete, expanded clay, fire resistance, elevated temperatures, transient heat, specific heat, thermal conductivity

## INTRODUCTION

Lightweight aggregate concrete (LWAC) has several advantages in comparison to normal-weight concrete (NWC). The most obvious one is lower bulk density and corresponding lower dead load of a construction. That can result in smaller cross-section of construction elements. In addition, cutting down transportation costs for precast elements is also a benefit. The lower bulk density corresponds with the lower thermal conductivity as well. This ability makes LWAC more suitable for heat insulating constructions as façade walls and precast panels. The most common use of in-situ pumping LWAC is for composite steel and concrete structures, especially for high-rise buildings when lesser loading for columns is needed.

These advantages are also disadvantages from another point of view. LWAC has higher porosity. It can result in higher absorbing capacity of water and lower compressive strength. Fire resistance of a structural member made of LWAC is mainly affected by parameters such as free water content, permeability, porosity of microstructure, coefficient of thermal expansion between cement paste and aggregate. Free water content accelerates pore pressure in concrete at elevated temperatures for instance. Together with low permeability, it can result in spalling phenomena.

This paper presents a numerical model of transient heat transport. The model is based on elementary thermo-dynamics equations to predict temperature profile of cross-section of a slab element during fire. Temperature profile of concrete is influenced by these material characteristics: bulk density, thermal conductivity, specific heat. Data for these characteristics (Constitutive relations-Models of material characteristics) are based on the fire test of the LWAC precast panels, several cited papers, literature and standards (Euro codes, ACI, BS). Fire resistance of LWAC panels is calculated with implementation of the assembled material models. Then comparison between the NWC and LWC is carried out.

## 1 FIRE RESISTANCE OF LWAC WITH EXPANDED CLAY AGGREGATE-STATE OF THE ART

There are several theories declaring fire resistance of LWAC is higher than NWC. These theories are based on the following three main statements.

- The first statement is that LWAC is less heat conductive than NWC. Therefore, gradient of temperature profile of cross-section is higher. This is caused by aggregate that is more porous.
- The second one is modul of elasticity. The modul of elasticity of expanded clay aggregates are similar to the modul of elasticity of hardened cement paste. That is a result of high temperature during manufacturing expanded clay aggregates that could exceed 1100°C. That temperature is similar to sintering temperature of cement. Therefore, LWAC with expanded clay aggregates is more compact under loading condition due to lower micro-cracking on the contact zone between lightweight aggregate and cement paste.
- The last statement is also derived from similar manufacturing temperature of cement and aggregate. Due to high temperature during manufacturing, expanded clay is more stable at elevated temperatures. Thus the coefficient of thermal expansion between a cement paste and aggregate is also similar.

## 2 FIRE TEST OF LWAC PRECAST PANELS

Many of further studies and assumptions are based on the fire tests of LWAC with expanded clay aggregate that were done in Czech Republic. The purpose of the fire test was to determine fire resistance of LWAC precast panels made of L25/28-D1,6 concrete (according to EN 1365-2:2000 and EN 1363-1:2000 ). The scheme of the test is in Fig. 1.

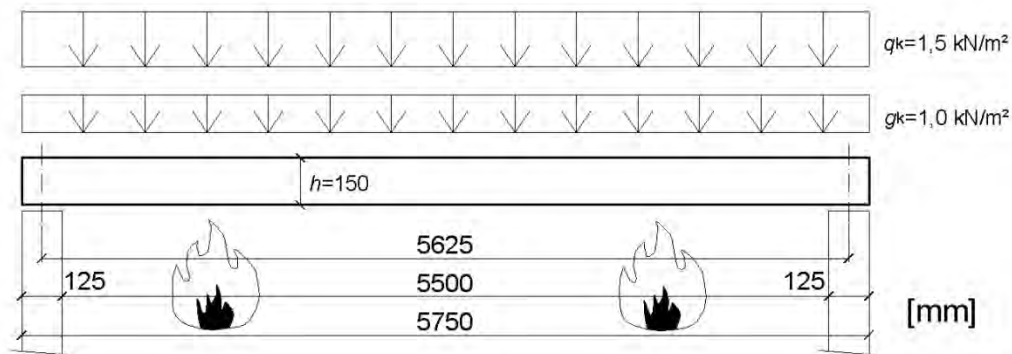


Fig. 1 Scheme of the fire test

Before the fire test was done, basic material characteristics had been measured (bulk density, moisture content, thermal conductivity). Those material characteristics are essential for further determination of material models at elevated temperatures and for simulation of behaviour LWAC panels at elevated temperatures. Temperatures on the unexposed side and deformation were measured during the fire test.

## 3 CONSTITUTIVE RELATIONS-MODELS OF MATERIAL CHARACTERISTICS

Generally, the temperature profile of cross-section of a construction is affected by three material characteristics: bulk density, specific heat and thermal conductivity. All of these characteristics are temperature and moisture dependent. Temperature is solved by numerical solution of transient heat. Development of moisture content during fire is indirectly implemented into material models. This approach brings simplification and there is no need to

solve a hydrothermal model of coupled temperature and moisture transport. In addition, less data of material characteristics are needed. Only data needed are the ones that have been measured on dry samples and samples with common temperature and common moisture content so that every laboratory could measure them.

Several models are assembled according to standards (EN 1992-1-2, EN 1994-1-2) or slightly modified. Other models are assembled in order to fit results obtained from the fire test. Empirical prediction of moisture content progress during fire loading is essential for all models.

#### 4 NUMERICAL SOLUTION AND FIRE RESISTANCE CALCULATION

The numerical solution of temperature distribution is implemented into MATLAB program. Its workspace provides effective tools for matrix equations.

The 1-D transient heat transport model is used. The dimension of the numerical model was chosen as 1-D in order to cover only slab or wall elements. Moisture content must not be omitted hence is implemented into constitutive relations (Constitutive relations-Models of material characteristics).

Fire resistance of a structural member (panel, slab) is calculated according to temperature distribution. The calculation is done using EN 1992-1-2 standard.

Fire resistance of slab members is based on flexural strength in concrete member during fire condition. The equilibrium on a cross section is calculated in every 10s (time increment) and then the resisting bending moment is calculated and compared with the applied internal bending moment (Fig 2).

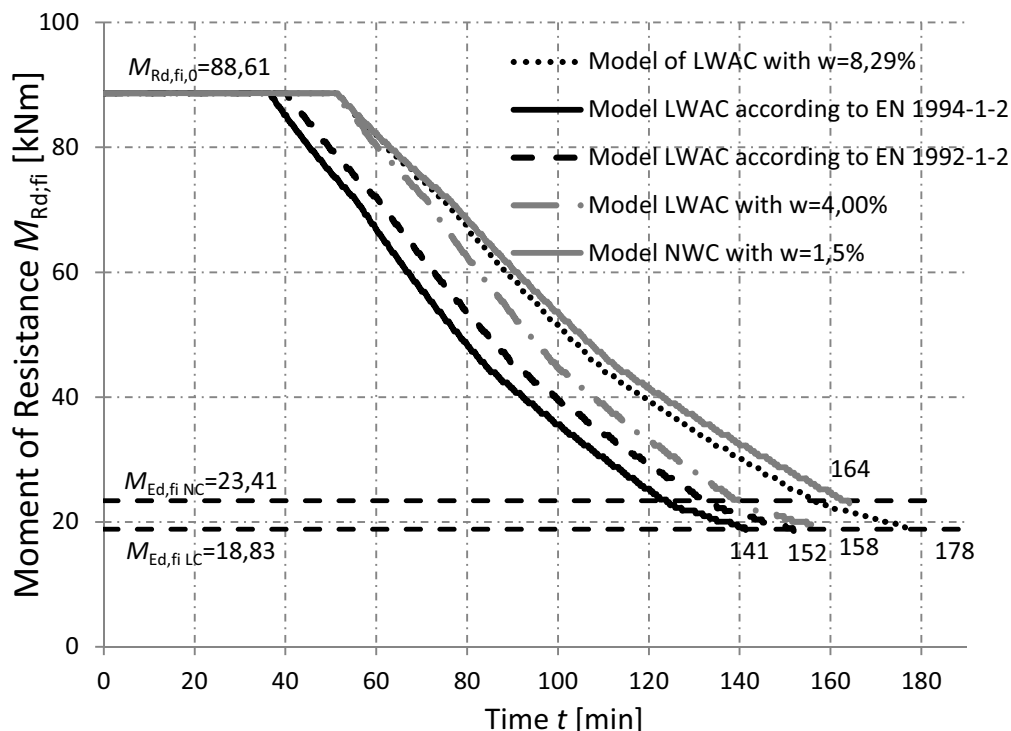


Fig. 2 Fire resistance comparison of panels with different material models

Apparently better fire resistance of LWAC panels is caused by lower dead load (lower bulk density) in case of heating the tensile side. The fact that LWAC has lower thermal conductivity is important for insulation on the unexposed side. Fire resistance in this case of fire (tensile side is heated) is determined by heating of reinforcement bars. So reduction coefficients of concrete at elevated temperatures are not used in this case because failure of reinforcement appears before. Every curve has different gradient of temperature as can be seen in Fig. 3. It is caused by different volumetric heat capacity (product of bulk density and

specific heat). This value is higher for NWC (higher bulk density) thus more time is needed to heat NWC. However, higher thermal conductivity of NWC causes higher temperatures on the fire-unexposed side. Volumetric heat capacity is also influenced by moisture content.

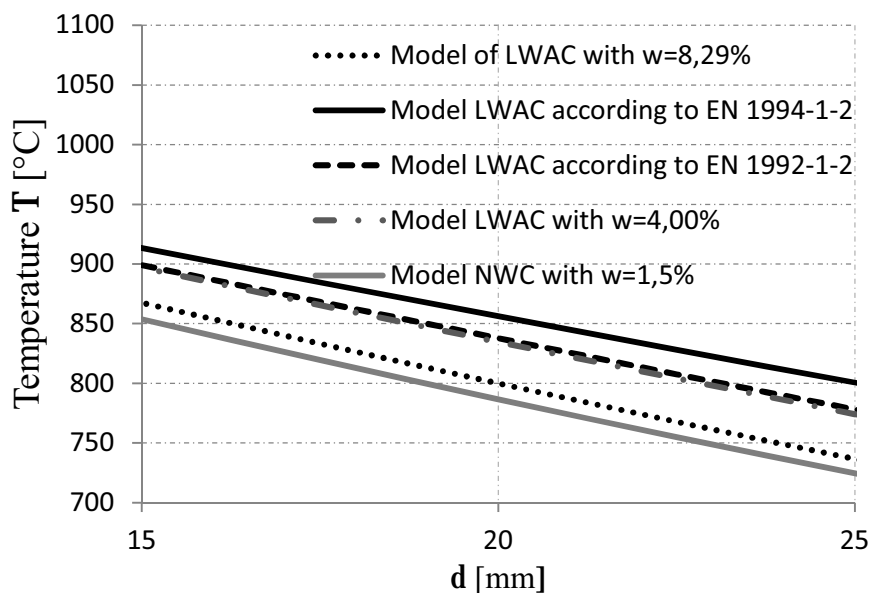


Fig. 3 Temperatures of reinforcement bars of panels with different material models

## 5 CONCLUSIONS

Fire resistance of slab member is highly influenced by location of fire, if it is on the tensile side or the side in compression. In condition of heating the tensile side of a member, fire resistance is determined by temperature of reinforcement bars. Slab member shows similar failure as in case of normal temperatures but with a few differences. The redistribution of internal forces is quicker and large deformations are observed.

Fire resistance of a slab member made of LWAC is mainly influenced by volumetric heat capacity. The higher volumetric heat capacity is, the lower temperatures of reinforcement bars are observed. Generally, materials with higher bulk density have higher volumetric heat capacity. Nevertheless, members made of LWAC has better insulating functions due to lower thermal conductivity.

### 5.1 Comparison between LWAC and NWC

The material models described in this paper were based on the fire test of LWAC with expanded clay and others materials with similar contain. All assumptions were made with neglecting explosive spalling.

Based on the results of this study, the following conclusions are written:

- Fire resistance of horizontal constructions (slabs, panels) made of LWAC with expanded clay aggregate is lower than NWC.
- Fire resistance of vertical constructions (columns) made of LWAC with expanded clay aggregate can be higher than NWC. It is caused by lower thermal conductivity results in lower temperatures in the centre of a member and higher values of the strength reduction coefficient ( $k_c$ ) of concrete at elevated temperatures.
- Fire insulating function is higher at LWAC panel than NWC panel.
- The moisture content should be limited due to high risk of spalling. Especially expanded clay aggregate is more likely to absorb water.

## REFERENCES

- Neville, A.M., Properties of Concrete, Paerson Education Limited, Edinburgh 2003, ISBN 0-582-23070-5.
- Chandra S., Berntsson L., Lightweight Aggregate Concrete–Science, Technology and Applications, Norwich, NY, USA: Noyes Publication, 2003, ISBN 0-8155-1486-7.
- Newman J., Choo Ban S., Advanced Concrete Technology: Constituent Materials, Oxford, UK, Elsevier, 2003, ISBN 0-7506-5103-2.
- Zhenai G., Xudong S., Experiment and Calculation of Reinforced Concrete at Elevated Temperatures, Tsingua University, 2011, ISBN: 978-0-012-386962-3.
- Jansson R., Measurement of thermal properties at elevated temperatures-Brandforsk project 328-031, SP Swedish National Testing and Research Institute, 2004, ISBN 91-85 303-22-4.
- EN 1992-1-2 Eurocode 2: Designing of concrete structures-Part 1-2: General rules for buildings–Structural fire design.
- EN 1992-1-1 Eurocode 2: Designing of concrete structures-Part 1-1: General rules for buildings.
- EN 1994-1-2 Eurocode 4: Designing composite steel and concrete structures-Part 1-2: General rules for buildings–Structural fire design.
- EN 1992-1-2 Eurocode 1: Action on structures-Part1-2: General actions-Actions on structures exposed to fire.
- EN 1996-1-2 Eurocode 6: Designing of masonry structures-Part 1-2: General rules-Structural fire design.
- ACI 213R-03: Guide for Structural Lightweight-Aggregate Concrete. American Concrete Institute, 2003.
- E119-00a: Standard Methods for Fire Tests of Building Construction and Materials. ASTM International
- BS 476-20: Fire Resistance Test to Building Material. British Standard
- Khoury A., Anderberg Y., Concrete spalling review, Fire Safety Design (FSD), Swedish National Road Administration, June 2000.
- Valore R.C., Insulating Concretes, Journal of the American Concrete Institute, 1957.
- Santos, W.N., Effect of moisture and porosity on the thermal properties of conventional refractory concrete, Journal of the European Ceramic Society 23 (2003) 745-755, Elsevier 2003.
- Wang Hong-Bo, Heat transfer analysis of components of construction exposed to fire, A Thesis submitted for degree of Doctor of Philosophy, Department of Civil Engineering and Construction, University of Salford, Manchester, M5 4WT, England, April, 1995.
- Othuman M.A., Wang Y.C., Elevated-temperature thermal properties of lightweight foamed concrete, Construction and Buildings Materials, Elsevier 2010.
- Lingard J., Hammer T.A., Fire resistance of structural lightweight aggregate concrete a literature survey with focus on spalling.
- Al-Sibahy A., Edwards R., Thermal behavior of novel lightweight concrete at ambient and elevated temperatures: Experimental, modeling and parametric studies, Construction and Building Materials, Elsevier 2011.
- Rahmanian I., Thermal and Mechanical Properties of Gypsum Boards and Their Influences on Fire Resistance of Gypsum Board Based Systems, A Thesis submitted for The degree of Doctor of Philosophy, Faculty of Engineering and Physical Sciences, University Manchester, M5 4WT, England, April, 2011.

- Nguyen T.D., Maftah F., Chammas R., Mebarri A., The behaviour of masonry walls subjected to fire: Modelling and parametrical studies in case of hollow burnt-clay bricks, *Fire Safety Journal* (Volume 44, Issue 4), Elsevier 2009.
- Sancak E., Sari Y.D., Simsek O., Effects of elevated temperature on compressive strength and weight loss of the light-weight concrete with silica fume and super plasticizer, *Science Direct Cement and Concrete Composites* 30 (2008) 715-721, Elsevier 2008.
- Andic-Cakir O., Hizal S., Influence of elevated temperatures on the mechanical properties and microstructure of self-consolidating lightweight aggregate concrete, *Construction and Building Materials*, Elsevier 2012.
- Tanyildizi H., Coskun A., Performance of lightweight concrete with silica fume after high temperature, *Construction and Building Materials*, Elsevier 2007.
- Demirel B., Kelestemur O., Effect of elevated temperature on the mechanical properties of concrete produced with finely ground pumice and silica fume, *Fire Safety Journal*, Elsevier 2010.

## **REINFORCED CONCRETE WALLS DURING FIRE**

### **Investigation of the Out-of-Plane Flexural Capacity**

William Hayhoe<sup>a</sup>, Maged A. Youssef<sup>a</sup>, Salah El-Fitiany<sup>a</sup>

<sup>a</sup> Western University, Department of Civil and Environmental Engineering, London, Ontario, Canada

#### **Abstract**

Current building codes address the design of concrete walls for fire by specifying minimum thicknesses and concrete covers based on required fire ratings. As building codes move towards performance-based design for fire, it is important to provide engineers with tools to design concrete walls to resist fire. The out-of-plane flexural capacity of a wall is critical to resist loads associated with the hose stream during fire-fighting efforts, wind loads, and movements perpendicular to the wall longitudinal axis. In this paper, a parametric study is conducted to evaluate the effect of different parameters on the out-of-plane flexural capacity. A simplified sectional analysis method is utilized to sketch the moment-curvature diagrams of different walls. Results are examined to assess the effect of each of the considered parameters on the wall out-of-plane performance and capacity.

**Keywords:** reinforced concrete, walls, fire resistance, elevated temperature, structural behaviour, out-of-plane, flexural capacity

#### **INTRODUCTION**

Reinforced concrete walls form an integral part of the structure of many buildings. They resist gravity, in-plane, and out-of-plane loads and provide fire separation between different compartments within a building. Designing concrete walls to resist the effects of fire is critical for the performance of structures and the safety of building occupants and fire fighters. Fire affects the performance of concrete members by reducing the strength and stiffness properties of concrete and steel and introducing new strains in the concrete in the form of thermal strains and transient creep strains. Currently, engineers design concrete walls for fire by specifying minimum thickness and concrete cover from applicable standards and building codes. However, building codes are moving towards performance-based design for fire and as a result there is a need to provide engineers with a simple method to design concrete walls for fire. One of the critical loads to be considered in this design is the pressure applied by the hose stream during fire fighting efforts (CPCI 2007). As this load is applied in the out-of-plane direction, it is critical to establish the out-of-plane capacity of concrete walls during fire. This paper addresses this need by utilizing a simplified sectional analysis method developed by El-Fitiany and Youssef (2009) to perform a parametric study and sketch moment-curvature diagrams for various walls. The effect of several different parameters, including axial load level, fire orientation, fire duration, concrete cover, and wall thickness, on the performance and capacity of the wall is noted and discussed.

#### **1 MODEL DESCRIPTION**

A detailed description of the method used to model concrete walls in this paper has been presented by El-Fitiany and Youssef (2009). In summary, the model uses the well-known sectional analysis method to predict the flexural and axial behaviour of reinforced concrete sections during exposure to elevated temperatures. The finite difference method is utilized to predict the temperature distribution throughout the section as a function of time. The section is divided into layers and temperature dependent properties of concrete and steel are then



calculated for each layer. The stress-strain relationship for concrete and steel at elevated temperatures proposed by Youssef and Mofteh (2007) is adopted in the model. This relationship accounts for the effects of transient creep by shifting the value of the strain at peak stress by the transient creep strain.

The average temperature of each layer is used to calculate the induced thermal strains. As the distribution of thermal strains is not linear throughout the section, an equivalent linear strain is evaluated such that the axial forces and bending moments in the concrete and steel are in self equilibrium. For each layer, the difference between the evaluated linear strain and the actual thermal strain represents the induced mechanical strain required to retain the linearity of the section. This procedure ensures that plane sections remain plane, which is still the case at elevated temperatures (El-Fitiany and Youssef 2009). These induced mechanical strains are included as initial strains in the model. Once the distribution of the thermal strains is known, the mechanical strain in each layer can be calculated by subtracting the thermal strain from the total strain. Sectional analysis can then be performed using temperature dependent properties and the stress-strain relationship mentioned above. The advantages of this model are its simplicity and efficiency as compared to finite element models.

## 2 MODEL VALIDATION

Although this sectional analysis model has been previously validated (El-Fitiany and Youssef 2009; El-Fitiany and Youssef 2008), these validations have only considered column and beam specimens. Additional validation of the model for the case of walls was performed in this paper. The wall specimen tested by Crozier and Sanjayan (2000) was 150 mm thick and 3.2 m long, and was exposed to fire on its tension side. Concrete strength was 52 MPa. Reinforcement ratio of 0.25% was arranged in two layers and was placed considering a clear cover of 30 mm. The specimen was placed on its side and simply supported at each end, and was thus laterally loaded by its own self-weight in addition to an applied eccentric axial load. Results were presented in terms of mid-span deflection of the wall for up to one hour of fire exposure. The specimen was modelled using the method described in section 1, and the resulting curvature at various temperatures was used to predict the mid-span deflection of the wall. The good agreement between the predicted deflection and the measured deflection, Figure 1, provides further validation for the model, specifically in the case of walls.

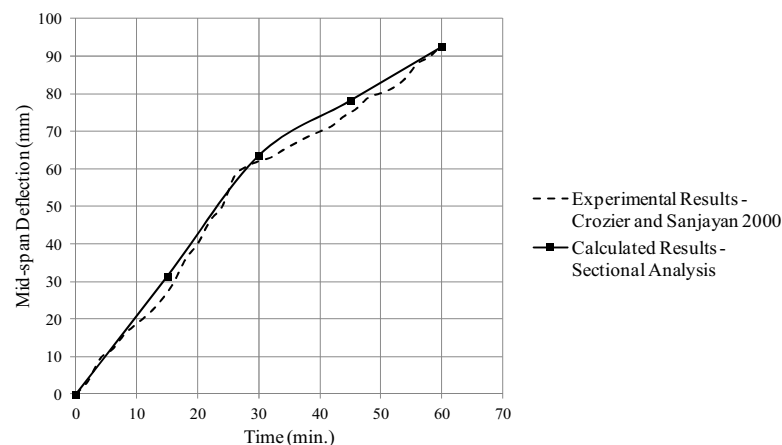


Fig. 1 Model Validation

## 3 PARAMETRIC STUDY

A parametric study was performed to investigate the effects of various parameters on the out-of-plane flexural capacity of concrete walls. A summary of the parameters included in the study, the range over which the parameters were considered, and the percentage effect on the

capacity is presented in Tables 1 to 3. Because the axial load level was found to have a significant influence, results are presented for two separate axial load levels, 0 and 0.4. An axial load level of 0 represents the pure flexural capacity of walls, and is valid as well for standard slabs. An axial load level of 0.4 corresponds to the approximate balance point on the interaction diagram for the wall. The results are presented for walls exposed to fire from their tension side, their compression side, or both sides. The tables show the percentages for the maximum change in capacity caused by varying each parameter within the range shown.

Tab. 1 Results - Fire on Tension Side of Wall

Parameter	Range	Effect on Flexural Capacity (axial load level = 0)	Effect on Flexural Capacity (axial load level = 0.4)
Fire Duration (hrs)	0-2	49.4%	79.7%
Concrete Clear Cover (mm)	20-60	65.6%	102.6%
Wall Thickness (mm)	210-400	32.8%	27.7%

Tab. 2 Results - Fire on Compression Side of Wall

Parameter	Range	Effect on Flexural Capacity (axial load level = 0)	Effect on Flexural Capacity (axial load level = 0.4)
Fire Duration (hrs)	0-2	73.5%	53.5%
Concrete Clear Cover (mm)	20-60	109.7%	108.4%
Wall Thickness (mm)	210-400	26.5%	22.6%

Tab. 3 Results - Fire on Both Sides of Wall

Parameter	Range	Effect on Flexural Capacity (axial load level = 0)	Effect on Flexural Capacity (axial load level = 0.4)
Fire Duration (hrs)	0-2	39.8%	46.9%
Concrete Clear Cover (mm)	20-60	69.2%	103.3%
Wall Thickness (mm)	210-400	28.2%	22.1%

Concrete and steel strength and reinforcement ratio were not included in the parametric study as previous studies had shown that these parameters have little effect on the capacity of a concrete wall (Crozier and Sanjayan 2000; O'Meagher and Bennetts 1991; Lee and Lee 2012). The walls were analyzed as sections only, and thus height-to-thickness ratios and buckling effects were not considered. All walls had a reinforcement ratio of 0.15%, concrete strength of 30 MPa, steel yield strength of 400 MPa, and were composed of siliceous type concrete. The reinforcement ratio of 0.15% corresponds to the minimum amount of reinforcement required by the Canadian concrete standard (CSA 2004). The effect of each of the different parameters is discussed in the following sections.

### 3.1 Axial load level

The presence of axial load had a significant effect on the moment capacity, increasing the capacity by up to 975%. This is due to the low reinforcement ratio in the walls, which results in lower moment capacity for walls with no axial load. The presence of a compressive axial load reduces or entirely eliminates any tension force in the wall. Results for a 210 mm thick concrete wall that was exposed to fire for one hour on its tension side and had a concrete cover of 20 mm are shown in Figure 2. As illustrated in the figure the presence of axial load had a large beneficial impact on the capacity of the wall. The figure also illustrates that an axial load level of 0.4 corresponds to the approximate balance point on the interaction diagram.

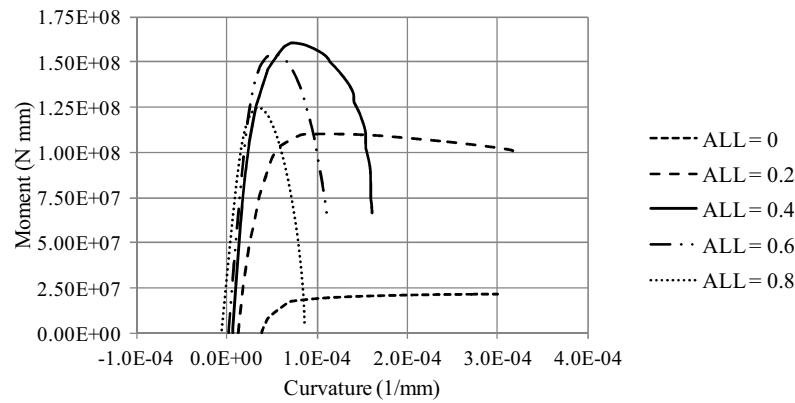


Fig. 2 Effect of Axial Load Level

The effects of higher axial load illustrated in Figure 2 were similar for all other fire orientations, fire durations, concrete covers, and wall thicknesses. As illustrated in Tables 1 and 3, the presence of axial load also had a significant impact on the effectiveness of concrete cover for walls exposed to fire on the tension side or from both sides. The flexural capacity of such walls with no axial load was significantly affected by increased cover, whereas the capacity of walls with higher levels of axial load was marginally affected by increased cover.

### 3.2 Fire Orientation

Changing the fire exposure from one to two sides was found to decrease the capacity of the wall up to 62% for walls exposed to fire on the tension side and up to 48% for walls exposed to fire from the compression side. As illustrated in Fig. 3, for the case of fire on the compression side of the wall the effect of two-sided fire exposure was markedly reduced by either increasing the axial load level or increasing the amount of concrete cover. All specimens shown in Figure 3 had a thickness of 210 mm, were exposed to fire for one hour, and in cases of one-sided fire exposure were exposed to fire on the compression side.

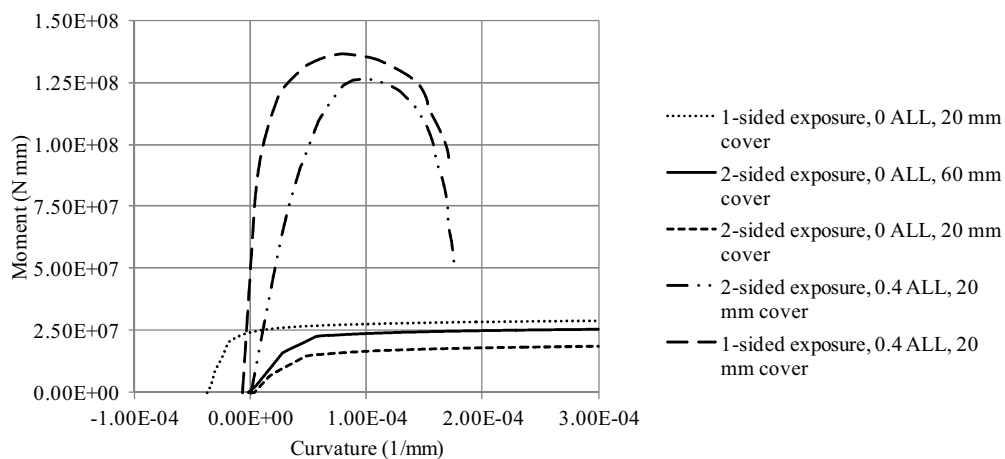


Fig. 3 Effect of Increased ALL or Cover on Reducing the Impact of Two-sided Fire Exposure

For cases of 20 mm cover and no axial load, walls exposed to fire on the tension side were approximately 70% weaker than the same walls exposed to fire on the compression side. Walls with 60 mm cover and no axial load had approximately the same capacity whether fire was applied to the tension or compression side. Walls with an axial load level of 0.4 performed approximately 20% better when exposed to fire on the tension side as opposed to the compression side. This is due to the fact that such walls failed in compression, with the compressive strength further reduced due to fire exposure.

### 3.3 Fire duration

As illustrated in Tables 1 and 2, increasing the fire duration from 0 to 2 hours in walls exposed to fire from either the tension or the compression side significantly lowered the moment capacity. As is expected and as illustrated in Figure 4, the effect of increasing the fire duration was slightly more pronounced in the cases of walls exposed to fire from both sides, up to a maximum of 40%. All walls shown in Figure 4 had a thickness of 210 mm, cover of 20 mm, and were exposed to fire from both sides.

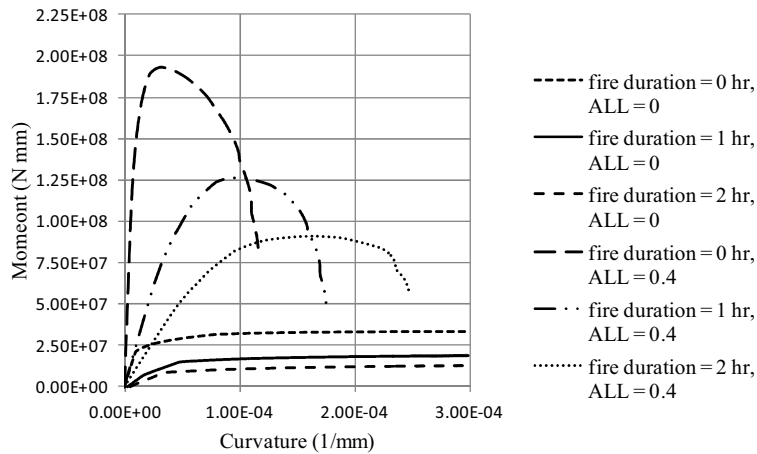


Fig. 4 Effect of Fire Duration on Walls Exposed to Fire on Both Sides

### 3.4 Concrete cover

As illustrated in Tables 1 and 3, decreasing the concrete cover from 60 mm to 20 mm decreased the capacity of the walls by a maximum of 65-70%. This is because an increased concrete cover provides better temperature insulation for the reinforcement, thus lowering the impact of the fire on the strength of the reinforcement. This reduction of capacity was only representative of walls with both a low axial load and exposure to fire on the tension side. As illustrated in Figure 5, the effect of increasing the concrete cover for cases of an axial load level equal to 0.4 was negligible, and in the majority of cases slightly decreased the capacity. All walls shown in Figure 5 had a thickness of 210 mm, were exposed to fire on the tension side only, and had an axial load level equal to 0.4.

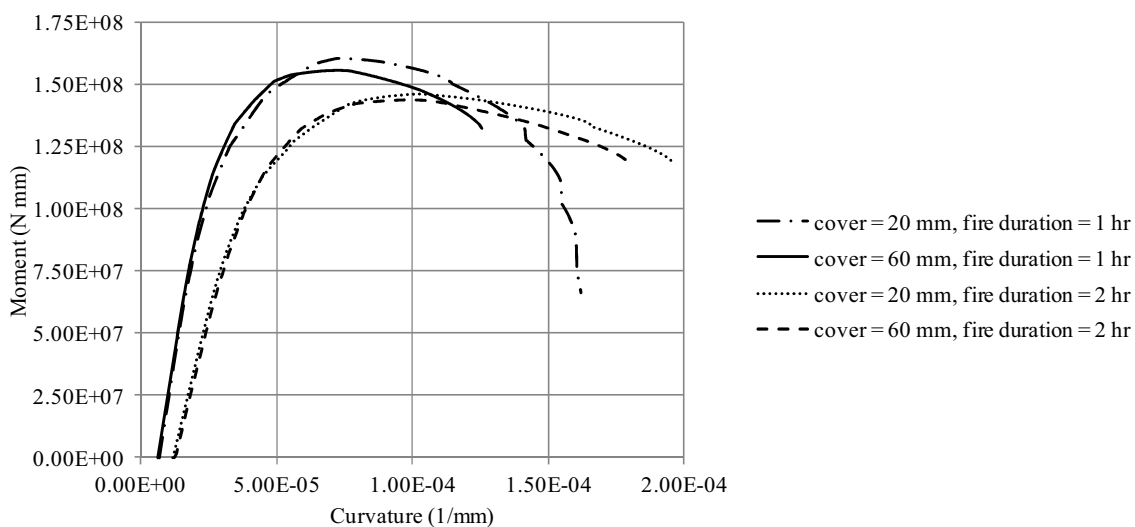


Fig. 5 Negligible Effect of Cover with a Higher Axial Load Level

### 3.5 Wall thickness

The results show that wall thickness is one of the most important parameters to be considered in the design of concrete walls for fire. As illustrated in Tables 1-3, the effect of varying the wall thickness from 400 mm to 210 mm was approximately uniform throughout all sections considered, ranging from 22% to 35%. In general the effect of the wall thickness on the capacity was approximately 5% greater for cases with an axial load level of 0 as opposed to cases with an axial load level equal to 0.4.

## 4 CONCLUSION

The results of this research show that all five parameters considered have a significant impact on the design of concrete walls for fire. Increasing the level of axial load up to a level of 0.4 significantly increased the out-of-plane flexural capacity of all walls considered. The significant effect of axial load level illustrates the importance of considering different load cases during the design of concrete walls for fire, as the case of minimum axial load will likely govern the out-of-plane capacity. Another reason to consider different axial load cases is the fact the failure mode of the wall is dependent on the axial load level.

Changing the fire exposure from one to two sides significantly reduced the capacity of many of the walls considered. In the case of fire on the tension side of the wall, this effect was less significant in walls with a thickness of 400 mm. In the case of fire on the compression side of the wall, this effect was less significant in walls with a higher axial load level or increased concrete cover. The varying effects of fire orientation illustrate the importance of considering all possible fire loading scenarios in the design of concrete walls.

The results show that concrete cover is a significant parameter only in cases where the tension side of the wall is exposed to fire and there is a low amount of axial load. In cases where these requirements are not met an increased amount of concrete cover was either negligible or slightly decreased the capacity of the wall.

Finally, the results show that wall thickness is one of the most important parameters to be considered. The beneficial effects of increased wall thickness were approximately uniform for all cases considered.

## REFERENCES

- Canadian Precast and Prestressed Concrete Institute, CPCI Design Manual 4, Canada, 2007.
- Canadian Standards Association, CSA A23.3-04 Design of Concrete Structures, 2004.
- Crozier, D. A., Sanjayan, J. G., Tests of Load-bearing Slender Reinforced Concrete Wall in Fire, *ACI Structural Journal*, vol. 97, pp. 243-253, 2000.
- El-Fitiany, S., Youssef, M. A., Assessing the Flexural and Axial Behaviour of Reinforced Concrete Members at Elevated Temperatures using Sectional Analysis, *Fire Safety Journal*, vol. 44, no. 5, pp.691-703, 2009.
- El-Fitiany, S., Youssef, M. A., Stress-block Parameters for Reinforced Concrete Beams during Fire Events, *ACI Fall 2008 Convention: Innovations in Fire Design of Concrete Structures*, 2008.
- Lee, S. Lee, C., Fire Resistance of Reinforced Concrete Bearing Walls Subjected to All-sided Fire Exposure, *Materials and Structures*, in-press, 2013.
- O'Meagher, A. J., Bennetts, I. D., Modelling of Concrete Walls in Fire, *Fire Safety Journal*, vol. 17, pp. 315-335, 1991.
- Youssef, M. A., Moftah, M., General Stress-strain Relationship for Concrete at Elevated Temperatures, *Engineering Structures*, vol. 29, no. 10, pp. 2618-2634, 2007.









## AN ALTERNATIVE SIMPLIFIED MODEL OF TENSILE MEMBRANE ACTION OF SLABS IN FIRE

Ian W. Burgess<sup>a</sup>, Xu Dai<sup>a</sup>, Shan-Shan Huang<sup>a</sup>

<sup>a</sup> University of Sheffield, Dept. of Civil and Structural Engineering, UK

### Abstract

This paper presents an initial re-examination of the mechanisms of tensile membrane action of thin concrete floor slabs. The study is based on a large-deflection plastic analysis, which can apply to either isolated or continuous slabs at ambient or high temperatures. The basic calculation method considers plain flat slabs, but is in no way limited to these, or to isotropic reinforcement. The new method is compared against the generic Bailey-BRE method, indicating for some typical examples that the actual enhancement of yield-line capacity due to TMA can be over-estimated by the latter.

**Keywords:** steel frames, fire, composite slab, tensile membrane action, Bailey-BRE method.

### INTRODUCTION

Before 2000, there was only one way of ensuring the fire resistance of steel-framed buildings with composite flooring systems, which was simple but over-conservative. This traditional method considers the composite floor as an array of parallel, simply supported, composite beams, and implies that each of the steel downstand sections which form the tension zone of a composite beam needs to be provided with an insulating cover, in the same way as the non-composite steel columns. This takes no account of the intrinsic fire resistance of the structure due to its continuity.

A simplified design method for composite slabs to resist fire was introduced by Bailey & Moore (2000a, b). This method was based very largely on a calculation of the enhanced load capacity of concrete slabs at high deflections, due to their membrane strength, which had been published by Hayes (1968). The method has since then become widely used in practical fire engineering design, and has recently been published in both the UK (Simms & Bake 2010) and New Zealand (Clifton 2006) as freely-available public-domain design software. Within the EU, the project FRACOF (Vassart & Zhao 2011a, b) has recently extended this simplified method to the Eurocode context, and this project has resulted in a design process which is extremely similar to that in the UK.

In fire conditions, when the temperatures of both unprotected and protected steelwork become extremely high, the mechanism which controls the load resistance of floor systems changes increasingly at high deflections, from the bending strength of the array of composite beams which applies in normal ULS design to tensile membrane action (TMA). In TMA the highly deformed concrete slab effectively carries the loading when the strength of the attached downstand steel beam sections has reduced dramatically at high temperatures. TMA enhances the floor system's load capacity compared with the usual small-deflection capacity based on the optimum plastic yield-line mechanism. However, the structural mechanics of the Bailey method is not completely transparent; at more than one stage purely empirical assumptions are made. The effects of these assumptions are by no means clear. This study takes a fresh look at TMA of thin concrete floor slabs at large deflections, with the prime objective of making kinematically consistent assumptions which eliminate the mechanical inconsistencies inherent in the existing methods..

### Load and deflection for a kinematically consistent TMA mechanism

A two-way spanning rectangular slab panel of aspect ratio  $r$ , which is transversely supported along all its four edges, is considered. The slab may either be considered as isolated (having no continuity with adjacent panels across these edges) or as continuous (adjacent panels on all four sides are assumed to deflect in the same way as the panel under consideration). The slab is lightly reinforced with a welded mesh, which for the purposes of this paper is considered to be isotropic, and the two layers of bars are assumed to lie at a single mean level within the slab.

The transverse loading intensity on the slab is increased until a plastic yield-line pattern of cracks forms, in the characteristic arrangement shown in Fig. 1. The optimum yield-line mechanism, giving the lowest possible failure load intensity, is given for either isolated or continuous cases by:

$$n = \frac{1}{2r} (-1 + \sqrt{1 + 3r^2}) \quad (1)$$

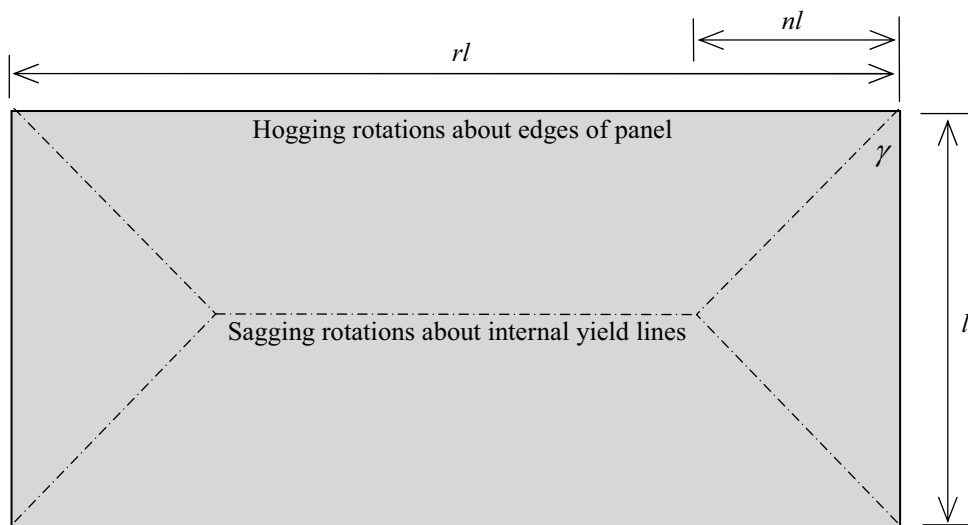


Fig 1: Small-deflection yield-line mechanism

If the load intensity is increased beyond the optimum small-deflection yield-line failure value at which this pattern of folds appears, any further deflection of the flat facets of the slab is assumed to be based on increasing the rotations about the yield lines. The existing simplified methods of calculating enhancement of load capacity due to TMA make use of the consistent observation from tests that a through-depth tensile crack subsequently appears across the shorter mid-span of the slab; in fire this tensile crack provides the possibility of a compartmentation integrity failure. If this crack is assumed to form, then six flat facets (four trapezoidal and two triangular) take part in the subsequent deformation of the slab. It can be seen from Fig. 2 that this mechanism causes four different crack types (denoted  $\alpha$ ,  $\beta_1$ ,  $\beta_2$  and  $\beta_3$ ) in different locations

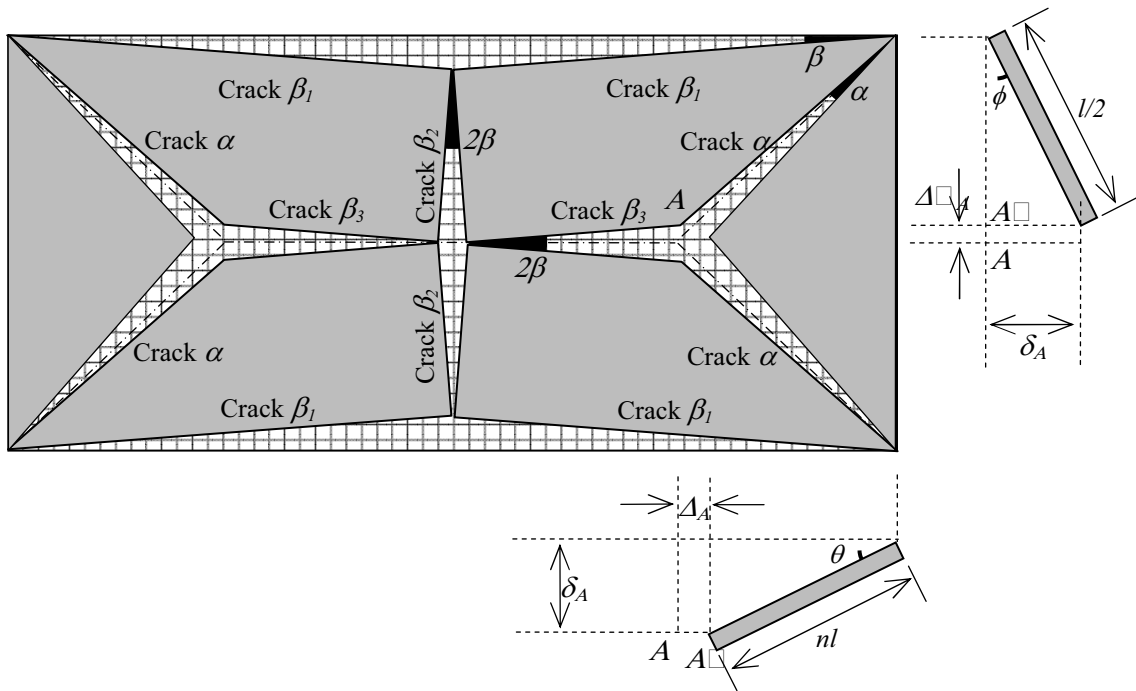


Fig 2: Plan and elevations of the slab facets at high deflection.

It is assumed that internal plastic work is done by stretching the reinforcing bars of the mesh across any relevant cracks; clearly in the case of an isolated slab panel no internal work is done either in cracks  $\beta_1$  or along the short-span panel edges. Across any crack the mesh bars in the long ( $x$ ) and short ( $y$ ) directions stretch independently, and the total internal work therefore consists of the aggregate for all bars which cross cracks of (*the yield force of a bar  $\times$  the crack crack opening at the level of the bar*). The relationships between the displacement  $\delta_A$  and the crack opening angles, assuming that the concrete compression zones at the ends of the cracks have negligible length, are:

$$\beta = \frac{1}{2r} \phi^2 \quad (2)$$

$$\alpha = n\theta^2 \cos^2 \gamma + \phi^2 \left[ \left( \frac{1}{2} - \frac{n}{r} \right) \sin \gamma \cdot \cos \gamma - \frac{1}{2r} \cos^2 \gamma \right] \quad (3)$$

in which

$$\theta = \frac{\delta_A}{nl} \quad \phi = \frac{2\delta_A}{l} \quad \gamma = \tan^{-1}(2n) \quad (4)$$

The crack opening in either the  $x$  or  $y$  directions at a particular rebar location is a function of the crack opening angle and of the rotation angle about the perpendicular axis between the slab facets which meet at the crack. The principle is illustrated in Fig. 3.

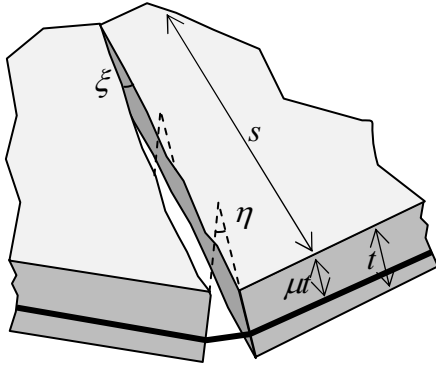


Fig. 3: Crack opening at rebar level.

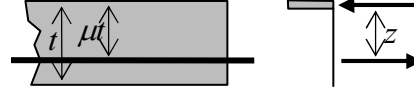


Fig. 4: Assumed reduced effective depth.

If the crack pivots about its top edge then the rebar extension is  $(\xi s + \eta \mu t)$ . However, a finite area of concrete at the top edge of the crack is actually needed to balance the tensile force across the crack. Although it may eventually be necessary to represent the exact size and shape of the compression area at the closed end of a crack, the assumption of balanced stress blocks, shown in Fig. 4, which is made in the existing simplified methods, is also used here to slightly reduce the lever arm from  $z = \mu t$  to

$$z = \mu t - \frac{1}{2} \left( \frac{f_y A_r}{f_c} \right) = \mu t - \frac{1}{2} \left( \frac{F_p}{f_c} \right) \quad (5)$$

in which  $A_r$  is the reinforcement area per unit slab width, and  $F_p$  is the yielded bar force per unit width of slab. It can be assumed that the reinforcement bars have a fracture ductility strain of  $\varepsilon_u$ , and that a bar anchors positively into the concrete where transverse bars are welded to it. The fracture strain is assumed to act on the transverse bar spacing to define a fracture crack width at the reinforcement level, with no diminution due to bond between the concrete and rebar. As a crack opens, the wide end will reach a width at which the bars begin to fracture, and with further opening the length of crack over which bars are fractured will increase. The components of the internal plastic work for the sagging yield lines are then expressed in terms of the dimensionless quantities:

$$\bar{t} = t/l \quad v = \frac{\Delta_{lim}}{l} = \frac{d_{sp}}{l} \varepsilon_u \quad (6)$$

in which  $d_{sp}$  is the inter-bar spacing in both directions and  $\Delta_{lim}$  is the crack width at which rebar fracture occurs.

For each yield line the plastic internal energy due to the  $x$ - and  $y$ -direction rebars can be calculated individually, over the length of the yield line (X or Y) for which the corresponding rebars are unfractured. Dimensionless versions of these unfractured lengths are denoted  $\bar{X} = X/l$  and  $\bar{Y} = Y/l$ .

The components of the internal plastic energy are then shown in Tab. 1. These are aggregated at each deflection step to form the total internal energy. Clearly, for an isolated slab, the components generated along the long and short slab edges are zero.

Tab. 1: Internal plastic energy components of slab at large deflections.

Crack	Rebar direction	Maximum rebar length/ $l$	Intact rebar length/ $l$ if bars fractured	Internal plastic energy	Factor for whole slab
$\alpha$	$x$	$\bar{Y} = 0.5$	$\bar{Y} = \frac{(v - \theta \mu \bar{t})}{\alpha}$	$W_{int, \alpha x} = F_p l^2 \bar{Y} \left( \frac{\alpha}{2} \bar{Y} + \theta \mu \bar{t} \right)$	4

	$y$	$\bar{X} = n$	$\bar{X} = \frac{(v - \phi\mu\bar{t})}{\alpha}$	$W_{int,\alpha y} = F_p l^2 \bar{X} \left( \frac{\alpha}{2} \bar{X} + \phi\mu\bar{t} \right)$	4
$\beta_1$	$y$	$\bar{X} = \frac{r}{2}$	$\bar{X} = \frac{(\frac{v}{2} - \phi(1 - \mu)\bar{t})}{\beta}$	$W_{int,\beta_1} = F_p l^2 \bar{X} \left( \frac{\beta}{2} \bar{X} + \phi(1 - \mu)\bar{t} \right)$	4c*
$\beta_2$	$x$	$\bar{Y} = 0.5$	$\bar{Y} = \frac{v}{2\beta}$	$W_{int,\beta_2} = F_p l^2 \bar{Y} (\beta\bar{Y})$	2
$\beta_3$	$y$	$\bar{X} = \left( \frac{r}{2} - n \right)$	$\bar{X} = \frac{(v - 2\phi\mu\bar{t})}{2\beta}$	$W_{int,\beta_3} = F_p l^2 \bar{X} \left( \frac{\alpha}{2} \bar{X} + \phi\mu\bar{t} \right)$	2
Short edge	$x$	$\bar{Y} = 1$	0	$W_{int,l} = F_p l^2 \bar{Y} (\theta(1 - \mu)\bar{t})$	2c*

\*  $c=0$  for isolated slab,  $c=1$  for continuous slab.

The aggregate internal energy is then

$$W_{int} = W_{int,\alpha x} + W_{int,\alpha y} + \sum_{i=1}^3 W_{int,\beta_i} + W_{int,l} \quad (7)$$

The external work (or loss of potential energy) of the uniform transverse loading, of intensity  $p$ , is expressed in the same way as for small deflections:

$$W_{ext} = p l^2 \delta_A \left( \frac{r}{2} - \frac{n}{3} \right) \quad (8)$$

Since rigid-perfectly plastic behaviour is being assumed for the reinforcing mesh,

$$W_{ext} = W_{int} \quad (9)$$

Thus the load capacity of the slab, at any deflection  $\delta_A$ , is therefore:

$$p = W_{int} / \left[ l^2 \delta_A \left( \frac{r}{2} - \frac{n}{3} \right) \right] \quad (10)$$

### Comparisons with the conventional simplified methods

Fig. 5 shows an example comparison between the load capacity enhancements given by the conventional methods and the new proposal. The example is for a 9m x 6m isolated slab 120mm thick, with A142 mesh (6mm bars at 200mm spacing in both directions) at the mid-depth (60mm from the top) of the slab. The steel grade is S500 and the concrete C30. In this case the fracture ductility of the reinforcing steel has been assumed to be 5%. In presenting the limiting deflection of the slab in the context of the conventional methods the component of that deflection which is derived from the assumed thermal bowing of the slab has been ignored, because the TMA is being considered independent of any temperature effects. It can be seen that the enhancement of capacity due to deflection differs between the methods; the new approach shows a lower rate of enhancement for this particular slab case. The new approach is capable of showing where reinforcement fracture begins and is completed for each yield line.

In this particular case the limiting deflection given in the Bailey/BRE or FRACOF methods occurs at roughly the same deflection as the peak load capacity which is caused by the start of rebar fracture in the longitudinal yield line  $\beta_3$ .

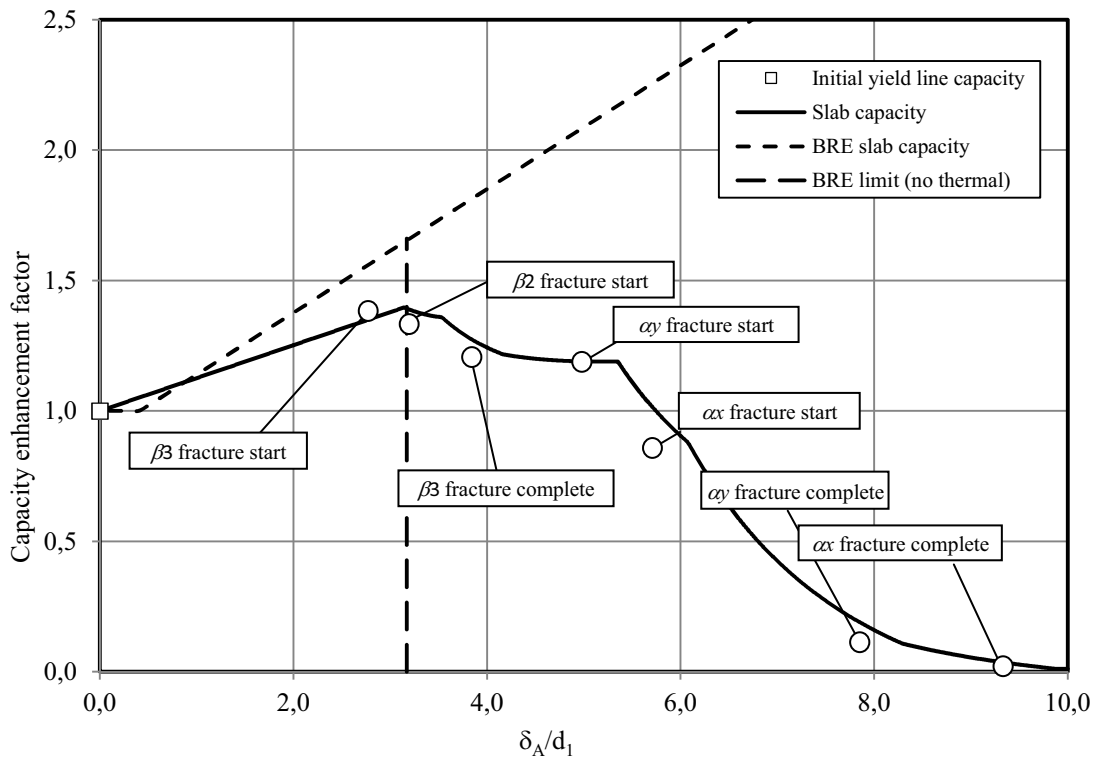


Fig. 6: Enhancement of yield-line capacity of a 9m x 6m slab by BRE and current approaches.

However Fig. 7, which considers different steel ductilities, shows that there is no inherent connection involved.

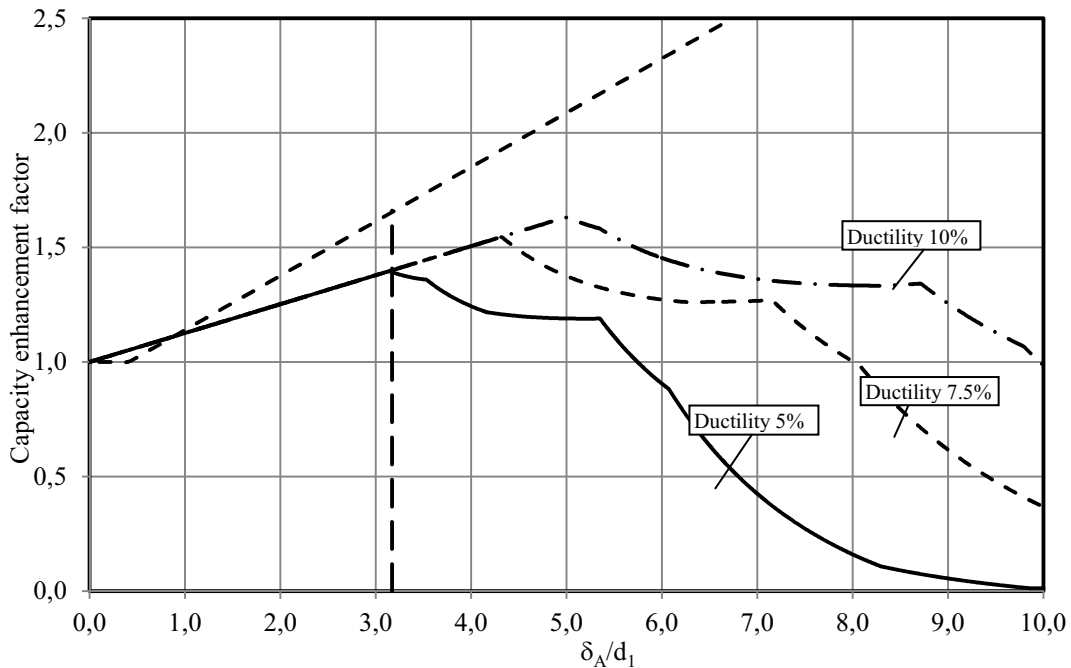


Fig. 7: Comparison between BRE method and the new approach with rebar fracture ductility.

In order to gauge how this approach correlates to the existing methods for slabs of different aspect ratio, the predicted enhancements of capacity for three slabs, 6m x 6m, 6m x 9m and 6m x 12m, reinforced as in the previous cases, are shown in Fig. 8. Clearly the actual yield-line capacities of the three cases are different, but since the enhancement factors are plotted, all of the curves begin at 1.0 enhancement at zero deflection. It can be seen that the gradients of the enhancements with intact reinforcement for any aspect ratio differ between the two

approaches; the discrepancy appears highest for the square panel, for which the ratio of the gradients is 0.45. For the slab of aspect ratio 2.0 the enhancement the enhancement gradients are almost identical.

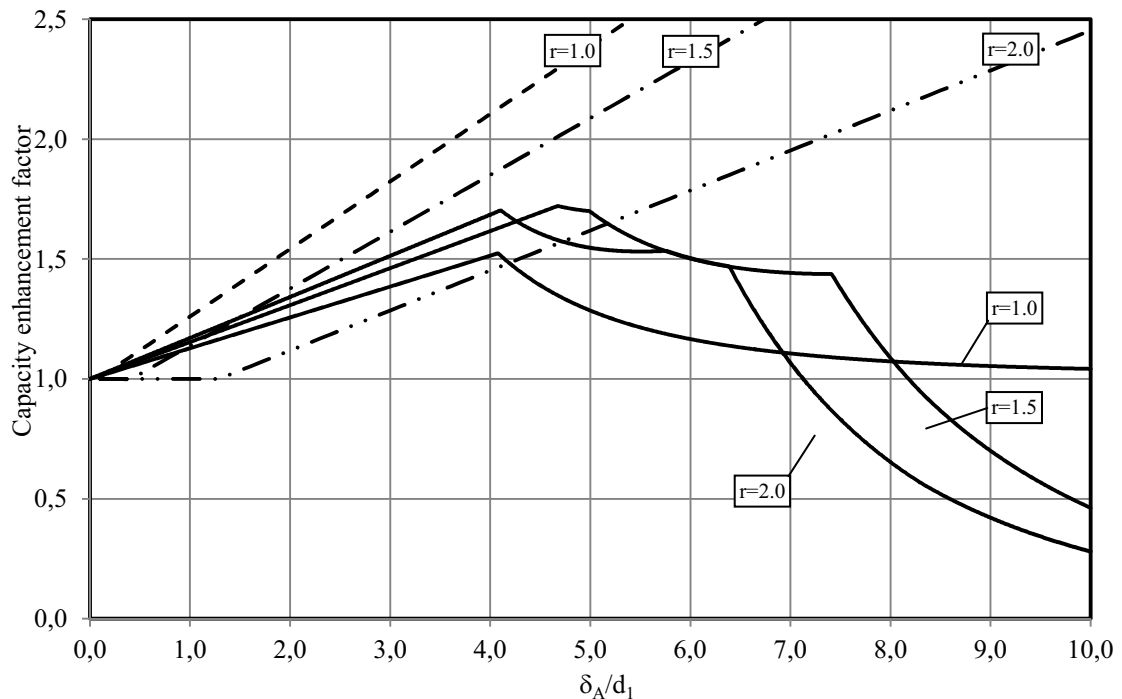


Fig. 8: Comparison between BRE enhancements and new approach with slab aspect ratio.

## DISCUSSION

The method developed here appears to have the advantage over the preceding approaches that it is clearly based on a kinematically admissible deflection model, and involves no arbitrary aggregation of “enhancements” from four different sources. The approach is easily capable of being extended to account for continuity, concrete crushing failure, orthotropic mesh and a rebar-concrete bond model. It can also examine different kinematically admissible deflection mechanisms without any change to its basic methodology; allowing lower-bound to be identified.

## REFERENCES

- Bailey, C.G. and Moore, D.B. (2000a), “The structural behaviour of steel frames with composite floor slabs subject to fire - Part 1 Theory”, *The Structural Engineer*, 78 (11), pp 19-27.
- Bailey, C.G. and Moore, D.B. (2000b), “The structural behaviour of steel frames with composite floor slabs subject to fire - Part2: Design”, *The Structural Engineer*, 78(11), pp28-33.
- Hayes, B. (1968), “Allowing for membrane action in the plastic analysis of rectangular reinforced concrete slabs”, *Magazine of Concrete Research*, 20 (65), pp205-212.
- Simms, W.I. and Bake, S. (2010), “TSLAB V3.0 User Guidance and Engineering Update”, SCI publication P390.
- Clifton, C. (2006), “Design of composite steel floor systems for severe fires”, HERA publication, Manukau City, New Zealand.
- Vassart, O. and Zhao, B. (2011a), “FRACOF : Fire resistance assessment of partially protected composite floors: Engineering Background”, Arcelor/Mittal & CTICM.
- Vassart, O. and Zhao, B. (2011b), “FRACOF : Fire resistance assessment of partially protected composite floors: Design guide”, Arcelor/Mittal & CTICM.

# **EFFECT OF UNPROTECTED INTERIOR BEAMS ON Membrane Behaviour of Composite Floor Systems in Fire. I: Experimental Investigation**

Kang-Hai Tan <sup>a</sup>, Tuan-Trung Nguyen <sup>a</sup>

<sup>a</sup> Nanyang Technological University, School of Civil and Environmental Engineering, Singapore

## **Abstract**

A number of previous studies on tensile membrane action have been conducted and they are very valuable towards understanding the behaviour of isolated slabs as well as of floor assemblies. However, the role of unprotected interior beams in the development of TMA still has not clearly determined. This paper presents an experimental study on the effect of unprotected interior beams on the behaviour of composite floor assemblies in fire. The experimental observations and results of two one-fourth scale composite slab-beam systems, 3.15 m by 3.15 m in plan, subjected to transient-heating test are presented.

The test results show that the presence of interior beams can reduce the slab deflection and greatly enhance the slab load-bearing capacity. The interior beams have a major role in helping the slab in passing through the 'transition' stage, and thus the slab can mobilize more tensile membrane forces. Without the interior beams, the compressive ring failure may occur resulting in a little contribution from TMA in the slab load-bearing capacity.

**Keywords:** tensile membrane action, slab-beam systems, composite slabs, fire

## **INTRODUCTION**

Composite slabs, which are commonly used in steel-framed buildings, have shown very good load-bearing capacities under fire conditions because of the mobilisation of tensile membrane action at large-deflection stage. Interior secondary beams can be left unprotected in fire without affecting the stability of the slabs. Recent years, interest in the tensile membrane behaviour of the overall floor assemblies in fire has increased (Vassart et al., 2010; Zhao and Roosefid, 2010; Stadler et al., 2011; Wellman et al., 2011). These studies are very valuable towards understanding the membrane behaviour of the floor assemblies. To investigate the influence of interior supporting beams between two slab panels, Stadler et al. (2011) conducted two medium-scale tests on composite beam-slab systems in fire. They found that tensile membrane forces changed considerably when the interior beams were taken into account. However, more research is still needed on the effect of unprotected interior beams on the development of tensile membrane action.

Therefore, part of a research project conducted in Singapore aims to investigate the effect of unprotected interior beams on membrane behaviour of the column-beam-slab systems in fire. This paper presents the test results and observations from two specimens, namely, one with two unprotected interior beams and one without any interior beams at all.

## **1 TEST ARRANGMENT**

### **1.1 Specimen Design**

The dimensions of two specimens were 2.25m long by 2.25m wide, giving an aspect ratio of 1.0. To simulate interior slab panels, the specimens were designed with a 0.45m outstand beyond the edge beams in both directions. The specimens were denoted S2-FR-IB and S3-FR. Specimen S3-FR were designed without interior beams (IB), while S2-FR-IB (denoted as S2



in a previous conference paper (Nguyen and Tan, 2012)) had two unprotected interior beams as shown in Fig. 1. In this figure, the notation MB, PSB, and USB denote the protected main beam, protected secondary beam, and unprotected secondary (interior) beam, respectively. The concrete slabs were supported by I-beams and four I-section steel columns. All the edge beams were protected with intumescent coating to a prescriptive fire-protection rating of 60 minutes.

Material and geometrical properties of the I-section steel beams are given in Tab. 1. The beams were designed for full-shear composite action using 40mm long, 13mm diameter headed shear studs at a spacing of 80mm to avoid premature failure at the studs. A common type of steel joints, i.e. flexible end plates, was used for beam-to-beam and beam-to-column connections.

Tab. 1 Properties of I-beams

Specimen		Depth <b>h</b> (mm)	Width <b>b<sub>f</sub></b> (mm)	Thickness		Yield stress <b>f<sub>y</sub></b> (MPa)	Ultimate stress <b>f<sub>u</sub></b> (MPa)	Elastic modulus <b>E<sub>s</sub></b> (MPa)
				Web <b>t<sub>w</sub></b> (mm)	Flange <b>t<sub>f</sub></b> (mm)			
S2-FR-IB	MB	131	128	6.96	10.77	302	437	197500
	PSB & USB	80	80	9.01	9.14	435	533	206900
S3-FR	MB	131	128	6.97	11.03	307	462	211364
	PSB & USB	80	80	10.26	10.02	467	588	210645

The concrete slab thickness was 55mm and 58mm for S2-FR-IB and S3-FR, respectively. Shrinkage reinforcement mesh with a grid size of 80mm x 80mm and a diameter of 3mm was placed within the slabs and 18mm from the top. The mesh of S2-FR-IB had a yield strength of 543MPa and a ultimate strength of 771MPa, while the corresponding values of S3-FR were 648MPa and 806MPa. The characteristic cylinder strengths of concrete were 36.3MPa and 31.3MPa for S2-FR-IB and S3-FR, respectively.

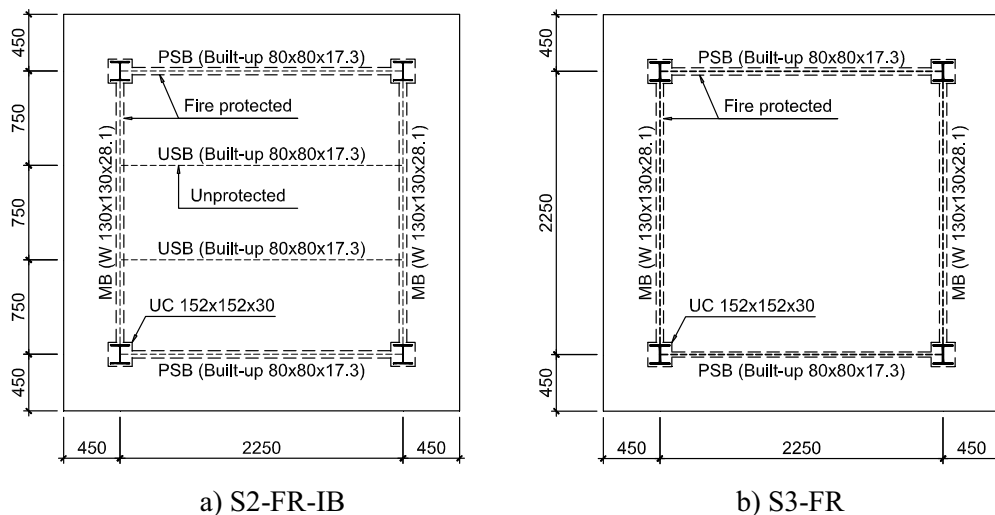


Fig. 1 Structural layout of the specimens

## 1.2 Test Setup

The test setup is shown in Fig. 2. The concentrated force from a 50-ton hydraulic jack was distributed equally to twelve-point loads by means of a loading system designed to simulate uniformly distributed loads. Slabs S2-FR-IB and S3-FR are considered as rotationally

restrained by the additional beam system on top of the outstand part which were fixed to the reaction frame via two plate stiffeners.

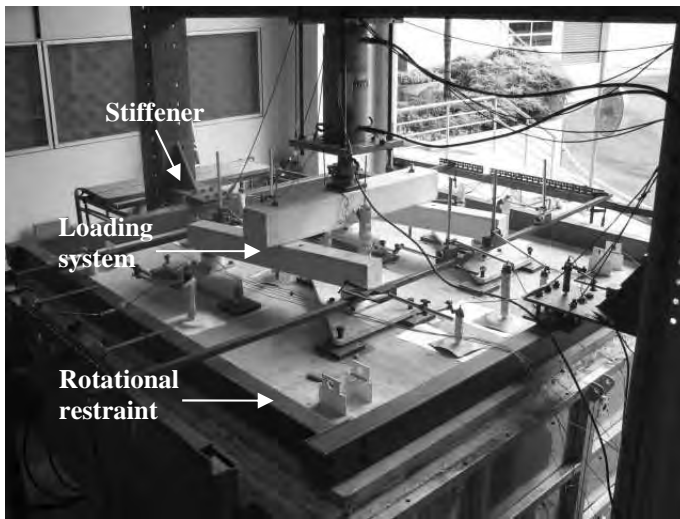


Fig. 2 Test setup



Fig. 3 Supporting columns

The edge and interior beams, which were totally enclosed inside the furnace, were able to deform freely. The specimens were connected to four supporting circular columns which were located outside the furnace and connected to the strong floor by pinned connections (Fig. 3). These pin-ended columns allow the specimens to move horizontally without any degree of restraint.

An electric furnace, of length 3m, width 3m and height 0.75m, was used to simulate fire conditions. Because of limitations on the power supply, the furnace could not simulate the ISO 834 standard fire curve. However, the furnace temperature could reach 1000°C within 50min, a heating rate of about 20°C/min which is within the practical range stipulated by BS 5950-8 for steel sections.

Transient-state heating was applied. The specimens were first loaded to a value of 15.8kN/m<sup>2</sup>, corresponding to a load ratio of 0.43 for S2-FR-IB, and 1.97 for S3-FR. The furnace temperature was then increased while the load was manually maintained constant. After failure had been identified, the test was ended.

Linear variable differential transducers (LVDT) were used to measure the vertical displacements of the slabs and beams. Temperatures at various locations of the slab and beams were captured with 21 K-type thermocouples. The furnace air temperature was also recorded by four thermocouples.

The load from the hydraulic jack was measured by a 300-kN load cell which was placed between the jack and the loading system.

## 2 TEST RESULTS AND OBSERVATIONS

### 2.1 Slab Deflection

Fig. 4 shows the relationships between the mid-span vertical deflections and temperature, plotted against time, together with the corresponding failure points of the slabs. 'Failure' was considered to have occurred when there was a significant drop in the mechanical resistance, and the hydraulic jack could no longer maintain the load level (violating criterion "R"). S2-FR-IB failed at a deflection of 177mm when the mesh temperature had reached 512°C, while S3 failed earlier at a deflection of 115mm when the mesh temperature was only 150°C.

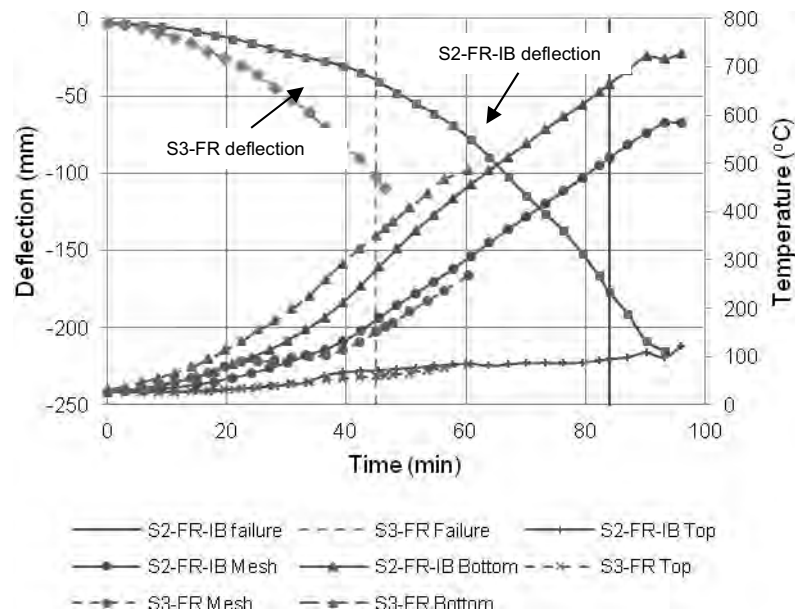


Fig. 4 Comparisons of temperatures and vertical deflection of the slabs

## 2.2 Behaviour of Edge Beams

Fig. 5 shows a comparison of the temperature development at the beam bottom flange and the vertical deflection against time. It can be seen that the temperature development of the beams was very close in both tests. Therefore the differences in the beam behaviour, if any, were definitely not caused by thermal effects. The limiting target temperature at 650°C of 60min for the edge beams was also observed.

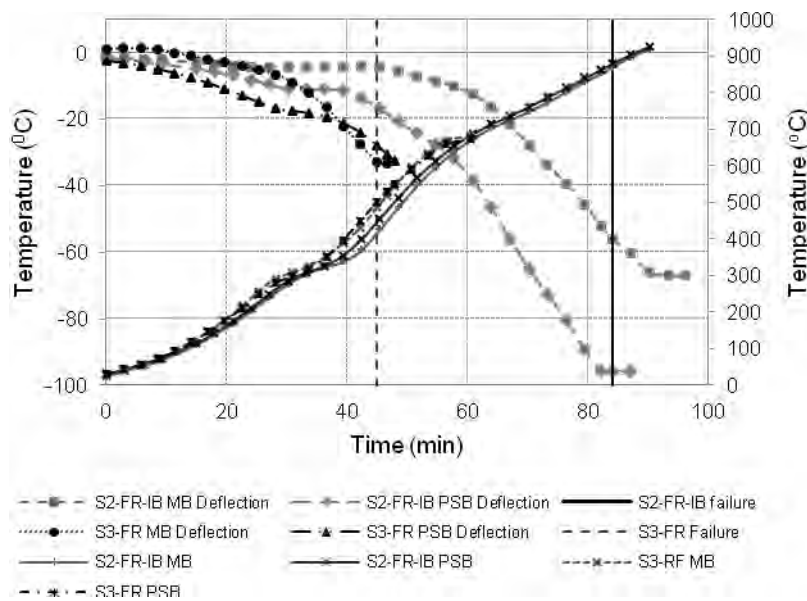


Fig. 5 Comparisons of temperatures and vertical deflection of the edge beams

At failure, the protected secondary beam (PSB) and the main beam (MB) of S2-FR-IB experienced very large deflections, 96mm and 56mm, respectively. The corresponding values of S3-FR were only 28mm and 33mm for PSB and MB, respectively. However, in S3-FR the recorded values for the main beam were not accurate. This was because severe cracks appeared at a very early stage (after only 20min of heating), directly above the main beams, as

shown in Fig. 7. Thus, composite action between the main beams and the slab could not be maintained, leading to inaccurate measurement of the beam deflection. It should be noted that the beam deflection was measured from the part of the concrete slab which remained intact and directly above the beams.

After cooling, it was observed that local buckling of the beam flanges had not occurred. This is due to discontinuous nature of the specimens, allowing the beams to expand to some extent through the flexible end plate connections and overall expansion of the slab system.

### 2.3 Failure modes

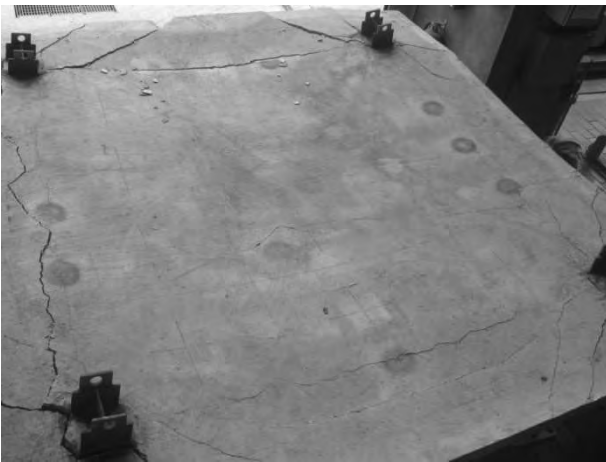


Fig. 6 Crack pattern of S2-FR-IB



Fig. 7 Crack pattern of S3-FR

In S2-FR-IB, the compression ring formed after 50min of heating. The test ended when fracture of reinforcement occurred and full-depth cracks appeared close to the edge beams, as shown in Fig. 6.

In S3-FR, the compression ring formed after 28min of heating with the appearance of curved cracks at the four corners (Fig. 7). However, at 45min three full depth cracks appeared suddenly, one at the slab corner near the column, and two above the main beams. These cracks led to 'brittle' failure of the compression ring and caused 'run-away' failure in the slab. In conclusions both of the slabs did not fail globally, but they lost their integrity and load bearing capacities (criteria "E" and "R").

## 3 DISCUSSION

In S2-FR-IB test, after 50min of heating, the compression ring began to form at a mesh temperature of 200°C. The corresponding deflection was 52mm, 0.95 of the slab depth. In S3-FR test, after 30min of heating, the compression ring was observed to begin to form when the mesh temperature had reached about 100°C, corresponding to a deflection of 52mm, equal to 0.95 of the depth. It can be concluded that that S2-FR-IB, which included interior beams, entered the tensile membrane action stage later than S3-FR, because the unprotected secondary beams enhanced the slab capacity during the bending stage. On the other hand, the compression ring formed at the slab deflection equal to 0.95 of the slab thickness, irrespective of the presence of interior beams.

Fig. 4 indicates clearly that S3-FR experienced larger deflection than S2-FR-IB. At failure S2-FR-IB had a greater enhancement factor, of 2.55 compared to 1.54 for S3-FR. This enhancement is defined in this paper as the ratio of the test failure load to the conventional yield-line failure load at the same mesh temperature. It is obvious that the presence of interior beams significantly reduces the slab deflection and enhances the load-bearing capacity of the slab.

As can be seen in Figs. 6 & 7, S2-FR-IB failed because of reinforcement fracture in the vicinity of edge beams which led to full-depth cracks, while S3-FR failed because of 'brittle' failure of compression ring. Therefore it can be concluded that the interior beams have a major role in helping the slab to transit smoothly from biaxial bending to membrane behaviour. Without the interior beams, failure of compression ring may occur, resulting in less contribution from tensile membrane action in the load-bearing capacity of the slab.

With regard to temperature distribution, the presence of interior beams did not have any effect on the temperature distributions of the edge beams as shown in Fig. 5, but they had effect on their deflection profiles. At similar temperatures, the protected secondary beams of S3-FR had greater deflection than those in S2-FR-IB, because of the difference in load path from the slabs to the beams. During the initial heating stage, in S3-FR load was transferred directly to the protected edge beams, while in S2-FR-IB the load was transferred via unprotected interior beams to the edge beams.

#### **4 CONCLUSIONS**

This paper presents the experimental results and observations of two one-quarter scale composite floor systems tested in fire, aiming to define the effect of interior beams on the membrane behaviour of the systems. The results show that the presence of interior beams greatly enhances the load-bearing capacity of the slab. Without interior beams, the slab may experience 'brittle' failure of the compression ring and caused 'run-away' failure in the slab. This work is part of an on-going research project which shall facilitate the use of membrane action for fire design of composite slabs in Singapore.

#### **5 ACKNOWLEDGEMENT**

The authors would like to acknowledge the support provided by Agency for Science, Technology and Research (A\*Star Singapore) for this work under Grant No. 0921420047.

#### **REFERENCES**

- Nguyen, T. T. and K. H. Tan, Testing of Composite Slab-beam Systems at Elevated Temperatures, 7th International Conference on Structures in Fire (SiF), Zurich, Switzerland, 2012.
- Stadler, M., M. Mensinger, et al., Munich Fire Tests on Membrane Action of Composite Slabs in Fire - Test Results and Recent Findings, Application of Structural Fire Engineering, Prague, Czech Republic, 2011.
- Vassart, O., C. G. Bailey, et al. (2010). Large-scale fire test of unprotected cellular beam acting in membrane action. 6th International Conference on Structures in Fire, SiF'10, June 2, 2010 - June 4, 2010, East Lansing, MI, United states, DEStech Publications Inc.
- Wellman, E., A. Varma, et al., Experimental Evaluation of Thin Composite Floor Assemblies under Fire Loading. Journal of Structural Engineering Vol 137, N0. 9 (2011), 1002-1012, 2011.
- Zhao, B. and M. Roosefid (2010). Experimental and numerical investigations of steel and concrete composite floors subjected to ISO fire condition. 6th International Conference on Structures in Fire, SiF'10, June 2, 2010 - June 4, 2010, East Lansing, MI, United states, DEStech Publications Inc.

## EFFECT OF UNPROTECTED INTERIOR BEAMS ON Membrane Behaviour of Composite Floor Systems in Fire. II: Numerical Assessment

Tuan-Trung Nguyen <sup>a</sup>, Kang-Hai Tan <sup>a</sup>

<sup>a</sup> Nanyang Technological University, School of Civil and Environmental Engineering, Singapore

### Abstract

The authors' companion paper presented the observations and results from two one-fourth scale composite beam-slab systems tested in fire. This paper introduces the numerical assessment based on these experimental results. A non-linear finite element model is developed using ABAQUS/Explicit to simulate the specimen behaviour. Material properties at elevated temperatures are assumed to vary according to EN 1994-1-2 (2005). The FE model was first validated with the test results, and then was used to examine the effect of unprotected interior beams on tensile membrane action. It is found that the numerical predictions agree well with the test results. The presence of interior beams significantly affects the magnitude as well as the distribution of stress of the slab elements, i.e. mesh reinforcement and concrete slab. The part with maximum tensile force is not necessarily at the slab centre. It may be part of the concrete slab above the edge beams. Shortcomings of the numerical model in predicting the failure modes are indicated.

**Keywords:** finite element analysis, composite floor systems, tensile membrane action, fire

### INTRODUCTION

This paper describes numerical assessments of the effect of unprotected interior beams on the membrane behaviour of composite beam-slab systems in fire. A nonlinear finite-element model is developed using ABAQUS/Explicit and validated against the experimental results presented in the companion paper in terms of temperature development, deflection response, and failure modes. The validated model provides valuable insight into the stress and strain distribution of concrete and reinforcement at the membrane stage of the systems.

This paper uses the experimental results from two tested specimens which are denoted as S2-FR-IB and S3-FR. S3-FR was designed without any interior beam, while S2-FR-IB had two interior beams. The layout of the two specimens is shown in Fig. 1, in which the notation MB, PSB, and USB denote protected main beam, protected secondary beam, and unprotected secondary (interior) beam, respectively.

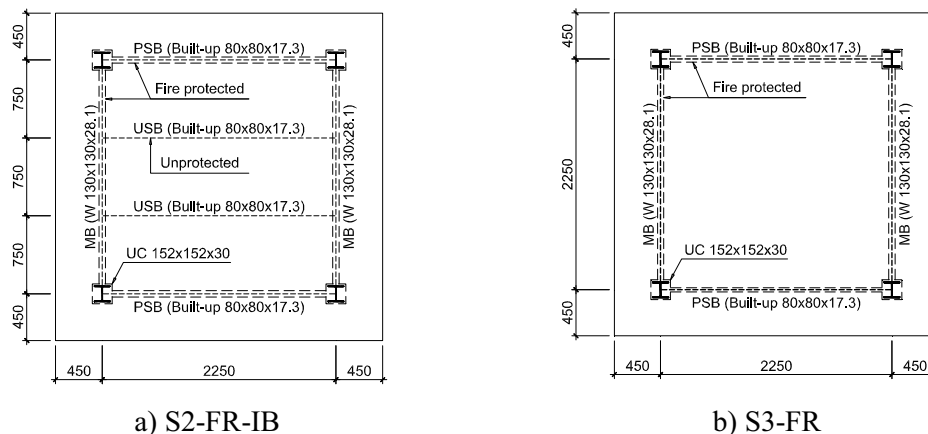


Fig. 1 Structural layout of the specimens

Both slabs are considered as rotationally restrained by the additional beam system placed on top of the outstand part. The beam system was fixed to the reaction frame. More details can be found in the authors' companion paper.

## 1 MODELLING TECHNIQUE

ABAQUS/Explicit was adopted because it uses consistent large-deformation theory which can overcome the numerical convergence difficulty caused by the simulation of large-deformation problems. **Sequentially coupled thermal-stress analysis procedure** is used because the thermal fields are the driving forces for the stress analysis but the thermal solution does not depend on the stress solution. Therefore, the simulation comprises two steps: (1) apply mechanical loading; (2) apply heating. **Concrete damaged plasticity model** was adopted, and reinforcement was modelled using the layered rebar technique.

S4R shell element was used to discretize both the beams and the slabs. Fully composite action between the beams and the slab was simulated using 'tied' technique via surface-based contact interactions.

Material properties of the steel and the concrete were obtained from tensile coupon tests and concrete cylinder tests at ambient temperature. The corresponding material properties at elevated temperatures were then obtained using the material reduction factors specified in EN 1994-1-2 (2005). For numerical purposes, the descending branches of concrete and reinforcement models were also adopted. Therefore ultimate compressive strain of concrete was taken from Table B.1 EN 1994-1-2, which depends on temperature of concrete slab; and ultimate tensile strain of reinforcement was taken as 0.2.

The simplified numerical model took into account the steel beams, the concrete slab, and the reinforcing mesh. Vertical support for the slab edges was provided by the protected edge beams. In turn, these beams were supported by the columns. Vertical restraint ( $U_3 = 0$ ) was imposed at the column locations; it is assumed that the vertical displacement at these positions is negligible. Vertical restraint along the edge outstands was applied to model the rotational restraint beam system, which was assumed to provide infinite vertical stiffness.

The temperature distribution at the slab bottom surface was incorporated into the numerical model. Based on the recorded temperatures at the mesh reinforcement and at the slab top surface, thermal gradient across the slab thickness was defined. For the beams, the recorded temperatures across the beam sections were incorporated into the model.

## 2 MODEL VALIDATION

### 2.1 Temperature Development

Figs. 2 and 3 show the comparisons of the temperature distribution of the slabs between the simulation and the test results. With a thermal gradient of  $10^\circ\text{C}/\text{mm}$ , the predicted temperatures agreed very well with the experimental results.

However, the results were not very good for the mesh temperature in S3-FR after 22min of heating. This is because severe cracks appeared in S3-FR resulting in significant heat losses. Consequently, the recorded mesh temperature increased at a lower rate after the cracks had appeared.

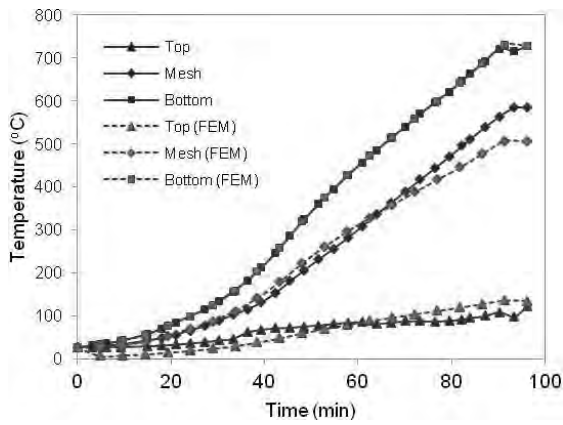


Fig. 2 Temperature distribution – S2-FR-IB

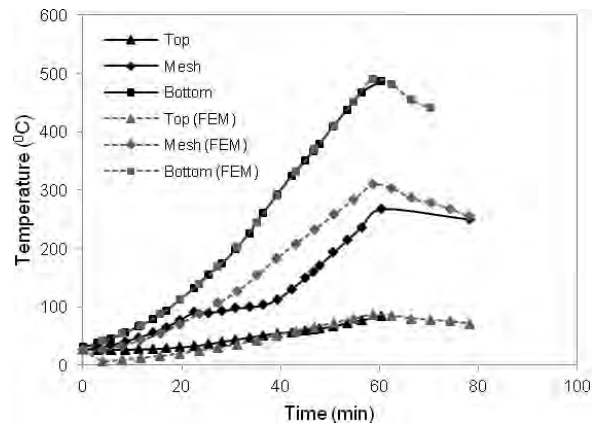


Fig. 3 Temperature distribution – S3-FR

## 2.2 Slab / Beam Deflection

Recorded temperature profiles of the flanges and the webs of the beams were input directly into the numerical models using the amplitude technique in ABAQUS. Consequently, structural behaviour can be obtained. Comparisons in terms of beam deflections versus time, as shown in Figs. 4 and 5, demonstrate that the model predicts the beam and the slab behaviour very well.

However, for the main beam of S3-FR the comparison is poor although the trend is similar. This is because in S3-FR severe cracks appeared at a very early stage (just 20min into the start of heating), directly above the main beams. Thus, composite action between the main beams and the slab could not be maintained, leading to inaccurate measurements of the beam deflection. These measurements were taken from the part of the concrete slab directly above the beams.

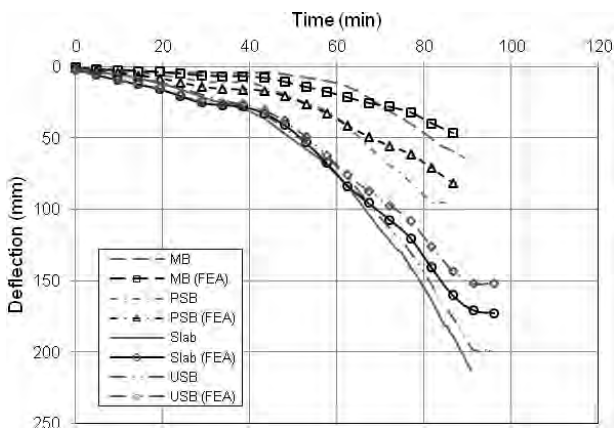


Fig. 4 Deflection vs. time curves for S2-FR-IB

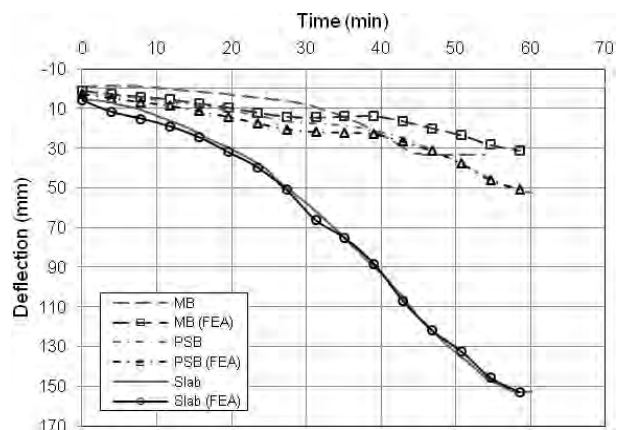


Fig. 5 Deflection vs. time curves for S3-FR

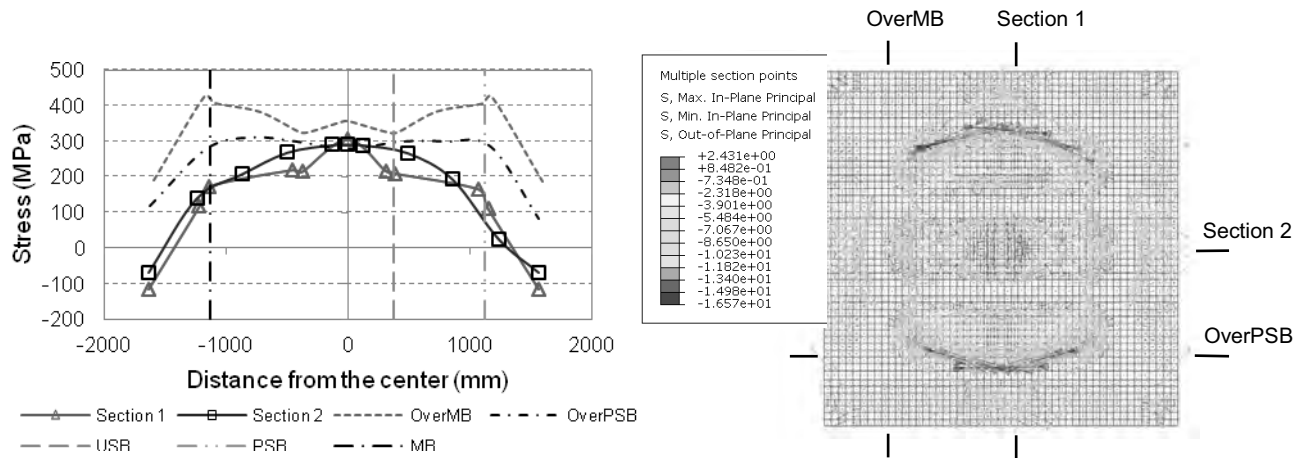
Fig. 4 also shows the deflection of unprotected interior beam of S2-FR-IB. As expected, the mid-span deflection of the beam was very close to that of the slab even though the beam was not at the slab centre. This indicates that the slab behaved as a membrane. This membrane was supported by the reinforcement mesh which anchored into the protected edge beams.

## 3 DISCUSSION

Figs. 6 and 7 show the stress distributions across the sections and at the top surface of the slabs at failure. In these figures, Section 1 denotes the mid-span slab section perpendicular to



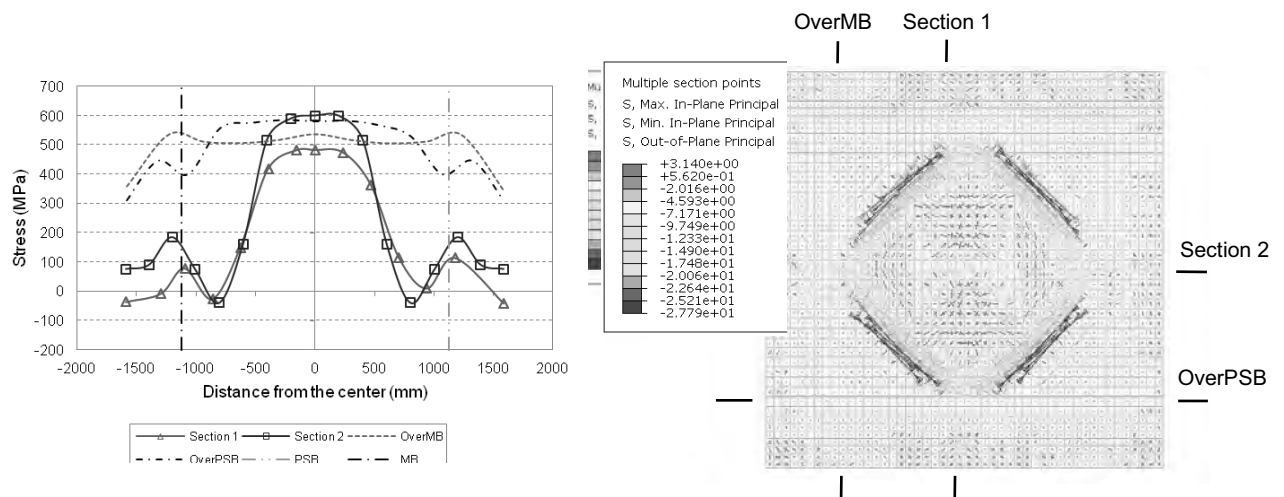
the protected secondary beams, Section 2 denotes the mid-span slab section perpendicular to the main beams, OverMB is the cross slab section above a main beam, and OverPSB is the cross slab section above a protected secondary beam. The positions of these cross sections are indicated in Figs. 6(b) and 7(b).



a) Stress distributions in reinforcement cross sections      b) Stress distribution at concrete top surface

Fig. 6 Stress distribution of S2-FR-IB at failure – 84.0min

It can be seen that, for S2-FR-IB, at 84.0min the maximum tensile stress of 425MPa in the reinforcement is found above the main beam. The maximum stress above the protected secondary beams is 310MPa, approximately equal to the stress in the reinforcement across the slab mid-span section. For S3-FR, the maximum tensile stress is found at the slab mid-span (Section2), followed by the section above the protected secondary beam (OverPSB).



a) Stress distributions in reinforcement cross sections      b) Stress distribution at concrete top surface

Fig. 7 Stress distribution of S3-FR at failure – 45.0min

The principal stress distributions at the top surface of the concrete slab are shown in Figs. 6(b) and 7(b), in which negative values indicate compressive stresses and positive values indicate tensile stresses. It can be seen that TMA was obviously mobilized in all specimens, with the formation of a tensile zone in the slab centre and a ‘compression ring’ consisting of the upper parts of the edge beams and part of the concrete slab directly above the edge beams.

The compression ring was most evident in S2-FR-IB, but it was not so clearly observed in S3-FR. This is possibly because the tensile stresses in the central zone of the slab in S3-FR were mainly equilibrated by the compressive stresses in the upper parts of the steel edge beams, with some contribution from the compressive stresses in the concrete slab. It should be noted that S3-FR was designed without any interior beam. Therefore tensile stress at the slab centre region in S3-FR is quite uniform and continuous, which is not observed in S2-FR-IB. In S2-FR-IB, part of concrete slab above the unprotected interior beams is still in compressive because of the effect of T-flange beam.

Therefore, on the basis of numerical simulations of S2-FR-IB (Fig. 6), the fracture of reinforcement above the edge beams would occur first, before the fracture of the reinforcement at the mid-span of the slabs; this failure mode concurs with the experimental observations.

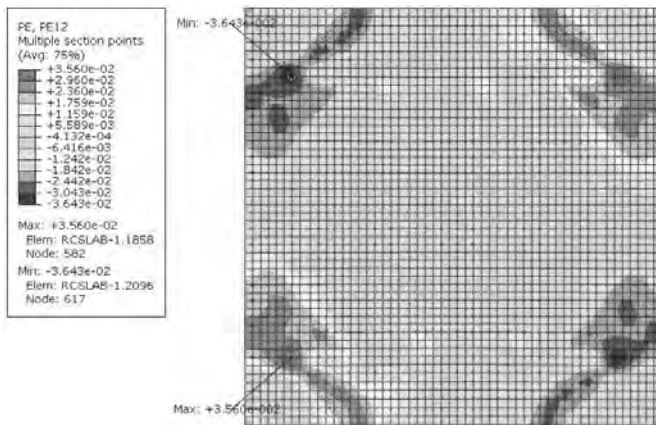


Fig. 8 Strain distribution at top surface – S2-FR-IB at failure – 84.0min

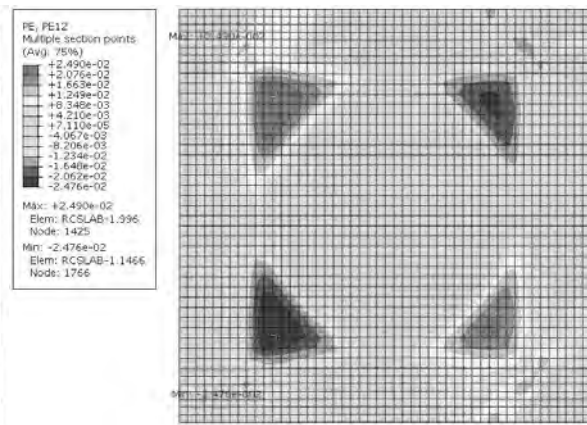


Fig. 9 Strain distribution at top surface – S3-FR at failure – 45.0min

In S3-FR, failure is predicted to be due to fracture of reinforcement at the slab mid-span. However, in the actual test, the failure mode was due to the failure of compression ring. On the other hand, as shown in Figs. 8 and 9, the maximum strain at the top surface of the concrete slab at its corners is 0.0356 and 0.0249 for S2-FR-IB and S3-FR, respectively. These values are higher than the failure compressive strain according to EN 1994-1-2, which are 0.0223 for S2-FR-IB and 0.0213 for S3-FR at the same temperature of the concrete slab. It means that at the slab corners, the stress in concrete top surface is almost zero, or failure would occur in these regions. Unfortunately, there is no obvious indication of which failure mode, i.e. reinforcement fracture at the slab mid-span or concrete crushing at the slab corner, would occur first. This is a shortcoming of the numerical model.

Although the comparisons show good correlation between test and numerical results for both specimens, there are still several limitations of the numerical model. Firstly, final failure modes of the beam-slab substructures could not be exactly identified from the stress or strain contours. Secondly, partial failures such as concrete crushing and fractures of rebars can not be taken into account. Also, heat loss caused by the appearance of concrete cracks could not be predicted.

#### 4 CONCLUSION

This paper presents numerical studies on the effect of interior beams on membrane behaviour of composite slab-beam systems in fire. The proposed numerical model was validated with the test results of two specimens, and the results show good correlation between the test and the numerical results.

It is found that the presence of interior beams significantly affects the magnitude as well as the distribution of stresses in the slab elements. The maximum tensile stress is not necessarily

located at the slab centre, but may be located in the concrete slab above the edge beams. This may cause different failure modes for the floor assemblies compared with those of isolated slab panels.

## **5 ACKNOWLEDGEMENT**

The authors would like to acknowledge the support provided by Agency for Science, Technology and Research (A\*Star Singapore) for this work under Grant No. 0921420047.

## **REFERENCES**

- Abu, A. K., I. W. Burgess, et al., Slab panel vertical support and tensile membrane action in fire. *Steel and Composite Structures* 8 3 (2008), 217-230, 2008.
- EN 1994-1-2: **Eurocode 4. Design of composite steel and concrete structures - Part 1-2: General Rules - Structural fire design.** Brussels, Belgium, European Committee for Standardization (CEN), 2005.

## THERMOMECHANICAL ANALYSIS OF COMPOSITE STRUCTURES USING OPENSEES

Jian Jiang <sup>a</sup>, Guo-Qiang Li <sup>a,b</sup> and Asif Usmani <sup>c</sup>

<sup>a</sup> Department of building Engineering, Tongji University, Shanghai, 200092, China

<sup>b</sup> China State Key Laboratory for Disaster Reduction in Civil Engineering, Tongji University, Shanghai 200092, China

<sup>c</sup> School of Engineering, The University of Edinburgh, Edinburgh EH9 3JF, UK

### Abstract

The OpenSees framework has been extended to deal with steel-concrete composite structures under fire conditions. The single section and rigid link methods can be used to model composite beams and slabs in OpenSees. The former models the composite beam by defining a single beam section including steel beam and concrete slab and the latter is to define them separately interconnected by rigid link element. The equivalence of these two methods is verified by mechanical tests and fire tests on simply supported composite beams. Good agreements achieved between OpenSees predictions and experimental measurements shows the robustness of the developed OpenSees.

**Keywords:** composite structures; OpenSees; thermomechanical analysis.

### INTRODUCTION

The fire performance of composite steel and concrete beams can be assessed by conducting standard fire tests (Wainman and Kirby 1988; Newman and Lawson 1991; Zhao and Kruppa 1995). Although the experimental investigation of composite beams in fire gives fundamental understanding of the fire behavior of composite beams, it is impossible to cover all application domains and robust numerical analysis should be used to make up the experimental limitation. A two-dimensional analytical model was proposed by Oven (1996) to consider the partial interaction in composite beams. Huang et al. (1999) developed a separate shear connector element permitting modelling of full, partial and zero interaction between the steel beam and concrete slab. Sanad et al. (2000) modeled the Cardington restrained beam test using a grillage of beam elements to investigate the influence of restrained thermal expansion and thermal bowing on the forces and moments developed in the composite structures in fire. Fakury et al (2005) presented two-dimensional finite element analysis of semi-continuous composite beam with different temperature distribution regimes. Benedetti and Mangoni (2007) extended the method of the Fourier series expansion to the fire analysis of composite beams concerning deformable shear connectors. Ranzi and Bradford (2007) presented an analytical model for structural analysis of composite beams in fire accounting for both longitudinal and transverse interaction by means of the principle of virtual work. Hozjan et al. (2011) presented a strain-based finite element to account for slip between steel beam and slab. Fang et al. (2011) proposed two robustness assessment approaches for steel-framed composite construction under localised fire using a grillage model of beam elements.

These numerical analyses of composite structures at elevated temperature were carried out based on specialist programs such as VULCAN, ADAPTIC, SAFIR, and commercial packages such as ABAQUS, ANSYS and DIANA. Although specialist programs are cost-effective to purchase and easy to use they lack generality and versatility. The commercial packages require substantial recurring investment for purchase and maintenance that often make them unaffordable for researchers and deter new entrants to the field.

OpenSees (McKenna 1997) is an open source object-oriented software framework developed at UC Berkeley and supported by PEER and Nees. OpenSees has so far been focussed on providing an advanced finite-element computational tool for analysing the non-linear response of structural frames subjected to seismic excitations. This paper presents an augmentation of OpenSees to enable two-dimensional thermomechanical analysis of composite beams. This involves creating a new thermal load class, modifying existing material classes to include temperature dependent properties and modifying methods in element and section classes in OpenSees. A composite beam can be modelled in two alternative ways in OpenSees. One is to define a fibred single beam section combining the steel beam and concrete slab. The other model is to define them separately using beam elements interconnected by rigid link element. Four mechanical tests and two fire tests on the composite beams are chosen to verify the performance of the developed OpenSees and the equivalence of the two modeling methods.

## 1 OPENSEES MODEL

New subclasses were implemented and new methods were developed that derive behavior from existing components in OpenSees. These involved creating a new thermal load pattern class, and modifying existing material classes to include temperature dependent properties. Fig.1 shows the class hierarchy of new classes added in OpenSees using the graphical Unified Modeling Language notation (Booch et al. 1998).

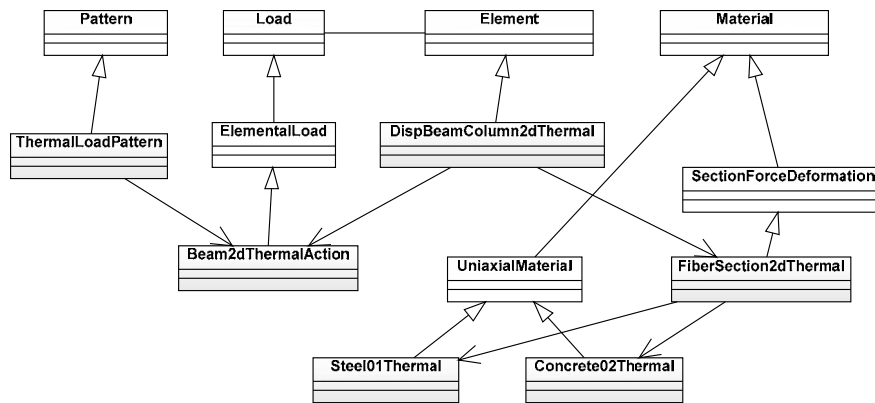


Fig. 1 Class diagram for thermomechanical analysis in OpenSees

A composite beam can be modeled in two alternative ways in OpenSees. One is to use a single section including steel I beam and concrete slab representing the composite beam. The other is to define steel beam and slab separately with rigid link connected between them to model the full shear connection condition. The command “rigidLink” was used to construct a single multi-point constraint between steel beam and slab to model the shear connection relation. Two rigid-link types “bar” and “beam” are offered in OpenSees. The “bar” type only constrains the translational degree-of-freedom and “beam” type constrains both translational and rotational degrees of freedom. In this paper, the “beam” type is used to model the full shear connection between the steel beam and concrete slab. The schematic of these two OpenSees models are shown in Fig. 2.

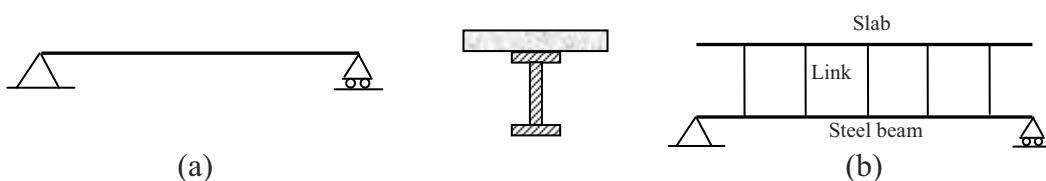


Fig. 2 Schematic of OpenSees models for composite beams: (a) single section model; (b) rigid link model.

## 2 VALIDATION

In this section, the performance of developed structural analysis of composite beams exposed to fire in OpenSees was verified by comparing with experimental results. These comparisons started from four tests on composite beams under mechanical load only followed by two tests on composite beams exposed to standard fire.

### 2.1 Composite beams at ambient temperature

Four simply-supported composite beams under mechanical load at ambient temperature were analysed using OpenSees. These tests included one tested beam (B4) from Amadio et al. (2004) and the other three beams (A3, A5, U4) reported by Chapman and Balakrishnan (1964). The beam U4 was subjected to uniformly distributed load and the others subjected to concentrated load. The test set up and beam dimensions are shown in Fig. 3. The existing 2D beam element `DispBeamColumn2d` was used to model the composite beams in OpenSees. The existing material classes `Steel01` and `Concrete02` in OpenSees were used to model the steel and concrete material respectively. Fig. 4 shows the comparisons of mid-span deflection from measured and predicted results of OpenSees as well as Oven (1996) and Huang et al. (1999). Good agreement achieved between the single section and rigid link models in OpenSees shows their equivalence to model two-dimensional composite beams under mechanical load. The OpenSees predictions agree well with experiment measurements.

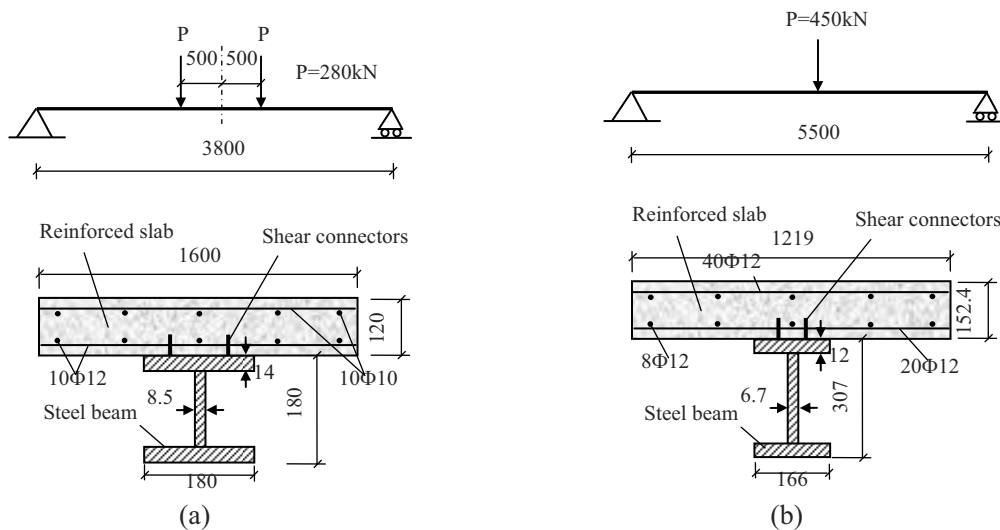
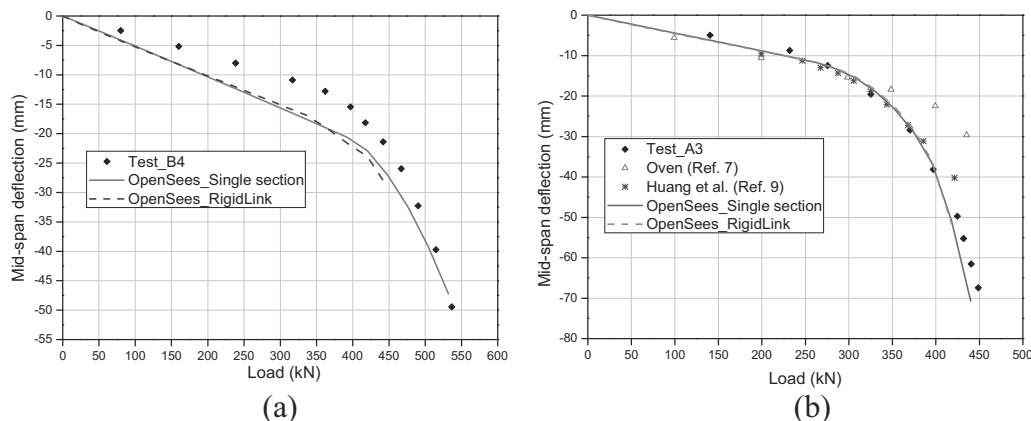


Fig. 3 Schematic of tested beams: (a) composite beam B4; (b) composite beam A3, A5 and U4. (all dimensions in mm)



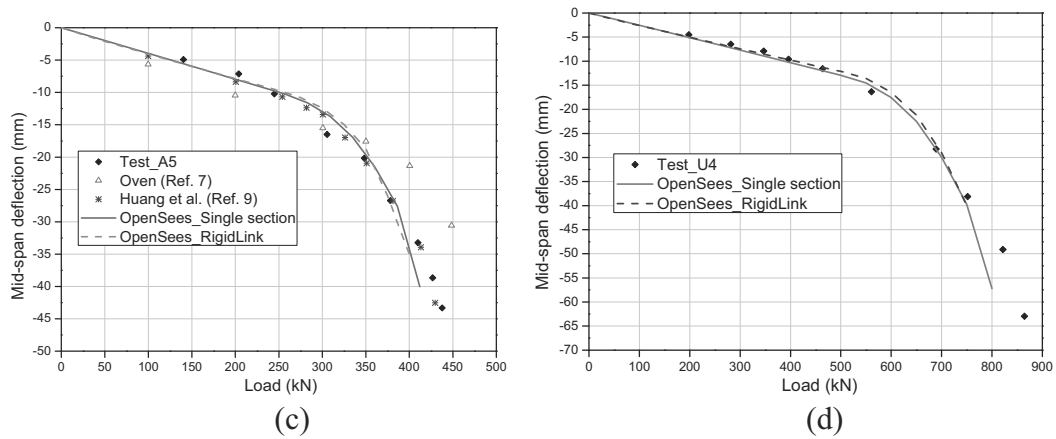


Fig. 4 Comparison of measured and predicted mid-span deflection of tested beams: (a) beam B4; (b) beam A3; (c) beam A5; (d) beam U4.

## 2.2 Composite beams at elevated temperature

Two ISO834 standard fire tests (Test 15 and 16) on simply supported composite beams were conducted by Wainman and Kirby (1988). The structural configuration is shown in Fig. 5. The material class Steel01Thermal and Concrete02Thermal in OpenSees were used to model the steel and concrete material in the composite beam. Their temperature dependent properties are shown in Fig. 6. The modified beam element `DispBeamColumn2dThermal` was used to model the composite beams in OpenSees. Fig. 7 shows the temperature distribution in different components of the two tested composite beams. No concrete slab temperature profiles were reported and therefore the temperature distributions through the thickness of the slabs were referred to Eurocode 4 (2005). Fig. 8 shows the comparisons of mid-span deflection from measured and predicted results of OpenSees and Huang et al. (1999). The OpenSees predictions show reasonable agreement with test results. The equivalence between single section and rigid link models in OpenSees is verified again for composite beams under fire conditions.

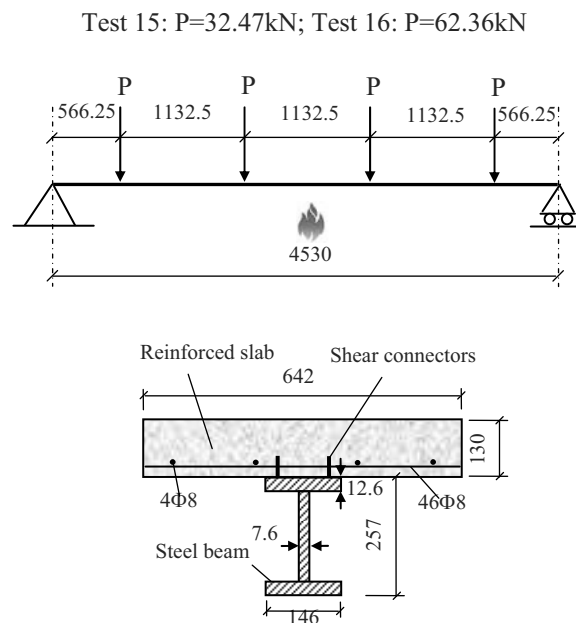


Fig. 5 Schematic of tested composite beam (Test 15 and Test 16) (all dimensions in mm)

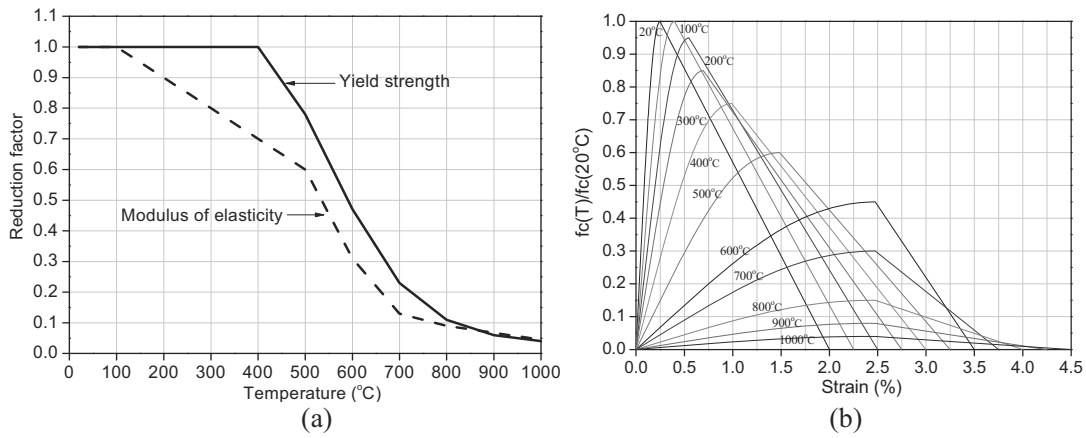


Fig. 6 Material properties at elevated temperature in OpenSees: (a) yield strength and elasticity modulus of steel; (b) compressive stress-strain relation of concrete

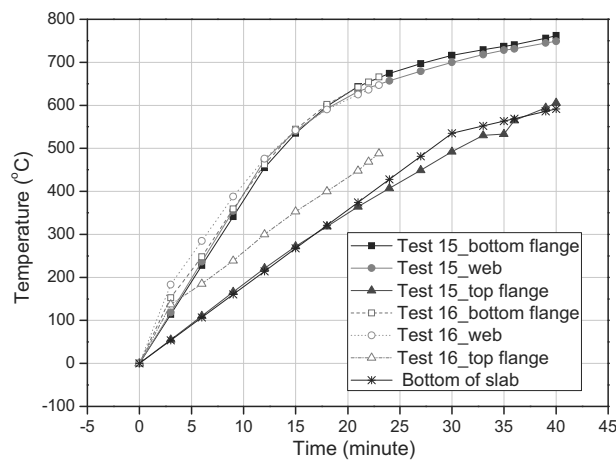


Fig.7 Temperature distribution in the composite beams against time

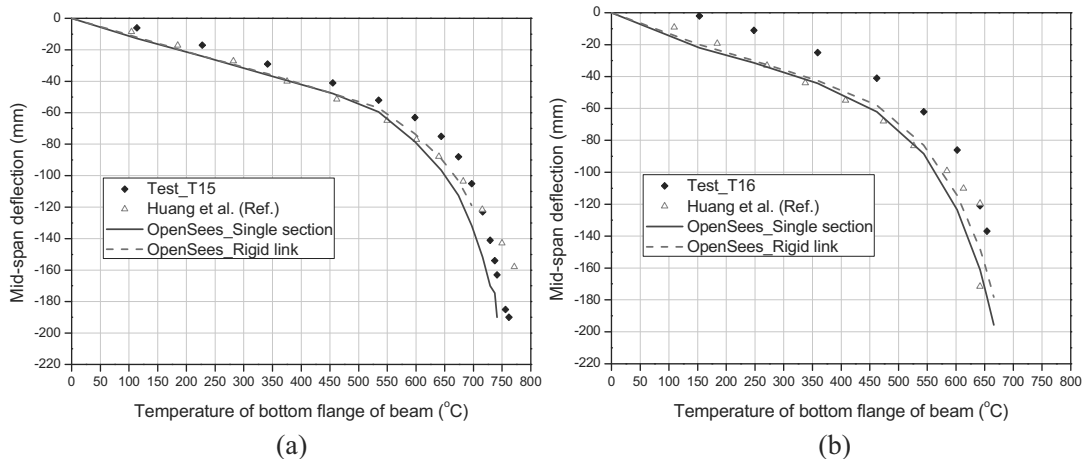


Fig. 8 Comparison of measured and predicted mid-span deflection of tested beams: (a) beam Test 15; (b) beam Test 16.

### 3 CONCLUSIONS

The OpenSees framework has been extended to perform thermomechanical analysis of composite structures. The performance of the developed capacity in OpenSees is verified by predicting mid-span deflection of tested composite beam under mechanical and thermal load respectively. Good agreement is achieved between OpenSees predictions and experimental



measurements. The single section and rigid link method is proved equivalent to model the composite beam in OpenSees. The further work will focus on modeling three-dimensional steel-framed composite structures using OpenSees (e.g. Cardington tests).

## REFERENCE

- Amadio C., Fedrigo C., Fragiaco M. and Macorini L. Experimental evaluation of effective width in steel-concrete composite beams. *Journal of Constructional Steel Research*, 60:199-220, 2004
- Benedetti A. and Mangoni E. Analytical prediction of composite beams response in fire situations. *Journal of Constructional Steel Research*, 63: 221-228, 2007
- Booch G, Rumbaugh J. and Jacobson I. *The unified modelling language user's guide*, Addison-Wesley, Reading, Mass, 1998.
- Chapman J.C. and Balakrishnan S. Experiments on composite beams. *The Structural Engineer*, 42(11): 369-383, 1964
- Eurocode 4. Design of composite steel and concrete structures: Part 1.2 General rules, Structural fire design, ENV 1994-1-2, Brussels, European Committee for Standardisation, 2005
- Fakury R.H., Las Casas E.B., Pacifico F. and Abreu L.M.P. Design of semi-continuous composite steel-concrete beams at the fire limit state. *Journal of Constructional Steel Research*, 61: 1094-1107, 2005
- Fang C., Izzuddin B.A., Elghazouli A.Y. and Nethercot D.A. Robustness of steel-composite building structures subject to localised fire. *Fire Safety Journal*, 46:348-363, 2011
- Hozjan T., Saje M., Srpac S. and Planinc I. Fire analysis of steel-concrete composite beam with interlayer slip. *Computers and Structures*, 89: 189-200, 2011
- Huang Z., Burgess I.W. and Plank R.J. Influence of shear connectors on the behaviour of composite steel-framed buildings in fire. *Journal of Constructional Steel Research*, 51(3): 219-237, 1999.
- McKenna, F. T., *Object-Oriented Finite Element Programming: Frameworks for Analysis, Algorithms and Parallel Computing*, PhD thesis, University of California, Berkeley, 1997.
- Newman G.M. and Lawson R.M. Fire resistance of composite beams. *The Steel Construction Institute Technical Report 109*, 1991
- Oven V.A. The behaviour of composite beams with partial interaction at elevated temperatures. PhD thesis, The University of Sheffield, UK, 1996.
- Ranzi G. and Bradford M.A. Composite beams with both longitudinal and transverse partial interaction subjected to elevated temperatures. *Engineering Structures*, 29:2737-2750, 2007
- Sanad A.M., Rotter J.M., Usmani A.S. and O'Connor M. Composite beams in large buildings under fire-numerical modeling and structural behaviour. *Fire Safety Journal*, 35: 165-188, 2000
- Wainman D.E. and Kirby B.R. *Compendium of UK standard fire test data unprotected structural steel-1*. British Steel Corporation, Ref. No. RS/RSC/S10328/1/98/B. Swinden Laboratories, Rotherdam, 1988.
- Zhao B. and Kruppa J. Fire resistance of composite slabs with profiled steel sheet and of composite steel concrete beams, Part 2: Composite beams. CEC, agreement No. 7219/SA/509, CTICM, France, 1995.

## STEEL FIBRE REINFORCED CONCRETE FOR FLOOR SLABS

Jan Bednář<sup>a</sup>, František Wald<sup>a</sup>, Jan Vodička<sup>b</sup>, Alena Kohoutková<sup>b</sup>

<sup>a</sup> Department of steel and timber structures, Czech Technical University in Prague, Czech Republic

<sup>b</sup> Department of concrete and masonry structures, Czech Technical University in Prague, Czech Republic

### Abstract

The composite steel and concrete floor slabs reinforced with steel fibres were tested at ambient and at elevated temperature at Czech Technical University in Prague. The slabs and secondary beams were fire unprotected during the tests at elevated temperatures. The edge beams only were protected. The concrete slabs were reinforced by steel fibres only without added steel bars. The tests demonstrated the suitable properties of the steel fibre reinforced concrete in fire, which enable creating the membrane action. The material properties of the fibre-concrete allowed forming a beam, the plate and tensile membrane mechanisms, which increase the fire resistance of the floor slabs. For the fire resistance of the floor slabs was utilised the tensile strength and ductility of the steel fibre reinforced concrete. The material properties tests at ambient and at elevated temperature, summarised in this contribution, approved the required ductility and tensile strength of the steel fibre concrete reinforced by 70 kg per cubic meter.

**Keywords:** steel reinforced fibre concrete, fire design, materials properties, composite steel and concrete floor

### INTRODUCTION

The design of concrete, composite steel and concrete and composite timber and concrete slabs for fire resistance is usually based on prescriptive ratings that specify the minimum slab thicknesses and the required concrete cover of the reinforcement. These ratings are generally based on standard fire resistance tests of particular elements using furnaces or simple design models of behaviour of slab as separated element. However, such approach does not represent

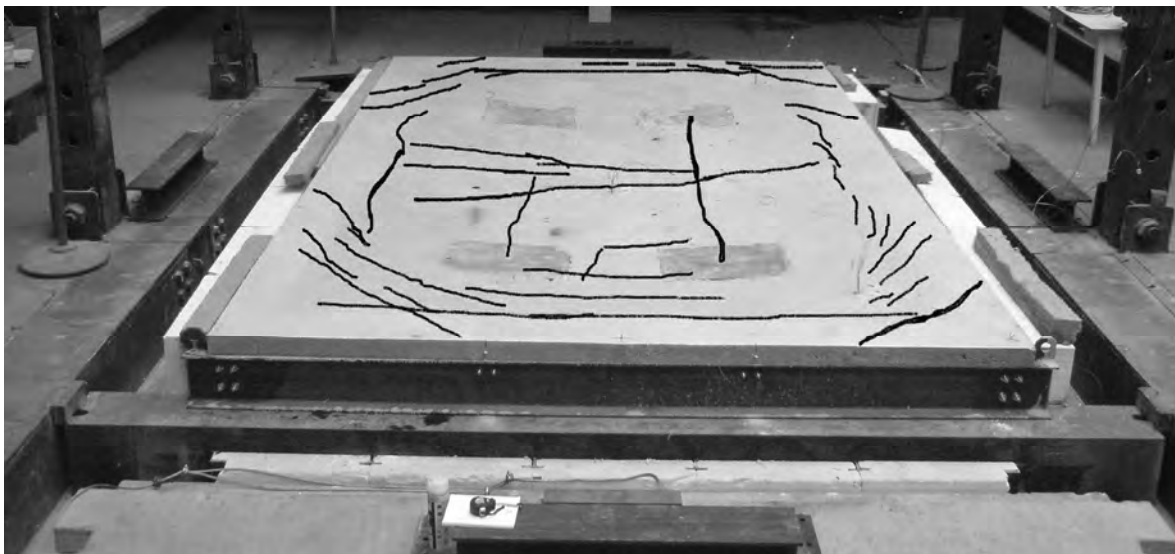


Fig. 1 Slab after fire test in PAVUS with marked cracks

a real structure as a whole as it does not account for overall floor behaviour, see (Bailey & Moore, 2000). Fire resistance ratings of properly designed full floor systems is higher than those of single elements because the compressive restraint in the edging of the slab allows in the central part of the slab for membrane action to develop increasing the time to failure of the elements compared to the standard tests. For design of floor slabs at elevated temperature based Eurocode rules, see (EN 1994-1-4, 2005), may be applied advanced procedures by FEM analyses and simple procedures, see (Vassart & Zhao, 2011). The ductility of steel fibre reinforced concrete (SFRC) broadens the range of application of the reinforced concrete and composite steel-concrete structures. These materials are characterized by high resistance to cracking, corrosion, abrasion, impacts, fatigue and good resistance in exposition to the high temperatures, see (Lie & Kodur, 1996). Steel fibre reinforcement helps to maintain the residual strength and fracture toughness after being heated, see (Rustin & Kodur, 2011). In the last years, composite SFRC floor slabs at ambient and at elevated temperature have been tested at the Czech Technical University in Prague. Concrete slabs were reinforced by steel fibres only without added steel bars. The main aim of the tests was to demonstrate the sufficient properties of the SFRC slab in fire. For the fire resistance of the floor slabs, it is important for the material to have sufficient ductility and adequate tensile and shear strength. These material properties of the SFRC allow for the slab to create a different load bearing mechanism, which increases its fire resistance.

## 1 FURNANCE TESTS

Six slabs were tested with sizes of 4.5 x 3 m. The slabs of the thickness 40 mm were concrete to trapezoidal sheets TR40/160/0.75. The concrete was reinforced by 70 kg per cubic meter. Added steel fibres had the sizes of 0.75 x 50 mm and its strength was 1100 N/mm<sup>2</sup>. Four slabs were tested at the ambient temperature and two at elevated temperature. The tests at ambient temperature were performed in Prague in UTAM and the tests at the elevated temperature in Veselí nad Lužnicí in PAVUS, see Fig. 1 and 2. The first floor slab tested at elevated temperature reached the collapse in 195 min of the test. Deflection of the slab was over 300 mm, see Fig. 3. Integrity of the slab was maintained during 75 min and criterion of isolation was transgressed after 65 min. The second floor slab tested at elevated temperature approved the resistance of R120.

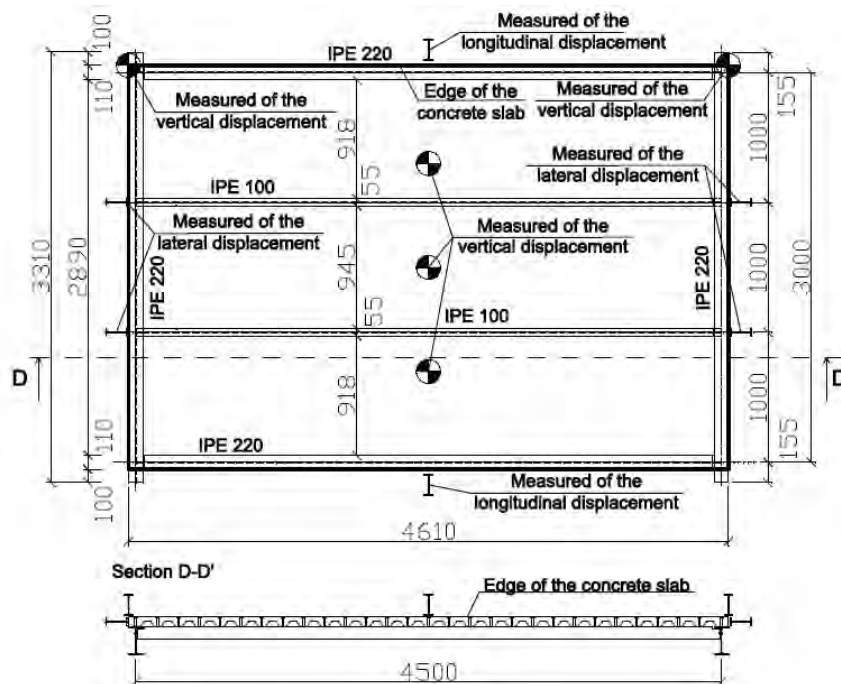


Fig. 2 Sizes of the specimen and location of the deflectometers by the test

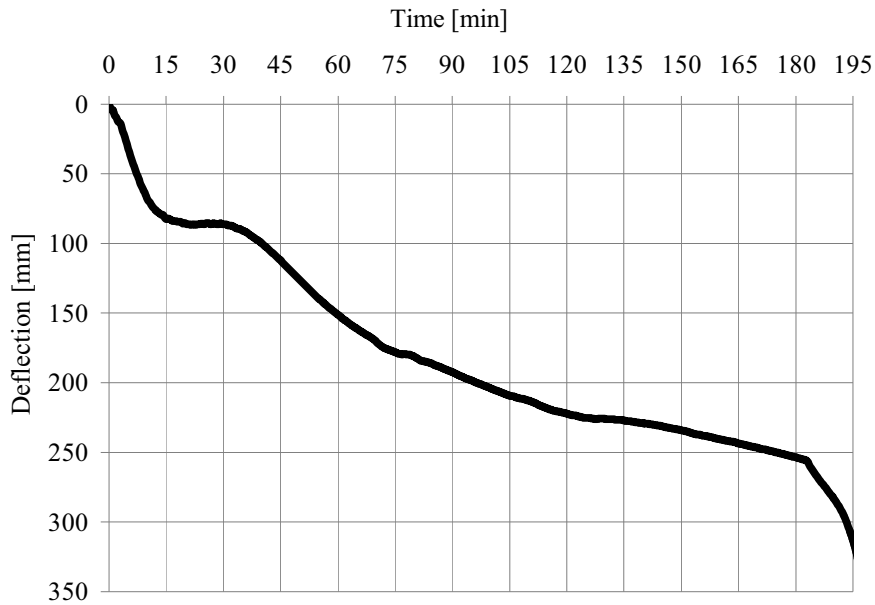


Fig. 3 Vertical deflection in the centre of the slab

## 2 MATERIAL TESTS

### 2.1 Material properties at ambient temperature

For the prediction model developed under the project were created tests of the materials properties. Concrete mixtures were two. In concreting plants, for each mixture there was made 9 cubes and 9 scantlings. Concreting plants were in the towns Jindřichův Hradec and Písnice. Sizes of the cubes were 150 x 150 x 150 mm and scantlings 150 x 150 x 700 mm. The cubes were tested in simple compression and scantlings by for point bending test to describe the tensile properties of concrete according (EN12390-5, 2009), see Fig. 4. The scantlings were tested at 20 °C, at 500 °C and 600 °C

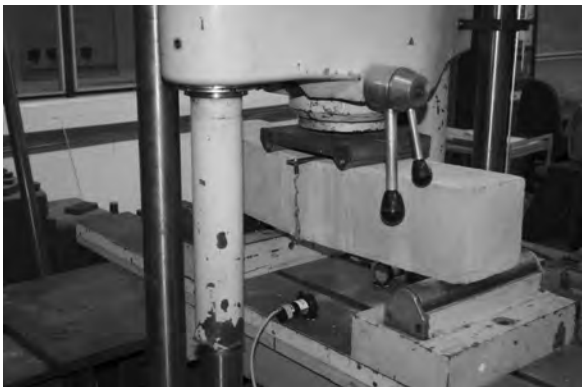


Fig. 4 Scantling H-1-20 after the test at ambient temperature

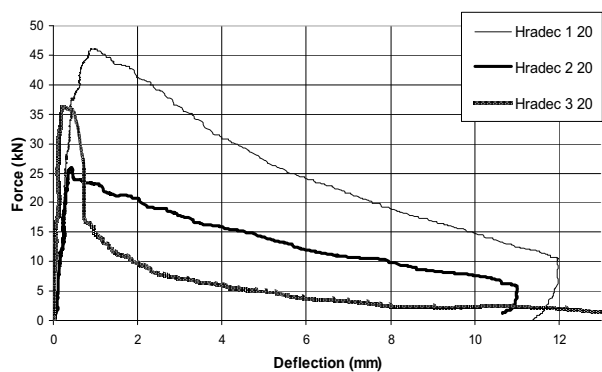


Fig. 5 Force – deflection relation from four point bending test at 20°C.

The six cubes from concreting plant Písnice reached an average compression strength of 80.9 N/mm<sup>2</sup> and three cubes in lateral tension showed by the tests an average tensile strength of 7.4 N/mm<sup>2</sup>. This concrete was used on the tests of the slabs at ambient temperature. The six cubes from concreting plant Jindřichův Hradec reached the average compression strength 68.3 N/mm<sup>2</sup> and three cubes in lateral tension showed by the tests an average tensile strength 7.1 N/mm<sup>2</sup>. This concrete was used on the test of the slab at elevated temperature.

There were tested 2 x 3 scantlings at 21 °C. The scantlings were tested by four-point bend, see Fig.3. There is shown a specimen after creation of the macro-crack. The fibre concrete achieved average tensile strength of 6.42 N/mm<sup>2</sup> and its average ductility was 1.1 % (concrete plant Jindřichův Hradec). Second concrete mixture achieved average tensile strength of 7.22 N/mm<sup>2</sup> and average ductility was 0.92 %. This ductility was measured at the initiation macro-cracks. After creating the macro-cracks, stretch was increasing and load bearing capacity was decreasing. The force - deflection relation from four point bending test at 20 °C is shown in Fig. 5.

## 2.2 Material properties at ambient temperature

Materials property tests were performed on the specimens, which were heated up by five electrical heaters. The specimens were heated to the temperature of 500 °C and 600 °C. The specimens were thermally protected and were heated up four hours so that the temperature in the scantling is uniformly distributed. The temperature was control by four thermocouples. The deflections were measured by two mechanical deflectometers, which were due to the temperature installed a little while before the loading of a specimen. The loading scheme was the same as by the test at ambient temperature. Fig. 6 shows the specimen during the heating. The heating was performed directly in the press. Tab. 1 shows the average values of tensile strengths at ambient and elevated temperature and reduction coefficients at selected relative deformation.



Fig. 6 The specimen during the heating

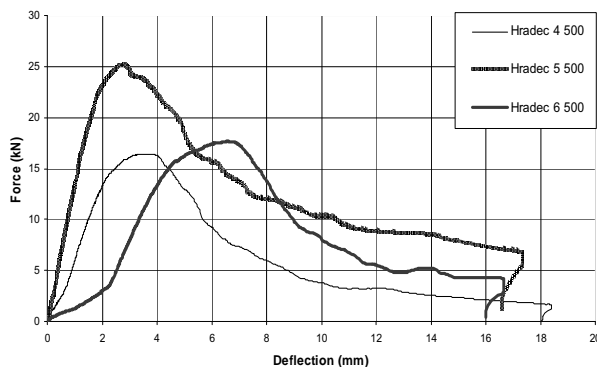


Fig. 7 Force – deflection relation from four point bending test at 500°C

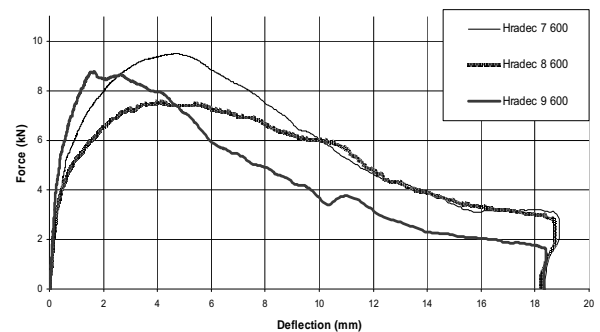


Fig. 8 Force – deflection relation from four point bending test at 600°C.

Tab. 1 Average values of tensile strengths at ambient and elevated temperatures

Temperature of specimen	Max tensile strength (N/mm <sup>2</sup> )	Tensile strength $\epsilon=6\%$ (N/mm <sup>2</sup> )	Tensile strength $\epsilon=10\%$ (N/mm <sup>2</sup> )	Tensile strength $\epsilon=14\%$ (N/mm <sup>2</sup> )	$k_{max}$	$k_{6\%}$	$k_{10\%}$	$k_{14\%}$
20 °C	5.8	3.2	2.2		1.00	0.55	0.38	-
500 °C	3.5	3.3	3.0	2.2	0.59	0.58	0.53	0.34
600 °C	1.5	1.4	1.4	1.3	0.26	0.25	0.25	0.24

There were tested 2 x 3 scantlings at 500 °C and 600 °C. The scantlings were tested also by four-point bend. The ductility was calculated at the initiation macro-cracks. The fibre concrete achieved at temperature 500 °C average tensile strength of 3.52 N/mm<sup>2</sup> and its average ductility was 8.77 %. At 600 °C it had 1.53 N/mm<sup>2</sup> and ductility was 6.99 %. Fig. 6 and 7 show force – deflection relation at four point bending tests.

### 3 CONCLUSIONS

Homogeneity of the results of material tests of fibre concrete was good. The steel fibre reinforced concrete demonstrated appropriate ductile behaviour. Based on experiments the reduction coefficient of decrease strength of SFRC was prepared, see (Bednář et al, 2011 and 2012). The ductility of SFRC by 500 °C was higher than by 20 °C but also than by 600 °C, see Fig. 9.

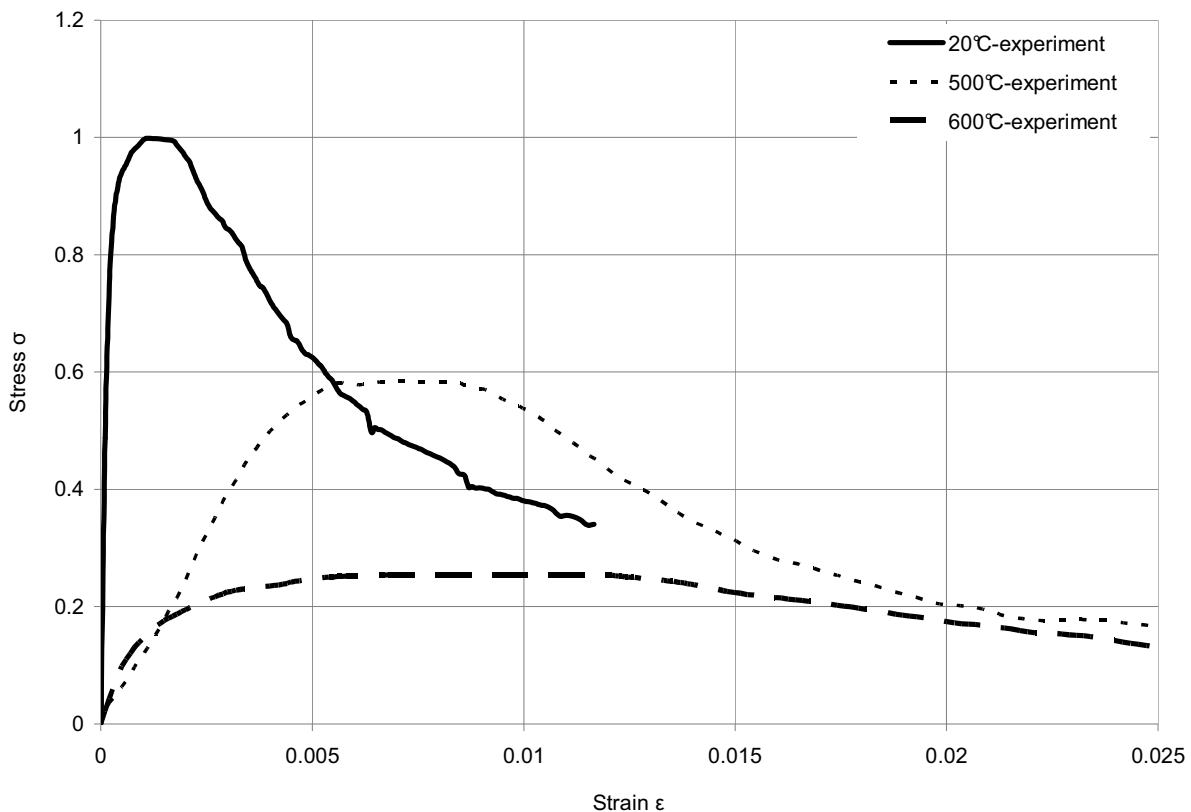


Fig.9 Relative stress-Strain diagram of the fibre concrete at 20°C, 500°C and 600°C

The evaluation of the material properties of SFRC and the tests with floor slabs allows the preparation of FEM model and analytical prediction model. The models are taking into account the contribution to the behaviour of the steel beam and SFRC slab in bending and the development of membrane behaviour at large deformation at elevated temperature.

## ACKNOWLEDGEMENT

This outcome has been achieved with financial support of the Grant Agency of Czech Republic No. P105/10/2159.

## REFERENCES

- Bailey C.G. & Moore D.B., The structural behaviour of steel frames with composite floor slabs subjected to fire: Part 1: Theory, *The Structural Engineer*, Vol. 78 (11), pp. 19-27, 2000.
- EN1994-1-4, Eurocode 4: Design of composite steel and concrete structures – Part 1-2: General rules – Structural fire design, CEN, Brussels, 2005.
- Vassart O., & Zhao B., Fire Resistance Assessment of Partially Protected Composite Floors, FRACOF+, 2011, <http://fire.fsv.cvut.cz/fracof>
- Lie T.T., Kodur V.R., Thermal and mechanical properties of steel-fiber-reinforced concrete at elevated temperatures, *Canadian Journal of Civil Engineering*, Vol. 23(4), pp. 511-517, 1996.
- Rustin F. & Kodur V.R., Enhancing the fire resistance of composite floor assemblies through the use of steel fibre reinforced concrete, *Engineering Structures*, pp. 2870-2878, 2011.
- EN 12390-5, Testing hardened concrete - Part 5: Flexural strength of test specimens, CEN, Brussels, 2009.
- Bednář J., Wald, F., Vodička J. & Kohoutková A., Membrane Action of Composite Fibre Concrete Slab in Fire. *Procedia Engineering*, online, 2012, vol. 40, no. 40, p. 498-503, ISSN 1877-7058.
- Bednář J., Wald F., Kohoutková A. & Vodička J., Properties of the fibre concrete in fire. In *6th International Conference Fibre Concrete 2011 - Technology, Design, Application*. Praha: vydavatelství ČVUT v Praze, 2011, p. 87-94. ISBN 978-80-01-04917-4.

## FIRE RESISTANCE OF STEEL-CONCRETE SIDE-PLATED BEAMS

Jerneja Kolšek <sup>a</sup>, Tomaž Hozjan <sup>a</sup>, Miran Saje <sup>a</sup>, Igor Planinc <sup>a</sup>

<sup>a</sup> University of Ljubljana, Faculty of Civil and Geodetic Engineering, Ljubljana, Slovenia

### Abstract

In the paper a novel three-phase finite-element numerical model for the fire analysis of side-plated reinforced concrete (RC) beams is presented. In addition, advantages of beam side reinforcing as a measure of structural retrofitting are explored for a selected case and an important contribution of the side plates to the ultimate fire resistance of the RC beam is observed.

**Keywords:** side-plated beam, fire, longitudinal slip, transversal slip, moisture transfer, heat transfer, high temperatures.

### INTRODUCTION

Over the course of the past few decades the technique of plating of flexural beams has become acknowledged as one of the peak engineering solutions of structural retrofitting. During this time a vast number of different plating solutions has been introduced in the market (i.e. the tension-face plating technique, the side-plating technique, the U wraps, etc.), yet it seems, that for every day engineering purposes only the tension face plating technique has been widely accepted. Undoubtedly, this is also a reflection of the current status of the scientific publications. While a vast number of favourable scientific findings have been presented in the field of the research of the tension face plated beams, the reports on the investigations of the alternatively plated beams are extremely rare and our understanding of their behaviour under different types of loading (especially such as in fire) is still poor.

When considering RC beams at high temperatures a complex numerical analysis cannot be avoided. To fully understand the complexity of the problem, the microscopic structure of concrete and changes, that it undergoes at high temperatures, need to be looked in detail. Concrete consists of not only the hardened cement paste but also of pores partially filled with water (liquid, adsorbed or chemically bound) and with the gaseous mixture of dry air and water vapour. Due to the presence of gas and water the heat capacity of the material is increased and, in addition, heat is not only conducted but also convected through the material and accompanied with chemical decomposition and phase changes (water evaporation and vapour condensation). On top of the temperature gradients, also the pressure and the concentration gradients are established inside the concrete body and free water and gas fluxes are evoked. Depending on the permeability of the thermally and mechanically damaged material, these are headed partially outwards, towards the heated surface, and partially inwards, towards the cooler layers of concrete where vapour condenses. Inside the concrete body, in the area where the permeability of the material is substantially diminished (e.g. due to high saturation levels), the gas and water flow is hindered and its speed is reduced. This (so called) plugged zone eventually causes a rapid rise of pore pressures in front of the zone, accelerated crack propagation in this area and, in most severe cases, explosive spalling (separation) of the damaged material.

Within the last decade, several different models have been suggested in scientific literature for analyses of concrete structures at high temperatures. Depending on whether 'mechanical' (stress induced) damage effects are accounted for in the heat and mass transfer inside the concrete element or not, two fundamental groups of such models can be distinguished. The first group represents the models (e.g., Davie et al., 2006), where the mechanical effects are



neglected in total. In line with this assumption, these models are only applicable for concrete structures with zero mechanical loading and where thermal dilatations of the concrete element are not (significantly) restrained, so that no (significant) stress is induced in the element during fire. For a general case of a mechanically loaded concrete structure in fire, however, only the alternative fully coupled thermo-hygro-mechanical models are commonly applicable (e.g. Gawin et al., 2003). Unfortunately, in these sophisticated models, extremely complex systems of governing equations and their respective constitutive relationships are usually observed and the accompanying numerical procedures are often found as unmanageably time consuming. As a result, the applicability of these models for different types of concrete and composite concrete structures is still limited and only specific problems with a small number of DOFs are mostly analysed in this way. In lieu of complex hydro-thermo-mechanical models, therefore, an empirically validated proposal for capturing the 'mechanical' effects in a pure hygro-thermal model indirectly has been recently presented by Dwaikat and Kodur (2010).

In the present paper a new three-phase numerical model for thermo-mechanically loaded side-plated RC beams is presented. In the first phase of the model, the time-dependent change of temperatures in the fire compartment surrounding the structure is defined, e.g. by engaging a CFD model of fire-driven fluid flows or by selecting an adequate fire curve prescribed in standards and regulations. For the sake of simplicity, the standard ISO 834 fire curve is engaged in this paper. The following hygro-thermal phase of the model is based on the model of Davie et al. (2006). Within the latter the proposal of Dwaikat and Kodur (2010) is additionally implemented capturing the effects of mechanical damage of concrete on its time-dependent permeability. Such combined model accounts for: (i) the porous and multiphase nature of concrete, (ii) phase and chemical transformations, and (iii) mutual interactions and couplings between the thermal, hygral and (indirectly) mechanical degradation of concrete. For the final, mechanical, part of the analysis, a new mathematical model and a strain-based FE formulation is proposed by the authors. In this part of the model the following phenomena are considered: (iv) partial longitudinal and transversal interlayer interaction, (v) stress-induced viscous creep of steel, and (vi) stress-induced creep and transient deformations of concrete. In zones where due to the changes in temperatures cyclic loading and reloading of the material is triggered, (vii) elastic reloading and (viii) kinematic hardening of the material are assumed. Since the separate phases of the proposed model have already been extensively validated against experiments elsewhere (see, e.g. Kolšek, 2013), this part of the presentation of the model is in the paper omitted. The paper concludes with a case study exploring the effects of the side strengthening of a selected RC beam on its fire resistance.

## **1 THERMO-HYGRO-MECHANICAL ANALYSIS OF A SIDE-PLATED RC BEAM**

In this paper, firstly, for the description of the time development of temperatures of the fire compartment surrounding the side-plated beam, the standard ISO 834 fire curve is selected. Secondly, the coupled heat and mass transfer in the beam is observed and, thirdly, the mechanical response of the structure during fire is pursued. For the second and the third phase of the model two mathematically independent submodels are suggested. Within each, the total duration time of the fire is divided into time intervals  $[t^{j-1}, t^j]$ , and for each of the intervals the basic unknowns of the problem are iteratively determined.

### **1.1 The heat and mass transfer submodel**

In the second phase of the proposed model the time and space distributions of temperatures and pore pressures in the side-plated RC beam are determined. For the non-porous side plates Fourier law of heat conduction is employed. For the heterogeneous RC beam the model of Davie et al. (2006) is selected comprising three governing equations of mass conservation of free water, water vapour and dry air:

$$\begin{aligned}\frac{\partial(\overline{\rho_{FW}})}{\partial t} &= -\nabla \mathbf{J}_{FW} - E_{FW} + \frac{\partial(\overline{\rho_D})}{\partial t}, \\ \frac{\partial(\overline{\rho_V})}{\partial t} &= -\nabla \mathbf{J}_V + E_{FW}, \\ \frac{\partial(\overline{\rho_A})}{\partial t} &= -\nabla \mathbf{J}_A,\end{aligned}\quad (1)$$

and the governing equation of energy conservation:

$$(\overline{\rho C}) \frac{\partial T}{\partial t} = -\nabla \cdot (-k \nabla T) - (\overline{\rho C \mathbf{v}}) \cdot \nabla T - \lambda_E E_{FW} - \lambda_D \frac{\partial(\overline{\rho_D})}{\partial t}. \quad (2)$$

In Eqs. (1)–(2),  $\mathbf{J}_i$  is the mass flux of phase  $i$ ,  $\overline{\rho_i}$  is the mass concentration of phase  $i$ ,  $E_{FW}$  the rate of evaporation of free water (including desorption), and  $t$  is time. Index  $i$  denotes phases of concrete:  $FW$  is free water,  $V$  is water vapour and  $A$  is dry air. In Eq. (2)  $\overline{\rho C}$  is heat capacity of concrete,  $k$  is its thermal conductivity,  $\overline{\rho C \mathbf{v}}$  relates to the energy transferred by fluid flow,  $\lambda_E$  is the specific heat of evaporation,  $\lambda_D$  specific heat of dehydration and  $T$  is temperature.

The mass fluxes  $\mathbf{J}_i$  are further expressed in terms of pressure and concentration gradients assuming that the Darcy's and Fick's laws are applicable. These and all of the other respective constitutive equations are in the model adopted as proposed by Davie et al. (2006), thus, they are not presented in this paper. Nevertheless, an exception regarding the time dependent concrete permeability evaluations is suggested. In contrast to case studies of Davie et al. (2006) dealing with problems, where zero 'mechanical' effects in the pressure-driven flow evaluations were assumed, such an assumption is no longer valid when a general case of a fire exposed side-plated RC beam is analysed. Instead, the 'mechanical' effects need to be explicitly considered. Indirectly, as recently proposed by Dwaikat and Kodur (2010), this can be performed by accounting for the gradients in the initial permeability of concrete,  $k_0$ :

$$k_0 = k_{top} \begin{cases} 10^{2y/D} & y \leq x \\ 10^{2y/D} \left( 10^{3(y-x)/(D-x)} \right) & y > x \end{cases}. \quad (3)$$

In Eq. (3)  $k_{top}$  refers to initial permeability in the top surface of the concrete section,  $D$  to the depth of the concrete cross-section,  $y$  is the distance from top of the cross-section, and  $x$  is the depth of neutral axis at service load and ambient temperature. Further, at each time station  $t > 0$ , the permeability of concrete,  $k$ , is evaluated in dependency on temperature,  $T$ , and the averaged pressure of liquids and gas inside the solid concrete matrix (i.e. pore pressure),  $P_{pore}$  (Dwaikat and Kodur, 2010, Gawin et al., 2002):

$$k = k_0 \left[ 10^{0.0025(T-T_0)} \left( \frac{P_{pore}}{P_0} \right)^{0.368} \right]. \quad (4)$$

The solution of the presented hygro-thermal submodel is finally obtained numerically with the Galerkin's type of the finite element method as proposed in Davie et al. (2006).

### 1.3 The stress-strain evolution submodel

Once the temperature and pore pressure variation in time and space has been obtained, the stress-strain state evolution in the beam during fire can be pursued. In the mechanical submodel both of the layers of the steel–concrete side-plated beam (i.e. the layer 'a' representing the RC beam and the layer 'b' representing the side plates) are modelled

separately, each by the geometrically exact theory of a planar beam but neglecting the effects of shear deformations. The related governing equations of the layer 'i' ( $i = a, b$ ) are:

$$\begin{aligned}
 & \bullet \text{ kinematic:} & \bullet \text{ equilibrium:} & \bullet \text{ constitutive:} \\
 1 + u^i{}' - (1 + \varepsilon^i) \cos \varphi^i = & R_X^i{}' + \mathcal{P}_X^i = 0, & N^i = \int_{\mathcal{A}_x^i} \sigma^i(D_\sigma^i, T) dA - N_p^i, \\
 w^i{}' + (1 + \varepsilon^i) \sin \varphi^i = 0 & R_Z^i{}' + \mathcal{P}_Z^i = 0, & M^i = \int_{\mathcal{A}_x^i} z \sigma^i(D_\sigma^i, T) dA - M_p^i. \\
 \varphi^i{}' - \kappa^i = 0, & M^i{}' - (1 + \varepsilon^i) Q^i + \mathcal{M}_Y^i = 0, & 
 \end{aligned} \tag{5}$$

(-)' in Eqs. (5) denotes the derivative with respect to material coordinate  $x$ .  $u^i$ ,  $w^i$  and  $\varphi^i$  represent, respectively, the  $X$ -displacement, the  $Z$ -displacement and the rotation of the reference axis of the layer 'i' and  $\varepsilon^i$  and  $\kappa^i$  are its extensional and bending strains (the curvature).  $R_X^i$  and  $R_Z^i$  are the components of the cross-sectional stress-resultants with respect to the fixed basis ( $\mathbf{E}_X, \mathbf{E}_Y, \mathbf{E}_Z$ ) and  $N^i$ ,  $Q^i$ , and  $M^i$  are the cross-sectional axial force, the shear force and the bending moment. Note, that  $R_X^i$  and  $R_Z^i$  relate to  $N^i$  and  $Q^i$  as follows:  $N^i = R_X^i \cos \varphi^i - R_Z^i \sin \varphi^i$  and  $Q^i = R_X^i \sin \varphi^i + R_Z^i \cos \varphi^i$ . Moreover,  $\mathcal{P}_X^i$ ,  $\mathcal{P}_Z^i$ ,  $\mathcal{M}_Y^i$  denote components of the traction vectors  $\mathcal{P}^i$  and  $\mathcal{M}^i$  representing static equivalents of surface and volume forces after being reduced to the layer's reference axis, and  $N_p^i$  and  $M_p^i$  are the contributions of pore pressures in the total stress of the layer 'i' (the well-known Terzaghi's principle). These are equal to zero when the non-porous steel side plates are considered (i.e. for  $i = b$ ). Furthermore,  $\sigma^i$  and  $D_\sigma^i$  are, respectively, stress and mechanical strain of a generic particle of the layer 'i', and the relationship  $\sigma^i(D_\sigma^i, T)$  is the material constitutive relationship of concrete/steel at elevated temperatures accounting also for elastic reloading and kinematic hardening of cyclically loaded and reloaded material. Based on the temperature of the time interval  $j$ , already determined within the hygro-thermal subanalysis, and the given stress and strain state in the time interval  $j-1$ , the mechanical strain of a generic particle,  $D_\sigma^{i,j}$ , is determined using the incremental equation:

$$D^{i,j} = D^{i,j-1} + \Delta D^{i,j}. \tag{7}$$

In Eq. (7)  $D^{i,j}$  is the increment of the total strain of the layer 'i' in the time interval  $j$ . Considering the principle of additivity of strains we assume that the strain increment,  $\Delta D^{i,j}$ , is the sum of the strain increments due to temperature,  $\Delta D_{th}^i$ , stress,  $\Delta D_\sigma^i$ , creep,  $\Delta D_{cr}^i$ , and (for concrete only) transient strains,  $\Delta D_{tr}^i$  (with  $\Delta D_{tr}^a \neq 0$  and  $\Delta D_{tr}^b = 0$ ):

$$\Delta D^{i,j} = \Delta D_{th}^{i,j} + \Delta D_\sigma^{i,j} + \Delta D_{cr}^{i,j} + \Delta D_{tr}^{i,j}. \tag{8}$$

By decomposing the traction (load) vectors of both layers with respect to their external (index 'e') and the contact (index 'c') contributions:

$$\mathcal{P}^i = \mathcal{P}_e^i \pm \mathcal{P}_c^i \quad \text{and} \quad \mathcal{M}^i = \mathcal{M}_e^i \pm \mathcal{M}_c^i, \tag{6}$$

the equations of the side plates and the equations of the beam are finally coupled. The contact contributions,  $\mathcal{P}_c^i$  and  $\mathcal{M}_c^i$  (where  $\mathcal{P}_c^a = -\mathcal{P}_c^b$  and  $\mathcal{M}_c^a = -\mathcal{M}_c^b$ ), depend on the longitudinal ( $\Delta U$ ) and transversal ( $\Delta W$ ) slips between the layers, i.e.  $\mathcal{P}_c^i = f(\Delta U, \Delta W)$  and  $\mathcal{M}_c^i = g(\Delta U, \Delta W)$ , where  $f$  and  $g$  are functions determined by experiments for the actual type of the contact connection.

Based on the modified principle of virtual work, the final system of equations of the mechanical submodel, briefly presented above, is finally solved by a novel strain-based FE method. For a detailed description of the proposed mechanical submodel, its governing as

well as its auxiliary equations and the numerical solving procedure a reader is referred to Kolšek et al. (2013).

## 2 THE CASE STUDY

We consider a simply supported RC beam externally strengthened with two symmetrically bolted side plates exposed to mechanical and thermal loads simulating ISO 834 fire conditions. The geometrical, loading, and reinforcement data of the problem along with its hygro-thermal boundary conditions are presented in Fig. 2. The initial relative humidity of air inside the concrete pores is chosen as 60% and the surrounding air relative humidity is 40%. Furthermore, initial porosity of concrete is set to  $p_{or,0}=0.12$  and the initial permeability in the top surface of the concrete section is  $k_{top}=3\cdot 10^{-15}m^2$ . The side plate and the beam are connected by 2 parallel rows of 8 (case ‘c1’) or 5 (case ‘c2’) bolts at each end and each side of the beam. For each of the connectors the constitutive law of contact as suggested by Huang et al. (1999) is used, where for the maximal bearing capacity of a shear connector at room temperature  $P_{max}=40kN$  is chosen. The material data at ambient temperature used in the analyses are: compressive strength of concrete  $f_{c,20} = 3.43kN/cm^2$ , elastic modulus of concrete  $E_{c,20} = 3250kN/cm^2$ , yield strength of steel  $f_{ys,20} = 33.5kN/cm^2$ , elastic modulus of steel  $E_{ys,20} = 21200kN/cm^2$ , yield strength of reinforcing steel  $f_{ya,20} = 53.7kN/cm^2$ , and elastic modulus of reinforcing steel  $E_{ya,20} = 18700kN/cm^2$ . In the analysis, the fire response of the both beams (cases ‘c1’ and ‘c2’) will be compared against the response of the unstrengthened beam (case ‘c3’) and further against each other.

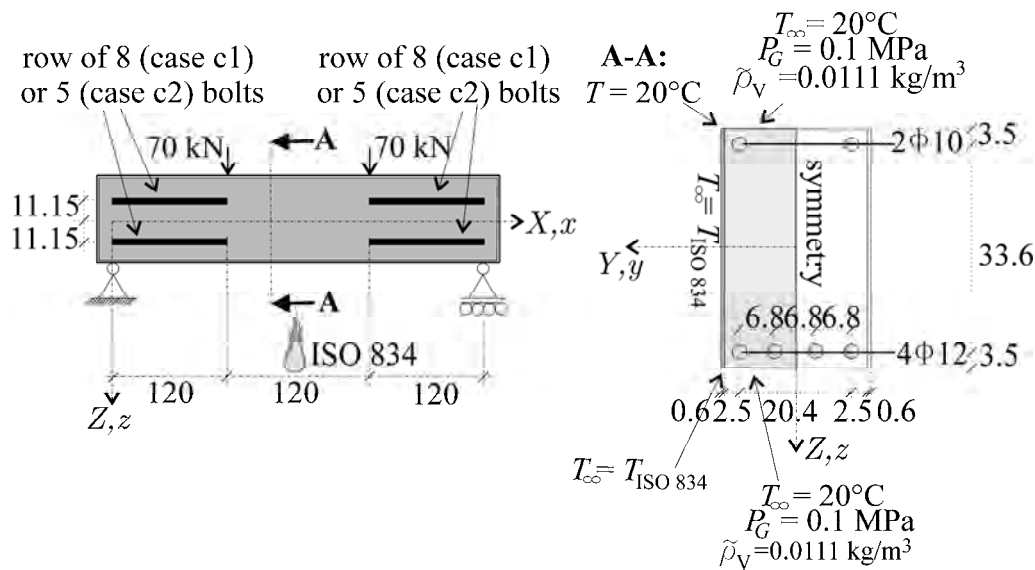


Fig. 1: Geometrical data, loading data, reinforcement data and the hygro-thermal boundary conditions.

The distributions of temperature and pore pressures over the concrete part of the cross section of the side-plated beam and over the cross section of the unstrengthened beam at 22 and 45 min are shown in Fig. 3a. The effect of the vapour-tight side plate preventing the vapour from escaping the side-plated beam is here seen clearly. In comparison to the unstrengthened beam, increased pore pressures are observed along the steel–concrete contact in the side-plated beam resulting in a slight reduction of temperatures of concrete (observe the hottest regions of the cross-section). Nevertheless, the rate of pore pressures evolved in concrete is small in both cases, therefore, their contribution to the total stress of the RC beam can be neglected from the proceeding mechanical subanalysis. Moreover, as confirmed by the criterion of concrete spalling, suggested by Dwaikat and Kodur (2010), in the presented cases spalling of concrete is only superficial and can be also neglected. As in the present analysis characteristics of normal strength concrete have been assumed, such conclusions are rather expected.

Fig. 4 shows the increase of the midspan deflection with time for the two observed cases ‘c1’ and ‘c2’. The bearing capacity of the strengthened beams ( $t_{cr} \approx 45$  min) is here obviously greater than that of the unstrengthened beam ( $t_{cr} = 23$  min) and almost a 100% increase in the fire resistance of the RC beam after its strengthening is observed. By comparing the results for the side-plated beams ‘c1’ and ‘c2’, however, higher number of bolts would appear unreasonable at first glance, especially since for both cases load-deflection curves as well as the predicted fire resistances ( $t_{cr}$ ) are almost identical. Nevertheless, as observed in the numerical analysis, by increasing the number of bolts (case ‘c1’), the pronounced creep deformations in the reinforcement bars of the RC beam would be discovered prior to the collapse and a material instability of the concrete part of the composite cross-section would be eventually reported. Because, in this way, the structure would not fail due to a contact failure (as it would in the alternative case of the ‘c2’ beam) the bearing capacity of the beam would be fully exploited. In contrast to the case shown in this paper, this could be of a special importance, if the RC beam was sufficiently strong.

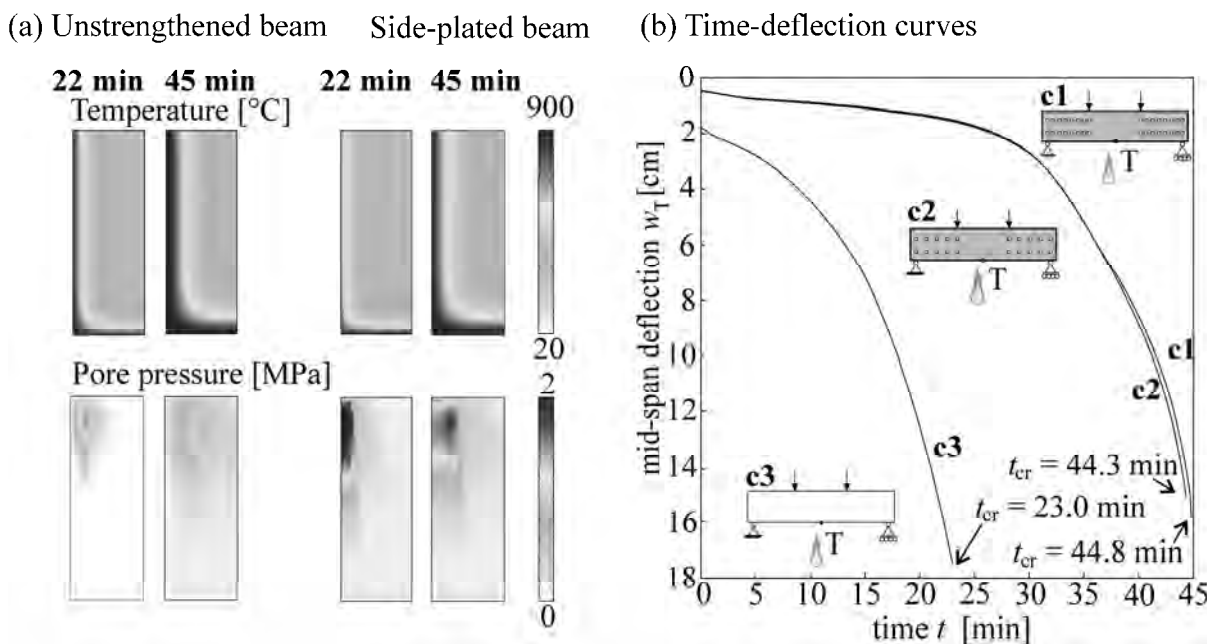


Fig. 2: (a) Temperature and pore pressure distributions in the mid-span cross-section of the analysed beams. (b) The time-deflection curves.

## REFERENCES

- Davie C.T., Pearce C.J., Bićanić N., Coupled heat and moisture transport in concrete at elevated temperatures - Effects of capillary pressure and adsorbed water. *Numerical Heat Transfer, Part A: Applications* 49 (2006) 733 – 763.
- Dwaikat M. B., Kodur V. K. R., Fire induced spalling in high strength concrete beams. *Fire Technology* 46 (2010) 251 – 274.
- Gawin D., Pesavento F., Schrefler B.A. Simulation of damage-permeability coupling in hygrothermo-mechanical analysis of concrete at high temperature. *Communications in Numerical Methods in Engineering* 18 (2002) 113 – 119.
- Gawin D., Pesavento F., Schrefler B.A. Modelling of hygro-thermal behaviour of concrete at high temperature with thermo-chemical and mechanical material degradation. *Computational Methods in Applied Mechanics and Engineering* 192 (2003) 1731 – 1771.
- Hozjan T., Saje M., Srpčič S., Planinc I. Fire analysis of steel-concrete composite beam with interlayer slip. *Computers and Structures* 89 (2011) 189-200.

- Huang Z., Burgess I., Plank R. The influence of shear connectors on the behaviour of composite steel-framed buildings in fire. *Journal of Constructional Steel Research* 51 (1999) 219 – 237.
- Kolšek J. Fire analysis of two-layered composite structures, University of Ljubljana, Faculty of Civil and Geodetic Engineering, Doctoral thesis (in Slovene), 2013.

# **FIRE PERFORMANCE OF AN UNPROTECTED COMPOSITE BEAM Behavior with Finite Beam End Restraints, Rebar Size and Locations**

Serdar Selamet <sup>a</sup>

<sup>a</sup> Bogazici University, Department of Civil Engineering, Bebek 34342 Istanbul, Turkey;  
email: serdar.selamet@boun.edu.tr; tel: +90-212-359-6430

## **Abstract**

The fire performance of steel connections is crucial to provide integrity and stability to floor systems. In full-scale fire tests, the steel frame systems experience large deflections and rotations, which in turn subject the connections to large axial forces and moments. The shear connections, which have limited rotational allowance due to a small gap distance between the beam and the supporting member, exhibit a semi-rigid behavior during fire. Further, the effect of the concrete slab is observed to be beneficial to the deflection behavior of the floor system in several experiments. In this study, the fire performance of a beam with a concrete slab is investigated with varying degrees of rotational rigidity and the tension capacity of the concrete slab with steel rebars. The thermo-mechanical analysis capability of Opensees is utilized.

**Keywords:** steel beam, composite beam, connection, restraints, Cardington, fire, Opensees

## **INTRODUCTION**

A recent capability in analyzing the thermo-mechanical problems is added to Opensees by the research team in University of Edinburgh in U.K, which is an open-source software framework to simulate the performance of structures subjected to earthquakes (Mazzoni et al., 2007). This paper contributes to the development of this newly added thermo-mechanical analysis capability by integrating the rotational end restraints to the composite beam elements. A part of the 2D unprotected steel frame subassembly is modeled and analyzed using Opensees. The frame consists of a two-floor and two-bay compartment consisting of two composite beams restrained by four columns. One bay is subjected to nonuniform temperature whereas the other bay is kept at ambient temperature to consider the catenary action of the concrete slab from the cold region. The springs with nonlinear moment-rotation curves are defined at the beam end restraints. These spring models take account the rotational allowance of shear connections as well as the decreased stiffness due to beam local buckling. Further, the rebar locations and sizes are varied to observed the effect on the global beam behavior.

## **1 CARDINGTON BUILDING TEST**

In 2003, a large full-scale test on an 8-story steel framed building at Cardington facility (Wald et al., 2006). The goal was to understand the behaviour of beam-to-column and beam-to-beam connections and to quantify the effect of concrete slab on the restrained beams. Fig. 1 illustrates the floor layout of the test. Previously, the subassembly with the single plate connection in the shaded compartment is modeled with three-dimensional solid elements in Abaqus (Selamet and Garlock, 2010). Although the detailed model was very useful to see the local buckling in the connection and the connection failure during the cooling phase, the finite element model required large amount of time to build and run. In this paper, the same secondary beam is represented with a much simpler model to study the effects of connection's rotational capacity and the tensile capacity of the concrete slab during the cooling phase.

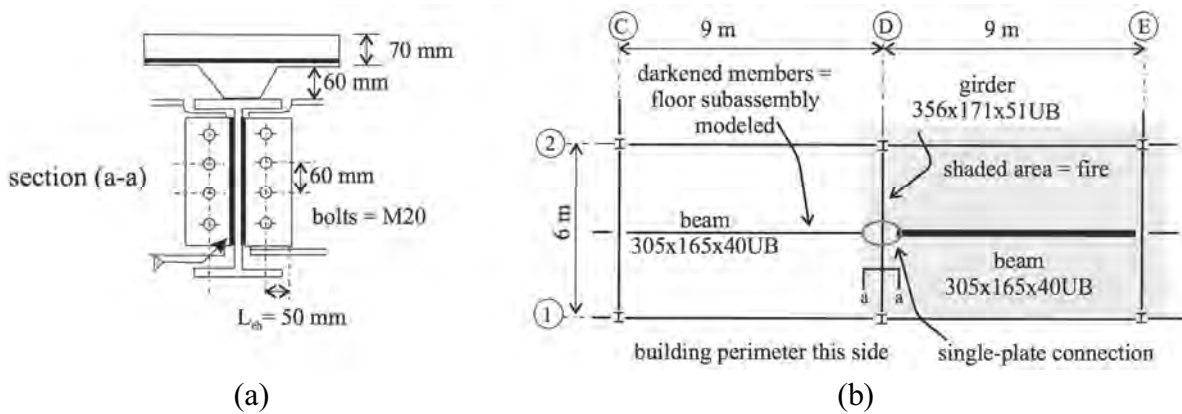


Fig. 1 Details of Cardington building test: (a) single plate connection and (b) the heated building compartment (the modeled beam with thick lines)

In Cardington test, the secondary beam 305x165x40UB is steel with 300 MPa yield strength, the concrete slab is composed of 35 MPa of lightweight concrete (no tensile strength) with A142 anti-crack mesh, which has 320 m<sup>2</sup>/m area of steel and 460 MPa of yield strength. The beam is loaded with 21.45 kN/m uniformly distributed load assuming its corresponding tributary area. The structural temperatures are read directly from the thermo-couple readings of Cardington test.

## 2 THE FINITE ELEMENT MODEL IN OPENSEES

### 2.1 Description

A recent capability in analyzing the thermo-mechanical problems is added to Opensees by the research team in University of Edinburgh in U.K (Usmani, 2012; Jiang, 2013). In this paper, the realistic scenario of Cardington test is simulated using the structural fire capability of Opensees. For this particular problem, only the secondary (restrained) beam in the heated compartment is investigated. The steel and concrete material properties are adopted from Eurocode 3 (CEN, 2005) by using the *Steel01Thermal* and *Concrete02Thermal* commands. The composite beam is modeled as one section with 8 fibers of concrete slab and 8 fibers of steel beam. The steel mesh is represented as one layer of 8 steel rebars with area of 40 m<sup>2</sup> as illustrated. The effective composite section width is taken from the Steel Construction Manual (AISC, 2005) as 2.25 m, which is one quarter of the total beam length. Only half of the rib area, which runs perpendicular to the beam direction, is added to the concrete slab as shown in Fig. 2.

From the previous research by the authors (Garlock and Selamet, 2010), it was concluded that the cool neighboring compartment (see Fig. 1) provided almost rigid axial constraint to the heated beam. Therefore, the heated beam is axially fully restrained. The *Zerolength Element* command is used to simulate the semi-rigid connection behavior of the single plate shear connection. The single plate connection, as other types of shear connections, has a gap distance that allows limited free rotation (pinned) as seen in Fig. 3. After the gap is closed, the connection behaves as fixed (with high rotational stiffness). Using *UniaxialMaterial ElasticPPGap* command, the realistic behavior of the connection is achieved. The force-deformation character of the *Zerolength Element* is shown in Fig. 4. After the gravity load is applied to the beam, the 'Fire Pattern' command is used to apply the structural temperatures at 7 different fiber locations across the composite beam section as shown in Fig. 2. The temperatures are obtained from Cardington test as shown in Fig. 5. The *Corotational* command is used to invoke geometrically nonlinear analysis. A full Newton analysis is done using *algorithm Newton* and *test NormUnbalance* commands.



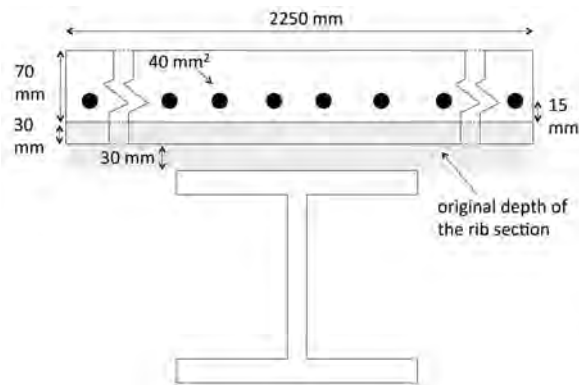


Fig. 2 Composite beam section in Cardington test

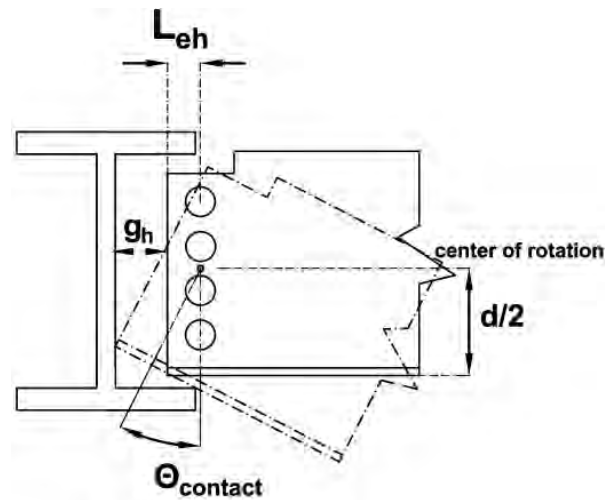


Fig. 3 Composite beam section model in Opensees

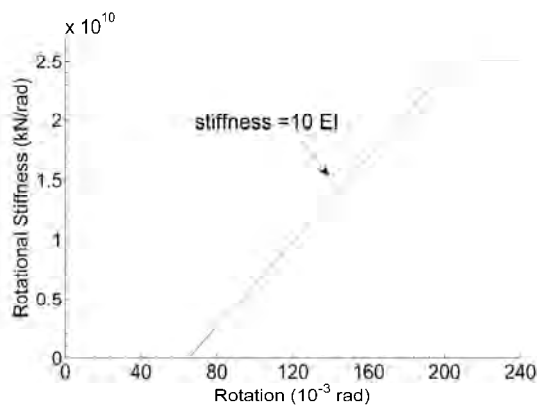


Fig. 4 Semi-rigid connection stiffness of the single-plate connection

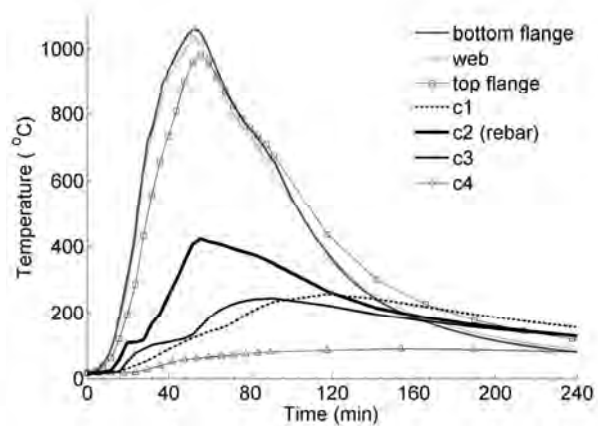


Fig. 5 Fire loading applied to the beam

## 2.2 Validation

The model in Opensees is compared with the vertical beam midspan deflection obtained from Cardington test. Since the full-scale single plate connection is represented by a 1D rotational spring at the beam end, the spring needs to be calibrated according to the vertical deflection result in the experiment. In addition, an allowable free rotation  $65 \times 10^{-3}$  rad is taken as estimated by Eq. (1) (Jaspart, 2003) and illustrated in Fig. 3. Fig. 6 shows that the model with a large rotational stiffness of  $10 \cdot EI$  (of the steel beam) and the experiment are in close agreement. The heated beam deflects as the stiffness of the steel material decreases. The semi-rigid connection behavior avoids a possible runaway behavior. As the region gets into the cooling phase, the beam contracts and regains some of the deflection but it is significantly limited due to plastic deformations in the beam and in the rebars.

$$\theta_{contact} = \sin^{-1} \left[ \frac{L_{eh} + g_h}{\sqrt{L_{eh}^2 + (d/2)^2}} \right] - \tan^{-1} \left[ \frac{L_{eh}}{d/2} \right] \quad (1)$$

### 3 PARAMETRIC STUDY

#### 3.1 Effect of concrete slab

A parametric study is conducted to investigate the effect of the concrete slab and the rebar to the vertical deflection behavior of the composite beam section. As seen in Fig. 6, the bare steel beam experiences runaway behavior and fails during the heating phase of the fire. Further, the composite beam without rebars deflects significantly larger due to the limited tensile capacity of the composite beam. The previously validated composite beam with rebars is in close agreement with the experiment.

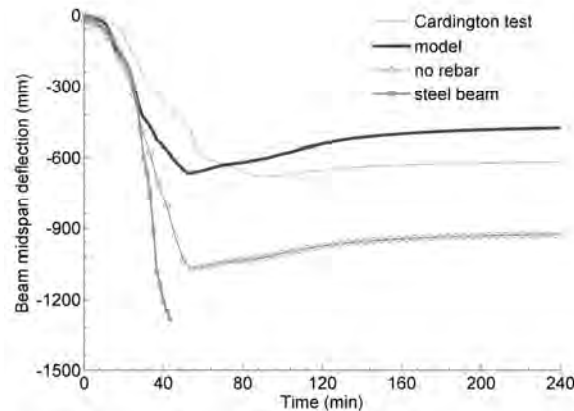


Fig. 6 Vertical deflection of the beam midspan of various parametric studies

#### 3.2 Effect of rebars

Fig. 7a) shows the stress-history in the beam web and in the rebar at the beam end (supports). Independent of the rebar size, it is observed that the rebar's tensile capacity (460MPa) is reached almost immediately after the steel beam yields due to large compression and degrading material properties at elevated temperatures at 300MPa. The stress-strain history of the rebar (not shown) points out that the rebar enters to the unloading (decreasing) stress state at around 2.5% strain during the cooling phase of the fire due to the significant strength regain of the steel beam. Therefore, the stress in the rebar decreases due to large strains after 80 minutes of fire and the regain of the strength is not observed. The increased rebar area increase the tensile stress in the rebar and in the beam web since the beam has deflected much less during the heating with larger rebar (tensile) contribution as clearly seen in Fig. 7b).

Fig. 8a) illustrates the effect of the rebar location on the fire performance of the composite beam. If the rebar is placed further from the beam (closer to the concrete top surface), the rebar carries nearly the same tensile stress as the beam web. As observed in Fig. 8b), the further away the rebar from the beam, it experiences smaller strains. This behavior is expected since the temperatures in the concrete slab are much lower than the temperatures in the steel beam. However, since the yield stress of the rebar is already reached at earlier stages, the strain deformation does not seem to affect the tensile stress development in the beam web during the heating and the cooling phase of the fire.

#### 3.3 Effect of end restraints

The rotational allowance  $\theta_{contact}$  is varied from 0 rad to  $90 \times 10^{-3}$  rad (see Fig. 4) with the gap parameter in *UniaxialMaterial ElasticPPGap* command in Opensees. The effect, though insignificant, is seen in early stages of fire in Fig. 9. The rotational spring does not seem to affect the global vertical deflection of the beam midspan mainly because the beam elements near the end supports yield and form a plastic hinge.

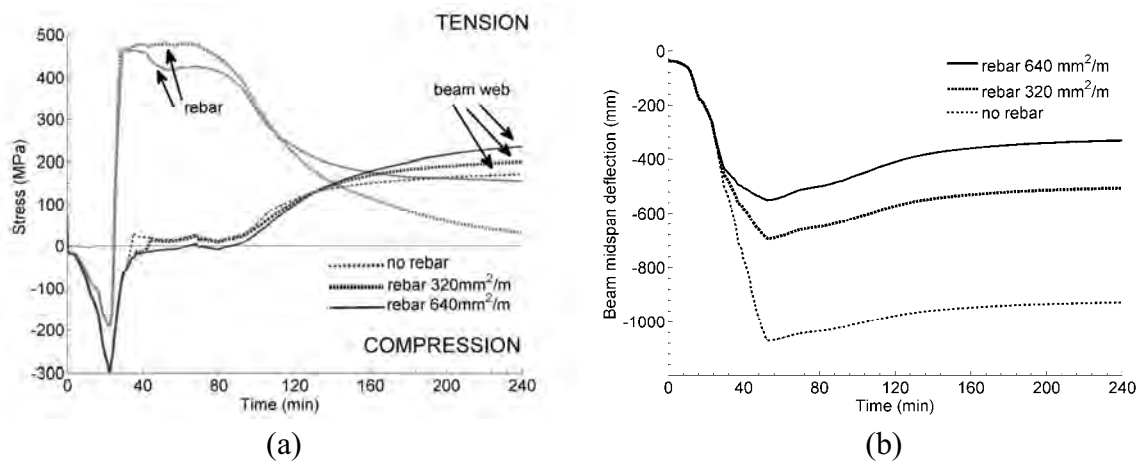


Fig. 7 Stress-strain history of the beam web and the rebar at the beam end with different rebar sizes

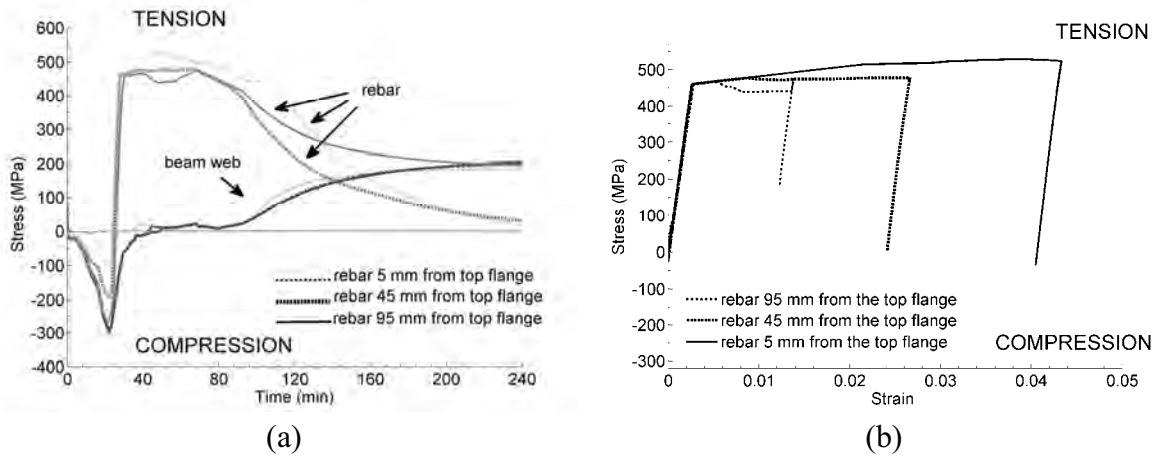


Fig. 8 Stress-strain history of the beam web and the rebar at beam end with different rebar locations

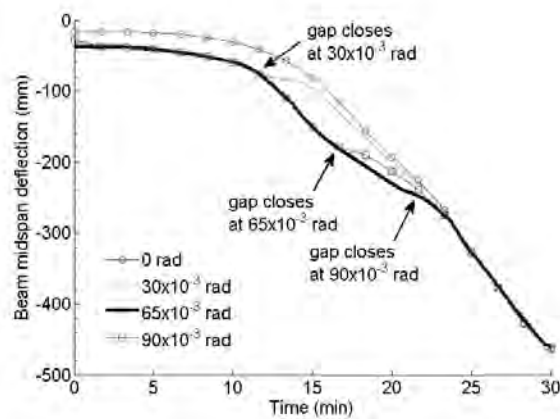


Fig. 9 The vertical beam midspan deflection for various rotational (gap) allowance with the *Zerolength Element*

## 4 SUMMARY AND ACKNOWLEDGMENT

This paper investigates the behavior of an axially restrained composite beam in Cardington test. A newly developed thermal capability of Opensees is utilized to model and run the analysis. The secondary beam is loaded with large gravity and thermal loading to test its ultimate capacity especially during the cooling phase of the fire. Due to the 1D nature of the beam elements, the full effect of the composite behavior is not observed. It is concluded that Opensees is especially an advantageous tool to create more realistic boundary conditions by using multi-purpose spring elements. However, some convergence problems are reported with using *Steel02Thermal* elements and with *Concrete02Thermal* elements with nonzero tensile capacity. Further, most of the analyses did not converge using *algorithm ModifiedNewton* command.

## REFERENCES

- AISC, Steel Construction Manual 13<sup>th</sup> Edition, Chicago, IL, 2005.
- CEN, Eurocode 3: Design of Steel Structures Part 1.2: General Rules Structural Fire Design ENV 1993-1-2:2005, Brussels, Belgium, 2005.
- Garlock M. and Selamet S., Modeling and Behavior of Steel Plate Connections Subject to Various Fire Scenarios, *Journal of Structural Engineering*, 136 (7), 897-906, 2010.
- Jaspart J.P., European design recommendations for simple joints in steel structures University of Liege, 2003.
- Jiang J., Usmani A., Modeling of Steel Frame Structures in Fire using Opensees, *Computers and Structures*, doi: 10.1016/j.compstruc.2012.07.013, 2013.
- Mazzoni S., McKenna F., Scott M. H., Fenves G. L. et al., Opensees Command Language Manual, 2007.
- Selamet S. and Garlock M., Robust Fire Design of Single Plate Shear Connections, *Engineering Structures*, 32 (8), 2367-2378, 2010.
- Usmani A., Zhang J., Jiang J., Jiang Y., May I., Using Opensees for Structures in Fire, *Journal of Structural Fire Engineering*, 3(1), 2012.
- Wald F., Simoes da Silva L., Moore D.B., Lennon T., Chladna M., Santiago A., Benes M., Borges L., Experimental Behaviour of a Steel Structure under Natural Fire, *Fire Safety Journal*, 41 (7), 506-522, 2006.

# **FIRE RESISTANCE OF STEEL FRAMES UNDER DIFFERENT FIRE-AFTER-EARTHQUAKE SCENARIOS BASED ON SCALED DESIGN ACCELEROGRAMS**

Dapnhe Pantousa<sup>a</sup>, Euripidis Mistakidis<sup>a</sup>

<sup>a</sup>Laboratory of Structural Analysis and Design, Dept. of Civil Engineering, University of Thessaly, 38334 Volos, Greece, web page: <http://lsad.civ.uth.gr/>

## **Abstract**

The scope of this paper is to examine the performance of a steel framed structure under fire conditions after earthquake events. Taking into account this combined scenario, it is clear that the fire behavior of steel structures depends on the intensity of the ground motion and the study should be based on the performance based design philosophy. For this purpose a three-dimensional beam finite element model is developed using the non-linear analysis code MSC Marc. The combined scenario involves two different stages: during the first stage, the structure is subjected to the ground motion record while in the second stage the fire occurs. Several time-acceleration records are examined, each scaled to multiple levels of the Peak Ground Acceleration (PGA). The objective is to relate, the level of damage of the structural members occurring due to earthquake, to the fire-resistance of the structure.

**Keywords:** fire-after-earthquake, steel structures

## **INTRODUCTION**

The design of structures according to the current codes is performed individually for the seismic and the thermal actions. Despite the significant progress of the worldwide scientific research on the earthquake response and on the fire-performance, the research concerning the combined scenario is rather limited. It is expected that the damage induced by earthquake can be present to both structural and non-structural members. The seismic damage to non-structural members can be related to different fire-after-earthquake (FAE) scenarios that should be considered at the fire design of the structure. Moreover, it is expected that the fire performance of structures will be different, depending on the level of damage caused to the structural members by the seismic loads.

Recently, some studies have been conducted, for the evaluation of the performance of structures under combined scenarios of FAE. For example, the post-earthquake fire resistance of steel moment resisting frames is evaluated in Zaharia et al (2009). Moreover, two different moment resisting steel frames are considered in Della Corte et al (2003) for the evaluation of the FAE resistance.

## **1 DESCRIPTION OF THE PROBLEM**

The aim of the current study is to evaluate and quantify the behaviour of the four-storey steel frame, which is illustrated in Fig. 1, for the combined scenario of fire after earthquake. Taking into account the fact that the behaviour of the structure for the combined scenario is strongly dependent on both structural and non-structural damage induced due to the seismic action, it is evident that the problem should be approached through the performance based philosophy. For this purpose, the multi-level design approach of FEMA which considers four different seismic performance levels (Operational, Immediate Occupancy, Life safety and Collapse Prevention), is adopted. Following the principles of the performance based seismic design, the intensity of the earthquake is scaled up in order to represent more severe seismic actions. For

this reason seven different accelerograms are selected, according to the criteria that are defined in Section 1.2. The earthquake records are scaled to multiple levels of the Peak Ground Acceleration (PGA). Each FAE scenario consists of two different stages. The first stage is defined from the time-acceleration record while in the second stage the fire is described using the ISO fire curve. It is noted that in the current study, the damage induced to the non-structural members due to earthquake (e.g. breakage of windows, broken sprinkler system etc.) is not taken into account.

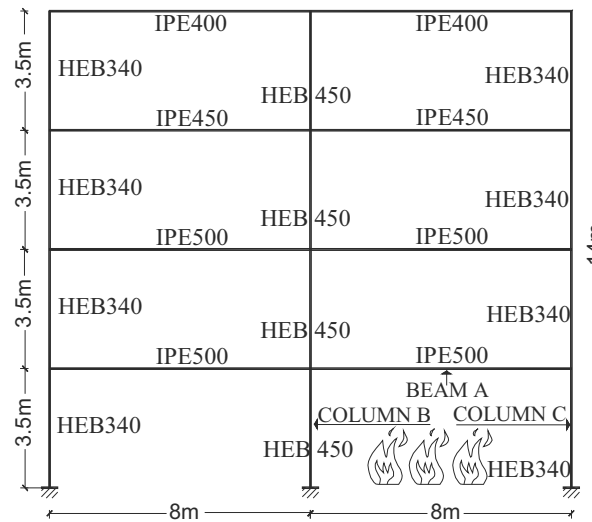


Fig. 1 The considered steel frame

The study here is focused on new buildings where the regulations of the current codes are applied. The first task is to design the steel frame for the ultimate limit state (ULS) combination of actions for the gravity loading. Regarding the design for the seismic actions, the principles of EN 1998-1-1 (2004) are followed and the lateral force method of analysis is used. Specifically, Type 1 elastic response spectrum is considered with  $a_g = 0.36 \text{ g}$  and soil type D ( $S=1.35$ ). The behaviour factor  $q$  was taken equal to 4.

The modelling of the seismic and the fire hazard follows. The seismic action is modelled through different time-history acceleration records. To this end, seven time-history acceleration records are selected from the European strong motion Database. These records are scaled to match the design spectrum using Rexel v3.5 (Ambraseys et al, 2002) following the guidelines of par. 3.2.3.1.2 of EN 1998-1-1 (2004). The considered records are summarized in the headings of Tab. 1. The fire action is represented through the ISO fire curve and it is supposed that the fire breaks out in the first level of the frame structure as it is illustrated in Fig. 1. In order to simplify the problem, it is assumed that the temperature inside the fire compartment is uniform. The temperature-time curves are calculated according to the guidelines of EN 1993-1-2 (2003), depending on the cross-section characteristics of the structural members. Finally, the FAE scenarios are defined. Regarding the seismic action, the time-history acceleration records, which were already modified as explained earlier, are further scaled to three levels of the Peak Ground Acceleration (PGA) using the scale factors 1, 1.5 and 2. It is noted that the reference fire scenario corresponds to the case where the structure is not damaged due to earthquake.

## 2 NUMERICAL SIMULATION

The numerical analysis is carried out using the nonlinear finite element code MSC-Marc (2011). The model for the simulation of the behaviour of the steel frame is developed using element 98 of the library of MSC Marc (2011). This is a straight beam in space which includes transverse shear effects. The cross-section of the finite element used for the numerical modelling, is a user-defined solid numerically integrated one. Four different

branches are defined for the sections of the structural members: the upper flange, the web (which is divided into two parts for more accurate results) and the lower flange branch. Depending on the order of the numerical integration that is selected for every branch of the cross-section, the stress strain law is integrated through solid sections using a Newton-Cotes rule. The output results are exported to different layers, corresponding to the position of the integration points. The results are exported to different layers corresponding to positions of integration points.

The yield stress of the structural steel is equal to 275 MPa at room temperature. All the material properties are supposed to be temperature dependent according to EN 1993-1-2 (2003). It is underlined that the strain hardening of the steel for temperature range 20 °C – 400 °C is neglected in order to simplify the problem.

The problem is solved through dynamic transient analysis with direct integration of the equations of motion and the Newmark-Beta operator is used.

The numerical analysis is divided into two different parts. In the first analysis the steel frame is subjected to the seismic action while in the second one the analysis restarts and the deformed structure is exposed to the standard fire ISO curve for 60 minutes.

### 3 RESULTS OF THE NUMERICAL ANALYSIS

The results of the time history analysis for the earthquake loading indicate that the steel frame fulfils the demands of the capacity design rules and the plastic hinges are formed at the beam ends and to the columns bases, as it is expected. The study is focused on the structural members which are exposed to the fire in the next stage of the analysis (beam A, column B and column C), as it is illustrated in Fig. 1. At the starting point of the fire analysis plastic hinges have already been formed at the ends of beam A. The fire-after earthquake analysis indicates that the failure occurs when one more plastic hinge is formed at the mid-span of the beam. It is evident that this is a local type failure. In this study it is considered that the global failure of the steel frame will follow immediately after the local failure.

In order to study more systematically the behaviour of the steel frame under the combined scenario of fire after earthquake, the results of the analyses are classified according to the amplitude of the maximum equivalent plastic strain that is developed to the plastic hinge locations, at the end of the seismic analyses. This classification characterizes the level of damage induced in the structural members. Tab. 1 summarizes maximum equivalent plastic strain at both ends of Beam A for the various FAE scenarios. It is noted that Beam A appears the higher degrees of damage, compared with all the structural members of the steel frame.

It is observed that the results corresponding to the scale factors (S.F.) 1 and 1.5, are reasonable. On the contrary, when the scale factor 2 is implemented in the analysis, the values of the equivalent plastic strain become very high. The results that produce values of equivalent plastic strain higher than 0.2 are not considered acceptable and the corresponding FAE scenarios are not further studied.

Tab. 1 Level of damage for the FAE scenarios (end of the earthquake)

S.F.	Fire-after-earthquake scenarios													
	FAE 290xa		FAE 293ya		FAE 612xa		FAE 1726xa		FAE 1726ya		FAE 5850xa		FAE 6142ya	
	x=0	x=8m	x=0	x=8m	x=0	x=8m	x=0	x=8m	x=0	x=8m	x=0	x=8m	x=0	x=8m
1.0	0.020	0.036	0.044	0.036	0.032	0.028	0.046	0.046	0.034	0.022	0.016	0.022	0.080	0.090
1.5	0.100	0.138	0.124	0.134	0.200	0.200	0.158	0.162	0.086	0.104	0.070	0.058	0.220	0.222
2.0	0.308	0.346	0.262	0.294	0.528	0.564	0.278	0.266	0.154	0.192	0.158	0.152	0.406	0.442

The distributions of the equivalent plastic strain along the height of the cross-section of Beam A, for both the beam ends, are presented in Fig. 2. These distributions correspond to the starting point of the fire analysis. It is observed the plastic hinges are “fully” developed at both beam ends at the end of the earthquake event, and this holds for all the FAE scenarios.

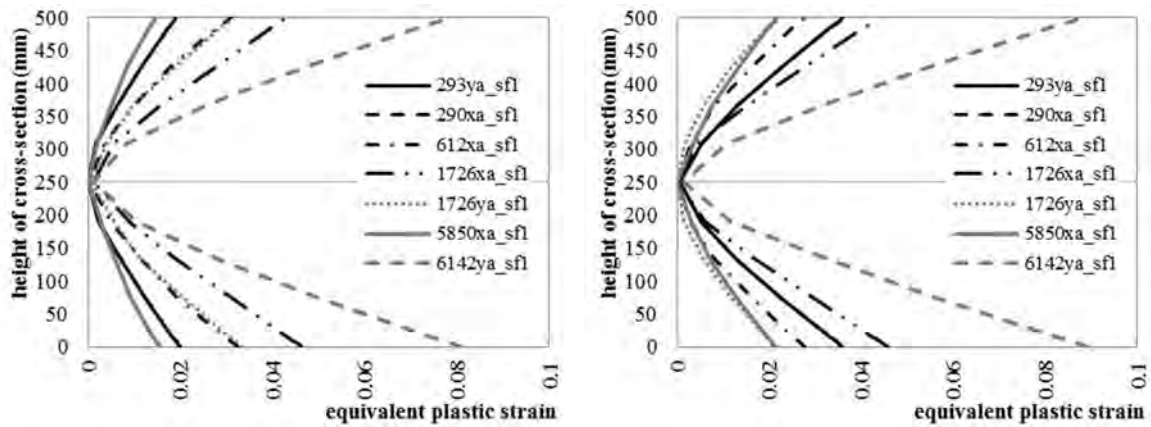


Fig. 2 Equivalent plastic strain distribution at  $x=0$  and  $x=8m$  for Beam A (S.F. 1.5)

The evaluation of the outcomes of the analyses, taking into account the equivalent plastic strain is a qualitative approach, for thoroughly understanding the behaviour of the structure during the combined scenario, but is not an objective criterion for the determination of the fire resistance of the steel frame. In this study the criterion that is proposed in order to assess the fire-resistance of the structure, is based on the rotational capacity of the structural members at elevated temperatures.

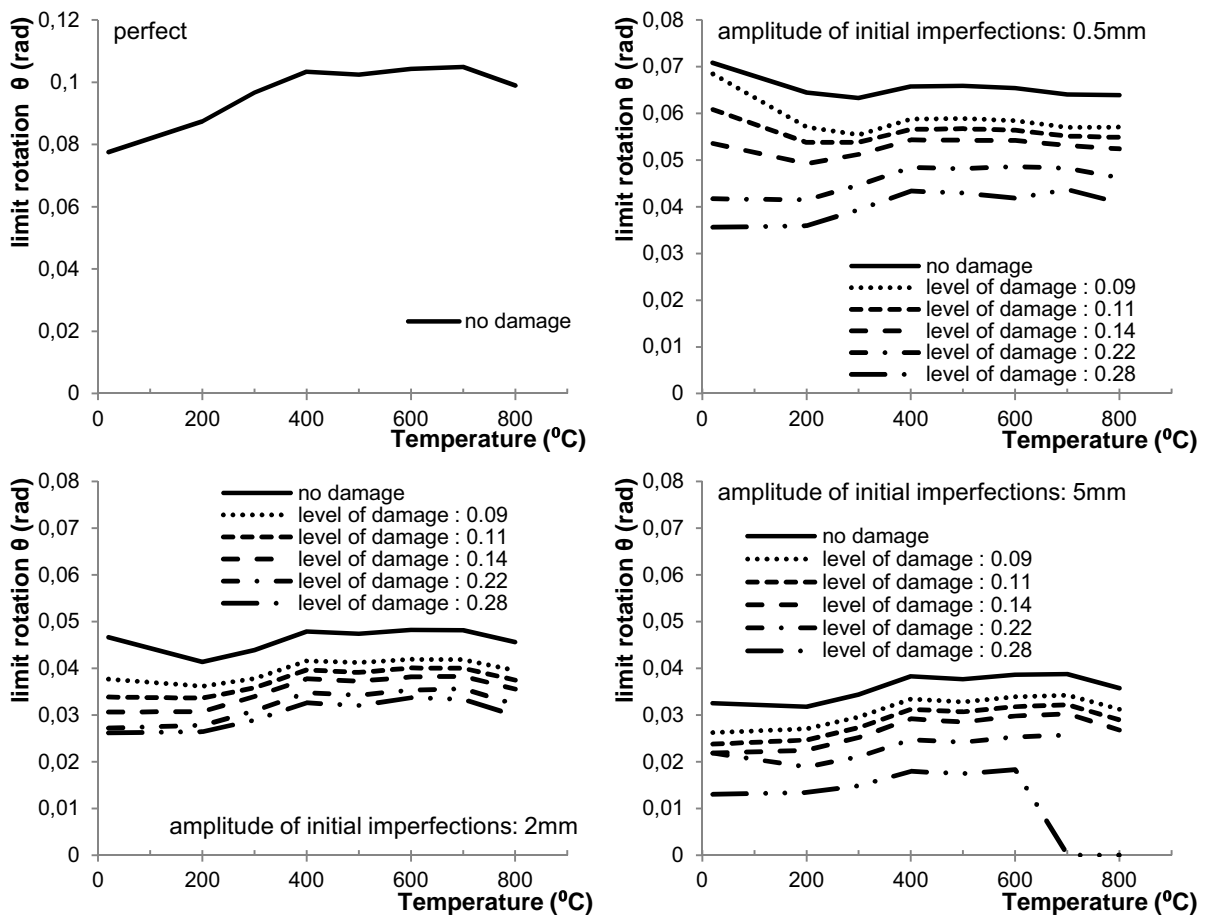


Fig. 3 Rotation limits

Advanced three-dimensional numerical models are developed for the determination of the rotational capacity of the steel beams under fire conditions (Pantousa D. et al, 2011). The three-dimensional models are based on shell finite elements and take into account the existing initial imperfections of the steel members. Parametric analyses are conducted with respect to the amplitude of the initial imperfections, in order to obtain moment – rotation curves for steel



IPE beams at elevated temperatures. The limit values for the rotation of the beam at the plastic hinges positions (beam ends) are represented in Fig. 3, for models that do not take into account initial imperfections (perfect models) and for models which include different levels of initial imperfections. In order to take into account the seismic damage, the limit values for rotation  $\theta$ , are also obtained for beams which are pre-damaged due to cyclic loading. Each curve corresponds to different level of damage which is classified according to the level of the equivalent plastic strain that develops. The perfect models are examined only for the case where the beams are not damaged due to cyclic loading. Comparing the evolution of the rotation of beam A as the temperature increases with the limit values of Fig. 3, the fire-resistance of the steel frame is obtained.

In order to explain the procedure that was followed, the example of Fig. 4a) is presented. Two different curves are depicted. The first curve corresponds to the plastic hinge rotation (beam end at  $x=8$  m) during the fire exposure in the case of FAE scenario 6142 ya, using S.F.=1, while the second curve represents the maximum acceptable rotation of the beam plastic hinge as a function of the temperature, for amplitude of initial imperfection equal to 0.5 mm. It is evident that this last curve corresponds to a specific level of damage induced to the end of the beam due to earthquake. In the specific case of Fig. 4a), as it is observed in Tab. 1, the level of damage for the beam end at the location  $x=8$ m, is equal to 0.09, thus the corresponding curve is selected in order to assess the fire-resistance time. The intersection of the two curves of Fig.4a indicates the temperature and the corresponding limiting rotation.

Taking into account the above, it is clear that the fire-resistance time of the steel frame depends on the level of initial imperfections. Tab. 2 summarizes the fire-resistance of the structure for the FAE scenarios, considering different amplitudes of initial imperfections. Concerning the reference scenario, the fire-resistance is obtained for different cases (Fig. 4b). First, the limit rotation curve that corresponds to the “perfect model” is used and the fire resistance is calculated equal to 1526 sec. Then, the limit rotation curves which are obtained through the analyses of the models that take into account initial imperfections, are used. Thus, the fire-resistance time is calculated equal to 1362 sec, 1526 sec and 1277 sec for amplitude of initial imperfections 0.5 mm, 2 mm and 5 mm respectively.

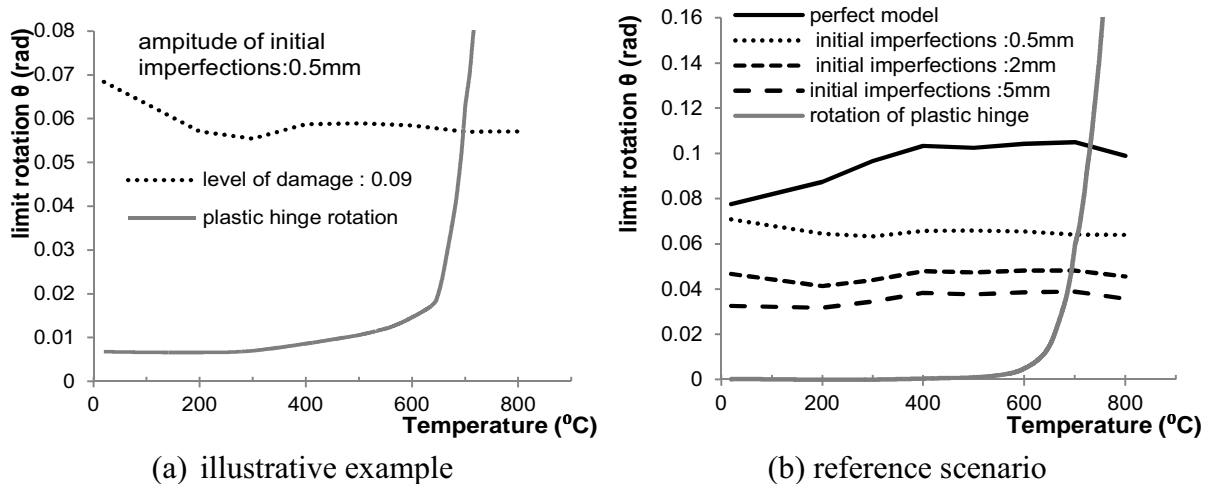


Fig. 4 Calculation of the fire resistance

Finally, the reduction of the fire resistance time of the steel frame for the combined scenarios is obtained for two different cases (Tab. 2). In the first case (Case 1) the reduction is obtained taking into account the fire-resistance times of the reference scenario that correspond to different amplitudes of initial imperfection. In the second one (Case 2) the reduction is calculated with respect to the fire-resistance of the reference scenario that does not include the initial imperfections.

Tab.2 Fire resistance time (sec) and the corresponding reduction for the FAE scenarios

Fire-resistance in time domain (sec)						
FAEscenario	Amplitude of initial imperfections					
	0.5mm		2mm		5mm	
	scale1	scale 1.5	scale1	scale 1.5	scale1	scale 1.5
290xa	1325	1299	1274	1235	1234	1194
293ya	1331	1313	1281	1257	1244	1216
612xa	1333	1296	1285	1241	1248	1191
1726xa	1324	1293	1273	1230	1232	1186
1726ya	1328	1306	1278	1245	1238	1206
5850xa	1342	1320	1294	1267	1259	1227
6142ya	1321	1281	1269	1222	1232	1171
<b>mean time</b>	<b>1329</b>	<b>1301</b>	<b>1279</b>	<b>1242</b>	<b>1241</b>	<b>1199</b>
Reduction of the fire resistance time for the FAE scenarios						
<b>Case 1</b>	<b>2.41%</b>	<b>4.47%</b>	<b>2.28%</b>	<b>5.09%</b>	<b>2.82%</b>	<b>6.13%</b>
<b>Case 2</b>	<b>12.90%</b>	<b>14.74%</b>	<b>16.18%</b>	<b>18.58%</b>	<b>18.68%</b>	<b>21.45%</b>

#### 4 CONCLUSIONS

In this paper the behaviour of a steel frame under the combined scenario of FAE is studied. The level of damage, induced due to earthquake is classified according to the values of the equivalent plastic strain in the plastic hinge locations. The fire-resistance of the frame, in time domain, is calculated using as criterion the rotational capacity of the structural members under fire conditions, which is obtained through appropriate 3D finite element models. The reduction of the fire resistance with respect to the undamaged steel frame increases as the level of damage induced by the seismic action becomes greater. The reduction of the fire-resistance strongly depends on the level of the initial imperfection that is taken into account.

#### 5 ACKNOWLEDGMENTS

The present work is financially supported by the National Research Program “HERACLITUS II”, the contribution of which is gratefully acknowledged.

#### REFERENCES

- Ambraseys N., Smit P., Sigbjornsson R., Suhadolc P. and Margaris B., Internet-Site for European Strong-Motion Data, European Commission, Research-Directorate General, Environment and Climate Programme, 2002.
- Della Corte G., Landolfo R., Mazzolani F. M., “Post earthquake fire resistance of moment resisting steel frames”, *Fire Safety Journal*, Vol. 38, pp. 593-612, 2003.
- European Committee for Standardization, Eurocode 8.EN 1998-1-1.Design of structures for earthquake resistance – Part 1. General rules seismic actions and rules for buildings, 2004.
- European Committee for Standardization, Eurocode 3. EN 1993-1-2.Design of steel structures – Part 1-2. General rules – structural fire design, 2003.
- MSC Software Corporation, MSC Marc, Volume A: Theory and User Information, Version 2010.
- Pantousa D., Mistakidis E., “The effect of the geometric imperfections on the rotational capacity of steel beams at elevated temperatures”, 7th GRACM international congress on computational mechanics, Athens, 2011
- Zaharia R., Pintea D., “Fire after earthquake analysis of steel moment resisting frames”, *International Journal of Steel Structures*, Vol. 9, pp. 275-284, 2009.

## **FIRE TEST OF TIMBER-FIBRE CONCRETE COMPOSITE FLOOR**

Eva Caldová <sup>a</sup>, František Wald <sup>a</sup>, Anna Kuklíková <sup>a</sup>

<sup>a</sup> Czech Technical University in Prague, Faculty of Civil Engineering, Prague, Czech Republic

### **Abstract**

Furnace test was performed on one full-size floor specimen at the Fire testing laboratory PAVUS. Floor specimen was 4.5 m long and 3 m wide, consisting of 60 mm fibre concrete topping on plywood formwork, connected to GL floor joists. It was subjected the standard fire for over 150 min. The membrane effect of the floor was progressively activated. The project is part of the experimental research that deals with the effect of membrane action of composite steel fibre reinforced floor slabs exposed to fire and continuous on previous research on steel fibre reinforced concrete slabs. The main objective of the project is the preparation of the analytical prediction model for the fire resistance of the steel-concrete and timber-concrete slab with steel fibre concrete.

**Keywords:** timber, fibre reinforced concrete, fire test, furnace

### **INTRODUCTION**

The use of timber-concrete structures has considerably increased especially in case of reconstructions and constructions of prefabricated residential houses. For this reason it is necessary to gain a deeper knowledge of the behaviour of timber-concrete structures in fire, to remove all unknown and to ensure safe use for the intended purpose.

In the concrete slab of the timber-concrete composite floor is necessary reinforcement for restrain caused by shrinkage of concrete and to obtain a sufficient resistance against tensile forces around the shear connectors. Consider the amount and the position of the reinforcement in the slab the thickness of the slab results in a minimum of about 60 mm which leads to an unnecessary high dead load of the composite floor, see Holschmacher, 2002. For this reasons several research studies during the last decades have been conducted, with focus on new timber-concrete composite floor. One of the new kinds of such floor is that the usual reinforced concrete is replaced by steel fibre reinforced concrete (SFRC). This innovative concrete with specific hardened concrete properties and fresh was developed to reduce the slab thickness and to help the construction procedure. With the use of fibres the experiment shows that the behaviour is more ductile and redistribution of stresses is better.

One of the most important requirements of floor structure is its fire resistance. The fire resistance of timber-fibre concrete composite elements is mainly influenced by the timber, the connectors and mixture of fibre concrete. The temperature inside the timber member depends particularly on the cross-sectional dimensions, on the density and moisture content of wood and on the fire load and temperature development during the fire. The temperature development in the place of the shear connection can be governed by the cross-sectional dimensions, particularly by the width, and by the sort of fire scenario. It is possible to use nominal, parametric or natural fire scenario. Fire resistance of SFRC can be increased by adding of plastic fibres (polypropylene, polyester) because the plastic fibres evaporate in temperature of 100 °C and rise continuous water pore to escape from concrete in case of fire. The results indicate that the influence of steel fibres on the mechanical properties is relatively greater than the influence on the thermal properties and is expected to be beneficial to the fire resistance of structural elements constructed of fibre-concrete. Experimental and theoretical studies shows that the compressive strength at elevated temperatures of fibre-reinforced

concrete is higher than that of plain concrete. The presence of steel fibres increases the ultimate strain and improves the ductility of fibre-reinforced concrete elements, see Kodur, 1996.

The experimental work of testing a composite timber-fibre concrete floor in fire is described in this report. For the experiments were made material properties tests at ambient and elevated temperature. There were detected tensile strength and ductility of fibre reinforced concrete. Thermal and mechanical properties of fibre reinforced concrete at elevated temperature and numerical modelling of timber-fibre concrete composite floor in fire will be the subject of further author's works and papers. The results obtained in the numerical simulations will be compared with results obtained from furnace tests, which were performed on one full-size floor specimens in the Fire testing laboratory PAVUS in October 2012. On the evaluating of results and comparing results and simulations author currently works.

## 1 TEST AT ELEVATED TEMPERATURE

The full scale floor specimen was designed to span 3,5 m by 4 m according to the furnace interior dimensions. The composite timber-concrete floor was composed of timber frame, two secondary beams and a 60 mm thick floor slab connected to glue laminated floor joists. Concrete slabs with a strength class 45/55 were reinforced by steel fibre only without added steel bars. The fibre content was  $70 \text{ kg/m}^3$  with type of fibres HE 75/50 Arcelor. As connectors were used TCC screws inclined 45 degrees to the beam axis in two rows, distance of screws in one row is 0,1 m. The timber frame was fire protected and the secondary beams in the centre of the floor slab were left unprotected. The design fire used in the tests was the standard fire. The mechanical load during fire was created by concrete blocks uniformly distributed over the floor. The arrangement of the test specimen is shown in Fig. 1.



Fig. 1 Fire test set-up

The behaviour of the composite slabs in the furnace was recorded by 27 thermocouples and 13 deflectometers. 13 thermocouples were concreted in the composite slab at 3 separate points across the slab, 4 were located on timber beams and 10 recorded the gas temperature in the furnace and were located just below the floor. Seven deflectometers measured the vertical deflections and six measured the horizontal deflections.

## 2 EXPERIMENTAL RESULTS

During the heating phase of this test, the standard fire curve was followed which lasted for 150 mins. After that, burners were turned off and the furnace was cooled down naturally. The unprotected timber beams located at the middle of the floor were heated up to 250 °C. The maximum recorded temperature occurred after 45 mins at the centre span of beam. Then the secondary beams failed, see Fig. 2. Integrity of this slab was maintained during the first 100 mins, when the first crack opened. The full collapse of the test was reached at 154 mins due to damage of the fire protection of edge beams, see Fig. 2.

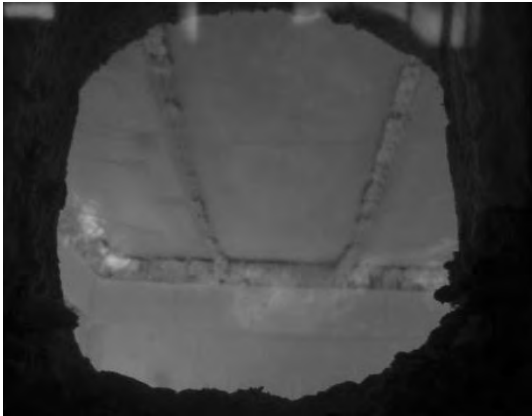


Fig. 2 Floor during the fire test from bottom



Fig. 3 Collapse of the composite slab

The temperature in the concrete slab continues to rise after the maximum atmosphere temperature, which occurred at 150 mins. The maximum temperature reached 845 °C in the middle of the slab 20 mm from the bottom surface of the slab. The temperature rise at the unexposed face of the composite slab after 150 mins of fire was slightly above 350 °C. The limit of 140 °C that defines the insulation criterion was exceeded at 52 mins.

At low temperatures, less than 400 °C, the beam deflection is predominantly due to thermal bowing. At higher temperatures, mechanical deflection will dominate and the deflection increases at a faster rate. At 150 minutes of fire, the total deflection of the floor reached 220 mm. Their flexural load bearing capacity with this level of heating would no longer allow them to bear the applied load alone. In consequence, the slab and membrane effect of the floor was progressively activated, to maintain the global resistance of the floor.

The supported concrete slab was not horizontally restrained around its perimeter and the supporting protected perimeter beams maintained their load carrying capacity. They were subjected to small vertical displacements and allowed membrane action to develop with the in-plane forces in the central region of the slab going into tension and in-plane equilibrium compressive forces forming in the slab around its perimeter.

Based on the experimental results, behaviour of timber-concrete floor in fire may be divided into three stages, as shown in Fig. 4. In the initial stage of fire, when the temperature is not very high, the slab carried applied load in a bending mechanism with small deflections (Stage 1). In addition to the thermally induced downward deflection, the unprotected beam was losing strength and stiffness due to the increasing temperatures from fire. With increasing temperature, between 30-45 mins, the strengths of timber and concrete of the slab were reduced, and the slab behaviour formed in the slab (Stage 2). The temperatures reached in the timber beam by the end of Stage 2 are in excess of 250 °C. When the temperature of the slab increased further (after 46 mins), the bending capacity of the slab was not enough, and the deflection of the slab had to be further developed, which created additional load-bearing capacity under membrane mechanism to maintain the resistance of the slab (Stage 3). How the deflection of the slab was larger, the tensile membrane action is higher. Finally, most of the vertical load on the slab was carried by membrane action.

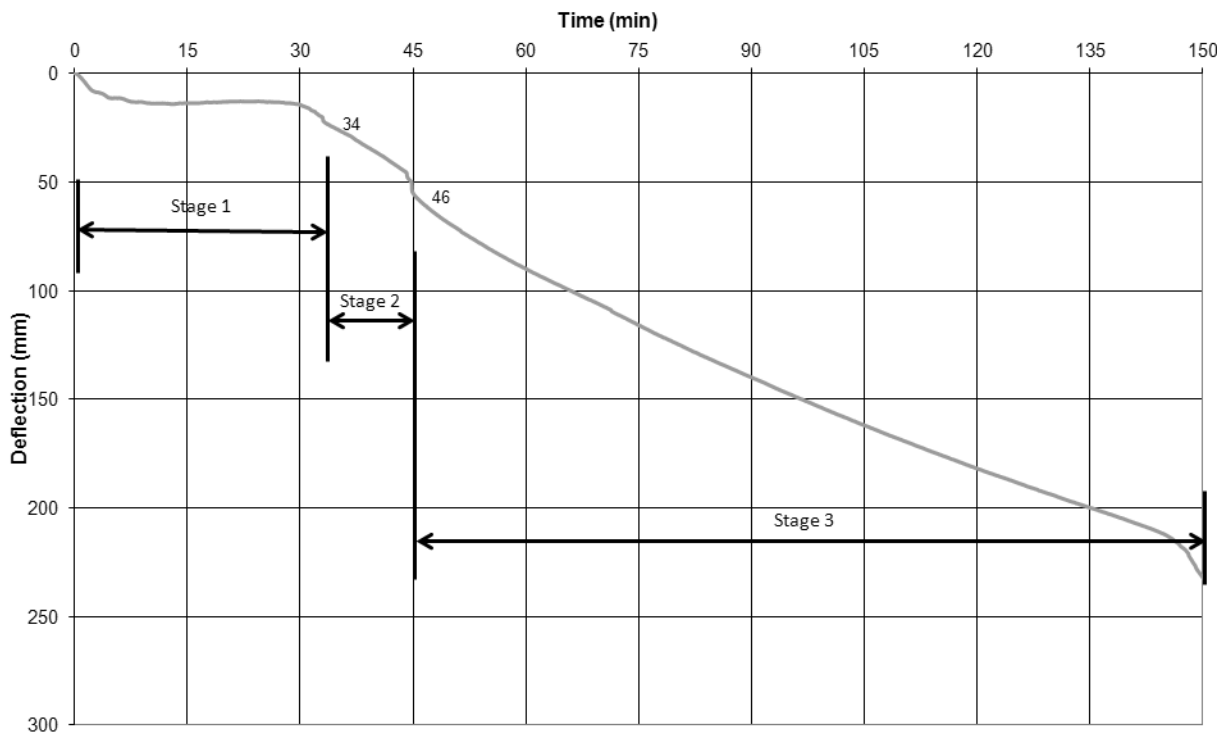


Fig. 4 Stages of timber-concrete composite floor during fire test

### 3 SUMMARY AND ACKNOWLEDGMENT

The timber-concrete slab performed well supporting the applied load for the duration of the test and pointed out the strength in the system due to membrane action. Due to membrane action, the existence of secondary timber beams to support the slab is not necessary in the fire condition and these beams can be left unprotected.

Based on current knowledge and the performed tests the analytical model is prepared for the fire resistance of the timber- concrete slab with steel fibre concrete.

This outcome has been achieved with financial support of the Grant Agency of Czech Republic No. P105/10/21591.

### REFERENCES

- Bailey C.G., Moore D.B., The structural behaviour of steel frames with composite floors slabs subject to fire - part 1 theory, *Struct Eng*, Vol. 78(11), pp. 19–27, 2000.
- Bednář J., Wald F., Vodička J., Kohoutková A., Membrane Action of Composite Fibre Concrete Slab in Fire. *Procedia Engineering* [online]. 2012, Vol. 40, no. 40, p. 498-503. Internet: <http://www.sciencedirect.com/science/article/pii/S1877705812025180>. ISSN 1877-7058.
- Vassart O., Zhao B., Fire Resistance Assessment of Partially Protected Composite Floors, *FRACOF+*, 2011, <http://fire.fsv.cvut.cz/fracof>.
- Holschmacher K., Klotz S., Weise D., Application of steel fibre reinforced concrete for timber-concrete composite constructions, *Lacer* No. 7.2002: 161-170, 2002.
- Kodur V.K., Lie T.T., Thermal and mechanical properties of steel-fibre-reinforced concrete at elevated temperatures, *Can. J. Civ. Eng.* 23:511-517, 1996.
- Guo-Qiang Li, Shi-Xiong Guo, Hao-Sheng Zhou, Modeling of membrane action in floor slabs subjected to fire, *Engineering Structures*, Vol. 29, pp. 880–887, 2007.







## NUMERICAL ANALYSIS OF TIMBER BEAM EXPOSED TO FIRE

Robert Pečenko<sup>a</sup>, Tomaž Hozjan<sup>a</sup>, Goran Turk<sup>a</sup>

<sup>a</sup> University of Ljubljana, Faculty of Civil and Geodetic Engineering, Ljubljana, Slovenia

### Abstract

In this paper the advanced calculation method to determine the response of timber beams during fire is presented. In the first phase of the advanced calculation method the development of temperature across the cross-section of the beam and the char dept are determined. The second phase consists of the mechanical analysis of timber beam. Char dept for one dimensional charring is compared to the empirical values from the literature. In addition, fire resistance calculated with advanced calculation model is compared with the fire resistance calculated with reduced cross-sectional method proposed by Eurocode (EN 1995-1-2 (2005)).

**Keywords:** heat transfer, advanced calculation method, reduced cross-sectional method, fire resistance, timber beam

### INTRODUCTION

Fire safety of timber structures is strongly dependent on fire safety of timber elements that compose it. Timber beams represent one of such elements. From the view of fire safety timber structures are relatively safe in comparison to other types of structures. This is mainly due to relatively low thermal conductivity of timber and char. However, the temperature increase is deteriorating the load bearing capacity of timber elements. The temperature increase results in a reduction of mechanical properties of timber in addition, timber is subjected to thermal degradation or so-called pyrolysis. Pyrolysis is a complex phenomenon which starts at temperatures about 200-300°C and represents the combined effect of various chemical processes with the process of heat and moisture transfer. The results of pyrolysis are the formation of char, various gases, acids and resins. As a results the material properties of timber change. Char layer has both a positive and negative impact. It has a relatively low thermal conductivity which contributes to a slower warming in the core of the cross section of the timber element. On the other hand, the char layer has almost negligible strength characteristics and thus does not contribute to the load bearing capacity of the timber elements.

Fire safety of a timber beam can be proved in several ways. Standard Eurocode (EN 1995-1-2 (2005)) proposes simplified rules for analysis of structural members and components and advanced calculation methods. Simplified rules are primarily intended for the approximate evaluation of fire resistance of timber elements, e.g. beams or columns. The reduced cross-sectional method represents one of such simplified procedures. Fire resistance is calculated based on the effective cross-section, which is determined by reducing the initial cross-section by the effective charring dept where the design charring rate depends on standard fire curve ISO 834 (1999). The advanced calculation method allows us to analyse the behaviour of the structure and its part during the fire. The analysis is divided in tree separated phases. In the first phase the development of temperatures with time in the fire room is determined. The standard fire curve ISO 834 (1999) is considered. In the second phase the temperature state of timber beam is analysed, taking into account the charring of timber. Here the coupled problem of heat and moisture transfer is not modelled but the moisture content is indirectly considered with higher specific heat in the temperature range between 100 and 120°C (EN 1995-1-2 (2005)). Based on the temperature state of timber beam the mechanical analysis is determined

in the third phase. Additive principle is adopted where the increment of the total geometric strain is divided on the increment of the mechanical and thermal strain.

The aim of this paper is to provide comparisons between both procedures which are proposed by Eurocode.

## 1 THERMAL ANALYSIS

### 1.1 Heat transfer

To determine time dependent temperature in cross section of timber element all three ways of heat transfer are considered: convection, radiation and conduction. Heat conduction over cross-section is described with Fourier partial differential equation:

$$\left( k_{ij} \cdot \frac{\partial T}{\partial x_j} \right) \frac{\partial}{\partial x_i} + Q - \rho \cdot c \cdot \frac{\partial T}{\partial t} = 0. \quad (1)$$

Heat transfer through outer surface of the beam due to convection and radiation is considered with appropriate boundary conditions. These are:

$$S_q : q^s = -k_{ij} \cdot \frac{\partial T}{\partial x_j} n_i, \quad S_T : T^s = T, \quad S : T(t=0) = T_0. \quad (2)$$

In equations (1) and (2)  $S$  denotes cross section of beam,  $S_q$  is a part of cross-section where specific surface heat flux  $q^s$  is prescribed,  $S_T$  represents a part of cross-section where temperature  $T_S$  is prescribed,  $t$  is time,  $k_{ij}$  constitutes the symmetric thermal conductivity tensor,  $\partial T/\partial x_j$  is the partial derivate of temperature over coordinate  $x_j$ ,  $n_i$  is a component of the unit vector perpendicular to the cross-section,  $Q$  is the internal heat source,  $\rho$  the density of material,  $c$  specific heat and  $T_0$  is the initial temperature at any point of the cross section. Specific surface heat flux consists of the share represented by the exchange of heat between the body and the surrounding area by convection ( $q_c$ ), the share of the radiation ( $q_r$ ) and from other sources ( $q_0$ ).

$$q^s = q_c + q_r + q_0. \quad (3)$$

Heat flux due to convection  $q_c$  depends on the temperature of gases in the vicinity of the fire exposed element  $T_s$ , the surface temperature of the element  $T$  and coefficient of heat transfer by convection  $\alpha_c$ . Heat flux due to radiation  $q_r$  depends on the emissivity of the surface of the element  $\varepsilon_m$ , Stefan-Boltzman constant  $\sigma$  and the difference between the effective radiative fire temperature  $T_r$  and the surface temperature of the element  $T$ .

$$q_c = \alpha_c \cdot (T_s - T), \quad q_r = \varepsilon_m \cdot \sigma \cdot (T_r^4 - T^4). \quad (4)$$

System of equations (1)-(4) is solved numerically by the finite element method in the *Matlab* environment.

### 1.2 Material properties of timber and the char layer at elevated temperatures

Temperature dependence of the specific heat of timber, density ratio for softwood and thermal conductivity for timber in accordance with standard EN 1995-1-2 (2005) are shown in Fig. 1. With the increase of the specific heat of timber in temperature range between 100 and 120°C the indirect impact of evaporation of water on the development of the temperature in timber is modelled. Thermal conductivity suggested by the EN 1995-1-2 (2005) takes into consideration increased heat transfer due to shrinkage crack at temperatures above 500°C.

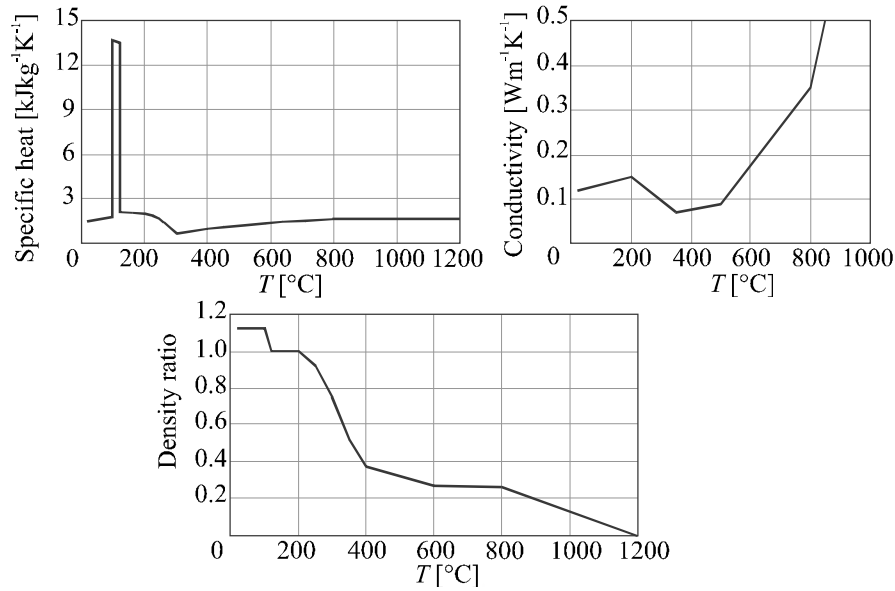


Fig. 1 Temperature-specific heat relationship for timber and char, temperature dependent density ratio for softwood (for initial moisture content of 12%) and temperature dependent thermal conductivity for timber and the char layer (EN 1995-1-2 (2005))

## 2 MECHANICAL ANALYSIS

The presented finite element formulation is based on Reissner's kinematically exact model of beam where large membrane and flexural deformations are allowed (Reissner, 1972). The effect of the shear strain is neglected. The geometric extensional strain is a function of extensional strain of centroidal axis  $\varepsilon$  and its pseudocurvature  $\kappa$ . The Bernoulli hypothesis is considered and the geometric extensional strain over the beam cross section can be written:

$$D(x, z) = \varepsilon(x) + z\kappa(x). \quad (5)$$

Basic equations for beam are presented by kinematic, equilibrium and constitutive equations:

$$\begin{aligned} 1 + u' - (1 + \varepsilon)\cos\varphi &= 0, & (N \cos\varphi + Q \sin\varphi)' + p_x &= 0, & N_c &= \int_A \sigma(D_m, T) dA, \\ w' - (1 + \varepsilon)\sin\varphi &= 0, & (-N \cos\varphi + Q \sin\varphi)' + p_z &= 0, & M_c &= \int_A z\sigma(D_m, T) dA, \\ \varphi' - \kappa &= 0, & M' - (1 + \varepsilon)Q + m_y &= 0, & & \end{aligned} \quad (6)$$

The prime ( )' denotes the derivative with the respect to  $x$ ,  $u$  and  $w$  are displacements of the centroidal axis in the  $x$  and  $z$  direction,  $\varphi$  is the rotation about  $y$ -axis.  $N$ ,  $Q$ ,  $M$  are equilibrium generalised internal forces,  $p_x$ ,  $p_z$  and  $m_y$  denotes conservative distributed loads of the element. Constitutive internal forces  $N_c$  and  $M_c$  depend on a chosen material model which is defined by the relationship between the longitudinal normal stress  $\sigma(D_m, T)$  and mechanical extensional strain  $D_m$ , of a longitudinal fibre at elevated temperature. The geometric extensional strain is determined using incremental equation:

$$D^j = D^{j-1} + \Delta D^j, \quad (7)$$

where  $D^j$  and  $D^{j-1}$  denotes the total geometric strains in the time intervals  $j$  and  $j-1$ ,  $\Delta D^j$  is the increment of the total geometric strain in the time interval  $j$  and it is assumed to be the sum of mechanical extensional strain increment  $\Delta D_m^j$  and thermal strain increment  $\Delta D_T^j$ .

$$\Delta D^j = \Delta D_m^j + \Delta D_T^j. \quad (8)$$

The final system of equations for finite element method is written based on modified principle of virtual work where quantities  $\varepsilon$  and  $\kappa$  are interpolated over finite element by Lagrangian

polynomials. A more detailed description of the finite element formulation is presented in Bratina et al (2003).

### 2.1 Mechanical properties of timber at elevated temperatures

Mechanical properties for strength and modulus of elasticity parallel to the grain of softwood are considered in accordance with EN 1995-1-2 (2005). Reduction factors are different for timber fibre in tension or compression. It is considered that the char layer doesn't have any strength. The char occurs at a temperature around 300°C therefore the reduction factors above this temperature are equal to zero.

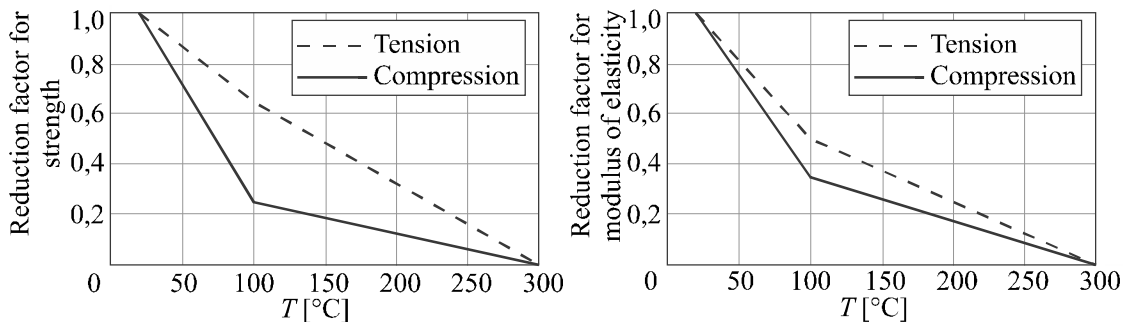


Fig. 2 Reduction factor for strength and modulus of elasticity parallel to the grain of softwood (EN 1995-1-2 (2005))

The normal stress  $\sigma$  and mechanical extensional strain  $D$  of a longitudinal fiber are connected thru linear relationship in tension and bi-linear relationship in compression (Fig. 3).

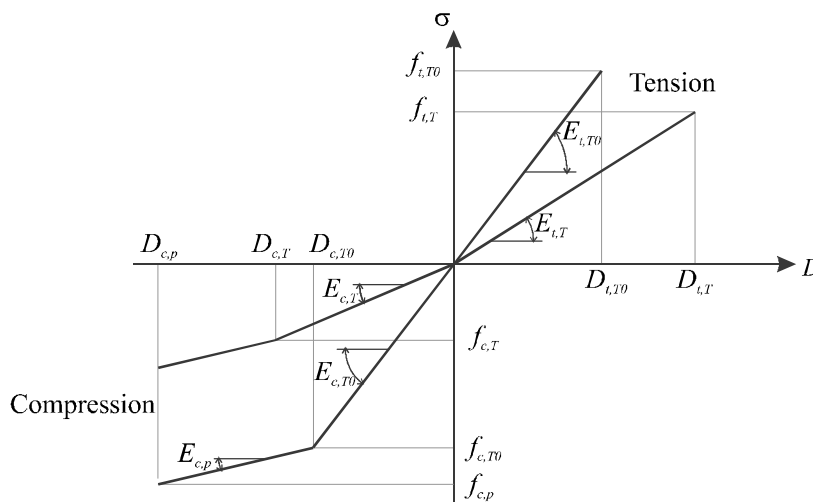


Fig. 3 Stress-strain relationship for timber at ambient and elevated temperature

In Fig. 3,  $D_{i,j}$ ,  $E_{i,j}$  and  $f_{i,j}$  ( $i = c, t; j = T, T_0$ ) are the limit elastic strains, the Young's modulus and the limit elastic stresses for timber in compression ( $c$ ) and tension ( $t$ ) at ambient ( $T_0$ ) and elevated temperatures ( $T$ ).  $E_{i,j}$  and  $f_{i,j}$  are determined according to Fig. 2 and  $D_{i,j}$  is determined from their relationship. The limit plastic stress  $f_{c,p}$ , is defined by Pischl (1980). Symbols  $E_{c,p}$  and  $D_{c,p}$  denotes plastic hardening modulus and limit plastic strain for timber in compression.

## 3 CASE STUDIES

### 3.1 One dimensional charring of timber beams

In this example comparison is made between present model of charring and different models of one-dimensional charring (EN 1995-1-2, 2005; Schnabl, 2007). In the present model we

consider that the charring occurs at a temperature of 300°C. Specific heat, conductivity and density are taken into account in accordance with EN 1995-1-2(2005) and are shown on Fig. 1. Standard ISO fire curve, coefficient of heat transfer by convection  $\alpha_c = 25 \text{ W/m}^2\text{K}$  and the emissivity of the surface  $\varepsilon_m = 0.8$  are considered in thermal analysis. The initial moisture content  $w$  is 0.12 and the initial density is  $\rho = 380 \text{ kg/m}^3$ . The cross section considered for the analysis is  $b/h = 5/30 \text{ cm}$ .

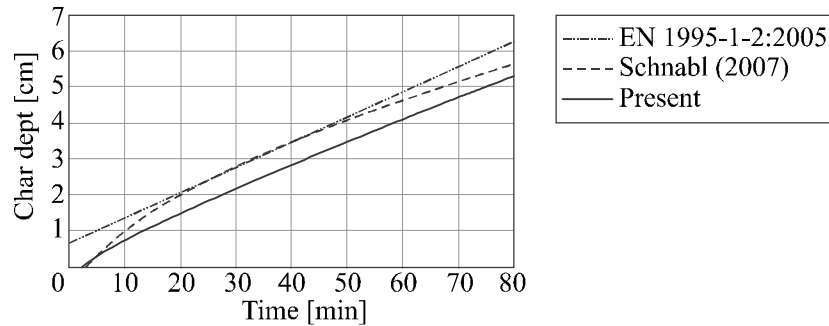


Fig. 4 Comparison of different one-dimensional charring models

The start of charring in the present model occurs at the approximate time of 3 min which is the same as by model proposed by Schnabl. In the model proposed by Eurocode, the charring begins simultaneously with the start of fire, which does not represent the actual state. Char depth increases almost linearly with time and it fits well with the values proposed by Schnabl in the beginning and at the end of the simulation, while bigger discrepancy can be observed for time between 20 and 70 minutes. In the present model the char depth at the time of 80 minutes is 5.34 cm, 5.56 cm for model presented by Schnabl and 6.1 cm in case of Eurocodes.

### 3.2 Fire resistance of timber beam

Subject of our analysis is simply supported timber beam with span of 3 m. It is loaded with uniform load of 5 kN/m. The cross section of the beam is  $b/h = 10/20 \text{ cm}$ . The strength class of timber is C30. The characteristic bending strength  $f_{m,k}$  and Young's modulus for selected timber at ambient temperature are  $3 \text{ kN/cm}^2$  and  $1200 \text{ kN/cm}^2$ .

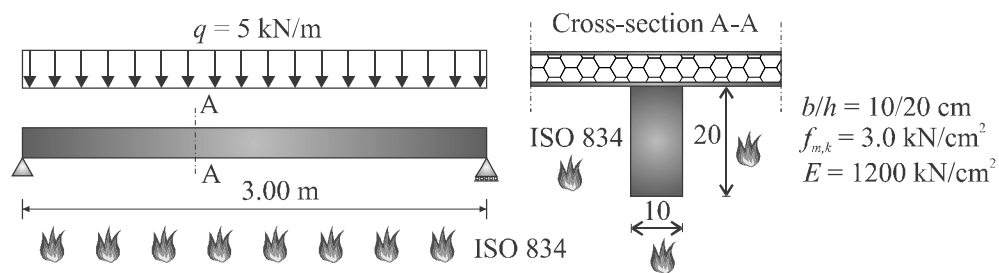


Fig. 5 Data for simply-supported timber beam

#### 3.2.1 Simplified rules - Reduced cross-sectional method

Method is well described in EN 1995-1-2(2005), therefore we present only the parameters needed for the calculation of the fire resistance of timber beam. The design notional charring rate under standard fire exposure,  $\beta_n$  is 0.7 mm/min, depth of layer with assumed zero strength and stiffness,  $d_0$  is 7 mm, coefficient  $k_0$  is 1, the modification factor for fire  $k_{mod,fi}$  is 1 and the design strength in fire  $f_{d,fi}$  is  $3 \text{ kN/cm}^2$ . Failure time of timber beam determined by reduced cross-sectional method is 33.5 min.

### 3.2.2 Advanced calculation method

For the thermal analysis, the specific heat, density and thermal conductivity are taken based on the Fig. 1, where the initial density is  $\rho = 380 \text{ kg/m}^3$ . Standard ISO 834 curve, the emissivity of the surface of the element  $\varepsilon_m = 0.8$  and the coefficient of heat transfer by convection  $\alpha_c = 25 \text{ W/m}^2\text{K}$  are taken into account. In mechanical analysis, the parameters for stress-strain relationship for timber are as follows:  $E_{t,T0} = E_{c,T0} = 1200 \text{ kN/cm}^2$ ,  $f_{t,T0} = f_{c,T0} = 3 \text{ kN/cm}^2$ ,  $D_{t,T0} = D_{c,T0} = 0.0025$ ,  $D_{c,p} = 0.0065$ ,  $E_{c,p} = 250 \text{ kN/cm}^2$  and  $f_{c,p} = 4 \text{ kN/cm}^2$ . Thermal strain is considered linear with a coefficient of linear thermal expansion  $\alpha_T = 5 \cdot 10^{-6} \text{ m/m}^\circ\text{C}$ .

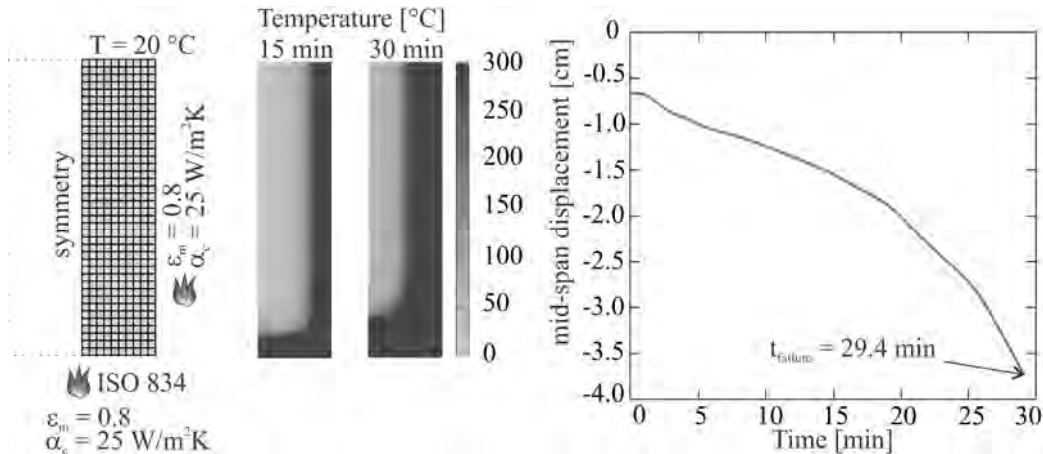


Fig. 6 Finite element mesh, temperature distribution in the cross-section and the time-displacement curve of the analyzed timber beam

The initial mid-span displacement is 0.66 cm. To the time of 20 minutes the mid-span displacement increases slower, after that time the increase is faster. The failure time of the timber beam occurs at 29.4 minutes where the mid-span displacement is 3.74 cm. Failure occurs when the longitudinal fibres are fully exploited and cannot provide any more to the bearing capacity of the cross-section of the beam. Compared to the reduced cross-sectional method the failure time is smaller but remains in the same rank. The difference in failure time for both methods is 4.1 minutes which is 12.2 %. From the view of fire-safety design the advanced calculation method for this case gives more conservative result.

### REFERENCES

- Bratina S., Planinc I., Saje M., Turk G. Non-linear fire-resistance of reinforced concrete beams. *Structural engineering and mechanics* 16 (2003), 6:695-712.
- EN 1995-1-2: 2005 – Eurocode 5: Design of timber structures - Part 1-2: General - Structural fire design.
- ISO 834. 1999. Fire-resistance Tests - Elements of Building Construction - Part 1: General Requirements. ISO 834-1. International Organization for Standardization, Geneva, Switzerland.
- Pischl R. Holzbau mit kritischen betrachtungen und neuen vorschlägen zur bemessung nach theorie 1. und 2. ordnung. Institut für Stahlbau, Holzbau und Flächentragwerke, Technische Universität Graz, 1980.
- Reissner E. On one-dimensional finite-strain beam theory: the plane problem. *J. Appl. Math. Phys. (ZAMP)* (1972), 23:795–804.
- Schnabl S. Analysis of composite beams exposed to fire, University of Ljubljana, Faculty of Civil and Geodetic Engineering, Doctoral thesis (in Slovene), 2007.

## NUMERICAL MODELLING OF THE BEHAVIOUR OF PROTECTED AND UNPROTECTED WOODEN MEMBERS UNDER FIRE

Magdaléna Dufková<sup>a</sup>, Petr Kuklík<sup>a</sup>

<sup>a</sup> Czech Technical University in Prague, Faculty of Civil Engineering, Department of Steel and Timber Structures, Czech Republic

### Abstract

Sufficient knowledge of the behaviour of wood under fire is necessary for the most effective, the most economical, but still safe design of timber structures. The subsequent numerical modelling leads to new computational methods with higher accuracy. This paper is focused on protected and unprotected wooden members, on the contribution of wooden constructions to fire resistance using calcium-silicate boards. On the basis of the fire test results, the comparison of the fire test results with a numerical model in ANSYS was carried out.

**Keywords:** wood, fire resistance, contribution to fire resistance, protected member, unprotected member

### INTRODUCTION

For elements which are protected by the fire shell, the beginning of charring is moved till the time  $t_{ch}$ . The charring of a timber element can occur before the deformation of the fire protection but with a lower speed than specified in Eurocode 5 (EN 1995-1-2). Using the testing method (EN 13381-7), a fire test was performed to determine the contribution to fire resistance. In Figure 1, there is a protected member and the location of thermocouples. The location of thermocouples in an unprotected member is the same.

The test standard specifies a test method for determining the contribution of fire protection systems to the fire resistance of structural timber members. Based on this standard, the ability of the fire protection system to delay the temperature rise throughout the timber member, to maintain coherence and a link to the timber member and to provide data of the thermal characteristics of the fire protection system is determined, during its exposition to the load according to the standard temperature/time curve. This test procedure is also applicable to timber structural members incorporating insulating materials between the timber members.

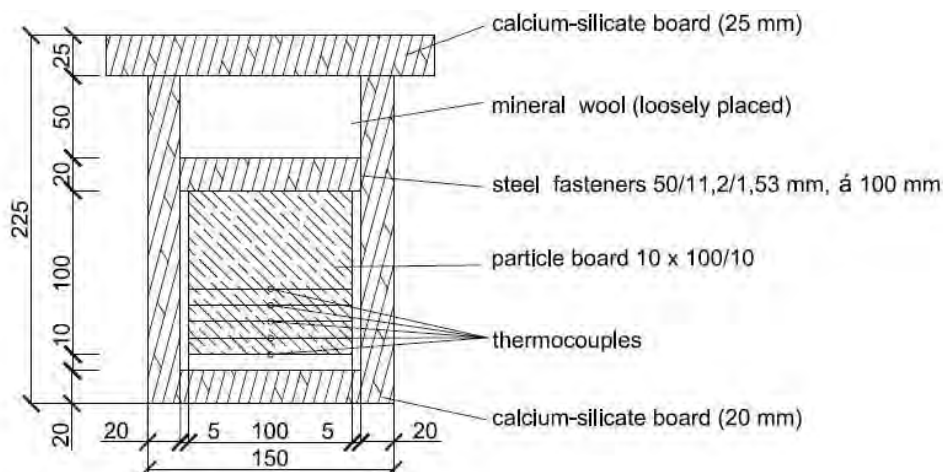


Fig. 1 Protected member and the location of thermocouples

## 1 FIRE TEST

The assessment and the numerical model based on the fire test of a calcium-silicate board were carried out. The results of the fire test were provided by the Promat, s.r.o. company.

In the test furnace, there were specimens with a calcium-silicate board and specimens without a lining. The total dimensions of the board (a specimen without the lining) were 2 000 x 1 200 x 100 mm and the total dimensions of the beam (a specimen with the lining) were 100 x 100 x 4 500 mm. The test specimen consisted of ten chipboard layers bonded by glue. The thickness of the fire protected board was 20 mm.

## 2 NUMERICAL ANALYSIS

The timber beam was modelled covered by a calcium-silicate board on three sides and these sides were exposed to the fire. The unprotected timber board was modelled with its exposure to the fire from one side. This 3D model was performed using the ANSYS Workbench programme, solved in thermal analysis (Transient thermal) using a fire of 60 minutes.

Material properties for wood at elevated temperatures were taken from the Eurocode (EN 1995-1-2) and for the calcium-silicate board they were supplied by the manufacturer based on testing. The result of this numerical calculation should provide the time when the temperature of the timber member reaches 300 °C, this is the temperature where timber begins to char. Eurocode 5 provides a very limited range of the time  $t_{ch}$  (time of the start of charring of timber) and  $t_f$  (failure time of the cladding), based on the determination of these values to arrive at a more accurate calculation of fire resistance.

The timber beam has dimensions identical to the test specimen (100 x 100 mm) and it was covered on three sides with a calcium silicate board, with a thickness 20 mm. The unprotected board was modelled a little smaller than in the real fire test specimen (1 000 x 1 000 mm).

Heat transfer by the construction is calculated using the heat-dependent coefficients according to EN 1991-1 -2. Thermal actions are given by the net heat flux  $h_{net}$  [W / m<sup>2</sup>] to the surface of the member. On the fire exposed surfaces, the net heat flux  $h_{net}$  should be determined by considering heat transfer by convection and radiation.

In Figures 2 and 3, there is a comparison between unprotected boards after 30 minutes and 60 minutes with exposure to the fire. The comparison between protected beams after 30 minutes and 60 minutes with exposure to the fire is shows in Figures 4 and 5. The depth of char has black colour in the Figures (temperature is higher than 300 °C).

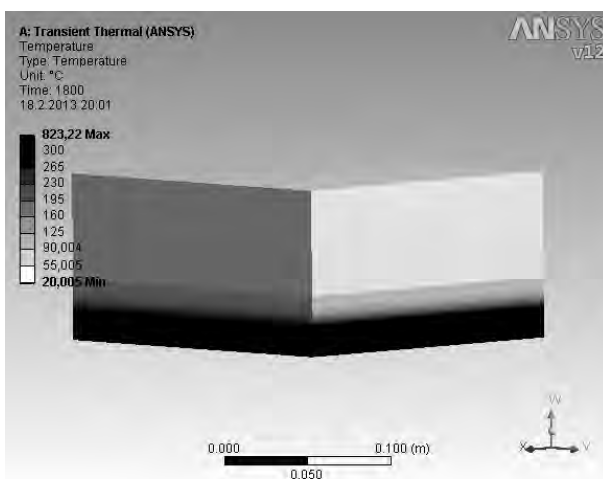


Fig. 2 Unprotected boards after 30 minutes

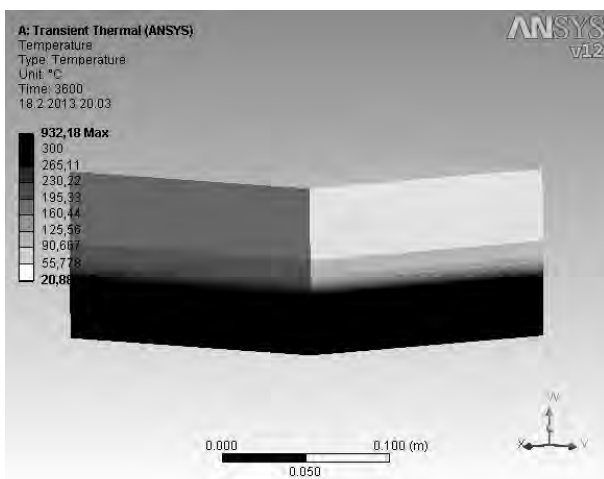


Fig. 3 Unprotected boards after 60 minutes



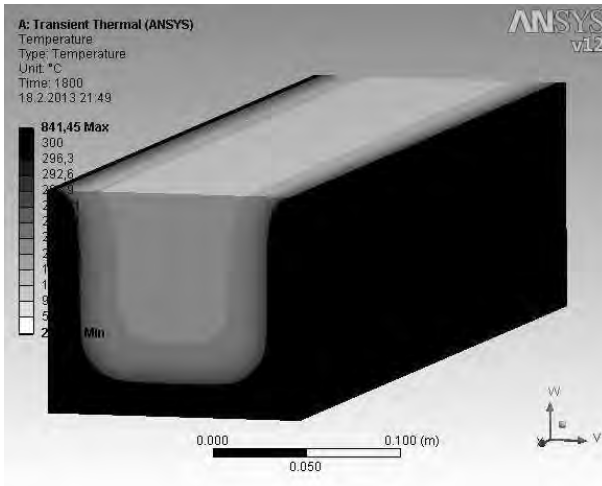


Fig. 4 Protected beam after 30 minutes

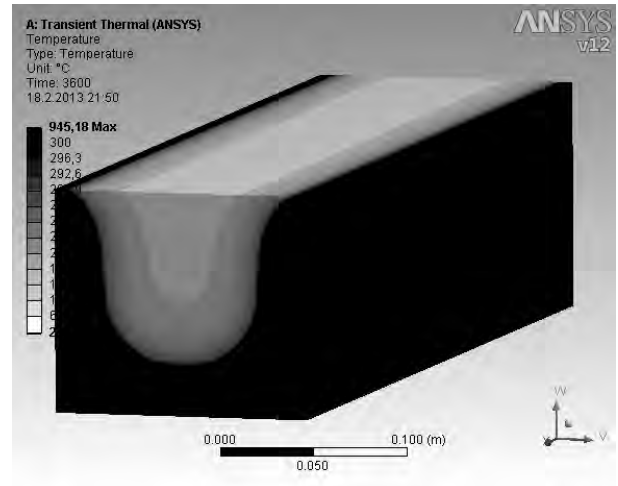


Fig. 5 Protected beam after 60 minutes

### 3 RESULTS

The results were available from two fire tests of unprotected members (test 1 - thermocouples were disconnected after reaching the temperature of 300 ° C and test 2 - thermocouples measured the temperature until the end of the test). The modelling was performed for 60 minutes. There is shown a very good agreement in comparing the results of the fire tests with numerical analysis in the following graph (Fig. 6).

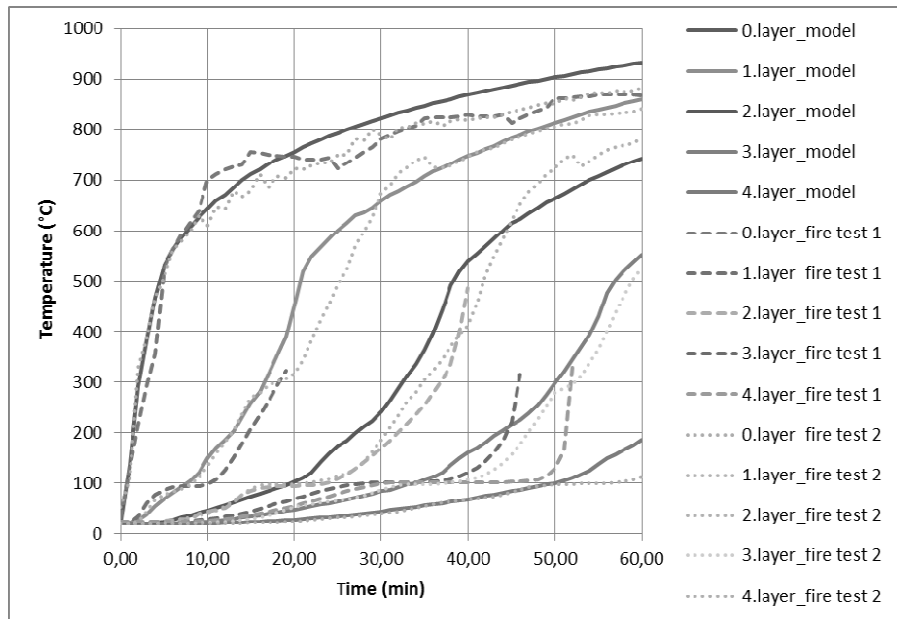


Fig. 6 Temperature in unprotected members obtained from fire tests and from numerical modelling

The protected beam was modelled with a calcium-silicate board 20 mm in thickness used by fire conditions for 60 minutes. In these results, there is also a very good agreement in comparing the results of fire tests with numerical analysis. The fire test result of the protected member was only available from one fire test. There is a problem with well defined mechanical characteristics of the calcium-silicate board, because its behaviour under fire is not predictable very well in comparison with wood.

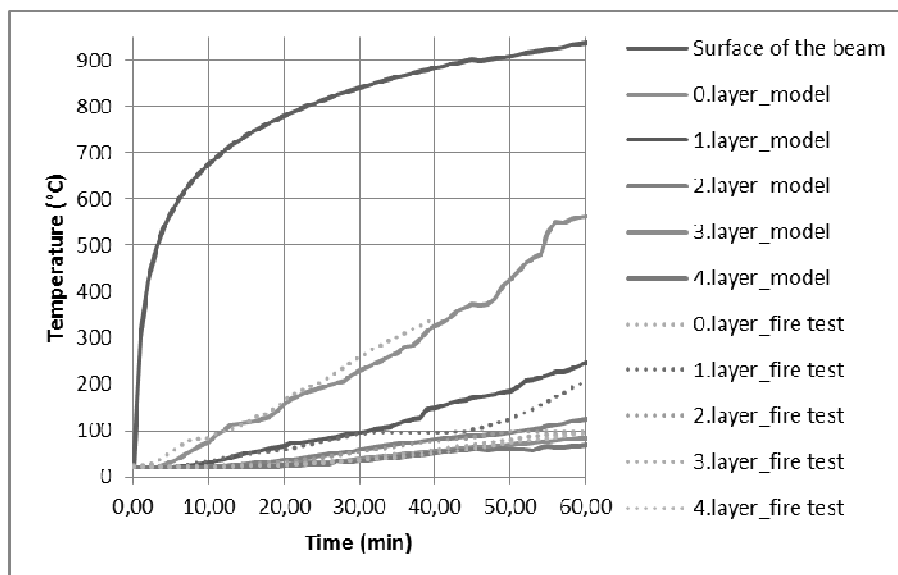


Fig. 6 Temperature in the protected member obtained from fire tests and from numerical modelling

#### 4 SUMMARY AND ACKNOWLEDGMENT

The behaviour of wood under fire is a very predictable phenomenon. Using simplified computational methods can determine the separating and load-bearing function of structures. For a load-bearing bar element it is the parameter R (resistance and stability), for a vertical or horizontal element the design criteria are R, E, I (resistance, integrity, insulation) limits. In many cases, according to Eurocode 5 (part 1-2), it is very difficult or nearly impossible to determine the starting time of charring of the timber element of the fire protection and the failure time of the cladding. In this area, there are still some deficiencies and it is necessary to perform fire tests in order to increase the level of knowledge and to be able to further develop more precise computational methods.

On the basis of numerical analysis, the following was determined:

- with higher density there is a lower growth in temperature;
- with higher heat conductivity there is a higher growth in temperature;
- with higher specific heat there is a lower growth in temperature.

This research is carried out with support from research project - SGS ČVUT, "Příspěvek k požární odolnosti dřevěných konstrukcí pomocí boardového materiálu".

#### REFERENCES

- ČSN EN 1995-1-2 Eurokód 5: Navrhování dřevěných konstrukcí – Část 1-2: Obecná pravidla – Navrhování konstrukcí na účinky požáru, ČNI, Praha 2006.
- ENV 13381 – 7 Test methods for determining the contribution to the fire resistance of structural members – Part 7: Applied protection to timber members, CEN, 2008.
- ČSN EN 1995-1-2 Eurokód 5: Navrhování dřevěných konstrukcí – Část 1-2: Obecná pravidla – Navrhování konstrukcí na účinky požáru, ČNI, Praha 2006.

## **ESTIMATION OF FIRE RESISTANCE BY MEANS OF CALCULATION Performed for Atypical Exterior Wall of a Woodstructure**

Kamil Vargovský<sup>a</sup>, Pavol Sedlák<sup>b</sup>, Martin Zachar<sup>b</sup>

<sup>a</sup> Fire engineering, Novozámocká 1350/40, 960 01 Zvolen, Slovakia

<sup>b</sup> Faculty of Wood Science and Technology, Technical University in Zvolen, Slovakia

### **Abstract**

The paper describes essential characteristics of a structural system for a wood structure, based on light composite wood stud, designed at Technical University in Zvolen.

The system was reviewed by means of calculation method to prove fire resistance, respecting various relevant current standards of Slovak Republic and in accordance to eurocodes series. The methodology considered wider aspects of evaluation (properties, methods, carbonisation, minimal dimensions, cross sections, thermal field).

Later, simple wall design alternatives were created by modification of inner part of the assembly, in order to examine the influence of the modifications to the total fire resistance of the wall.

**Keywords:** estimation of fire resistance, calculation method, timber buildings construction, composite wood stud

### **INTRODUCTION**

Development in the building industry and construction brings new designs of external walls, with particular focus on systems using renewable materials – in this case wood. Such walls are subject to proper testing by means of experimental testing and/or by computational methods.

New timber structural system was developed, with light composite wood stud and minimised number of layers within the wall (utility models PUV 219-2011 and PUV 220-2011), at the Department of Woodstructures, Technical University in Zvolen.

The assembly was verified by strength and heat laboratory testing, together with computational methods regarding water vapour transition, environmental impact, production technology, cost analysis and basic structural details of a house.

In order to provide complex view, there was a need for fire resistance evaluation. Fire properties were evaluated by various calculation methods according to relevant Slovak standards, with later option to compare these to experiments.

### **1 STRUCTURAL SYSTEM**

The reviewed system is based on composite stud (Fig. 1), on which there is a board material fixed from interior, to guarantee shear rigidity within the wall. Another board material is fixed to the studs from exterior and therefore closes the cavity filled with insulation (Fig. 2). This board material meets required diffuse water vapour properties.

It is possible to add layers to this basic assembly to modify interior and exterior appearance (Fig. 3). The base assembly itself remains unchanged, as it fulfils insulation, vapour diffuse and load bearing properties.

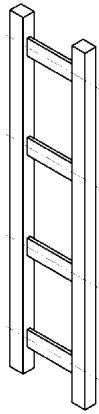


Fig. 1 Composite wood stud

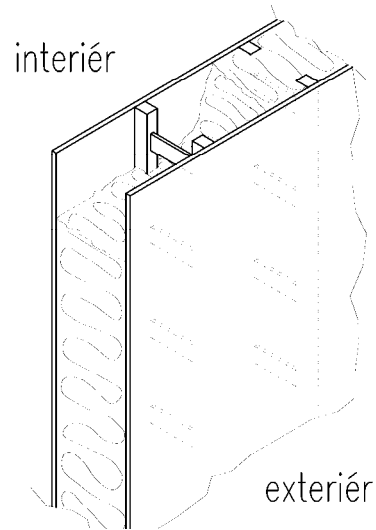


Fig. 2 Basic assembly of the wall

Main advantages of the system:

- Material efficiency
- Utilisation of short-sized timber
- Limiting the layers of the wall
- Simple wall thickness increase by changing only length of the cross-piece within the composite stud
- Design avoiding thermal bridges



Fig. 3 Optional assembly of the wall



Fig. 4 Experimental shear testing

This structural system was subjected to multiple examinations, in order to find out and refine assumed static and thermal properties (Fig. 4). These were verified by calculations, and later widened to vapour diffuse properties, manufacturing technology, cost analysis, environmental impact analysis.

## 2 FIRE RESISTANCE DETERMINATION

### 2.1 Fire resistance determination methods – calculation and evaluation of critical phases of fire resistance

Fire resistance of a building structure is determined (§ 8 promulgation MV SR no. 94/2004 statute):

- on the basis of initial type testing (act no. 90/1998 statute about building products as amended)
- by calculation according to technical standards (in cases where it is possible to express all the relevant factors by calculation, for example under the so-called „Eurocodes for the design of constructions to the effects of fire “)
- by test and calculation (in those cases where the examination is not possible to express and show all the relevant factors affecting the fire resistance test of a building construction)

The decisive factors:

All the important building-physical properties, thermal and mechanical parameters depending on the temperature, at which the known dimensions and for the construction element (structure) allow simplifying the determination of fire resistance.

Reviewed building construction is designed to:

- effects of mechanical loading at normal ambient temperature according to Eurocodes,
- the various factors in the tables for each building element,
- the temperature curve,
- to determine the fire resistance of a structural element.

### 2.2 Selection of the wall assemblies for the evaluation

There were total 5 assemblies selected (Fig. 5 to 9).

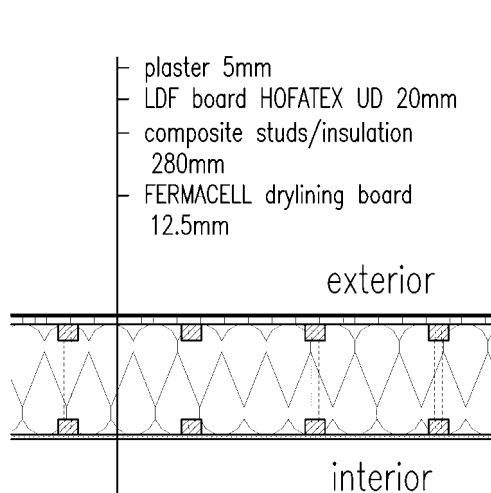


Fig. 5 Assembly 1A, 1B, 1C

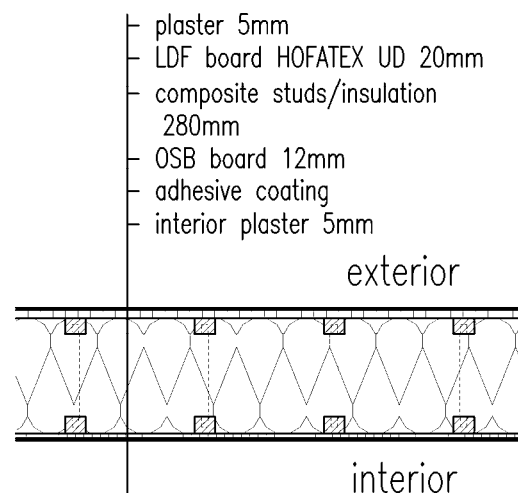


Fig. 6 Assembly 2A, 2B, 2C

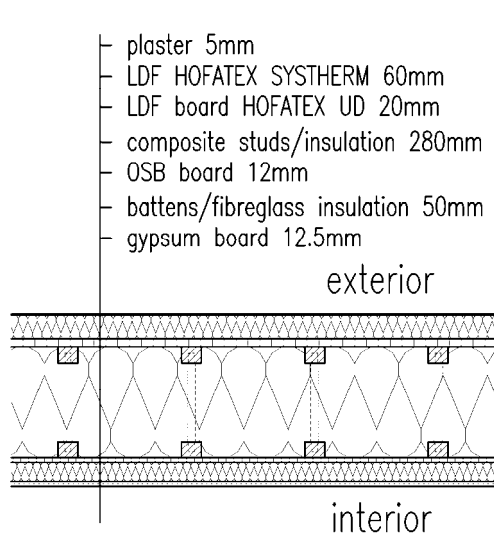


Fig. 7 Assembly 3A, 3B, 3C

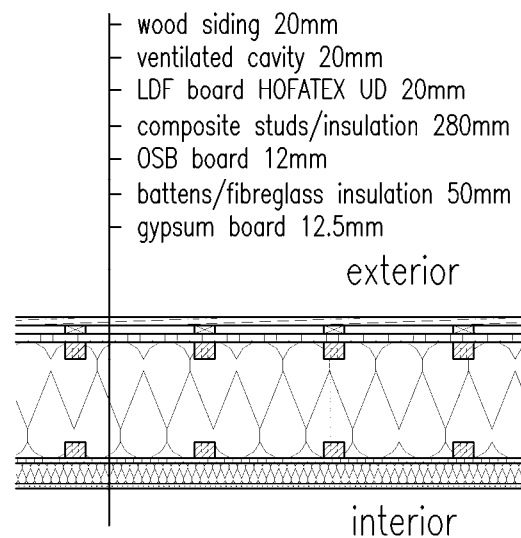


Fig. 8 Assembly 4A, 4B, 4C

For each assembly, there were three options considered:

- A. with insulation Isover DOMO ( $12 \text{ kg/m}^3$ ,  $REI_{\max} = 15 \text{ min}$ )
- B. with insulation Isover UNIROL PROFI ( $23.5 \text{ kg/m}^3$ ,  $REI_{\max} = 40 \text{ min}$ )
- C. with cellulose insulation CLIMATIZER PLUS ( $50 \text{ kg/m}^3$ ,  $REI_{\max} = 60 \text{ min}$ )

Fifth assembly represented typical structure of a timberframe house wall, and was shown to compare to the above structural system (Fig. 5 to 8).

For all of the assemblies, load to a single stud is set to  $1.2 \text{ kN}$  - that means to one part of the composite stud with cross-section  $50 \times 40 \text{ mm}$ . The height of the wall is assumed to be  $2750 \text{ mm}$ .

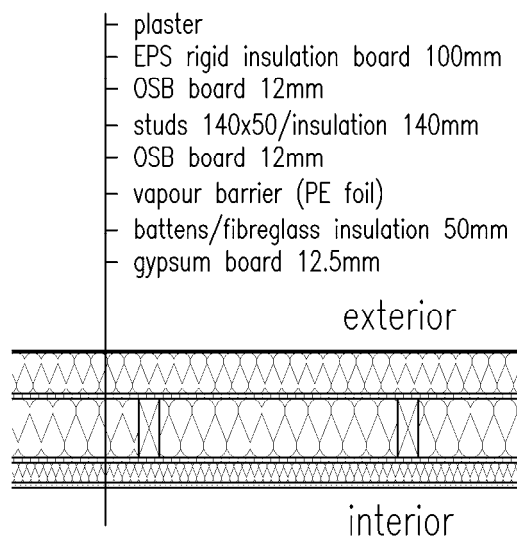


Fig. 9 Assembly 5A, 5B, 5C

### 2.3 Material properties

Density of the mineral fibre insulation between load bearing studs has to be as follows, according to fire resistance R requirements (EN 1995 – 1 – 2):

- response type reaction to fire tests A1 for assemblies required R 60 -min. density  $50 \text{ kg/m}^3$
- response type reaction to fire tests A1 for assemblies required R 60 -min. density  $85 \text{ kg/m}^3$
- response type reaction to fire tests A1 for assemblies required R 45 -min. density  $30 \text{ kg/m}^3$
- response type reaction to fire tests A1 for assemblies required R 30 -min. density  $20 \text{ kg/m}^3$
- response type reaction to fire tests A1 for assemblies required R 15 -min. density  $12 \text{ kg/m}^3$

Density of a fibre material forming fire protection external envelope (e.g. thermal facade Hofatex) has to be min.  $210 \text{ kg/m}^3$  for  $50 \text{ mm}$  thickness and fire resistance W 60 (i → o).

### 2.3 Modification of the assemblies to improve fire resistance

To improve the assemblies, following simple modifications were performed:

- in assembly 1C, thickness of the drylining board Fermacell was increased to 15mm (assembly 1C1) and to 18mm (assembly 1C2)
- in assembly 2C, thickness of the OSB board was increased to 15mm (assembly 2C1)

## 3 RESULTS

### 3.1 Fire resistance of the proposed walls

There were several values calculated and evaluated (fire resistance at 100% cross-section utilisation, fire resistance at max. load of a stud to 3kN, depth of carbonisation, keeping minimal dimensions of boards and studs, corruption time of board material), for each assembly. For simplicity, there are only fire resistance values shown, at 100% cross-section utilisation, in order to show and compare the most negative state. This was evaluated as load bearing timberframe external wall - exposure from interior (by STN EN 1991 – 1 – 2).

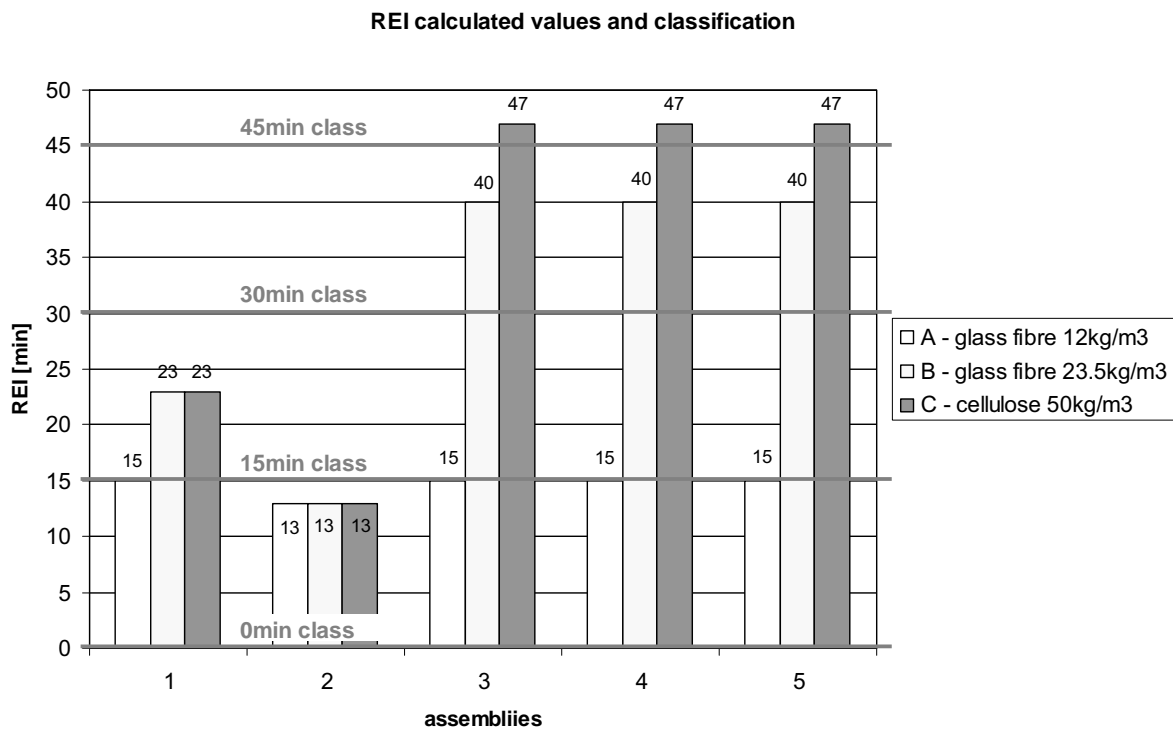


Fig. 10 Calculated values of the fire resistance and the classification according to EN 13501-2

Fig. 10 shows importance of interior layers during internal fire. Thus, fire resistance is basically the same for different structures (composite studs, typical timber stud) while having equal interior layers with fire properties – in this case closed space (usually for wiring, piping, etc) filled with insulation.

Using solely OSB board with plaster from interior proved to be absolutely inappropriate, as 2A, 2B and 2C assembly classification was 0min.

### 3.2 Effect of the assemblies modification to the fire resistance

It is possible to say, that even simple modification (increasing thickness of the shear-bearing board) can bring an assembly to a higher class of fire resistance (Fig. 11).

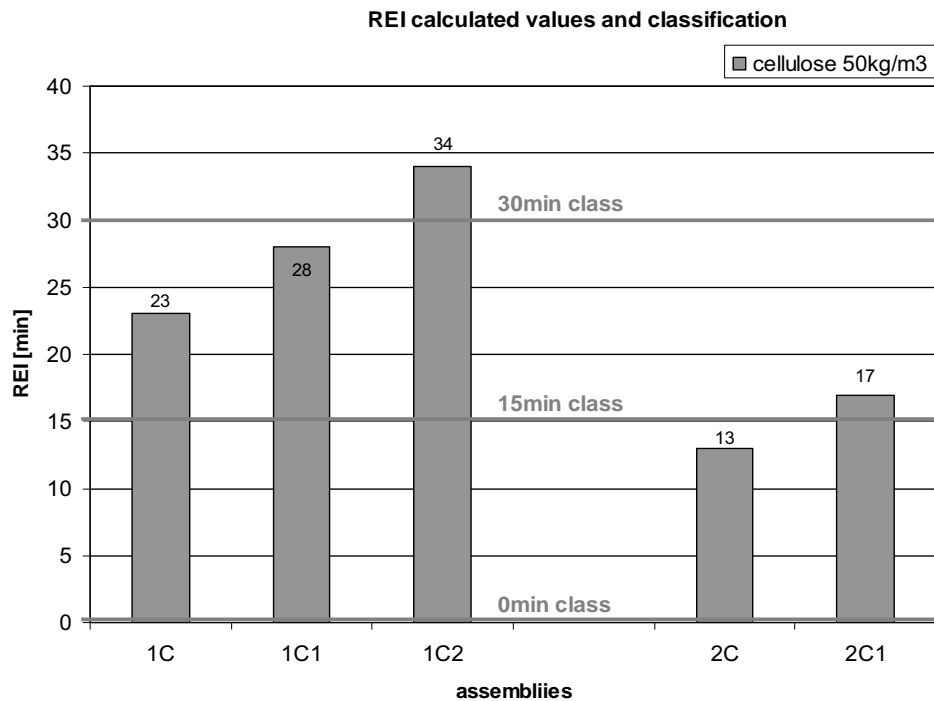


Fig.11 Calculated values of the fire resistance and the classification according to EN 13501-2

## SUMMARY

The purpose of the assembly variation and modification was to evaluate fire protection properties, for alternatives of the atypical wood-based external wall. This information is essential at the very early stage of a design process, as appropriate selection of particular materials has to be performed, according to total fire resistance requirements.

## REFERENCES

- Decree no. 94 of the Ministry of Interior of the Slovak Republic No. 94/2004 Z. z. – Technical requirements for the fire safety by building and using the buildings.
- EN 13501-2, Fire classification of construction products and building elements- Part 2: Classification using data from fire resistance tests, excluding ventilation services.
- EN 1990, Eurocode: Basis of structural design (E), including Attachment A1: Buildings(S)
- EN 1991 – 1 – 2, Eurocode 1: Actions on structures -Part 1 -2: General actions –Actions on structures exposed to fire.
- EN 1995 – 1 – 2, Eurocode 5: Design of timber structures. Part 1 -2: General. Structural fire design.
- F. Wald et al.: Calculation Fire resistance of buildings constructions, ČVUT Praha 2/2005. ISBN 80-01-03157-8.
- Ed.: Wald F. et al.: Design of construction the Fire influence according to EN, ČVUT Praha 2/2007. ISBN 978-80-01-03580-1.
- Karpaš J., Directives for calculation the Fire resistance of constructions, VÚPS Praha No. 15/84.
- Kupilík V., Buildings constructions from Fire view, Grada Publishing, a.s., Praha 2006, ISBN 80-247-1329-2.



# CONE CALORIMETER TESTS ON FR TREATED NORWAY SPRUCE

## Comparison of Different Fire Retardant Products for Timber Structures

Paul Hartmann<sup>a</sup>, Josef Kögl<sup>a</sup>, Wilfried Beikircher<sup>a</sup>

<sup>a</sup> University of Innsbruck, Department of Engineering Science, Timber Engineering Unit, Innsbruck, Austria

### Abstract

Fire retardants are effective in reducing different reaction to fire parameters of wood such as the ignitability, the heat release, the burning rate and the flame spread. This paper discusses the different mechanisms of fire retardant products as pressure impregnated wood, non-intumescence surface coatings and intumescence coatings on Norway spruce (*Picea abies*). The tests were performed by using the cone calorimeter test. The comparison of the investigated products will describe the mechanisms of action to reduce combustion by using the heat release rate of 25 kW/m<sup>2</sup> and 50 kW/m<sup>2</sup> and the standard ISO 834 test curve. As result information on the ignition time, the heat release rate, the mass loss and the temperature profile over the material thickness will be presented in this paper.

**Keywords:** fire retardant treatment, intumescent coatings, Norway spruce, heat release rate, cone calorimeter test, oxygen consumption

### INTRODUCTION

For centuries, wood has been used in construction both structurally and as a decorative material. Due to its natural combustibility, timber burns if exposed to severe fire conditions. However, wood products can be used safely by improving their fire performance which includes chemical, biochemical and physical modification. At present, the level of knowledge of wood products with improved fire performance is not high enough for their extensive utilization. The main problems are not clear defined technical requirements in building standards and minor existing investigation regarding the long term behaviour under different environmental conditions. Even though some wood products with improved fire performance show excellent fire properties and reach in the European classification system class B, examples of products with hardly any benefit compared to ordinary wood also exist, which typically fall into class D (Hakkarainen et al. 2005). Another problem is the selection of an unsuitable product for a certain application. But the fire retardant treatment, if correctly specified, provides added value to the wood based substrates and extends the market potential of the world's most natural building material.

The purpose of this project is to assist the wood construction with selection criteria for FRT and fire retardant coating products for wood by systematically assembling data on the flammability and other fire related properties of these materials. The ultimate use of such a data base assembly is input for a method for accurately predicting the real fire performance and flammability characteristics of products from bench-scale tests. The cone calorimeter test as used in this investigation is widely used to evaluate the flammability characteristics of materials.

### 1 MATERIALS

The materials used in this study are listed in Tab. 1. Untreated and treated test specimens made of defect free Norway spruce was cut into 100 mm by 100 mm squares and generally at 30 mm thickness. With exception the samples of FRT-wood (C2-Series) were only in 20 mm thickness available by the supplied product. For each test series three replications were

performed. Each test series were cut out of the same three boards s. Fig. 1. The underlying wood was selected in that way to have twin samples and the influence on the natural wood properties is minimized. The samples were prepared for testing perpendicular to the grain orientation. The series of impregnated wood is not fully comparable with the other series as the material was supplied by the providing company. The grain orientation and the material itself (density) do not correspond to the other test samples. Commercial fire retardant products were chosen instead of model formulations so that the effects of single chemicals and other additives are included in the fire performance results. All selected fire retardant products have a classification certificate according the EN 13501 of class B. The compounded formulations were provided by different manufacturers. The coatings were applied by spraying the required amount of 350 g/m<sup>2</sup> resp. 300 g/m<sup>2</sup> on the surface. For the FR impregnation a concentration of 20,9 % and an amount of 91,2 kg/m<sup>3</sup> was brought into the wood.

Tab. 1 Fire retardant treated Norway spruce - test series

Test series	Test Replications	Fire retardant product	colour	applied quantity [g/m <sup>2</sup> ]	Sample thickness [mm]
A1	3	intumescent coating	transparent	350	30
A2	3	intumescent coating	transparent	350	30
B1	3	intumescent coating	white	350	30
B2	3	intumescent coating	white	350	30
C1	3	fire retardant solution	transparent	300	30
C2	3	fire retardant treatment	transparent	91,2 kg/m <sup>3</sup>	20
D (REF)	3	Natural Wood - reference	-	0	30

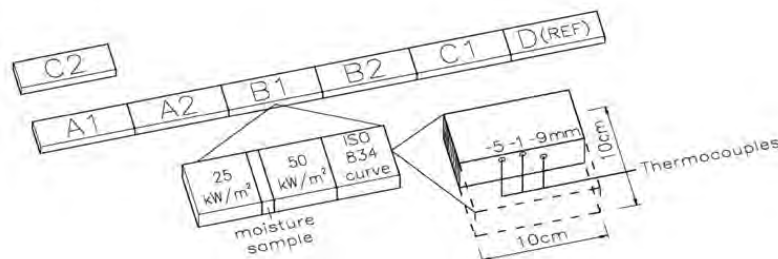


Fig. 1 Schematic representation of the sample preparation procedure

After the coating resp. the impregnation the samples were conditioned at laboratory conditions at 65 % RH and 20 °C for at least for weeks prior to testing to meet equilibrium moisture content (EMC). Before testing the moisture content was determined according to ISO 3130:1975 and the density was determined according to ISO 3131:1975. For the determination of the temperature profile within the sample thermocouples (Type-K) were placed on different depth measured from the exposed surface. The thermocouples were at the depth of -1 mm, -5 mm and – 9 mm. For the cone test the specimen were placed in an aluminium foil with a lip 5 mm above the top surface of the sample.

## 2 METHODS

The data reported here were obtained using the adapted Conical Heater from FTT (Fire Testing Technology) with respect of the requirements on the Cone Calorimeter Test as described in accordance to the guidance in ISO 5660-1 on choosing a heat flux for cone calorimeter experimentation. The Cone Calorimeter and its function have been previously

described by Babrauskas (1982) and Babrauskas and Parker (1987). Briefly, it is a bench-scale test for determining the rate of heat release based on the principle of oxygen consumption. The energy release rate is computed from the measurements of mass flow rate and oxygen depletion in the gas flow through the exhaust stack. The cone calorimeter brings quantitative analysis to materials flammability research by investigating parameters such as heat release rate (HRR), time to ignition ( $t_{ig}$ ), total heat release (THR) and mass loss rate (MLR). The HRR measurements can be further interpreted by looking at average HRR, peak HRR and time to peak HRR. Cone calorimeter test results can be used as prediction for the results in the SBI test according to EN 13501-1 (Kristoffersen et al, 2003).

In this study the tests were performed in the horizontal orientation, with the conical radiant electric heater located above the specimen and the retainer frame over the test specimen. The electric spark igniter has not been used in these investigations. The time measured for ignition is the time until the auto-ignition is observed. Heat flux levels of 25 kW/m<sup>2</sup> and 50 kW/m<sup>2</sup> and the standard ISO 834 test curve are used to test the wood products. The real standard ISO 834 test curve was not possible to regulate with the available equipment and therefore a simplified regulation by using target temperatures was used. The ISO 834 test curve was stepwise actuated as shown in Fig.2 for generating the time-temperature curve. For all tests the duration was 600 s.

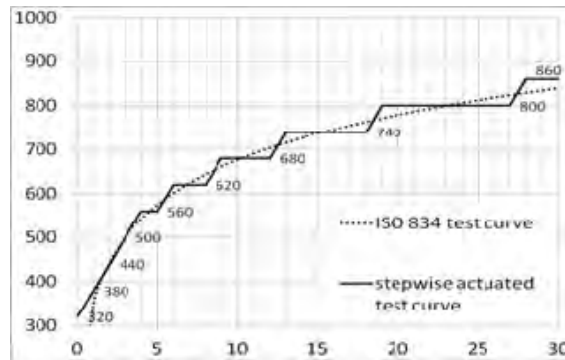


Fig.2 Regulation steps for the standard ISO 834 test curve

A ‘‘Specimen shield’’ is used to prevent radiation exposure to the specimen before the start of the test ( $t = 0$ ). In the closed position, it completely covers the opening in the heater base plate. The specimen shield is manually opened via a mechanical lever. The start of the test,  $t = 0$  is defined by the moment the specimen shield is opened exposing the specimen to the radiant heat flux. The time to ignition is measured from the start of the test. A load cell was used to continuously measure changes in sample mass, while products of decomposition, (i.e., CO, CO<sub>2</sub> and total unburned hydrocarbons) were monitored by appropriate gas analysers. The accuracy of the oxygen measurement is  $\pm 420$  ppm. The measurements were logged every second. Heat release calculations were based on the oxygen consumption principle, which states that for complete combustion of a wide range of fuels, 13.1 ( $\pm 5\%$ ) kJ of energy is produced for every 1 g of oxygen consumed by the fire (Hugget, 1980). The heat release was calculated according to the ISO 5660 standard as

$$\dot{q}(t) = (\Delta h_c / r_o)(1,10)C \sqrt{\frac{\Delta P}{T_c}} \cdot \frac{X_{O_2}^0 - X_{O_2}}{1,105 - 1,5X_{O_2}} \quad (1)$$

and the value of the rate of heat release per unit area is

$$\dot{q}'' = \dot{q} / A_s \quad (2)$$

Nomenclature:

- $\dot{q}$  heat rate (kW)  $T_c$  temperature for orifice meter (K)  
 $t$  time (s)  $X_{O_2}^0$  oxygen content input  
 $\Delta h_c$  net heat of combustion ( $\text{kJ kg}^{-1}$ )  $X_{O_2}$  oxygen content in the exhaust gas  
 $r_0$  stoichiometric oxygen/fuel mass ratio  $\dot{q}''$  heat release rate per unit area ( $\text{kW/m}^2$ )  
 $C$  orifice meter calibration constant  $A_s$  specimen exposed area ( $\text{m}^2$ )  
 $\Delta P$  orifice meter pressure differential (Pa)  
 $\frac{\Delta h_c}{r_0}$  is the expression that rates the heat of combustion release per unit mass of oxygen which

Hugget (1980) has shown to be sensibly constant with  $13.1 \times 10^3 \text{ kJ kg}^{-1}$ . The oxygen content  $X_{O_2}^0$  is calculated with  $0.2095 (\pm 0.0001)$ . The HRR curves values were calculated from the data recorded on the computer. The results are reported in  $\text{kW/m}^2$  of the exposed surface area. The areas beneath the HRR curves were integrated to give cumulative heat release as total heat release THR in  $\text{MJ/m}^2$  for the test duration of 600 s.

### 3 RESULTS AND DISCUSSION

The cone calorimeter test results are shown in Tab. 2 as averages values of the three replication tests. Please note that most of the tests performed did not auto-ignite during the 600 s testing.

Tab. 2 Results of the cone calorimeter tests

Test series	Test	Density ( $\text{kg/m}^3$ )	Moisture content (%)	Irradiance: 25 $\text{kW/m}^2$				Irradiance: 50 $\text{kW/m}^2$				Standard time-temperature curve acc. ISO 834						
				$t_0$ [s]	HRR $\dot{q}''_{100}$ [ $\text{kW/m}^2$ ]	HRR $\dot{q}''_{300}$ [ $\text{kW/m}^2$ ]	HRR $\dot{q}''_{600}$ [ $\text{kW/m}^2$ ]	THR $Q''_{600}$ [ $\text{MJ/m}^2$ ]	$t_{ig}$ [s]	HRR $\dot{q}''_{100}$ [ $\text{kW/m}^2$ ]	HRR $\dot{q}''_{300}$ [ $\text{kW/m}^2$ ]	HRR $\dot{q}''_{600}$ [ $\text{kW/m}^2$ ]	THR $Q''_{600}$ [ $\text{MJ/m}^2$ ]	$t_{ig}$ [s]	HRR $\dot{q}''_{100}$ [ $\text{kW/m}^2$ ]	HRR $\dot{q}''_{300}$ [ $\text{kW/m}^2$ ]	HRR $\dot{q}''_{600}$ [ $\text{kW/m}^2$ ]	THR $Q''_{600}$ [ $\text{MJ/m}^2$ ]
A1	A	563	12.1	-	4.55	4.58	4.72	2.67	-	4.80	10.05	15.96	5.54	-	4.29	10.80	22.54	6.94
	B	572	10.8	-	4.48	9.34	9.35	4.19	-	9.12	13.56	28.34	8.68	-	13.34	22.97	35.62	11.90
	C	511	11.9	-	17.55	22.87	28.19	12.40	-	8.97	13.56	23.31	8.50	-	4.41	4.49	13.16	3.21
A2	A	472	11.6	-	0.05	4.59	4.50	1.73	-	4.74	0.09	8.45	2.77	-	4.23	4.36	4.65	3.14
	B	465	11.2	-	0.05	4.33	4.52	1.89	429	4.81	10.09	56.98	11.30	-	4.47	4.44	9.15	2.93
	C	570	12.7	-	4.50	9.27	9.17	3.80	-	4.52	9.00	15.91	5.68	-	4.38	8.93	22.07	6.00
B1	A	484	11.2	-	9.09	13.60	27.70	8.45	-	13.73	14.96	38.55	12.00	-	4.34	8.71	13.52	4.47
	B	508	10.6	-	9.07	8.99	4.66	5.51	-	8.82	13.84	28.90	10.10	-	4.47	4.58	4.72	2.22
	C	529	12.2	-	8.45	12.92	17.31	7.26	-	9.58	19.34	45.61	11.30	-	10.10	13.50	31.08	8.77
B2	A	486	10.9	-	8.81	8.58	4.46	5.20	-	4.65	9.76	17.55	5.94	-	9.00	9.12	27.64	7.39
	B	579	12.2	-	15.04	16.02	9.23	7.54	-	17.11	13.14	15.74	8.81	-	4.41	8.82	18.12	5.59
	C	473	10.6	-	9.53	8.00	11.97	5.74	-	8.31	8.79	15.65	6.41	-	6.92	13.53	22.92	6.59
C1	A	508	12.0	-	4.86	10.52	31.62	8.70	71	72.63	74.71	82.43	42.40	-	4.13	8.67	40.47	8.11
	B	517	10.8	-	9.36	20.14	41.52	11.60	62	76.76	82.47	83.97	45.40	-	13.40	18.41	45.69	12.20
	C	548	11.6	-	5.04	15.33	33.74	9.58	-	40.68	50.28	52.54	24.20	-	0.00	4.76	31.51	4.24
C2	A	468	13.1	-	4.45	8.79	9.09	4.32	-	18.99	29.03	46.85	15.90	-	4.33	8.86	18.69	4.93
	B	510	13.0	-	8.81	8.96	4.73	4.92	-	19.20	24.89	42.15	14.40	-	19.00	36.01	62.65	20.80
	C	555	13.8	-	17.51	27.14	35.81	13.70	-	23.67	33.89	49.91	19.40	-	17.61	32.14	56.65	19.80
REF	A	490	10.8	-	11.26	23.18	59.64	15.50	86	72.57	64.50	75.86	38.90	-	8.78	13.40	74.38	13.90
	B	454	11.2	-	22.90	39.70	87.08	24.20	48	105.45	106.40	120.61	62.30	-	9.02	13.96	62.92	12.30
	C	580	11.6	-	6.32	13.62	45.65	9.50	64	108.61	112.68	132.05	63.00	580	4.51	9.57	120.88	8.72

The results of the mass loss rate in Fig. 3 show that at the heat flux of  $25 \text{ kW/m}^2$  and for the standard ISO 834 curve the rates are very similar. However the mass loss rate at  $50 \text{ kW/m}^2$  show higher differences between the tested products. The intumescence coatings in between show quite similar results and the non-intumescence coating and the FR impregnation are in the range of the untreated reference sample regarding the mass loss rate. Note: The mass loss rate at  $t_0 = 0$  is not fully correctly given in the diagrams Fig. 3 due to the calculation method used.

The results of the heat release rate in Fig. 4 show that at the heat flux of  $25 \text{ kW/m}^2$  and for the standard ISO 834 curve the rates are very similar. At the heat flux of  $50 \text{ kW/m}^2$  the product C1 show some similarities to the reference but at lower level and the other products have considerable lower heat release rates. By consider the suggestion from Kristoffersen et al (2003) for the prediction of the classification of FRT wood products after running the cone calorimeter test at heat exposure levels of  $50 \text{ kW/m}^2$  for the most of the tested products the class B can be predicted which should be expected as all products have a positive testing

certificate as class B according to EN 13501-1. But for the product C1 the results of two samples show  $HRR > 80 \text{ kW/m}^2$ . This testing results lead to the question whether the product does not fulfil the class B, or the suggested limiting values according to Kristoffersen et al (2003) are not always valid and have to be determined by further tests.

The results of the temperature measurements at the heat flux of  $50 \text{ kW/m}^2$  in Fig. 5 show that at the depth of  $-1 \text{ mm}$  the intumescent coatings show a very clear insulation effect. The temperature at  $-5 \text{ mm}$  and at  $-9 \text{ mm}$  depth rise some questions as the untreated reference series show similar temperatures as the intumescence coated products but the non-intumescence coated and the impregnated product show quite higher temperatures at this depth.

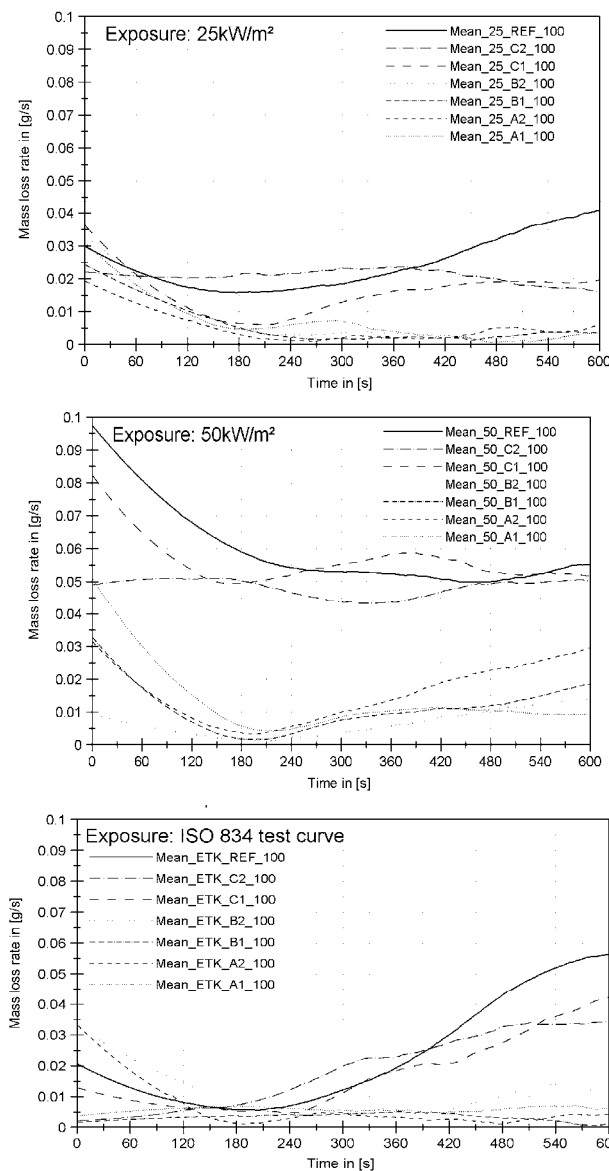


Fig. 3 Mass loss rate curves (mean value of 3 replications) during the cone test with the irradiance of  $25 \text{ kW/m}^2$ ,  $50 \text{ kW/m}^2$  and the standard ISO 834 curve for the test duration of 600 s for the different fire retardant products and the untreated reference series

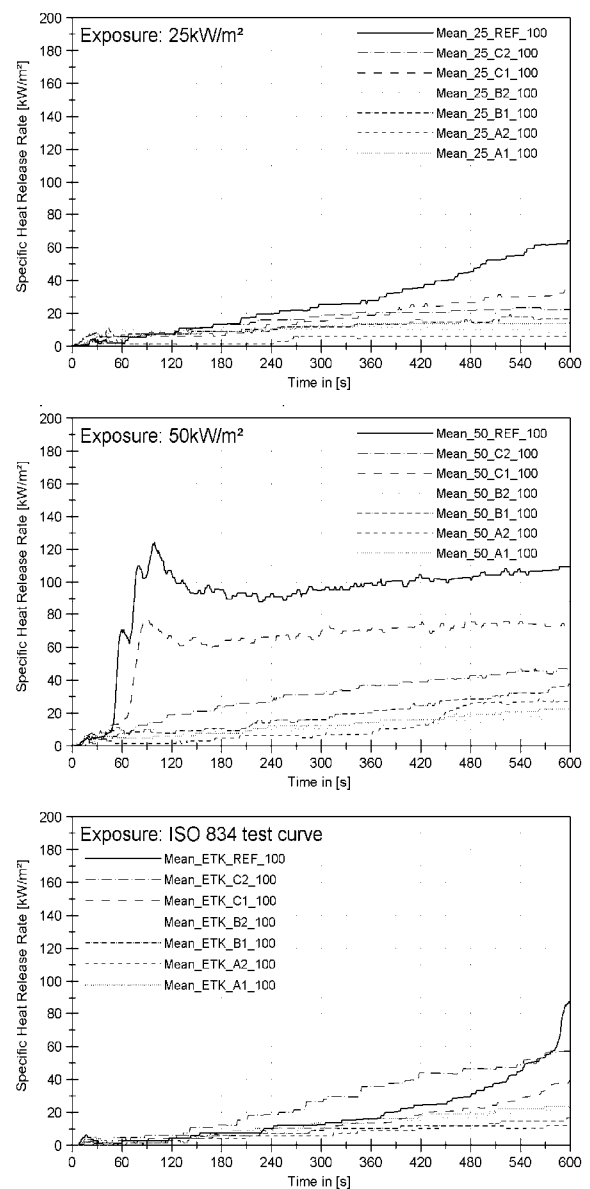


Fig. 4 Rate of heat release curves (mean value of 3 replications) during the cone test with the irradiance of  $25 \text{ kW/m}^2$ ,  $50 \text{ kW/m}^2$  and the standard ISO curve for the test duration of 600 s for the different fire retardant products and the untreated reference series

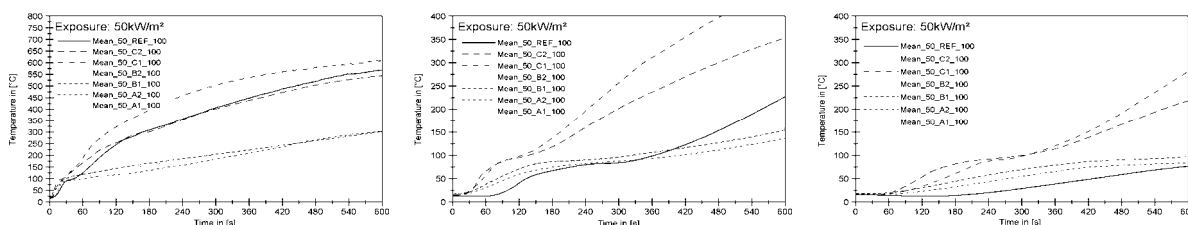


Fig. 5 Temperature profiles (mean value of 3 replications) in the sample at the depth of -1 mm, -5 mm and -9 mm during the cone test with the irradiance of 50 kW/m<sup>2</sup>

#### 4 SUMMARY AND ACKNOWLEDGMENT

In this paper we have shown the HRR data on various fire retardant treatments on Norway spruce tested in the cone calorimeter. Intumescence coatings on wood reduce significantly the HRR and the temperature in the substrate. Almost no difference between transparent and coloured intumescence coatings in the behaviour under heat load could be determined. The non-intumescence coating and the FR impregnation show quite similar results within the cone calorimeter test as the untreated reference sample. Hence the question arises if those products are useful where fire resistance is required for the protection of structural elements. Further investigations show that the data generated with the cone calorimeter can be used to estimate the fire reaction behaviour according to Euro classes but are limited applicable on intumescent coatings. The Standard ISO 834 curve for 600 s shows that the results could be useful for generating information on the behaviour of fire retardant treated wood for simulation purposes as this curve describes a natural fire.

The authors gratefully acknowledge the support from the manufacturer those supplied the test materials. They also thank Franz Haas for writing a software program for running and data collection out of the cone calorimeter experiments. This work was partially supported by the “Innovative Wood Protection” project, which is funded by the Tyrolean Government and the European Regional Development Fund (ERDF).

#### REFERENCES

- Babrauskas V., Development of the Cone Calorimeter A Bench-Scale Heat Release Rate Apparatus Based on Oxygen Consumption (NBSIR 82-2611), (1982).
- Babrauskas V. and Parker W.J., Ignability Measurements with the Cone Calorimeter, Fire and Materials 11, 31-43 (1987).
- Hakkarainen T., Mikkola E., Östman B., Tsantaridis L., Brumer H., Piispanen P., InnoFireWood: Innovative ecoefficient high fire performance wood products for demanding applications. State of the art, Project Report: Inno Fire Wood, March 2005.
- Huggett C., Estimation of Rate of Heat Release by Means of Oxygen Consumption Measurements. Fire and Materials 4, 61-65 (1980).
- Kristoffersen B., Steen Hansen A., Hakkarainen T., Östman B., Johansson P., Pauner M., Grexa O. & Hovde P. J. Using the Cone Calorimeter for screening and control testing of fire retarded wood products. Report Nordtest project 1526-01. Trondheim: Norwegian Fire Research Laboratory, 2003. 63 p. + app. 18 p. (NBL A03119.)
- ISO 3130:1975, Wood -- Determination of moisture content for physical and mechanical tests
- ISO 3131:1975, Wood -- Determination of density for physical and mechanical tests.
- ISO 5660:1993, Fire Tests; Reaction to Fire; Part 1: Rate of Heat Release from Building Products (Cone Calorimeter Method).
- EN 13501-1:2002, Fire classification of construction products and building elements – Part 1: Classification using test data from reaction to fire tests. Brussels: European Committee for Standardization







# **BEHAVIOUR OF THE HEADED STUD SHEAR CONNECTORS ON Composite Steel-Concrete Beams under Elevated Temperatures Utilising Carbon Nanotube**

Olivia Mirza<sup>a</sup>, Kathryn Wilkins<sup>a</sup>

<sup>a</sup> University of Western Sydney, School of Computing Engineering and Mathematics, Locked Bag 1797, Penrith, 2751, New South Wales, Australia

## **Abstract**

This paper describes the ultimate loads and failure modes of composite steel-concrete specimens when carbon nanotube is implemented. This paper also compares the load versus slip relationship of push tests under ambient temperature, at-fire exposure and post-fire exposure. Results from the experimental study demonstrated that the reduction of ultimate load and stiffness as temperatures increased. The at-fire exposure specimens showed a decrease in ductility as temperatures increased. Whilst, the post-fire exposure specimens showed an increase in ductility as temperatures increased. Even though carbon nanotube did not show increment in ultimate load, however the carbon nanotube reduced concrete spalling and cracking when compared to normal concrete under elevated temperatures.

**Keywords:** composite steel-concrete, push tests, shear connectors and elevated temperatures

## **INTRODUCTION**

Composite steel-concrete beams consist of a concrete slab connected to a steel beam via headed stud shear connectors located at the interface of the components. Composite steel-concrete beams are considered effective due to the high concrete compressive strength complementing the high tensile strength of the steel component (Uy & Liew 2003). The headed stud shear connectors are used to prevent the vertical separation of the components, and also to transfer the normal and shear loads between the components (Lam & El-Lobody 2005).

The integrity of fire-exposed structures is of high importance to understand. When exposed to elevated temperatures, the concrete and steel mechanical properties decrease with increasing temperature (Mirza and Uy 2009). As the headed stud shear connectors are indirectly exposed to the elevated temperatures, axial tensions are experienced from the imposed vertical uplift forces (Wang 2005). Research regarding the integrity of post-fire exposed structures is limited.

Carbon nanotubes are considered a smart material with research suggesting effective properties to be gained. When added to concrete mixture, the carbon nanotubes are expected to increase the compressive strength of the concrete component, and overcome concrete durability issues (Potapov et al. 2011). However, the experimental research regarding carbon nanotube concrete at elevated temperatures on composite steel-concrete structures has not been explored. This paper is to look at the effect of carbon nanotube on headed stud shear connectors for composite steel-concrete beam under elevated temperatures.

## **1 EXPERIMENTAL STUDIES**

The push test method was conducted according to Eurocode 4 (British Standards Institution EC4 2005). The push test method involved applying a shear load directly to the headed stud shear connectors. The push test specimens were formed by a reinforced concrete slab standing vertically with two structural steel beams connected via the flanges by welded headed stud

shear connectors. Two types of push tests were conducted, including normal concrete material and carbon nanotube concrete material.

For this experimental study, 400mm long 150UB14.0 Grade 300MPa structural steel beams were used. The reinforced concrete slabs had dimensions of 400mm wide, 400mm long and 200mm deep. The concrete used was 25MPa concrete. The nanotube concrete mixture had an addition of 1% carbon nanotube to concrete material. Three N12 reinforcing bars were spaced at 170mm centre to centre in the concrete slab. 19mm diameters with 100mm long headed stud shear connectors were used. The push test specimen setup for the normal concrete and carbon nanotube concrete materials are shown in Fig. 1.

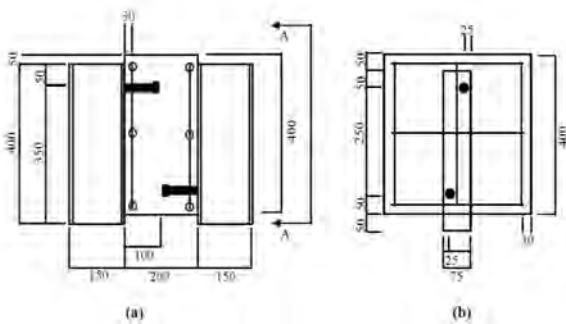


Fig. 1 Push test specimens

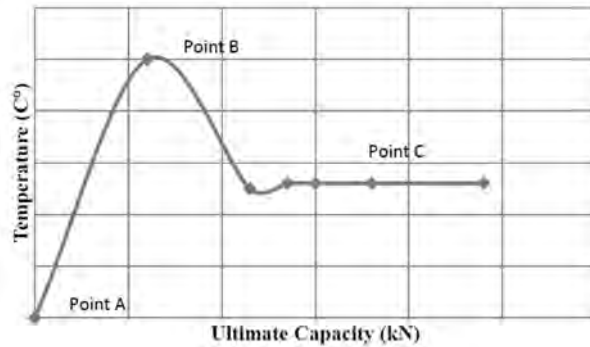


Fig. 2 Push test specimens under different conditions

Eurocode 4 (British Standards Institution EC4 2005) requires push test specimens using concrete to be of 600mm wide, 600mm long and 150mm deep dimensions. However due to the size limitation of the furnace, modifications to the push test specimens have been made. Hence the concrete component is 400mm wide, 400mm long and 200mm deep.

A total of 28 push test specimens were tested: 14 normal concrete and 14 carbon nanotube concrete materials. The three temperature conditions to be considered include Point A – ambient temperature, Point B – at-fire and Point C – post-fire exposure. The specimens were tested under ambient temperature, 200°C, post 200°C, 400°C, post 400°C, 600°C and post 600°C. Fig. 2 shows the push test experiment details and temperature conditions.

## 2 RESULTS AND DISCUSSIONS

### 2.1 Comparison of Push Tests Results for Normal Concrete at Fire

Generally, the specimens at ambient temperatures, 200°C and 400°C failed due to headed stud shear failure. The failure was signified by a large bang as the stud sheared off the steel flange, separating the concrete slab and steel beam components. For specimens at 600°C, the failure mode was caused by the combination of headed stud failure, concrete cracking and spalling failure. At the same time, it was also observed that the structural steel beam buckled due to the elevated temperatures.

Fig. 3 illustrates the comparison of push tests for the normal concrete at-fire exposure. Comparing the stiffness of the normal concrete at ambient temperature to 200°C, 400°C and 600°C, a reduction of 4%, 6% and 38% were observed, respectively. Overall, the ambient push test had the greatest stiffness. According to Mirza and Uy (2009) this is to be expected, as the increase in temperature steadily reduces the stiffness of the steel components. This is also due to the bond failure between concrete and steel surface when subjected to elevated temperatures.

The normal concrete ambient temperature push test achieved an ultimate load of 253kN. The 200°C, 400°C and 600°C normal concrete push test achieved an ultimate load of 223kN, 156kN and 89kN, respectively. This large reduction illustrates the increased danger of failure

of composite steel-concrete beams when subjected to elevated temperatures. Overall the normal concrete ambient temperature specimen achieved the greatest ultimate load. This is due to the increased temperatures decreasing the mechanical properties of the composite steel-concrete specimens; specifically the compressive strength of the concrete component and the rigidity of the steel beam.

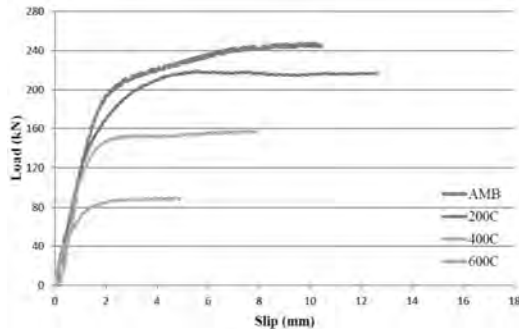


Fig. 3 Load versus slip relationships for normal concrete at fire exposure

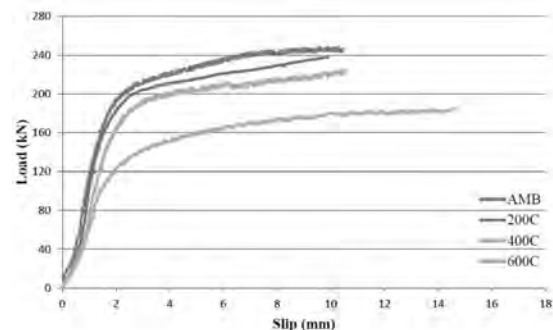


Fig. 4 Load versus slip relationships for normal concrete for post fire exposure

The normal concrete 200°C push test achieved the greatest ductility followed by the ambient temperature, 400°C and 600°C. Overall the ductility of the at-fire exposure specimens decreased as the temperature increased. This trend illustrates how the tensile strength of the headed stud shear connectors decreases as the temperature increases. The decreasing ductility of the specimens means the integrity of the structure reduces, as shorter failure periods occur.

## 2.2 Comparison of Push Tests Results for Normal Concrete at Post Fire

Similar failure modes were observed for normal concrete at post fire. The specimens at ambient temperatures, post-200°C and post-400°C failed due to headed stud shear failure. The failure was signified by a large bang as the stud sheared off the steel flange, separating the concrete slab and steel beam components. For specimens at post-600°C, the failure mode was caused by the combination of headed stud failure, concrete cracking and spalling failure. However buckling of the steel beam did not occur for the post-600°C specimen. This is because the specimen was not loaded whilst exposed to the elevated temperatures.

Fig. 4 demonstrates the comparison of push tests for the normal concrete at post fire exposure. The stiffness reduction of 11%, 39% and 45% between the normal concrete ambient temperature and post-200°C, post-400°C and post-600°C was observed. When compared to the normal concrete ambient temperature to at-fire push tests, similar trends of stiffness were observed. However, the normal concrete ambient temperature to at-fire push tests achieved a greater stiffness overall when compared to the ambient temperature to post-fire push tests. This suggests that the stiffness of the specimens continues to decrease and is not regained, once exposed to elevated temperatures.

An ultimate load of 253kN was achieved by the normal concrete ambient. The post-200°C, post-400°C and post-600°C normal concrete achieved an ultimate load of 237kN, 227kN and 183kN, respectively. This demonstrates an ultimate load reduction of 6%, 10% and 28% compared to the ambient temperature. In comparison to the normal concrete ambient temperature to at-fire push tests, the ambient temperature to post-fire push tests reduced in ultimate load at a significantly lower rate. This suggests that the ultimate load of the composite steel-concrete beams after exposure to elevated temperatures is greater than exposure during elevated temperatures. According to Fike and Kodur (2011), this is to be expected as the decreasing temperatures allow for the ultimate strength of the concrete and steel components to be regained.

The greatest ductility was achieved by the post-600°C push test. The ambient temperature and post-400°C push tests achieved similar ductility whilst the post-200°C push test achieved the

lowest ductility. Overall the ductility of the normal concrete post-fire push tests increased as the temperature increased. This trend illustrates how the tensile strength of the headed stud shear connectors increases as the temperature increases. This trend is opposite to the at-fire exposure specimens. This suggests that greater tensile strength is regained as the specimens cool to ambient temperature. The increasing ductility of the specimens suggests the integrity of the structure also increases. This allows for longer periods of failure to occur, thus increasing safety.

### 2.3 Comparison of Push Tests Results for Carbon Nanotube Concrete at Fire

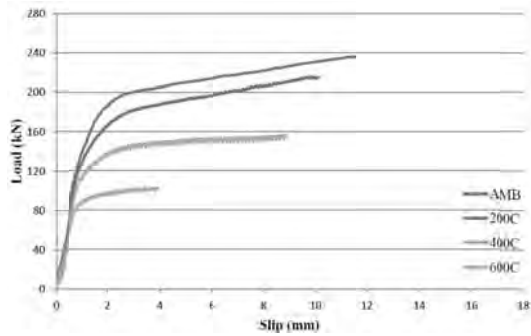


Fig. 5 Load versus slip relationships for carbon nanotube concrete at fire exposure

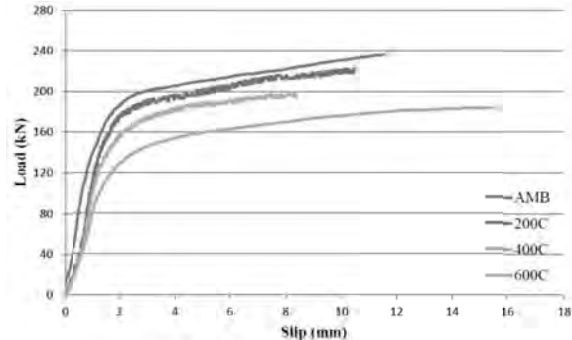


Fig. 6 Load versus slip relationships for carbon nanotube concrete for post fire exposure

The failure modes for carbon nanotube are similar to normal concrete. This is due to the carbon nanotube not taking affect in increasing the compressive strength of the concrete. However, it was observed that the reduction of concrete cracking and spalling was observed when compared to the normal concrete at elevated temperatures. This is due to the nanotube concrete being able to prevent nano-cracks from occurring, by requiring a greater amount of energy to form the cracks (Konsta-Gdoutos et al. 2010).

Fig. 5 demonstrates the comparison of push tests for the carbon nanotube concrete at fire exposure. When compared with ambient temperatures, the stiffness of the nanotube concrete at 200°C, 400°C and 600°C illustrated an 8%, 18% and 38% reduction, respectively. When compared to the normal concrete ambient temperature to at-fire exposure push tests, similar trends of stiffness are observed. However the 200°C and 400°C normal concrete push tests achieved greater stiffness when compared to the nanotube 200°C and 400°C.

The nanotube concrete ambient temperature, 200°C, 400°C and 600°C achieved an ultimate load of 244kN, 204kN, 153kN and 100kN, respectively. When compared to ambient temperature, the ultimate load reduced 16%, 37% and 59%, respectively. In comparison to the normal concrete ambient temperature to at-fire push tests, the nanotube ambient temperature to at-fire push tests showed a similar trend in ultimate load reduction. More specifically, the nanotube at-fire push tests achieved a slightly lower ultimate load from ambient temperature to 400°C. However, from 400°C to 600°C, the nanotube at-fire push tests achieved a slightly higher ultimate load.

Overall the ductility of the at-fire exposure specimens decreased as the temperature increased. This trend in ductility is similar to the ductility trend of the normal concrete ambient temperature to at-fire push tests. The decreasing tensile strength of the headed stud shear connectors means the integrity of the specimen also decreases.

### 2.4 Comparison of Push Tests Results for Carbon Nanotube Concrete at Post Fire

The specimens at ambient temperatures, post-200°C, post-400°C and post-600°C failed due to headed stud shear failure. The failure was signified by a large bang as the stud sheared off the steel flange, separating the concrete slab and steel beam components. One improvement to these specimens, there were no sign of concrete cracking or spalling failure. This is due to the calcium-

silicate hydro-crystals decomposing, allowing for the chemically bound water to be released and evaporated.

Fig. 6 demonstrates the comparison of push tests for the carbon nanotube concrete at post fire exposure. A 22%, 30% and 63% stiffness reduction was observed between the nanotube concrete ambient temperature and post-200°C, post-400°C and post-600°C, respectively. When compared to the normal concrete under ambient temperature and post-fire, the carbon nanotube ambient temperature and post-fire push tests achieved similar trends of stiffness. However, the normal concrete post-fire push tests achieved a greater stiffness. Greater stiffness was also achieved by the nanotube ambient temperature to at-fire exposure push tests when compared to the nanotube ambient temperature to post-fire push tests.

An ultimate load of 244kN was achieved by the nanotube concrete ambient temperature specimens. The post-200°C, post-400°C and post-600°C nanotube concrete demonstrated an ultimate load of 233kN, 197kN and 183kN, respectively. This illustrates an ultimate load reduction of 5%, 19% and 25% when comparing the ambient temperature push test to the post-200°C, post-400°C and post-600°C, respectively. Compare to the nanotube concrete ambient temperature to at-fire push tests, the ambient temperature to post-fire push tests reduced in ultimate load at a significantly lower rate. This is similar to the ultimate load trend between the normal concrete at-fire and post-fire push tests.

The greatest ductility was achieved by the post-600°C push test followed by the ambient temperature, the post-200°C and the post-400°C. This trend is opposite to the nanotube concrete ambient temperature to at-fire push tests, as the at-fire 600°C push test achieved the lowest ductility. Similarly, both the normal concrete and nanotube post-600°C push tests achieved the highest ductility when compared to the lower temperatures.

### **3 SUMMARY**

The experimental studies showed that the failure modes for push tests were generally headed stud shear failure. Even though adding carbon nanotube into the concrete did not increase the compressive strength of the concrete, however, when the specimens were exposed to elevated temperatures, the reduction in concrete cracking and spalling were observed.

When comparing the normal concrete to the carbon nanotube concrete, it was observed that similar ultimate capacities were achieved. Similar rates in the reduction of the ultimate capacities were also achieved. Even though the carbon nanotube concrete had similar ultimate capacity as the normal concrete, the carbon nanotube concrete showed that there was a great reduction in spalling and cracking when exposed to elevated temperatures.

Furthermore, it can be concluded that the carbon nanotube material did not have any effect until temperatures reached 400°C or above. This is observed by the change in colour from the carbon nanotube concrete ambient temperature specimen to the 600°C specimen. This suggests that at greater elevated temperatures, the carbon nanotube concrete material would be a more effective choice, particularly with the reduced concrete spalling and cracking achieved.

In comparison of the at-fire exposure results to the post-fire exposure results, it was observed that greater ultimate loads and ductility were achieved by the post-fire exposed specimens, with similar stiffness achieved. This suggests that the strength of the components regains during the cooling process of the post-fire testing.

### **ACKNOWLEDGMENT**

The authors would like to acknowledge the funding and financial assistance provided by Institute for infrastructures Engineering, University of Western Sydney. The authors also would like to acknowledge the technical staff at the University laboratory at the University of Western Sydney for their assistance, effort, hard work and overall dedication to the preparation of the experimental study push test specimens and to the conducting of the push test study. Lastly, the authors would like to acknowledge the School of Computing

Engineering and Mathematics at the University of Western Sydney for providing an exceptional learning environment, research facilities and materials.

## REFERENCES

- British Standards Institution EC4 2005, Eurocode 4 1994-1-1:2005, London.
- Fike, R & Kodur, V, Enhancing the Fire Resistance of Composite Floor Assemblies Through the use of Steel Fiber Reinforced Concrete, *Engineering Structures*, vol. 33, pp. 2870-2878, 2011.
- Konsta-Gdoutos, MS, Metexa, ZS & Shah, SP 2010, 'Multi-scale mechanical and fracture characteristics and early-age strain capacity of high performance carbon nanotube/cement nanocomposites', *Cement & Concrete Composites*, vol. 32, pp. 110-5.
- Lam, D & El-Lobody, E, Behaviour of Headed Stud Shear Connectors in Composite Beam, *Journal of Structural Engineering*, pp. 96-107, 2005.
- Mirza, O & Uy, B, Behaviour of headed stud shear connectors for composite steel-concrete beams at elevated temperatures, *Journal of Constructional Steel Research*, vol. 65, no. 3, pp. 662-74, 2009.
- Potapov, VV, Shitikov, ES, Trutnev, NS, Gorbach, VA & Portnyagin, NN, Influence of Silica Nanoparticles on the Strength Characteristics of Cement Samples, *Glass Physics and Chemistry*, vol. 37, no. 1, pp. 98-105, 2011.
- Uy, B & Liew, RJY, *The Civil Engineering Handbook*, eds WF Chen & RJY Liew, CRC Press, Chapter 51, via CRC netbase <http://www.crcnetbase.com.ezproxy.uws.edu.au>, 2003
- Wang, YC, Performance of Steel–Concrete Composite Structures in Fire, *Progress in Structural Engineering and Materials*, vol. 7, no. 2, pp. 86-102, 2005.

# INVESTIGATIONS OF STEEL ELEMENTS WITH INTUMESCENT COATING CONNECTED TO SPACE-ENCLOSING ELEMENTS IN FIRE

## Fire tests on intumescent coated steel members

Peter Kraus<sup>a</sup>, Martin Mensinger<sup>a</sup>, Florian Tabeling<sup>b</sup>, Peter Schaumann<sup>b</sup>

<sup>a</sup>Technische Universität München, Chair of Metal Structures, Munich, Germany

<sup>b</sup>Leibniz Universität Hannover, Institute for Steel Construction, Hannover, Germany

### Abstract

The current status of the research program “Optimized use of intumescent coating systems on steel members” (AiF 17200) is presented. The aim of the project is to quantify the influence of space-enclosing elements on the thermal behaviour of supporting steel members. Those elements cause partially restrained expansion of the fire protection system. Experimental investigations on beams and columns directly connected to space-enclosing elements are presented. Additionally, numerical simulations are performed for temperature field calculations of steel elements with intumescent coating. As a new development, the numerical model takes into account the expansion process of intumescent painting. The setup of the numerical model is introduced.

**Keywords:** intumescent coating, numerical simulation, fire tests

### INTRODUCTION

The fire resistance of steel members protected by intumescent coating (IC) depends strongly on the expansion behavior of the fire protection system. In practical application, structural steel elements are often connected to space-enclosing elements like trapezoidal sheeting, liner trays and sandwich elements. Consequently, parts of the cross-sections are covered by adjacent space-enclosing elements (compare Fig. 1 and 2). In these regions the intumescent coating system is restrained in its expansion and is not able to develop an effective fire protection for the steel elements. As a consequence, the cross-section will be heated up not only in response to the behavior of the intumescent char but also depending on the isolation and the additional heat transfer provided by adjacent elements. This may lead to a non-uniform temperature distribution in the cross-section.

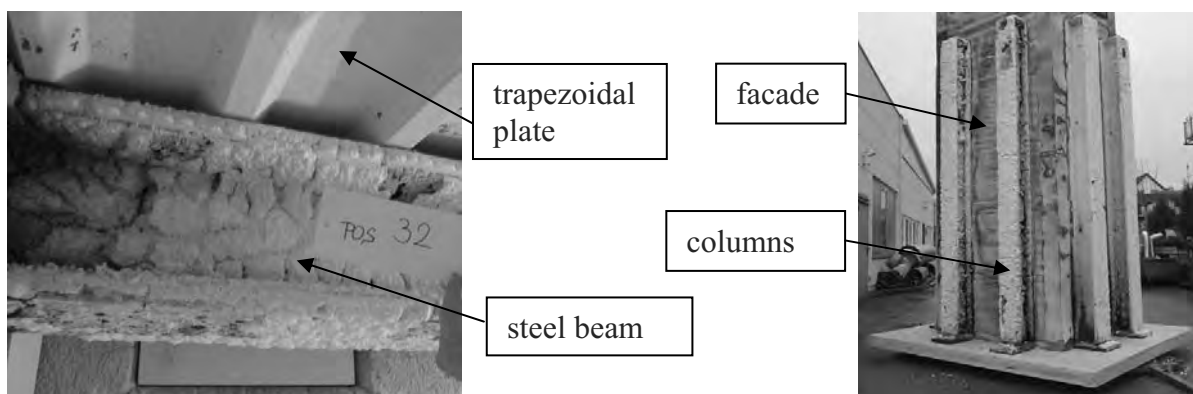


Fig. 1 Loaded Beam with IC and trapezoidal plate after test

Fig. 2 Column with IC and connected facade after test

Usually, a uniform temperature distribution is assumed in structural fire design of steel elements. This simplification enables comparably simple calculation methods for the heating of steel sections in case of fire. SuiTab. formulae are given in [DIN EN 1993-1-2] for instance. However, for steel elements protected by IC and located adjacent to space-enclosing elements it is not clear, if this assumption is valid due to a possible non-uniform temperature distribution caused by the aforementioned effects.

The main research approach aims to investigate, if the covered parts of the steel elements (e.g. the flanges) need to be protected by IC or may be left unprotected. Therefore, full scale fire tests of steel beams and columns with adjacent trapezoidal plates have been performed. The test setup and first results are presented in this paper. Additionally, these investigations are supported by numerical analyses. In these analyses the temperature field of steel elements with IC is calculated taking into account the expansion process of IC. Furthermore, shrinkage procedures due to combustion of the organic parts of IC are considered as well. The numerical model and the material parameter for IC used in the thermal calculations are presented in this paper.

## 1 TEST ARRANGEMENTS

In the experimental program two different setups were carried out: loaded beam tests and unloaded column tests. All tests were carried out over a period of 30 minutes ISO-Standard fire. The thickness of the intumescent coat on all test specimens has also been designed for 30 minutes fire resistance in regard to German regulations.

### 1.1 Loaded beam tests

The furnace used at the Fire Test Laboratory of the Technische Universität München is 3m wide 4m long and 3m high. For the tests on the loaded beams it was enlarged up to 5m length. In order to investigate the behaviour of beams in industrial halls 10 specimens HEA 200 and 10 specimens HEM 200 with a span of 4.5 m and two different types of trapezoidal sheeting were tested.

In order to achieve a constant bending moment over the length of more than 1m the beams were loaded with single loads in the third points of the span.

The load level chosen led to a bending moment in the beam sup to 60 % of the plastic bending capacity. The total load (applied with hydraulic cylinders) for HEA 200 beam sreached 80 kN, for HEM 200 beams220 kN.

Care was taken to realize a hinged support and an assembly typically used for industrial halls.



Fig. 3 View from outside; the blue and grey columns and beams are the load admission

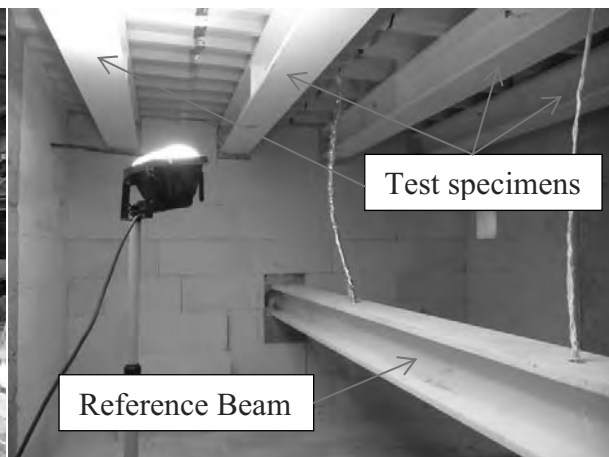


Fig. 4 View into the furnace short before fire-test

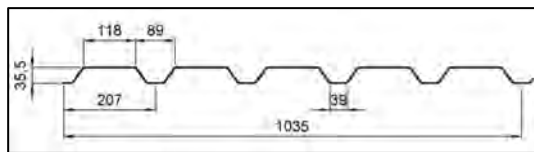


120 thermocouples per test were used to obtain temperature gradients in the steel members and in the trapezoidal sheets. The trapezoidal sheets (thickness 0,88 mm) were fixed on the beams with Hilti powder actuated fasteners. The isolation material on the top of the sheets was 120 mm mineral wool (non-flammable, melting point higher than 1000°C) which is typical for industrial halls in Germany.

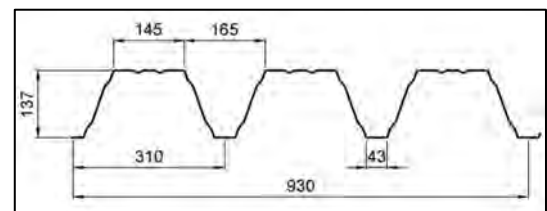
Tab. 1 Number of test specimens (beams), in combination with the trapezoidal sheets.

BEAM	FischerTRAPEZ 35/207	FischerTRAPEZ 135/310	Without sheets (Reference)
HEA 200	4	4	2
HEM 200	4	4	2

“FischerTRAPEZ 35/207”



“FischerTRAPEZ 135/310”



## 1.2 Unloaded column tests

The column tests were also performed at the fire test site of TUM. A tower (columns with connected façade) was constructed which was slightly higher than the furnace (see Fig. 6-8) in order to simulate a typical situation at fires of industrial buildings where columns and the inner part of the façade sheets are exposed to the fire, but not the outer part of the façade. The measurement equipment was installed in the cool inner part of the tower.



Fig. 5 Column setup before the test

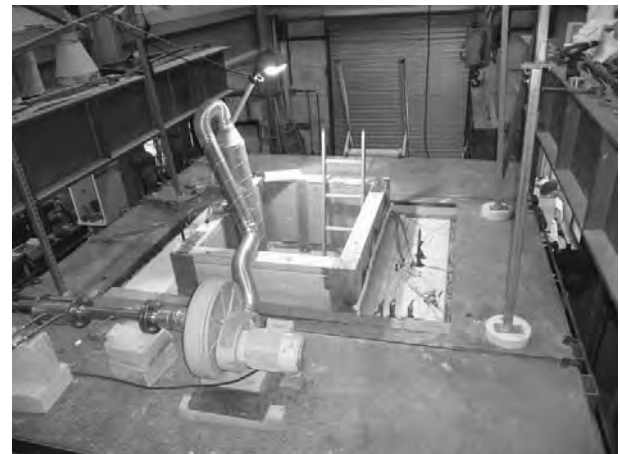


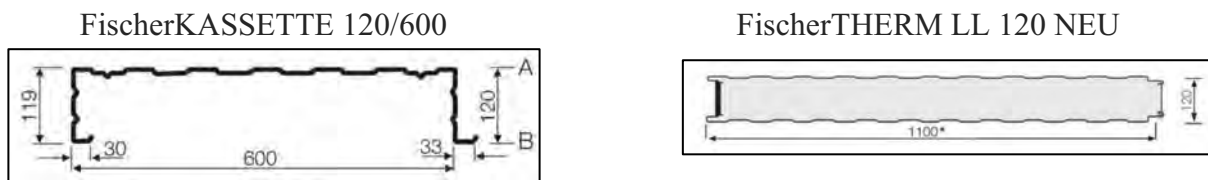
Fig. 6 Façade elements, which come through the furnace ceiling. In order to prevent an overheating in the tower a ventilator, blowing air into the lower area of the tower, guaranteed a continuous slow air draft from the tower floor to the ambient air

In total eight columns (four columns HEA 200 and four columns HEM 200) connected with two different types of industrial cladding were tested. For the first test a liner tray façade, filled with 120 mm mineral wool (non-flammable, melting point higher than 1000°C) and for the second test a standard sandwich panel consisting of two steel sheets (0,75 mm) and between 120 mm polyurethane foam was used.

Temperatures of the steel columns and the temperature of the directly flamed steel sheets were measured. The evaluation of the test results is on-going und will be published later.

Tab. 2 - Number of test specimens (columns), in combination with the façade sheets.

COLUMN	FischerKASSETTE 120/600	FischerTHERM LL 120 NEU	Without sheets (Reference)
HEA 200	4	4	2
HEM 200	4	4	2



### Pre-Evaluation of a beam

After 6 to 7 minthe intumescent coating starts to foam up.

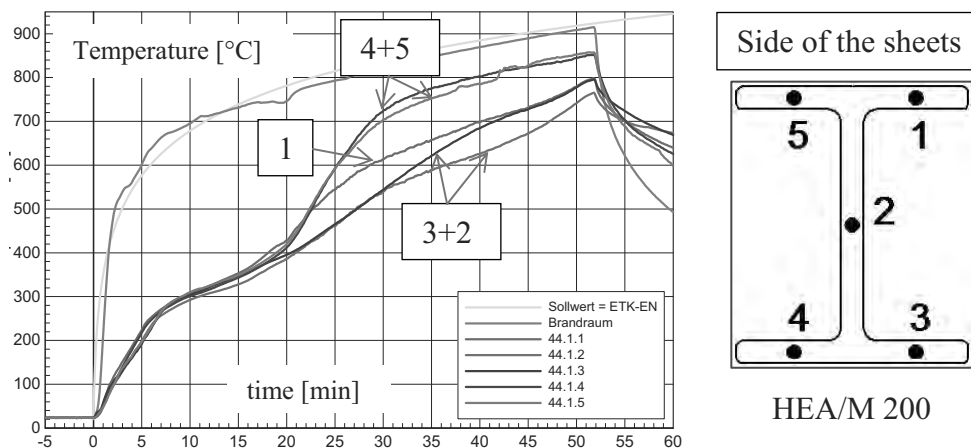


Fig. 7Example of a time-temperature course (test specimen 44)

Furthermore, an additional steel beam with intumescent coating has been tested under ISO fire conditions to investigate the thermal behaviour without any influences due to space-enclosing elements. Moreover, the numerical investigations will be validated against this test. In this test, an IPE 200 profile (S235) with a length of 1000 mm has been coated with a solvent based intumescent coating system and exposed to fire from all sides. The coating thickness amounted about 700 µm. The steel temperatures have been measured during the tests at different cross-section points. The evaluation of the steel temperatures in web and flange are depicted in Fig. 3.

## 2 NUMERICAL SIMULATIONS OF INTUMESCENT COATINGS

The performed fire tests indicate the importance of the expansion process of intumescent coating concerning the fire protection of steel elements. Regarding regions in which parts of the flanges are covered by space-enclosing elements, the intumescent coating is restrained in its expansion and is not able to develop effective fire protection behavior. Consequently, there are areas with fully developed char and areas in which the expansion of IC is restrained. As a result, it is absolutely necessary to take into account the expansion process in order to consider a restrained expansion process. In this context, a numerical model is introduced in which the expansion process is simulated explicitly.

In the numerical model which bases on the finite-element method (FEM), the expansion process of intumescent coating has been taking into account for thermal analysis. Influences of a restrained expansion process are not considered in the model yet. An implementation of these effects is in process. However, the numerical model represents a basis to take these special effects into account later. Besides the expansion process of intumescent coating, shrinkage as described in [Zhang et al, 2012] is considered as well.

The numerical simulations are performed using the finite-element software [ABAQUS] in a fully coupled 2D thermal-stress analysis. The expansion process has been implemented by defining a thermal expansion coefficient  $\alpha$  according to the expansion behavior observed in the tests. The porosity can be calculated using the following expression:

$$\psi = 1 - \frac{1}{\alpha} \quad [-] \quad (1)$$

Based on this equation, the thermal conductivity can be calculated using an equation developed by [Spitzner, 2001].

$$\lambda_{\text{eq}} = \frac{1}{1 + \frac{1}{3}(1-\psi)} \cdot \lambda_{\text{air}} + \frac{2 \cdot \frac{1}{3}(1-\psi)}{1 + \frac{1}{3}(1-\psi)} \cdot \lambda_{\text{IC}} + \frac{4 \cdot b}{1 + \frac{1}{3}(1-\psi)} \cdot \varepsilon_{\text{res}} \cdot \sigma \cdot T_{\text{m}}^3 \quad [\text{W}/(\text{m} \cdot \text{K})] \quad (2)$$

with:	$\lambda_{\text{eq}}$	equivalent thermal conductivity	[W/(m·K)]
	$\psi$	porosity	[-]
	$b$	diameter of a pore	[m]
	$\lambda_{\text{air}}$	thermal conductivity within of air the pores	[W/(m·K)]
	$\lambda_{\text{IC}}$	thermal conductivity of IC (20°C)	[W/(m·K)]
	$\varepsilon_{\text{res}}$	emissivity	[-]
	$\sigma$	Stefan-Boltzmann-constant	[W/(m <sup>2</sup> ·K <sup>4</sup> )]
	$T_{\text{m}}$	average temperature of pores	[K]

For the determination of the thermal heat capacity of intumescent coating the *mixture-rule* is used:

$$C = (\rho \cdot c_p) = \psi \cdot (\rho \cdot c_p)_{\text{air}} + (1-\psi) \cdot (\rho \cdot c_p)_{\text{IC}} \quad [\text{J}/(\text{m}^3 \cdot \text{K})] \quad (3)$$

The diameter of the pores is assumed as 0.5 mm according to [Staggs, 2010] and the thermal conductivity of IC for room temperature conditions is assumed to  $\lambda_{\text{IC}} = 0.5 \text{ W}/(\text{m} \cdot \text{K})$ . The specific heat of intumescent coating for room-temperature conditions is assumed as  $c_p = 1600 \text{ J}/(\text{kg} \cdot \text{K})$  and the density as  $\rho = 1300 \text{ kg}/\text{m}^3$ . The expansion factor and the porosity versus temperature as well as the thermal conductivity and the heat capacity versus temperature are shown in Fig. 1.

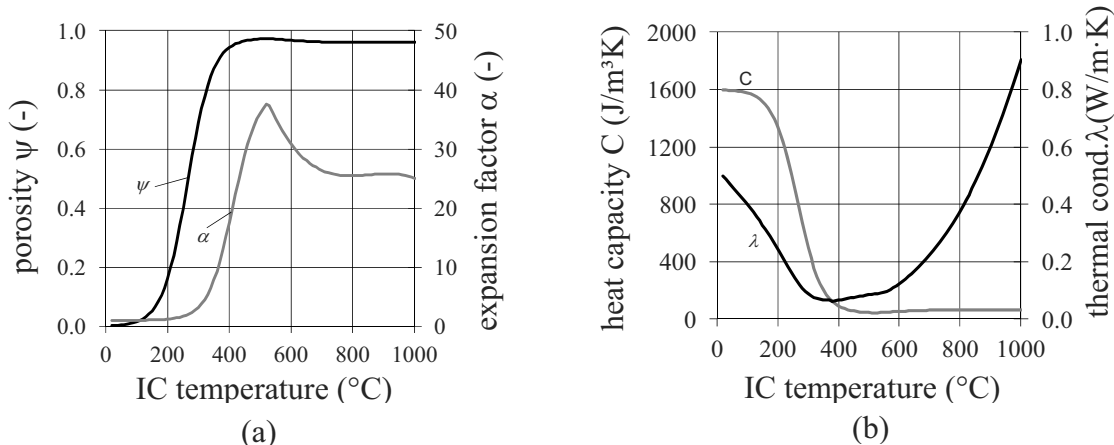


Fig. 8 – Evaluation of a) porosity and expansion and b) heat capacity and thermal conductivity versus intumescent coating temperature

In the thermal analysis the material behavior of steel, as well as the thermal boundary conditions for convection and radiation are set according to [DIN EN 1993-1-2]. Based on the aforementioned specifications, the expansion model will be applied to an I-section (IPE200) fire protected by intumescent coating without any influences from space-enclosing elements. In this context, the model will be validated against the experimental investigations described before.

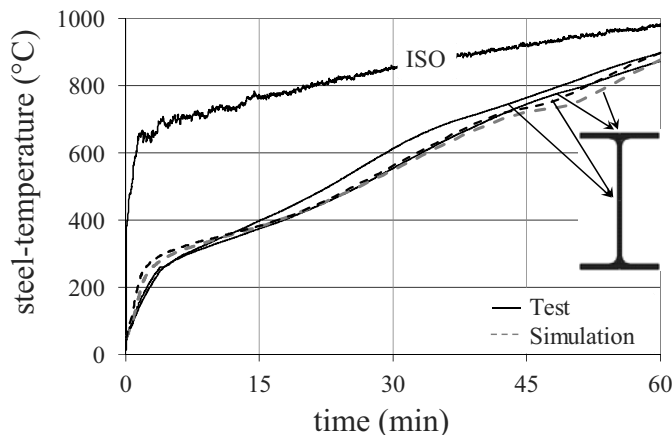


Fig. 9 – Comparison of simulated and measured steel temperatures of a IPE200 profile

Simulated and measured temperatures are compared in two cross-section points as indicated in Fig. 3. In particular the simulated temperatures in the flanges show very good agreement to the temperatures measured in the test. The temperatures in the web are slightly underestimated by the numerical simulation with a maximum deviation of about 25 C to the test. This small deviation is acceptable.

Summing up, the prognosticated temperatures are in good agreement with the measured ones and can be predicted by the model in good agreement.

### 3 CONCLUSIONS

In this paper, experimental investigations of steel elements with intumescent coating where parts of the cross-sections are covered by adjacent space-enclosing are presented. In additional numerical investigations, temperature field calculations of I-profiles with intumescent coating are performed taking into account the expansion process of intumescent coating. Furthermore, shrinkage procedures of the intumescent char are considered as well. Comparing the calculated steel temperatures to the measured temperatures from fire tests show good accordance. Consequently, the fire protection behavior of intumescent coating as well as the expansion process can be predicted. Based on the introduced model effects as a restrained expansion of intumescent coating due to space-enclosing elements will be implemented in further investigations.

### 4 OUTLOOK

The remaining work of the research project is focused on the evaluation and interpretation of the extensive test data. After these phase it will be possible to make correct declarations about the heating behaviour from steel members, connected with space-enclosing elements both experimentally and numerically.

### 5 ACKNOWLEDGEMENT

The authors would like to thank the sponsors of the project. Special thanks go to the German steel construction association DAST, the German ministry of economy and technology represented by the AiF, the construction company Goldbeck GmbH, that enabled with big

effort the assembly of the tests and the team of the fire test laboratory of the Technische Universität München in Dachau. Further industrial partners of the project are: Sika Deutschland GmbH, Rüttgers Organics GmbH and Hilti Deutschland AG.

The results have been produced within the German research project: „Optimierter Einsatz intumeszierender Anstriche im Stahlbau“ (IGF 17200 N). The IGF project was funded by the “Federal Ministry of Economics and Technology” via AiF.

## REFERENCES

- ABAQUS. Abaqus/Standard Version 6.10. Pawtucket: Hibbit, Karlsson & Sorensen, Inc. 2011.
- Di Blasi, C.; Branca, C.: Mathematical Model for the Nonsteady Decomposition of Intumescent Coatings. American Institute of Chemical Engineers Journal Vol. 47. Wiley, 2001, P. 2359–2370
- Eurocode 3: Design of steel structures - Part 1-2: General Rules – Structural fire design; German version EN 1993-1-2:2005 + AC:2009, Beuth Verlag, Berlin, 2010
- Spitzner, M. (2001): Untersuchungen zur Wärmeleitfähigkeit geschäumter Massen, Technische Universität Clausthal, Dissertation, Fraunhofer IRB Verlag.
- Staggs, J. E. J. (2010): Thermal Conductivity Estimates of Intumescent Chars by Direct Numerical Simulation, Fire Safety Journal, 45 (2010), Elsevier, S. 228-237.
- Zhang, Y.; Wang, Y.C.; Bailey, C.G.; Taylor, A.P. (2012): Global modelling of fire protection performance of intumescent coating under different cone calorimeter heating conditions, Fire Safety Journal, 50 (2012), Elsevier, S. 51-62.
- Schaumann, P.; Tabeling, F.: Experimentelle und numerische Untersuchungen von reaktiven Brandschutzsystemen im Stahlbau. (English: Experimental and Numerical Investigations on Intumescent Coatings in Steel Constructions) In: Deutscher Ausschuss für Stahlbau DAST (Hrsg.): 18. DAST-Kolloquium in Aachen, 2012, S. 64–69
- Allgemeine bauaufsichtliche Zulassung Rüttgers Organics GmbH Z-19.11-1889 Reaktives Brandschutzsystem „pyroplast-ST 200“
- Allgemeine bauaufsichtliche Zulassung Sika Deutschland GmbH Z-19.11-1319 Reaktives Brandschutzsystem „Sika Unitherm LSA eco“

# NUMERICAL AND EXPERIMENTAL ANALYSIS OF REACTIVE FIRE PROTECTION SYSTEMS APPLIED TO SOLID STEEL RODS IN TENSION

Dustin Häbler<sup>a</sup>, Sascha Hothan<sup>a</sup>

<sup>a</sup> Federal Institute for Materials Research and Testing (BAM), Division 7.3 – Fire Engineering, Berlin, Germany

## Abstract

The application of intumescent coatings for fire protection of steel constructions is increasing. Thanks to the relative thin thickness of the coatings, the typical visual appearance of the structures can be preserved. In Germany, the applicability of the systems is regulated by the national as well as European technical approvals. According to the approvals, the application on steel members in tension is only allowed with limitations. Especially, the application on solid steel rods in tension is currently not covered. The paper will explain the actual state of the art of the application of reactive fire protection systems applied to steel structures. Physical and technical background information will be provided. After that, the latest scientific results of an on-going research project funded by the German National Institute of Building Technology (DIBt) and conducted by the Federal Institute for Materials Research and Testing (BAM) will be described.

**Keywords:** steel structure, solid rod, tension, fire protection, reactive fire protection systems, structural analysis, finite element method (FEM), experimental testing

## INTRODUCTION

Unprotected steel structures exposed to fire can lose their load-carrying capacity at an early stage due to the relatively rapid heating rate. For steel structures that need to fulfill requirements concerning fire resistance, appropriate protection systems can be used in order to prevent a premature loss of the load-carrying capacity. In case of visible steel constructions, coatings with reactive fire protection systems are often used for architectural reasons. Thanks to the low thickness of the coatings, the visual appearance of the steel structure can be preserved. In case of fire, the increase of temperature causes a chemical reaction of the fire protection system that leads to expansion and the forming of a heat-insulating layer on the surface of the steel structure. This layer reduces the heating rate of the steel and thus delays the reduction in the load-carrying capacity.

Currently, the regulations in the European as well as in the German standards for the application and testing of reactive fire protection systems applied to solid steel members in tension are not adequately regulated. Therefore, a research project with the objective to explore the possibilities for the use of reactive fire protection systems applied to solid steel tension members is carried out at the Federal Institute for Materials Research and Testing (BAM) in Berlin. First results of this research are presented in this paper.

## 1 REACTIVE FIRE PROTECTION SYSTEMS

According to the approval guidelines of the German Institute of Building Technology (DIBt, 1998), reactive fire protection systems can be applied as a coating on steel members to increase the fire resistance. Generally, a system consists of a primer and corrosion protection, a reactive component and a top coating. The reactive component may be an intumescent, an ablation, a sublimation or a combination of these products. The coating materials can be applied in one layer or several layers by spraying, brushing, dipping or in a similar vein.

## 1.1 General regulations

Since reactive fire protection systems are not regulated building and construction types, their application in Germany is based on technical approvals (abZ), European technical approvals (ETA) or approvals on a case-by-case basis (ZiE) (Stopp et al, 2011). In the scope of these approvals released by the DIBt, the use of reactive fire protection systems is defined. The application of reactive fire protection systems are currently limited to open and closed sections. In addition, the application is restricted to steel grades S235 and S355 and a particular range of the section factor  $A_m/V$  (according to ETA) or rather  $U/A$  (according to abZ). Further limitations arise from the maximum possible fire resistance of the individual reactive fire protection system and the static load type for the steel member, i.e. bending, compression or tension. Based on the mentioned criteria, the minimum dry film thickness of the reactive fire protection system that was assessed on the basis of fire tests can be determined. For applications of reactive fire protection systems different from the regulations given in the approvals, a case-by-case permission is required.

## 1.2 Application on tension members

In accordance with the approvals published by the DIBt until December 2010, which are in some cases still valid, the use of reactive fire protection systems on steel members in tension was not in the scope of the approvals and a verification by adequate tests was required. Starting from January 2011, the restrictions for all new approvals were changed in such a way that reactive fire protection systems can be applied also to tension members with open and closed profiles. However, the maximum load utilization factor ( $\mu_{fi}$ ) for the steel member is limited to 0.5 (Hothan, 2011). Tension members with solid cross-section are still excluded from the scope of the approvals (Stopp & Proschek, 2011). Currently a European standard for the implementation of fire tests on tension members with solid cross sections is an on-going works (CEN prEN 13381-10(V1), 2012).

## 1.3 Requirements

According to the approval guidelines of the DIBt, reactive fire protection systems have to fulfill different requirements (DIBt, 1997). These include, among other requirements, a durable effectivity against fire exposure, sufficient adhesion to the steel member and a perfect corrosion protection. Therefore, reactive fire protection systems have to fulfill certain thermal and mechanical requirements. For example, the thermal conductivity must be small enough to slow down the heating rate of the steel in order to keep the strength of the steel as long as possible. The determination of the mechanical and thermal properties of the reactive fire protection system is difficult due to the foaming behaviour. In particular, the adhesion to the steel surface is difficult to describe. Therefore, the adhesion of the reactive fire protection system to the steel (stickability) is considered sufficient when the coating remains on the surface of the steel for the entire length of the fire tests (DIN 4102-2, 1977). Another difficulty results from partially large differences in the behaviour and properties between the different products of the reactive fire protection systems, which makes it difficult to give general statements. Instead of determining the thermal properties of the reactive fire protection system, often the heating rate of the steel is used, which can be determined much easier by measurements (DIN EN 1993-1-2, 2010). The heating rate of the steel basically depends on the gas temperature in the furnace, the section factor of the steel section as well as the thermal properties and thickness of the reactive fire protection system. To determine the material properties of the steel, the heating rate is also important because it affects the creep behavior of the steel.

In contrast to the use of reactive fire protection systems on beams and compression members, other special aspects have to be taken into account for tension members. For instance, it must be verified whether the heating rates that occur for tension members meet the requirements

given in the standard EN1993-1-2 (DIN EN 1993-1-2, 2010) in order to apply the material properties for steel recommended by this standard. Furthermore, circular solid sections are often used for tension members. The cross-sectional curvature and its effect on the adhesion of the reactive fire protection system have to be examined. Another issue for the adhesion results from the elongation of tension member. Moreover, the failure mechanism, i.e. local necking, and the influence of small defects and damages to the reactive fire protection system on the load bearing and deformation behavior of the tension members have to be investigated. Following, the robustness of the entire system can be assessed.

## 2 RESEARCH ON SOLID STEEL RODS IN TENSION

A research project funded by the DIBt and carried out by the BAM aims to develop recommendations and guidelines for the use and testing of reactive fire protection systems applied to solid steel members in tension. The investigation consists of fire tests and numerical simulations based on the finite element method (Hothan & Häßler, 2012).

### 2.1 Experimental Analysis

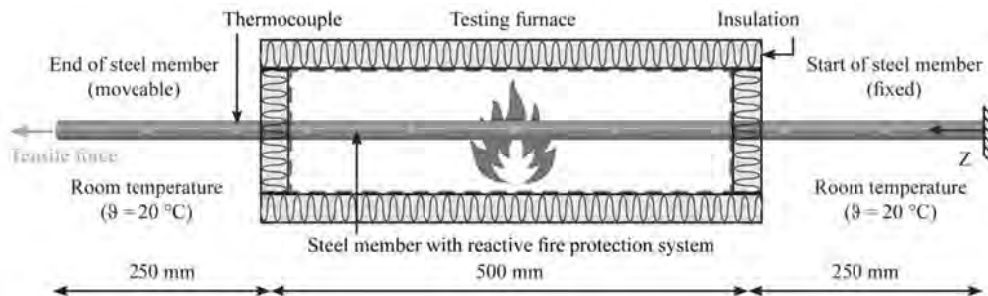


Fig. 1 Schematic experimental setup for the real scale fire tests

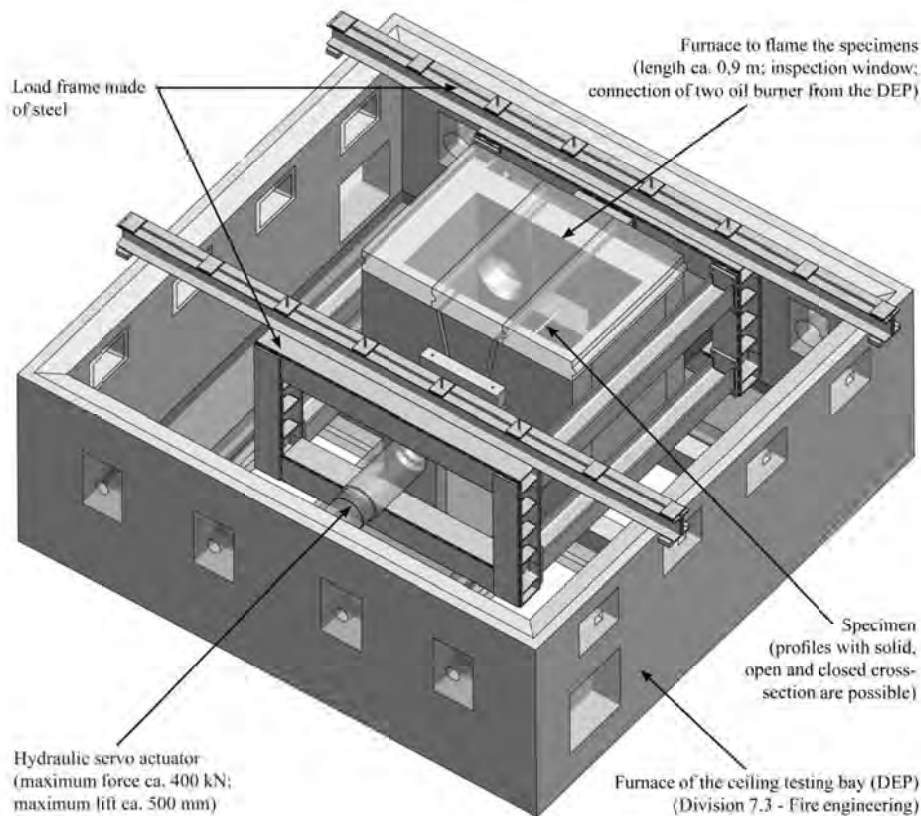


Fig. 2 Detailed experimental setup for the real scale fire tests in the ceiling testing bay of BAM



Currently no studies exist for the use of reactive fire protection systems applied to solid steel tension members. Therefore, appropriate experimental tests as well as numerical analysis will be carried out. For the experimental analysis, real scale fire tests on steel members subjected to tension will be performed at the testing facilities of BAM. The experimental setup is schematically presented in Fig. 1. A reactive fire protection system will be applied and tested on various solid steel sections. Especially, circular cross-sections, which are typically used for tension members, will be analysed. The specimens consist of steel S355. Thermocouples on the surface of the steel specimen are used to measure the temperature during the experiment. In Fig. 2, a detailed 3D-model of the entire testing bay at BAM is presented. In addition to the real scale tests, small scale tensile tests at room and elevated temperatures will be performed in order to characterise the relevant material properties of the steel.

## 2.2 Numerical Analysis

In addition to the fire tests, the applicability of reactive fire protection systems on tension members with solid cross-section will be also analysed by numerical simulations. For this purpose, a numerical model based on the finite element method (FEM) will be developed in order to describe the behaviour of the specimens used in the real scale fire tests. The data obtained in the fire tests will be used as input for the numerical simulation as well as for the validation of the finite element model. Afterwards, the validated numerical model will be used for parametric studies. The aim of the comparison between the experimental and numerical analysis is to develop an appropriate design method for the application of reactive fire protection systems to tension members with solid cross-section.

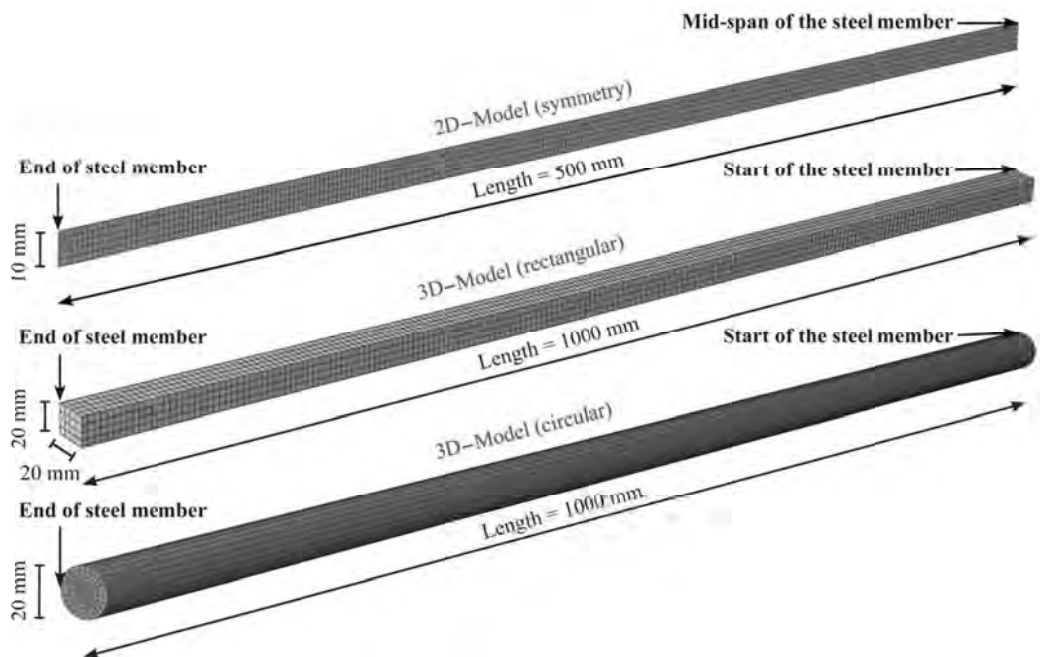


Fig. 3 Overview of the developed numerical models

At the present time, several two and three dimensional finite element models of solid tension members were developed using assumptions in the material properties. In total, there are three models with different cross-sections. Because the small scale tensile tests were not yet carried out in laboratory, as a first assumption the material properties for steel at room and elevated temperatures were assumed according to DIN EN 1993-1-2 (DIN EN 1993-1-2, 2010). An overview of the created FEM models is presented in Fig. 3. The finite element program ABAQUS<sup>®</sup> was used.

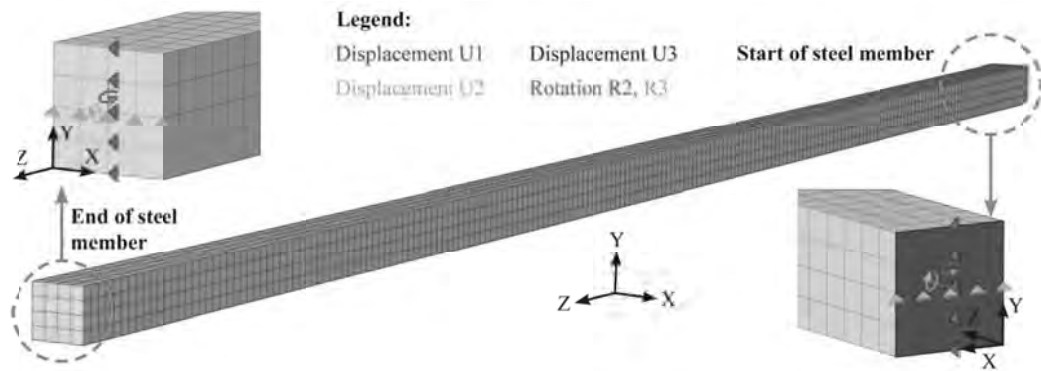


Fig. 4 Example of the applied restraints to the 3D-model with rectangular cross-section

The calculation of the temperatures of the steel resulting from fire exposure (temperature model) is separated from that according to the mechanical behaviour due to the axial load and elevated temperatures (mechanical model). Both models have the same geometry mesh. However, the type of element used in the models is different. For the investigation, time and local variable temperature fields were studied. Because the temperature data from the experiment was not available at the current moment, the steel temperature was assumed to be the same as in the Standard ISO 834 fire curve. After carrying out the real scale real scale fire tests the steel temperature can be taken directly from the measurements of the thermocouples, which are located on the surface of the specimens. As an advantage of this method, it is not necessary to model the difficult foaming process of the reactive fire protection system. One end of the specimen is fixed and the other end can move in longitudinal direction. The axial tensile force is applied at the moveable end of the steel member. In all models, stresses from the applied restraints were minimised. In Fig., the boundary conditions for the 3D-model with rectangular cross-section are presented.

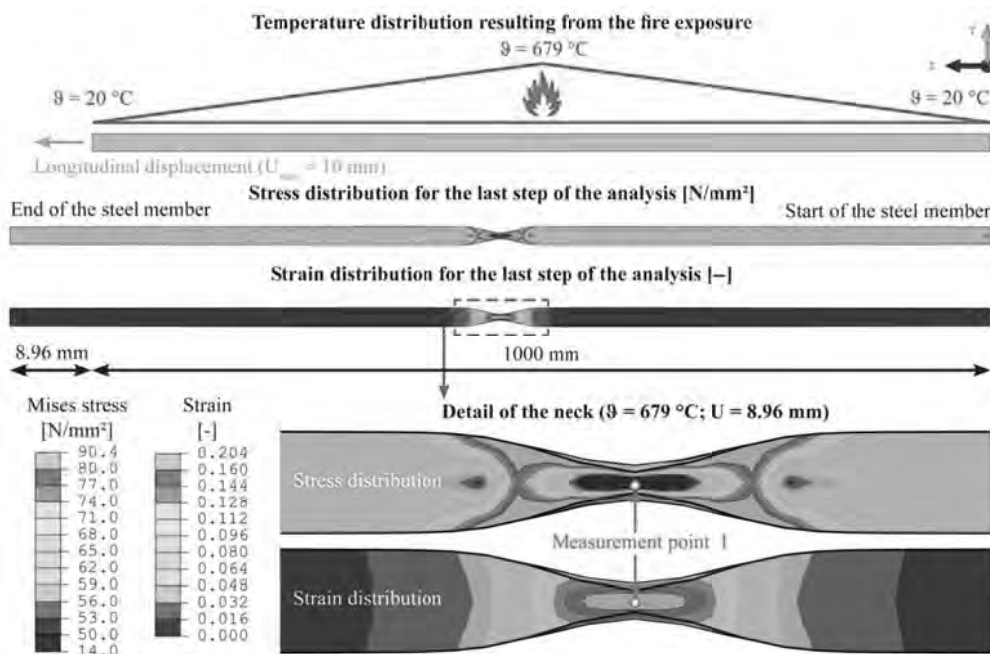


Fig. 5 Stress and strain distribution at the time of failure [last analysis step, scaling factor = 10]

In addition to the magnitude of the loads, the sequence of the loads can be also changed. This allows the simulation of non-stationary ( $\sigma = \text{const.}, \vartheta \neq \text{const.}$ ), as well as stationary ( $\sigma \neq \text{const.}, \vartheta = \text{const.}$ ) tensile tests. In the numerical simulation, the failure of the tension member is emerged by the formation of a neck. Because of its complexity, the fracture mechanism

occurring in reality is not included in the developed numerical models. In the simulation, the process terminates automatically when no more convergence in the calculation can be achieved. Fig. 5 shows the stress and strain distribution of a tensile test at elevated temperatures at the time of failure. After the temperature field resulting from the fire exposure was applied to the steel member, an additional longitudinal displacement started at the end of the specimen (stationary tensile test). The calculation stopped before reaching the maximum displacement of 10 mm due to the high temperatures in the mid-span of the steel member and the resulting low strength of the material. The failure of the specimen is announced by the formation of a neck.

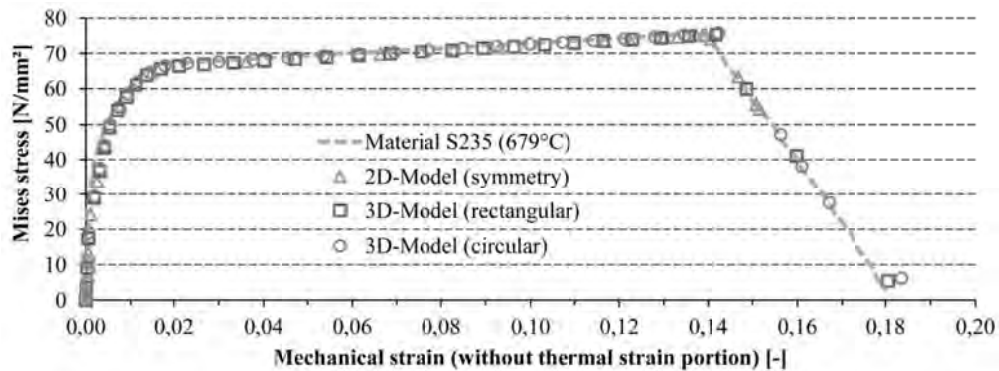


Fig. 6 Stress-strain diagram for measurement point 1

In order to check the three developed numerical models for accuracy, the stress-strain relationship in measurement point 1 was analysed. The corresponding curves are presented in Fig. 6. For all models, the stress-strain curves follow the material behaviour of S235, which was implemented in the numerical models. In addition, it can be noticed that only the 3D-models are capable to display the fracture area up to nearly no stress. The calculation of the 2D-model is already stopped shortly after reaching the maximum stress. To conclude, all developed numerical models are capable to describe the structural behaviour of the steel member subjected to tension and fire exposure.

### 3 SUMMARY

The application of reactive fire protection systems to tension members in Germany is currently only regulated by European and national technical approvals for open and closed profiles. As an additional restriction, the maximum load utilisation factor in the case of fire is limited to  $\mu_{fi} \leq 0.5$ . This corresponds to a load utilisation in the normal design situation of 0.78. The regulations given in the current approval are based on numerical analysis of a comparison between the deformation of bending members and tension members (Hothan, 2011). For higher load utilisation factors and for profiles with solid cross-sections, a use of reactive fire protection systems can only be allowed in an approval on a case-by-case basis, which requires in general additional experimental investigation. In particular, the adhesion of the intumescent coating on the surface of the steel member (stickability) has to be proved. A research project funded by the DIBt and carried out by the BAM aims to develop recommendations and guidelines for the use and testing of reactive fire protection systems applied to solid steel members subjected to tension. The investigation consists of fire tests and numerical simulations based on the finite element method (Hothan & Häßler, 2012). Numerical models have been already created and the first results have been explained in this paper. The models are able to describe the global load-deformation behaviour at elevated temperatures as well as local effects, such as the failure by necking. The appropriate material properties used as input for the numerical analysis will be determined by small scale tensile tests in laboratory. In particular, the effect of different heating and load rates will be studied. Real scale fire tests on unloaded and loaded tension members with reactive fire protection system will be performed to validate the numerical models. Based on the result of the research

project, an extension of the scope of the technical approvals might be possible. The practicability, relevance and expected benefits from the project encourage the possibility of a technical and substantial cooperation of BAM with third parties, especially producers of reactive fire protection systems.

## REFERENCES

- DIBt – Deutsches Institut für Bautechnik, Zulassungsgrundsätze für reaktive Brandschutzsysteme auf Stahlbauteilen, Edition November 1997, DIBt Mitteilungen, issue 4, Ernst & Sohn, 1998.
- Stopp V., Proschek P., Reaktive Brandschutzsysteme auf Stahlbauteilen mit reiner Zugbeanspruchung, DIBt Mitteilungen, issue 42, Ernst & Sohn, 2011.
- CEN – European Committee for Standardisation: Technical Committee CEN/TC 127, prEN 13381-10 (V1), Test methods for determining the contribution to the fire resistance of structural members, Applied protection to solid steel rods, 2012.
- DIN EN 1993-1-2, Design of steel structures, General rules – Structural fire design, DIN e.V., 2010.
- DIN 4102-2, Behaviour of building materials and components in fire, building components, definitions, requirements and tests, DIN e.V., 1977.
- Hothan S., Grundlagen zur Erweiterung des Anwendungsbereiches für reaktive Brandschutzsysteme auf Stahlbauteilen im nationalen Zulassungsverfahren, DIBt Mitteilungen, issue 42, Ernst & Sohn, 2011.
- Hothan S., Häßler D., Zur Anwendung reaktiver Brandschutzsysteme auf Stahlzuggliedern, Bauphysik, issue 6, Ernst & Sohn, 2012.

## **LEAN DUPLEX STAINLESS STEEL MATERIAL TESTS At Elevated Temperatures Using Steady State Method**

Yuner Huang<sup>a</sup>, Ben Young<sup>a</sup>

<sup>a</sup> Department of Civil Engineering, The University of Hong Kong, Pokfulam Road, Pokfulam, Hong Kong, China

### **Abstract**

A test program to investigate the material properties of a relatively new cold-formed lean duplex stainless steel under elevated temperatures is presented. A total of 44 tensile coupon tests were carried out by steady state method for temperatures ranged from 24 to 900 °C. Material properties including Young's modulus, yield strength, ultimate strength and ultimate strain were obtained. The test results and available data were compared with the design values in the European Code as well as a unified equation by Chen & Young for stainless steel. The lean duplex stainless steel is not covered in these existing design rules. It is shown that the material properties of lean duplex stainless steel under elevated temperatures cannot be well predicted by the existing design rules.

**Keywords:** elevated temperatures, fire resistance, lean duplex, material properties, stainless steel, steady state tests

### **INTRODUCTION**

Fire is destructive for stainless steel structures, due to its significantly reduced strength and stiffness under elevated temperatures. Accurate design rules are required to predict the material properties under elevated temperatures, which is important in structural design. Cold-formed lean duplex stainless steel (EN 1.4162), a recently developed high strength stainless steel with a relatively low price, has a great potential to be used in construction. However, little research has been carried out on the material properties of lean duplex stainless steel under elevated temperatures, and this material is not covered in the existing design specifications for stainless steel structures. Therefore, it is necessary to investigate the material properties of cold-formed lean duplex stainless steel.

A test program to investigate the material properties of cold-formed lean duplex stainless steel (EN 1.4162) at elevated temperatures using steady state method is carried out. The test specimens were heated to a specified temperature then imposed tensile stress to the specimens until failure. Tensile coupon tests were conducted for cold-formed lean duplex stainless steel specimens extracted from three different sections, which are under different level of residual stresses due to the cold-forming process. The nominal temperatures used in the test program were ranged from 24 – 900 °C. The test results were compared with the design values by EC3 (2005) and Chen & Young (2006). It should be noted that these two design rules do not cover the lean duplex stainless steel. Therefore, the duplex stainless steel (EN 1.4462) was used for comparison. Reliability analysis was also conducted to assess the design rules for lean duplex stainless steel. It is shown that the EC3 generally provides unconservative prediction, which may lead to an unsafe design of structures, while the unified equation provides generally conservative prediction to lean duplex stainless steel material properties under elevated temperatures.

### **1 STEADY STATE TESTS**

Coupon tests were conducted under elevated temperatures to determine the material properties of the coupon specimens. The specimens were extracted from cold-formed lean duplex stainless steel rectangular hollow sections (RHS) and square hollow section (SHS) with

nominal dimension ( $D \times B \times t$ )  $50 \times 30 \times 2.5$ ,  $50 \times 50 \times 1.5$ , and  $150 \times 50 \times 2.5$ , where  $D$ ,  $B$ ,  $t$  are the depth, width, and thickness in millimetre of the cross-section, respectively. The coupons were taken from the centre of the face at  $90^\circ$  angle from the weld for all specimens. The dimensions of coupon specimens conformed to the Australian Standard AS 2291 (1979) and the American Standard ASTM E 21 (1992) for the tensile testing of metals at elevated temperatures using a 6 mm wide coupon and a gauge length of 25 mm. The location of coupon and weld in cross-section as well as dimensions of the coupon specimens are shown in Fig. 1.

The test set-up is shown in Fig. 2. An MTS testing machine was used to conduct the coupon tests. The MTS high temperature furnace with a maximum temperature of  $1400^\circ\text{C}$  was used to specify the required temperatures during testing, with an accuracy of  $1^\circ\text{C}$ . There are six heating elements located at the upper, middle and lower part of each side of the furnace. Three internal thermal couples were located inside the furnace to measure the air temperature, and one external thermal couple was attached on the specimen surface to measure the temperature of the specimen. The calibrated extensometer of 25 mm gauge length with the range limitation of  $\pm 2.5$  mm was mounted onto the specimens to measure the longitudinal strain during the tests. For specimens with large deformation under high temperatures, the strain may exceed the range limit of the extensometer. The extensometer was reset manually when it approached approximately 80% of the range limit during testing to avoid any damage to the apparatus.

In the steady state tests, a specimen is heated up to a specified temperature and then loaded until it fails. The temperature is maintained when the tensile load is applied during testing. Coupons extracted from each hollow section are loaded under 10 different nominal temperatures from 24 to  $900^\circ\text{C}$  with an interval of  $100^\circ\text{C}$ . Firstly, the lower end of the specimen is free to expand during the heating process until it reaches the specified temperature. When the temperature on the specimen, which is measured by the external thermal couple, is stabilized at the specified temperature for 10 minutes, the lower end of the specimen is then gripped. Secondly, tensile load is applied to the specimen by displacement control with a constant loading rate of  $0.5$  mm/min until it fails. The strain rate of the tests measured by the extensometer conformed to the Australian Standard AS 2291 (1979) and American Standard ASTM E 21 (1992). A total of 44 coupon specimens were tested using steady state method.

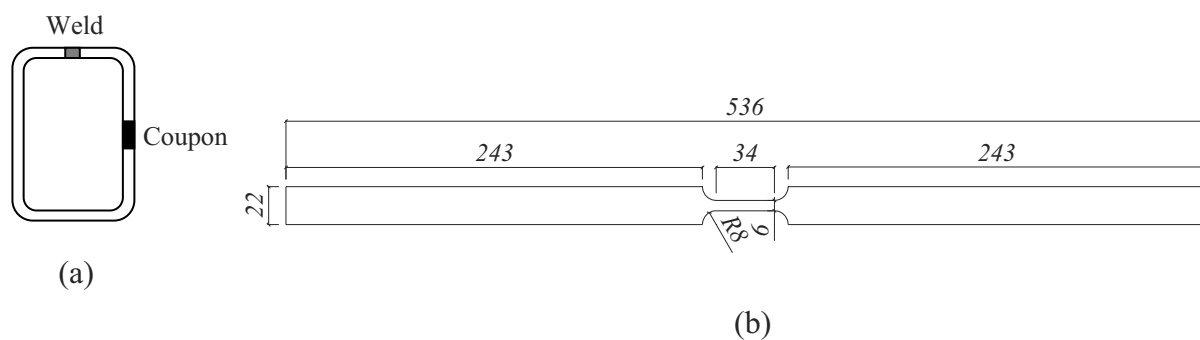


Fig.1: (a) Location of coupon and weld in hollow section (b) Dimensions of coupon specimens

## 2 TEST RESULTS

The material properties measured at room temperature including Young's modulus ( $E_o$ ), 0.2% yield strength ( $f_y$ ), which is also known as the 0.2% proof stress, ultimate tensile strength ( $f_u$ ), elongation at ultimate strength ( $\epsilon_u$ ) and fracture ( $\epsilon_f$ ) of a gauge length of 25 mm, and the Ramberg-Osgood parameter ( $n$ ) using the Ramberg-Osgood expression  $n = \ln(0.01/0.2)/\ln(f_{0.01}/f_y)$  are summarized in Tab. 1. The 0.2% yield strength and 0.01% stress ( $f_{0.01}$ ) are the intersection points on the stress-strain curve, which are the proportional lines off-set by 0.2% and 0.01% strains, respectively. It is well known that the material properties

reduce as the temperature increases. The reduction factors of Young's modulus ( $E_T/E_o$ ), 0.2% yield strength ( $f_{y,T}/f_y$ ), ultimate strength ( $f_{u,T}/f_u$ ) and ultimate strain ( $\varepsilon_{u,T}/\varepsilon_u$ ) determined from the ratio of material properties under elevated temperatures to those at room temperature are shown in Fig. 3. Some specimens were failed outside the measuring range of the extensometer, and therefore the ultimate strains for these specimens are not reported. The actual specimen temperature was obtained by the average value of the specimen temperatures measured by the external thermal couple at the beginning, middle and the end of each test. The actual specimen temperatures are close to the nominal temperatures with the maximum difference of 6.6%. The reduction factors of Young's modulus ( $E_T/E_o$ ), 0.2% yield strength ( $f_{y,T}/f_y$ ), ultimate strength ( $f_{u,T}/f_u$ ) and ultimate strain ( $\varepsilon_{u,T}/\varepsilon_u$ ) are plotted against the actual specimen temperatures in Figs 3(a), (b), (c), (d), respectively.

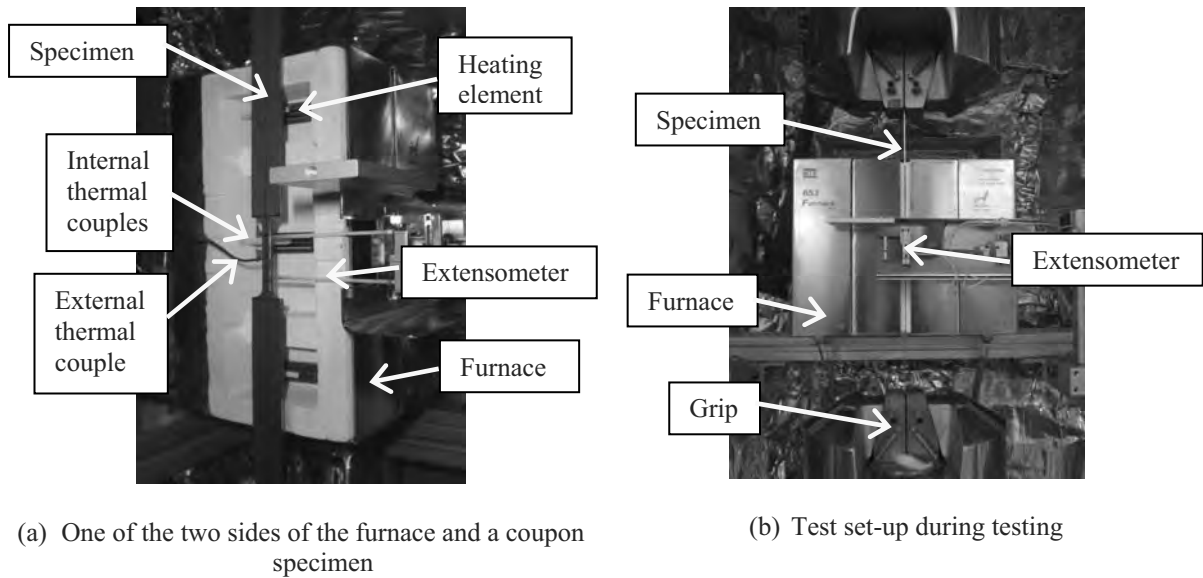


Fig. 2: Typical test set-up of a coupon specimen

Tab. 1 Material properties obtained from coupon tests at room temperature

Specimen	$T$ (°C)	$E_o$ (GPa)	$f_y$ (MPa)	$f_u$ (MPa)	$\varepsilon_u$ (%)	$\varepsilon_f$ (%)	$n$
50×30×2.5T24	24.6	203	722.1	829.7	16.4	27.2	5.9
50×50×1.5T24	24.2	199	682.4	828.1	21.5	30.6	6.4
150×50×2.5T24	25.0	199	693.0	830.4	21.7	33.0	6.9

### 3 COMPARISON OF TEST RESULTS WITH DESIGN PREDICTIONS

A total of 11 data of the reduction factors of 0.2% yield strength (0.2% proof stress) and ultimate strength for lean duplex stainless steel sheets under transient state tests were reported by Gardner et. al. (2010). Test results of lean duplex stainless steel material properties under elevated temperatures obtained from this study and the available data are compared with design values by European Code (2005) and unified equations (Chen & Young, 2006). For the European Code, the reduction factors of Young's modulus, 0.2% yield strength and ultimate strength under elevated temperatures for various stainless steel grades are provided in Tab. C.1 of the Code. However, the lean duplex stainless steel of Grade 1.4162 is not covered by the Code. Therefore, the reduction factors of duplex stainless steel (EN 1.4462) are used to compare with the test results to assess its suitability for lean duplex stainless steel (EN 1.4162). The reduction factors in European Code are provided for discrete temperatures only, thus linear interpolation was required to obtain the reduction factors corresponding to the actual temperatures on the test specimens. Chen & Young (2006) proposed four unified equations to predict the reduction factors of Young's modulus, 0.2% yield strength, ultimate

strength and ultimate strain for stainless steel under elevated temperatures. Two sets of coefficients are calibrated for stainless steel types EN 1.4462 (Duplex) and EN 1.4301 (AISI 304). The unified equations with coefficients for stainless steel type EN 1.4462 (Duplex) are used to compare with the test results in this study and the available data, in order to assess its suitability for lean duplex stainless steel.

The reliability of the design rules to predict the lean duplex stainless steel material properties under elevated temperatures was evaluated using reliability analysis, which is detailed in the Commentary of the ASCE (2002). However, target reliability index ( $\beta_0$ ) and the resistance factor ( $\phi_0$ ) for stainless steel material property are not suggested by the design specification. Therefore, the target reliability index of 2.50 for stainless steel material property is adopted in this study. The resistance factors of the two design rules corresponding to this target reliability index 2.50 are calculated by Eq. 6.2-2 of the ASCE Specification (2002). The load combinations of 1.35DL+1.5LL and 1.2DL+1.6LL, as specified in the EC3 (2005) and ASCE (2002) respectively, were used in calculating the resistance factors ( $\phi_0$ ) for EC3 and the unified equations (Chen & Young, 2006), where DL = dead load and LL = live load. For the purpose of direct comparison, a load combination of 1.2DL + 1.6LL as specified in the ASCE was used to calculate the resistance factors ( $\phi_l$ ), as shown in Tab. 2.

The reduction factors of Young's modulus of the test specimens under elevated temperatures are compared with those predicted by EC3 (2005) and unified equation for Young's modulus (Chen & Young, 2006) for duplex stainless steel of Grade EN 1.4462. The comparison of the reduction factors are shown in Tab. 2 and Fig. 3(a), where  $k_{E,Test}$ ,  $k_{E,EC3}$ , and  $k_{E,Chen\&Young}$  are the reduction factors of Young's modulus obtained from the test results, prediction values by EC3 and prediction values by the unified equation, respectively. It is observed that the predictions by EC3 are unconservative for the test specimens, which may lead to an unsafe design. However, the unified equation provides quite conservative and scattered predictions to the Young's modulus of lean duplex stainless steel under elevated temperatures. It is found that these two design rules cannot provide accurate predictions of Young's modulus for lean duplex stainless steel under elevated temperatures, and thus further research on this topic is required.

The reduction factors of yield strength of the test specimens and the available data under elevated temperatures are also compared with the design values by the two design rules, as shown in Tab. 2 and Fig. 3(b), where  $k_{y,Test}$ ,  $k_{y,EC3}$ , and  $k_{y,Chen\&Young}$  are the reduction factors of 0.2% yield strength obtained from the test results, prediction values by EC3 and prediction values by the unified equation for yield strength (Chen & Young, 2006), respectively. Once again, the EC3 is unconservative in predicting the reduction factors of 0.2% yield strength of lean duplex stainless steel under elevated temperatures. On the other hand, the predictions by the unified equation for yield strength provide a conservative prediction. The mean value of  $k_{y,Test}/k_{y,Chen\&Young}$  equals to 1.02, with the COV of 0.203. The target reliability of 2.50 can be achieved by adopting the resistance factor of 0.75. It is shown that the unified equation is generally capable to predict the reduction factor of yield strengths of lean duplex stainless steel under elevated temperatures, by adopting the resistance factor of 0.75.

Comparison between the reduction factors of ultimate strength of the test specimens and the available data with the design values are shown in Tab. 2 and Fig. 3(c), where  $k_{u,Test}$ ,  $k_{u,EC3}$ , and  $k_{u,Chen\&Young}$  are the reduction factors of ultimate strength obtained from the test results, prediction values by EC3 (2005) and prediction values by the unified equation for ultimate strength (Chen & Young, 2006). It is shown that the predictions by both design rules are generally unconservative. Therefore, it is recommended that further research should be carried out for lean duplex stainless steel ultimate strength under elevated temperatures.

Chen & Young (2006) proposed an equation to predict the reduction factor of ultimate strain ( $\epsilon_{u,T}/\epsilon_u$ ) for duplex stainless steel EN 1.4462. Such predictions are compared with the test results, as shown Fig. 3(d). The design rule provides a generally conservative prediction to the reduction factor of the ultimate strain of the lean duplex stainless steel under elevated



temperatures. Therefore, the design equation for duplex stainless steel (EN 1.4462) is also recommended for lean duplex stainless steel (EN 1.4162) in predicting the ultimate strain under elevated temperatures.

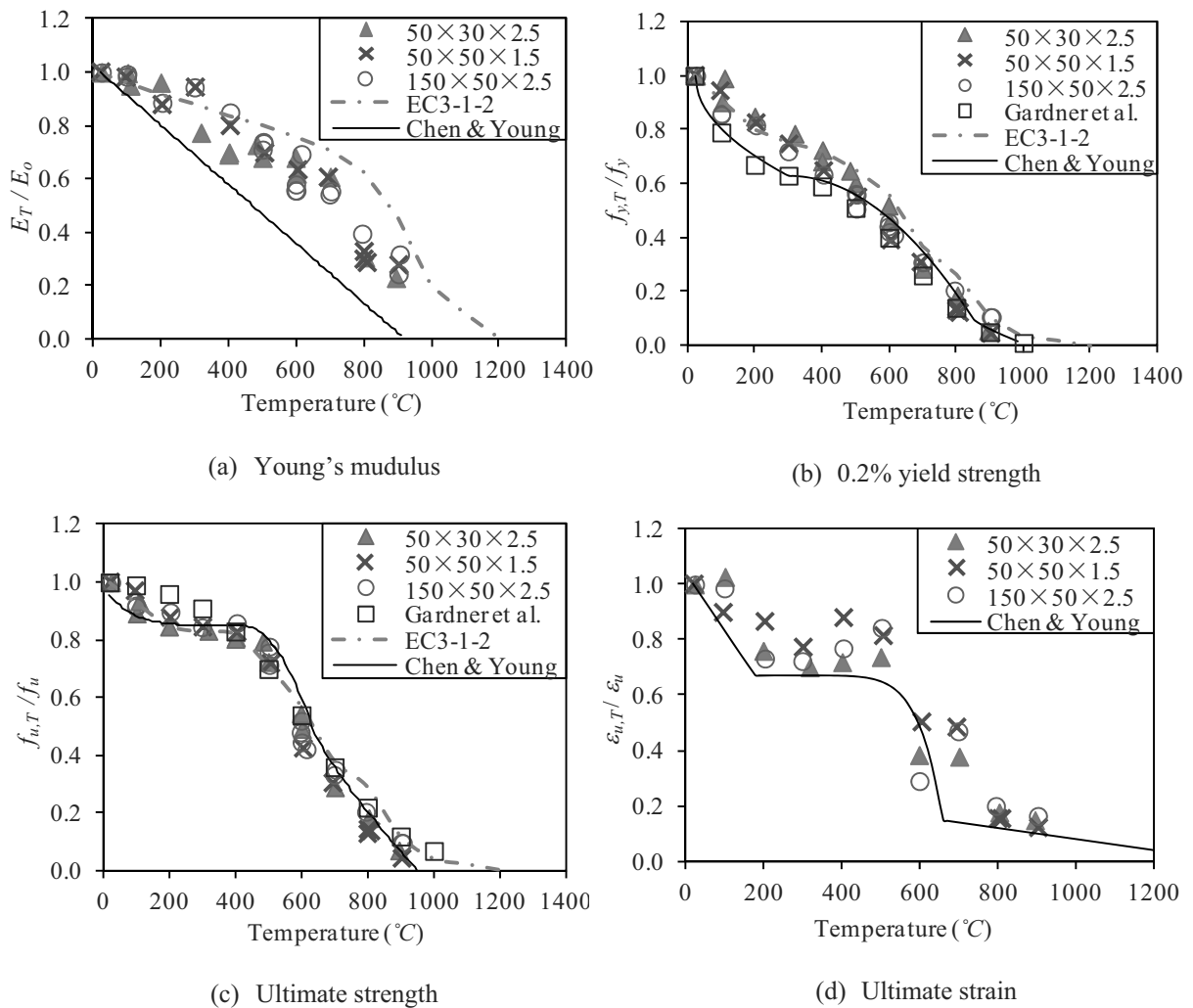


Fig. 3: Comparison of material properties obtained from design rules and test results

Tab. 2 Material properties obtained from coupon tests at room temperature

	$\frac{k_{E,Test}}{k_{E,EC3}}$	$\frac{k_{E,Test}}{k_{E,Chen\&Young}}$	$\frac{k_{y,Test}}{k_{y,EC3}}$	$\frac{k_{y,Test}}{k_{y,Chen\&Young}}$	$\frac{k_{u,Test}}{k_{u,EC3}}$	$\frac{k_{u,Test}}{k_{u,Chen\&Young}}$
	# of data	44	44	55	55	55
Mean ( $P_m$ )	0.84	1.60	0.85	1.02	0.90	0.87
COV ( $V_p$ )	0.209	0.318	0.193	0.203	0.200	0.186
Resistance factor ( $\phi_o$ )	0.59	0.95	0.61	0.75	0.68	0.70
Reliability index ( $\beta_o$ )	2.50	2.50	2.50	2.50	2.50	2.50
Resistance factor ( $\phi_I$ )	0.61	0.95	0.64	0.75	0.71	0.70
Reliability index ( $\beta_I$ )	2.50	2.50	2.50	2.50	2.50	2.50

#### 4 CONCLUSIONS

An experimental investigation of material properties of lean duplex stainless steel at elevated temperatures has been presented. The test specimens are extracted from three square and rectangular hollow sections of type EN 1.4162. Coupon tests using steady state method at different temperatures ranging from 24 to 900 °C were conducted. Material properties

including Young's modulus, yield strength, ultimate strength and ultimate strain under elevated temperatures were obtained. The test results obtained in this study together with available data were compared with design values by current design rules. It is shown that the ultimate strain of lean duplex stainless steel under elevated temperatures can be well predicted using the unified equation proposed by Chen & Young (2006), in which the lean duplex stainless steel material was not covered by the proposed equation. It is also shown that the EC3 provides generally unconservative predictions to the Young's modulus, yield strength and ultimate strength. The unified equations provide quite conservative predictions for Young's modulus, conservative predictions for yield strength, but unconservative predictions for ultimate strength. It is apparently shown that the current design rules are generally inappropriate to be used for lean duplex stainless steel under elevated temperatures. It is suggested that further research is required for lean duplex stainless steel under elevated temperatures for both steady and transient state tests.

## **5 ACKNOWLEDGEMENTS**

The authors are grateful to STALA Tube Finland for supplying the test specimens. The authors are also thankful to Mr. Kwai-Mo Tse for his assistance in the experimental program as part of his final year undergraduate research project the The University of Hong Kong. The research work described in this paper was supported by a grant from the Research Grants Council of the Hong Kong Special Administrative Region, China (Project No. HKU718612E).

## **REFERENCES**

- EC3, Design of steel structures – Part 1-2: General rules – Structural fire design. European Committee for Standardization, CEN, 2005.
- Chen J., Young B., Stress-strain curves for stainless steel at elevated temperatures, *Engineering Structures* 28(2): 229-39, 2006.
- AS 2291, Methods for the tensile testing of metals at elevated temperatures, Australian Standard, Standard Association of Australia, Australia, 1979.
- ASTM E 21, Standard test methods for elevated temperature tension tests of metallic materials, American Society for Testing and Materials, West Conshohocken, USA, 1992.
- Gardner L., Insausti A., Ng K. T., Ashraf M., Elevated temperature material properties of stainless steel alloys, *Journal of Constructional Steel Research* 66(5): 634-47, 2010.
- ASCE, Specification for the design of cold-formed stainless steel structural members, SEI/ASCE 8-02, American Society of Civil Engineers, Reston, VA, 2002.

# MECHANICAL PROPERTIES OF SELF-COMPACTING CONCRETE WITH DIFFERENT MINERAL ADITIVES AFTER HIGH TEMPERATURE EXPOSURE

Marija Jelcic Rukavina <sup>a</sup>, Dubravka Bjegovic <sup>a</sup>, Ivan Gabrijel <sup>a</sup>

<sup>a</sup> University of Zagreb, Faculty of Civil EGINEERING, Zagreb, Croatia

## Abstract

This paper presents an experimental research on the performance of high-strength self-compacting concrete (SCC) with different mineral additives after exposure to high temperature of up to 600°C. For this purpose, four SCC mixtures were studied: one reference and three mixtures where the Portland cement was replaced with mineral additive (fly ash, metakaolin and limestone) in certain proportions. After natural cooling in the furnace, compressive strength and static modulus of elasticity were determined and compared to results obtained from other studies and those provided in EN 1992-1-2 and EN 1994-1-2 for normal-vibrated concrete. Additionally, in order to characterize the damage of the specimens caused by high temperatures, AE parameters during compression test of heated and unheated specimens were also obtained.

**Keywords:** self-compacting concrete, high temperature, metakaolin, fly ash, limestone

## INTRODUCTION

Self-compacting concrete (SCC) is a special type of high performance concretes that fill the formwork with its own weight without need for vibration. There is trend for its increased use in the structural applications, because of the many benefits of SSC compared to conventional concrete. Although SCC consists of the same components as normal and high - strength types of concrete, higher amounts of powder materials are necessary to obtain satisfactory stability of the mixture. For that purpose usually pozzolanic or filler materials such as fly ash, granulated ground blast furnace slag, metakaolin, limestone powder etc. are used. Thus, compared to traditional normal vibrated concrete, increased paste volume and specific placing condition can modify SCC properties on ambient and high temperature.

Although concrete is considered as an excellent thermal-resistant material among various construction materials, high temperature cause physical and chemical changes that result in deterioration of concrete mechanical and thermal properties (Bazant and Kaplan, 1996). Up to now, results of the influence of high temperature on the properties of SCC are rather limited, but show behaviour similar to that of normal-vibrated concrete with increased risk of spalling (Persson, 2004; Bamonte & Gambarova, 2012).

In order to help better characterisation of the performance of SCC mixtures after exposure to high temperature, this preliminary study is focused on testing of mixtures with similar compressive strength where part of Portland cement is replaced with different mineral additive.

## 1 EXPERIMENTAL PROGRAM

Experimental program includes determination of following residual concrete properties of SCC obtained by uniaxial loading

- compressive strength,
- static modulus of elasticity,

- AE parameters during compression tests,

before exposure to high temperatures and immediately after cooling down to the ambient temperature. In addition, weight loss and ultrasonic pulse velocity tests were also obtained before and after high temperature exposure.

### 1.1 Concrete mixtures composition

Details of studied concrete mixtures are given in Tab. 1. All mixtures were designed in accordance to CBI method developed in Sweden (Billberg 2002). CEM I 42.5 R and dolomite powder were used for all mixtures. In addition, the mineral additives, namely fly ash (FA), metakaolin (MK) and limestone (LF) were used as a partial replacement of cement by weight as indicated in Tab. 1. The fine and coarse aggregate used was dolomite aggregate with a nominal maximum size of 16 mm. Constant powder quantity ( $670 \text{ kg/m}^3$ ) and constant water-powder ratio ( $w/p=0,27$ ) were selected for all mixtures, in which the powder content,  $p$ , is defined as the sum of the cement, mineral additive and dolomite filler content. All concrete mixtures were designed to give slump flow of  $700 \pm 50$  mm which was achieved by using the superplasticizer based on polycarboxylic ether polymers and viscosity modifying agent at amounts as indicated in Table 1. Other fresh properties required for SCC mixtures were also examined in order to guarantee a good flowability, workability and segregation resistance of studied mixtures according to HRN EN 206-9. The actual compressive strength and static modulus of elasticity at ambient temperature, indicated in Table 1, is the average of three tests on identical cylinders ( $\emptyset/L = 75/225$  mm where the variability of each mix was limited to  $\pm 2$  MPa or 2 GPa respectively.

Tab. 1 Concrete mixture proportioning for  $1 \text{ m}^3$

Mix ID	M1 - ref	M2 (MK5)	M3 (FA30)	M4 (LF10)
Cement, <i>kg</i>	450	427,5	315	405
Metakaolin (5% c.w), <i>kg</i>	-	22,5	-	-
Fly ash, (30% c.w), <i>kg</i>	-	-	135	-
Limestone, (10 % c.w.), <i>kg</i>	-	-	-	45
Dolomite filler, <i>kg</i>	220	220	220	220
Water, <i>l</i>	180	180	180	180
w/c	0,40	0,42	0,57	0,44
Fine aggregate, <i>kg</i>	862	862	862	862
Coarse aggregate, <i>kg</i>	696	696	696	696
SP, <i>l</i>	5,6	4,5	3,6	4
VMA, <i>l</i>	0,7	0,7	0,7	1,0
Hardened concrete properties				
Compressive strength, <i>MPa</i>	83,5	85	82	69,5
Static modulus of elasticity, <i>GPa</i>	48	47	44	46

Prepared specimens for high temperature exposure were also cylinders with dimensions of  $\emptyset = 75$  mm and  $L = 225$  mm (i.e. with slenderness equal to 3). All specimens were demoulded one day after casting and were kept at a temperature of  $20 \pm 3^\circ\text{C}$  and relative humidity of 95% in a curing room for another 27 days. Then the specimens were moved to the ordinary environmental conditions ( $T=15\text{-}25^\circ\text{C}$ ; R.H. = 50-70%) until testing. Testing programme was initiated at an age of more than 180 days.

### 1.2 Testing

Temperature exposure and procedure of testing followed recommendations of the RILEM Technical Committee TC-129. The specimens were subjected to three different temperature

cycles up to 200°C, 400°C and 600°C in an electrical furnace ( $T_{\max} = 1000^{\circ}\text{C}$ ). The temperature 600°C was chosen as maximum because above this temperature decarbonation occurs and mechanical properties of concrete usually rapidly decrease. The first part of the temperature cycle consisted of heating rate  $\Delta T/\Delta t$  of 2°C/min (inside the furnace) up to target temperature in order to avoid dangerous self-stresses. After that, the temperature was kept constant until steady-state thermal conditions throughout the specimens were ensured, while the last part of the cycle consisted of a slow cooling down to ambient temperature in closed furnace in order to avoid thermal shock. Specimens were tested immediately after cooling down to ambient temperature. For each temperature cycle, eight cylindrical specimens were used where one specimen was equipped with NiCr thermocouples monitoring temperature evolution, surface and centre temperature, according to mentioned RILEM recommendations. No spalling of the specimens was observed which can be attributed to slow heating rate as also as low moisture content of the specimens. Compressive strength and modulus of elasticity were tested using hydraulic Toni Technik testing machine with 3000 kN capacity and speed of applied load of 0,5 MPa/s. Elastic modulus is measured between 0,5 MPa and 1/3 of ultimate compressive strength. Ultrasonic pulse velocity measurement were determined using commercial device of Proceq company (Tico), while weight losses were determined by weighing specimens with precision balance. Acoustic emission system consisted of resonant R6 sensor from Physical Acoustics Corporation (PAC), 8 channel  $\mu$ -disp unit and a PAC 1220 preamplifier. Studied initial and residual concrete properties were expressed as the mean value of three measurements per each temperature.

## 2 RESULTS AND DISCUSSION

### 2.1 Compressive strength

Fig. 1a) and b) show the results of relative residual compressive strength vs. temperature of the studied concrete along with models proposed by EN 1992-1-2, EC2, for high-strength normal-vibrated concretes, EN 1994-1-2, EC 4, for carbonate normal-vibrated concrete aggregate concretes and results obtained by two other study based on testing SCC concretes with limestone filler (Persson 2004; Bamonte and Gambarova 2012).

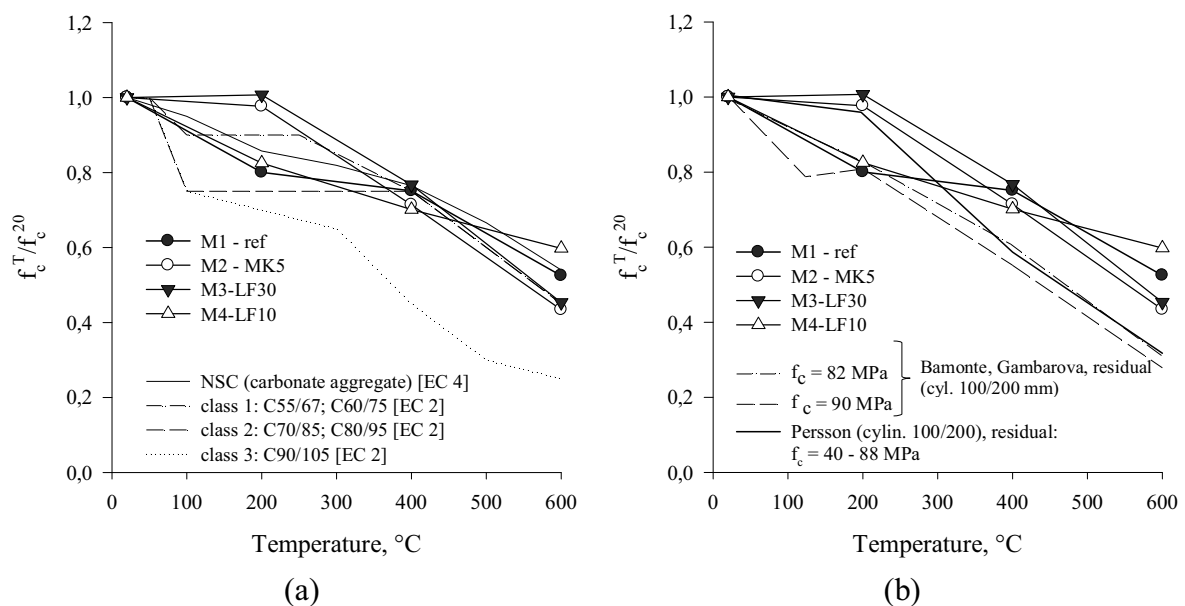


Fig. 1 Plots of the residual compressive strength vs. temperature: a) this study and models in EC2 and EC4 and b) this study and results in Persson, 2004 and Bamonte 2012

From the figures, it is visible that there are two important stages in residual strength-temperature relationship: 1) 0-200°C with negligible strength loss up to 2% for mixtures with metakaolin, M2, and fly ash, M3, on one side, and reference mixture, M1, and mixture with limestone, M4, on the other side with strength loss of 20 and 18% respectively and 2) 200 – 600°C with permanent strength loss. In the later, mixtures M2 and M3 show sharp loss up to temperature of 400°C, at point which all mixtures have similar relative residual compressive strength (from 70% for M1 to 77 % for M3). Positive influence of fly ash in the whole temperature range and metakaolin up to 200°C on the residual strength is in line with results obtained for normal-vibrated concrete with the same mineral additives in (Poon et al, 2003; Xu et al, 2001). Relating proposed models in EC2 and EC4, results obtained within mixtures M1 and M4 are in good agreement with that proposed with EC 4 for carbonate aggregate in the whole temperature range, while results of M1 and M4 follow it at higher temperature, 400-600°C. Results of all mixtures are in good agreement with the models proposed in EC2 for class 1 and 2 in the temperature range 400 – 600°C. Relating comparison to other studies presented at Fig. 1b) the agreement is satisfactory in the temperature range 0 – 200°C, while at higher temperatures, results of other studies are lower which can be attributed to aggregate type (crushed gneiss and gravel in Persson` s study and river gravel in Bamonte`s study).

## 2.2 Modulus of elasticity

Fig. 2a) and b) show the results of relative residual modulus of elasticity vs. temperature. Results obtained in this study show that all mixtures have very similar trend of loss no matter which mineral additive were used in the mixture.

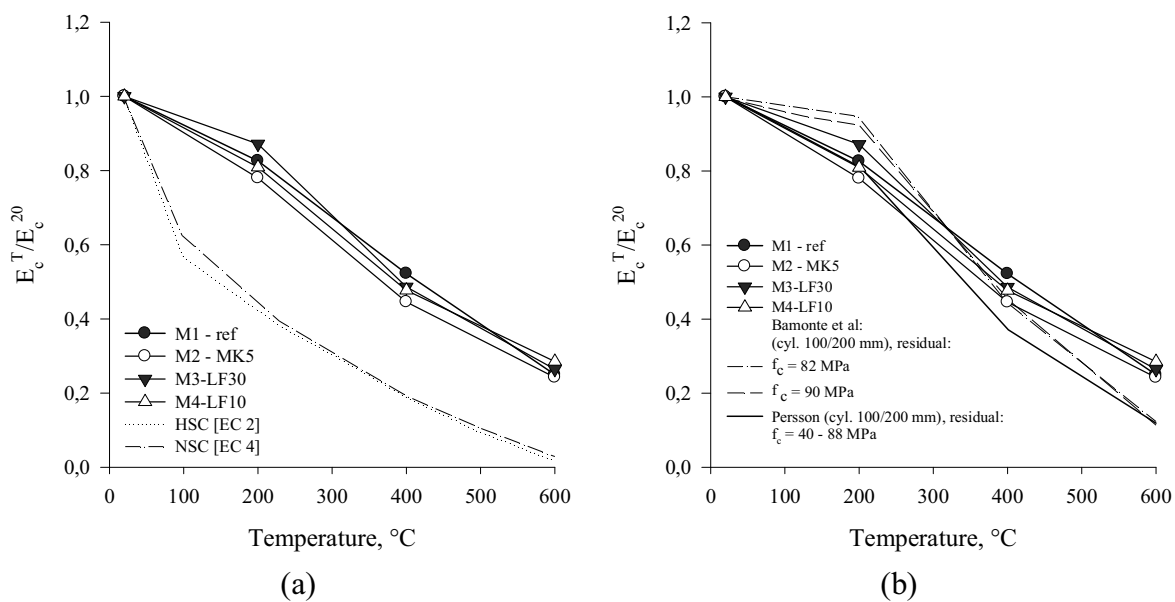


Fig. 2 Plot of the relative secant modulus of elasticity vs. temperature: a) this study and models in EC2 and EC 4 and b) this study and results in Persson, 2004 and Bamonte 2012

Large discrepancy exists between the experimental results and the values obtained from the initial point of stress-strain curves in EC-s (Fig. 2a), because the stress-strain curves from EC implicitly account for additional strains occurring during first heating of concrete, i.e. transient thermal creep, which is beyond the scope of this study. There is good agreement between results obtained in this study and results obtained in other studies presented in Fig. 2b.

### 2.3 Ultrasonic pulse velocity and mass loss

The weight losses of the SCC mixtures with increasing temperatures are given in Fig. 3 which show that evolution of the weight losses versus temperature is very close for all studied concrete mixtures.

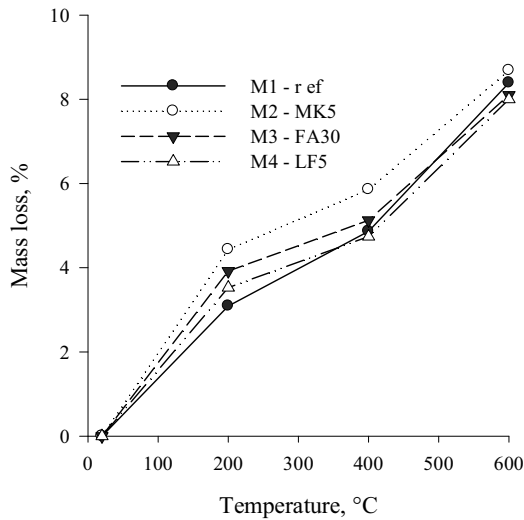


Fig. 3 Plot of mass loss vs. temperature

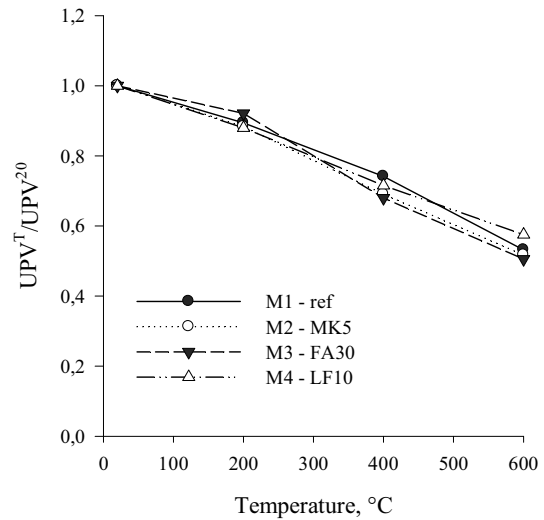


Fig. 4 Plot of UPV vs. temperature

At around 120°C only a small amount of water escaped from the specimens, but at the 200°C the mass loss is up to 4,5 % (for mixture M3). Fig. 4 presents the results of the relative residual pulse velocities as a measure of the extent of deterioration of the concrete microstructure. As for modulus of elasticity, it can be concluded that the studied types of concrete have very similar decrease in UPV no matter which mineral additive is used in the particular mixture.

### 2.4 AE measurement

On Figs. 5a) – d) the relative signal strength of AE is plotted against relative stress applied during compression tests of the specimens heated to different high temperatures. AE parameter signal strength represents area under rectified waveform or more generally it represents energy released during crack propagation. Results presented are average values obtained on three specimens with AE sensor positioned on side of cylindrical specimens during compression test.

From presented figures, it can be seen that, apart for temperature 400°C, all studied mixtures have almost the same relationship relative signal strength-relative stress. After exposure to temperature of 400°C, this relation is different for different mixtures where the highest values of relative signal strength were obtained for mixture with fly ash, M3, which, in the same time, have the highest value of the residual strength (77%), Fig.1. For other studied mixtures, also can be stated that relationship relative signal strength-relative stress follow the values of the residual strength after exposure to 400°C. These preliminary observations need further detailed research in the next step of the study, but certainly represent good tool for identifying exposure temperature in dependence of the proposed relationship.

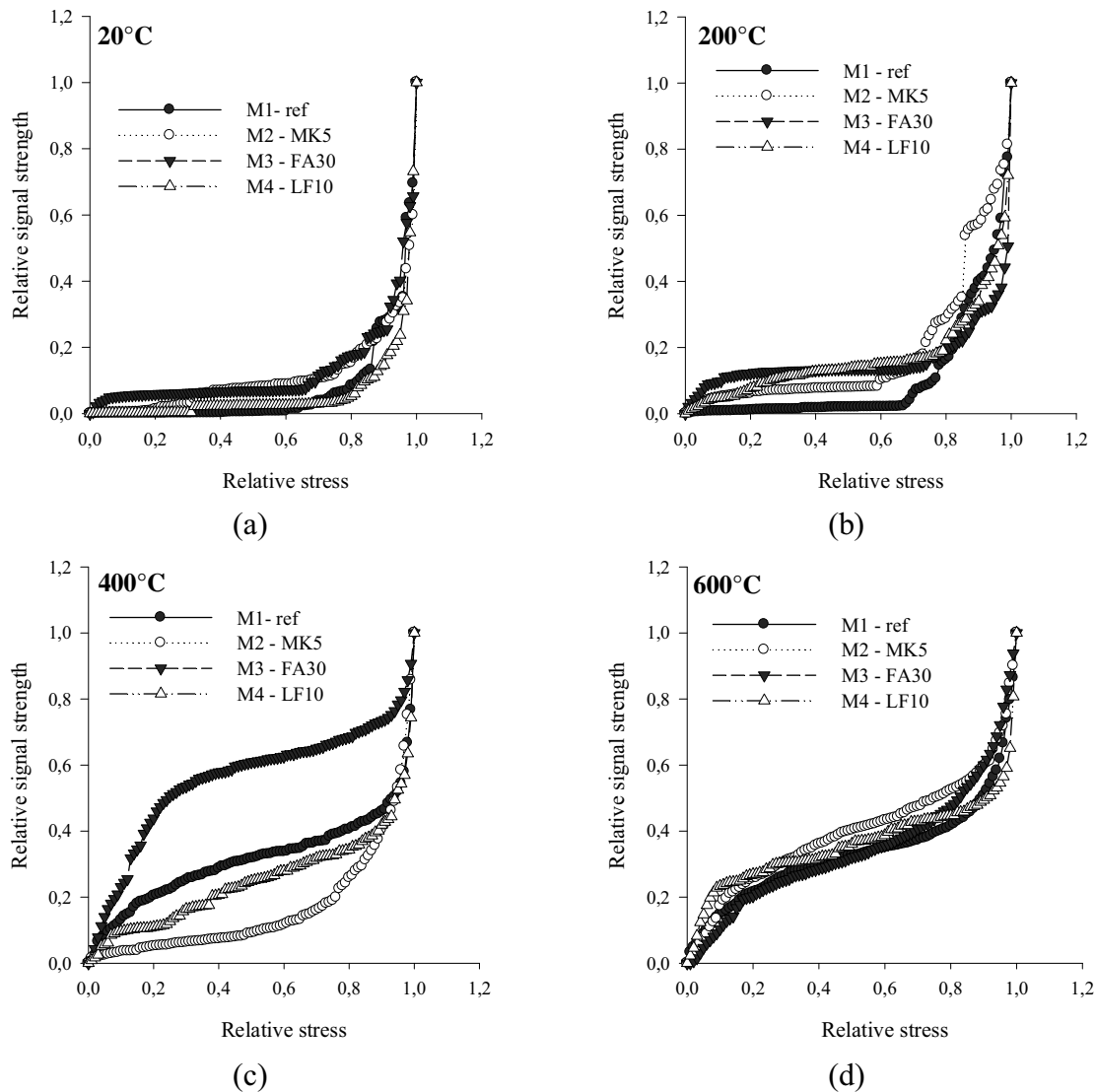


Fig. 5 Plot of relative signal strength vs. relative stress obtained during compression tests of the specimens: a) at ambient temperature, b) after heated to 200°C; c) after heated to 400°C; d) after heated to 600°C

### 3 CONCLUSIONS

The following conclusions may be stated on the basis of the results obtained in this study:

- Mineral additives have great influence on the residual compressive strength between ambient temperature and 400°C; at temperatures above 400°C, the decrease of the residual compressive strength is similar for all studied mixtures and is in good agreement with the model proposed of EC 4 for normal-vibrated calcareous aggregate concretes.
- Higher temperatures have more influence on the residual modulus of elasticity compared to the compressive strength; related to different mineral additives, results show that they have not significant effect on modulus, because all studied mixture show almost the same trend of decrease in dependence of the applied temperature.
- As for residual modulus of elasticity, there is very similar trend in decrease of residual UPV for all studied mixtures which indicates that mineral additive has no particular effect on the residual UPV.
- In order to withdraw general conclusions about the influence of the different mineral additives in concrete mixtures on mechanical properties of self-compacting concrete after exposure to high temperatures (compressive strength and modulus of elasticity, in



particular) there is need for further research with mixtures containing different percentage of each mineral additive. This research is currently underway.

- Preliminary results of AE parameters (signal strength in particular) obtained during compression test of specimens after heating to high temperatures show good tool for identifying exposure temperature of the concrete needed for assessment of concrete structures after fire.

## REFERENCES

- Bamonte P., Gambarova P.G., A study on the mechanical properties of self-compacting concrete at high temperature and after cooling. *Materials and Structures* 45, 2012.
- Bazant Z. P., Kaplan M. F., *Concrete at high temperatures: materials properties and mathematical models*. Longman Group Limited, 1996.
- Billberg P., *CBI Mix Design Model for Self-Compacting concrete*, PhD course. Lingby, 2002.
- CEN, European Comitee for standardisation, EN 1992-1-2; Eurocode 2: Design of concrete structures - part 1-2: general rules - structural fire design, Brussels, Belgium, 2004.
- CEN, European Comitee for standardisation, EN 1992-1-2; Eurocode 2: Design of composite steel and concrete structures - part 1-2: general rules - structural fire design, Brussels, Belgium, 2005.
- HRN EN 206 - 9, *Concrete -- Part 9: Additional Rules for Self-compacting Concrete (SCC)* (EN 206-9:2010). 2010.
- Persson B., Fire resistance of self-compacting concrete, SCC. *Materials and Structures* 37 (273): 575–584. 2004.
- Poon C., Azhar S., Anson M., Wong Y. Performance of metakaolin concrete at elevated temperatures. *Cement and Concrete Composites* 25(1):83–89. 2003.
- RILEM TC 129 MHT: Test methods for mechanical properties of concrete at high temperatures, Part 3: Compressive strength for service and accident conditions, *Materials and Structures* 28 (181): 410-414. 1995.
- Part 5: Modulus of elasticity of for service and accident conditions, *Materials and Structures* 33, 219-223. 2000.
- Xu Y., Wong Y., Poon C., Anson M., Impact of high temperature on PFA concrete. *Cement and Concrete Research* 31: 1065–1073, 2001.

# MICROSTRUCTURAL AND MECHANICAL CHARACTERISATION OF POST-TENSIONING STRANDS FOLLOWING ELEVATED TEMPERATURE EXPOSURE

Lucie Robertson<sup>a</sup>, Zuzana Dudorova<sup>a</sup>, John Gales<sup>a</sup>, Esther Vega<sup>a</sup>,  
Holly Smith<sup>a</sup>, Tim Stratford<sup>a\*</sup>, Jane R. Blackford<sup>b</sup>, Luke Bisby<sup>a</sup>

<sup>a</sup> BRE Centre for Fire Safety Engineering, School of Engineering, Univ. of Edinburgh, Edinburgh, EH9 3JL, UK

<sup>b</sup> Institute for Materials and Processes, School of Engineering, Univ. of Edinburgh, Edinburgh, EH9 3JL, UK

## Abstract

Prestressing strands lose strength and become more susceptible to creep deformation when they are heated during a fire. The consequent loss in prestressing force could under certain conditions result in structural collapse, potentially outwith the heated region of the structure. This paper describes a test programme characterising the changes in microstructure of steel prestressing tendons exposed to elevated temperatures. The residual strength tests, hardness testing, and elevated temperature mechanical test were performed to demonstrate how recovery and recrystallisation of the initially work-hardened steel produce changes in its mechanical properties at elevated temperatures. The research results of this paper are beneficial not only in the fire design of post-tensioned structures using modern prestressing steel, but also in the assessment of the tendons' residual strength after being affected by fire.

**Keywords:** Prestressing steel, microstructure, hardness, residual strength, creep.

## 1 INTRODUCTION

The prestressing tendons used in pre-tensioned and post-tensioned concrete construction can be greatly affected by elevated temperature, potentially resulting in catastrophic collapse of a structure. Even if collapse does not occur, heating can reduce both the strength of the tendon at elevated temperature, and the residual strength after it has cooled down, and the tendon can undergo creep deformation. The extent of damage is often not visually quantifiable and another means of assessment must therefore be sought.

This paper reports a study of the changes in physical and mechanical properties of a modern prestressing steel at high temperatures. It examines how the microstructure, hardness and residual tensile strength of the steel is affected by temperature. The aims are to (a) provide fundamental information on the behaviour of prestressing steel subjected to fire temperatures, and to (b) allow the post-fire condition of a tendon to be assessed by means of a simple, cheap, and non-destructive hardness test.

### 1.1 Previous Work Characterising the Effect of Temperature upon Prestressing Steel

The tendons in pre- or post-tensioned concrete are embedded in concrete that provides good insulation; however it is possible for the tendon to reach temperatures over 400°C, and well above this temperature if the tendon or the tendon duct are exposed directly to fire following spalling or cracking of the cover concrete (Gales *et al.*, 2011).

The strength of prestressing steel decreases significantly when exposed to temperatures above 300°C (Holmes *et al.* 1982; Neves *et al.*, 1996; Maclean, 2007), and can lose 50% of its strength at high temperatures. Preloading the strands prior to testing makes little difference to its behaviour. There is a slight increase in strength, however, for temperatures above 700°C (Abram & Erlin, 1967; Holmes *et al.*, 1982).

The mechanical performance of prestressing steel follows from the changes in microstructure that occur as it is heated. Prestressing steel is a cold-drawn, pearlitic steel (a eutectoid mixture of iron carbide and ferrite). At ambient temperature its microstructure consists of thin, elongated pearlite grains. Between 400°C and 700°C, spheroidisation occurs (in which the iron carbide in the pearlite forms globules), accompanied by recovery (in which the dislocations present due to cold working are annihilated). Upon heating to temperatures above 700°C, the matrix recrystallises completely and forms new grains, which then grow over time (Abrams & Erlin, 1967).

A correlation between hardness, tensile strength, microstructure and temperature was established for prestressing steel in the 1960s by Abrams & Erlin (1967). Modern steel, however, has a different chemical composition; the composition of the prestressing steel studied in this paper is compared to those used in previous studies in Tab. 1. The current BS 5896 steel has a higher carbon content and a lower phosphorus and sulphur content than the steel tested by Abrams & Erlin. Gales *et al.* (2012) have identified that existing design guidance may overestimate creep deformation, as a result of the changes in the steel used for prestressing tendons. Consequently, the design guidance may be non-conservative for predicting tendon rupture during a fire, and it is important to re-examine the performance of prestressing steels at high temperatures.

Tab. 1 Carbon and main alloy content in the steels used in previous and current studies

	C (%)	Mn (%)	P (%)	S (%)	Si (%)
Abrams & Erlin (1967)	0.794	0.498	0.0118	0.0376	0.288
Neves <i>et al.</i> (1996)	0.824	0.712	0.02	0.013	0.235
MacLean (2007)	0.80	0.868	0.023	0.012	0.45
Current Tests (BS 5896, 2000)	0.90	0.66	0.007	0.014	0.25

## 2 PROCEDURE

The tests were performed on prestressing steel strands and core wires made to British Standard BS 5896 (2000). The hardness, residual strength and microstructure of the steel were studied after cooling.

### 2.1 Heat Treatment

Unloaded and unrestrained strands were heated to temperatures of 200, 400, 500, 600, 700 and 800°C. Two samples were tested for each exposure temperature. The samples were placed in a furnace and heated from room temperature to the target temperature at 10°C/min, using four thermocouples to monitor the furnace and sample temperatures. The specimens were then held at the target temperature for 1.5 hours, followed by air-cooling to simulate natural cooling following a fire. This heating regime matched previous tests by MacLean (2007).

An additional four samples were heated to 400°C and held for periods of 4 and 8 hours (corresponding to the study by Abrams & Erlin, 1967). These samples allowed the effect of soak time upon microstructure and hardness to be studied at 400°C, for which significant changes in mechanical properties start to occur (Neves *et al.*, 1996; MacLean, 2007; Myers & Bailey, 2009).

### 2.2 Hardness

Vickers hardness tests were performed on all the heated core wires. 30 mm long samples were ground using P400 silicon carbide paper to produce a flat, clean surface at least 2 mm wide. The samples were mounted in a special stand, tested under the equivalent of a 30kg mass, and the appropriate conversion used to obtain the Diamond Pyramid Hardness (DPH) value. Four

hardness tests were performed in the centre of each sample (to eliminate the influence of the sample edges) and the results were averaged.

### 2.3 Microstructure

Microstructural observation of both transverse and longitudinal sections of the samples were conducted through a Zeiss Axioscope light microscope. Two 10 mm long sections were cut from each sample and mounted in EpoxiCure resin. These were ground using gradually finer grit paper and then polished with cloths and diamond paste, to obtain a flat, scratch-free surface. The samples were etched with 2% Nital to expose the grain structure.

### 2.4 Residual Tensile Strength

Residual tensile strength tests were performed on the core wires after cooling using an Instron 600LX universal testing machine. The samples were tested using a free length of 50 mm, at a strain rate of 2 mm/min (to avoid creep effects). Digital Image Correlation (DIC) was used to measure the steel strains during the tests (see Gales *et al.* (2012) for details).

### 2.5 Tension test

The core wire from a prestressing strand was heated at 10°C/min to a temperature of 500°C and held for 15 mins. The sample was loaded at 1mm/min whilst maintaining the temperature at 500°C. The test was stopped before failure to observe necking, which occurred in two distinct places. The necked sections were tested for hardness and prepared for microscopy as described above.

## 3 RESULTS AND DISCUSSION

The results obtained during this study are compared with prior research by Abrams & Erlin (1967), Holmes (1982), Neves (1996), MacLean (2007), and Myers & Bailey (2009). These authors studied the change in residual mechanical and material properties of loaded and/or unloaded prestressing steel samples with temperature.

### 3.1 Microstructure

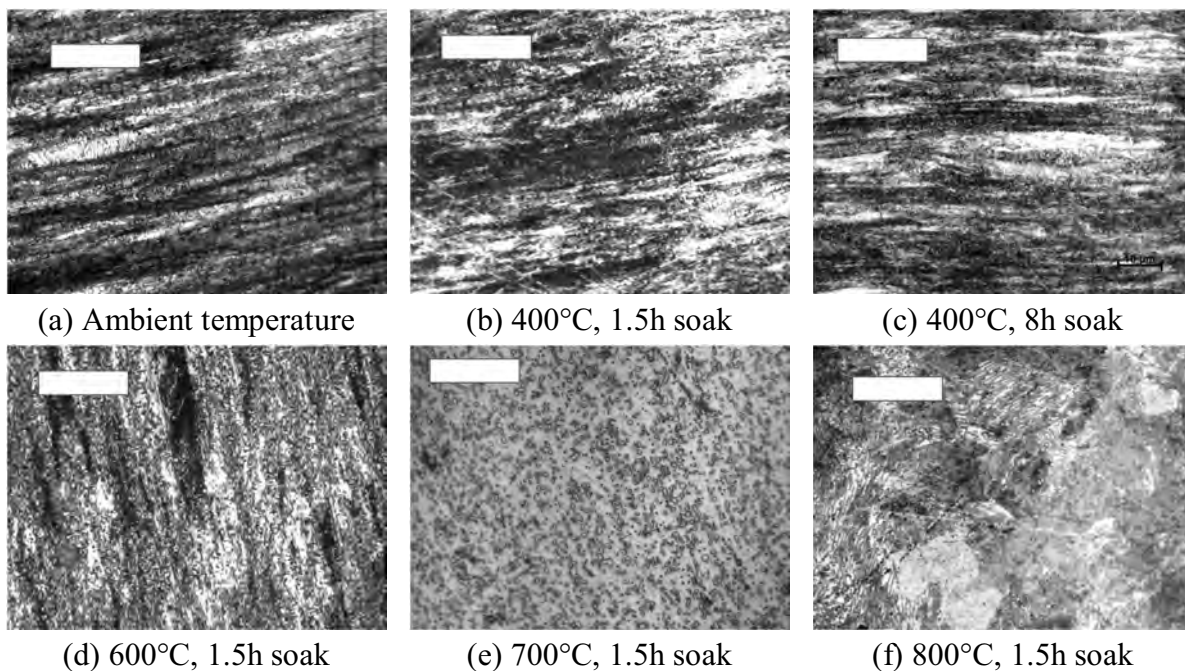


Fig. 1 Longitudinal sections for different exposure temperatures and times; the length bar is 20  $\mu\text{m}$  long.

Fig. 1 shows the microstructure of the longitudinal sections at different temperatures and soak times. The elongated pearlite grains are clearly shown in the non-heated prestressing steel (Fig. 1a). The extensive cold-drawing during manufacture of the steel wire results in very fine grains that cannot be distinguished in the transverse direction.

A similar microstructure with long, fine grains is evident for samples that have been heated up to 500°C (Fig. 1b and 1c), and it is not possible to resolve the individual grains in the transverse view. However, the pearlitic banding is less clear in the 400°C samples. Whilst (even at 1000× magnification) it was difficult to discern this banding, it is possible to see that the proportion of pearlitic banding was lower. For the 8h soak time, the original structure is still visible, but the clear pearlitic structure has disappeared and slightly grainier dark and light bands are visible. This suggests that the effect of this temperature upon the steel is time dependent.

For temperatures above 500°C pearlite starts to dissociate into ferrite and globular iron carbide, and the microstructure is a mixture of the pearlite grain structure and the new globular structure. This is evident at 600°C in both longitudinal (Fig. 1d) and transverse directions.

At temperatures above 700°C the directionality of the original grain structure is lost. Above the eutectoid temperature ( $\approx 727^\circ\text{C}$ ), the steel transforms to austenite, but re-forms into coarse pearlite colonies upon cooling (Fig. 1e and 1f). Decarburisation is also observed for these temperatures; after heating, the samples were coated in a carbon layer and the proportions of ferrite in the microstructure near the surface were higher.

Similar trends were observed by Abrams & Erlin, Neves *et al.* and MacLean, despite the different compositions of the steels that they tested (Tab. 1).

### 3.2 Hardness vs. Temperature

The results from the Vickers hardness tests are shown in Fig. 2, which plots the reduction in hardness with exposure temperature.

There is no significant change in hardness for temperatures up to 300°C, with a marked decrease in hardness above 400°C. A minimum hardness (equal to 40% of the un-heated hardness) occurs for steel heated to 700°C. At 800°C, the hardness increases slightly (to 60%) due to recrystallization. These results correlate with those obtained by Abrams & Erlin (1967).

The multiple points at 400°C in Fig. 2 are due to the soak times of 1.5, 4 and 8h. The longest exposure resulted in the lowest hardness value, with a difference of not more than 8% (55 DPH) between the longest and shortest exposure times.

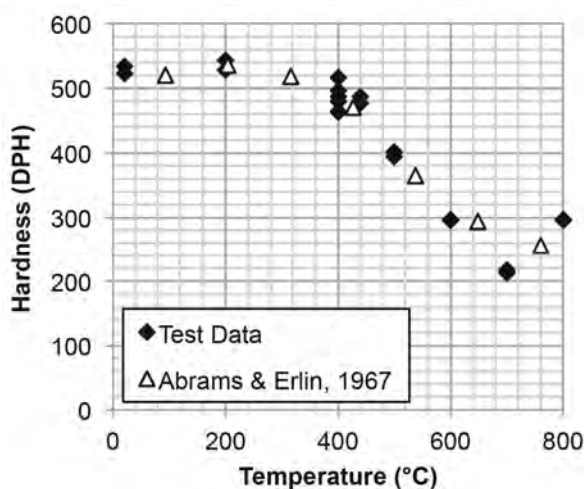


Fig. 2 Hardness variation with temperature

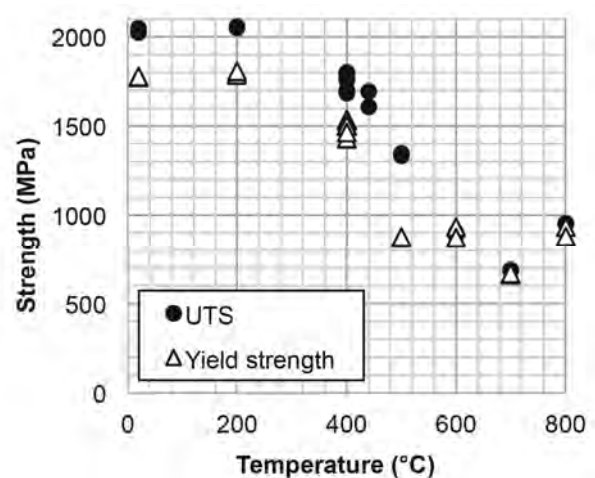


Fig. 3 Strength variation with temperature

### 3.3 Residual Strength vs. Temperature

Fig. 3 shows how the residual yield tensile strength and ultimate tensile strength (UTS) varied with exposure temperature. The yield strength was the stress at which the prestressing steel samples ceased to behave linearly. There is very strong similarity between Fig. 2 and 3, confirming the correlation between strength and hardness.

As with hardness, significant change in tensile strength occurs for temperatures below 300°C. The strength is reduced at 400°C, but neither the yield or ultimate tensile strengths are significantly affected by the exposure times at this temperature (the results are within 120MPa of each other). The minimum strength occurs at 700°C, where the UTS has reduced by nearly 70%, and the yield strength by around 60%. The strength recovers slightly at 800°C, with a residual UTS around 50% of the unheated strength.

Stress-strain curves were plotted using the DIC measurements of strain (but are not included here). The elastic portion of the response gave a Young's modulus ( $E$ ) close to 210GPa, which is in the range defined by the manufacturer. The residual value of  $E$  did not vary significantly with exposure temperature. The stress-strain curves for the majority of the specimens had clear elastic-plastic regions with very little hardening. Those exposed to 800°C, however, were similar to those for mild steel, with hardening, a consequence of the un-worked microstructure of the steel following heating to 800°C (Fig. 1f).

Fig. 4 compares the UTS results from the present study (from Fig. 3) to the results from previous studies, normalised with respect to the unheated strength. The trend is the same as for previous work except for that of MacLean, who obtained higher residual UTS values for temperatures above 400°C. A recovery of residual UTS is also observed for 800 °C by Neves *et al.* and Abrams & Erlin.

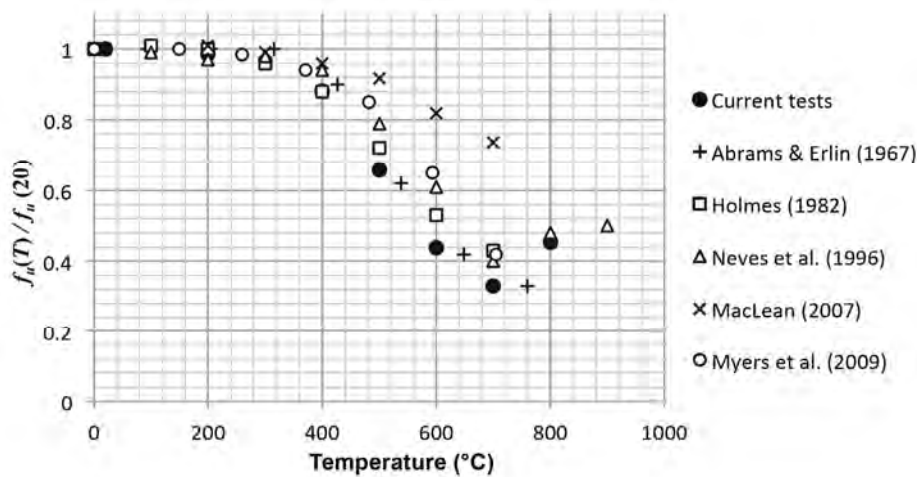


Fig. 4 Comparison of test data with previous studies

### 3.4 Heated Tension Test at 500°C

The strength test conducted at 500°C was used to determine whether loading at elevated temperature affects the hardness or microstructure of the steel (after it has been cooled). There was a small decrease in hardness of 8.3% compared to the unloaded sample. The loaded tests by Abrams & Erlin (1967) gave a similar result, which they deemed to be negligible, but it should be noted that the difference in hardness is similar in magnitude to that resulting from the different exposure times at 400°C.

The microstructure of samples taken from the necked region was similar to that of unloaded test, although the plastic deformation would have caused the formation of microcavities in the necked region.

### 3.4 Hardness as an Assessment of Residual Strength

The results demonstrate that the hardness of the modern prestressing steel (to BS 5896) correlates very well with the residual UTS, in a similar manner to historic prestressing steel (Abrams & Erlin, 1967).

Portable hardness testing may allow the residual tensile strength of a post-tensioning tendon to be assessed following a fire without needing to recourse to destructive test methods that require samples of steel to be removed from the structure.

Care is required, due to the non-unique values of hardness that occur between 600°C and 800°C, because hardness testing cannot distinguish steel exposed to these two temperatures. The ductility of the 800°C exposed steel will be higher, but this would require microstructural examination or mechanical testing. It is unlikely, however, that prestressing tendons exposed to any temperature in the 600°C to 800°C could be retained because of the consequent large reduction in strength.

## 4 SUMMARY

This study has examined how exposure to elevated temperatures up to 800°C affects the microstructure, hardness, and residual tensile strength of a modern prestressing steel.

Whilst the chemical composition of the British Standard steel examined here differs from the prestressing steels examined in previous studies (from the 1960s onwards), its elevated temperature performance is similar. Residual strength loss occurs from 400°C, with a maximum ultimate tensile strength of 70% at 700°C. The exposure time does not greatly affect its residual properties.

The residual strength loss is accompanied by a reduction in the steel's hardness, and this may allow hardness testing as a non-destructive method to establish the residual strength of a prestressing tendon following fire.

## REFERENCES

- Abrams M. S. & Erlin B. (1967). Estimating Post-Fire Strength and Exposure Temperature of Prestressing Steel Using Metallographic Method. Portland Cement Association, Skokie, USA.
- BS 5896 (2000). Specification for High Tensile Steel Wire and Strands for the Prestressing of Concrete, BSi, London.
- Gales J., Bisby L. A. & Gillie M. (2011). Unbonded Post-Tensioned Concrete in Fire: A Review of Data from Furnace Tests and Real Fires. *Fire Safety Journal*, 46(4), 151-163
- Gales, J. Bisby L. A. & Stratford T. (2012). New Parameters to Describe High-Temperature Deformation of Prestressing Steel Determined Using Digital Image Correlation. *Structural Engineering International*, 2(4), 476-486
- Holmes M. E., Anchor, R., Cook, G., & Crook, R. (1982). The Effects of Elevated Temperatures on the Strength Properties of Reinforcing and Prestressing Steels. *The Structural Engineer*, 60(13), 7-13
- MacLean K. J. (2007). Post-Fire Assessment of Unbonded Post-Tensioned Concrete Slabs: Strand Detioration and Prestress Loss. Master's Thesis, Queen's Univ., Kingston, Ontario, Canada.
- Myers J. J., & Bailey W. L. (2009). Residual Properties of Seven-wire Low Relaxation Prestressing Tendon Subjected to Extreme Temperatures. PCI National Bridge Conference, San Antonio.
- Neves C. I., Rodrigues, J. & de Padua Loureiro, A. (1996). Mechanical Properties of Reinforcing and Prestressing Steels after Heating. *Journal of Materials in Civil Engineering*, 8(4), 189-194

## MODELLING OF THE INFLUENCE OF CREEP STRAINS ON THE FIRE RESPONSE OF STEEL ELEMENTS

Torić N.<sup>a</sup>, Harapin A.<sup>a</sup>, Boko I.<sup>a</sup>, Peroš B.<sup>a</sup>, Ban M.<sup>a</sup>

<sup>a</sup> University of Split, Faculty of Civil Engineering, Architecture and Geodesy, Matice Hrvatske 15, HR-21000 Split, Croatia; e-mails: neno.toric@gradst.hr, alen.harapin@gradst.hr, ivica.boko@gradst.hr, bernardin.peros@gradst.hr, maja.ban@gradst.hr

### Abstract

The paper presents a numerical model for the behaviour of steel structures exposed to fire capable of taking into account the effect of steel creep at high temperatures by using a simple implicit model. The objective of the simple implicit model is to modify the material stationary stress-strain curves. After reaching temperatures above 400°C, stress-strain curves are modified by stretching the curves using a calculated value of creep strain at current stress, temperature and time. Described numerical procedure was tested by modelling the behaviour of two simply supported steel elements that were partially exposed to high temperatures in an in-house experiment. Authors are claiming that the implicit model is applicable for modelling the behaviour of steel elements with free thermal expansion or with a low level of restriction to thermal expansion.

**Keywords:** fire, heat transfer, finite element, steel, creep strains

### INTRODUCTION

Behaviour of steel structures at high temperatures is greatly influenced by the level of creep strains that occur after reaching the temperature above one third of the melting point of steel. For structural carbon steel, this occurs after reaching the steel temperature of approximately 400°C. Generally, for simply supported steel elements with no axial restraints, the creep strain affects the vertical deflections, while in the elements which are axially restrained, the creep strain induces development of additional forces in the structure (Kodur, Dwaikat 2010). Consequently, creep strains have significant effect on the load bearing capacity of steel structures exposed to fire. Most of the creep models are derived based on material stationary creep tests, in which the steel specimen is heated while the stress is kept constant (Harmathy 1967, Williams-Leir 1983). Implementation of creep strains into the calculation of the structural response is achieved through explicit or implicit creep models. Explicit creep models include creep strains directly into the strain profile of the cross section, where the calculation procedure involves finding the strain profile for which the internal forces are in equilibrium with the applied load forces at one cross section. Afterwards, the moment-curvature relationship for every cross section is calculated, and in dependence on the equilibrated strain profile (curvature), the bending stiffness of the structure member is calculated. Implicit creep models include creep strains directly into the stress-strain curves of the material, thus creating effective relationships in which stress-strain curves are highly nonlinear. However, implicit creep models only partially take into account high temperature creep strain at elevated temperatures, since no calculation of creep strain exists in implicit creep models (Kodur et al 2010). This paper presents a newly developed implicit creep model that calculates creep strains with the help of the existing creep material models in order to modify the stress-strain curves of the material. Consequently, the implicit model creates stress-strain curves that are modified according to the level of stress and temperature that the cross section is exposed to after reaching the critical temperature of steel creep development.



# 1 NUMERICAL MODEL FOR STRUCTURAL FIRE ANALYSIS

The model is generally based on a spatial beam-column element analysis (spatial frame structures), which has a detailed description in (Torić et al 2012). The model consists of three submodels: a model for structural analysis (Bernoulli beam elements with six degrees of freedom), a model for calculation of the nonlinear stress-strain distribution in the cross-section and a 3D transient nonlinear heat transfer model (eight node cube element). In the calculation procedure the structure is divided into elements and subelements. (Fig. 1, a-b). Each of these elements and subelements has a cross-section consisting of one material or one composite section (Fig. 1-c), and each of the materials of the cross-section has its constitutive material behaviour law (stress-strain curve). Once the model for structural analysis has been formed and the element cross-section defined, the spatial 3D model for heat transfer analysis is automatically formed (Fig. 1-d).

## 1.1 Structural calculation procedure

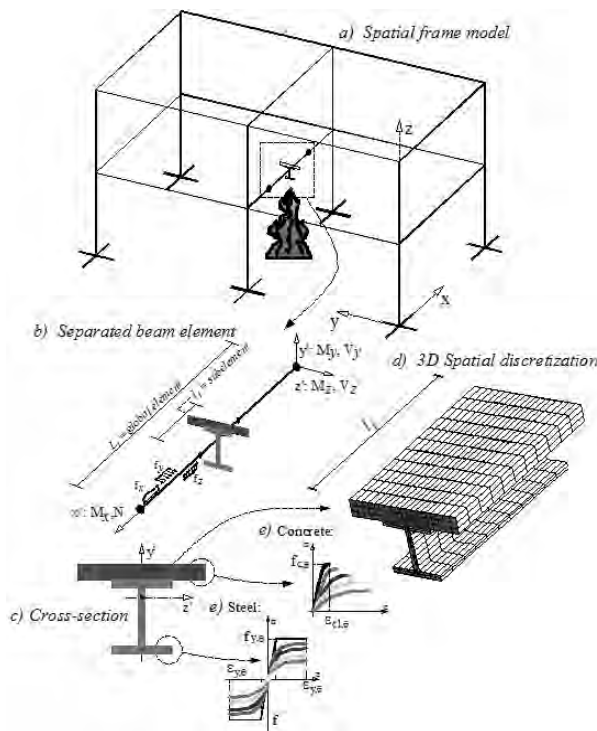


Fig. 1 Presentation of the numerical model

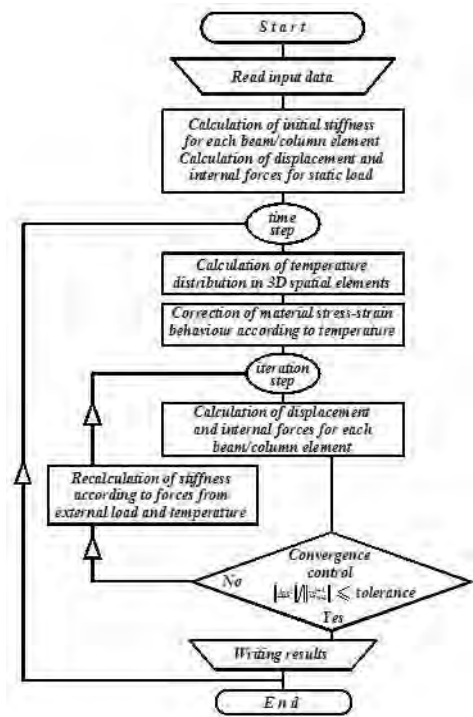


Fig. 2 Structural fire analysis flow-chart

The calculation procedure starts with a linear elastic structural analysis. The structure is loaded with a static load, for which displacements and internal forces are calculated (quasi static analysis). Afterwards, depending on the level of internal forces in each subelement, the structure stiffness matrix is modified according to the nonlinear stress-strain distribution in the cross-section. Strain components in the steel cross-section during fire exposure are comprised of three components (Purkiss 2007):

$$\varepsilon_{tot} = \varepsilon_{th}(\mathbf{T}) + \varepsilon_{\sigma}(\sigma, \mathbf{T}) + \varepsilon_{cr}(\sigma, \mathbf{T}, t) \quad (1)$$

where:  $\varepsilon_{tot}$  – total strain,  $\varepsilon_{th}(\mathbf{T})$  – thermal strain (function of temperature  $\mathbf{T}$ ),  $\varepsilon_{\sigma}(\sigma, \mathbf{T})$  – stress related strain (function of both the applied stress  $\sigma$  and the temperature  $\mathbf{T}$ ) and  $\varepsilon_{cr}(\sigma, \mathbf{T}, t)$  – creep strain (stress, temperature and time dependent strain). Creep strains are excluded from Eq. (1) if an implicit creep model is utilized in the structural analysis. In that case, creep strains are implicitly included in the material stress-strain curves. The implicit model is described in the following chapter. Thermal strains are converted into displacements or internal forces depending on the end restraints of the element. Once the modified stiffness

matrix of the structure is assembled, new structure displacements are calculated until the convergence of the displacement vector is achieved (norm of displacement vector lower than norm limit). This phase can be described as a stationary state of the structure, for the time period before the structural fire analysis starts. Flowchart of the numerical model is presented in Fig. 2.

## 2 NEW IMPLICIT CREEP MODEL

### 2.1 Introduction

The idea for a new implicit creep model was developed from the observation of results obtained from classical stationary and transient material tests. For steel, stress-strain curves obtained from transient test differ from those obtained by stationary test, mainly because of the influence of steel creep. Steel creep develops because steel specimens are heated with slow thermal gradient while under stress, which results in a distorted stress-strain curve due to existence of implicitly included creep strain in comparison to stationary curves (Lu et al 2003, Mäkeläinen et al 1998). The main difference is observed in the reduced modulus of elasticity  $E_{y,\theta(\text{trans})}$  over the whole stress range, and depending on the temperature level, in a slightly lower yield strength  $f_{y,\theta(\text{trans})}$ . Fig. 3 presents a typical stress-strain curve obtained by stationary and transient steel testing for a fixed temperature level  $\theta$ .

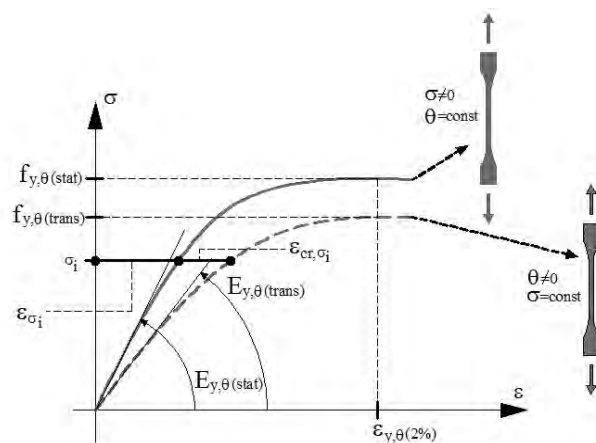


Fig. 3 Comparison of typical stress-strain curves obtained from stationary and transient steel tests

From Fig. 3 it is evident that for each stress level on the curve  $\sigma_i$ , the total deformation on the transient stress-strain curve can be divided into two components: stress related strain  $\varepsilon_{\sigma_i}$  and creep strain  $\varepsilon_{cr,\sigma_i}$  (thermal deformation excluded). In case of the classical transient test, the level of creep strain that is implicitly included in the stress-strain curve depends upon the level of stress that is kept constant during the test and the imposed heating gradient on the specimen.

### 2.2 Implementation of the new implicit creep model

The new implicit creep model is based on the observation of dual deformation division of the total sum of deformation observed on the transient stress-strain curve (Fig. 3). The model is based on the calculation of realistic values of creep strains depending on the level of stress and temperature to which the cross section is exposed. Realistic values of creep strain are then used to modify the stationary stress-strain curves. The modification is obtained by adding the calculated creep strain to the value of stress related strain in order to reach values that should correspond in maximum degree to the observed total sum of deformation on transient stress-strain curves from Fig. 3. By adding the calculated creep strain to the stress related strain for each stress level  $\sigma_i$ , the new modified stress-strain curve is obtained which reduces the

modulus of elasticity on the curve and creates a ductile material curve that is similar to stress-strain curve obtained by transient testing of the material.

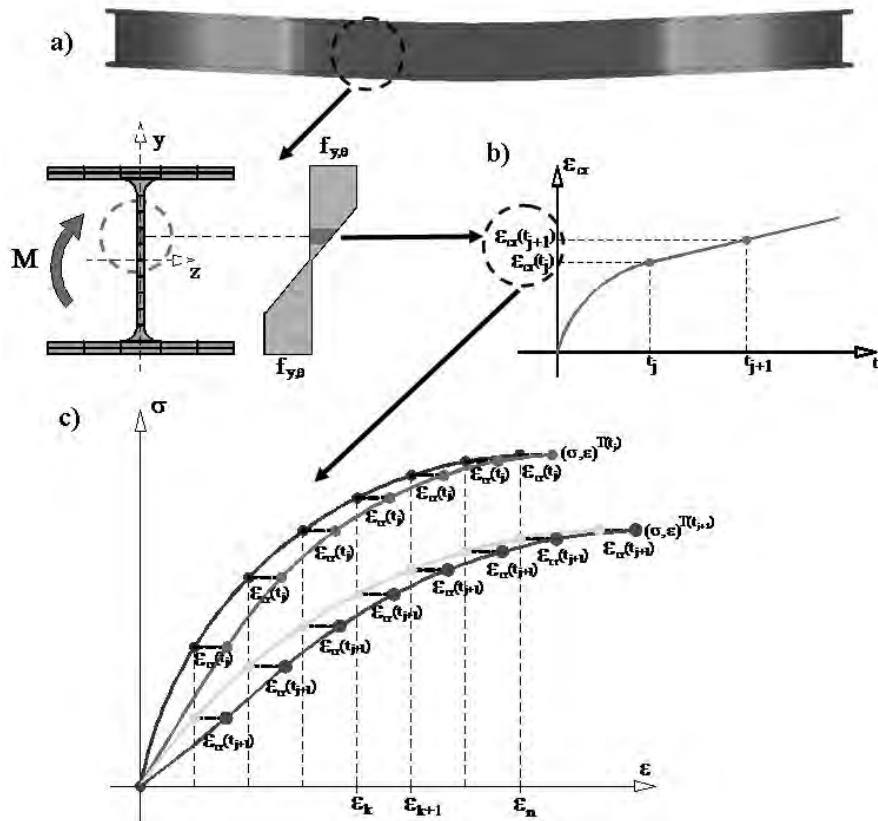


Fig. 4 New implicit creep model for stress-strain curve modification: (a) Temperature calculation; (b) creep strain calculation; (c) strain modified curve

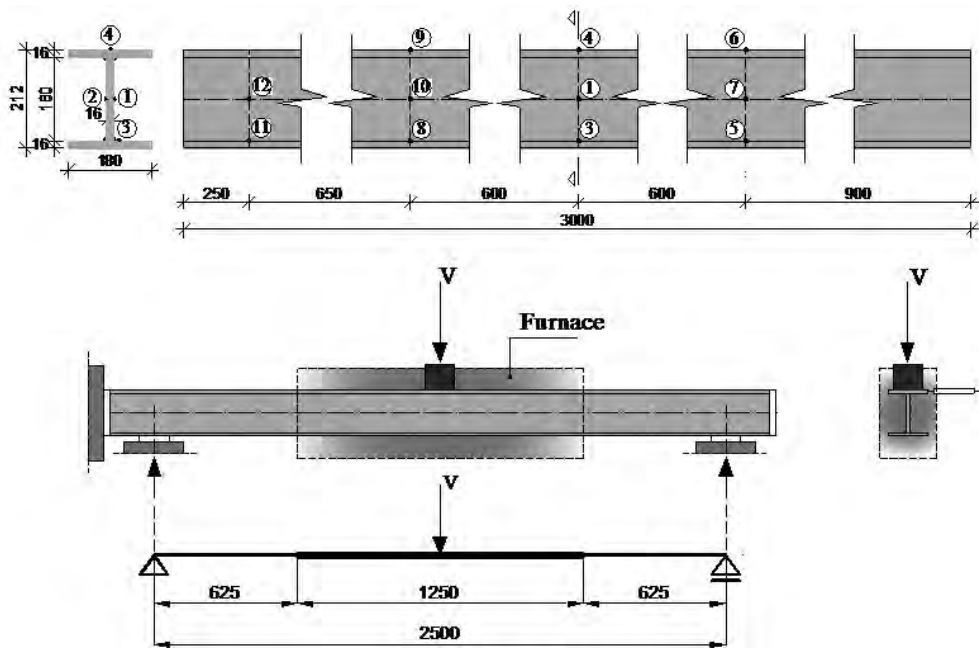


Fig. 5 Temperature measuring points and structure model

Fig. 4 summarizes the proposed implicit calculation procedure. The proposed implicit calculation procedure is modifying stress-strain curves obtained from stationary tests and using them to recreate equivalent transient stress-strain curves. The procedure in this manner creates curves which are influenced by a creep strain that is likely to occur in a certain part of the cross section. The model for calculation of creep strains applied in this study is based on Harmathy's research (Harmathy 1967). Parameters for calculating creep strains are derived for steel grade A36 (Harmathy et al. 1970), which is equivalent to steel grade S275.

### 3 NUMERICAL VERIFICATION

Verification of the proposed implicit creep model was conducted on the results of two fire tests (Boko et al 2012). Two simply supported steel beams I 212/180, steel grade S355, with 2.5 m span were previously loaded and then heated on all four sides of the element inside the furnace (Fig. 5). First element (E1) was loaded with concentrated vertical force  $V = 200$  kN at midspan and the second element (E2) was loaded with concentrated vertical force  $V = 200$  kN and horizontal compressive force  $H = 400$  kN. Fig. 5 presents the disposition of discrete temperature measuring points in which temperature development was observed over time, and the structure model used for numerical modelling. Tab. 1 presents basic input parameters for the heat transfer analysis.

Tab. 1 Basic input parameters for heat transfer analysis

Thermal conductivity $\lambda$	Specific heat capacity $C$	Density $\rho_a$ [kg/m <sup>3</sup> ]	Convection $\alpha_c$ [W/m <sup>2</sup> K]	Config. factor $\Phi$	Emissivity $\epsilon_{res}$	$\Delta t$ [s]
EN1993-1-2	EN1993-1-2	7850.0	50.0	1.0	0.8	0.5

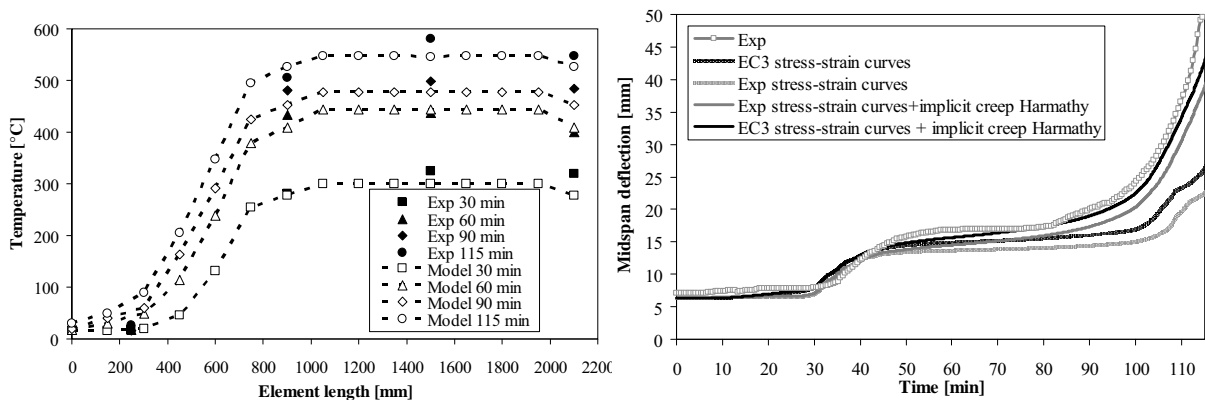


Fig. 6 Comparison of results obtained by model and experiment (Element E1)

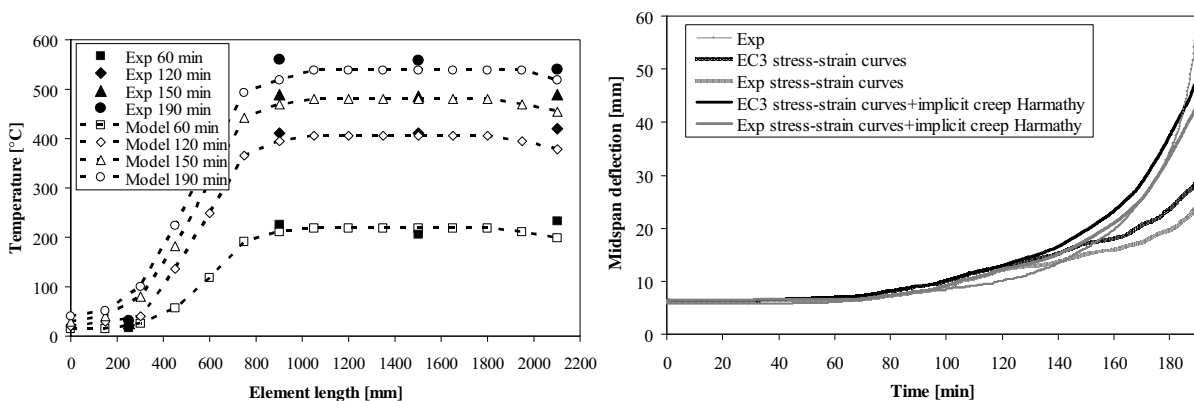


Fig. 7 Comparison of results obtained by model and experiment (Element E2)

The numerical analysis was done by using two different sets of stress-strain curves: experimental stationary stress-strain curves which were determined for steel that was used in the steel beam itself (Boko et al 2012) and the stress-strain curves proposed by EN1993-1-2, generally used for engineering analysis of the behaviour of steel structures under fire. Figs. 6 and 7 present the comparison of results between the conducted experiment and the model predictions.

#### **4 DISCUSSION OF RESULTS**

Figs. 6 and 7 show good agreement between the temperatures predicted by the 3D heat transfer model and the measured temperatures during element testing, indicating higher level of precision for temperature predictions if using 3D heat transfer modelling in case of local heating of the element. Both of steel elements were exposed to temperatures above 400°C for at least 70 minutes, thus enabling the development of high temperature creep strains. Figs. 6 and 7 show unconservative results when using both experimental stationary stress-strain curves and steel curves from Eurocode in structural analysis. The unconservative results are obtained without the inclusion of the implicit creep model, for the time period in which steel element is heated above 400°C. The presented implicit creep model is used to modify the initial elasto-plastic steel material model and creates an equivalent visco-plastic material model by modifying stationary stress-strain curves. Results of the deflections obtained by the numerical model show good agreement with the experiment when using the proposed implicit creep model, and therefore, indicate the validity of the applied implicit creep model. However, some discrepancies exist because the applied creep calculation model (Harmathy 1970) is sensitive to input parameters, which are highly variable depending on the type of steel. Creep model was used with the help of experimental parameters derived for steel grade S275. However, steel beams were made of steel grade S355. The present study is focused on the behavior of unrestrained steel elements. Further tests are necessary to confirm the validity of the proposed implicit creep model, especially for the case of restrained steel elements.

#### **REFERENCES**

- Boko I., Torić N., Peroš B., *Materialwissenschaft und Werkstofftechnik*, Vol. 43, 2012.
- EN 1993-1-2:2005 Eurocode 3 - Design of steel structures - Part 1-2: General Rules - Structural fire design, European Committee for Standardization, Belgium 2005.
- Harmathy T. Z., *Journal of Basic Engineering*, Vol. 89, p. 496, 1967.
- Harmathy T. Z., Stanzak W. W., *Elevated-Temperature Tensile and Creep Properties of Some Structural and Prestressing Steel*, National Research Council of Canada, Division of Building Research, Canada, 1970.
- Kodur V., Dwaikat M., Fike R., *ASCE Journal of Materials in Civil Engineering*, Vol. 22, p. 423, 2010.
- Kodur V. K. R. , Dwaikat M. M. S., *Materials and Structures*, Vol. 43, p. 1327, 2010.
- Lu W., Mäkeläinen P., *Advanced Steel Structures TTK-TER 29 Report*, Laboratory of Steel Structures, Helsinki University of Technology, 2003.
- Mäkeläinen P., Outinen J., Kesti J., *Journal of Constructional Steel Research*, Vol. 48, p. 47, 1998.
- Purkiss J. A., *Fire Safety Engineering Design of Structures Second edition*, Butterworth-Heinemann, UK, 2007.
- Torić N., Harapin A., Boko I., *Građevinar* Vol. 64, p. 1, 2012.
- Williams-Leir G., *Fire and Materials*, Vol. 7, p. 73, 1983.

## STRENGTHENING OF HEAT DAMAGED REINFORCED CONCRETE CYLINDERS

A.B. Danie Roy<sup>a</sup>, U. K. Sharma<sup>b</sup>, P. Bhargava<sup>c</sup>

<sup>a</sup> Indian Institute of Technology Roorkee, Research Scholar Dept. of Civil Engineering Roorkee, India

<sup>b</sup> Indian Institute of Technology Roorkee, Associate Professor Dept. of Civil Engineering Roorkee, India

<sup>c</sup> Indian Institute of Technology Roorkee, Professor Dept. of Civil Engineering Roorkee, India

### Abstract

The purpose of this study is to investigate the effectiveness of various strengthening techniques in restoring heat damaged reinforced concrete. A series of 40 reinforced concrete cylinders were tested under concentric compression after being jacketed externally with high strength fiber reinforced concrete (HSFRC), Ferrocement (FC) and Glass fiber reinforced polymer (GFRP) jackets. Concrete specimens were exposed to elevated temperatures ranging from room temperature to 900 °C. The overall response of strengthened specimens was investigated vis-à-vis un-strengthened specimens in terms of axial compression, axial displacement and axial stress strain behaviour. The results indicate that important gains in strength and ductility can be achieved by strengthening heat – damaged R.C cylinders by HSFRC, FC and GFRP external Jacketing. GFRP jacketing was found to be the most effective method of strengthening fire or heat damaged concrete structures.

**Keywords:** concrete cylinders, strengthening, GFRP, Ferrocement, HSFRC

### INTRODUCTION

Reinforced Concrete structures (RCC) may require strengthening for a various reasons. Heating or fire accidents in buildings demands repair and rehabilitation. Many experimental techniques have been used in recent years to strengthen RCC columns under ambient condition using suitable retrofitting and strengthening techniques. Materials of strengthening include FRP wrapping, FC jacketing, HSFRC, Steel plate bonding etc. Apart from low maintenance cost and improvement in the service life of buildings, Fibre Reinforced polymer (FRP) wrapping have several benefits like high strength, light weight, resistance to corrosion, low cost, and versatility (Ehsani et al, 1998). Also the interaction between concrete and fiber enhances concrete strength and ultimate strain (Luca et al, 2011). Effectiveness of FRP jacketing is significant in columns with circular cross section (Lam et al, 2003). Many researchers have emphasized the potential usage of FC laminates in repair and rehabilitation of concrete structures. Increased strength and ductility were observed in FC encased short circular and square concrete columns with unreinforced and reinforced cores for both axial and eccentric loading conditions (Kaushik et al, 1990). Apparent stiffness and ultimate load carrying capacity has been increased due to FC retrofit coating in new structures, repair and rehabilitation of existing structures and marine environment (Nedwell et al, 1990, Mourad et al, 2012). HSFRC provides a better alternative to normal concrete, with high strength/weight ratio, high toughness, excellent durability, and moreover cost effective than conventional materials. Utilization of composite materials in rehabilitating structures can greatly reduce maintenance, improved life safety and service life (Haddad et al, 2011). Literature review on HSFRC exhibits the possibility of designing structures with new geometries and shapes with great improvement in strength (Martinola et al, 2010). However, literature indicates that the

repair of heat damaged reinforced concrete elements with these strengthening techniques have not been investigated in detail (Haddad et al, 2011, Yaqub et al, 2011, 2012).

The main aims of this research are to investigate the effectiveness of applying HSFRC, FC and GFRP jackets on heated one-sixth-scale reinforced concrete cylinder; and to study the behavior of damaged and repaired elements in terms of strength gain, ductility and failure modes.

## 1 EXPERIMENTAL PROGRAMS

The experimental program consists of testing one-sixth- scale cylinder (150 mm dia) specimens with a height of 450 mm in three phases as follows; Level 1: Control specimens without any damage and without jackets, Level 2: Specimens were induced with heat damage and without jacking, and Phase 3: Heat damaged specimens strengthened with HSFRC, FC, and GFRP jackets. The RC cylinders numbers and details are given in Table 1. The dimension and reinforcement details are shown in Fig.1.

Tab. 1 Specimen Details

Temperature	300	600	900
Designation & Wrapping Methods	CC3 CC3 HSFRC CC3 FC CC3 GFRP	CC6 CC6 HSFRC CC6 FC CC6 GFRP	CC9 CC9 HSFRC CC9 FC CC9 GFRP CC9MC

### 1.1 Materials properties

Concrete was prepared with ordinary Portland cement, Natural River sand, and crushed limestone aggregate of maximum size 12.5 mm with tap water. Cylinder compressive strength of 37.19 MPa was obtained after 28 days. The concrete mix consisted of 450 kg/m<sup>3</sup> Portland cement, 658 kg/m<sup>3</sup> washed sand, 1034 kg/m<sup>3</sup> crushed limestone, and 202.5 kg/m<sup>3</sup> tap water. The steel used for longitudinal reinforcement was 10 mm diameter with 520 MPa yield strength and while that used for lateral ties 6 mm diameter bars of 590 MPa. Hook end steel fibers were used in preparing the HSFRC jacket. The fibers were used at volumetric fraction of 2%. The steel fiber used in the jacket was 0.60mm diameter, 30mm length with yield strength of 1120 MPa. It was planned to use locally available weld mesh as a low cost material in rehabilitation and upgrading of RC Cylinders. The weld mesh used in the jackets had square openings of (13\*13 mm) and wire diameter of 0.96 mm, tensile tests was performed on three coupons and the average yield strength was 385 MPa. The properties of GFRP used for the investigation was unidirectional with nonstructural weaves in the secondary direction to hold the fabrics together, which was glued using epoxy resin, with thickness of about 0.324mm, average tensile strength of 3400 N/mm<sup>2</sup>, and an ultimate elongation of 4.33%. The materials used in preparing slurry specimens included ordinary Portland cement, natural sand which was less than 600 micron and silica fume. The slurry mix proportions were 1:0.6:0.15:0.35:0.01 by weight of cement, sand, silica fume, water and super plasticizer correspondingly. Prepared slurry mix had a high compressive strength of about 68.06 MPa and a high flow as measured by a standard ASTM C939 flow cone (about 32 seconds).

### 1.2 Casting, Curing and Thermal Testing

A concrete cover of 12.5 mm was provided at side in all the cylinders. A cover of 15 mm was also provided between the ends of the longitudinal bars at the top and bottom surfaces of the specimens to prevent direct loading. The water curing period lasted for 28 days after which

the specimens were kept in the laboratory at ambient temperature and humidity conditions for another 122 days.

A programmable electrical furnace intended for a maximum temperature of 1200°C was used for heating the specimens. The temperature inside the furnace was measured and recorded with specially installed thermocouples. After 150 days, the specimens are heated in the furnace to different target temperatures ranging from ambient temperature to 900°C. Rate of heating was set at 10°C/min and each target temperature was maintained for 3 hrs to achieve a thermal steady state (Fig. 2). After exposing the specimens (CC3, CC3CY, CC6, and CC9 NA) to target temperatures for the desired time duration, the specimens were allowed in the furnace for natural cooling till room temperature.

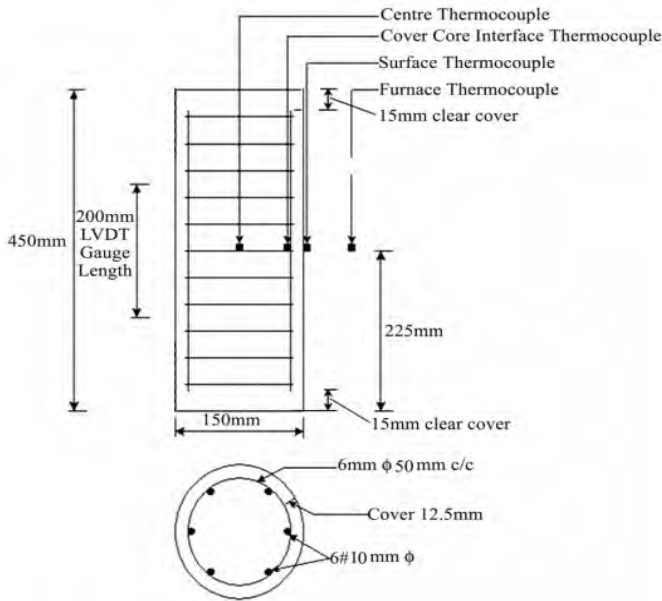


Fig. 1 Reinforcement details and position of thermocouple

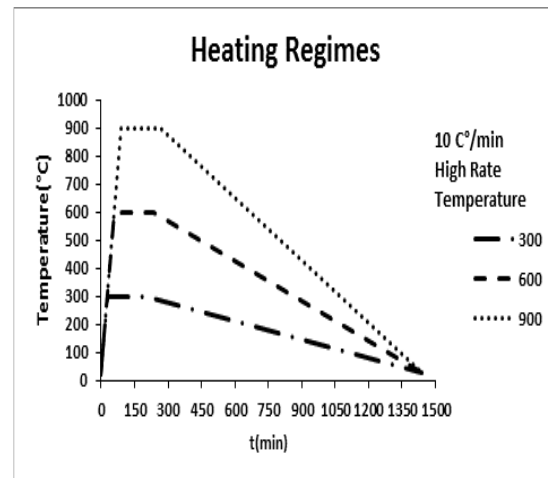


Fig. 2 Heating Regimes

### 1.3 Observation during heating

Assessment of fire damaged concrete usually starts with visual observation of colour change, cracking and spalling of concrete surface. The colour of concrete cylinder changed to pink when the specimens were exposed to 300°C temperature and became light greyish at 600°C. However, the specimen's changed to ash white colour when exposed to 900°C. There was no visible crack on the surface of the specimens heated up to 300°C. However while insignificant hairline cracks were observed at 600°C. The number of crack became relatively pronounced at 900°C. No spalling was observed in 300°C and 600°C temperatures. On exposure to temperature of 900°C no instant spalling was recorded in any of the specimens and spalling occurs after few days.

### 1.4 Installation of Strengthening Schemes

The heat damaged cylinders were strengthened with 1) HSFRC, 2) FC and 3) GFRP jacketing. The columns which were heated to 900°C temperature were repaired before wrapping. The loose concrete was removed with steel wire brush and the surfaces of specimens were cleaned thoroughly to remove dust or oil stains and a primer coat of bonding was applied over the surface to achieve good bonding between the old concrete and new micro concrete (MC) (BS EN1504, Technical report no. 69). Also, for the specimens exposed



to 300°C and 600°C, a primer epoxy bonding was applied after the surface was cleaned in order to provide good bonding between the substrata and the new strengthening material. Dr.fixit Epoxy bonding agent was applied on the surfaces of cylinder specimens to provide good bond between the heat damaged specimens and the HSFRC jacket. The specimens were placed in the mould containing 25 mm thick HSFRC slurry. A gap of 20 mm was left at the ends of concrete cylinders to prevent HSFRC jacket from direct loading condition while testing. FC jacketing was similar as in HSFRC jacketing in cleaning, bonding and curing process. The specimens were wrapped with two layers of welded wire mesh. At several places, the first and the second layers of the wire mesh were tied together with the same diameter of steel wire. An overlap of 100 mm was provided in the lateral direction of the wire mesh. The slurry was forced into the mesh by hand to form 25mm thick FC jacket. Before GFRP jacketing, the surface of the specimens were scraped lightly to remove surface contaminants. Firstly the surface of the concrete was coated with a layer of epoxy primer on the external surfaces of the concrete to fill air voids and provide high bond strength. Secondly, a thin layer of the two part saturant solution consisting of resin was applied over the specimens. Later first layer of GFRP sheets were wrapped around the specimens carefully with a lap of 100 mm in length. A roller was used to remove the entrapped air between the fiber and excess saturant so as to allow better impregnation of the saturant. After the application of the first wrap, a second layer of saturant solution was applied on the surface of the first layer.

### **1.5 Instrumentation and test setup**

Instrumentations were put in place to measure the axial and transverse displacements during concentric loading. A special kind of steel-frame was used to mount the LVDTs away from the surface of the specimens at the central zone to monitor the axial contraction and lateral displacements of the cylindrical specimens. Monotonic concentric compression was applied at a very slow rate (0.1 mm/min) to capture the complete post peak behavior of the measured load deformation curves.

## **2 RESULTS AND DISCUSSION**

Heat damaged columns and heat damaged strengthened columns are subjected to axial compression and the axial load versus displacement behavior has been studied.

### **2.1 Failure modes of Control Specimens and Heat Damaged specimens**

In the unheated control specimens shear failure was observed. Cracks formed near to the top and bottom ends due to batten effect (Kumutha et al, 2007), and as the displacement increased, the flexural cracks perpendicular to the cylinder axis widened with a sudden separation failure. In case of heat damaged cylinders, as reported in previous studies (Yaqub et al, 2011) the failure was gradual and exhibited ductility with increase in load and the lateral ties opened because of the spalling produced due to high temperature. The vertical cracks formed at the top and bottom ends of the cylinders, which eventually propagated and lead to crushing.

### **2.2 Failure modes of Heat damaged Strengthened specimens**

Failure of the HSFRC specimens was mainly due to the vertical and diagonal cracks in the jacket. The vertical cracks got widened with increase in load as shown in (Fig. 3). Further increase in load created noise due to breaking of steel fibers, thereby indicating the stress transfer from the dilated concrete to the jacket. In FC Strengthened cylinders the initial cracks formed at the ends, while the number of cracks increased with loading. Beyond peak loading the mesh wires started bulging out with breaking noise in all the specimens. The failure mode

of repaired FC jacketed specimens is shown in (Fig. 3). The steel wires of the welded mesh in the vertical direction bulged, while wires in horizontal direction got broken in entire length of the specimen. The failure of specimens occurred due to the cracks in the core concrete and the yielding of transverse wires. The failure mode clearly indicates that the transverse wires were subjected to hoop tension and thereby produced passive confinement pressure. In the specimens repaired with GFRP, the column failure was due to rupture. Clicking sounds were heard during the loading stage, and failure occurs at top and bottom of the specimens as shown in (Fig. 3). In this region, the stress attentiveness is attributed to high energy release, in the form of sudden failure of GFRP sheets. The damaged specimens exhibited good contact between the jackets and the concrete indicating no de-bonding.

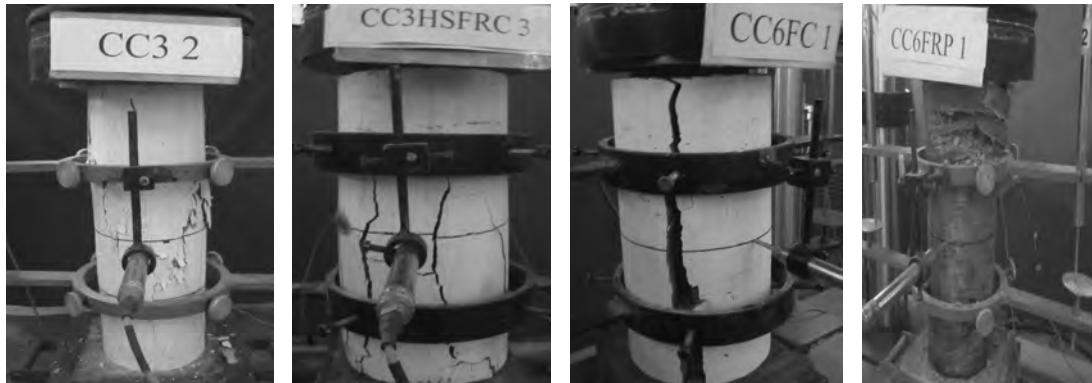


Fig. 3 Failure pattern of heat damaged cylinder and strengthened specimens

### 2.3 Strength of Heat damaged Strengthened Specimens

In this study heat damaged cylinders are repaired using number of methods comprising of HSFRC, FC and GFRP. Specimens were tested under axial compression & strength & deformability of repaired specimens were evaluated. Fig. 4 shows the effect of these methods on axial compressive strength. It shows that the post heating effect causes drastic reduction in strength of cylinders (Fig. 4). The strength was restored considerably by the various strengthening techniques (Fig. 5, 6, 7).

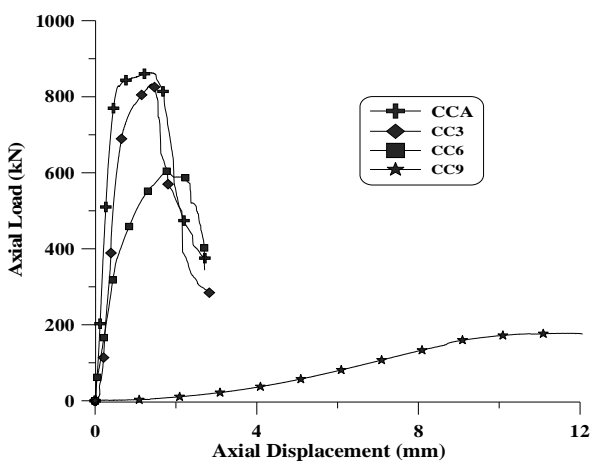


Fig. 4 Axial load- displacement comparison of control and heat damaged cylinders

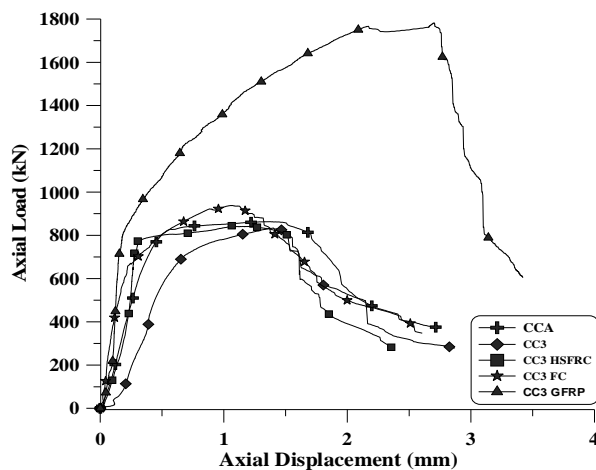


Fig. 5 Comparison of control and heat damaged specimens with 600°C strengthened cylinders

HSFRC jackets provide confinement effect to heat damaged specimens. Such confining effect is produced due to the fact that the heat damaged concrete dilates more under axial compression due to micro crack and porosity. HSFRC jackets restrain the heat damaged concrete, from radial bulging. When the heat damaged concrete reaches its ultimate unconfined compressive strength, the activation of jackets confines the columns in a three – dimensional state of stress, and consequently, increase the load carrying capacity of cylinder till the failure at its confined compressive strength. It can be seen that the strength of the heat damaged and HSFRC jacketed specimens are higher than the unstrengthened heat damaged specimens, but still remains less than the control specimen.

FC jacketing introduced hoop tension in the heat damaged cylinders, which eventually caused passive confinement. The effects of FC jacketing in strength enhancement is almost similar with HSFRC jacketing method, but the volume of variation is more prevalent in FC jacketing (Fig. 5-7). In GFRP Strength specimens the core concrete failed due to the compressive forces on the concrete. GFRP wrapping became active after this point. Expansion of the concrete core in the lateral direction made the GFRP more and more active in resisting the axial compressive force. Considerable strengthening was introduced due to double layer GFRP wrapping. The strength of the jacketed cylinder was greater than the control specimen.

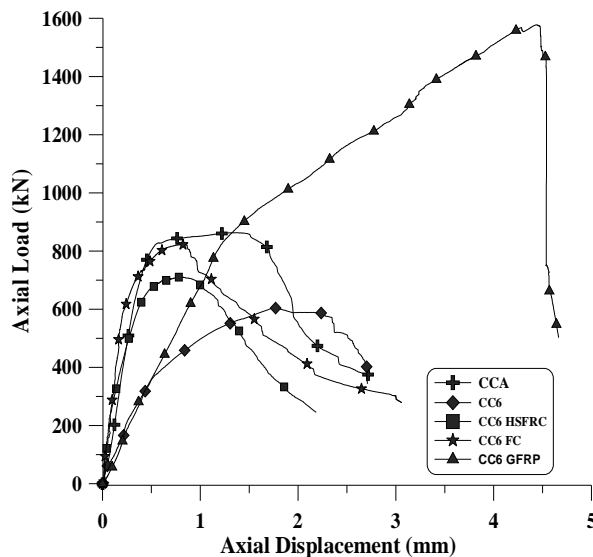


Fig. 6 Comparison of control and heat damaged specimens with 600°C strengthened cylinders

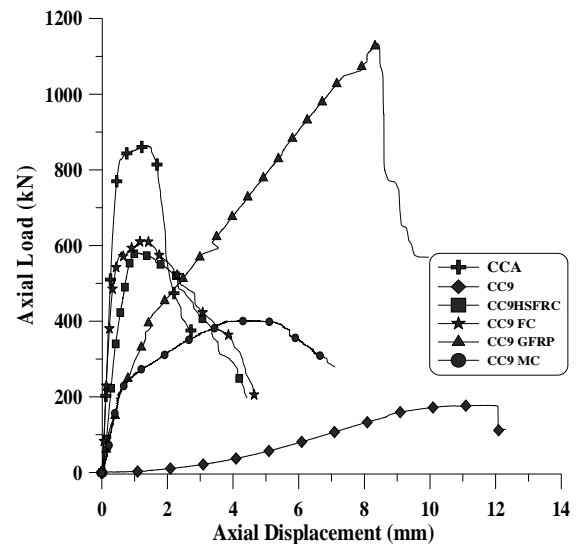


Fig. 7 Comparison of control and heat damaged specimens with 900°C strengthened cylinders

## 2.4 Ductility of heat damaged & strengthened Specimens

HSFRC and FC jacket repairing exhibits less amount of deformation ability in comparison to heat damaged columns. Above effect is due to the increase in cross section area in these methods. Increase in load carrying capacity and deformation by GFRP wrapping improves ductility of the specimen. Relative column load versus displacement is shown in Fig. 5-7. It can be seen that the enhancement of ductility of heat damaged columns wrapped with GFRP jacket was more noticeable than other jacketing methods. The Ultimate axial and lateral strains increased manifold, representing the ductility enhancement. This enhancement in the ductility is due to significant confinement to micro cracked heat damaged columns.

### 3 CONCLUSIONS

Following conclusions can be made based on the study. HSFRC, FC and GFRP composites can be utilized as strengthening technique for increasing the axial load carrying capacity of heat damaged reinforced concrete columns. The axial compressive strength of heat damaged cylinders increased significantly with GFRP when compared to other two strengthening techniques. Specimens repaired with HSFRC and FC jacketing exhibit less amount of deformation ability than the heat damaged specimens. Ductility of heat damaged specimens wrapped with GFRP jacket was more noticeable than other jacketing methods. Increase in ductility and strength of GFRP jacketed specimens is higher than the HSFRC and FC strengthened specimens

### REFERENCES

- Ehsani, M. R., & Jin, L. Repair of Earthquake-Damaged RC Columns with FRP Wraps, *ACI Structural Journal*, 94(2), 206-214, 1998.
- Luca, A. D., Asce, M., Nardone, F., Matta, F., Asce, A. M., Nanni, A., Asce, F. Structural Evaluation of Full-Scale FRP-Confined Reinforced Concrete Columns. *Journal of Composites for Construction*, 15(1), 112-123, 2011.
- Lam, L., and Teng, J. G. Design –Oriented Stress-Strain Model for FRP Confined Concrete. *Construction and Building Materials*, 17, 471-489, 2003.
- Kaushik S, Prakash A, Singh A. Inelastic Buckling of Ferrocement Encased Columns. In: *Proceedings of the Fifth International Symposium on Ferrocement*, 327–41, 1990.
- Nedwell P, Ramesht M, Rafei-Tanhanaki S. Investigation into the Repair of Short Square Columns Using Ferrocement. *Proceedings of the Fifth International Symposium on Ferrocement*, 277–85, 1990.
- Mourad, S. M., & Shannag, M. J. Repair and strengthening of reinforced concrete square columns using ferrocement jackets. *Cement and concrete composites*, 34(2), 288-294, 2012.
- Haddad, R H, Shannag, M. J., & Hamad, R. J. Repair of heat-damaged reinforced concrete T-beams using FRC jackets. *Concrete*, 9831(3), 223-231, 2011.
- Martinola, G., Meda, A., Plizzari, G. A., & Rinaldi, Z. Strengthening and Repair of RC Beams with Fiber Reinforced Concrete. *Cement and Concrete Composites*, 32(9), 731-739, 2010.
- Haddad, R H, Al-mekhlafy, N., & Ashteyat, A. M. Repair of heat-damaged reinforced concrete slabs using fibrous composite materials. *Construction and Building Materials*, 25(3), 1213-1221. 2011.
- Yaqub, M., & Bailey, C. G. Repair of fire damaged circular reinforced concrete columns with FRP composites. *Construction and Building Materials*, 25(1), 359-370, 2011.
- Yaqub, M., Bailey, C.G, Nedwell, P., Khan, I. Strength and stiffness of post-heated columns repaired with ferrocement and fibre reinforced polymer jackets. *Composites: Part B* 44 200–211, 2013.
- The Concrete Society. Repair of concrete structures with reference to BS EN1504. Technical report no. 69.
- Kumutha, R., Vaidyanathan, R., Palanichamy, M.S Behaviour of Reinforced Concrete Rectangular Columns Strengthened using GFRP, *Cement & Concrete Composites*, 29, 609–615, 2007.

## COMPARATIVE FIRE PERFORMANCE OF HIGH STRENGTH CONCRETE COLUMNS WITH DIFFERENT TYPES OF FIBER REINFORCEMENT

Wasim Khaliq <sup>a</sup>, Venkatesh Kodur <sup>b</sup>, Nikhil Raut <sup>c</sup>

<sup>a</sup>NUST Institute of Civil Engineering (NICE), School of Civil and Environmental Engineering (SCEE), National University of Sciences and Technology (NUST), Islamabad 44000, Pakistan

<sup>b</sup>Department of Civil and Environmental Engineering, 3546 Engineering building, Michigan State University, East Lansing, MI 48824, USA

<sup>c</sup>Bentley Systems Inc., Metairie, LA 70002, USA

### Abstract

Reinforced concrete (RC) columns made of high strength concrete (HSC) experience faster degradation of capacity and spalling when exposed to fire. To mitigate such fire induced spalling and enhance fire resistance, fibers are often added to HSC mix. This paper presents results from fire resistance tests to illustrate the comparative fire performance of HSC columns with different fiber combinations. Four reinforced concrete (RC) columns made of HSC with plain, polypropylene, steel, and hybrid fibers were tested under design fire conditions and data from tests is utilized to evaluate the comparative fire behaviour of these columns. Results from these fire resistance experiments show that hybrid fiber reinforced HSC columns exhibit improved performance as compared to plain, polypropylene, and steel fiber reinforced columns.

**Keywords:** fire response, high strength concrete columns, polypropylene fibers, steel fibers, hybrid fibers, spalling

### INTRODUCTION

Fire represents one of the most severe environmental conditions to which structures may be subjected, and hence, provision of appropriate fire safety measures is an important aspect in high rise buildings. In recent years there is an increased use of high strength concrete (HSC) for structural members in buildings. However, various studies show that HSC columns exhibit lower fire resistance than that of normal strength concrete (NSC) columns (Ali, Nadjalet al., 2004, Kodur, Chenget al., 2003, Kodur and McGrath, 2003). The lower fire resistance of HSC columns is attributed to faster degradation of strength of HSC with temperature and occurrence of fire induced spalling (Diederichs and Schneider, 1995, Kodur, Chenget al., 2003, Hertz, 2003).

Fire induced spalling is attributed to dense microstructure and lower permeability of HSC that prevents dissipation of pore pressure generated from water vapor in HSC members when exposed to high temperatures (Kodur and Dwaikat, 2008). When this pore pressure build-up exceeds the tensile strength of concrete, pieces of concrete break-off from the surface of concrete structural member (Kodur and Dwaikat, 2008). With increasing temperature, tensile strength of concrete also decreases and thus the risk of spalling increases. The faster degradation of compressive strength with temperature, combined with occurrence of spalling, leads to lower fire resistance in HSC members.

To mitigate fire induced spalling in HSC members, researchers have recommended the addition of polypropylene fibers to concrete (Ali, Nadjalet al., 2004, Kodur, 2000, Kodur and Phan, 2007). These polypropylene fibers melt at relatively low temperatures (about 167-170°C) and create randomly oriented micro and macro channels inside concrete. These channels facilitate dissipation of high vapor pressure generated in concrete members. Another approach to overcome spalling is through enhancing tensile strength of concrete which is

facilitated through adding steel fibers(Kodur, 1999). Alternatively, hybrid fibers comprising of both polypropylene and steel fibers can be added to HSC to mitigate fire induced spalling in HSC members (Ali and Nadjai, 2008). There have been numerous studies on fire performance of HSC columns with polypropylene fibers, but there are only limited studies on fire performance of HSC columns with steel and hybrid fiber reinforcement. Further there is lack of information on comparative fire performance of HSC columns made with different fibers.

To illustrate comparative fire performance of HSC columns with different fiber combinations, fire resistance tests were carried out on HSC columns with different fiber reinforced concrete mixes. Data generated in fire resistance tests is utilized to discuss the effect of different fiber combinations on fire performance of HSC columns.

## 2 EXPERIMENTAL PROGRAM

To generate data on HSC columns with different fiber combinations, fire resistance experiments were carried out on four HSC columns fabricated with plain, polypropylene fiber, steel fiber and hybrid fiber reinforced high strength concrete.

### 2.1 Mix Proportions and Column Characteristics

The experimental program consisted of conducting fire resistance tests on four reinforced concrete columns designated as HSC (plain – without fibers), HSC-P (with polypropylene fibers), HSC-S (with steel fibers) and HSC-H (with hybrid fibers). All four columns were 3300 mm long and were of square cross section of 203×203 mm. The columns had four 19 mm dia bars as longitudinal reinforcement and 10 mm ties, at 200 mm spacing, as transverse reinforcement. The steel of main reinforcing bars and stirrups had specified yield strength of 420 MPa. Steel plates of size 406×406×25 mm were attached to the top and the bottom of the column in order to fix the column in position and for facilitating load transfer from the actuator. The actual support conditions of columns were close to partially fixed, however pin-pin end condition were assumed for conservative load calculations.

The size of the test columns was dictated by dimensions of furnace and loading equipment and thus the columns had to be designed as slender (with slenderness ratio 61) as per ACI 318 specifications(2011). As per ACI 216.1 (2007) specifications, these columns were designed for two hour fire resistance rating. A summary of column characteristics, test parameters and results from fire resistance tests on these columns is tabulated in Tab. 1.

Tab. 1 Summary of column characterises, test parameters and results

Column designation	Fire exposure (ASTM E119 – decay)	Total test duration (minutes)	Concrete strength (MPa)		Column capacity (kN)	Load ratio (%)	Applied load (kN)	Relative humidity (%)	Failure time (minutes)	Extent of Spalling (% exposed volume)
			28 Day	Test day						
HSC	SF- decay @8°C/min	180	91	107	1260	60	760	86.6	75	Severe (40)
HSC-P	LF- decay @11°C/min	270	85	93	1260	60	760	92.5	221	Minor (10)
HSC-S	LF- decay @11°C/min	270	72	77	1060	60	640	91.25	No Failure	Nil (0)
HSC-H	LF- decay @11°C/min	270	75	80	1100	60	660	89.65	No Failure	Nil (0)

The columns were fabricated from four batches of HSC mix, one with no fibers and the other three columns with different fiber types. For fiber reinforced HSC mixes, commercially available fibers, NOVOCON XR type steel fibers and MONOFILAMENT (multi-plus) polypropylene fibers were added. Steel fibers were 38 mm in length and 1.14 mm equivalent diameter and had a specified tensile strength of 966 MPa. Polypropylene fibers in HSC-P and HSC-H batch mix were of nonabsorbent type with 20 mm length, 0.91 specific gravity and 162°C melting point. Steel fibers in HSC-S and HSC-H mix comprised of 42 kg/m<sup>3</sup> of

concrete representing 0.54% by volume. In HSC-P and HSC-H mix, polypropylene fibers weighing 1 kg/m<sup>3</sup> of concrete representing 0.11% by volume were added. The columns were cast horizontally and were moist cured in the forms for 7 days. Then the specimens were lifted from the forms and stored at ambient conditions, maintained at about 25°C and 40% relative humidity. Three cylinders from each concrete batch mix were tested to evaluate compressive strength at 7, 28 and 90 days respectively. The average compressive strength of concrete measured on 100×200 mm cylinders at 28 days ranged from 72-91 MPa and is given in Table 1. Just prior to undertaking fire tests, the room temperature moisture conditions (relative humidity) and compressive strength of concrete were also measured and this is also given in Tab. 1.

## 2.2 Instrumentation

The instrumentation in the test columns included thermocouples (TC), strain gauges (SG), and linear position transducers (LPT). Thirteen type-K (Chromel-alumel) thermocouples of 0.91 mm thickness were installed in columns for measuring concrete and rebar temperatures. Also strain gauges were mounted on three main longitudinal rebars. The location and numbering of thermocouples and strain gauges in the cross-section are shown in Fig. 1. The lateral deformations were also measured by placing two LPTs outside of furnace attached to columns with chromelwires.

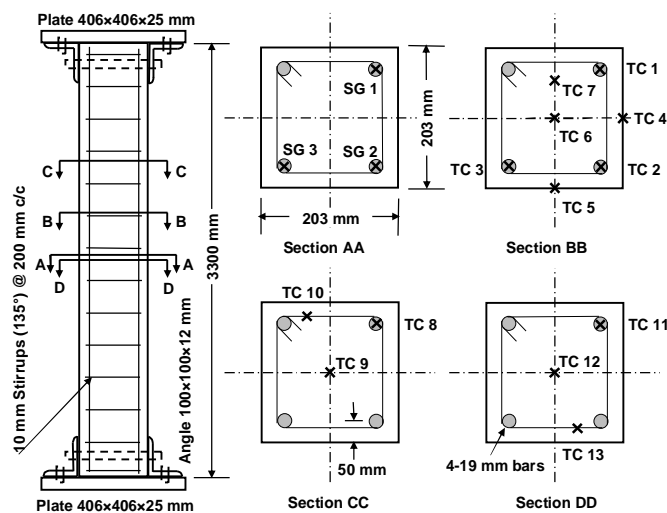


Fig. 1 Column dimensions and location of thermocouples (TC) and strain gauges (SG)

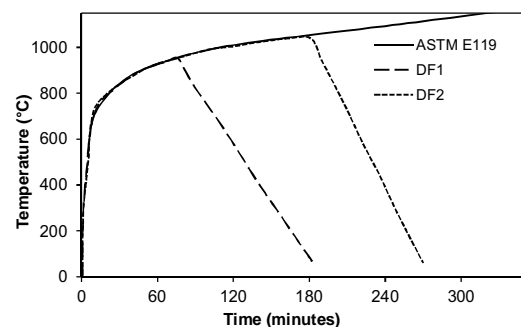


Fig. 2 Fire scenarios and furnace

## 2.3 Test Conditions and Procedure

The fire resistance tests were carried in the structural fire test furnace at Michigan State University (MSU). The test furnace has been specially designed to produce conditions, such as temperature, loads and heat transfer, to which a structural member might be exposed during a fire. The furnace has the capacity to supply both heat and applied loads that are present in a typical structural member exposed to fire. The furnace accommodates two columns at a time and different load level can be applied on each column. Full details on the furnace are given by Kodur and Fike (2009).

The fire resistance tests were carried out by exposing middle 1.68 m of the 3.3 m high columns from all four sides. HSC column without fibers was exposed to ASTM E119 (2008) standard fire exposure (DF1) for 90 minutes followed by a decay phase (8°C/min) as shown in Fig. 2. HSC-P, HSC-S, and HSC-H columns were tested under a parametric (design) fire exposure, comprised of a growth phase as per ASTM E119 (2008) standard fire exposure (DF2) for 3 hours, followed by a decay phase (11°C/min) as shown in Fig. 2. The well-

defined decay (cooling) phase was obtained by controlling temperatures to decay at a predetermined cooling rate (DF1 or DF2), to represent typical fire in a building.

All four columns were tested under a concentric axial load equivalent to 60% (load ratio) of the capacity of the column. The load ratio is the ratio of the applied (test) load to the column capacity at ambient conditions, computed according to ACI 318 (2011). The load was applied approximately 30 minutes before the start of the fire resistance test and was maintained until the column failed under fire exposure. During the test, the columns were exposed to heat controlled in such a way that the average temperature in the furnace followed, as closely as possible, the parametric fire curve. The load was maintained constant throughout the fire test duration. The columns were considered to have failed when the actuator could no longer maintain the load.

### 3 RESULTS AND DISCUSSION

A summary of results of fire resistance tests on four columns (HSC, HSC-P, HSC-S, and HSC-H) is tabulated in Table 1. The fire performance of these columns is evaluated in the form of thermal response, structural response, spalling progression and failure times.

#### 3.1 Thermal Response

The thermal response of all four columns is shown in Fig. 3 by plotting comparative temperatures profiles in rebar, and concrete (at mid depth) as a function of fire exposure time. In all columns, an initial plateau can be seen in rebar and concrete temperatures around 100°C and this can be attributed to heat from fire being utilized for evaporation of free water in concrete. After this initial plateau, the temperatures in concrete and rebars increase with fire exposure time. It can be noted that, in all four columns, the progression of temperatures in concrete (at mid-depth) is lower than that in rebars. This can be attributed to lower thermal conductivity and higher specific heat of concrete which delays temperature rise to inner layers of concrete.

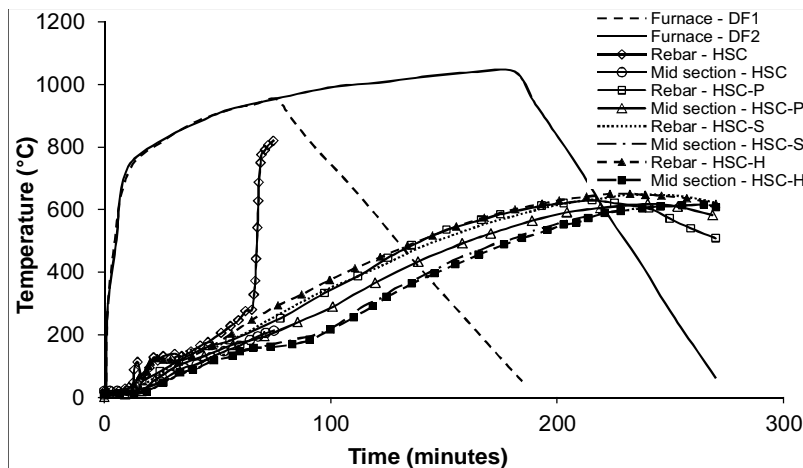


Fig. 3 Comparative temperature progression in HSC columns with different fibers

In HSC column without any fibers, severe spalling occurred which led to loss of concrete cross-section. This loss of concrete resulted in rapid rise of temperatures in rebars as shown in Fig 3. The spalling and loss of concrete cross-section in HSC column can be attributed to pore pressure build-up resulting from lower porosity in HSC.

HSC column with polypropylene fibers experienced some level of surface scaling and resulted in minor loss of concrete cross-section that led to slightly faster rise in temperatures in HSC-P column as seen in Fig. 3. The temperature progression in both HSC-S and HSC-H columns follow similar trends to that of HSC-P column, however HSC-P column experienced



lower temperature rise both in rebars and concrete at mid-section. The higher temperature in HSC-P can be attributed to slightly higher thermal conductivity and specific heat of HSC with polypropylene fibers (Kodur and Khaliq, 2011).

### 3.2 Structural Response

Structural response of concrete column can be assessed by monitoring axial and lateral deformations in columns. Only axial deformations were measured in the first two tests on HSC and HSC-P columns due to lack of expertise initially for measuring lateral deformations. However, both axial and lateral deformations were recorded in the case of HSC-S and HSC-H columns. The structural response of four columns is evaluated by comparing measured axial deformations as a function of fire exposure time, which is shown in Fig. 4.

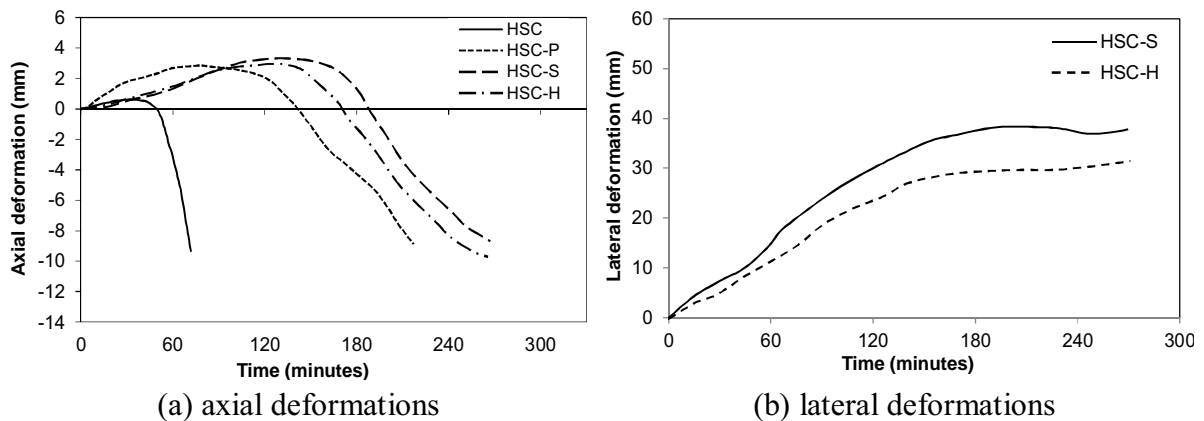


Fig. 4 Comparative structural response in HSC columns with different fiber combinations

A reinforced concrete column, when exposed to fire, expands initially due to thermal expansion occurring both in steel rebars and in concrete. With increasing fire exposure time, strength loss occurs in both steel and concrete (Kodur and McGrath, 2003). With further increase in temperature, the loss of strength and stiffness properties in concrete lead to increased load induced mechanical strains which in turn results in significant contraction of the columns.

The axial deformation of the columns plotted in Fig 4(a) illustrates that all four columns exhibit initial expansion phase followed by contraction with increasing fire exposure time. It can be noted that HSC column without fibers had earliest onset of axial deformation and failed through excessive contraction in about 75 minutes. This can be attributed to capacity degradation that resulted from loss of concrete cross-section due to severe spalling (Raut and Kodur 2010). HSC column with polypropylene fibers also endured axial deformation and failed in about 221 minutes. The axial deformations in HSC-P column was not abrupt as in the case of HSC column without fibers. This can be attributed to spalling mitigation facilitated by melting of polypropylene fibers present in concrete. The overall progression of axial deformation in both HSC-S and HSC-H columns was similar to that in HSC-P column. The onset of both expansion and contraction in these columns was slower which can be attributed to slow degradation of compressive and tensile strength in HSC-S and HSC-H columns facilitated by presence of steel fibers (Khaliq and Kodur, 2011, Lie and Kodur 1996). Also, no fire induced spalling was observed in HSC-S and HSC-H columns, and this in turn led to better fire performance in these columns as compared to that in HSC and HSC-P columns.

Fig. 4(b) illustrates the progression of lateral deformation in HSC-S and HSC-H columns as a function of fire exposure time. The lateral deformation in these columns increased gradually and reached to a maximum of 35 to 40 mm in about 150-180 minutes of fire exposure time. The lateral deformations then remained almost constant till the end of the test. This constant

lateral deformation in HSC-S and HSC-H columns can be attributed to slower degradation of strength and no loss of concrete cross-section due to absence of fire induced spalling.

### 3.3 Fire Induced Spalling

The progression and extent of spalling in tested columns was recorded qualitatively through visual observations during fire tests and was also evaluated by measuring the volumetric loss of concrete in fire exposed columns after fire tests and this is tabulated in Tab. 1. Fig. 5 shows pictures of all four columns after fire resistance test.

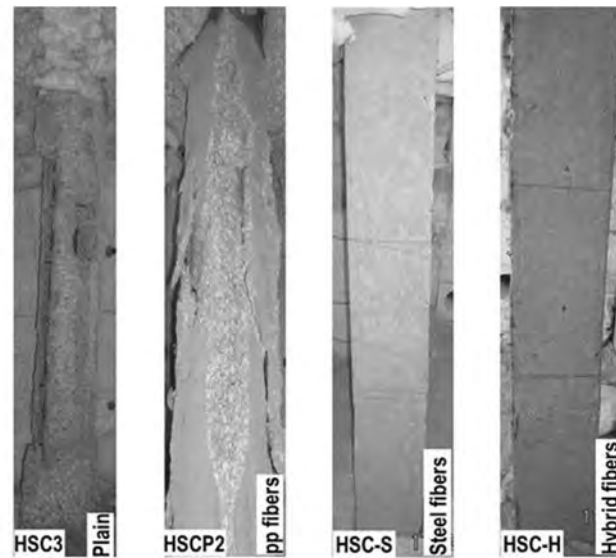


Fig. 5 State of high strength concrete columns after the fire resistance tests

Significant spalling occurred in HSC column without fiber sand this can be attributed to higher compactness and lower permeability of high strength concrete which results in the pore pressure build-up within the cross section. When this pore pressure exceeds the tensile strength of concrete, chunks of concrete break-off from the surface (Bilodeau, Koduret al., 2004, Dwaikat and Kodur, 2010). Reduced spalling in HSC-P column can be attributed to presence of polypropylene fibers. These polypropylene fibers melt at about 160°C and create micro channels in concrete that help to diffuse pore pressure build-up and thus reduce spalling (Kodur, 2000). No fire induced spalling was observed in HSC-S and HSC-H columns. This can be attributed to increased tensile strength facilitated by the presence of steel fibers in HSC-S and HSC-H and also increased permeability achieved through melting of polypropylene fibers in the case of HSC-H column (Khaliq and Kodur, 2011).

## 4 FIRE RESISTANCE

A comparison of fire resistance of four columns is given in Table 1. The time to reach failure is defined as the fire resistance and failure is said to occur when the strength of the column decreases to a level at which the column cannot sustain the applied load. HSC column without fibers failed only 75 minutes while HSC-P column failed in 221 minutes. This shows that significant increase in fire resistance of HSC columns can be achieved through adding polypropylene fibers to concrete mix.

In the case of HSC-S and HSC-H columns, fire induced spalling was not encountered and consequently these columns did not fail and survived burnout conditions. The steel fibers in HSC-S, and HSC-H columns helped to slowdown degradation of compressive and tensile strength of concrete and polypropylene fibers in HSC-P column mitigated spalling. The higher fire resistance in HSC-S and HSC-H columns can therefore be attributed to presence of steel and hybrid fibers respectively.

## 5 SUMMARY

Results from fire resistance tests clearly show that fiber reinforced HSC columns exhibit improved fire resistance as compared to HSC column without fibers. The fire resistance of plain HSC column was significantly lower due to the occurrence of fire induced spalling. Presence of polypropylene fibers in HSC-P column, help mitigate fire induced spalling by relieving the pore pressure and enhance its fire resistance. Presence of steel fibers in both HSC-S column help enhance tensile strength of HSC at elevated temperatures and thus minimize spalling and enhance fire performance. Presence of hybrid fibers in HSC-S column not only benefits from improved tensile strength (through steel fibers), but also through higher permeability in concrete (through polypropylene fibers) and this leads to significant increase in fire performance. Thus HSC columns with hybrid fibers exhibit superior performance under fire conditions.

## REFERENCES

- Ali, F., Nadjai, A., Silcock, G., Abu-Tair, A. Outcomes of a major research on fire resistance of concrete columns. *Fire Safety Journal*, Vol 39, pp 433-45, 2004.
- Kodur, V. R., Cheng, F. P., Wang, T. C., Sultan, M. A. Effect of strength and fiber reinforcement on the fire resistance of high strength concrete columns. *Journal of Structural Engineering*, ASCE, Vol 129, pp 253-9, 2003.
- Kodur, V. R., McGrath, R. Fire endurance of high strength concrete columns. NRCC-45141, : National Research Council Canada, Ottawa, Canada, p. 1-13, 2003.
- Diederichs, U. M., Schneider, U. High temperature properties and spalling behaviour of high strength concrete. 4th Weimar workshop on high performance concrete, HABp. 219-35, 1995.
- Hertz, K. D. Limits of spalling of fire-exposed concrete. *Fire Safety Journal*, Vol 38, pp 103-16, 2003.
- Kodur, V. K. R., Dwaikat, M. B. Effect of fire induced spalling on the response of reinforced concrete beams. *International Journal of Concrete Structures and Materials*, Vol 2, pp 71-81, 2008.
- Kodur, V. R. Spalling in high strength concrete exposed to fire - concerns, causes, critical parameters, and cures. *Proceedings of the ASCE Structures Congress*. Philadelphia, PAp. 1-9, 2000.
- Kodur, V. K. R., Phan, L. Critical factors governing the fire performance of high strength concrete systems. *Fire Safety Journal*, Vol 42, pp 482-8, 2007.
- Kodur, V. R. Fiber reinforced concrete for enhancing structural fire resistance of columns. *American Concrete Institute*, Vol SP 182-12, pp 215-34, 1999.
- Ali, F., Nadjai, A. Fire resistance of concrete columns containing polypropylene & steel fibers. *Special Publication, SP-255-9*, American Concrete Institute, Farmington Hills, MI, Vol 255, pp 199-216, 2008.
- ACI 318-11. *Building Code Requirements for Reinforced Concrete and Commentary*. Farmington Hills, MI: American Concrete Institute, 2011.
- ACI 216.1. *Code requirements for determining fire resistance of concrete & masonry construction assemblies*. ACI 216.1-07. American Concrete Institute, Farmington Hills, MI:p. 1-32, 2007.
- Kodur, V. K. R., Fike, R. Guidelines for improving the standard fire resistance test specifications. *Journal of ASTM International (JAI)*, Vol 6, pp 16, 2009.

- ASTM E119-08b. Standard test methods for fire tests of building construction and materials. West Conshohocken, PA: ASTM International, 2008.
- Kodur, V., Khaliq, W. Effect of temperature on thermal properties of different types of high strength concrete. *Journal of Materials in Civil Engineering*, ASCE, Vol 23, pp 793-801, 2011.
- Khaliq, W., Kodur, V. K. R. Effect of high temperature on tensile strength of different types of high-strength concrete. *ACI Materials Journal*, Vol 108, pp 394-402, 2011.
- Bilodeau, A., Kodur, V. R., Hoff, G. C. Optimization of the type and amount of polypropylene fibers for preventing the spalling of lightweight concrete subjected to hydrocarbon fire. *Cement and Concrete Composites*, Vol 26, pp 163-74, 2004.
- Dwaikat, M. B., Kodur, V. K. R. Fire induced spalling in high strength concrete beams. *Fire Technology*, Vol 46, pp 251-74, 2010.
- Lie, T.T., Kodur V.K.R., Thermal and mechanical properties of steel-fibre-reinforced concrete at elevated temperatures, *Canadian Journal of Civil Engineering* 23 (2), 511-517, 1996.
- Raut, N. Kodur V.K.R., Response of high-strength concrete columns under design fire exposure, *Journal of Structural Engineering* 137 (1), 69-79, 2011.

## ON THE THERMO-MECHANICAL CHARACTERIZATION OF CEMENT MORTARS EXPOSED TO HIGH TEMPERATURE

Patrick Bamonte <sup>a</sup>, Pietro G. Gambarova <sup>a</sup>

<sup>a</sup> Department of Civil and Environmental Engineering, Politecnico di Milano, Milano, Italy

### Abstract

Some recent technical documents on fire-resistant walls made of either cementitious blocks or clay bricks are bringing onto the stage the thermo-mechanical behavior of the mortars. Information on mortars decay at high temperature, however, is either contradictory or can hardly be found in the technical-scientific literature. This study aims to provide information on the thermo-mechanical behaviour of mortars in residual conditions. Three mortars are investigated (a **reference** mortar, cube strength  $f_{cc} \approx 5$  MPa, and two higher-grade mortars,  $f_{cc} \approx 10$  MPa and  $f_{cc} \approx 15$  MPa, respectively). All mortars are tested past a high-temperature cycle at 200, 400 and 600°C. On the whole, the mechanical decay turns out to be very close to that of typical ordinary concretes, while the thermal diffusivity is markedly lower. A worked example about a concrete-block fire-resistant wall ends the paper.

**Keywords:** mortars, residual tests, mechanical properties, thermal diffusivity.

### INTRODUCTION

Increasing attention has been devoted in the last years by the scientific and professional communities, and by code makers, to the risk of fire and high temperature in constructions, and to the ensuing detrimental effects on structural safety. In most cases, however, the structural damage due to a fire is more or less limited, especially in concrete and masonry structures, and people are more endangered by the smoke (in the early phases of a fire, when temperatures are still rather low) than by the weakening of the bearing structure.

Focusing on human safety, and leaving aside the structural behaviour as such, compartmentation is a major issue (= subdivision of the space inside a building into a number of sub-spaces, so that the fire and its effects remain confined to a single compartment).

Compartmentation is generally achieved by means of 2-D load-bearing or non-load bearing members (slabs, floors, partitions and walls, or windows and doors), whose compartmentation capacity requires two fundamental criteria to be met for any fire duration (Buchanan, 2002):

- Criterion E = Integrity: the given member should exhibit no cracks, no spalling, no excessive out-of-plane displacements, no disconnections along the boundaries, to avoid flame, gas and smoke transmission to nearby compartments.
- Criterion I = Insulation: the given member should limit heat transmission, from the internal hot surfaces (exposed to the fire) to the external cold surfaces, in order to avoid any spread of the combustion.

To meet Criterion E laboratory tests are required, as there are no other means to ascertain whether smoke and flames pass through walls or floors (due to cracking, open joints, ...).

Meeting Criterion I implies that any given member used in compartmentation should keep the average differential temperature between the hot surface and the cold surface, and the maximum differential temperature below certain limits, for any given fire duration ( $\Delta T_{av} \leq 140^\circ\text{C}$  and  $\Delta T_{max} \leq 180^\circ\text{C}$ , according to Eurocode 2 – EN 1992-1-2).

As for **stability** or **resistance** (Criterion R), meeting this criterion requires the preliminary determination of the thermal field inside the structural member, under one of the more or less realistic fire curves specified by the codes. Knowing the thermal field allows evaluating the

mechanical decay of the material in each point, provided that materials mechanical properties at high temperature – and past cooling – are known. Then structural analysis makes it possible to assess the loss in terms of bearing capacity and to check whether the actual reduced bearing capacity guarantees an adequate safety level face to the loads applied in fire conditions (Bamonte et al., 2008).

Among the most common structures used in compartmentation, fire-resistant walls take the lion’s share, especially in industrial buildings (Dal Lago, 2002). Firewalls generally consist of hollow bricks made of concrete (vibrated under pressure) or clay, with mortar layers interposed along the vertical and horizontal joints. The compartmentation capacity is partly due to the good insulating properties of the materials (concrete, clay and mortar) and partly to the voids of the blocks or bricks.

Within this context, the thermo-mechanical characterization of three commercial cementitious mortars is performed in this paper, in order to assess their compatibility with the properties of ordinary concrete, often used in the manufacture of hollow blocks. The three mortars, called “M5”, “M10” and “M15” throughout the paper, belong to the classes M5, M10 and M15 of the Italian standard, with  $f_{cc} \approx 5, 10$  or  $15$  MPa, respectively. Furthermore, M5 can be considered as a reference mortar, in spite of its fibre content (polypropylene fibres,  $v_f = 0.1\%$  by volume), while M15 is a high-strength mortar.

## 1 EXPERIMENTAL PROGRAM

The thermo-mechanical characterization of any cementitious material generally requires the evaluation of such parameters as compressive strength, tensile strength, elastic modulus, mass per unit volume and thermal diffusivity as a function of the temperature (Felicetti and Gambarova, 1998; Bamonte and Gambarova, 2010).

In this project, twenty-four cylindrical specimens were required by the tests in compression and for the evaluation of the elastic modulus ( $\varnothing \times h = 80 \times 160$  mm). Three further cylinders ( $\varnothing \times h = 100 \times 300$  mm) were instrumented with two thermocouples each, to evaluate the thermal diffusivity.

All cylinders were stored for 28 days in quasi-sealed conditions at 20-25°C and 60-70 R.H. (The cylinders were left inside plastic pipes, without plugs at the extremities). Later, the specimens were sawn at the desired length and the end sections were ground and polished.

The same curing process was adopted for the prisms to be tested in bending ( $40 \times 40 \times 160$  mm). The two stumps resulting from the fracture of each prism were tested in compression, to evaluate the cube compressive strength.

In Fig. 1a) one of the three specimens instrumented for the evaluation of the thermal diffusivity is placed inside the electric furnace, whose heating rate is controlled via a proportional integro-differential procedure. The uniformity of the thermal field is guaranteed by a steel pipe, whose temperature is the control parameter of the furnace.

Tab. 1 Main properties of the mortars

Lime, cement and siliceous aggregate (0-4 mm)	see EN 13139 (2006)
Soluble chloride	$\approx 0.05\%$
Mass per unit volume (fresh/hardened state)	$\approx 2000/1850$ kg/m <sup>3</sup>
Thermal conductivity (hardened state)	0.80-0.90 W/m°C

## 2 THERMAL CHARACTERIZATION

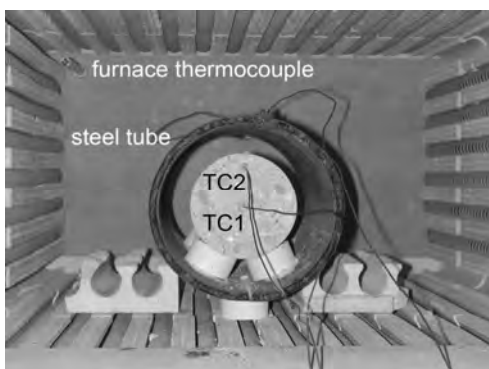
The thermal diffusivity is defined as:  $D = \rho/(c \lambda)$ , where  $\lambda$  is the thermal conductivity,  $c$  is the specific heat and  $\rho$  is the mass per unit volume. In a long cylinder ( $h \geq 2\varnothing$ ) subjected to a constant heating rate ( $v_h =$  mean heating rate inside the specimen), the thermal diffusivity can be evaluated by means of the following equation:

$$D = v_h R^2 / (4 \Delta T) \quad (1)$$

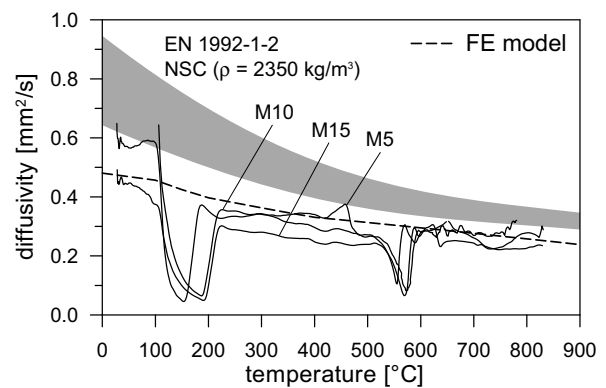
where  $\Delta T = T_2 - T_1$  is the difference between the temperatures measured close to the heated surface and along the axis in the mid-height section, and  $R$  is the distance between the two measurement points (Fig. 1a).

Each of the three cylinders instrumented with 2 thermocouples was slowly heated from 20 to 900°C, and  $T_1$  and  $T_2$  were measured at regular intervals. As shown in Fig. 1b, between 200 and 550°C the thermal diffusivity of the three mortars is roughly constant ( $= 0.25\text{-}0.35 \text{ mm}^2/\text{s}$ ) and by 30-35% lower than that of ordinary concrete, represented in Fig. 1b by the grey envelope. Hence, ordinary and high-strength mortars never act as thermal bridges in a firewall, thanks to their good insulation properties.

Water vaporization in the pores and crystalline changes in the quartz contained in the aggregate are responsible for the downward spikes at 150-200°C and 550-600°C, respectively. Below 100-150°C and above 700°C the values are dubious because of the thermal transients and of calcination ( $=$  dissociation of calcium carbonate), respectively.



(a)



(b)

Fig. 1 (a) Cylinders inside the electric furnace instrumented with 2 thermocouples (TC1 and TC2); and (b) thermal diffusivity versus temperature

### 3 RESIDUAL COMPRESSIVE STRENGTH

Twenty-four cylinders (diameter  $\times$  height = 80  $\times$  160 mm) were tested in compression in displacement-controlled conditions, with the mortars either undamaged ( $T = 20^\circ\text{C}$ ) or past a thermal cycle ( $T = 200, 400$  and  $600^\circ\text{C}$ ). For each mortar and temperature, two tests were carried out, all characterized by an outstanding repeatability.

The thermal cycles were performed in quasi-steady conditions to guarantee the uniformity of the thermal field, and to avoid any self-stress. The heating/cooling rate and the rest at the reference temperature were 1.0/-0.25°C/minute and 120 minutes.

The displacement rate adopted in the tests was 2.5  $\mu\text{m/s}$  (up to the peak load), 5.0  $\mu\text{m/s}$  in the softening branch down to 50% of the peak load and 10.0  $\mu\text{m/s}$  down to the crushing of the specimen. All specimens were instrumented with 3 LVDTs placed at  $120^\circ$  astride the mid-height section ( $L = 50 \text{ mm}$ ), to measure the shortening of the specimen and to make the drawing of the stress-strain diagrams feasible (Fig. 2a). Though rather low, the values of the cylindrical strength at  $20^\circ\text{C}$  ( $f_c = 5.1, 8.4$  and  $12.1 \text{ MPa}$ ) agree with producer's indications on small cubes ( $f_{cc} = 8, 14$  and  $17 \text{ MPa}$ ) and with the tests performed by the authors on small cubes ( $f_{cc} = 8.5, 16.1$  and  $18.0 \text{ MPa}$ , not shown in the following), provided that the differences between small cubes (side = 40 mm) and rather large cylinders ( $h = 2\varnothing = 160 \text{ mm}$ ) are taken care of (in terms of size effect and platen-to-cube friction), and between curing in a controlled environment and in quasi-sealed plastic pipes, as done in this project.

Mortar M15 appears to have the best performance at any temperature, Fig. 2a. (At  $600^\circ\text{C}$  the residual strength of Mortar M15 is twice as much that of the reference Mortar M5).

In terms of normalized compressive strength (Fig. 2b), M10 and M15 behave somewhat better than M5 up to 300°C, while there are no practical differences above 400°C. The most important indication given by Fig. 2b, however, is that at any temperature mortars decay is very close to that of ordinary concrete (shaded envelope referring to hot concrete: mortars curves are lower as it should be, because they are residual curves, always lower by 15-25% compared to hot curves). As in certain concretes, the strength increase up to 250-300°C is nothing new, but – as in concretes – it is of no practical relevance.

Summing up, the strength decay similar to that of ordinary concrete is a clear indication that in any walls made of concrete blocks mortar layers are not the weakest link of the resistant chain.

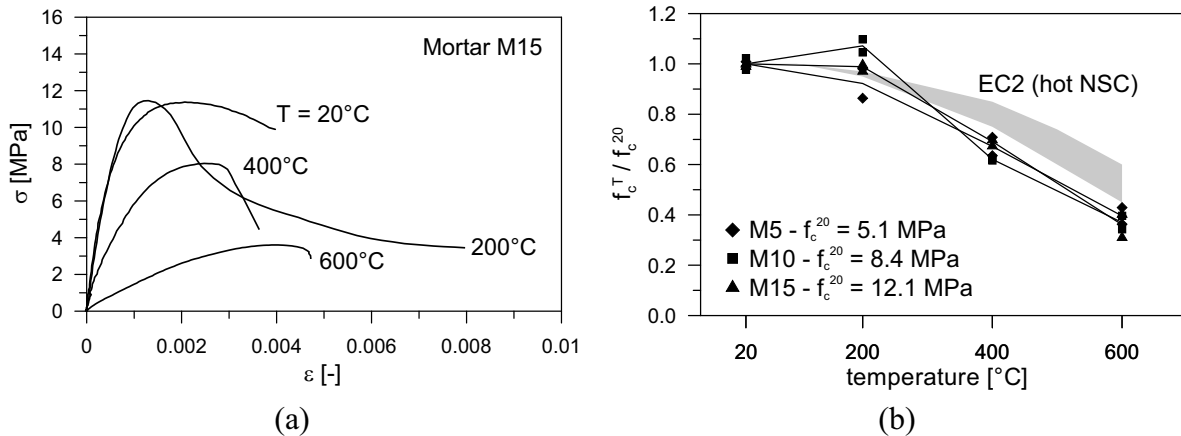


Fig. 2 (a) Stress-strain curves for the high-strength mortar M15; and (b) normalized plots of the cylinder strength as a function of the temperature; the gray band refers to EC2 provisions at high temperature, for calcareous (top curve) and siliceous (bottom curve) aggregates

#### 4 RESIDUAL ELASTIC MODULUS AND TENSILE STRENGTH IN BENDING

The secant modulus was evaluated starting from the stress-strain curves, in the stress range 30-50% with respect to the peak of the stress-strain curves.

The values at 20°C are very low compared to those of ordinary concrete, something well known for mortars (Neville, 2002; see the values indicated in the insert of Fig. 3a).

The normalized curves (Fig. 3a) show that the decay of the modulus of M15 is the least up to 300°C; beyond this temperature, the values of the three mortars are very close and similar to those of ordinary concrete (grey envelope). Up to 200°C, however, the mechanical decay of the mortars is even lower than that of ordinary concrete, as shown by the grey envelope (Phan and Carino, 1998).

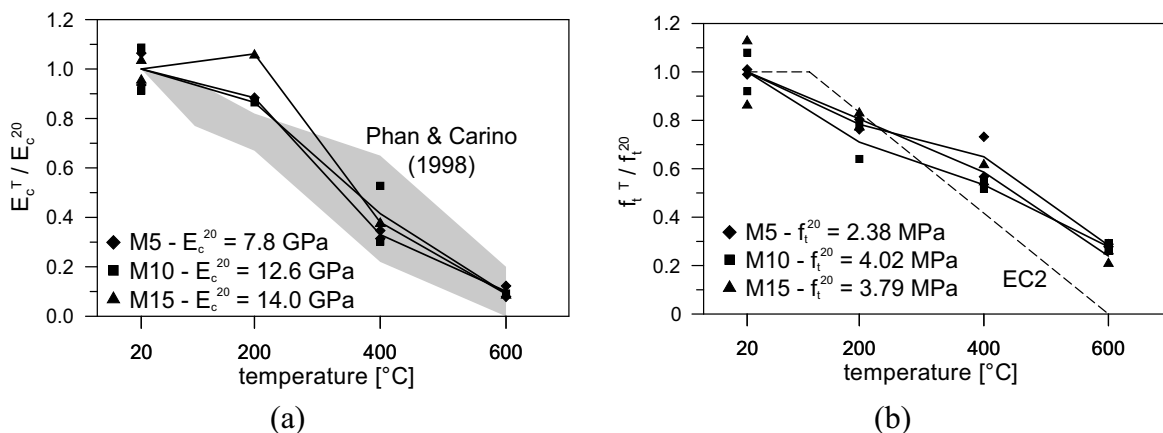


Fig. 3 (a) Normalized plots of the secant elastic modulus as a function of the temperature; (b) plots of the normalized strength in tension by bending as a function of the temperature



The tensile strength was measured by testing in bending a number of prisms ( $40 \times 40 \times 160$  mm) loaded at mid-span, in agreement with the Italian standard UNI EN 1015-11. The normalized curves (Fig. 3b) are very close and exhibit a rather linear decay with the temperature. As a reference, the normalized decay of the direct tensile strength of ordinary concrete at high temperature (from EC2) is reported as well in Fig. 3b. On the whole, above  $250^\circ\text{C}$  mortars seem to be less affected by high temperature. Such fact, however, may be more apparent than real, because the specimens loaded in direct tension and those loaded in indirect tension by bending behave differently at collapse, something that is well known.

## 5 APPLICATION

A rather simple example is worked out in the following to demonstrate that the three mortars in question allow Criterion I to be met in a typical fire-resistant wall made of concrete blocks. Let us consider a block-type firewall, whose lateral view and cross section are indicated in Figs. 4a,b. The nominal dimensions of the blocks are  $L \times h \times b = 500 \times 200 \times 180$  mm; the thickness of the front and back plates of each block, as well as that of the ribs, is 30 mm; the thickness of the mortar layers is 20 mm. Because of the symmetries of the problem, only the shaded portion (Fig. 4a) is considered in the 3D thermal analysis (extended to 150 minutes). The boundary conditions of the thermal problem are indicated in Fig. 4b.

A preliminary analysis (A0) was performed assuming the walls of the voids to be perfectly adiabatic, and the mean temperature of the walls was worked out as a function of the fire duration :  $T_{AV} = F_0(t)$ . Then, in the first analysis (A1) the average temperature in the voids was introduced through the function  $F_0(t)$ , and the updated time-evolution of the mean temperature of the walls was worked out:  $T_{AV} = F_1(t)$ . A second analysis was started having  $F_1(t)$  as imposed mean temperature in the voids, and again the updated time-evolution of the mean temperature of the walls was worked out:  $T_{AV} = F_2(t)$ . A third analysis was performed and so on. After a rather limited number of analyses ( $n = 3$ ), the perfect coincidence of the imposed mean temperature in the voids  $F_{n-1}(t)$  with the actual mean temperature  $F_n(t)$  allowed to stop the iterative process, since the solution had been reached.

The thermal analysis was performed by giving the concrete the thermal properties indicated in EC2 and the mortar those found in this project (mass per unit volume, not plotted in this paper, and diffusivity, see the dashed curve in Fig. 1b). As for the thermal conductivity of the mortar, the values indicated by the producer at  $20^\circ\text{C}$  were adopted ( $= 0.80 \text{ W}/[\text{m}\times\text{K}]$ ), while its temperature dependence was assumed to be the same as in concrete. In the analysis, 3D tetrahedric finite elements were used within the code ABAQUS.

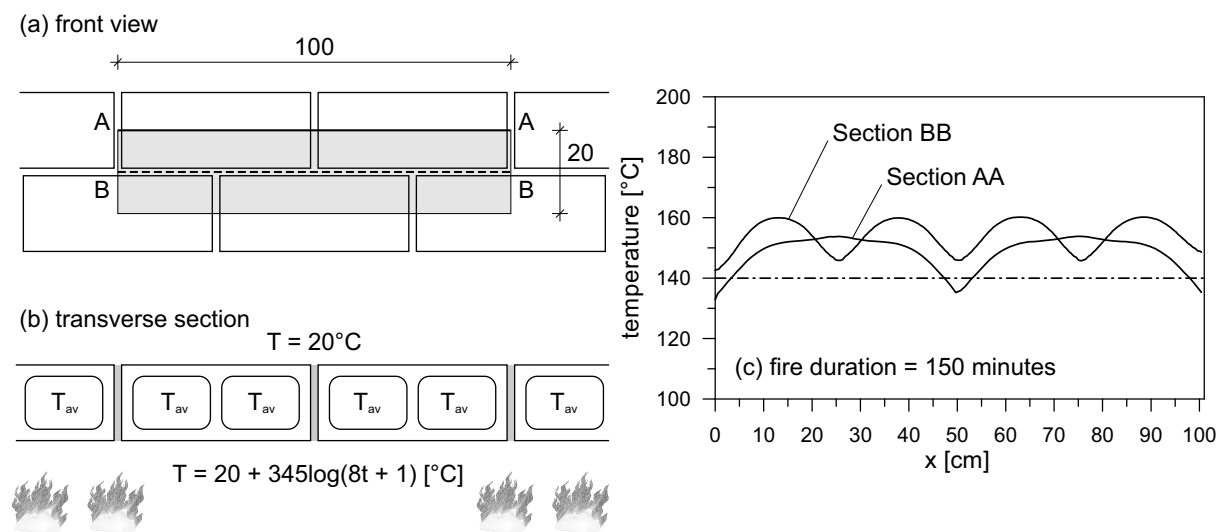


Fig. 4 (a) Portion of the fire wall discretized by finite elements; (b) boundary conditions of the thermal problem; and (c) plots of the temperature in Sections AA and BB along the cold face, for a fire duration of 150 minutes (the dash-dotted line refers to a 180 mm-thick concrete wall)

The results of the analysis are summarized in Fig. 4c, where the cold-face temperature is plotted along AA (thick curve) and BB (dashed curve), see Fig. 4a, 150 minutes after the beginning of the standard fire. (As the thermal properties and the mass per unit volume are very close for the three mortars, the analytical values hold for all three mortars).

In both sections AA and BB, assuming 20°C for the initial temperature of the cold face, the mean temperature at the cold face ( $T_{av} = 148$  and 154°C) is below  $140 + 20 = 160$ °C, and the maximum local temperature ( $T_{max} = 154$  and 160°C) is below  $180 + 20 = 200$ °C. (Note that the maximum temperature is reached in correspondence with the brick cavities, and not in correspondence with the vertical concrete ribs and mortar layers). Hence the system hollow blocks + mortar layers meets Criterion I, for a fire duration of 150 minutes. For the same fire duration, should the 180 mm-thick wall be made of solid concrete, the temperature at the cold face would be close to 140°C (dash-dotted line in Fig. 4c).

## 6 CONCLUDING REMARKS

The residual tests carried out on three cementitious mortars (M5, M10 and M15) exhibiting a cube strength in excess of 5, 10 and 15 MPa confirm their good thermo-mechanical properties at high temperature ( $T \leq 600$ °C), in terms of thermal diffusivity, compressive strength on cubes and cylinders, secant elastic modulus and tensile strength by bending. In detail:

- The three mortars exhibit a thermal diffusivity lower – on the whole – than that of ordinary concrete (from -25 to -40%), which is an indicator of the high insulation properties of the mortars.
- The two higher-grade mortars (M10 and M15) have definitely better residual-strength properties in compression than the reference mortar (M5), at any temperature; the normalized curves, of the compressive strength, however, are very close and rather similar to those of ordinary concrete, up to 600°C, while the normalized curves of the secant elastic modulus are very close, and better than those of ordinary concrete below 200°C; at higher temperatures, mortars are aligned with ordinary concrete.
- In terms of residual strength in indirect tension by bending, the three mortars behave similarly to ordinary concrete.
- The thermal analysis of a firewall made of hollow concrete blocks and mortar layers show that the better insulation properties of the mortar offset the thermal bridge created by the continuity of the layers across the wall; hence, mortar layers are never the weakest link of the chain in terms of strength (Criterion R) and insulation (Criterion I).

## REFERENCES

- Bamonte P., Gambarova P.G. and Meda A., Today's Concretes Exposed to Fire – Test Results and Sectional Analysis. *Structural Concrete*, 2008, V. 9, No. 1, pp. 19-30.
- Bamonte P. and Gambarova P.G., Thermal and Mechanical Properties at High Temperature of a Very High-Strength Durable Concrete. *ASCE - Journal of Materials in Civil Engineering*, 2010, Vol. 22, No. 6, pp. 545-555.
- Buchanan A.H., *Structural Design for Fire Safety*, John Wiley & Sons, 2002, 421 pp.
- Dal Lago A., Manufacturing Problems in Fire-Resistant Walls and Panels Certified for REI 120-180 (in Italian), In Proc. 14th Nat. Conf. of the Soc. of Building Technicians – CTE, Mantua (Italy), November 7-9, 2002, pp. 485-491.
- Felicetti R. and Gambarova P.G., Effects of High Temperature on the Residual Compressive Strength of High-Strength Siliceous Concretes, *ACI Materials Journal*, V. 95, No. 4, July-August 1998, pp. 395-406.
- Neville A.M., *Properties of Concrete*. Pub. by Dorling Kindersley on behalf of Pearson Education (South Asia), 2008, 844 pp.
- Phan L. and Carino N., Review of Mechanical Properties of HSC at elevated Temperature. *ASCE J. of Materials in Civil Eng.*, 1998, V. 10, No. 1, pp. 58-64.

## EVALUATION OF THE FIRE SEPARATING WALL AFTER THE FIRE

### Technical assessment of the loadbearing masonry wall exposed to high temperatures

Paweł A. Król <sup>a</sup>

<sup>a</sup> Warsaw University of Technology, Faculty of Civil Engineering, Warsaw, Poland

#### Abstract

The paper presents a procedure for an assessment of the technical condition of the loadbearing fire wall made of hollow silicate blocks after the fire. The wall in addition to its fire-separating function was one of two loadbearing walls in the three-story office building, carrying the load from the roof and intermediate floors. The wall was designed as structure satisfying the requirements of REI120 class. During the severe fire the wall fulfilled its task, and its technical fire parameters in reality turned out to be better than projected ones. As a result of the fire which, in spring 2011 completely destroyed the adjacent part of the warehouse building (Fig. 1), and as a result of the two-day intensive fire-fighting, the integrity of the wall was violated. The wall suffered extensive damage, which decreased the strength parameters, and its ability to carry loads.

**Keywords:** technical assessment, firewall, fire, masonry, silicate, carbonation, sample, test

#### INTRODUCTION

The building described in the paper was built in 2006 as part of the complex consisting primarily of warehouse and the administrative-office part, which was playing a supporting role to the warehouse facility. The administrative part of the building was designed in shape of the elongated rectangle with dimensions of approximately 7.0 x 174.0 m as a building of three storeys above the ground, without a basement, with traditional masonry construction of walls, and with reinforced concrete floors, made mostly of precast hollow panels, (Fig. 1).



Fig. 1 View of the complex during the firefighting (internet source); in the foreground the administrative-office part of the building is seen

The main loadbearing system of the building consists of two longitudinal loadbearing walls made of hollow silicate blocks 6 NFD W+W, grade 15, (Fig. 2) insulated from the outside with polystyrene plates. One of these walls, located on the side of the warehouse, was designed as a typical firewall satisfying the requirements of REI120 class, separating two zones with different purposes.

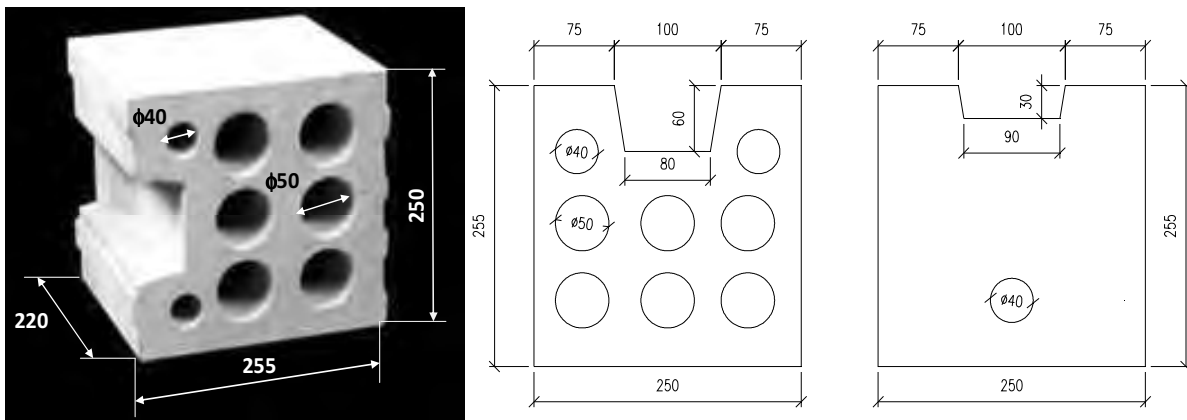


Fig. 2 The shape and nominal dimensions of the silicate block, type 6 NFD W+W

The building was divided on its length by four expansion joints, spaced about 30 m. The aforementioned warehouse burned down in a fire, which broke out in the building on May 10, 2011, (Fig. 1). The rescue action lasted uninterrupted for more than two days. Due to the presence of fire separation wall located between two parts of the building and smoothly conducted firefighting, flames did not spread to an office premises, but the construction of the wall - in a result of the simultaneous action of high temperatures and coolant - suffered quite extensive damage, which decreased the strength parameters and its ability to carry loads.

## 1 DESCRIPTON OF THE WALL'S DAMAGES

On a large wall area it has been observed a violation of its structure through the crack spreading along the designated location of hollow channels in the silicate blocks, (Fig. 3). Some parts of the wall have suffered mechanical damage, most likely as a result of being hit by the falling roof structure elements. Relatively large lateral displacements of individual silicate blocks observed on site reinforced this assessment, (Fig. 3).

Quite similar picture of damage, but occurring in the middle of the floor, could be seen on the fragments of the wall, located near the middle of the distance between expansion joints. Here, however, the deformation of the wall was more uniform in nature and tended to indicate wall buckling out of its plane – rather than other reasons - as a result of inability to compensate for the thermal elongation strains due to too long distance between the expansion joints. Deformation of the wall that was measured on the height of a single story reached about 20 mm whilst the standard deviation limits allowed for thick walls (> 24 cm) should not exceed 6 mm. The deformations that occurred as a result of thermal effects were so significant that existing compensation joints were not able to compensate for them, leading to pressing interaction between the two wall portions, located on opposite sides of the joint. To be more strict, with temperature increase of 400°C, the wall 30 m long and made of silicate blocks is able to increase its length of about 12 cm, which confirms the observations made on site, during inspection, (Fig. 3).

In addition, as a result of high temperature exposure of the floor ring beams, there was a concrete spalling observed, not only within the concrete cover, but also in the deeper layers. Due to the explosive nature of the phenomenon of spalling, on certain passages also some silicate wall blocks were significantly damaged, especially those ones located in the immediate vicinity of the ring beam. In many places, the wall material losses reach about 50% of the wall thickness, (Fig. 3). There could be also found some wall sections in which, for various reasons, the wall thickness defects reached even 75-80% of its original thickness. Not only spalling itself but also the concrete color change indicated during the inspection proved the change of the internal structure and mechanical properties of concrete paste. Some secondary damage within the wall material was caused by the firefighting itself, causing dampness of walls, destruction of internal gypsum plasters, lime efflorescence and mold beginnings.



Fig. 3 Examples of the structural damage to the wall

## 2 LABORATORY TESTS ON SAMPLES OF THE WALL MATERIALS

### 2.1 Tests on silicate wall blocks

During sampling, it was found out that due to the significant degree of cracking only just below 20-30% of items were suitable to be used as a material for carrying out further research. Totally five selected silicate blocks were collected. Despite the pre-selection in the wall on site, only three out of five blocks collected were qualified to the strength tests. The degree of cracking of two elements prevented unambiguous determination of their mechanical properties, and there were no further testing done on those components.

The nominal strength of silicate blocks obtained during tests reached, respectively, (PN-EN 771-2:2006 and PN-EN 772-1:2011):

- for test sample No. 1: 12.33 N/mm<sup>2</sup>
- for test sample No. 2: 8.16 N/mm<sup>2</sup>
- for test sample No. 3: 13.03 N/mm<sup>2</sup>
- average value: **11.18 N/mm<sup>2</sup>**

The compressive strength can be recalculated for the purposes of computing to the normalized strength,  $f_b$ . The normalized strength for tested samples, following the available conversion procedures, has achieved the following values, (PN-EN 772-1:2011):

- for test sample No. 1: 11.04 N/mm<sup>2</sup>
- for test sample No. 2: 7.32 N/mm<sup>2</sup>
- for test sample No. 3: 11.68 N/mm<sup>2</sup>
- average value: **10.01 N/mm<sup>2</sup>**

The tested blocks were certified for the declared strength of class 15, which meant that the average normalized compressive strength should not be less than 15.0 N/mm<sup>2</sup>. This condition in case of tested samples was not met. Silicate masonry elements examined could be classified at most to class 10. It should be pointed out, that in case when the manufacturer declares an average compressive strength or class, the individual values of normalized compressive strength within the sample should not be less than 80% of the declared value (in this case 80% x 15.0 N/mm<sup>2</sup> = 12.0 N/mm<sup>2</sup>), which was not met in any case of the samples in question. It should be also noted, that the results for the sample marked No. 2 stands out quite significantly from the values obtained for sample No. 1 and No. 3. If the results of these studies were the nature of the statistical surveys, the results should be formally discarded and not included when calculating the average value. Due to the small sample size, the result obtained for the test item No. 2 is a valuable source of information on differentiation of the strength parameters of the various elements, depending on the individual level of damage of each of them.

On the basis of the tests results it can be said that the silicate masonry blocks did not meet the requirements assumed in the design project of class 15. At most, in the present state they can

be classified as class 10. Such a value of the normalized compressive strength was adopted in the calculations carried out in the next step to check the capacity of the wall damaged by fire.

## 2.2 Tests on drilled concrete cores

In addition some test were also carried out on four drilled concrete cores with a nominal diameter of 95 mm and a depth of about 300 mm each, taken from the ring beam surrounding the floor above the ground floor, just to verify its strength parameters. Average compressive strength of the inner layer of the ring beam achieved the level of  $36.10 \text{ N/mm}^2$ , while the same parameter assessed for the surface layer reached only the value of  $21.91 \text{ N/mm}^2$ , which is about of 40% lower. Based on the test results and the code procedures the characteristic value of compressive strength of the concrete built into the structure was specified, which in the analyzed case was equal, respectively to:

- for inner layer:  $29.10 \text{ N/mm}^2$
- for surface layer:  $14.91 \text{ N/mm}^2$

According to PN-EN 13791:2008 testing of the drilled concrete cores of length equal to the nominal diameter yields a value corresponding to the characteristic strength  $f_{ck, is, cube}$  for the cubic standardized sample. Based on the results and according to PN-EN 13791:2008 the concrete samples satisfy the following classes of concrete compressive strength developed according to PN-EN 206-1:2003:

- for inner layer: C25/30 ( $f_{ck, is, cube} < 31 \text{ N/mm}^2$ )
- for surface layer: C12/15 ( $f_{ck, is, cube} < 17 \text{ N/mm}^2$ )



Fig. 4 Discoloration depth corresponding to the depth of destruction of the drilled concrete cores

As can be seen from the above given analyzes the concrete surface layer has been destroyed in a result of high temperatures exposure and sudden cooling down, and its strength was significantly reduced by 3 classes.

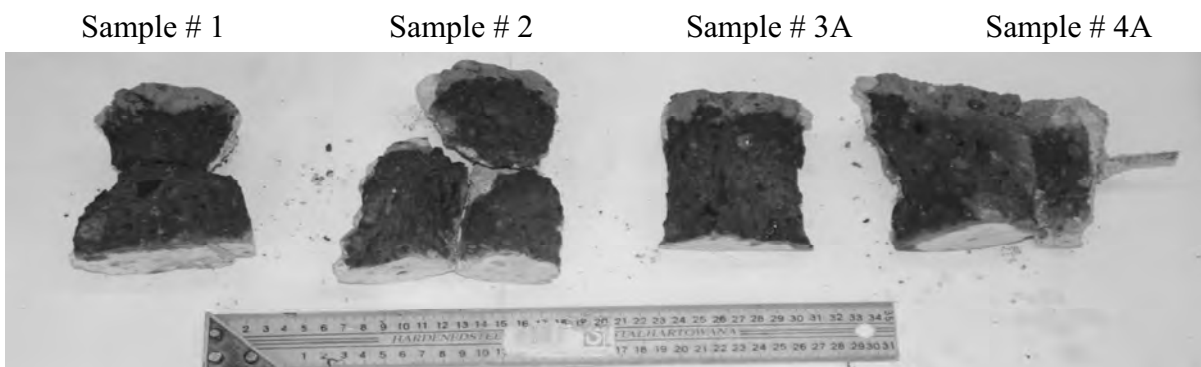


Fig. 5 Depth of carbonation in drilled core breakthroughs

Since, during sampling, some clear discolorations of subsurface of cores were observed and in addition to strength testing also some detailed visual analysis of the four samples were carried out, (Fig. 4). It was supposed that the visible discoloration was the most likely caused by the damage of concrete internal structure. To accurately determine the depth of discoloration, samples were evenly moistened, and then after 3 minutes the destruction range was marked with the marker. Discoloration depth corresponding to the depth of destruction reached from 1.5 up to 5 cm. After the cores destruction an additional test of concrete carbonation depth of breakthroughs were done. The depth of carbonation ranged from 1.5 to 2.5 cm. In addition, it was found that the extent of carbonation range in sample No. 1 has already reached more than a size of concrete cover of stirrups, which may cause rapid corrosion of reinforcing steel, deprived of protective covering layer, (Fig. 5).

### **3 ANALYTICAL EVALUATION OF THE LOADBEARING CAPABILITIES**

#### **3.1 Assumptions for the calculations**

Wall loadbearing calculation analyzes were carried out for two design situations:

- for the wall in perfect technical condition (as initially designed) and
- for the real wall in the weakened condition reflecting the destruction after the fire.

Calculations performed in perfect technical conditions, assumed the initial characteristics of the wall material and strength parameters of the idealized structure, were carried out totally consistently with the original design documentation. In the second design situation, the reduced strength values of the silicate blocks, based on the results obtained from the real compression tests of the wall elements, were adopted. Additionally, due to the numerous vertical cracks parallel to the wall surface, for the calculation model it was assumed, that the wall is made with longitudinal mortar seam, which allows for the inclusion in the procedure of computing the potential danger of delamination of the wall through its thickness. Furthermore, for each of the variants, the calculations were performed twice - including the articulated (simple) model of wall in which the wall is modeled as the separate bar, pivotally supported by a horizontal slabs or alternatively - a model of a continuous wall.

Having regard to the current state of the building and its exclusion from the use after the fire, all the calculations (due to legal expectations) were carried out in accordance with the actual state of standardization, (Eurocode 6, 2010). In addition, after the declaration of conformity it was adopted that the wall blocks correspond to the parameters established for the Group 1 (for which the capacity of all openings shall not exceed 25% of the gross volume) and Category I of masonry elements. Additionally, a category B of the masonry works execution standard was assumed, which affects the size of the partial safety factors to be adopted in the calculation of the wall.

Calculations were carried out assuming the vertical wall straightness, without taking into consideration any deviations or eccentricities measured during an on-site inspection. Their influence, in fact, increases the level of capacity utilization of the wall in relation to the values obtained from the calculations, and presented in the further part of this study.

#### **3.2 Results of calculations for the assumption of perfect technical condition**

After the calculations, the following results reflecting the capacity utilization level of the fire separating wall were achieved:

- for a simple model, pivotally supported by slabs; wall considered as the inner structure (without the wind load): 50.8 %,
- for a simple model, pivotally supported by slabs; wall considered as the external structure (with the wind load applied): 59 %,
- for the continuous model of the wall, considered as the inner structure (without the wind load): 118.5%,

- for the continuous model of the wall, considered as the external structure (with the wind load applied): 135.6%.

### 3.3 Results of calculations reflecting the real weakened condition of the wall, after a fire

After the calculations the following results reflecting the capacity utilization level of the fire separating wall were achieved:

- for a simple model, pivotally supported by slabs; wall considered as the external structure (with the wind load applied): 98 %,
- for a continuous model of the wall, considered as the external structure (with the wind load applied): 162%.

## 4 SUMMARY AND FINAL CONCLUSION

Based on the conducted analyzes the following summarizing conclusions can be formulated:

- the capacity utilization rate of the wall evaluated taking into account the damage caused by the fire and the reduced value of a standard compression strength of the wall material exceeded by 62% the maximum acceptable values in terms of design standards and could not be considered safe,
- through the degradation of the concrete ring beams and the decrease of the mechanical properties of reinforcing steel bars, some basic principles of legal certainty and predictability of the behavior of the structure have been violated, in particular:
  - the stability of structural elements (walls and floors),
  - the expected level of reliability,
  - performance and load-carrying mutual cooperation between the structural elements,
- there was a concern that the ring beams, whose job was to ensure the overall compactness of the object, and - if necessary - recreation of the secondary supporting structure of the building in the event of local damage (e.g. collapse of the wall underneath the ring beam), may not satisfy its role,
- the wall that suffered the poor technical condition after the fire, because of the number of defects and leaks, no longer could serve as a reliable fire separating partition.

On the way of expert activities a few different variants of the wall and office building restoration were considered. Due to the nature of the building construction and the unsatisfactory condition of the wall, the majority of the proposals to extend the life of the object have been dismissed as technologically difficult or unjustified because of economic reasons. Finally, the building inspection authorities decided to pull down the entire building.

## REFERENCES

- PN-EN 13791:2008 - Assessment of in-situ compressive strength in structures and precast concrete components, Polski Komitet Normalizacyjny, Warszawa, 2008, (in Polish),
- PN-EN 206-1:2003 - Concrete - Part 1: Specification, performance, production and conformity, Polski Komitet Normalizacyjny, Warszawa, 2003, (in Polish).
- PN-EN 1996-1-2:2010 - Eurocode 6 - Design of masonry structures - Part 1-2: General rules - Structural fire design, Polski Komitet Normalizacyjny, Warszawa, 2010, (in Polish),
- PN-EN 772-1:2011 – Methods of test for masonry units - Part 1: Determination of compressive strength, Polski Komitet Normalizacyjny, Warszawa, 2011, (in Polish),
- PN-EN 771-2:2006 – Specification for masonry units - Part 2: Calcium silicate masonry units, Polski Komitet Normalizacyjny, Warszawa, 2006, (in Polish),
- PN-EN 1052-1:2000 – Methods of test for masonry - Part 1: Determination of compressive strength, Polski Komitet Normalizacyjny, Warszawa, 2000, (in Polish).



## AUTHOR INDEX

Abramowicz M., <i>Poland</i> .....	307	Gales J., <i>United Kingdom</i> .....	474
Anderson K., <i>United Kingdom</i> .....	36	Gambarova P.G., <i>Italy</i> .....	501
Armstrong C., <i>United Kingdom</i> .....	258	Gillie M., <i>United Kingdom</i> .....	36, 301
Arrais F., <i>Portugal</i> .....	244	Glasa J., <i>Slovak Republic</i> .....	340
Bamonte P., <i>Italy</i> .....	501	Glema A., <i>Poland</i> .....	220
Ban M., <i>Croatia</i> .....	480	Glowacki M., <i>Poland</i> .....	307
Bednář J., <i>Czech Republic</i> .....	386	Guiliani L., <i>Denmark</i> .....	265
Beikircher W., <i>Austria</i> .....	433	Guo Q., <i>USA</i> .....	96
Bhargava P., <i>India</i> .....	486	Halada L., <i>Slovak Republic</i> .....	340
Bilotta A., <i>Italy</i> .....	326	Harapin A., <i>Croatia</i> .....	480
Bisby L., <i>United Kingdom</i> .....	474	Hartmann P., <i>Austria</i> .....	433
Bjegovic D., <i>Croatia</i> .....	467	Hasalová L., <i>Czech Republic</i> .....	42
Blackford R., <i>United Kingdom</i> .....	474	Häßler D., <i>Germany</i> .....	454
Bojanowski C., <i>Poland</i> .....	13	Hayhoe W., <i>Canada</i> .....	352
Boko I., <i>Croatia</i> .....	480	Heinisuo M., <i>Finland</i> .....	23
Burgess I., <i>United Kingdom</i> .....	9, 207, 214, 361	Heistermann T., <i>Sweden</i> .....	272
Byström A., <i>Sweden</i> .....	290	Hora M., <i>Czech Republic</i> .....	346
Caldová E., <i>Czech Republic</i> .....	411	Horová K., <i>Czech Republic</i> .....	102
Couto C., <i>Portugal</i> .....	232	Hothan S., <i>Germany</i> .....	454
Craveiro H.D.S., <i>Portugal</i> .....	251	Hozjan T., <i>Slovenia</i> .....	314, 392, 417
Dai X., <i>United Kingdom</i> .....	361	Hricák J., <i>Czech Republic</i> .....	226
Davison B., <i>United Kingdom</i> .....	207, 214	Huang S-S., <i>United Kingdom</i> .....	361
De Sanctis G., <i>Switzerland</i> .....	89	Huang Y., <i>China</i> .....	461
Dehn F., <i>Germany</i> .....	49	Huang Z., <i>United Kingdom</i> .....	166
Del Prete I., <i>Italy</i> .....	326	Choi S., <i>Korea</i> .....	320
Dobrucky M., <i>Slovak Republic</i> .....	340	Iqbal N., <i>Sweden</i> .....	272
Dondera A., <i>Denmark</i> .....	265	Ira J., <i>Czech Republic</i> .....	42
Dong G., <i>United Kingdom</i> .....	207	Jadhav S., <i>USA</i> .....	125
Drosopoulos G.A., <i>Germany</i> .....	193	Jahoda M., <i>Czech Republic</i> .....	42
Du Y., <i>China</i> .....	284	Jána T., <i>Czech Republic</i> .....	278
Dudorova Z., <i>United Kingdom</i> .....	474	Jandera M., <i>Czech Republic</i> .....	173, 226
Dufková M., <i>Czech Republic</i> .....	423	Jeffers A.E., <i>USA</i> .....	96
El-Fitiany S.F., <i>Canada</i> .....	334, 352	Jiang J., <i>China</i> .....	380
Entler S., <i>Czech Republic</i> .....	102	Jirků J., <i>Czech Republic</i> .....	294
Faggiano B., <i>Italy</i> .....	138	Johnson L., <i>United Kingdom</i> .....	214
Fan M., <i>United Kingdom</i> .....	166	Johnston R.P.D., <i>United Kingdom</i> .....	258
Fontana M., <i>Switzerland</i> .....	89	Khaliq W., <i>Pakistan</i> .....	493
Formisano A., <i>Italy</i> .....	138	Kim S., <i>Korea</i> .....	320
Gabrijel I., <i>Croatia</i> .....	467	Kirsch T., <i>Germany</i> .....	200
		Klinzmann C., <i>Germany</i> .....	114

Kodur V., <i>USA</i> .....	108, 493	Prachař M., <i>Czech Republic</i> .....	173
Kögl J., <i>Austria</i> .....	433	Procházka J., <i>Czech Republic</i> .....	346
Kohler J., <i>Norway</i> .....	89	Raut N., <i>USA</i> .....	493
Kohoutková A., <i>Czech Republic</i> .....	386	Ribeiro J., <i>Portugal</i> .....	186
Kolšek J., <i>Slovenia</i> .....	392	Rigueiro C., <i>Portugal</i> .....	186
Kowalski R., <i>Poland</i> .....	307	Robertson L., <i>United Kingdom</i> .....	474
Kraus P., <i>Germany</i> .....	447	Rodrigues J.P.C., <i>Portugal</i> .....	79, 251
Król P.A., <i>Poland</i> .....	507	Roy Danie A.B., <i>India</i> .....	486
Kuklík P., <i>Czech Republic</i> .....	423	Rukavina M.J., <i>Croatia</i> .....	467
Kuklíková A., <i>Czech Republic</i> .....	411	Ružić D., <i>Slovenia</i> .....	314
Kurzawa Z., <i>Poland</i> .....	73, 220	Saje M., <i>Slovenia</i> .....	314, 392
Kwaśniewski L., <i>Poland</i> .....	13, 29	Salaverri M., <i>United Kingdom</i> .....	301
Laim L.M.S., <i>Portugal</i> .....	79, 251	Saleta D., <i>Poland</i> .....	55
Li G-Q., <i>China</i> .....	380	Sandström J., <i>Sweden</i> .....	153, 290
Lim J.B.P., <i>United Kingdom</i> .....	258	Santiago A., <i>Portugal</i> .....	186, 272
Lin S., <i>United Kingdom</i> .....	166	Sawicki B., <i>Poland</i> .....	29
Lopes F., <i>Portugal</i> .....	272	Sedlák P., <i>Slovakia</i> .....	427
Lopes N., <i>Portugal</i> .....	232, 244	Sekret R., <i>Poland</i> .....	55
Łukacz M., <i>Poland</i> .....	238	Selamet S., <i>Turkey</i> .....	399
Malendowski M., <i>Poland</i> .....	73, 220	Sharma U.K., <i>India</i> .....	486
Maślak M., <i>Poland</i> .....	238	Schaumann P., <i>Germany</i> .....	200, 447
Mazzolani F.M., <i>Italy</i> .....	138	Schlee S., <i>Germany</i> .....	49
Mensing M., <i>Germany</i> .....	447	Schmidt J., <i>Germany</i> .....	49
Mirza O., <i>Australia</i> .....	441	Simoos da Silva L., <i>Portugal</i> .....	272
Mistakidis E., <i>Greece</i> .....	131, 405	Simon P., <i>Germany</i> .....	49
Molkens T., <i>Belgium</i> .....	61, 144	Smardz P., <i>Poland</i> .....	55
Morgado H.J.L., <i>Portugal</i> .....	79	Smith H., <i>United Kingdom</i> .....	474
Naser M., <i>USA</i> .....	108	Sonebi M., <i>United Kingdom</i> .....	258
Nguyen T-T., <i>Singapore</i> .....	368, 374	Stavroulakis G.E., <i>Greece</i> .....	193
Nigro E., <i>Italy</i> .....	326	Stratford T., <i>United Kingdom</i> .....	474
Outinen J., <i>Finland</i> .....	160	Sun R., <i>United Kingdom</i> .....	207
Ozyurt E., <i>United Kingdom</i> .....	179	Szilagyi C., <i>Hungary</i> .....	67
Paliga K., <i>Germany</i> .....	114	Sztarbała G., <i>Poland</i> .....	55
Palmiere E., <i>United Kingdom</i> .....	214	Szumigala M., <i>Poland</i> .....	73
Pantousa D., <i>Greece</i> .....	131, 405	Štefan R., <i>Czech Republic</i> .....	346
Partanen M., <i>Finland</i> .....	23	Tabaddor M., <i>USA</i> .....	125
Pečenko R., <i>Slovenia</i> .....	417	Tabeling F., <i>Germany</i> .....	447
Pełczyński J., <i>Poland</i> .....	29	Tan K-H., <i>Singapore</i> .....	368, 374
Peroš B., <i>Croatia</i> .....	480	Thackray R., <i>United Kingdom</i> .....	214
Planinc I., <i>Slovenia</i> .....	314, 392	Torić N., <i>Croatia</i> .....	480
Polus L., <i>Poland</i> .....	73, 220	Tsapara K., <i>Greece</i> .....	193

Tsatsoulas D., <i>Greece</i> .....	120
Turk G., <i>Slovenia</i> .....	417
Usmani A., <i>United Kingdom</i> .....	380
Vaari J., <i>Finland</i> .....	160
Valasek L., <i>Slovak Republic</i> .....	340
Vargovský K., <i>Slovakia</i> .....	427
Vega E., <i>United Kingdom</i> .....	474
Veljkovic M., <i>Sweden</i> .....	272, 290
Vila Real P., <i>Portugal</i> .....	232, 244
Vodička J., <i>Czech Republic</i> .....	386
Wald F., <i>Czech Republic</i> .....	9, 173, 226, 278, 294, 386, 411
Wang Y.C., <i>United Kingdom</i> .....	179
Weisenpacher P., <i>Slovak Republic</i> .....	340
Wickström U., <i>Sweden</i> .....	153, 290
Wilkins K., <i>Australia</i> .....	441
Wrzesien A.M., <i>United Kingdom</i> .....	258
Yom K., <i>Korea</i> .....	320
Young B., <i>China</i> .....	461
Youssef M.A., <i>Canada</i> .....	334, 352
Zachar M., <i>Slovakia</i> .....	427
Zehfuss J., <i>Germany</i> .....	114
Zhao B., <i>France</i> .....	232
Zografopoulou K., <i>Greece</i> .....	131

## **SCIENTIFIC COMMITTEE**

BURGESS Ian, *United Kingdom*  
Chairman  
BLOCK Florian, *United Kingdom*  
DE LA QUINTANA Jesus, *Spain*  
DEHN Frank, *Germany*  
FRANSSEN Jean-Marc, *Belgium*  
FARIS Ali, *United Kingdom*  
GAMBAROVA Pietro, *Italy*  
KHOURI Gabriel A., *United Kingdom*  
KODUR Venkatesh, *USA*  
LI Guo Qiang, *China*  
LUO Ming Chun, *China (Hong Kong)*  
MAHENDRAN Mahen, *Australia*  
MORENTE Fernando Belmez, *Spain*  
OKSANEN Tuuli, *Finland*  
OUTINEN Jyri, *Finland*  
REIN Guillermo, *United Kingdom*  
SCHAUMANN Peter, *Germany*  
TAERWE Luc, *Belgium*  
TAN Kang Hai, *Singapore*  
VASSART Olivier, *Luxembourg*  
VELJKOVIC Milan, *Sweden*  
VILA REAL Paulo, *Portugal*  
WANG Yong, *United Kingdom*  
ZAHARIA Raul, *Romania*  
ZHAO Bin, *France*

## **ORGANIZING COMMITTEE**

BEDNÁŘ Jan, *Czech Republic*  
DUDÁČEK Aleš, *Czech Republic*  
HOROVÁ Kamila, *Czech Republic*  
JÁNA Tomáš, *Czech Republic*  
KAISER Rudolf, *Czech Republic*  
KREGL František, *Czech Republic*  
KUČERA Petr, *Czech Republic*  
KUKLÍK Petr, *Czech Republic*  
PROCHÁZKA Jaroslav, *Czech Republic*  
SOKOL Zdeněk, *Czech Republic*  
VAŠKOVÁ Jitka, *Czech Republic*  
WALD František, *Czech Republic*  
Chairman